STUDIES OF IONIC MECHANISMS IN MODEL CELL LINES OF PROSTATE CANCER

Nahit Rizaner

Imperial College London

Division of Cell and Molecular Biology

Ph.D.

For my family.

This dissertation is the result of my own work unless otherwise acknowledged in the text or by references.

Signed: Nahit RIZANER

Date: November 8, 2010

Acknowledgements

This PhD was financially supported by Pro Cancer Research Fund (PCRF).

First of all, I would like to thank my supervisor, Prof Mustafa Djamgoz for his greate support and advice. This PhD would not have been possible without him.

I would like to thank my advisors Dr H. Keun and Dr R.O.J. Weinzierl for their help and advice; Dr Scott Fraser, Dr James Diss, Dr. Dongmin Shao and Rustem Onkal for their assistance and discussion; Dr Kenji Okuse and Alessandro Pristera for advice on Ca^{2+} imaging.

I would also like to thank each member of the Neuroscience Solution to Cancer Research Group for their friendship.

Finally I would like to thank to my family for their endless support.

Abstract

Metastasis is the major problem in clinical management of cancer, including prostate cancer (PCa). Biochemical conditions in tumour microenvironment (especially O_2 and Ca^{2+} levels) are important for modulating metastatic cell behaviours (MCBs). Ionic mechanisms, in particular voltage-gated sodium channel (VGSC) and intracellular Ca^{2+} activities, were shown previously to be involved in MCBs in PCa. This PhD tested the hypotheses (1) that MCBs would be sensitive to hypoxia and be inhibited by VGSC blockers including those selective for the persistent current and (2) that VGSC activity would control intracellular Ca^{2+} signalling. Experiments were carried on a variety of model cell lines in a comparative approach: strongly metastatic Mat-LyLu and weakly metastatic AT-2 rat PCa cells, and analogous human PCa cell lines (PC-3M and LnCaP, respectively). Experiments on Mat-LyLu cells showed that hypoxia (2 % O_2, 24 h) increased mRNA expression of Nav1.7, the predominant VGSC α-subunit expressed in PCa; however, both plasma membrane and intracellular VGSC protein levels were reduced. There was no change in cellular proliferation, Matrigel invasion or lateral motility, whilst transverse migration increased significantly. Treatment (24 h) with the VGSC blockers ranolazine, riluzole, lidocaine and procaine (micromolar concentrations) decreased Nav1.7 mRNA and total VGSC protein levels, and suppressed Matrigel invasion in both normoxia (~21 % O_2) and hypoxia. PC-3M (but not LNCaP or Mat-LyLu) cells showed spontaneous, transient elevations of intracellular Ca^{2+} ("Ca^{2+} oscillations"). Ionic substitution and pharmacological experiments suggested that Ca^{2+} influx and release from intracellular stores both contributed to the oscillations. Importantly, acute treatment with tetrodotoxin and ranolazine decreased the oscillation amplitude and frequency. Thus, both hypotheses were confirmed, i.e. (1) that hypoxia increases

PCa (Mat-LyLu) cell migration and VGSC expression and (2) that intracellular Ca^{2+} oscillations are downstream to VGSC activity. Overall, the thesis concludes that VGSC blockers could serve clinically as anti-metastatic agents.

Table of Contents

Acknowledgements 4

Abstract 5

Table of Contents 7

List of Figures 15

List of Tables 22

List of Videos 23

Abbreviations 25

Chapter 1 GENERAL INTRODUCTION 30

1.1 Voltage-gated sodium channels 31

1.1.1 Basic structure and molecular diversity 31

1.1.1.1 VGSCα 32

1.1.1.2 VGSCβ 41

1.2. Regulation of VGSCs 44

1.2.1 Transcription 44

1.2.2 Alternative splicing 46

1.2.3 Post-translational modification: Glycosylation 52

1.2.4 Protein synthesis and trafficking 53

1.2.5 Protein degradation 56

1.2.6 Phosphorylation 57

1.3. Metastatic disease 58

1.3.1 The case of prostate cancer 60

1.3.2 The metastatic cascade 63

1.3.3 VGSC expression in metastatic disease 68

1.3.3.1 In vitro 68

1.3.3.2 In vivo 71

1.3.4 Involvement of VGSCs in metastatic disease 71

1.3.5 Other ion channels expressed in prostate and breast cancers 77

1.3.6 Possible downstream mechanisms involved in VGSC activity-dependent promotion of MCBs 83

1.4 Aims and scope of the present study 85

Chapter 2 MATERIALS AND METHODS 87

2.1 Cell lines and culture conditions. 88

2.1.1 Dunning rat PCa cell lines 89

2.1.2 Human PCa cell lines 89

2.2 Pharmacology 90

2.2.1 Pharmacological agents 90

2.2.2 Toxicity assay 90

2.3 Polymerase chain reaction (PCR) 92

2.3.1 RNA extraction 92

2.3.2 cDNA synthesis 93

2.3.3 Real-time PCR 93

2.3.4 Agarose gel electrophoresis 95

2.4 Western blotting 99

2.4.1 Extraction of total protein 99

2.4.2 Sodium dodecyl sulphate polyacrylamide gel electrophoresis (SDS-PAGE) and immunoblotting 99

2.4.3 Densitometry 101

2.5 Immunocytochemistry 105

2.5.1 Confocal microscopy 106

2.6 Morphological analysis 107

2.7 Measurement of cell number - MTT assay 109

2.8 Lateral motility (wound-heal) assay 111

2.9 Transwell migration assay 112

2.1 Matrigel invasion assay 112

2.11 Intracellular calcium imaging 113

2.12 Data analyses 114

Chapter 3 EFFECTS OF CHRONIC HYPOXIA ON VOLTAGE-GATED Na^+ CHANNEL EXPRESSION AND METASTATIC CELL BEHAVIOURS OF DUNNING PROSTATE CANCER 116

3.1 Introduction 117

3.1.1 Aims and scope of the present study 119

3.2 Results 119

3.2.1 Some initial observations: Effects of chronic hypoxia on cell morphology 119

3.2.2 Effects of chronic hypoxia 134

3.2.2.1 Cell viability 134

3.2.2.2 Cellular proliferation 134

3.2.2.3 Nav1.7 mRNA expression 134

3.2.2.4 VGSCβ subunit mRNA expression 138

3.2.2.4.1 Normoxia 138

3.2.2.4.2 Hypoxia 140

3.2.2.5 Expression of VGSCα protein 144

3.2.2.5.1 Control experiments 147

3.2.2.5.2 Plasma membrane VGSCα protein level 147

3.2.2.5.3 Intracellular VGSCα protein level 147

3.2.2.5.4 Subcellular distribution 152

3.2.2.6 VGSCβ1 protein expression 152

3.2.2.6.1 Plasma membrane VGSCβ1 protein level 152

3.2.2.6.2 Intracellular VGSCβ1 protein level 152

3.2.2.6.3 Subcellular distribution 156

3.2.2.7 Studies on metastatic cell behaviours 156

3.2.2.7.1 Lateral motility 156

3.2.2.7.2 Transwell migration 160

3.2.2.7.3 Matrigel invasion 160

3.3 Discussion 163

3.3.1 Effect of hypoxia on morphological development 163

3.3.2 Effect of hypoxia on proliferation 165

3.3.3 Regulation of VGSCα subunit expression by hypoxia 166

3.3.3.1 Nav1.7 mRNA expression 166

3.3.3.2 VGSCα protein expression 167

3.3.3.3 Relative subcellular distribution of VGSC protein 168

3.3.4 VGSCβ subunit expression in Mat-LyLu and AT2 cells 169

3.3.5 Regulation of VGSCβ expression by hypoxia 172

3.3.5.1 VGSCβ mRNA expression 172

3.3.5.2 VGSCβ1 protein expression 173

3.3.5.3 Relative subcellular distribution of VGSCβ1 protein 173

3.3.6 Hypoxic regulation of metastatic activity of Mat-LyLu cells and possible involvement of VGSC activity 174

3.3.6.1 Lateral motility 174

3.3.6.2 Transverse migration 174

3.3.6.3 Matrigel invasion 175

3.4 Concluding remarks 177

Chapter 4 EFFECTS OF PHARMACOLOGICAL BLOCKERS ON VOLTAGE-GATED Na+ CHANNEL EXPRESSION AND METASTATIC CELL BEHAVIOURS OF DUNNING PROSTATE CANCER 178

4.1 Introduction 179

4.1.1 Aims and scope of the present study 181

4.2 Results 182

4.2.1 Effects of ranolazine 182

4.2.1.1 Some initial observations: Cell morphology 182

4.2.1.2 Cell viability 185

4.2.1.3 Cellular proliferation 185

4.2.1.4 Nav1.7 mRNA expression 185

4.2.1.5 Subcellular VGSCα protein expression 189

4.2.1.5.1 Relative distribution 189

4.2.1.5.2 Plasma membrane VGSCα protein level 189

4.2.1.5.3 Internal VGSCα protein level 193

4.2.1.6 Matrigel invasion 193

4.2.1.7 Summary of the effects of ranolazine 198

4.2.2 Effects of riluzole 198

4.2.2.1 Some initial observations: Cell morphology 202

4.2.2.2 Cell viability 202

4.2.2.3 Cellular proliferation 202

4.2.2.4 Nav1.7 mRNA expression 207

4.2.2.5 Subcellular VGSCα protein expression 209

4.2.2.5.1 Relative distribution 209

4.2.2.5.2 Plasma membrane VGSCα protein level 209

4.2.2.5.3 Internal VGSCα protein level 215

4.2.2.6 Matrigel invasion 215

4.2.2.7 Summary of effects of riluzole 220

4.2.3 Effects of procaine 220

4.2.3.1 Some initial observations: Cell morphology 220

4.2.3.2 Cell viability 221

4.2.3.3 Cellular proliferation 221

4.2.3.4 Nav1.7 mRNA expression 226

4.2.3.5 Subcellular VGSCα protein expression 226

4.2.3.5.1 Relative distribution 226

4.2.3.5.2 Plasma membrane VGSCα protein level 230

4.2.3.5.3 Internal VGSCα protein level 230

4.2.3.6 Matrigel invasion 236

4.2.3.7 Summary of effects of procaine 236

4.2.4 Effects of lidocaine 236

4.2.4.1 Some initial observations: Cell morphology 239

4.2.4.2 Cell viability 239

4.2.4.3 Cellular proliferation 239

4.2.4.4 Nav1.7 mRNA expression 244

4.2.4.5 Subcellular VGSCα protein expression 244

4.2.4.5.1 Relative distribution 244

4.2.4.5.2 Plasma membrane VGSCα protein level 246

4.2.4.5.3 Internal VGSCα protein level 246

4.2.4.6 Matrigel invasion 252

4.3 Discussion 252

4.3.1 Effects of hypoxia alone 258

4.3.2 Observations on cell morphology 258

4.3.3 Effects on cell number 259

4.3.4 mRNA versus protein expression 260

4.3.5 Effects of ranolazine 261

4.3.6 Effects of riluzole 263

4.3.7 Effects of procaine 266

4.3.8 Effects of lidocaine 267

4.4 Concluding remarks 268

Chapter 5 STUDY OF INTRACELLULAR Ca^{2+} OSCILLATIONS IN HUMAN METASTATIC PROSTATE CANCER PC-3M CELLS 269

5.1 Introduction 270

5.2 Aims and scope of the present study 273

5.3 Results 273

5.3.1 Spontaneous oscillations of intracellular Ca^{2+} in PCa cells: Basic 274

5.3.2 Effects of VGSC blockers on Ca^{2+} oscillations in PC-3M cells 277

5.3.2.1 Effect of TTX 277

5.3.2.2 Effect of ranolazine 277

5.3.3 Effects of Na^{+}-free conditions on Ca^{2+} oscillations 282

5.3.3.1 Effect of Li^{+}-substituted Na^{+}-free solution 282

5.3.3.2 Effect of choline-substituted Na^{+}-free solution 285

5.3.4 Involvement of extracellular Ca^{2+} in spontaneous Ca^{2+} oscillations 285

5.3.5 Effects of thapsigargin and EGTA on spontaneous Ca^{2+} oscillations 289

5.3.6 Effects of caffeine and ryanodine on spontaneous Ca^{2+} oscillations 292

5.4 Discussion 293

5.4.1 Calcium signalling in PCa cells 297

5.4.2 A model of intracellular Ca^{2+} oscillations in PC-3M cells 301

5.4.3Role of the various subcellular mechanisms in Ca^{2+} signalling / 304

5.4.3.1 VGSC and cation (Na^{+}) influx 304

5.4.3.2 Extracellular Ca^{2+} 305

5.4.3.3 Thapsigargin 305

5.4.3.4 Ryanodine receptor 306

5.4.4 Possible pathophysiolgical consequence of Ca^{2+} oscillations in PCa (PC-3M) cells and future perspectives 307

Chapter 6 GENERAL DISCUSSION 310

6.1 Summary of key findings 311

6.2 Hypoxic regulation of VGSC expression and MCB in PCa 313

6.3 Ca^{2+} signalling downstream to VGSC activity possibly leading to MCB regulation 315

6.4 Pharmacological VGSC inhibition and clinical implications 317

6.5 Future perspective 318

References 321

Publications 406

Appendice 408

List of Figures

Figure 1.1 Structure of voltage-gated Na^+ channels 33

Figure 1.2 Functional states of voltage-gated sodium channels 39

Figure 1.3 Mechanism of fast inactivation 40

Figure 1.4 Levels of regulation of VGSC expression and activity 45

Figure 1.5 VGSC regulatory sites 49

Figure 1.6 The metastatic cascade 65

Figure 2.1 Visual assessment of RNA quality by agarose gel electrophoresis. 94

Figure 2.2 Real-time PCR amplification and melting curves (typical examples). 97

Figure 2.3 Standard calibration (dilution) curves to validate PCR efficiency. 98

Figure 2.4 Protein standard calibration curve. 100

Figure 2.5 Protein dilutions and standard curves used to study Western blot band intensities. 104

Figure 2.6 Micrographs of a Mat-LyLu cell illustrating morphologic parameters used. 108

Figure 2.7 Examples of typical standard curves for MTT assay. 110

Figure 3.1 Phase-contrast light-photomicrography of Mat-LyLu cells. 120

Figure 3.2 Phase-contrast light-photomicrography of AT2 cells. 121

Fig. 3.3 Phase-contrast light-photomicrography of Mat-LyLu cells in high magnification. 123

Figure 3.4 Studies effects of hypoxia on number of non-process bearing Mat-LyLu cells. 125

Figure 3.5 Studies effects of hypoxia on number of monopolar Mat-LyLu cells. 126

Figure 3.6 Studies effects of hypoxia on number of bipolar Mat-LyLu cells. 128

Figure 3.7 Studies effects of hypoxia on number of multipolar Mat-LyLu cells. 129

Figure 3.8 Bar diagram showing quantitative effect of hypoxia on cell body diameter. 130

Figure 3.9 Bar diagram showing quantitative effect of hypoxia on cell area. 131

Figure 3.10 Histograms showing quantitative effect of hypoxia on process thickness. 132

Figure 3.11 Histograms showing quantitative effect of hypoxia on process length. 133

Figure 3.12 Bar diagram showing treatments had no toxic effect. 135

Figure 3.13 Time dependent effect of hypoxia (2 % O_2) on Mat-LyLu (A) and AT-2 (B) cell number. 136

Figure 3.14 Effect of hypoxia (2 % O_2) on Mat-LyLu and AT-2 Nav1.7 mRNA expression. 137

Figure 3.15 Basal mRNA expression profiles of VGSCβ subunits in Mat-LyLu and AT-2 cells. 139

Figure 3.16 Comparison of VGSCβ subunits mRNA expression, using Cytb5R as normalising/control gene, between Mat-LyLu and AT-2 cells. 141

Figure 3.17 Comparison of VGSCβ subunits mRNA expression, using α-actin as normalising/control gene, between Mat-LyLu and AT-2 cells. 142

Figure 3.18 Effect of hypoxia (2 % O_2) on VGSCβ subunits mRNA expression in Mat-LyLu cells. 143

Figure 3.19 Effect of hypoxia (2 % O_2) on VGSCβ subunits mRNA expression in AT2 cells. 145

Figure 3.20 Effect of hypoxia (2 % O_2) on VGSCα protein expression in Mat-LyLu cells. 146

Figure 3.21 Controls for Immunocytochemistry with Mat-LyLu cells. 148

Figure 3.22 Confocal images from immunochemistry of Mat-LyLu cells incubated in normoxia and hypoxia (2 % O_2) with pan-VGSC antibody. 149

Figure 3.23 Effect of hypoxia (2 % O_2) on VGSCα protein levels in plasma membrane of Mat-LyLu cells. 150

Figure 3.24 Effect of hypoxia (2 % O_2) on internal VGSCα protein levels of Mat-LyLu cells. 151

Figure 3.25 Effect of hypoxia (2 % O_2) on VGSCα protein distribution along typical cellular cross-section in Mat-LyLu cells. 153

Figure 3.26 Confocal images from immunochemistry of Mat-LyLu cells incubated in normoxia and hypoxia (2 % O_2) with VGSCβ1 antibody. 154

Figure 3.27 Effect of hypoxia (2 % O_2) on VGSCβ1 protein levels in plasma membrane of Mat-LyLu cells. 155

Figure 3.28 Effect of hypoxia (2 % O_2) on internal VGSCβ1 protein levels of Mat-LyLu cells. 157

Figure 3.29 Effect of hypoxia (2 % O_2) on VGSCβ1 protein distribution along typical cellular cross-section in Mat-LyLu cells. 158

Figure 3.30 Effect of hypoxia (2 % O_2) on lateral motility of Mat-LyLu cells. 159

Figure 3.31 Effect of hypoxia (2 % O_2) on migration of Mat-LyLu cells. 161

Figure 3.32 Effect of hypoxia (2 % O_2) on invasion of Mat-LyLu cells. 162

Figure 4.1 Phase-contrast light-photomicrography of Mat-LyLu cells treated with ranolazine. 183

Figure 4.2 Phase-contrast light-photomicrography of Mat-LyLu cells, treated with ranolazine in high magnification. 184

Figure 4.3 Bar diagram showing ranolazine treatments had no toxic effect. 186

Figure 4.4 Dose dependent effect of ranolazine on Mat-LyLu cell number. 187

Figure 4.5 Effect of ranolazine on Mat-LyLu Nav1.7 mRNA expression. 188

Figure 4.6 Confocal immunocytochemistry study of Mat-LyLu cells incubated with ranolazine. 190

Figure 4.7 Typical image showing effect of ranolazine on VGSCα protein distribution along typical cellular cross-section in Mat-LyLu cells. 191

Figure 4.8 Effect of ranolazine on VGSCα protein distribution along typical cellular cross-section in Mat-LyLu cells. 192

Figure 4.9 Typical image showing effect of ranolazine on VGSCα protein levels in plasma membrane of Mat-LyLu cells. 194

Figure 4.10 Effect of ranolazine on VGSCα protein levels in plasma membrane of Mat-LyLu cells. 195

Figure 4.11 Typical image showing effect of ranolazine on internal VGSCα protein levels of Mat-LyLu cells. 196

Figure 4.12 Effect of ranolazine on internal VGSCα protein levels of Mat-LyLu cells. 197

Figure 4.13 Typical images of invaded cells showing the effect of ranolazine on invasion of Mat-LyLu invesiveness. 199

Figure 4.14 Effect of ranolazine on invasion of Mat-LyLu cells. 200

Figure 4.15 Phase-contrast light-photomicrography of Mat-LyLu cells, treated with riluzole. 203

Figure 4.16 Phase-contrast light-photomicrography of Mat-LyLu cells, treated with riluzole, in high magnification. 204

Figure 4.17 Bar diagram showing riluzole treatments had no toxic effect. 205

Figure 4.18 Dose dependent effect of riluzole on Mat-LyLu cell number. 206

Figure 4.19 Effect of riluzole on Mat-LyLu Nav1.7 mRNA expression. 208

Figure 4.20 Confocal immunocytochemistry study of Mat-LyLu cells incubated with riluzole. 210

Figure 4.21 Typical image showing effect of riluzole on VGSCα protein distribution along typical cellular cross-section in Mat-LyLu cells. 211

Figure 4.22 Effect of riluzole on VGSCα protein distribution along typical cellular cross-section in Mat-LyLu cells. 212

Figure 4.23 Typical image showing effect of riluzole on VGSCα protein levels in plasma membrane of Mat-LyLu cells. 213

Figure 4.24 Effect of riluzole on VGSCα protein levels in plasma membrane of Mat-LyLu cells. 214

Figure 4.25 Typical image showing effect of riluzole on internal VGSCα protein levels of Mat-LyLu cells. 216

Figure 4.26 Effect of riluzole on internal VGSCα protein levels of Mat-LyLu cells. 217

Figure 4.27 Typical images of invaded cells showing the effect of riluzole on invasion of Mat-LyLu invasiveness. 218

Figure 4.28 Effect of riluzole on invasion of Mat-LyLu cells. 219

Figure 4.29 Phase-contrast light-photomicrography of Mat-LyLu cells, treated with procaine. 222

Figure 4.30 Phase-contrast light-photomicrography of Mat-LyLu cells, treated with procaine, in high magnification. 223

Figure 4.31 Bar diagram showing procaine treatments had no toxic effect. 224

Figure 4.32 Dose dependent effect of procaine on Mat-LyLu cell number. 225

Figure 4.33 Effect of procaine on Mat-LyLu Nav1.7 mRNA expression. 227

Figure 4.34 Confocal immunocytochemistry study of Mat-LyLu cells incubated with procaine. 228

Figure 4.35 Typical image showing effect of procaine on VGSCα protein distribution along typical cellular cross-section in Mat-LyLu cells. 229

Figure 4.36 Effect of procaine on VGSCα protein distribution along typical cellular cross-section in Mat-LyLu cells. 231

Figure 4.37 Typical image showing effect of procaine on VGSCα protein levels in plasma membrane of Mat-LyLu cells. 232

Figure 4.38 Effect of procaine on VGSCα protein levels in plasma membrane of Mat-LyLu cells. 233

Figure 4.39 Typical image showing effect of procaine on internal VGSCα protein levels of Mat-LyLu cells. 234

Figure 4.40 Effect of procaine on internal VGSCα protein levels of Mat-LyLu cells. 235

Figure 4.41 Typical images of invaded cells showing the effect of procaine on invasion of Mat-LyLu invasiveness. 237

Figure 4.42 Effect of procaine on invasion of Mat-LyLu cells. 238

Figure 4.43 Phase-contrast light-photomicrography of Mat-LyLu cells treated with lidocaine. 240

Figure 4.44 Phase-contrast light-photomicrography of Mat-LyLu cells, treated with lidocaine, in high magnification. 241

Figure 4.45 Bar diagram showing lidocaine treatments had no toxic effect. 242

Figure 4.46 Dose dependent effect of lidocaine on Mat-LyLu cell number. 243

Figure 4.47 Effect of lidocaine on Mat-LyLu Nav1.7 mRNA expression. 245

Figure 4.48 Confocal immunocytochemistry study of Mat-LyLu cells incubated with with lidocaine. 247

Figure 4.49 Typical image showing effect of lidocaine on VGSCα protein distribution along typical cellular cross-section in Mat-LyLu cells. 248

Figure 4.50 Effect of lidocaine on VGSCα protein distribution along typical cellular cross-section in Mat-LyLu cells. 249

Figure 4.51 Typical image showing effect of lidocaine on VGSCα protein levels in plasma membrane of Mat-LyLu cells. 250

Figure 4.52 Effect of lidocaine on VGSCα protein levels in plasma membrane of Mat-LyLu cells. 251

Figure 4.53 Typical image showing effect of lidocaine on internal VGSCα protein levels of Mat-LyLu cells. 253

Figure 4.54 Effect of lidocaine on internal VGSCα protein levels of Mat-LyLu cells. 254

Figure 4.55 Typical images of invaded cells showing the effect of lidocaine on Mat-LyLu invasiveness. 255

Figure 4.56 Effect of lidocaine on invasion of Mat-LyLu cells. 256

Figure 5.1 Spontaneous Ca^{2+} oscillations in PC3M cells. 275

Figure 5.2 Spontaneous changes in $[Ca^{2+}]_i$ in LNCaP and Mat-LyLu cells 276

Figure 5.3 Effect of TTX on spontaneous Ca^{2+} oscillations in PC-3M cells 278

Figure 5.4 Summary of the effects of TTX on spontaneous Ca^{2+} oscillations in PC-3M cells. 279

Figure 5.5 Effect of ranolazine on spontaneous Ca^{2+} oscillations in PC-3M cells. 280

Figure 5.6 Summary of the effects of ranolazine on spontaneous Ca^{2+} oscillations in PC-3M cells. 281

Figure 5.7 Effect of Na^+ free (Li^+ substituted) conditions on Ca^{2+} oscillations in PC-3M cells. 283

Figure 5.8 Summary of the effects of Na^+ free (Li^+- substituted) conditions on spontaneous Ca^{2+} oscillations in PC-3M cells. 284

Figure 5.9 Effect of Na^+ free (choline-substituted) MPS on Ca^{2+} oscillations in PC-3M cells. 286

Figure 5.10 Summary of the effects of Na^+ free (choline-substituted) MPS on spontaneous Ca^{2+} oscillations in PC-3M cells. 287

Figure 5.11 Effect of varying the extracellular $[Ca^{2+}]$ on spontaneous Ca^{2+} oscillations in PC-3M cells. 288

Figure 5.12 Effect of thapsigargin on Ca^{2+} oscillations in PC-3M cells. 290

Figure 5.13 Effect of extracellular and intracellular $[Ca^{2+}]$ on Ca^{2+} oscillations in PC-3M cells. 291

Figure 5.14 Effect of caffeine on Ca^{2+} oscillations in PC-3M cells. 294

Figure 5.15 Effect of ryanodine on Ca^{2+} oscillations in PC-3M cells. 295

Figure 5.16 Summary of the effects of ryanodine on spontaneous Ca^{2+} oscillations in PC-3M cells. 296

Figure 5.17 A basic model explaining possible mechanisms underlying spontaneous Ca^{2+} oscillations in PC3M cells. 302

List of Tables

Table 1.1 VGSCα -binding toxins and drugs 35

Table 1.2 VGSCα-subunit gene family 36

Table 1.3 VGSCβ isoforms 43

Table 1.4 Alternative splice variants of VGSCαs 47

Table 1.5 Expression/activity of VGSCs in metastatic cancer cells 69

Table 1.6 Changes in expression of Ca^{2+} channels and pumps in cancer 82

Table 2.1 Summary of pharmacological agents used in the present study. 91

Table 2.2 PCR primer related details. 96

Table 2.3 Primary antibodies. 102

Table 2.4 Secondary antibodies. 103

Table 3.1 Summary of effect of hypoxia on Mat-LyLu cell morphology and morphological heterogeneity 124

Table 4.1 Summary of results 201

Table 5.1 Synopsis of results 298

List of Videos

Supplementary Video 1- Spontaneous Ca2+ oscillations in PC3M cells. Signal from Fluo-4	DVD
Supplementary Video 2-Spontaneous Ca2+ oscillations in PC3M cells. Bright field images	DVD
Supplementary Video 3- Spontaneous changes in [Ca2+]i in LNCaP cells. Signal from Fluo-4	DVD
Supplementary Video 4- Spontaneous changes in [Ca2+]i in LNCaP cells. Bright field images	DVD
Supplementary Video 5- Spontaneous changes in [Ca2+]i in Mat-LyLu cells. Signal from Fluo-4	DVD
Supplementary Video 6- Spontaneous changes in [Ca2+]i in Mat-LyLu cells. Bright field images	DVD
Supplementary Video 7- Effect of TTX on spontaneous Ca2+ oscillations in PC-3M cells. Signal from Fluo-4	DVD
Supplementary Video 8- Effect of TTX on spontaneous Ca2+ oscillations in PC-3M cells. Bright field images	DVD
Supplementary Video 9- Effect of ranolazine on spontaneous Ca2+ oscillations in PC-3M cells. Signal from Fluo-4	DVD
Supplementary Video 10- Effect of ranolazine on spontaneous Ca2+ oscillations in PC-3M cells. Bright field images	DVD
Supplementary Video 11- Effect of Na+ free (Li+ substituted) conditions on Ca2+ oscillations in PC-3M cells. Signal from Fluo-4	DVD
Supplementary Video 12- Effect of Na+ free (Li+ substituted) conditions on Ca2+ oscillations in PC-3M cells. Bright field images	DVD
Supplementary Video 13- Effect of Na+ free (choline substituted) conditions on Ca2+ oscillations in PC-3M cells. Signal from Fluo-4	DVD
Supplementary Video 14- Effect of Na+ free (choline substituted) conditions on Ca2+ oscillations in PC-3M cells. Bright field images	DVD
Supplementary Video 15- Effect of varying the extracellular [Ca2+] on spontaneous Ca2+ oscillations in PC-3M cells. Signal from Fluo-4	DVD

Supplementary Video 16- Effect of varying the extracellular [Ca2+] on spontaneous Ca2+ oscillations in PC-3M cells. Bright field images DVD

Supplementary Video 17- Effect of thapsigargin on Ca2+ oscillations in PC-3M cells. Signal from Fluo-4 DVD

Supplementary Video 18- Effect of thapsigargin on Ca2+ oscillations in PC-3M cells. Bright field images DVD

Supplementary Video 19- Effect of extracellular and intracellular [Ca2+] on Ca2+ oscillations in PC-3M cells.Signal from Fluo-4 DVD

Supplementary Video 20- Effect of extracellular and intracellular [Ca2+] on Ca2+ oscillations in PC-3M cells. Bright field images DVD

Supplementary Video 21- Effect of caffeine on Ca2+ oscillations in PC-3M cells. Signal from Fluo-4 DVD

Supplementary Video 22- Effect of caffeine on Ca2+ oscillations in PC-3M cells. Bright field images DVD

Supplementary Video 23- Effect of ryanodine on Ca2+ oscillations in PC-3M cells. Signal from Fluo-4 DVD

Supplementary Video 24- Effect of ryanodine on Ca2+ oscillations in PC-3M cells. Bright field images DVD

Abbreviations

AIS	Axon initial segment
Ank_G	Ankyrin G
ANOVA	Analysis of variance
AP	Action potential
ATX-II	Anemone toxin II
AU	Arbitrary unit
BAC	Bovine adrenal chromaffin
BCa	Breast cancer
BFA	Brefeldin A
Bp	Base pair
BSA	Bovine serum albumen
$[Ca^{2+}]_i$	Intracellular calcium concentration
CaC	Cervical cancer
CAM	Cell adhesion molecule
CaM	Calmodulin
CaMK	Calmodulin-dependent protein kinase
cAMP	Cyclic adenosine monophosphate
CELEX	Cellular excitability
CHO	Chinese hamster ovary
CNS	Central nervous system
con A	Concanavalin A
Cytb5R	Cytochrome b5 reductase
D	Domain of voltage-gated sodium channel

dbcAMP	Dibutyryl cyclic AMP
DEKA	Aspartate-glutamate-lysine-alanine
DMSO	Dimethyl sulfoxide
DRG	Dorsal root ganglion
EBNA	Epstein-Barr virus nuclear antigen
ECM	Extracellular matrix
EDTA	Ethylenediaminetetraacetic acid
EEDD	Glutamate-glutamate-aspartate-aspartate
EGF	Epidermal growth factor
EGFR	Epidermal growth factor receptor
EGTA	Ethylene glycol tetraacetic acid
ER	Endoplasmic reticulum
FBS	Foetal bovine serum
FITC	Fluorescein isothiocyanate
HEK	Human embryonic kidney
HIF	Hypoxia-inducible factor
HRP	Horseradish peroxidase
IC_{50}	50% inhibition concentration
ID	Inter-domain linker of voltage-gated sodium channels
IFM	Isoleucine-phenylalanine-methionine
Ig	Immunoglobulin
IGSF	Immunoglobulin superfamily
I_{Na}	Na^+ current
I_{NaP}	Persistent Na^+ current

I_{NaT}	Transient Na^+ current
IP3R	Inositol 1,4,5-triphosphate receptor
LEMS	Lambert–Eaton myasthenic syndrome
MAPK	Mitogen-activated protein kinase
MCB	Metastatic cell behaviour
MMP	Matrix metalloproteinase
MPS	Mammalian physiological saline
MRI	Magnetic resonance imaging
mRNA	Messenger RNA
MTT	Thiazolyl blue tetrazolium bromide
MW	Molecular weight
NCX	Na^+/Ca^{2+} exchanger
NESOpAb	Polyclonal nNav1.5-specific antibody
NGF	Nerve growth factor
nNav1.5	'neonatal' Nav1.5
NSCLC	Non small cell lung carcinoma
NTC	No treatment control
OD	Optical density
PBS	Phosphate buffered saline
PC12	Pheochromocytoma 12
PCa	Prostate cancer
PCR	Polymerase chain reaction
PFA	Paraformaldehyde
PKA	Cyclic AMP-dependent protein kinase

PKC	Protein kinase C
PKCI	Protein kinase C inhibitor peptide
P-loop	Pore-loop
PNS	Peripheral nervous system
PMCA	Plasma membrane Ca^{2+} ATPase
RE1	Repressor element 1
REST	RE1 binding silencer protein
RNAi	RNA interference
RPMI-1640 medium	Roswell Park Memorial Institute 1640 medium
rt-PCR	Real-time PCR
RyR	Ryanodine receptor
S	Segment of voltage-gated sodium channel
SBFI	Sodium-binding benzofuran isophthalate
SCLC	Small cell lung carcinoma
ScTX	Scorpion toxin
SDS-PAGE	Sodium dodecyl sulphate polyacrylamide gel electrophoresis
SEM	Standard error
SERCA	Sarcoplasmic-endoplasmic reticulum Ca^{2+} ATPase
siRNA	Small-interfering RNA
SS	Short-segment
STX	Saxitoxin
TBE	Tris-HCl-borate-EDTA
TRP	Transient receptor potential
T-tubules	Transverse tubules

TTX	Tetrodotoxin
TTX-R	Tetrodotoxin-resistant
TTX-S	Tetrodotoxin-sensitive
UV	Ultra-violet
V_0	Coefficient of voltage-dependence of time to peak
VEGF	Vascular endothelial growth factor
VGCC	Voltage-gated calcium channel
VGPC	Voltage-gated potassium channel
VGSC	Voltage-gated sodium channel
V_m	Membrane potential

Chapter 1

GENERAL INTRODUCTION

This General Introduction is subdivided into three sections. The first two sections summarize the structure and regulation of voltage-gated sodium channels (VGSCs). The third section introduces metastatic disease and discusses current evidence on the involvement of VGSCs and other ion channels in metastatic progression. The main emphasis is upon prostate cancer (PCa).

1.1 Voltage-gated sodium channels

VGSCs are widely expressed in 'excitable' tissues (e.g. neurons and muscle), where they mediate the initiation and propagation of actions potentials (APs) (e.g. Ogata and Ohishi, 2002). Increasing evidence suggests, however, that VGSCs are also expressed in classically 'non-excitable' cell types, including glia, endothelial cells, fibroblasts and metastatic cancer cells of epithelial origin, where their functional role is less well defined (Diss *et al*., 2004). For instance, in metastatic colon cancer cells, functional VGSC activity was recently shown to regulate gene expression levels and patterns, the conclusion being that "… VGSC is a key regulator of a gene transcriptional network that controls cancer invasion" (House *et al*., 2010). In vascular endothelial cells, Na^+ influx through VGSCs was found to upregulate intracellular Ca^{2+} level (i.e. via Na^+/Ca^{2+} exchange), which in turn played a key role in angiogenesis (Sage *et al*., 1991; Gosling *et al*., 1998).

1.1.1 Basic structure and molecular diversity

VGSCs are multimeric membrane proteins comprising a central α-subunit (VGSCα) and one or more auxiliary β-subunit(s) (Catterall, 2000). Basic channel functionality is achieved by the VGSCα, which forms the channel pore. VGSCβs modulate the

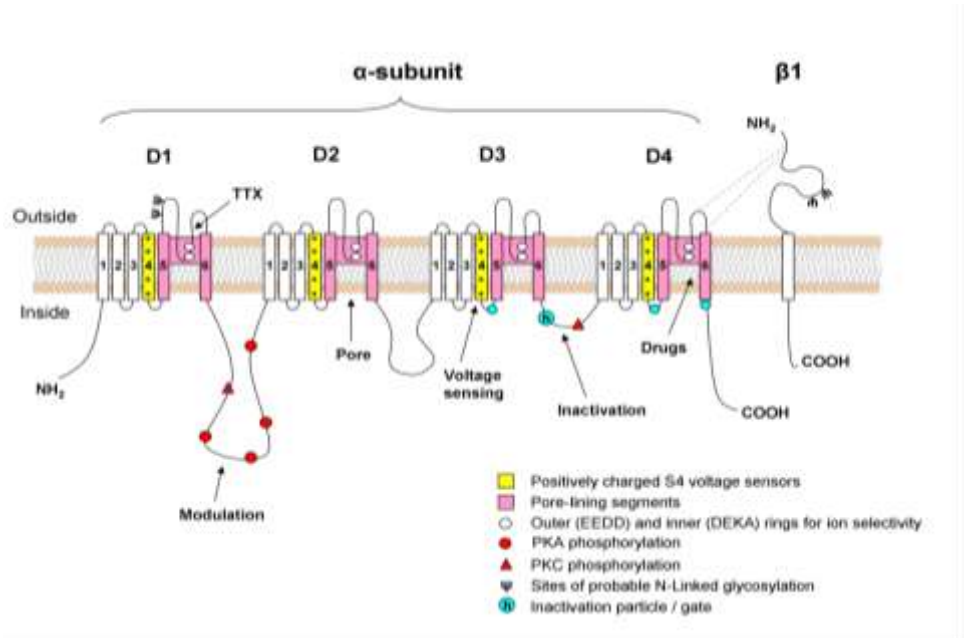
electrophysiological properties of VGSCαs and regulate their functional expression levels (Brackenbury and Isom, 2008).

1.1.1.1 VGSCα

The pore-forming VGSC α-subunit (220-260 kDa) is composed of four structurally homologous domains (D1-D4), each containing six α-helical transmembrane segments (S1-S6) of 19-27 amino acids (Figure 1.1A) (Yu and Catterall, 2003). The S4 segments in each of the four domains, which contain positively charged amino-acid residues (Arg or Lys) at every third position, serve as the voltage-sensors for activation (Swartz, 2008). Extracellular re-entrant pore-loops (P-loops or SS1-SS2 region) between helices S5 and S6 form the narrow entry to the Na^+-conducting pore and act as an ion-selectivity filter containing a critical amino acid sequence: aspartate-glutamate-lysine-alanine (DEKA) (Catterall, 2000). The wider intercellular end of the pore is formed mainly by the inner S6 residues (Goldin *et al*., 2000; Catterall, 2010). Mutations in the DEKA motif have been shown to affect ion selectivity and permeability (Sun *et al*., 1997), such that a change from DEKA to EEEE switched selectivity of a VGSCα from Na^+ to Ca^{2+} (Heinemann *et al*., 1992).

The 3-dimensional (3D) image of the VGSCα, obtained from helium-cooled cyro electron microscopy and single-particle image analysis, revealed four transmembrane masses (i.e. D1-D4) arrayed symmetrically around a central hydrophilic pore (Figure 1.1B; Sato *et al*., 2001). The VGSCα protein appeared bell-shaped, with 24% of its mass on the extracellular side and 47% on the intracellular side of the membrane (Catterall, 2001). Most of the intracellular mass was attributed to the large N- and C-termini and the large intracellular linkers connecting D1, D2 and D3 (Figure 1.1.A; Catterall, 2001). In addition, Sato *et al*. (2001) found that the

A



B

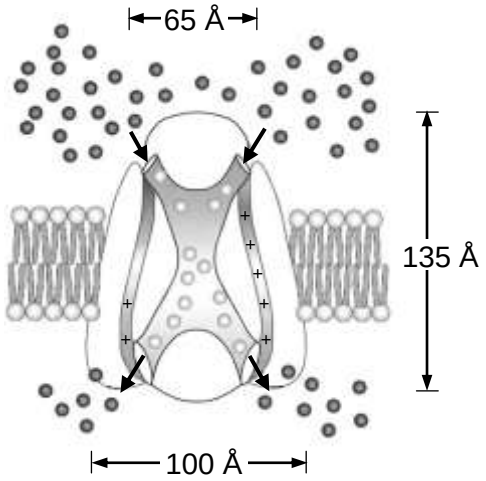


Figure 1.1 Structure of voltage-gated Na^+ channels
(A) VGSC α-subunit is shown together with the β1-subunit. VGSCα has four domains (D1-D4), each with six α-helical transmembrane segments (S1-S6). S5-S6 (pink) are the pore-lining segments and the S4 helices (yellow) form the voltage-sensors. The extracellular domain of the β1 is shown as an immunoglobulin-like fold, which interacts non-covalently with the α-subunit. Adapted from Onkal and Djamgoz, 2009. (B) 3D illustration of VGSCα structure: a, central ion permeation pore; b, gating pores. Modified from Ogata and Ohishi (2002).

central ion permeation pore branched into four ‘inlets’ and ‘outlets’ on both sides of the membrane rather than connecting directly to the intracellular and extracellular spaces (Figure 1.1B) (Catterall, 2001).

The VGSCα pore is permeable to several monovalent cations in the order of $Na^+ \sim Li^+ > Tl^+ > K^+ > Rb^+ > Cs^+$ (Hille, 1972, 2001). The channel is also permeable to a number of non-metallic cations including hydroxylamine and guanidinium but impermeable to organic cations such as choline (Hille, 1971). Five classes of toxins, including the highly specific guanidine-based natural toxin, tetrodotoxin (TTX), bind to VGSCα at various sites and modify its activity by discrete modes of action (Table 1.1) (Cestèle and Catterall, 2000; Catterall *et al*., 2007). In addition, various small-molecule VGSC blocker drugs, including local anaesthetics, anticonvulsants and antiarrhythmics, bind to a ‘drug-pocket’ formed by multiple residues in inner D1:S6, D3:S6 and D4:S6 (Table 1.1) (England, 2008; Clare, 2010).

To date, ten VGSCα subunits (Nav1.1-Nav1.9 and Nax) have been identified, each having subtle but potentially significant electrophysiological and pharmacological variability due to variable amino acid sequences (Table 1.2) (Plummer and Meisler 1999; Catterall, 2000; Diss *et al*., 2004). Additional VGSCα diversity is achieved at transcriptional, pre-translational (i.e. alternative splicing) and post-translational levels (i.e. phosphorylation), and these are detailed separately in Section 1.2. VGSCαs can be broadly characterized by their biophysical (e.g. activation/inactivation kinetics) properties and sensitivity to TTX. Thus, most VGSCαs (Nav1.1-Nav1.4, Nav1.6 and Nav1.7) are blocked by nanomolar concentrations of TTX (TTX-S), activate around -40 mV and have fast inactivation kinetics (Diss *et al*., 2004). On the other hand, a second subset of VGSCαs (Nav1.5, Nav1.8, Nav1.9) show sensitivity to TTX only at micromolar concentrations (TTX-

Table 1.1 VGSCα -binding toxins and drugs

Site #	Agent (Toxin / Drug)	Effect	Binding site
1	Tetrodotoxin, saxitoxin, μ-conotxoin	Blockage of pore: inhibition of conductance	SS1-SS2
2	Aconitine, veratridine, batrachotoxin, grayanotoxin	Hyperpolarization of activation: persistent activation	D1&D4:S6
3	α-scorpion toxin, β-pompilidotoxin, sea anemone toxin	Prevention of outward movement of D4:S4	D4:S3-S4
4	β-scorpion toxins	Trapping of D2:S4 in outward position	D2: S3:S4
5	Brevetoxins, ciguatoxins	Hyperpolarization of activation: persistent activation	DI:S6, D4:S5
6	Local anaesthetics, antiarrythmic drugs, antiepileptic drugs	Resting and use-dependent blockage of conductance	D1&D3&D4: S6

Abbreviations: D, domain; S, segment; SS, short-segment. Modified from Catterall *et al*. (2007).

Table 1.2 VGSC α-subunit gene family

VGSCα subunit	Former names	Gene symbol	Chromosomal location	Major site of expression
Nav1.1	rat I, HBSCI, GPBI, Scn1a	*SCN1A*	M: 2; H: 2q24	CNS
Nav1.2	rat II, HBSCII, HBA	*SCN2A*	M: 2; H: 2q23-24	CNS
Nav1.3	rat III	*SCN3A*	M: 2; H: 2q24	CNS, PNS
Nav1.4	SkM1, μ1	*SCN4A*	M: 11; H: 17q23-25	Skeletal muscle
Nav1.5	SkM2	*SCN5A*	M: 9; H:3p21	Heart
Nav1.6	NaCh6, PN4, Scn8, CerIII	*SCN8A*	M: 15; H: 12q13	CNS
Nav1.7	NaS, hNE-Na, PN1	*SCN9A*	M: 2; H: 2q24	PNS
Nav1.8	SNS, PN3, NaNG	*SCN10A*	M: 9; H: 3p22-24	DRG
Nav1.9	NaN, SNS2, PN5, NaT, SCN12A	*SCN11A*	M: 9; H: 3p21-24	DRG
Nax	Nav2.2, NaG, SCL11, Nav2.3	*SCN6A, SCN7A*	M: 2; H: 2q21-23	Heart, uterus, skeletal muscle

Abbreviations: CNS, central nervous system; PNS, peripheral nervous system; DRG, dorsal root ganglia. Modified from Goldin *et al.* (2000).

R), activate at more hyperpolarized potentials (-60 mV or more negative) and exhibit slower inactivation kinetics (Plummer and Meisler 1999; Goldin, 2001). Sensitivity to TTX is determined by an aromatic residue (Tyr or Phe) in the D1:S5-S6 loop; TTX-R VGSCαs have a polar residue (Cys or Ser) in this position (Figure 1.1A) (Satin *et al*., 1992; Heinemann *et al*., 1992; Fozzard and Lipkind, 2010).

Expression of different VGSCαs is tissue-specific and can be developmentally regulated (Table 1.2; Plummer and Meisler 1999; Catterall 2000). For instance, Nav1.1, Nav1.2 and Nav1.6 are expressed predominantly in central nervous system (CNS); Nav1.6 is mainly present in axon initial segments (AIS) and nodes of Ranvier; Nav1.2 is expressed in unmyelinated axons and AIS in myelinated axons; and Nav1.1 is localized mainly in the somata (Trimmer and Rhodes, 2004; Mantegazza *et al*., 2010). Nav1.3 is expressed in the CNS and also in dorsal root ganglion (DRG) neurons following peripheral nerve damage (Waxman *et al*., 1994; Black *et al*., 1999; Whitaker *et al*., 2001). Nav1.4 is the major VGSCα in adult skeletal muscle (Kraner *et al*., 1989), and Nav1.5 is the cardiac VGSCα (Gellens *et al*., 1992). Finally, Nav1.7, Nav1.8 and Nav1.9 are mainly expressed in the peripheral nervous system (PNS), where their function is thought to be critical for nociception (Toledo-Aral *et al*., 1997; Dib-Hajj *et al*., 1998; England, 2008). Thus, expression of multiple VGSCα isoforms can occur in single cells (both 'excitable' and 'non-excitable'), and it is thought that specific cell types may achieve their unique functional output based on the subtle functional differences in the VGSCα isoform(s) that they express (Goldin, 2001; Diss *et al*., 2004). In other words, controlled expression of a combination of different isoforms of VGSCs is hypothesized to allow a cell to modulate and 'fine-tune' its response patterns (Waxman, 2007).

VGSCs have 3 main functional states: 1) closed, (2) open/activated and (3) inactivated, and cycle between these states depending on the value of the membrane potential and time (Figure 1.2). According to the "sliding helix" model of activation, upon membrane depolarization, the spiral outward movement of the S4 helices initiates the conformational change of the protein structure that leads to the opening of the channel pore (Tombola *et al*., 2006; Catterall, 2010). Fast inactivation of the VGSC occurs within milliseconds of channel opening and the highly conserved hydrophobic amino acid triad known as the "IFM motif" (Iso-Phe-Met) in the short intracellular loop between D3 and D4 (ID3-4) mediates rapid inactivation of the channel (Figure 1.3) (Yu and Catterall, 2003). Thus, the 'hinged-lid' IFM motif folds into the inner mouth of the channel pore, occluding it and hence inactivating Na^+ conductance during sustained depolarization of the membrane (West *et al*., 1992; Goldin, 2003). The fast inactivation gate is believed to derive its voltage dependence through coupling to the outward movement of the D4:S4 during channel activation (Kontis and Goldin, 1997). Upon membrane repolarisation, VGSCs recover from inactivation due to relaxing of the inactivation gate (Figure 1.2) (Catterall, 2000). In the case where membrane repolarises before inactivation has occurred, VGSCs could undergo deactivation, directly transiting from open/activated to the closed state (Figure 1.2) (Kuo and Bean, 1994). In the case of the depolarization of the membrane for an extended period of time, VGSCs may undergo a separate form of inactivation, termed 'slow' inactivation (Vilin and Ruben, 2001; Goldin, 2003); this type of inactivation does not involve the fast inactivation particle in the ID3-4 linker and is hypothesized to result from a structural rearrangement of the pore (Goldin, 2003; Tikhonov and Zhorov, 2007). However, further studies are required to elucidate the precise mechanism and molecular determinant of slow inactivation.

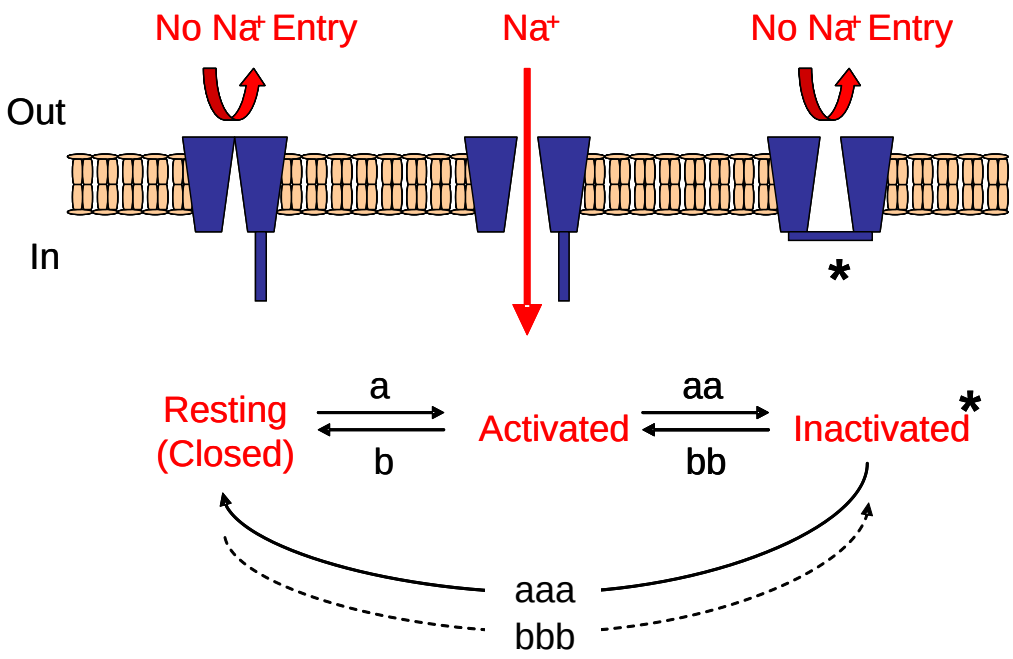


Figure 1.2 Functional states of voltage-gated sodium channels
Schematic representation of the three functional modes of voltage-gated Na^+ channels. At rest, the channels are in their resting (closed) state. Upon depolarization, channels activate (a) and then inactivate (aa) within milliseconds of activation. The inactivated state of the VGSCs through the binding of the inactivation gate (IFM motif) to the channel pore structure is indicated by (*). From the inactivated state, channels recover from inactivation (aaa) upon membrane repolarization. 'Reverse' transitions between these gating states are also possible (b, bb, bbb), but occur much less frequently: b, deactivation; bb, activation, bbb, closed-state inactivation.

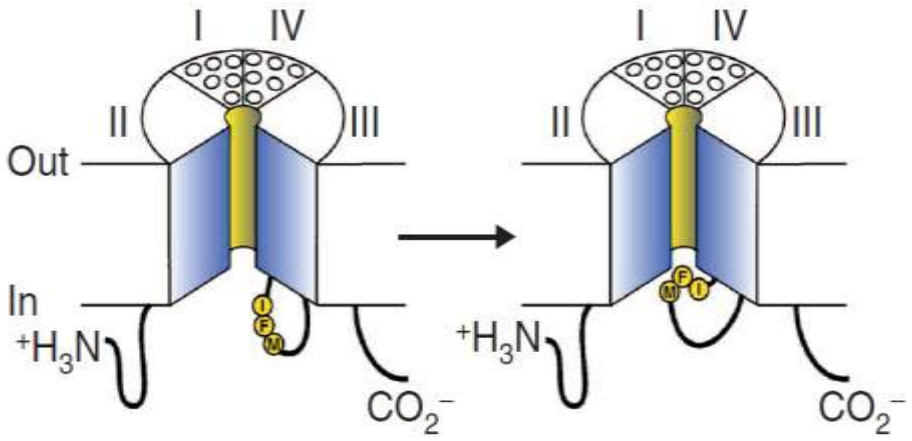


Figure 1.3 Mechanism of fast inactivation
The cytoplasmic linker between domains 3 and 4 (ID3-4) forms a 'hinged lid' that is responsible for fast inactivation of the VGSC. The critical Phe[1489] within the hydrophobic IFM motif (Ile[1488]-Phe[1489]-Met[1490]) occludes the intracellular mouth of the pore during the inactivation process (right). Adapted from Yu and Catterall (2003).

As described above, upon membrane depolarization, VGSCs typically activate, rapidly inactivate, and remain closed/non-conducting until repolarization occurs. However, it has become increasingly apparent that a small portion of VGSCs may inactivate and re-open during prolonged depolarisations, thereby resulting in a small but persisting Na^+ current (I_{NaP}). Such I_{NaP} could be recorded from neurons and cardiomyocytes as well as in heterologous systems expressing a single VGSCα subtype (Crill, 1996; Maltsev *et al*., 1998; Magistretti *et al*., 1999; Qu *et al*., 2001; Taddese and Bean, 2002; Maltsev and Undrovinas, 2006; Saint, 2008; Aman *et al*., 2009). Notably, I_{NaP} typically has a magnitude of < 1% of the peak Na^+ current; however, because it is very-slowly inactivating (or non-inactivating), the amount of charge (i.e. Na^+) it carries is considerable (Saint *et al*., 1992; Maltsev *et al*., 1998; Zygmunt *et al*., 2001). Furthermore, various (patho)physiological conditions can significantly enhance I_{NaP} in cardiomyocytes and neurons; among these are inactivation-modifying neurotoxins (e.g. sea anemone toxin ATX-II; Chahine *et al*., 1996), hypoxia (Ju *et al*., 1996), and Nav1.5 mutations associated with the long QT-3 syndrome (Bennett *et al*., 1995; Fredj *et al*., 2006).

1.1.1.2 VGSCβ

Whilst the VGSCα subunit is sufficient for functional expression, it is usually complexed with one or more smaller auxiliary VGSCβs (Figure 1.1), which can (1) modulate several aspects of VGSC function including channel activation/inactivation by shifting the voltage dependence of activation and inactivation, and (2) increase the level of functional VGSC expression on the plasma membrane through enhancing the intracellular trafficking of the VGSCα protein to the plasma membrane and/or

through increasing the cell surface stability of VGSCαs via association with cytoskeletal molecules such as ankyrin (Isom *et al*., 1994; Brackenbury *et al*., 2008).

To date, four VGSCβ isoforms have been identified: β1-4 (33-45 kDa) (Table 1.3). The β1- and β3- subunits associate non-covalently with the α-subunit, whereas β2- and β4- subunits are covalently linked to a cysteine residue on an extracellular linker of the α-subunit (Isom *et al*., 1992, 1995; Morgan *et al*., 2000; Yu *et al*., 2003). Each VGSCβ possesses an extracellular N-terminal domain with an immunoglobulin (Ig)-like fold, a single membrane-spanning segment, and a cytoplasmic C-terminal region (Isom 2001; Chahine *et al*., 2005). Importantly, VGSCβs are unique among ion channel subunits in containing Ig-like folds, giving them structural homology to certain types of cell-adhesion molecules (CAMs). This property was first discovered for β2 (whose Ig-like domain shares 45% sequence homology with one of the six Ig motifs in the extracellular domain of neuronal CAM, contactin; Isom *et al*., 1995). Further experiments showed that VGSCβs can function as Ig superfamily cell adhesion molecules (IGSF-CAMs), e.g. both β1 and β2 were shown to interact *trans*-homophilically, facilitating cellular aggregation and ankyrin recruitment to cell-to-cell contacts (Malhotra *et al*., 2000, 2002). Moreover, heterophilical interaction of β1 has been documented with contactin, NrCAM, N-cadherin, neurofascin-155, neurofascin-186 and VGSCβ2, and shown to potentiate functional VGSC expression in plasma membrane (Kazarinova-Noyes *et al*., 2001; McEwen and Isom, 2004; McEwen *et al*., 2004). Finally, both β1 and β2 were found to interact with and repelled from tenascin-C and tenascin-R (both extracellular matrix (ECM) molecules), thereby suppressing cell migration (Srinivasan *et al*., 1998; Xiao *et al*., 1999).

Table 1.3 VGSCβ isoforms

Isoform	MW (kDa)	Gene symbol	Chromosomal location	Tissue location
β1	36	*SCN1B*	19q13	Heart, skeletal muscle, CNS, glia, PNS
β1A	45	*SCN1B*	19q13	Heart, skeletal muscle, adrenal gland, PNS
β2	33	*SCN2B*	11q22	CNS, PNS, heart, glia
β3	36	*SCN3B*	11q23	CNS, adrenal gland, kidney, heart, PNS
β4	38	*SCN4B*	11q23	Heart, skeletal muscle, CNS, PNS

Abbreviations: CNS, central nervous system; DRG, dorsal root ganglion; PNS, peripheral nervous system. Modified from Brackenbury *et al*. (2008).

VGSCβ diversity is achieved by developmental and tissue-specific expression of the four subtypes as well as alternative splicing (Table 1.3) (Isom, 2001; Meadows and Isom, 2005). For instance, a partially developmentally regulated intron retention event generates the β1A splice variant, which (i) shares little amino acid homology with β1 apart from the N-terminal Ig domain, and (ii) is developmentally down-regulated and replaced by β1 in rat brain (Kazen-Gillespie *et al*., 2000). As with VGSCαs, multiplicity of VGSCβ expression occurs in given cell types, where each isoform may have a distinct role (e.g. modulation of particular VGSCαs or interaction with differing sets of extracellular matrix of cytoskeletal proteins) (Table 1.3) (Isom, 2001; Chahine *et al*., 2005; Brackenbury *et al*., 2008).

1.2. Regulation of VGSCs

Regulation of VGSC expression/activity is highly complex and occurs at multiple stages: (1) transcriptional, (2) pre-translational (e.g. alternative splicing), and (3) post-translational (e.g. glycosylation, phosphorylation, association with other membrane-bound proteins) (Figure 1.4).

1.2.1 Transcription

VGSC gene expression can be regulated by various stimuli such as electrical activity (Sashihara *et al*., 1994), hormones (Tabb *et al*., 1994) and growth factors (Black *et al*., 1997; Toledo-Aral *et al*., 1995; Choi *et al*., 2001; Fanger *et al*., 1997), Some of these effects may occur during injury (Black *et al*., 1999; Iwahashi *et al*., 1994; Waxman *et al*., 1994), For example, nerve growth factor (NGF) induced expression of Nav1.7 was shown in PC12 cells (Rudy *et al*., 1987; Toledo-Aral *et al*., 1995). On the other hand, NGF induced upregulation of Nav1.8 and down regulation of Nav1.3

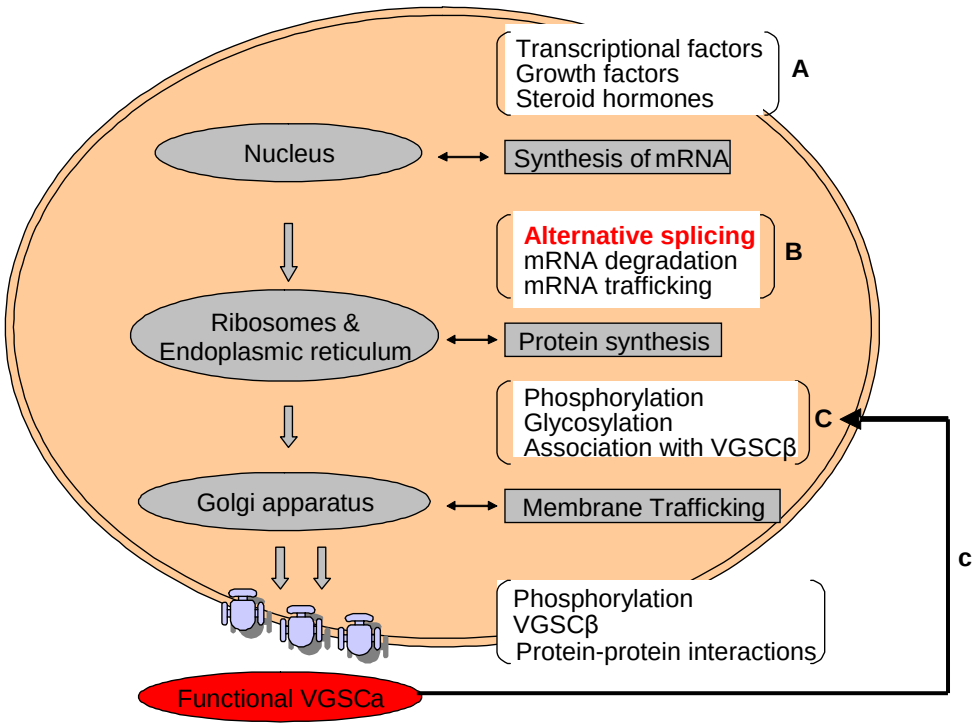


Figure 1.4 Levels of regulation of VGSC expression and activity
Regulation of VGSCs occur at (A) transcriptional level (e.g. transcriptional factors), followed by pre-translational modifications (B) (e.g. mRNA trafficking and splicing). Then, the channel protein is synthesized, and trafficked to the plasma membrane. Post-translation modifications (C) include phosphorylation, glycosylation, and interaction with other proteins including VSGCβs. Recycling and degradation of VGSC protein (c) is another important factor in keeping a steady-state balance of available functional VGSCs at the plasma membrane.

was reported for DRG neurons (Black *et al*., 1997). Interestingly, some pathological transcriptional re-expression of VGSCs can involve embryonic splice variants, as in the case of kainic acid-induced damage to mammalian brain and Nav1.3 (Gastaldi *et al*., 1997; Waxman *et al*., 1994)

Transcriptional factors are principal modulators of gene expression, and one transcription factor has been shown to effect expression of a VGSCα subtype (Chong *et al*., 1995). Nav1.2 expression was restricted to neurons by REST, a transcription silencer (Chong *et al*., 1995). REST is expressed in most tissues and binds to a specific receptor element 1 (RE-1) in the promoter region of Nav1.2 and causes suppression of its expression (Chong *et al*., 1995). On the other hand, absence of REST in neurons permits expression of Nav1.2 in these cells (Marban *et al*., 1998; Chong *et al*., 1995). Functioning of REST is also depends on other co-repressor proteins, CoREST and mSin3A (Andres *et al*., 1999; Grimes *et al*., 2000). Furthermore, another transcription factor Brn-3a, a POU-family homeobox protein, was shown to upregulate Nav1.7 expression in PC-3 cell line (Diss *et al*., 2006). Recent work has also characterized the transcriptional promoter region of Nav1.7 (Diss *et al*., 2008).

1.2.2 Alternative splicing

Functional diversity of the VGSC α-subunits is significantly increased by alternative mRNA splicing, which generates two or more different mRNAs from a single gene (McKeown, 1992; Blencowe, 2006). Within the modulatory region of the VGSCα subunit, there exist five major sites where alternative splicing is known to occur (Table 1.4) (Diss *et al*., 2004). Variability among the splice variants can be generated by inclusion, exclusion or substitution of amino acid residues in the coding sequence.

Table 1.4 Alternative splice variants of VGSCαs

Site	Nav	Event	Functional consequence	Reference
D1:S3	1.1, 1.2, 1.3, 1.5, 1.6, 1.7	Substitution of negative Asp in 'adult' to a neutral or positive residue in 'neonatal'	Modify voltage-dependence and kinetics activation/inactivation	Copley *et al*., 2004; Sarao *et al*. 1991; Gustafson *et al*., 1993; Chioni *et al*., 2005; Plummer *et al*., 1998; Belcher *et al*., 1995.
ID1-2	1.1., 1.3, 1.6, 1.7	Multiple splice forms with different ID1-2 regions	Modify (add / remove) phosphorylation sites	Schaller *et al*., 1992; Dietrich *et al*., 1998; Thimmapaya *et al*., 2005; Plummer *et al*., 1998; Toledo-Aral *et al*., 1997; Raymond *et al*., 2004.
ID2-3	1.5, 1.8	Shortened ID 2-3	Modify voltage-dependence of activation/inactivation; produce non-functional proteins	Gersdorff-Korsgaard *et al*., 2001; Zimmer *et al*., 2002; Camacho *et al*., 2006; Makielski *et al*., 2003
D3	1.1, 1.6	Alternative exon 18	Predominantly produce truncated 'fail-safe' proteins	Plummer *et al*., 1997; Oh and Waxman 1998; Schaller *et al*., 1995.
D4:S3	1.5, 1.9	Shortened intron in D4:S3	Produce truncated proteins	Gellens *et al*., 1992; Jeong *et al*., 2000

Abbreviations: D, domain; S, segment; ID, interdomain region.

These may be the consequence of (i) the alternative usage of 5' (donor) / 3' (acceptor) splice sites, (ii) exon skipping events (involving one or more exons) in the coding region, (iii) mutually exclusive exon usage, (iv) the alternative usage of 5' or 3' untranslated regions, and (v) intron to exon conversion events (McKeown, 1992; Chen and Manley, 2009).

Alternative splicing of the VGSCα genes results either in full-length, functional proteins that exhibit regulatory, electrophysiological and/or pharmacological variability (e.g. Dietrich *et al*., 1998; Onkal *et al*., 2008), or quite commonly, in highly truncated non-functional proteins (e.g. Schaller *et al*., 1992; Plummer *et al*., 1997) (Table 1.4). The role of the truncated VGSCαs has not been fully explained, but could involve the following: (1) functional interaction and association with other truncated VGSCαs in the right orientation to form 'heteromeric' sodium channels, and/or (2) a 'fail-safe' mechanism producing truncated proteins, preventing the synthesis and/or activity of functional, full-length VGSCα channels (Plummer *et al*., 1997; Diss *et al*., 2004; Schroeter *et al*., 2010).

Alternative splicing resulting in modified but full-length VGSCαs contributes significantly to functional VGSC diversity (Table 1.4) (Schroeter *et al*., 2010). Since cytoplasmic ID linkers are crucial for channel modulation (e.g. via phosphorylation or protein-protein interactions; Figure 1.5), splicing in ID1-2 and ID2-3 would be expected to produce VGSCα splice isoforms with differing functional characteristics. Indeed, an alternative splice form of Nav1.5 (Nav1.5c), which was first detected in mouse DRG neurons, was found to encode an extra glutamate residue in the ID2-3 linker region, which disrupted a putative casein kinase 2 (CK2) phosphorylation site (Kerr *et al*., 2004). Also, splicing in the ID1-2 linker resulted in splice variants of Nav1.1, Nav1.3, Nav1.6 and Nav1.7 with shortened ID1-2 linkers, which excluded

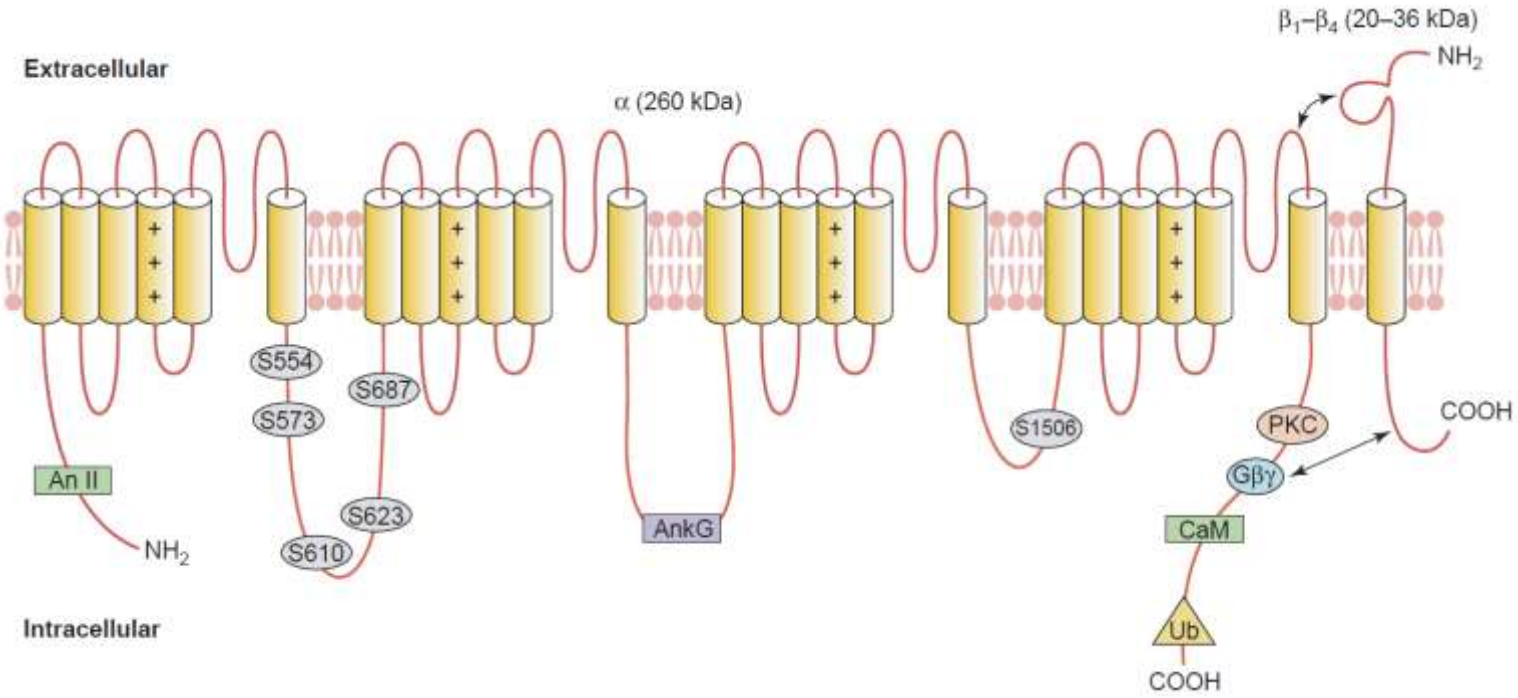


Figure 1.5 VGSC regulatory sites
Serine residues (S) phosphorylated by PKA or PKC are numbered (Nav1.2 numbering). Arrows indicate possible interaction sites between the VGSC α- and β-subunits. Abbreviations: An II, annexin II; Ub, ubiquitin; CaM, calmodulin; AnkG, ankyrin G; Gβγ, G-protein β-γ complex; Modified from Chahine *et al*. (2005).

multiple sites for putative PKA and PKC phosphorylation (Table 1.4 and Figure 1.5) (Diss *et al*., 2004). Moreover, Thimmapaya *et al*. (2005) over-expressed these Nav1.3 ID1-2 splice variants in *Xenopus* oocytes and showed that they exhibit slightly different (3-5 mV) voltage-range for activation and inactivation.

Apart from the modulatory effects of splicing in ID linkers, alternative splicing within the transmembrane VGSCα regions generally produce variants with significant electrophysiological distinction. A particularly important splicing site in this regard is D1:S3/S4 (Table 1.4) (Diss *et al*., 2004). Developmentally controlled splicing of two mutually exclusive alternative exons in D1:S3/S4 was first described for Nav1.2 and Nav1.3 in rat brain (Sarao *et al*., 1991; Gustafson *et al*., 1993). The two alternative exons encode part of the transmembrane segment S3, most of S4, and the S3/S4 extracellular linker (Diss *et al*., 2004; Chioni *et al*., 2005; Onkal and Djamgoz, 2009). The transcripts with the upstream (5') exon were found to be expressed predominantly during the neonatal period, whilst the transcripts with the downstream (3') exon were expressed only in the adult. Accordingly, for Nav1.2 and Nav1.3, the upstream exon was designated 'neonatal' and the counterpart downstream 'adult'. Similar D1:S3 splicing has also been reported for Nav1.1, Nav1.5, Nav1.6 and Nav1.7 (Diss *et al*., 2004).

Except for Nav1.5, the 'adult' and 'neonatal' exon 6 variants differ by 19-21 nucleotides resulting in only 1-3 amino acids changes; a single amino acid in the extracellular S3-S4 linker changes consistently from a neutral to a negatively-charged residue during development (Plummer and Meisler, 1999; Diss *et al*., 2004). On the other hand, Nav1.5 D1:S3 variants differ from each other by 31 nucleotides and 7 amino acids, where the key amino acid switch in the extracellular D1:S3/S4 linker is a charge-reversing one: from a positive lysine in 'neonatal' to a negative

aspartate in the ‘adult’ (Fraser *et al*., 2005; Ou *et al*., 2005). Because of these larger differences, Chioni *et al*. (2005) could generate a polyclonal antibody (NESOpAb) that was selective for ‘neonatal’ Nav1.5. Using NESOpAb in immunohistochemical studies, these authors also confirmed the developmental regulation of Nav1.5 D1:S3 splicing in mouse heart (Chioni *et al*., 2005).

Human Nav1.7 is expressed primarily in sensory neurons of the peripheral (i.e. DRG) and sympathetic nervous systems, and in Schwann cells (Goldin, 2001). D1:S3 splice variants of $Na_v1.7$ were identified in human (Klugbauer *et al*., 1995, Raymond *et al*., 2004), rabbit (Belcher *et al*., 1995), and rat (ToledoAral *et al*., 1997). D1:S3 splice variants of Nav1.7 differ in 21 of their 92 nucleotides. The resulting ‘adult’ and ‘neonatal’ Nav1.7 proteins differ by two amino acids, i.e. at positions 201 (Leu in ‘neonatal’ and Val in ‘adult’) and 206 (Asn in ‘neonatal’ and Asp in ‘adult’) (Belcher *et al*., 1995; Diss *et al*., 2004). The low expression of the ‘adult variant’ in neonatal rabbits suggested that the D1:S3 splicing in Nav1.7 is developmentally regulated, as for Nav1.2, Nav1.3 and Nav1.5 (Sarao *et al*., 1991; Gustafson *et al*., 1993; Belcher *et al*., 1995; Chioni *et al*., 2005). Interestingly, expression of Nav1.7 ‘adult’ and ‘neonatal’ variants appears to be tissue-specific in humans: the ‘neonatal’ isoform is preferentially expressed in the PNS and CNS of adult tissues, whereas the ‘adult’ variant is found predominantly in the DRG neurons (Raymond *et al*., 2004). Interestingly, Fraser *et al*. (2005) reported that strongly metastatic MDA-MB-231 breast cancer cell line selectively expressed relatively high levels of D1:S3 ‘neonatal’ splice form Nav1.7 mRNA (which subsequently contributed ~ 20% of total Na^+ current), indicating that this ‘neonatal’ isoform may be involved in the progression of metastasis in breast cancer cells (Section 1.3.3). Furthermore, in particular relevance to the present project, the predominant ‘culprit’

VGSCα expressed in strongly metastatic human (PC-3M) and rat (Mat-LyLu) prostate cancer cells in also the 'neonatal' D1:S3 variant of Nav1.7 (Section 1.3.3) (Diss *et al*., 2001; Onkal and Djamgoz, 2009).

At present, mechanisms controlling alternative splicing of VGSCα (and other ion channel) genes is not fully known but could involve changes in membrane potential (Xie and Black, 2001), growth factors (Akopian *et al*., 1999), and phosphorylation (Shipston, 2001) (reviewed in Diss *et al*., 2004). For instance, in adult rat DRG neurons, nerve growth factor (NGF) was found to upregulate a splice variant of Nav1.8 that contained a partial repeat of domain 2 (Akopian *et al*., 1999). In GH3 pituitary cells, membrane depolarization by adding KCl was shown to repress splicing of 'STREX', an exon conferring Ca^{2+} sensitivity in large-conductance K^+ (BK) channel mRNAs (Xie and Black, 2001). Notably, alternative splicing of VGSCα mRNAs can be regulated by various mechanisms in different cell types. Thus, for example, in spinal cord astrocytes, the expression of three Nav1.6 D3 splice variants was upregulated by 48 h exposure to the membrane-permeant dibutyryl cAMP (dbcAMP), whereas a similar treatment had no effect in cerebral astrocytes (Oh and Waxman, 1998).

1.2.3 Post-translational modification: Glycosylation

All VGSCαs possess number of potential extracellular glycosylation sites located at the putative pore lining regions of D1 and D3 (Bennett, 2002 and Marban *et al*., 1998). Five of these sites are highly conserved and therefore it was proposed that carbohydrate have essential role in structure and localisation of VGSC (Diss et al., 2004). The extend of glycosylation is subtype specific. For example, Nav1.1 - Nav1.4 are 15 - 30 % glycosylated whilst Nav1.5 and Nav1.9 are 5 % glycosylated

(Marban *et al*., 1998; Tyrrell *et al*., 2001). In addition, β1 and β2 subunits of VGSC are heavily glycosilated (Isom *et al*., 1992). Glycosylation was shown to effect electrophysiological properties of VGSC (Bennett et al., 1997). For instance, addition of negatively charged carbohydrate molecules has been shown to hyperpolarize voltage –dependence of VGSC gating (Marban *et al*., 1998; Cronin *et al*., 2005). Reduced sialyation depolarized the gating of Nav1.4 but not Nav1.5 in transfected Chinese hamster ovary (CHO) cells indicating that functional effect of glycosylation is subtype specific (Bennett, 2002). In addition, in CHO cells, highly sialylated β1-subunit hyperpolarizes the voltage dependence of Nav1.2, Nav1.5 and Nav1.7 but non- sialylated β1 had no effect (Johnson *et al*., 2004).

1.2.4 Protein synthesis and trafficking

Regulation of mRNA levels and protein level can be controlled separately and independently (Orphanides and Reinberg, 2002). For example, Brackenbury and Djamgoz (2006) showed that TTX treatment decreased Nav1.7 mRNA expression in Mat-LyLu cells but did not change total protein level. On the other hand, TTX induced increase in VGSCα expression at plasma membrane of Mat-LyLu suggested the role of trafficking. In separate study it was suggested that activation of cAMP – dependent protein kinase A (PKA) increased plasma membrane VGSC level via protein synthesis in BAC cells (Yuhi *et al*., 1996). However it should be noted that trafficking could play a role in this process.

VGSC protein level at plasma membrane can be regulated by protein trafficking via vesicular exocytosis (Herfst *et al*., 2004). It was show that PKA activity regulates VGSC externalisation from ER (Muniz *et al*., 1996, 1997; Zhou *et al*., 2000, 2002). For example, application of cAMP (1 h) resulted in elevation in

functional expression of VGSC in Nav1.5 expressing *Xenopus* oocytes (Frohnwieser *et al*., 1997). In addition, disruption of intracellular protein trafficking with monensin and chloroquine (Tietze *et al*., 1980; Mollenhauer *et al*., 1990) diminished the PKA-induced increase in functional expression of VGSC in *Xenopus* oocytes (Zhou *et al*., 2000).

Ca^{2+} signalling has been shown to play role in VGSC trafficking. For instance, cytosporin-A induced inhibition of calcineurin (a Ca^{2+}-and calmodulin–dependent protein phosphatase 2B) resulted in increase binding of [^{3}H]STX to VGSC at BAC cell surface. Furthermore, co-application of cytosporin-A and trans-Golgi network transport inhibitor brefeldin A (BFA) reduced cell surface VGSC level implying that calcineurin plays role in reduction in externalisation of newly synthesised proteins (Shiraishi *et al*., 2001b). In another study, increase in $[Ca^{2+}]_i$ with A23287, a Ca^{2+} ionophore, was documented to reduce BAC cell surface expression of VGSC (Shiraishi *et al*., 2001a). On the other hand, this decrease in cell surface expression was prevented by Ca^{2+}-dependent PKC (PKC-α) inhibition (Shiraishi *et al*., 2001a). In addition, in the presence of BFA, activation of PKC-α with thymeleatin (TMX) reduced [^{3}H]STX binding therefore it was proposed that PKC-α promote endocytotic internalisation in BAC cells (Yanagita *et al*., 2000; Kobayashi *et al*., 2002). In addition, A23187 induced decrease in cell surface VGSC level was abolished by calpastatin peptide, a calpain (a family of Ca^{2+}-dependent cycteine proteases) inhibitor (Shiraishi *et al*., 2001a).

It was proposed that interaction between VGSC and scaffolding proteins affects channel trafficking (Herfst *et al*., 2004). For example, it was documented that N-terminal of Nav1.8 binds to light chain (p11) of the cytoskeletal binding protein annexin II (Figure 1.5) and expression of p11 in stably transfected CHO cells

promotes trafficking of Nav1.8 to plasma membrane (Okuse *et al*., 2002). In addition, it was shown that Nav1.5 is coupled to dystrophin and the actin cytoskeleton via scaffolding protein syntropin (Ou *et al*., 2003). Co expression of CAM contactin and Nav1.9 in CHO cells was show to increase cell surface expression of Nav1.9 (Shah *et al*., 2004).The membrane skeletal protein ankyrin G (Ank_G) was shown to be essential for clustering of VGSC to axon initial segment (AIS) (Zhou *et al*., 1998). In addition, mutation in Ank_G binding site (E1053K at ID2-3 linker, Figure 1.5) caused reduced and disorganised expression of Nav1.5 at the sarcolemma, intercalated discs and T-tubules in cardiomyocytes (Mohler *et al*., 2004)

In addition, VGSC activity was show to effect protein trafficking. For example, long term treatment with VGSC 'opener' veratridine, batrachotoxin and α-scorpion toxin (α-ScTX) was shown to decrease cell surface expression of VGSCs in feta rat brain (Dargent and Couraud, 1990). Furthermore, reduction in cell surface expression of VGSC by [125I] α-ScTX was proposed to be mediated by increased internalisation (Dargent *et al*., 1994; Paillart *et al*., 1996). On the other hand, Brackenbury and Djamgoz (2006) showed by electrophysiology and confocal immunocytochemistry experiments that in strongly metastatic prostate cancer (PCa) Mat-LyLu cells long-term TTX application reduced plasma membrane expression of VGSC whilst not effecting total protein level. Similarly, long-term application of TTX reduced plasma membrane VGSC expression while not effecting total protein level in strongly metastatic human breast cancer (BCa) MDA-MB-231 cells (Chioni *et al*., 2010).

VGSCβs were also suggested to be involved in trafficking of VGSCα (Isom, 2002). For example, co-expression of β1 and Nav1.5 in human embryonic kidney (HEK) 293 cells revealed that they form complex in ER and β1 facilitate trafficking

of Nav1.5 to plasma membrane (Zimmer *et al*., 2002a). In addition, β2-knockout mice experiments revealed that DRG neurons have decreased VGSC expression at the plasma membrane (Chen *et al*., 2002). Therefore, it was suggested that β2 plays role in trafficking of VGSCs. Furthermore, mutagenesis experiments revealed that β3 interacts and masks ER-retention signal located on Nav1.8 and increase cell surface expression (Zhang *et al*., 2008).

1.2.5 Protein degradation

An important process mediating internalization and subsequent degradation of VGSCs is ubiquitination (Herfst *et al*., 2004; Shao *et al*., 2009). Thus, for example, Nedd4 family of ubiquitin-protein ligases were found to interact with the PY motifs in the C-termini of VGSCαs, targeting the channel protein for degradation via ubiquitination (Figure 1.5) (Ingham *et al*., 2004). In particular, when co-expressed with Nav1.5 in *Xenopus* oocytes, Nedd4 reduced peak current density, suggesting removal of functional channels from the plasma membrane (Abriel *et al*., 2000). In addition, in HEK-293 cells, cell surface expression of Nav1.5 was reduced upon co-expression with Nedd4-2, and this effect occurred faster upon co-application of the *trans*-Golgi network transport inhibitor, brefeldin A (BFA), suggesting that Nedd4-2 accelerated VGSC internalisation (van Bemmelen *et al*., 2004; Rougier *et al*., 2005). Furthermore, Nedd4-2 was shown to have a similar 'depressing' effect on functional expression of other VGSCαs, indicating that ubiquitination is a general mechanism for VGSCα internalisation and degradation. For instance, Nedd4-2 co-expression has been found to reduce the peak current amplitude of Nav1.2 and Nav1.3 in HEK-293 cells (van Bemmelen *et al*., 2004; Rougier *et al*., 2005) and Nav1.2, Nav1.7 and Nav1.8 in *Xenopus* oocytes (Fotia *et al*., 2004).

1.2.6 Phosphorylation

VGSCαs are phosphorylated by major kinases, including cAMP-dependent protein kinase (PKA), protein kinase C (PKC), calcium calmodulin kinase II (CAM kinase II) and tyrosine kinase (Cantrell and Catterall, 2001; Carr *et al*., 2003; Chahine *et al*., 2005). Phosphorylation by PKA can occur on five sites (serine residues) in the intracellular loop connecting domains 1 and 2 (Figure 1.5) (Murphy *et al*., 1993; Marban *et al*., 1998). PKA has VGSCα subtype-specific effects; it typically reduces current amplitude of TTX-S VGSCαs whilst increasing that of TTX-R channels, without drastically affecting voltage dependence and kinetics of VGSCα gating (Catterall, 2000; Zhou et al., 2000, 2002; Carr *et al*., 2003; Diss *et al*., 2004). In particular, PKA phosphorylation was found to reduce the current amplitude of Nav1.1, 1.2 and 1.7 (Li *et al*., 1992; Smith and Goldin 1997, 1998; Vijayaragavan *et al*., 2004), whilst the effect of Nav1.5 and 1.8 was the opposite (Marban *et al*., 1998; Zhou *et al*., 2000, 2002; England *et al*., 1996). The differential effect of PKA on different VGSCαs is thought to be due to the dual effect of PKA: (1) direct phosphorylation of serine residues in the ID1-2 linker, and (2) modulation of VGSCα trafficking via phosphorylation of yet unidentified modulatory proteins (e.g. Section 1.2.3) (Chahine *et al*., 2005; Brackenbury and Djamgoz, 2006; Shao *et al*., 2009).

VGSCαs are also phosphorylated by PKC at a conserved serine residue in the ID3-4 linker (located near the inactivation gate particle 'IFM') (West *et al*., 1991; Murray *et al*., 1997; Chahine *et al*., 2005). PKC phosphorylation was found to slow inactivation and reduce peak current amplitude of several heterologously expressed VGSCαs including Nav1.2, Nav1.4, Nav1.5, Nav1.7 and Nav1.8 (Schreibmayer *et al*., 1991; Bendahhou *et al*., 1995; Cantrell *et al*., 1996; Murray *et al*., 1997;

Tateyama *et al*., 2003; Vijayaragavan *et al*., 2004). Notably, Murray *et al*. (1997) showed that mutating the ID3-4 linker serine to alanine in Nav1.5 expressed in *Xenopus* oocytes reduced but did not abolish the effect of PKC on channel function, suggesting that additional PKC phosphorylation site(s) may exist. Consistently, mutagenesis studies in Nav1.2 revealed that maximal reduction of current amplitude required PKC phosphorylation of multiple serine residues in the ID1-2 linker as well as the 'classic' PKC site the ID3-4 linker (Cantrell *et al*., 2002). This was in agreement with the observation that PKA and PKC phosphorylation may interact, in a convergent manner, in modulating VGSC activity (Cantrell *et al*., 2002; Chahine *et al*., 2005; Chen *et al*., 2006). Thus, for example, in rat DRG neurons, PKC inhibitor peptide $PKCI_{19-36}$ attenuated the PKA-induced increase in VGSC current, suggesting convergence of PKA and PKC effects (Gold *et al*., 1998). Furthermore, mutagenesis experiments revealed that the inhibitory effect of PKA on Nav1.2 expressed in Chinese hamster ovary (CHO) cells was enhanced by PKC phosphorylation of two serine residues in the ID1-2 and ID3-4 linkers (Li *et al*., 1993; Cantrell *et al*., 2002).

1.3. Metastatic disease

Altered expression/activity of VGSCs contributes to several pathologies, such as neuropathic pain, epilepsy, cardiac conduction disorders, and metastatic disease (Diss *et al*., 2004; Onkal and Djamgoz, 2009). Such pathologies can occur as a result of either (i) genetic mutations in the VGSC protein (e.g. long QT syndrome, epilepsy) or (ii) dysregulation of VGSC gene expression (e.g. chronic pain, metastatic cancer) (Meisler *et al*., 2002; Waxman, 2007). Given its central importance to this PhD project, involvement of VGSCs in metastatic disease is described in detail as follows.

Worldwide, cancer is a leading cause of death, second only to cardiovascular diseases. In the developed Western countries, one in every four deaths is due to cancer (Edwards *et al*., 2005; Jemal *et al*., 2010). The most commonly diagnosed forms of cancer in males and females are prostate and breast cancers, respectively, and these cancer types have mortality rates second only to lung cancer in both genders (Edwards *et al*., 2005; Pruthi *et al*., 2007; Jemal *et al*., 2010). Most simply, normal cells become cancerous and form tumours as a result of genetic mutations (i.e. in proto-oncogenes or tumour suppressor genes) and/or epigenetic changes (i.e. hypo- or hyper-methylation) occurring in their DNA, which can result in the cells losing the control of their proliferative state (i.e. they become hyper-proliferating and apoptosis resistant) (Hanahan and Weinberg, 2000). In addition, it was proposed that cancerous cells would not be able to acquire metastatic phenotype by only genetic alteration without supporting microenvironment (Chung *et al.,* 2005). Following primary tumorigenesis, tumor cells with invasive (metastatic) potential spread to local or distant sites and, ultimately, form secondary neoplasms (i.e. metastasis). Overall, cancer cell genotype was described by at least 6 essential alterations in normal cell physiology that result in tumorigenesis and malignant spread/growth (Hanahan and Weinberg, 2000). These "hallmarks of cancer" include: (1) self-sufficiency in growth signals, (2) insensitivity to growth-inhibitory (antigrowth) signals, (3) evasion of programmed cell death (apoptosis), (4) unlimited replicative potential, (5) sustained angiogenesis, and (6) tissue invasion and metastasis (Section 1.3.2) (Hanahan and Weinberg, 2000). It is important to note that primary tumorigenesis (steps 1-5 above) and metastasis (step 6) are two distinct processes, which depend on separate sets of molecular/cellular determinants; supporting this phenomenon is the existence of a number of metastasis suppressor genes that

block/inhibit metastasis without affecting primary tumor formation (Steeg, 2003; Weigelt *et al*., 2005).

Most therapeutic strategies against cancer include excision of the primary tumour usually after some initial chemotherapy. Surgery may be followed by further pharmaco-, radio- and/or immuno-therapy to destroy any residual cancer cells (Vaidya and Welch, 2007). Metastasis, which is the spreading of cancer from the primary neoplasm to form tumours in secondary sites, is the cause of cancer-related deaths in approximately 90% of cases and is usually inoperable (Stetler-Stevenson *et al*., 1993; Sporn, 1996; Pantel and Brakenhoff, 2004). The discovery of metastasis suppressors (Berger *et al*., 2004; Vaidya and Welch, 2007) has raised the possibility that metastatic disease may also be treatable by drugs. Accordingly, much research time and effort has been directed in determining the genes/proteins and signalling pathways that regulate the metastatic behaviour of cancer cells (Schwirzke *et al*., 1999; Weigelt *et al*., 2005). In this regard, ion channels have emerged as promising novel targets (Prevarskaya *et al*., 2010). In particular, VGSCs, which are expressed and functionally expedient in a wide variety of metastatic carcinomas, have become an exciting new class of novel anti-metastatic drug targets (Roger *et al*., 2006; Onkal and Djamgoz, 2009). In the following, we aim to describe the evidence regarding (i) VGSC expression in metastatic carcinomas and (ii) functional contribution of VGSCs to metastatic cell behaviours (MCBs).

1.3.1 The case of prostate cancer

Prostate cancer (PCa) is a heterogeneous and complex disease and is generally accepted to start as a prostatic intraepithelial neoplasia (PIN) (Tennant *et al*., 2000; Maitland and Collins, 2005). PIN is characterized by cancer-related genetic and

phenotypic changes, but is non-invasive (initially); it can be detected by biopsy only (Bostwick and Qian, 2004). Typically, the subsequent metastatic adenocarcinoma develops within 10 years and this may be paralleled by an increased level of prostate specific antigen (PSA) (Bostwick and Qian, 2004). Prostate cancer treatment strategies are designed according to prognostic evaluation of PCa. Mainstream prognostic indicators are (i) clinical stage, (ii) prostate specific antigen (PSA) levels in blood, and (iii) histological stage, i.e. Gleason grade (Rosenthal and Sandler, 2010). According to these analyses, one or a combination of the following treatment methods may be used:

I. *Active surveillance (watchful waiting)*: This method involves constant surveillance of progression of cancer. If risk of cancer increases then other treatment options can be considered.

II. *Prostatectomy*: Early-stage PCa could be treated by surgically removal of all or part of the prostate with some surrounding tissue.

III. *Radiation therapy*: In this method cancer cells are destroyed by using directed radiation (X-rays) or radioactive seeds ("brachytherapy").

IV. *Chemotherapy*: Use of chemical to kill or stop growing of PCa.

V. *Hormone therapy*: Androgen-deprivation therapy (ADT) is the main therapy for PCa treatment. Huggins and Hodges (1941) showed that surgical castration or oestrogen injection induced PCa tumour regression. In the same study, androgen was shown to increase growth of prostate tumours. Therefore, surgical castration was used as an ADT with decreasing popularity with time because of irreversibility and gradual availability of pharmacological drugs that induce chemical castration by reducing level or

activity of testosterone (Schulman *et al.*, 2010). Chemical castration can be achieved as follows:

i. Luteinising hormone-releasing hormone (LHRH) receptor agonist: LHRH receptor (found in pituatary gland) induces release of luteinising hormone (LH) which in turn induces secretion of testosterone. LHRH can be downregulated by its agonist after initial increase in activity. Downregulation of LHRH receptor expression causes reduction in LH release and therefore in testosterone levels and androgen receptor (AR) activity.

ii. LHRH receptor antagonist: These antagonists compete with LHRH binding to its receptor and reduce endogenous LHRH receptor activity. This reduced receptor activity results in reduction of LH and testosterone levels.

iii. Antiandrogens: These drugs reduce directly androgen receptor activity by competing with testosterone and reducing its binding to AR.

In addition to castration, oestrogen therapy was shown to be effective against PCa growth (Huggins and Hodges, 1941). Therefore, oestrogen was used for PCa therapy. It was first applied orally but because of its side effects such as gynecomastia and cardiovascular toxicity, popularity of this therapy declined (Rosenthal and Sandler 2010). On the other hand, recent advances in application techniques resulted in renewed interest in this therapy (Langley *et al*., 2010).

ADT in combination with radiation therapy is the recommended treatment strategy for advanced PCa (Schulman *et al.*, 2010). However, following ADT, because of the presence of some ADT-resistant cells, PCa can return as more aggressive castration-

resistant prostate cancer (CRPC). CRPC cells are resistant to ADT because of mutations, overexpression or genomic amplification of AR (Koochekpour, 2010). Interestingly, the androgen receptor cascade of some CRPC cells can be activated by subcastration level of androgens, produced by adrenal cortex and prostate cancer itself (Brawer, 2008). In combination with improved chemotherapy, this technique became popular treatment for CRPC (Rosenthal and Sandler 2010).

In a subset of PCa tumours, cells may undergo neuroendocrine differentiation, which results in (i) castration resistance, (ii) growth factor dependence, and (iii) an aggressive phenotype (invasive / metastatic potential) (Kim *et al.,* 2002). Aggressive PCa cells metastasize mainly to bone, which is presumed to provide a hospitable microenvironment (e.g. growth factor and high Ca^{2+} content) that favours secondary tumour formation (Keller *et al.,* 2001; Fidler, 2002; Liao *et al.,* 2006).

1.3.2 The metastatic cascade

Metastasis is a complex process involving a series of interactive steps, in which primary tumour cells spread to secondary sites, where they ultimately form secondary tumours if provided with a favourable microenvironment with the right chemotactic agents and growth factors (i.e. 'seed and soil hypothesis') (Paget, 1889; Fidler, 2003). Only some tumour cells have ability to metastasize and only a minority of these metastatic cells (~ 0.01%) survive the multi-step metastatic cascade to form secondary tumours in distant body part(s) (Hunter, 2004). Moreover, each step of the metastatic cascade can be rate-limiting and failure to complete any of the steps can stop the entire process (Fidler, 2003). Notably, metastasis of solid tumours is

different than that of blood cancers (i.e. leukaemias), which do not require all the essential stages of metastasis described as follows (Figure 1.6):

1. Single cells or cell aggregates ***detach*** from primary tumour and degrade the basement membrane, by releasing proteolytic enzymes, and ***invading*** through local host stroma.
2. ***Intravasation***: embolization of single or aggregated tumour cells through endothelium into vascular and/or lymphatic systems. Thin-walled lymphatic channels provide the most common route for tumour-cell entry into the circulation, since they offer little resistance to penetration by tumour cells.
3. ***Transport in circulation***. After entering circulation, cells may be subject to immune defence and mechanical stress, and will often aggregate with other cancer cells or platelets, which may help their survival.
4. The surviving tumour cells become ***arrested*** in the capillary beds of distant organ(s) (secondary sites) and ***re-attach*** to the endothelial cells.
5. ***Extravasation*** and invasion into secondary sites (i.e. organ parenchyma). Extravasation requires the tumour cells that are attached to the endothelium to release certain protolytic enzymes and migrate through the basement membrane surrounding the blood vessel.
6. Invading tumour cells then migrate through stroma and ***proliferate*** within the organ parenchyma, which results in the formation of secondary tumours (micro-metastases").
7. ***Angiogenesis***: secondary tumor growth requires development of a new vascular network, which facilitates the growth by supplying O_2, survival factors, etc. and removing waste products. This essentially completes the metastatic process.

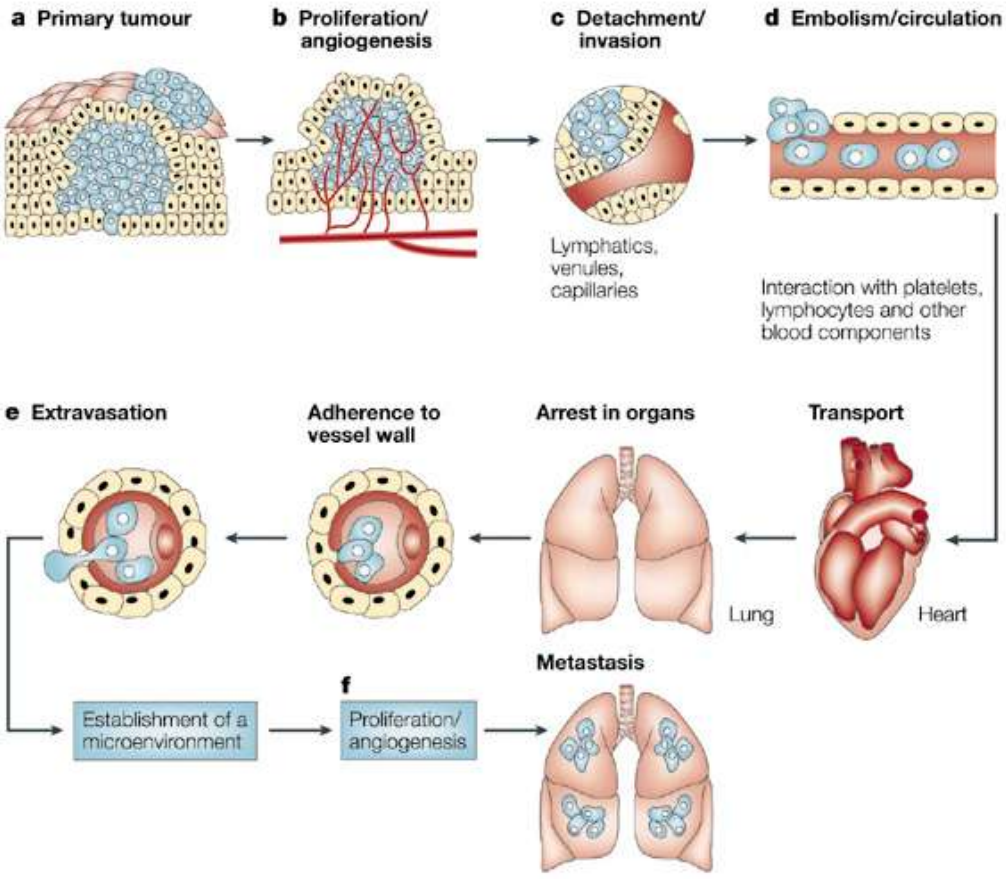


Figure 1.6 The metaststic cascade
a, Cellular transformation and primary tumorigenesis; b, extensive vascularization and tumor expansion; c, migration and invasion through local stroma; d, detachment and embolization followed by circulation and adherance to capillary endothelium of single or aggregated tumor cells; e, extravasation; f, secondary tumorigenesis and tumor expansion following angiogenesis. Adapted from Fidler (2003).

The tumour cells can then re-enter the circulation and produce additional metastases.

In spite of this cascade appearing well-organized, in fact, metastasis is a highly inefficient process (Hunter, 2004). A generally held "progression" model of metastasis explains this insufficiency, stating that a primary tumour progress to a premalignant state from which cells with metastatic ability arise due to stochastic genetic events (Fidler and Kripke, 1977; Hunter, 2004). Discovery of at least 11 metastasis suppressor genes, which inhibit the metastatic cascade without interfering primary tumourigenesis supports this model (Berger *et al*., 2004; Vaidya and Welch, 2007). The finding of consistent chromosomal aberrations specifically associated with malignant rather than benign tumours also supports this hypothesis (Goodison *et al*., 2005). However, more recent evidence has challenged the progression model, suggesting that metastatic ability may be "pre-coded" in primary tumours (Bacac and Stamenkovic, 2008, Bernards and Weinberg, 2002). For example, gene expression of a subset of primary tumours was found to be similar to that of metastatic secondary tumours, suggesting that metastatic potential may be encoded within the primary tumour tissue (Ramaswamy *et al*., 2003). In addition, 5% of metastatic disease cases have no clinically detectable primary tumour, which is also in support of the "pre-coded" model of metastasis (Hunter, 2004).

An 'integrative' model reconciles the two conflicting theories of metastasis (Hynes, 2003; Hunter, 2004; Weigelt *et al*., 2005). According to this model, primary tumours can be distinguished according to their metastatic potential, but rare subpopulations of variant cells, which are capable of forming metastases, are found within the primary tumours. The 'integrative' model encompasses three principles, as follows. First and foremost, tumour cells constitute a very heterogeneous population

in terms of their metastatic potential (Nguyen and Massague, 2007). For example, it has been shown that genes/proteins associated with various steps of metastasis such as proliferation, angiogenesis, cohesion, motility and invasion vary among different regions of neoplasms (Poste and Fidler, 1980; Simone *et al*., 1998). Second, during disease progression, the pre-existing metastatic tumour acquire further genetic variability, which may result in additional changes in their metastatic potential (Fidler, 2003; Vecchi *et al*., 2008; Gupta *et al*., 2007). Third, the cross-talk between the variant, metastasizing cells and the homeostatic mechanisms of the surrounding microenvironment can also influence the biologic behaviour of the metastatic cells (Fidler, 2002; Hunter, 2004). For instance, O_2 deprivation (hypoxia), a major tumour microenvironmental stress condition, has been associated with increased risk of metastatic dissemination *in vivo* (Pouyssègur *et al*., 2006; Bertout *et al*., 2008) and was shown to enhance invasiveness of several cancer cells *in vitro* (e.g. via upregulating expression/activity of various matrix metalloproteinase (MMPs) and cathepsins) (Canning *et al*., 2001; Burke *et al*., 2003; Brat *et al*., 2004; Ridgway *et al*., 2005). Furthermore, it has been shown that cancer cells prepare a "fertile ground" for their arrival in the secondary sites (Kaplan *et al*., 2005, Vaidya and Welch, 2007). Thus, melanoma cells were found to release soluble factors that stimulated lung fibroblasts to secrete fibronectin, thereby creating an attachment site for the arrival of vascular endothelial growth factor receptor (VEGFR) positive hematopoietic progenitor cells (Kaplan *et al*., 2005). These progenitor cells then secreted metalloproteinases that attracted chemokine receptor 4 (CXCR4) positive tumour cells (Kaplan *et al*., 2005).

Collectively, the observations summarised above support the view that new therapies and prognostic markers of metastasis should be targeted against not only

the metastatic cancer cells but also the surrounding microenvironmetal (host) factors that interact with metastasizing tumour cells, promoting different stages of metastasis (Fidler, 2002). A better understanding of the metastasis as a multi-step process, with respect to such host homeostatic factors, could lead to identification of more effective diagnostic and/or therapeutic anti-metastasis targets. Clearly, therefore, an important task would be to identify novel genes/proteins involved in the mediation of the metastatic cascade. One promising target in this regard is the VGSC (Onkal and Djamgoz, 2009).

1.3.3 VGSC expression in metastatic disease

1.3.3.1 *In vitro*

Functional VGSC expression has been shown to be up-regulated significantly in metastatic cancers of various epithelial origins (i.e. breast, prostate) both *in vitro* and *in vivo*, and correlated with the potentiation of a number of metastatic cell behaviours (MCBs) *in vitro* (e.g. invasion, adhesion, etc.) (Table 1.5; Roger *et al*., 2006; Brackenbury *et al*., 2008; Onkal and Djamgoz, 2009). Functional VGSC expression in metastatic cancer cells was initially detected in the Dunning rat model of PCa, whereby strongly metastatic Mat-LyLu cells expressed TTX-S Na^+ currents, whereas the weakly metastatic AT-2 cells did not (Grimes *et al*., 1995). Similarly, strongly metastatic human PCa cell line, PC-3, expressed functional VGSCs whereas there was no/little expression of VGSCs in weakly metastatic LNCaP cells (Laniado *et al*., 1997). Furthermore, TTX-R VGSCs were found in the strongly metastatic MDA-MB-231 human breast cancer (BCa) cells, but not in the weakly metastatic MCF-7 cells (Fraser *et al*., 2005). To date, VGSC expression has also been evidenced in several other carcinomas *in vitro* and, in some cases, *in vivo*, including, melanoma

Table 1.5 Expression/activity of VGSCs in metastatic cancer cells

Cancer (cell line)	Major VGSC(s)[1]	MCB(s)	Reference(s)
BCa (MDA-MB-231)	**nNav1.5** (1800x), Nav1.6, Nav1.7	Transwell migration, Matrigel invasion, lateral motility, galvanotaxis, endocytic membrane activity	Fraser *et al*. (2005); Roger *et al*. (2003); Brackenbury *et al*. (2007); Gillet *et al*. (2009); Chioni *et al*. (2010)
PCa (PC-3M, LNCaP, Mat-LyLu)	**nNav1.7** (1100x), Nav1.2, Nav1.3, Nav1.6	Process extention, galvanotaxis, lateral motility, endocytosis; detachment, gene expression, Matrigel invasion	Fraser *et al*. (1999, 2003); Djamgoz *et al*. (2001); Mycielska *et al*. (2003, 2005); Palmer *et al*. (2008); Grimes *et al*. (1995); Laniado *et al*. (1997); Bennett *et al*. (2004); Nakajima *et al*. (2009)
SCLC (H69, H209, H510)	**TTX-R**[2], Nav1.3, Nav1.5, Nav1.6, Nav1.9	Endocytic membrane activity	Blandino *et al*. (1995) ; Onganer and Djamgoz (2005)
NSCLC (H23, H460, Calu-1)	**Nav1.5**, Nav1.6, Nav1.7	Matrigel invasion	Roger *et al*. (2007)
Lymphoma (Jurkat)	**Nav1.5**, Nav1.6, Nav1.7, Nav1.9	Matrigel invasion	Fraser *et al*. (2004)
Mesothelioma (MPM)	Nav1.2, Nav1.6, Nav1.7	Lateral motility	Fulgenzi *et al*. (2006)
Colon cancer	**Nav1.5**	Matrigel invasion	House *et al*. (2010)
Ovarian cancer (Caov-3, SKOV-3)	**Nav1.5**, Nav1.2, Nav1.4, Nav1.7	Matrigel invasion, Transwell migration	Gao *et al*. (2010)
Neuroblastoma (nB1)	**nNav1.5**	ND	Ou *et al*. (2005)
Cervical cancer (JP, 085, 354)	**Nav1.2, Nav1.7** Nav1.4, Nav1.6	ND	Diaz *et al*. (2007)
Melanoma (C8161, C8146)	ND	ND	Allen *et al*. (1997)

Abbreviations: BCa, breast cancer, MCB, metastatic cell behaviour; ND, not determined; nNav1.5, neonatal Nav1.5; NSCLC, non-small cell lung cancer; PCa, prostate cancer; SCLC, small cell lung cancer; VGSC, voltage-gated sodium channel. [1] Pre-dominant isoforms are denoted in bold. Number in brackets indicates fold upregulation compared with corresponding weakly metastatic cells. [2] Predominant isoform unknown, but IC_{50} for TTX was 215 nM (Blandino *et al*., 1995). Modified from Onkal and Djamgoz (2009).

(Allen *et al*., 1997), small-cell lung cancer (SCLC) (Blandino *et al*., 1995; Onganer *et al*., 2005), non-small-cell lung cancer (NSCLC) (Roger *et al*., 2007), lymphoma (Fraser *et al*., 2004), neuroblastoma (Ou *et al*., 2005), cervical cancer (Diaz *et al*., 2007), mesothelioma (Fulgenzi *et al*., 2006), ovarian cancer (Gao *et al*., 2010) and colon cancer (House *et al*., 2010) (Table 1.5).

As regards the molecular identity of the VGSCα(s) expressed in metastatic PCa and BCa cell-lines, the predominant subtypes were Nav1.7 and Nav1.5, respectively, with much lower expression of various other VGSCα subtypes, as detailed in Table 1.5 (Diss *et al*., 2001; Fraser *et al*., 2005; Onkal and Djamgoz, 2009). Nav1.7 mRNA expression was ~1000-fold higher in strongly metastatic Mat-LyLu and PC-3 cell-lines, compared with the corresponding weakly metastatic cells (Diss *et al*., 2001). Similarly, Nav1.5 expression was found to be upregulated ~1800-fold in MDA-MB-231 cells, compared with the weakly metastatic MCF-7 cells (Table 1.5; Fraser *et al*, 2005; Chioni *et al*., 2009). Interestingly, in both Mat-LyLu and MDA-MB-231 cells, Nav1.7 and Nav1.5 were expressed primarily in their D1:S3 'neonatal' splice-forms (Diss *et al*., 2001; Chioni *et al*., 2005; Fraser *et al*., 2005). In particular, there are 7 amino acid differences between 'neonatal' and 'adult' Nav1.5 in D1:S3/S4 linker region of the channel protein, which enabled the generation of a novel 'neonatal' Nav1.5 selective polyclonal antibody, NESOpAb that was used to confirm that functional 'neonatal' Nav1.5 expression was higher in MDA-MB-231 *vs.* MCF-7 cells (Section 1.2.2; Diss *et al*., 2004; Chioni *et al*., 2005; Fraser *et al*., 2005). 'Neonatal' Nav1.5 mRNA expression has also been detected in human neuroblastoma cells (Ou *et al*., 2005). As regards PCa, 'neonatal' and 'adult' D1:S3 splice variants of Nav1.7 differ only by two amino acids (Section 1.2.2), which would make the production of an antibody selective for 'neonatal' Nav1.7 more difficult.

1.3.3.2 *In vivo*

Consistent with *in vitro* evidence, 'neonatal' Nav1.5 expression was found to be upregulated in metastatic BCa biopsy samples using immunohistochemistry with NESOpAb (Fraser *et al*., 2005). Real-time PCR data revealed that Nav1.7 was upregulated at the mRNA level in PCa biopsy samples compared with normal epithelium and benign hyperplasia (Diss *et al*., 2005; Onkal and Djamgoz, 2009). Moreover, immunohistochemical staining of normal prostate and metastatic PCa specimens on a tissue microarray slide has shown that overall VGSC expression was upregulated in a subset of metastatic PCa tissues (Abdul and Hoosein, 2002). Similar immunohistochemical results were also obtained using SCLC biopsies (Onganer *et al*., 2005). Diss *et al*., (2005) performed an analysis of "receiver operator characteristics" of Nav1.7 mRNA expression in PCa samples concluded that Nav1.7 has sufficient selectivity and sensitivity to be viable prognostic marker of metastatic PCa. More recently, (i) multiple VGSCαs (i.e. Nav1.2, 1.4, 1.6, 1.7) have been identified in primary cultures as well as biopsy samples of cervical cancer (Diaz *et al*., 2007), (ii) strong immunohistochemical Nav1.5 staining have been detected in colon cancer specimens but not in normal colon tissues (House *et al*., 2010), and (iii) Nav1.5 and Nav1.4 expression have been found by real-time PCR to be upregulated in cancerous *vs.* normal ovarian tissue; immunohistochemistry experiments also revealed that grade and metastasis of ovarian cancer correlated well with VGSC expression (Gao *et al*., 2010).

1.3.4 Involvement of VGSCs in metastatic disease

There is substantial evidence, obtained using various independent techniques, for VGSC-mediated upregulation of a range of MCBs *in vitro* (Table 1.5). On the main

part, TTX, a highly selective VGSC blocker, has been employed to show that VGSC activity potentiates cellular behaviours related to metastatic cascade, including process extension (Fraser *et al*., 1999), galvanotaxis (Djamgoz *et al*., 2001; Fraser *et al*., 2005), lateral motility (Fraser *et al*., 2003), Transwell migration (Roger *et al*., 2003; Fraser *et al*., 2005), detachment (Palmer *et al*., 2008; Chioni *et al*., 2009), gene expression (Mycielska *et al*., 2005; House *et al*., 2010), secretory membrane activity (Mycielska *et al*., 2003), and Matrigel invasion (Grimes *et al*., 1995; Laniado *et al*., 1997; Bennett *et al*., 2004; Fraser *et al*., 2005; Brackenbury and Djamgoz, 2006, 2007; Brackenbury *et al*., 2007; Gillet *et al*., 2009; Chioni *et al*., 2010; House *et al*., 2010).

Changes in cell morphology is important in terms of migratory activities of cancer cells and TTX has been shown to reduce cellular process extension of strongly metastatic Mat-LyLu, but not weakly metastatic AT-2 rat PCa cell line, which do not express functional VGSCs (Fraser *et al*., 1999). Such effect of VGSCs on cell morphology has also been described in neurons (e.g. Wilkemeyer and Angelides 1996). VGSCs also play a role in motility of metastatic cancer cells; TTX (1 μM) decreased lateral motility of Mat-LyLu cells by 47% whilst aconitine (a VGSC 'opener') increased motility by 15%; neither drug had any effect on motility of AT-2 cells (Fraser *et al*., 2003). The directional movement of Mat-LyLu cells in direct-current electric field ('galvanotaxis') was also dependent on VGSC activity, since it was suppressed by TTX and enhanced by veratridine (another VGSC 'opener' drug) (Djamgoz *et al*., 2001). TTX also suppressed galvanotaxis and Transwell migration of highly metastatic MDA-MB-231 BCa cells (Roger *et al*., 2003; Fraser *et al*., 2005; Brackenbury *et al*., 2007; Chioni *et al*., 2009, 2010). Possible mechanisms of *in vitro* involvement of VGSC activity in motility of metastatic cancer cells can be explained

as follows: 1) Intracellular enzymes implicated in cellular motility, such as protein kinase C (PKC) (Glauthier *et al.,* 2003) and/or protein kinase A (PKA) (Chioni *et al.,* 2010) may be stimulated by VGSC activity. (2) Cell-surface pH may change (acidify) which may promote proteolytic enzyme (e.g. cathepsin) activity, digestion of the tumour periphery and invasion (Gillet *et al.,* 2009; Li *et al.,* 2011). (3) Association with cytoskeletal elements, e.g. through VGSCβs which has significant structural homology with immunoglobulin-type cell adhesion molecule (CAM) (Brackenbury and Isom, 2008). (4) VGSC-mediated regulation of expression of genes involved in cellular motility, such as CAMs (Itoh *et al.*, 2004; House *et al.*, 2010).

Cancer cells are known to synthesize and release protolytic enzymes during various stages of the metastatic cascade, particularly during the process of local invasion (Fidler, 2002; 2003; Nguyen and Massague, 2007; Roger *et al*., 2007). Secretory membrane activities of Mat-LyLu and AT-2 cell lines were investigated by employing a non-cytotoxic secretory tracer, horseradish peroxidase (HRP) (Mycielska *et al*., 2003). It was shown that HRP uptake into strongly metastatic Mat-LyLu cells was approximately twice that of weakly metastatic AT-2 cells. Importantly, TTX significantly reduced uptake into Mat-LyLu cells without affecting that of AT-2 cells, which suggested a role for VGSCs in secretory (endocytic) membrane activities of metastatic cancer cells (Mycielska *et al*., 2003). Similar results were obtained from SCLC cell lines (Onganer and Djamgoz, 2005). In addition, Krasowska *et al*. (2004) showed that VGSC activity was also involved in patterning of endocytic/vesicular activity of rat PCa cell lines. Also, in LNCaP and PC-3 human PCa cell lines, it was found using immunoanalytical techniques that VGSC-blocking anticonvulsants carbamazepine and phenytoin inhibited secretion of PSA (Abdul and Hoosein, 2001).

There is also strong evidence that VGSC activity enhances *invasiveness* of metastatic cancer cells. Originally, Grimes *et al*. (1995) showed that treatment of Mat-LyLu cells with TTX (600 nM) significantly reduced the Matrigel invasiveness of this cell line *in vitro*. The same dose of TTX had no effect on weakly metastatic AT-2 cells. Parallel studies on human PCa cells (highly metastatic PC-3 and lowly metastatic LNCaP) revealed similar results (Laniado *et al*., 1997; Smith *et al*., 1998). In a particularly significant study, three human PCa LNCaP cell lines with increasing invasive potential (/LC, C4 and C4-2) were shown to express corresponding increasing levels of VGSC protein (Bennett *et al*., 2004). Importantly, transient expression of Nav1.4 in these three cell lines significantly enhanced their invasive potential, whilst treatment with TTX reduced their invasiveness back to control levels. This suggested that functional VGSCs are "necessary and sufficient" to enhance invasive phenotype of metastatic cancer cells (Bennett *et al*., 2004). An important implication of this study was that although the predominant VGSCα expressed in metastatic human PCa cells is Nav1.7, over-expression of another VGSCα isoform (Nav1.4) was adequate to enhance invasiveness. This raised the question of whether the precise VGSCα subtype expressed is important to enhancement of MCBs or whether functional expression of any VGSC would suffice (Onkal and Djamgoz, 2009).

VGSC activity was also shown to play a role in the invasive behaviour of highly metastatic MDA-MB-231 BCa cells (Roger *et al*., 2003; Fraser *et al*., 2005; Gillet *et al*., 2009). Both of these studies have shown that Matrigel invasion of MDA-MB-231 cells was reduced by up to some 50% following TTX treatment. Importantly, 'neonatal' Nav1.5, the predominant VGSCα in metastatic BCa cells (Fraser *et al*., 2005; Chioni *et al*., 2005), has been shown to be primarily responsible for the VGSC-

dependent enhancement of migration and invasion of MDA-MB-231 cells (Brackenbury *et al*., 2007; Chioni *et al*., 2010). Suppression of 'neonatal' Nav1.5 activity with (i) small interfering RNA (siRNA) or (ii) NESOpAb alsoreduced migration of MDA-MB-231 cells by ~40 %. Both treatments also significantly reduced Matrigel invasion of MDA-MB-231 cell line (Brackenbury *et al*., 2007). Consistently, the role of VGSC in cell invasiveness has also been reported for Jurkat cells, a human T-cell leukemia cell line (Fraser *et al*., 2004). In NSCLC cell lines, H23, H460 and Calu-1, where multiple isoforms of VGSCs are expressed (predominantly Nav1.5, Nav1.6 and Nav1.7), TTX reduced *in vitro* invasion by 40-50% (Roger *et al*., 2007). This study proposed that VGSCs may play a role in the enhancement of metastatic processes, such as invasion, through their involvement in the regulation of intracellular [Na^+] homeostasis (Roger *et al*., 2007). More recently, through TTX and siRNA experiments, VGSCs were found also to control invasiveness in ovarian and colon cancer cell lines *in vitro* (Gao *et al*., 2010; House *et al*., 2010).

The cellular mechanism(s) though which VGSCs participate in the modulation of invasiveness remains unknown. VGSCs have been shown to be involved in secretory activities of cancer cells (as noted above; also Mycielska *et al*, 2003). Thus, VGSC activity may control additional substances, such as presently unidentified proteases, growth factors etc. The invasive properties of non-small cell lung cancer (NSCLC) cell lines, as well as the metastatic breast cancer cell line MDA-MB-231 have been shown to be under control of proteolytic enzymes, such as metalloproteinases (MMPs) and cathepsins (Egeblad and Werb, 2002; Roger *et al.*, 2003; Gillet *et al.*, 2009, 2011). Moreover, VGSC ('neonatal' Nav1.5) activity was shown to result in acidification of the 'perimembrane' pH, which in turn enhanced the

proteolytic activity of secreted cysteine cathepsins, thereby ultimately upregulating the invasiveness of MDA-MB-231 BCa cells (Gillet *et al.*, 2009, 2011).

It has also been suggested that VGSC activity is involved in hyper-proliferative state of cancer cells. For example, various VGSC blockers (e.g. hydroxyamides and hydantoin) have been shown to inhibit PC-3 cell proliferation in a reversible, non-cytotoxic manner (Anderson *et al*., 2003). VGSC blocking drugs riluzole and flunarizine were found to inhibit the proliferation of LNCaP, MDA-PCA-2B, PC-3 and DU145 PCa cell lines, whereas the VGSC 'opener' veratridine increased proliferation, suggesting a role for VGSC in the hyper-proliferating state of cancer cells (Abdul and Hoosein, 2002). However, these drugs are not specific for VGSC and are known to affect other ion channels (e.g. Duprat *et al*., 2000; Fraser *et al*., 2000). In fact, when the highly specific VGSC blocker TTX was applied to Mat-LyLu, PC-3 or MDA-MB-231 cells, no effect on proliferation was seen (Laniado *et al*., 1997; Fraser *et al*., 2000; Roger *et al*., 2003; Fraser *et al*., 2005; Chioni *et al*., 2009, 2010; Nakajima *et al*., 2009).

In contrast to the plethora of evidence for functional VGSC expression in metastatic cancer cells, the mechanism(s) responsible for the upregulation of VGSCs in these cells is not fully known. It has recently been shown that epidermal growth factor (EGF) increased VGSC current density and was partially responsible for the enhancement of migration in Mat-LyLu cell line (Ding *et al*., 2008). Serum factors are also known to be important in the upregulation of VGSCs in Mat-LyLu cells (Ding and Djamgoz, 2004). Increasing serum concentration from 0% to 5% for 24 h reduced VGSC current density and increased TTX sensitivity, which suggests that serum components may be responsible for transcriptional and/or post-translational modifications of VGSC expression *in vitro*. It has been shown that nerve growth

factor (NGF) upregulated the total VGSC α-subunit protein level, increased VGSC current density in a dose- and time- dependent manner, and produced currents with faster kinetics of activation (Brackenbury and Djamgoz, 2007). This study also showed that PKA activity was involved in NGF induced increase in VGSC current density, since PKA inhibitor KT5720 completely abrogated the effect of NGF on VGSC current enhancement (Brackenbury and Djamgoz, 2007). In addition, in the strongly metastatic Mat-LyLu cell line, activity dependent (auto) upregulation of VGSCs (Nav1.7) was described, and this shown to occur via a positive feedback mechanism involving PKA as a signalling intermediate (Brackenbury and Djamgoz, 2006). A similar positive auto-regulatory loop was also reported for functional VGSC ('neonatal' Nav1.5) expression in MDA-MB-231 BCa cells (Chioni *et al*., 2010). Overall, VGSC autoregulation through positive feedback is unusual, and would suggest that blockage of VGSC activity in the short-term could lead to suppression of functional VGSC activity and expression in the long term. Clearly, this characteristic could contribute to VGSCs being an ideal anti-metastatic target.

1.3.5 Other ion channels expressed in prostate and breast cancers

Ion channels other than VGSCs have been shown to be involved in metastatic BCa and PCa. Both Mat-LyLu and AT-2 rat PCa cell lines expressed delayed-rectifier type voltage-gated potassium channel (VGPC) currents; however, the VGPC current density was significantly bigger for the weakly metastatic AT-2 cell line, in contrast to the higher / functional VGSC expression / activity in strongly metastatic Mat-LyLu cells (Fraser *et al*., 2000; 2003). Similar results were obtained in human PCa cell lines; weakly metastatic LNCaP cells possessed a larger VGPC current density compared to the corresponding strongly metastatic PC-3 cell line (Laniado *et al*., 2001). Fraser *et al* (2003) reported that the predominant VGPC isoform was Kv1.3,

alongside Kv1.4 and Kv1.6 in rat and human PCa cell lines. Consistently, in human BCa cells, weakly metastatic MCF-7 cells expressed much larger outward currents (consistent with VGPCs) as compared to small outward currents of the strongly metastatic MDA-MB-231 cells (Fraser *et al*., 2005). Combined pharmacology and immunocytochemistry data revealed that the primary isoform expressed in MCF-7 cell line was Kv1.1 (Ouadid-Ahidouch *et al*., 2000). Importantly, Kv1 family specific blocker α-dendrotoxin (α-DTX) reduced proliferation of MCF-7 cells, suggesting a role for Kv1.1 in growth regulation in this cell-line (Ouadid-Ahidouch *et al*., 2000). Several other studies have also observed this VGPC-dependent upregulation of proliferation in cancer cells (Wonderlin and Strobl, 1996; Fraser *et al*., 2000; 2003). It has been proposed that VGPCs may control/promote progression through the cell cycle G1 checkpoint by hyperpolarizing the membrane potential, which, in turn, might promote Ca^{2+} release from intracellular stores, and/or Na^{+}-dependent membrane transport (Wonderlin and Strobl, 1996; Pardo *et al*., 2005).

Taken together, weakly metastatic cells have higher VGPC, but lower VGSC expression/activity, compared to strongly metastatic PCa and BCa cells. Interestingly, a similar phenomenon occurs also in the case of NSCLC (Roger *et al*., 2007). This implies that there may be swift down-regulation of VGPCs, concomitant with the upregulation of VGSCs during the progression of the metastatic disease (Onkal and Djamgoz, 2009). It would follow from such pairing of channel activities that the reduced VGPC activity may depolarize the resting membrane potential, which would favour VGSC activity (Onganer and Djamgoz, 2005; Fraser *et al*., 2005; Prevarskaya *et al*., 2007). Based on these observations, a "cellular excitability" (CELEX) hypothesis of cancer metastasis was recently proposed (Djamgoz and Isbilen, 2006; Onkal and Djamgoz, 2009); this agrees favourably with the well-

evidenced ‘neuronal’ phenotype of aggressive cancer cells (Liotta and Clair, 2000; Hagel and Stavrou, 2007; Brackenbury *et al*., 2008; Onganer *et al*., 2005). Another important aspect of the pairing between VGSC-VGPC activities is that the proposed role of VGPCs in proliferation might be important in terms of tumourigenesis, whilst the VGSC activity has been shown to enhance various metastatic cell behaviours, including motility and invasion. This is a clear example of primary tumourigenesis and metastatic being driven by non-identical sets of molecular controls. Targeting/inhibition of VGSC expression and activity may thus present novel diagnostic markers and therapeutic approaches that are specifically directed at the metastatic disease (Sikes *et al*., 2003; Rogers *et al*., 2006; Onkal and Djamgoz, 2009).

Apart from VGSCs and VGPCs, Ca^{2+} channel and pump activity has also been implicated in metastatic behaviour of cancer cell lines such as those of prostate cancer, breast cancer, head and neck squamous cell carcinoma, pulmonary adenocarcinoma, rhabdomyoblastoma, fibrosarcoma and retinoblastoma (Wang *et al.*, 2010; Liao *et al.*, 2006; Huang *et al.*, 2004; Zhong *et al.*, 2010; Wu *et al.*, 1997; Amuthan *et al.*, 2002; Amuthan *et al.*, 2001; Cook and Lockyer, 2006; Wertz and Dixit, 2000; Lehen’kyi *et al.*, 2007). Changes in intracellular Ca^{2+} level have been shown to play important role in cellular processes including fertilization (Ozil and Swann, 1995), cell cycle (Ding *et al.*, 2010), apoptosis (Norberg *et al.*, 2008), mitochondrial redox state (Hajnóczky *et al.*, 1995), differential gene expression (Wang *et al.*, 2010; Liao *et al.*, 2006; Dolmetsch *et al.*, 1998; Li *et al.*, 1998; Haisenleder *et al.*, 2001; Buonanno and Fields, 1999; Olson and Williams, 2000), motility / invasion (Amuthan *et al.*, 2002; Wei *et al.*, 2009; Huang *et al.*, 2004; Komuro and Rakic, 1996), muscle contraction (Baylor and Hollingwoth, 2010),

pacemaker activity (Méry *et al.,* 2005), growth cone turning / migration (Gomez *et al.,* 1995; Gomez *et al.,* 2001), axonal growth (Tang *et al.,* 2003), development of neurotransmitter phenotype (Ciccolini *et al.,* 2003), formation of nodules in plant root hairs (Ehrhardt *et al.,* 1996), development of muscles (Ferrari *et al.,* 1998), release of cytokines (Uhlén *et al.,* 2000), exocytosis (Tse *et al.,* 1993), adhesion (Giannone *et al.,* 2002; Liao *et al.,* 2006), chemotaxis (Mycielska *et al.,* 2004), and synaptic plasticity (Parkash and Asotra, 2010; Berridge, 1998, 2009).

Basal $[Ca^{2+}]_i$ is tightly controlled and maintained at ≤ 100 nM (higher level / long periods of $[Ca^{2+}]_i$ rise can be cytotoxic), while extracellular Ca^{2+} concentration is at mM level. The intracellular Ca^{2+} is maintained by a complex set of mechanisms including channels, exchangers and pumps (Parkash and Asotro, 2010; Berridge *et al.,* 2003; Berridge *et al.,* 1998). Accordingly, Ca^{2+} signals must be re mediated only by brief changes in $[Ca^{2+}]_i$ (Parkash and Asotro, 2010; Rey *et al.,* 2010; Clapman, 2007; Berridge *et al.,* 1998). These brief changes can be mediated by influx of extracellular Ca^{2+} and/or release of Ca^{2+} form intracellular stores (Roderck and Cook, 2008; Clapham, 2007; Berridge *et al.,* 2003; Berridge *et al.,* 1998). Channels that are responsible for influx of Ca^{2+} can be divided into three groups: Voltage-gated, receptor-operated and store-operated Ca^{2+} channels (Berridge *et al.,* 1998). Another significant mediator of Ca^{2+} influx is Na^+ - Ca^{2+} exchanger (NCX) operating in reverse-mode. Under resting conditions, following an increase in $[Ca^{2+}]_i$, NCX works by extruding one Ca^{2+} ion in exchange of three Na^+ ions (Blaustein and Lederer, 1999). Importantly, it was shown that influx of Na^+ through opening of VGSCs can significantly raise localized intracellular Na^+ concentration and can consequently slow or reverse NCX activity and thus significantly increase the intracellular Ca^{2+} concentration (Sagel *et al.,* 1991; Gosling *et al.,* 1998) as well as

TRP channels (Poburka, *et al.,* 2007; Eder *et al.,* 2005; Rosker *et al.,* 2004; Arnon *et al.,* 2000). In addition, two channels, ryanodine receptor (RyR) and inositol-triphosphate receptor (IP_3R) have been implicated in release of Ca^{2+} from intracellular stores (Campbell *et al.,* 1987; Streb *et al.,* 1983). Furthermore, sarcoplasmic-endoplasmic reticulum Ca^{2+}-ATPase (SERCA), plasma membrane Ca^{2+}-ATPase (PMCA) and mitochondrial Ca^{2+} uniporter can also contribute to Ca^{2+} signalling (Berridge *et al.,* 2003; Berridge *et al.,* 1998).

Changes in expression profiles of these Ca^{2+} channels and pumps have been documented in various cancer types (Table 1.6) and it has been proposed that such changes can play an important role in carcinogenesis (Parkash and Asotor, 2010; Monteith *et al.,* 2007). For example, various cation-permeant transient receptor potential (TRP) channel family members, including TRPC1, TRPC3, TRPC4, TRPV2, TRPV6 and TRPM8, were detected in PCa cells (Abeele *et al.,* 2003a; Abeele *et al.,* 2003b; Abeele *et al.,* 2004; Fixemer *et al.,* 2003; Schmidt *et al.,* 2006; Thebault *et al.,* 2005). Importantly, increases in TRPM8 (Tsavaler *et al.,* 2001; Fuessel *et al.,* 2003; Schimidt *et al.,* 2006) and TRPV6 (Zhuang *et al.,* 2002; Fixemer *et al.,* 2003; Wissenbach *et al.,* 2001; Peng *et al.,* 2001) mRNA expression were documented in prostate cancer tissue samples. Interestingly, in Mat-LyLu and AT-2 cells, voltage gated calcium channel (VGCC) activity was not present (Ding *et al.,* 2008). However, using Indo-1 microfluorimetry, AT-2 cells were found to have higher $[Ca^{2+}]_i$ than Mat-LyLu cells (Ding *et al.,* 2008). That study also found that raising extracellular $[Ca^{2+}]$ increased while raising extracellular $[K^+]$ decreased $[Ca^{2+}]_i$ in AT-2 but had no effect on Mat-LyLu cells. It was proposed, therefore, that the weakly metastatic AT-2 cells possessed a voltage-independent Ca^{2+} permeation mechanism, which was down-regulated/absent in the strongly metastatic Mat-LyLu

Table 1.6 Changes in expression of Ca^{2+} channels and pumps in cancer

Ca^{2+} Channel/pump	Type of cancer	mRNA level	Protein level	Reference(s)
Voltage gated channels				
CaV1.2	Colon cancer	↑	n.d.	Wang *et al*., 2000
CaV1.1	Colorectal cancer	↑	n.d.	Zhang *et al*., 1997
CaV3.1	Glioma	↑	n.d.	Latour *et al*., 2004
	Colorectal cancer	↓	n.d.	Toyota *et al*., 1999
CaV3.3	Colon cancer	↓	n.d.	Paz *et al*., 2003)
TRP channels				
TRPV1	Bladder cancer	n.d.	↓	Lazzeri *et al*., 2005
	Glioma	↑	↑	Contassot *et al*., 2004
TRPV6	Prostate, breast, ovary, thyroid and colon cancer	↑	n.d.	Fixemer *et al*., 2003; Zhuang *et al*., 2002
TRPM1	Melanoma	↓	n.d.	Deeds *et al*., 2000
TRPM8	Prostate, colorectal cancer	↑	n.d.	Schmidt *et al*., 2006 ; Tsavaler *et al*., 2001
Pumps				
SERCA2	Colon and lung cancer	↓	n.d.	Korosec *et al*., 2006
	Tyroid, oral, cancer; squamous cell carcinoma	↓	↓	Pacifico *et al*., 2003; Endo *et al*., 2004
	Colorectal cancer	↑	n.d.	Chung *et al*., 2006
SERCA3	Colon cancer	n.d.	↓	Brouland *et al*., 2005
PMCA	Skin and lung cancer	n.d.	↓	Reisner *et al*., 1997
PMCA1	Oral cancer, squamous cell carcinoma	↓	↓	Saito *et al*., 2006
	Breast cancer	↑	n.d.	Lee *et al*., 2002
	Skin cancer	↓	n.d.	Reisner *et al*., 1997
PMCA2	Breast cancer	↑	n.d.	Lee *et al*., 2005
PMCA4	Skin cancer	↓	n.d.	Reisner *et al*., 1997
Store-release channels				
RyR1	Thyoma	↓	n.d.	Kusner *et al*., 1998
IP3R2	Non-small-cell lung cancer	↑	n.d.	Heighway *et al*., 1996
IP3R3	Gastric cancer	↑	↑	Sakakura *et al*., 2003

CaV, voltage-gated Ca^{2+} channel; TRPC, transient receptor potential canonical; TRPM, transient receptor potential melastatin; TRPV, transient receptor potential vanilloid; SERCA, sarcoplasmic/endoplasmic reticulum Ca^{2+}-ATPase; PMCA, plasma membrane Ca^{2+}-ATPase; RyR, ryanodine receptor; IP3R, inositol 1,4,5-triphosphate receptor; n.d., not determided; ↑, increase; ↓, decrease. Modified from Parkash and Asotro, 2010.

cells (Ding *et al.,* 2008). On the other hand, VGCC expression was detected in LNCaP cell line in one study (Mariot *et al.,* 2002; Toyota *et al.,* 1999; Steinsapir *et al.,* 1991), but not in another (Skryma *et al.,* 1997).

It was suggested that extracellular Ca^{2+} concentration is a possible mediator of PCa bone metastasis (Liao *et al.,* 2006). Thus, Liao *et al.* (2006) showed that extracellular Ca^{2+} enhanced proliferation of skeletal metastatic PC-3 and C4-2B cells but not non-skeletal metastatic LNCaP human prostate cells. In addition, extracellular Ca^{2+} was shown to increase adhesion of PC-3 cells via the anti-apoptotic Akt signalling pathway (Liao *et al.,* 2006). As mentioned above, Ca^{2+} signalling was shown to be important in MCBs of cancer cell lines, including in PCa (Wang *et al.,* 2010; Monet *et al.,* 2010; Gkika *et al.,* 2010; Liao *et al.,* 2006; Mycielska and Djamgoz, 2003; Mycielska and Djamgoz, 2004). For example, Mycielska and Djamgoz (2003, 2004) proposed that Ca^{2+} signalling plays important role in galvanotaxis and endocytosis membrane activity of Mat-LyLu cells. In addition, Ca^{2+} signalling was shown to regulate PCa cell motility via the Ca^{2+}/calmodulin-dependent protein kinases II (CaM kinases II) pathway (Wang *et al.,* 2010). TRP channels were shown to be involved in MCBs of PCa cells. For instance, silencing of TRPV2 by siRNA reduced growth and invasion of PC-3 cells (Monet *et al.,* 2010). On the other hand, TRP8M activation by PSA was reported to decrease motility of PC-3 cells (Gkika *et al.,* 2010).

1.3.6 Possible downstream mechanisms involved in VGSC activity-dependent promotion of MCBs

The possible cellular mechanism(s) which are downstream to VGSC activity that lead to modulation of MCBs remains unknown. However, a number of possible mechanisms can be suggested, as follows:

I. VGSC mediated change in gene expression: House *et al.* (2010) showed that Nav1.5, predominant VGSCα subunit functionally expressed in colon cancer cells, activity regulates genes expression including genes involved in cell migration, invasion and cycle control.

II. Association with other proteins: Multiple proteins were shown to interact with VGSC such as ankyrin, calmodulin, VGSCβ and annexin and these were suggested to play role in MCBs. For example, VGSCβs that have homology with immunoglobulin CAMs can associate with cytoskeletal elements (Brackenbury and Isom 2008).

III. Activating of the cAMP/PKA pathway: Blackenbury and Djamgoz (2006) showed that increase in intracellular Na^+ (including by VGSC activity) leads to increase in phosphorylated PKA level. In turn, the increase in PKA activity could phosphorylate cytoskeletal proteins that is involved in MCBs (Mycielska *et al.,* 2003).

IV. VGSC mediated change in pH: Na^+ influx through activity of VGSC was suggested to be capable of altering intracellular pH by disrupting activity of Na^+/H^+ exchange (Mycielska *et al.,* 2003). On the other hand, Gillet *et al.,* (2009) showed that VGSC activity results in perimembrane acidification and intracellular alkalization which leads to increased proteolytic activity of cathepsins and therefore increased invasiveness of MDA-MB-231 cells.

V. Modulation Ca^{2+} signalling by VGSC activity: The influx of Na^+ can slow or even reverse Na^+/Ca^{2+} exchanger (NCX) activity which, in turn, can result in increased intracellular Ca^{2+} ($[Ca^{2+}]_i$) (Poburko *et al.,* 2007; Eder *et al.,* 2005; Rosker *et al.,* 2004; Arnon *et al.,* 2000; Blaustein and Lederer, 1999; Matsuka and Hilgemann; Miura and Kimura, 1989). This increase in $[Ca^{2+}]_i$ may activate Ca^{2+}-sensitive signalling mechanisms and modulate MCBs (Parkash and Asotro, 2010; Monteith *et al.,* 2007). For instance an increase in $[Ca^{2+}]_i$ on the anodal side was suggested to determine the directionality of galvanotaxis in metastatic cells (Mycielska and Djamgoz 2004). Similarly, Mycielska and Djamgoz (2003) proposed that an increase in $[Ca^{2+}]_i$ could lead to increased endocytosis and secretion by activation of protein kinase C and/or CaM kinase.

1.4 Aims and scope of the present study

It is clear from this Introduction that ionic mechanisms such as VGSC expression/activity and Ca^{2+} signalling are important in the control of MCBs in PCa. Therefore, it was suggested that targeting ionic mechanisms could be useful in cancer therapy. Importantly, Ca^{2+} signalling may be downstream to VGSC activity leading to potentiation of MCBs. In addition, microenvironmental factors, such as O_2 level, were proposed to regulate VGSC expression/activity. The main aim of this study was to elucidate cellular / ionic mechanisms related to functional VGSC expression in PCa cells. A multi-faceted approach was used, including real-time PCR (to measure changes in mRNA expression), Western blotting (to measure total protein level),

immunocytochemistry and confocal microscopy (to measure sub-cellular distribution of proteins), live Ca^{2+} imaging (to measure changes in intracellular Ca^{2+} level), and *in vitro* lateral motility, transverse migration, and Matrigel invasion assays (to evaluate effects on MCBs). The specific aims were as follows:

1. To investigate VGSC α- and β- subunit regulation by long-term hypoxia (24 h, 2 % O_2) in strongly metastatic (Mat-LyLu) and weakly metastatic (AT-2) rat PCa cell lines;
2. To evaluate possible effects of clinical pharmacological blockers of VGSCs on (i) VGSC α expression and (ii) MCBs in Mat-LyLu cells under normoxic (21 % O_2) and hypoxic (2 % O_2) conditions; and
3. To characterise intracellular Ca^{2+} signalling and its dependence on VGSC activity in human metastatic PCa PC3M cells.

Chapter 2

MATERIALS AND METHODS

The present study employed a variety of materials and techniques. These are detailed in this chapter.

2.1 Cell lines and culture conditions

The following prostate cancer (PCa) cell lines were used: Dunning rat, AT-2 and Mat-LyLu, and human LNCaP and PC-3M. Mat-Lylu and PC-3M cells are strongly metastatic; AT-2 and LNCaP are weakly/non-metastatic (Isaacs *et al*., 1981; Chu *et al*., 2001). The Dunning cell lines at least partially reflect clinical behaviour. Mat-LyLu cells are strongly metastatic whilst AT-2 cells are weakly metastatic cells, corresponding to a central issue in clinical management of PCa, i.e. which tumour cells would metastasise and which would not. A possible limitation of the Dunning (Mat-LyLu) cells is that, when injected into Copenhagen rats, they tend not to metastasise to bone, one of the main secondary sites of human PCa. Human PC-3M cells were used in order to increase the clinical relevance of the effects observed. All cells were seeded into 100 mm Falcon tissue culture dishes (Becton Dickinson Ltd.) and grown in an incubator (Sanyo, IncuSafe MCO-18AIC) at 37 ^{o}C, 100 % relative humidity and 5 % CO_2. Cells were grown to confluence and serially passaged every 24 h using fresh culture medium. In 'chronic hypoxia' experiments, cells were grown in a dedicated hypoxia chamber (RSBioptech, Galaxy 14S), which maintained 2 % O_2 by flow of nitrogen which was regulated by built-in calibrated O_2 meter. In order to avoid passage-dependent effects on cultured cells' phenotype, passage numbers of cells were restricted to a maximum of 15. In addition, cell lines were monitored routinely by checking morphology and expression/activity of VGSC, as indirect controls for any change in phenotype. Finally, our collaborators at Istanbul

University showed routinely that Mat-LyLu cells injected subcutaneously into Copenhagen rats induced extensive lung metastases (within about 3 weeks).

2.1.1 Dunning rat PCa cell lines

AT-2 and Mat-LyLu were derived originally from a spontaneously occurring prostatic tumour of a Copenhagen rat; the tumour was well-differentiated, slow growing and heterogeneous, i.e. composed of both androgen–dependent and androgen–independent tumour cells (Dunning 1963; Isaacs *et al*., 1981). Both AT-2 and Mat-LyLu cells are androgen-insensitive, fast-growing and anaplastic. AT-2 cells are associated with a low rate of metastasis (less than 1 %); Mat-LyLu cells are strongly metastatic (75-90 %) (Isaacs *et al*., 1981). The cells were cultured in Roswell Park Memorial Institute (RPMI) 1640 medium (Invitrogen) supplemented with 2 mM L-glutamine (Invitrogen), 250 nM dexamethasone (Sigma-Aldrich) and 1 % foetal bovine serum (FBS) (Invitrogen), as described previously (e.g. Grimes *et al*., 1995). These cells lines were selected since they are well characterized, had markedly different metastatic ability (as mentioned above) and had significantly different VGSC expression/activity profiles. In particular, the strongly metastatic Mat-LyLu cells express a high level of functional VGSC (Grimes *et al.*, 1995). Intracellular Ca^{2+} measurements were made on PC3M cells, which also express functional VGSCs (Laniado *et al.*,1997), in order to be able to relate increase the clinical relevance of the data.

2.1.2 Human PCa cell lines

The PC-3M cells were originally isolated from a liver metastasis produced in nude mice by injection of the parental human PCa PC-3 cells (Kaighn *et al*., 1979; Kozlowski *et al*., 1984). The LNCaP cell line was isolated originally from a lymph

node metastasis of a 50-year old Caucasian male PCa patient (Horoszewicz *et al.*, 1980). LNCaP cells are generally much less aggressive than the PC-3M cells (Chu *et al*., 2001). Both PC-3M and LNCaP cells were maintained in RPMI 1640 medium (Invitrogen) supplemented with 4 mM L-glutamine (Invitrogen) and 10 % foetal bovine serum (FBS) (Invitrogen), as described previously (Laniado *et al*., 2001). Intracellular Ca^{2+} measurements were made on PC3M cells, which also express functional VGSCs (Laniado *et al.*,1997), in order to be able to relate increase the clinical relevance of the data.

2.2 Pharmacology

2.2.1 Pharmacological agents

Pharmacological agents were prepared as stock solutions in appropriate solvents (Table 2.1) and stored at -20 ^{o}C. Stock solutions were diluted to working concentration in culture medium or mammalian physiological saline (MPS) minutes before application. In all treatments that lasted longer than 24 h, culture medium ± pharmacological agents was replaced every 24 h.

2.2.2 Toxicity assay

In order to determine the possible cellular toxicicity of the pharmacological agents used at their working concentrations, trypan blue exclusion assay was used as described previously (Fraser *et al*., 2003). Briefly, cells were plated into 35 mm Falcon tissue culture dishes at a density of 3 x 10^4/ml and allowed to settle overnight before treatment. Cell culture medium ± pharmacological agent was then replaced with 0.1 % trypan blue (Sigma-Aldrich) in normal medium. Following incubation for 10 min at 37 ^{o}C, the solution was replaced with 1 ml fresh cell culture medium and the cells were viewed at 40x magnification under an inverted microscope (Carl

Table 2.1 Summary of pharmacological agents used in the present study.

Drug	Solvent	Working concentration	Supplier
TTX	Water/MPS	1 μM	Alomone
Lidocaine	Water	1 – 1000 μM	Sigma
Procaine	Water	1 – 1000 μM	Sigma
Ranolazine	Water	20 – 300 μM	Sigma
Riluzole	DMSO (30%) in water	1 – 100 μM	Sigma
Thapsigargin	MPS	5 μM	Sigma
Caffeine	MPS	10 mM	Sigma
Ryanodine	MPS	50 μM	Sigma

Abbreviations: TTX (tetrodoxin), MPS (mammalian physiological saline), DMSO (dimethyl sulfoxide)

Zeiss). For each treatment, the percentage of dead cells was determined from 30 randomly selected fields of view which had at least 30 cells. This procedure was repeated in three separated dishes. Data are presented as averages of 3x30 measurements.

2.3 Polymerase chain reaction (PCR)

2.3.1 RNA extraction

Total RNA was extracted from cells using TRIzol® reagent (Invitrogen), according to the manufacturer's instructions. Briefly, after washing the cells with ice-cold phosphate buffered saline (PBS) (Invitrogen), cells were lysed by adding 1 ml of TRIzol® reagent and homogenised by pippetting several times. Samples were mixed with 0.2 ml chloroform (Sigma-Aldrich) after 5 min incubation at room temperature. Following centrifugation (Labofuge 400R, Heraus) at 12,000 x *g* for 15 min at 4 ^{o}C, the top aqueous phase, which contains the RNA, was transferred to a fresh tube and mixed with 0.5 ml isopropyl alcohol (Sigma-Aldrich). Samples were incubated at room temperature for 10 min and centrifuged at 12,000 x *g* for 10 min at 4 ^{o}C. After removing supernatant, precipitated RNA was washed with 1 ml of 75 % (v/v) ethanol (Sigma-Aldrich) and centrifuged at 7,500 x *g* for 5 min at 4 ^{o}C. Supernatant was removed and RNA samples were air dried for 30 min before redissolving in RNase and DNase free water (Invitrogen). RNA samples were treated with DNaseI (Amersham Biosciences) in order to remove any DNA contamination. The quantity of the extracted RNA was checked by spectrophotometric absorbance at 260 nm (NanoDrop 1000A, Thermo Scientific). The quality of the RNA was confirmed by the 260 : 280 nm spectrophotometric absorbance ratio, where a value of $\geq$ 2.0 indicated good quality of extracted RNA (Sambrook *et al*., 1989). In addition, RNA

quality was assessed visually by agarose gel electrophoresis by observing 28S and 18S rRNA bands (Section 2.3.4; Figure 2.1). All RNA samples were stored at -20 ^{o}C for 1 month.

2.3.2 cDNA synthesis

One µg of RNA was used as a template for reverse-transcription into cDNA, as described previously (Mycielska *et al*., 2005). Each reaction contained 1 µg RNA, 250 ng random hexamer mix (Amersham Biosciences), 1 µl Superscript II reverse-transcriptase (Invitrogen), 2 µl 0.1 M DTT (Invitrogen), 4 µl Superscript II first strand buffer (x5) (Invitrogen), 1 µl 10 mM dNTP mix (Pharmacia Biotech), 1 µl (33.8 U) porcine RNA guard (Amersham Biosciences), and DNase and RNase free distilled water to make up final volume to 20 µl. For each sample, a control reaction was performed in which Superscript II reverse transcriptase was replaced with H_2O as a control for any genomic contamination. Synthesized cDNA was stored at -20 ^{o}C after it was diluted (x5) in DNase and RNase free distilled water.

2.3.3 Real-time PCR

Real-time PCR employing SYBR I Green technology was used to study and quantify gene expression, as described previously (Mycielska *et al.,* 2005). Briefly, 10 µl of QuantiTech SYBR Green PCR mix (Qiagene), 5 µl cDNA, 0.5 µM of both sense and antisense primers (Eurofin MWG) were mixed. Final volume was made up to 20 µl with RNase and DNase free distilled water. Amplification was performed using the DNA Engine Opticon 2 System (MJ Research). Reaction was started by heating at 95 ^{o}C for 15 minutes to activate HotStar Taq. This was followed by 3-step 40 cycles of

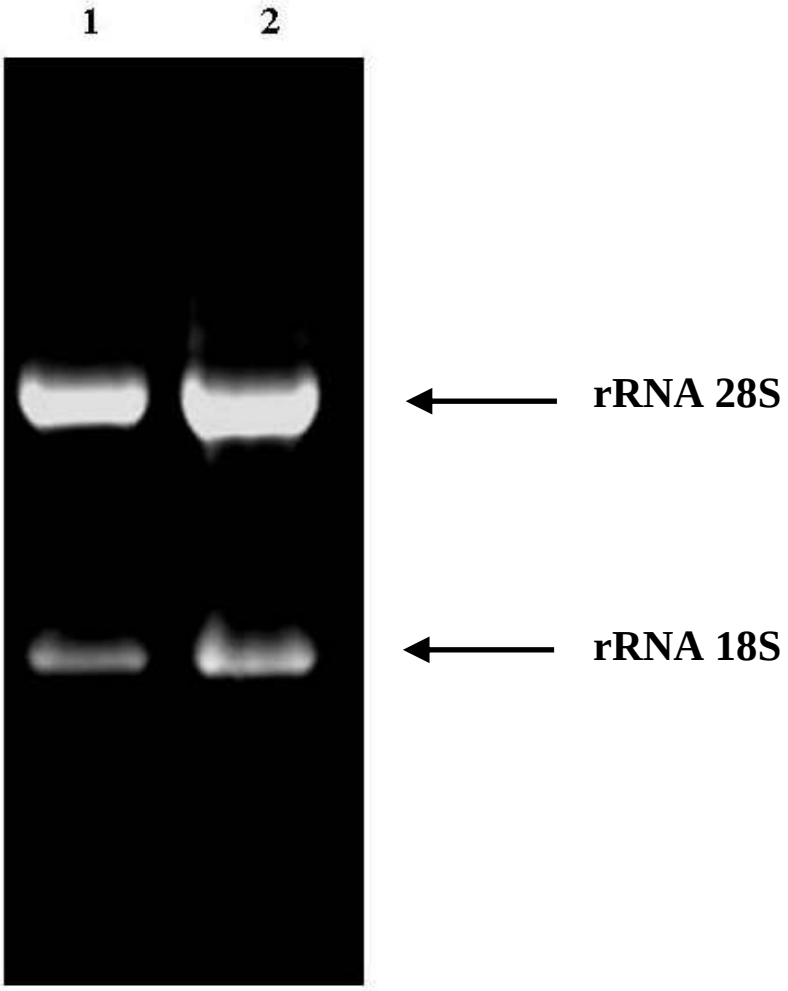


Figure 2.1 Visual assessment of RNA quality by agarose gel electrophoresis.
The quality of the extracted RNA was characterized by observing higher intensity of 28S rRNA band and low intensity 18S rRNA band. 5 µl of total RNA from AT-2 cells (lane 1) and Mat-LyLu cells (lane 2) were run on a 0.8 % agarose gel.

95 ^{o}C for 30 seconds, annealing temperature depending on the primer used for 30 seconds (Table 2.2) and 72 ^{o}C for 30 seconds. After each cycle, the fluorescence emitted by incorporation of SYBR Green to double stranded DNA was measured (Figure 2.2A-D). In order to verify the product composition, a melting curve was carried out from 65 ^{o}C to 95 ^{o}C with 0.3 ^{o}C steps at the end of the reaction (Figure 2.2E-H). For each cDNA sample, duplicate reactions were performed for both the target gene and the normalizing (control) gene (Cytb5R/ β-actin) simultaneously. Each set of reaction also included a non-template control, where the cDNA was replaced by DNase- and RNase-free distilled water. Standard calibration curve for each target gene using four serial dilutions of a cDNA template was also carried out (Figure 2.3). PCR product sizes were controlled by agarose gel electrophoresis (see Section 2.3.4). Opticon Monitor 2 software (MJ Research) was used to determine the threshold amplification cycles (C_T). The $2^{-\Delta\Delta C_T}$ method (Livak and Schmittgen, 2001) was used to analyze the data using following equation:

$$y = 2^{-([mean\,\Delta C_T] - [mean\,\Delta C_T\ control])}$$

equation 2.1

where y is the target gene mRNA level relative to control sample, and ΔC_T is the difference in amplification threshold cycle numbers between target and normalizing genes. The relative target gene levels were expressed as mean ± standard error (SEM) from at least three separate repeats.

2.3.4 Agarose gel electrophoresis

PCR products were separated by agarose gel electrophoresis. Five µl samples were mixed with 1 µl of loading buffer (x6; containing bromophenol blue and glycerol) and loaded on 0.8 % (w/v) agarose (Sigma-Aldrich), 1 x Triz-HCl-Borate EDTA (TBE; Invitrogen) gel containing 5 µl of SYBRSafe™ DNA gel stain (Invitrogen).

Table 2.2 PCR primer related details.

Target gene	Primer sequence		T_a (°C)	Product size (bp)	Reference(s)
rNav1.7	Sense Antisense	5'-TGACTTGGAAGCTGGGAAAC-3' 5'-TTCCAAGGGTCACGGAGGA-3'	60	414	-
VGSCβ1	Sense Antisense	5'-AACCACTCTGGCGACTACGA-3' 5'-TTCCGAGGCATTCTCTTGTG-3'	60	258	Seda *et al*. (2007)
VGSCβ2	Sense Antisense	5'-TGGACTTACCAGGAGTGTAGCAA-3' 5'-AGGCACCCACGATGACTG-3'	60	295	Seda *et al*. (2007)
VGSCβ3	Sense Antisense	5'-TCCTCACCTTGTGGCTGTTT-3' 5'-ACCTGGGGCACTTCCTGATA-3'	60	233	Seda *et al*. (2007)
VGSCβ4	Sense Antisense	5'-TCCTACAATAACAGCGAAACATCC-3' 5'-TCCTTCTCCTTGGGGTTCCT-3'	60	215	Seda *et al*. (2007)
β-actin	Sense Antisense	5'-TCCCTGGAGAAGAGCTACGA-3' 5'-ATCTGCTGGAAGGTGGACAG-3'	60	362	Seda *et al*. (2007)
Cytb5R	Sense Antisense	5'-ACACGCATCCCAAGTTTCCA-3' 5'-CATCTCCTCATTCACGAAGC-3'	60	425	Diss *et al*. (2001) Brackenbury *et al*. (2007)

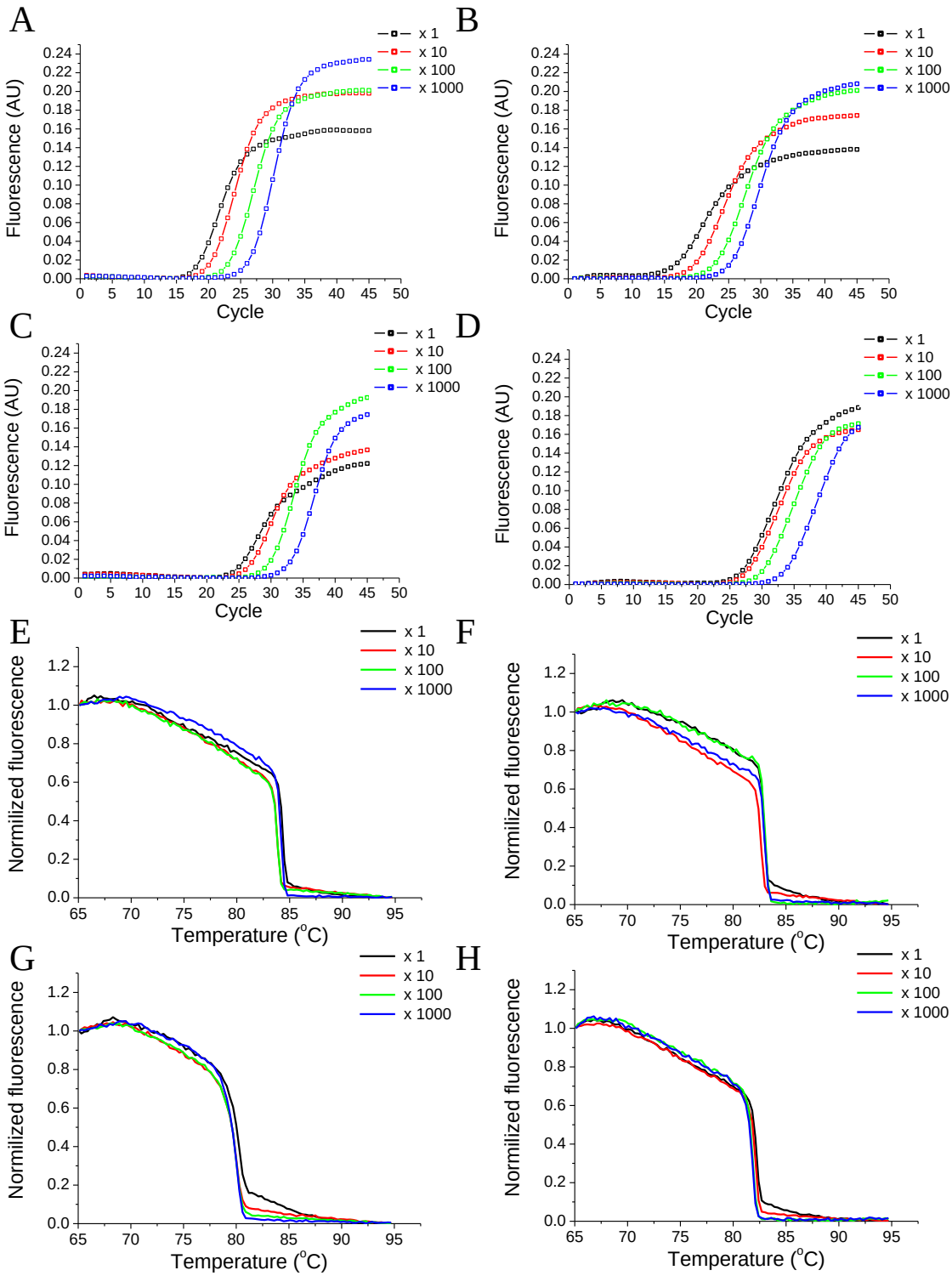


Figure 2.2 Real-time PCR amplification and melting curves (typical examples). Fluorescence from SYBER green incorporation to double stranded DNA was measured after each PCR cycle (A-D). PCR product composition was verified by heating from 65 °C to 95 °C in 0.3 °C steps at the end of the PCR amplification (E-H). These experiments carried out using x1, x10, x100 and x1000 diluted cDNA which was synthesized from RNA of Mat-LyLu cells grown (24 h) at control conditions. Amplified products were, Cytb5R (A and E), β-actin (B and F), Nav1.7 (C and G) and VGSCβ1 (D and H).

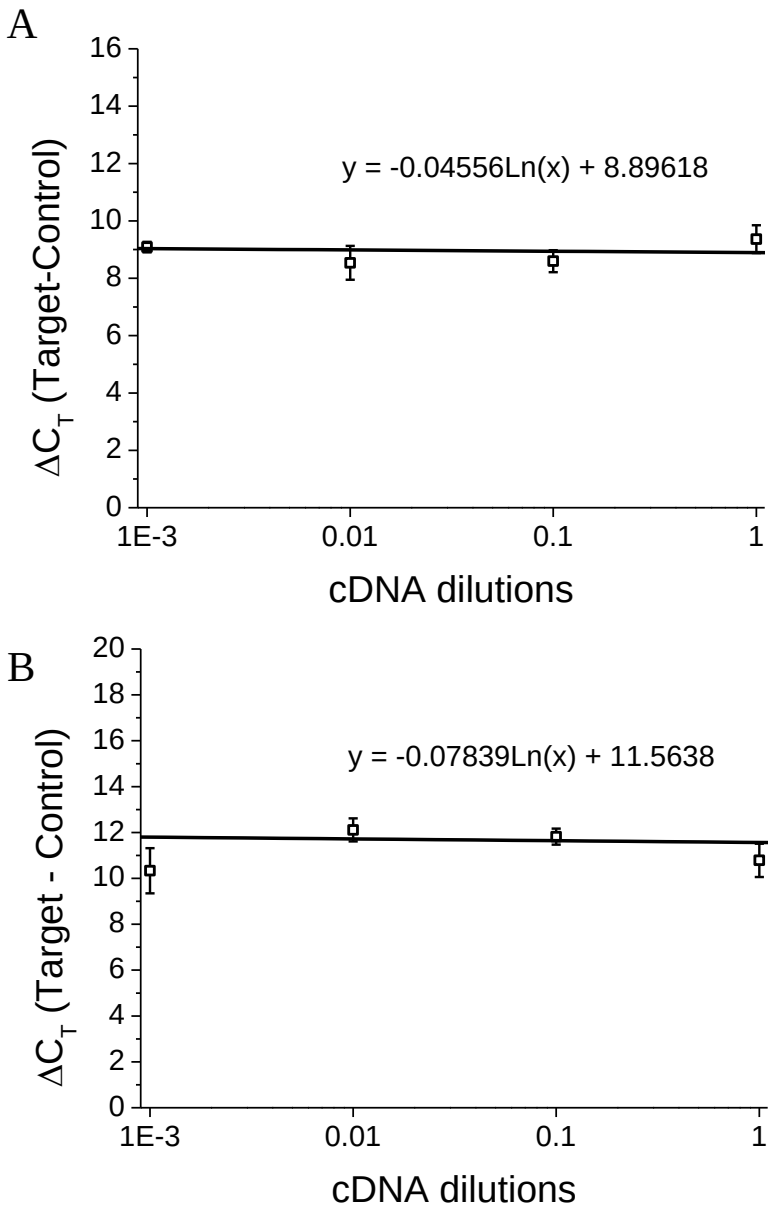


Figure 2.3 Standard calibration (dilution) curves to validate PCR efficiency.

Four dilutions (x1, x10, x100, and x1000) of cDNA, synthesised from Mat-LyLu cells which were grown in control conditions, were amplified using PCR reaction in order to determine efficiency of each primer set used. Two sample ΔC_T calibration curves are shown, where target genes are Nav1.7 (A) and VGSCβ1 (B), and normalizing gene is β-actin. ΔC_T was calculated by subtracting threshold amplification cycle of normalizing gene from target gene. Data are presented as means ± SEM (n = 3) and were fitted using linear regression analysis (solid line). Slopes of linear regression lines were statistically (non-paired t-test, p >0.05) not different from zero, indicating that efficiency of primers used are similar, validating the $2^{-\Delta\Delta C_T}$ method (Livak and Schmittgen, 2001).

Samples were visualised with an ultraviolet (UV) imager (Uvitec system, Jencons-Pls).

2.4 Western blotting

2.4.1 Extraction of total protein

Cells from 70-80 % confluent 35 mm Falcon tissue culture dishes were washed twice in ice cold PBS and lysed in ice-cold lysis buffer (Upstate Biotechnology) containing 50 mM Tris-HCl (pH 7.4), 1 % NP-40, 0.25 % Na-deoxycholate, 150 mM NaCl, 1 mM EDTA, 1 mM NaF, 1 µg/ml aprotinin, 1 µg/ml leupeptin, 1 µg/ml pepstatin and 1 mM phenylmethanesulfonylfluoride (PMSF) as described previously (Laniado *et al.,* 1997). Lysate was gently mixed on a rocker for 15 min at 4 ^{o}C. Lysates were centrifuged (Labofuge 400R, Heraus) at 13000 x *g* at 4 ^{o}C for 15 min and supernatant was transferred to a fresh tube. Protein yield was determined using a Bradford dye binding assay (Bio-Rad) according to manufacturer's instructions. Briefly, cell lysates were mixed with Bradford assay dye reagent and spectrophotometric absorbance at 595 nm was recorded (Cecil, CE 1020). Protein yield was calculated from standard calibration curve produced by measuring absorbance of serial dilutions of bovine serum albumin (BSA; Sigma-Aldrich) at 595 nm (Figure 2.4).

2.4.2 Sodium dodecyl sulphate polyacrylamide gel electrophoresis (SDS-PAGE) and immunoblotting

Unles otherwise stated, all chemicals were from Sigma-Aldrich. Equivalent amounts of protein from different lysates samples (50 µg) and a wide- range prestained molecular marker (Page Ruler protein ladder; Fermentas) were separated as

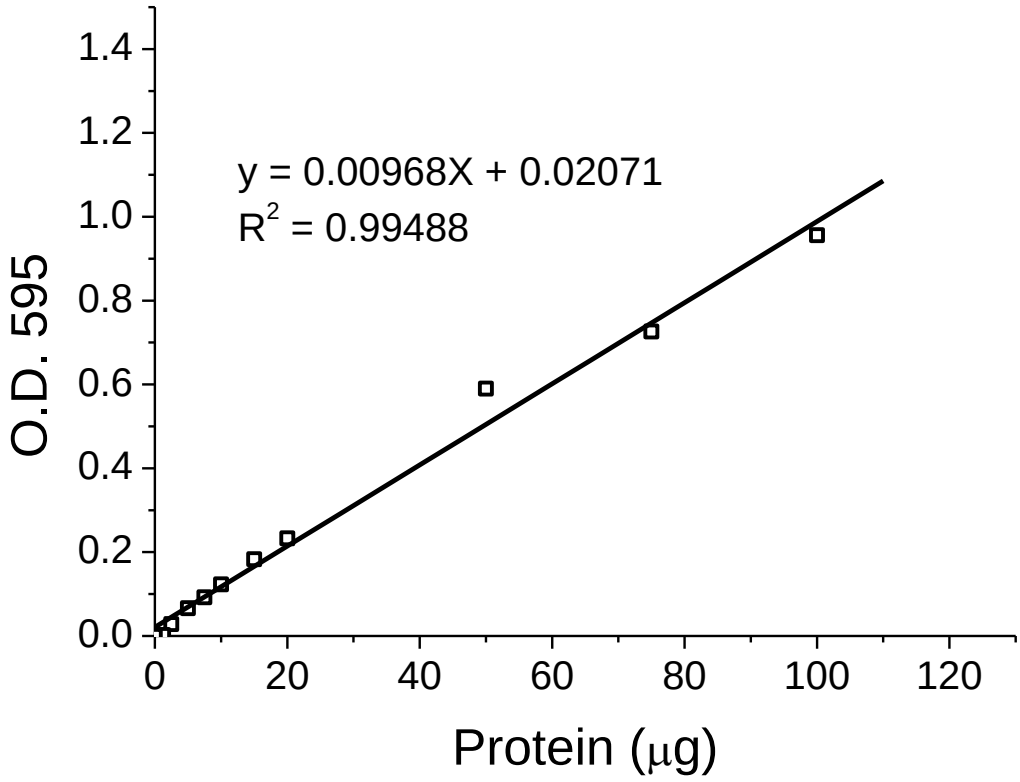


Figure 2.4 Protein standard calibration curve.

Eleven dilutions (0 to 100 µg) of BSA were used to construct standard calibration curve with a Bradford dye binding assay (BioRad). Spectrophotometric absorbance was measured at 595 nm. For each experiment, a new curve was constructed. Data were fitted using linear regression analysis (solid line).

described previously (Brackenbury and Djamgoz, 2006). Protein samples were mixed with LAEMMLI sample buffer incubated for 10 min at 37 ^{o}C and boiled for 5 min immediately before loading. Samples were separated using a 5 % acrylamide stacking gel and a 7.5 % acrylamide running gel, in a buffer containing 25 mM Tris, 192 mM glycine and 0.1 % (w/v) SDS at 100 V for 2 h and electroblotted onto nitrocellulose membrane (Hybond ECL, GE Healthcare) at 4 ^{o}C in a buffer containing 25 mM Tris and 192 mM glycine at 80 V for 2 h. Following the transfer, blots were blocked for 1 h in 5 % (w/v) non-fat dried milk (Marvel) in PBS and 30 min in 2 % (w/v) BSA/PBS. Blots were than incubated with primary antibodies (all antibodies were diluted in 2 % BSA/PBS; Table 2.3) for 16 h at 4 ^{o}C. Blots were washed three times in 0.2 % (v/v) Tween-20/PBS for 15 min before incubating with appropriate horseradish peroxidise (HRP)-conjugated secondary antibodies (Table 2.4) for 1 h at room temperature. Finally, blots were washed three times in 0.2 % (v/v) Tween-20/PBS for 15 min. The following negative controls were used: (i) blots were probed with pan-VGSC that had been pre-absorbed with 5x excess immunizing peptide for 30 min at room temperature, and (ii) blots were incubated with 2 % (w/v) BSA/PBS with no primary antibody added.

2.4.3 Densitometry

Blots were developed using the ECL chemiluminescence (Amersham) and protein bands were visualized by exposure to Super RX100NF film (Fujifilm). Densitometric analysis was performed using ImageJ software (NIH) on 600 dpi scanned images. Anti-actinin antibody was used as loading control and the pan-VGSC signal intensity was normalized to anti-actinin intensity. The linearity of the relationship between protein loading and signal intensity was confirmed for the pan-VGSC and the anti-actinin antibodies using serial dilution of protein extracts (20-100 μg) (Figure 2.5).

Table 2.3 Primary antibodies.

ICC: Immunocytochemistry; WB: Western blot; MW: Molecular weight; kDa: Kilo daltons

Primary antibody	Species	Stock concentration	Dilution for ICC	Dilution for WB	MW (kDa)	Source	Reference
Pan-VGSC	Rabbit polyclonal	1 µg/µl	1:100	1:1000	220	Upstate	Brackenbury *et al*. (2007)
VGSCβ1	Rabbit polyclonal	-	1:500	-	36	L. Isom	Malhotra *et al*. (2000); Xiao *et al*. (1999)
Anti-actinin	Mouse monoclonal	1 µg/µl	-	1:1000	100	Sigma	-

Table 2.4 Secondary antibodies.

Secondary antibody	Species	Stock Concentration	Dilution	Source
Anti-rabbit Alexa 568 (H+L)	Goat	2 mg/ml	1:100	Invitrogen
Anti-rabbit HRP	Goat	13.1 µg/µl	1:10000	Sigma
Anti-mouse HRP	Goat	1 µg/µl	1:1000	DAKO

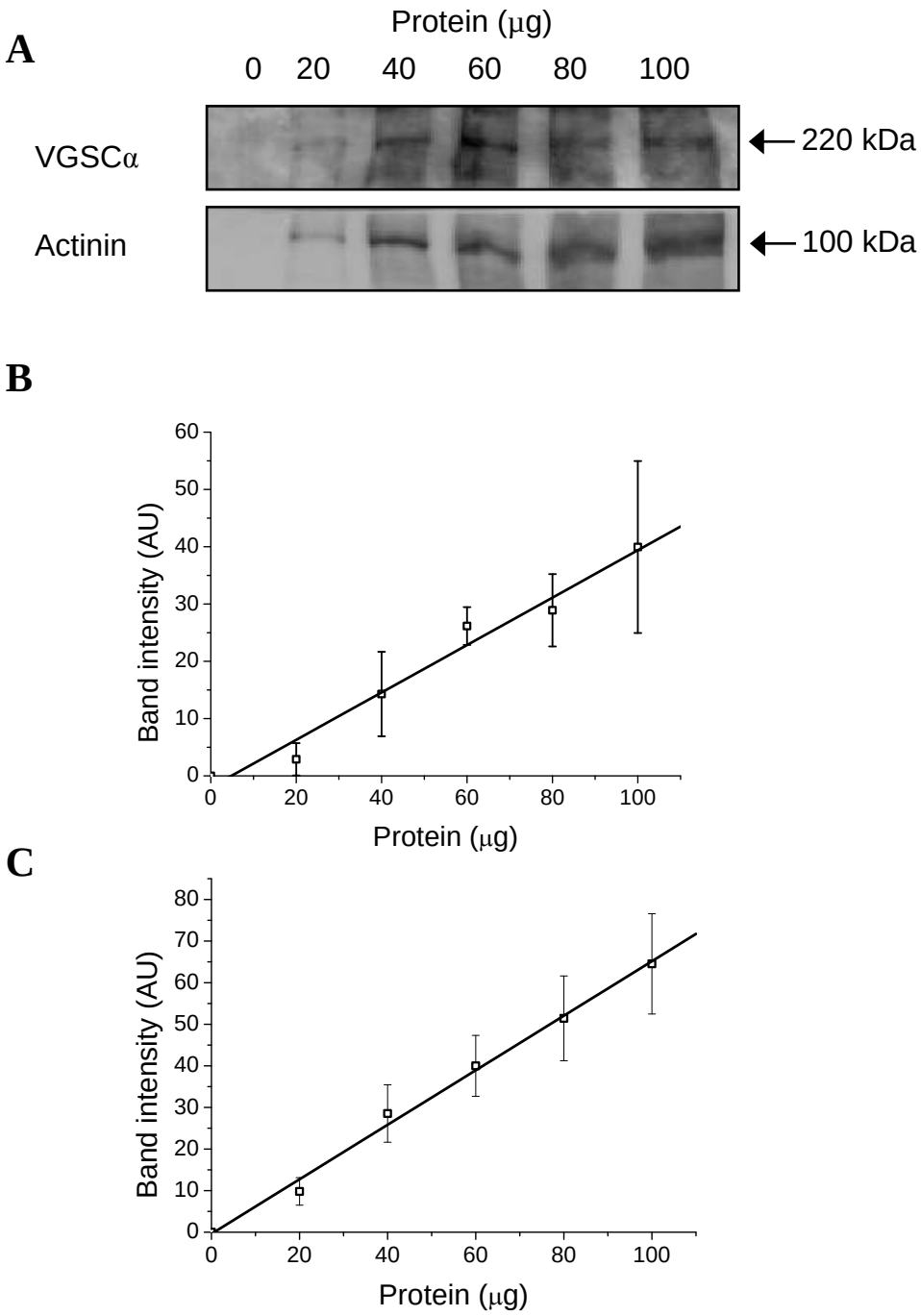


Figure 2.5 Protein dilutions and standard curves used to study Western blot band intensities.

Examples of Western blotting images of pan-VGSC and anti-actinin bands for serial dilution of protein extracted from Mat-LyLu cells (A). Band intensity, determined using ImageJ software, was plotted against protein concentration and fitted by linear regression line (solid line) for pan-VGSC (B) and anti-actinin (C). Data are presented as means ± SEM (*n* = 3). Linear relationship between protein level and band intensity within working range (50 μg) validated densitometric analysis.

2.5 Immunocytochemistry

Unles otherwise stated, all chemicals were from Sigma-Aldrich. Cells (5×10^4) were plated onto 0.025 mg/ml poly-L-lysine coated glass coverslips (13 mm, BDH) in 24-well Falcon tissue culture plates (Becton Dickinson) and allowed to settle overnight. After treatment samples were fixed in 4 % paraformaldehyde (PFA)/PBS for 15 min. Where appropriate, cells were labelled with 20 µg/100 µl fluorescein isothiocyanate (FITC)-conjugated concanavalin A, prepared in 5 % (w/v) BSA/PBS, for 45 min as a plasma membrane marker (Brackenbury and Djamgoz, 2006). Coverslips were washed three times with PBS for 10 min before permeabilization in 0.1 % (w/v) saponin/PBS for 4 min. Following permeabilization, samples were washed three times with PBS for 10 min. Cells were blocked for 1 h with 5 % BSA/PBS at room temperature and incubated with primary antibody (Table 2.3), prepared in 5 % (w/v) BSA/PBS, for 1 h. Coverslips were washed three times with PBS for 10 min, and then incubated with Alexa-568 conjugated goat anti-rabbit secondary antibody (Table 2.4), prepared in 5 % (w/v) BSA/PBS, for 1 h. Coverslips were washed three times in PBS and once in water. Vectashield mounting medium (Vector Laboratories) was used for mounting the samples. Mounted samples were stored at 4 ^{o}C in dark for 16 h before microscopy. The following negative controls were used:

i. Primary antibody specificity: Immunocytochemistry was performed as above except that primary antibody was substituted with an equal amount of 5 % BSA/PBS.

ii. Non-specific rabbit IgG: Immunocytochemistry was performed as above except that primary antibody was substituted with 0.002-0.004 µg/µl non-specific rabbit IgG (Dako).

iii. Pre-absorbed primary antibody: Immunocytochemistry was performed as above except that the pan-VGSC primary antibody was pre-absorbed with 5x excess of the immunizing peptide for 30 min at room temperature.

2.5.1 Confocal microscopy

Immunostained cells were examiner using a Leica SP5 MP microscope under oil immersion (x63 magnifications). Fluorescence was studies using a Leica Confocal laser scanner (Leica TCS-NT with an Ar/He laser). Antibodies conjugated with FITCY and/or Alexa568 were exited with the 488 nm and 568 nm laser lines, respectively. Images (1024 x 1024 pixels) were obtained simultaneously from the two channels using a Confocal pinhole of 229.96 µm. The following densitometric analyses were performed using the Leica LAS AF Lite software (Brackenbury and Djamgoz, 2006):

a. **Freeform line profile.** This determined the cell-surface expression of protein. For this function, the cell periphery was traced using the concanavalin A staining as a guide. Data were presented as total staining in arbitrary unit (AU) per µm. Measurements were taken from randomly chosen cells ($n \geq 30$) per condition, from at least three independent repeat experiments.

b. **Area histogram.** This covered a 16 μm^2 rectangular section of cytoplasm avoiding the nucleus and was used to measure the intracellular protein level (Brackenbury and Djamgoz, 2006; Chioni *et al*., 2010). Data were presented as total staining (AU). Measurements were taken from randomly chosen cells ($n \geq 30$) per condition, from at least three independent experimental repeats.

c. **Cross-sectional profile.** For this function, a straight line was drawn across the cell avoiding nucleus in order to study the relative subcellular distribution of the protein under investigation (Okuse *et al*., 2002; Shah *et al*., 2004, Brackenbury and Djamgoz, 2006). Peripheral (i.e. plasma membrane region) signal intensity was set to cover 1.5 µm inward from the edge of the concanavalin A staining. Internal (i.e. cytoplasmic) signal intensity was specified as the central 30 % of the line profile. Both peripheral and internal protein signals were normalised to total staining and expressed as percentages. Measurements were taken from randomly chosen cells ($n \geq 15$) per condition, from at least three independent experimental repeats.

2.6 Morphological analysis

Possible morphological effects of pharmacological treatment on several cellular parameters were studied as described previously (Fraser *et al*., 1999) with some modifications. Briefly, cells (3×10^4/ml) were plated in to 35 mm Falcon tissue culture dishes and allowed to settle overnight. After treatment, randomly selected cells were viewed under an inverted microscope (Axiovert 200, Carl Zeiss) and photographed under x200 magnification with a digital camera (Power-Shot G5, Canon). Images were quantitatively analysed using ImageJ software (NIH). The "cell body diameter" was defined as the diameter of the largest circle that could be fitted into the cell body (Figure 2.6A). An extension from a cell body which was at least one and half times the diameter of the cell body was accepted as a cell process. "Process length" was determined as the distance between tip of the process and centre of the cell body (Figure 2.6B). "Process thickness" was determined at the

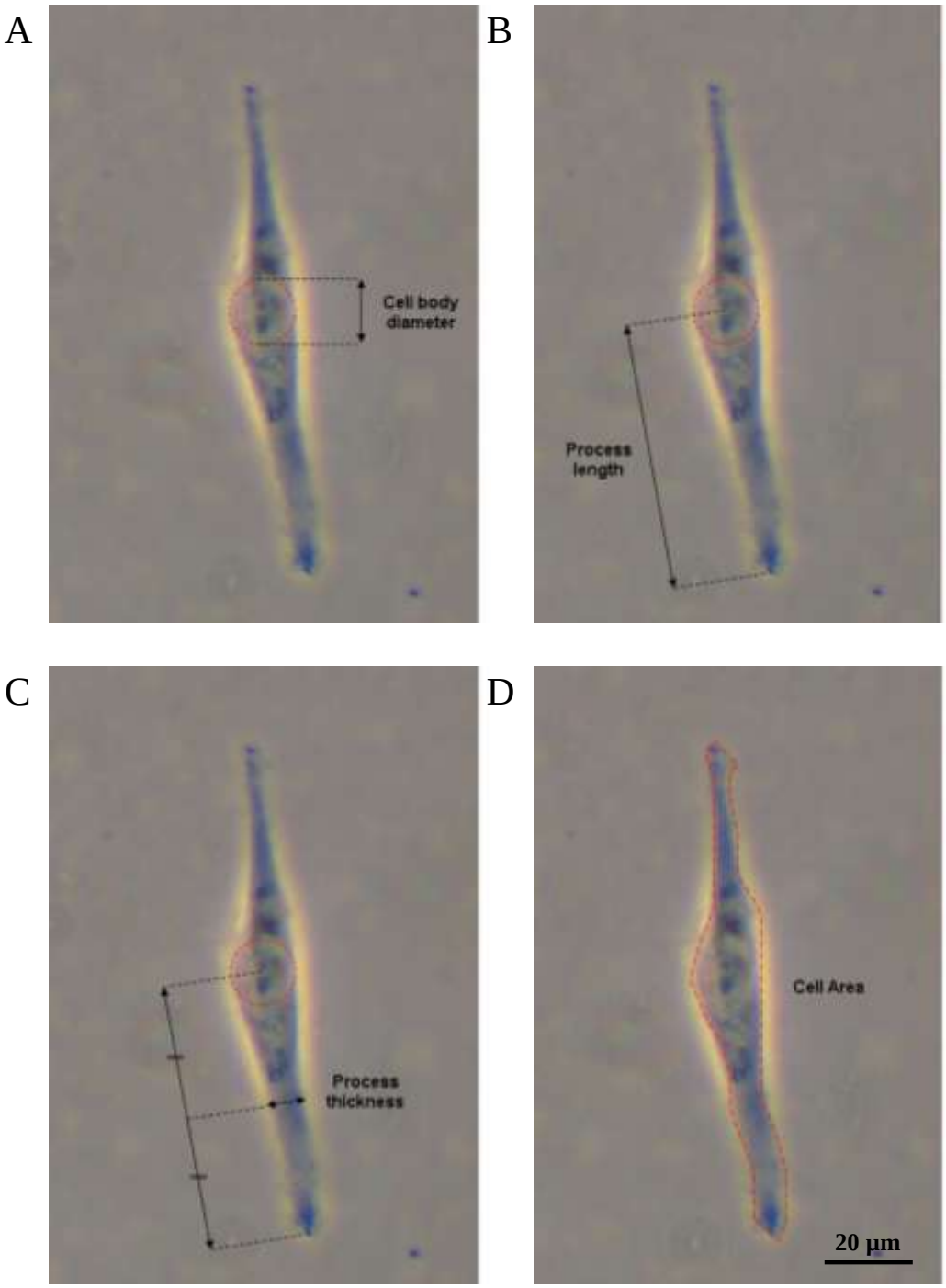


Figure 2.6 Micrographs of a Mat-LyLu cell illustrating morphologic parameters used.

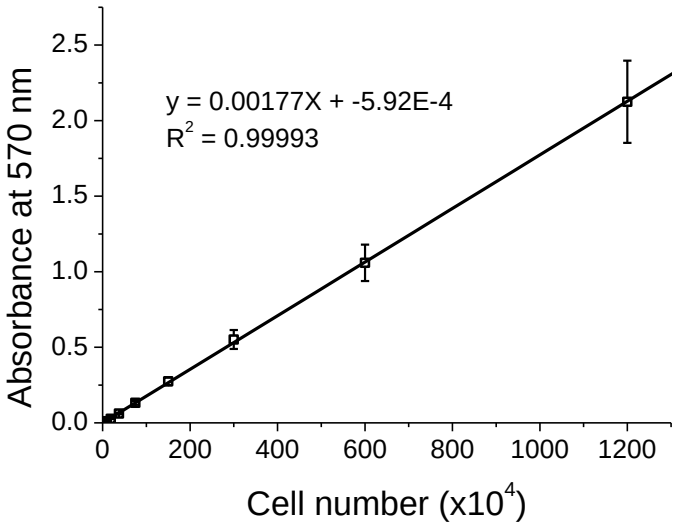
Cell body diameter (A) - diameter of the largest circle that could be fitted in to the cell. Process length (B) - distance between tip of the process and centre of the cell body. Process thickness (C) - thickness of the process at its half length; cell area (D). Scale bar (20 µM) applicable to all panels.

halfway point in the length of process (Figure 2.6C). Finally, the total "cell area" was calculated by tracing the cell outline (Figure 2.6D).

2.7 Measurement of cell number - MTT assay

Any change in cell number after long-term pharmacological treatment was assessed by the colorimetric 3-[4,5-dimethylthiazol-2-yl]-2,5-diphenyltetrazolium bromide (MTT) (Alfa Aesar) assay as described previously (Grimes *et al.,* 1995). Briefly, cells (4×10^4) were plated in 12-well Falcon tissue culture plates (Becton Dickinson) allowed to settle 24 h and treatment was applied. After the treatment period, culture medium was replaced with a control medium containing 1 mg/ml MTT and incubated at 37 ^{o}C for 2 h. MTT was removed and replaced with 0.89 ml DMSO and 0.11 ml glycine buffer (0.1 M glycine and 0.1 M NaCl, pH 10.5). Following 10 min incubation at room temperature, absorbance at 570 nm was measured on a multi-well plate reader (ELx800, BioTek Instruments). The measurements were carried out in dark in duplicates and each treatment was repeated at least three times. Spectrophotometric absorbance readings were normalized to the zero-hour recording measured after the initial 24 h. Standard calibration curves was created in order to verify linear relationship between cell number and absorbance at 570 nm (Figure 2.7). Briefly, eleven serial dilutions of cells (from 1200000 cells) were plated in to 12-well plates, allowed to settle for 4 h and MTT assay was performed as described above. For every freshly prepared MTT solution, the calibration was performed three times.

A



B

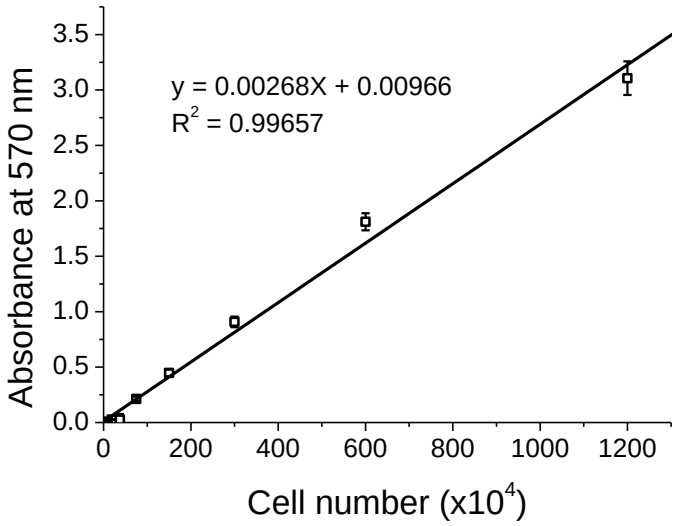


Figure 2.7 Examples of typical standard curves for MTT assay.

Relationship between cell number and absorbance at 570 nm was determined by MTT assay for (A) Mat-LyLu and (B) AT2 cells. Data are presented as means ± SEM ($n \geq 4$) and were fitted using linear regression analysis (solid line).

2.8 Lateral motility (wound-heal) assay

Lateral motility of the cells was assessed as described previously (Fraser *et al.*, 2003). Briefly, three parallel vertical lines and fifteen intersecting lines were marked under the 35 mm culture dishes. Cells were seeded into these dishes and incubated for 24 h which produced a near-monolayer culture. Then, three wounds of 0.5 - 0.8 mm width were created, guided by the vertical lines, using a sterile 200 µl Gilson pipette tips. The medium was replaced with fresh medium ± pharmacological agent and the wounds (3 x 15) were photographed using a digital camera (Power-shot G5, Canon) mounted on an inverted microscope (Axiovert 200, Zeiss) at x10 magnification. Wound widths were measured from these images using ImageJ software (NIH). Media (± treatment) were replaced and wounds were re-photographed every 24 h. Each experiment was carried out in triplicate and repeated at least three times. Lateral motility was calculated as the motility index (MoI), defined as follows:

$$MoI = 1 - \left(\frac{W_t}{W_0} \right) \qquad \textbf{equation 2.2}$$

where W_t is the width of the wound at time t (24 or 48 h), while W_0 is the initial wound width (time = 0 h). Thus, as limits, MoI = 0 corresponded to no movement of cells into the wound, whilst MoI = 1 represented complete closure of the wound.

2.9 Transwell migration assay

Migration of Mat-LyLu cells were studied using Transwell migration assays. Briefly cells (4 x 10^5) were plated on to Transwell migration filters (8µm pores) (Becton Dickinson). Cells were incubated in medium ± pharmacological agent in 0.5-5 % FBS chemotactic gradient for 24 h. Following the treatment, non-migrated cells were removed by swapping the upper surface of the Transwell filter. Migrated cells were stained with 0.5 % (w/v) crystal violet (Sigma-Aldrich) in 25 % methanol for 15 min at room temperature after fixation with 100 % ice-cold methanol for 15 min. Transwell filters were washed in water and let to air dry for 1 h. For each inserts randomly selected 3 fields of view were photographed using a digital camera (Power-shot G5, Canon) mounted on an inverted microscope (Axiovert 200, Zeiss) at 10x magnification. Images were analysed using ImageJ software (NIH). Experiments were performed in duplicates. Average of cell counts obtained from six fields of view (2 duplicate x 3 fields of view) represents one repeat. Experiments were repeated at least 3 times and results were normalised to corresponding controls.

2.10 Matrigel™ invasion assay

Invasion of Mat-LyLu cells were studied using Matrigel™ invasion assays. Briefly cells (4 x 10^5) were plated on to Transwell migration filters (8µm pores) (Becton Dickinson) which were coated with 1.25 mg/ml Matrigel™ basement membrane matrix (Becton Dickinson) and incubated at 37 ^oC for 30 min before cell plating as described previously (Zhu *et al.,* 2009). Cells were incubated in medium ± pharmacological agent in 0.5-5 % FBS chemotactic gradient for 24 h. Following the treatment, non-invaded cells were removed by swapping the upper surface of the Transwell filter. Invaded cells were stained with 0.5 % (w/v) crystal violet in 25 % methanol for 15 min at room temperature after fixation with 100 % ice-cold methanol for 15 min. Transwell filters were washed in water and let to air dry for 1 h.

For each inserts randomly selected 3 fields of view were photographed using a digital camera (Power-shot G5, Canon) mounted on an inverted microscope (Axiovert 200, Zeiss) at 10x magnification. Images were analysed using ImageJ software (NIH). Experiments were performed in duplicates. Average of cell counts obtained from six fields of view (2 duplicate x 3 fields of view) represents one repeat. Experiments were repeated at least 3 times and results were normalised to corresponding controls.

2.11 Intracellular calcium imaging

Changes in the concentration of intracellular free calcium ion ($[Ca^{2+}]_i$) were measured using a membrane soluble fluorescent Ca^{2+}-indicator dye (Fluo-4 AM; Invitrogen) as described previously (Lioudyno *et al.*, 2008). Cells (5×10^4) were plated on a glass coverslip, embedded on a 35 mm tissue culture dish (MatTek corporation), after coverslip was coated with 0.25 µg/ml poly-L-lysine (Sigma). Cells were allowed to settle for 24 h. An hour before recording, cells were washed three times with MPS and incubated in 4 µM Fluo-4 AM for 30 min in the dark. The cells were then rinsed twice and bathed in MPS for 30 min in the dark before imaging started. Cells were placed on a 37 ^oC heated chamber and imaged with a Leica SP5 confocal microscope with a x20 objective. Excitation of fluo-4 AM was provided by the 488 nm line of an argon laser. Images were acquired at 1 sec intervals. Data were analysed by Leica LAS AF Lite software. For each cell under investigation, mean intensity of fluorescence (F) was calculated for a sampling area of 9 x 9 μm^2, located centrally in the cell. The baseline reading was subtracted and the change in $[Ca^{2+}]_i$ was calculated as follows:

$$\Delta F / F_o = 100 \times \frac{F_t - F_0}{F_0} \qquad \textbf{equation 2.3}$$

where F_t is mean intensity of fluorescence at time t, F_0 is mean intensity of fluorescence at `baseline` level calculated by averaging mean intensity of 20-50 consecutive images in the absence of transient and $\Delta F/F_0$ (%) is a relative measure of free intracellular calcium as described previously (Williams and Sims, 2007). An increase in fluorescence was considered to be a transient when $\Delta F/F_0 \geq 50$ %. Cells were accepted as "oscillating" when at least three transients were recorded under control conditions within 10 min recording.

2.12 Data analyses

All quantitative data were presented as means ± standard errors of the mean (SEMs). Data analysis were performed using Excel 2003 (Microsoft), Origin 6.1 (Origin Lab) and SigmaStat 2.0 (Systat Software Inc.). Pairewise statistical significance were determined using paired or unpaired Student's t-test, or Mann-Whitney rank sum test, as appropriate (Krawetz, 2009). For comparisons involving more than two groups, statistical significance were determined using analysis of variance (ANOVA) followed by Newman-Keuls post hoc analysis, or Kruskal-Wallis analysis of variance as appropriate (Krawetz, 2009). Comparisons of linear regression slopes were performed using the following equation:

$$t = \frac{P_1 - P_2}{\sqrt{(SE\ of\ P_1)^2 + (SE\ of\ P_2)^2}} \qquad \textbf{equation 2.4}$$

where P_1 and P_2 are parameters (slopes) being compared. Real-time PCR data were analyzed using the $2^{-\Delta\Delta C_T}$ method (Livak and Schmittgen, 2001). Results were considered significant at $P < 0.05$ (*) and highly significant at $P < 0.001$ (**).

Chapter 3

EFFECTS OF CHRONIC HYPOXIA ON VOLTAGE-GATED Na^+ CHANNEL EXPRESSION AND METASTATIC CELL BEHAVIOURS OF DUNNING PROSTATE CANCER

3.1 Introduction

Hypoxia, reduced tissue oxygen level, has been detected in various human cancers, including cancers of prostate, breast, lung, pancreas, rectum, cervix, vulva, head and neck, brain, skin, liver and kidney (Vaupel *et al.,* 2007; Harrison and Blackwell, 2004). Accordingly, oxygen measurements from prostate tissue of patients showed that cancerous tissue has significantly lower O_2 level (9.9 mmHg / ~1.5 % O_2) compared to the normal muscle tissue (28.6 mmHg / ~4 % O_2; Movsas *et al.*,2000). In addition, hypoxia is a natural characteristics of aging organs (Tanaka *et al.,* 2006; Aalami *et al.,* 2003). Tissue hypoxia is caused by poor/altered vascularisation, deterioration of diffusion geometry or anaemia (Vaupel *et al.,* 2007). In carcinomas of cervix, head and neck, and soft tissue sarcomas, primary tumour hypoxia has been associated with increase incidence of metastases (Cairns *et al.,* 2001). In prostate cancer, significant positive correlations between hypoxia level and clinical stage and patient age were reported (Movsas *et al.,* 2000). Hypoxia is considered to be a crucial event promoting invasion and metastasis of many human cancer cells, including MDA-MB-231, MDA-MB-468, MCF7 and 4T1 (breast cancer), HCT116 and HT-29 (colon carcinoma), HepG2 (hepatoblastoma) and PANC-1 (pancreatic carcinoma) (Cronin *et al.,* 2010; Lester *et al.,* 2007; Graham *et al.,* 1999, Krishnamachary *et al.,* 2003). Although hypoxia can contribute to death of some tumour cells, it selects mainly for dedifferentiation, apoptosis resistance, cells with mutated p53 and increased metastatic capacity (Alqawi *et al.,* 2007; Watson *et al.,* 2009; Salnikow *et al.,* 2000; Ghafar *et al.,* 2003; Butterworth *et al.,* 2008; Harris 2002; Graeber *et al.,* 1996; Yu *et al.,* 2002; Subarsky and Hill 2003).

Hypoxia can regulate gene expression and regulate many signalling pathways, including those involving: 3`-5` adenosine monophosphate (cAMP) / protein kinase A (PKA), Ca^{2+}-calmodulin, mitogen-activated protein kinase (MAPK), stress-activated protein kinase (SAPK) and phosphatidylinositol 3-kinase (PI3K) - Akt (Seta *et al.,* 2002). Genome-wide DNA methylation and histone acetylation caused by hypoxia was documented in human prostate cancer cells (Watson *et al.,* 2009).

As reviewed in the General Introduction (Chapter 1, Section 1.3.3), functional voltage-gated Na^+ channel (VGSC) expression has been associated with several metastatic carcinomas (Grimes *et al.,* 1995; Laniado *et al.,* 1997; Grimes and Djamgoz, 1998; Abdul and Hoosein, 2002; Brackenbury and Djamgoz, 2006; Nakajima *et al.,* 2009; Fraser *et al.,* 2005; Roger *et al.,* 2003; Gao *et al.,* 2009; Fraser *et al.,* 2004; Blandino *et al.,* 1995; Onganer and Djamgoz 2005; Onganer *et al.,* 2005; Roger *et al.,* 2007; Fulgenzi *et al.,* 2006; Ou *et al.,* 2005; Allen *et al.,* 1997; Diaz *et al.,* 2007; Gao *et al.,* 2010; House *et al.,* 2010). The sodium current generated by VGSC activity has two components: transient current (I_{NaT}) and inactivation-resistant persistent current (I_{NaP}). Amplitude of I_{NaP} is generally 0.1 - 1 % of I_{NaT}; however, much greater amounts of Na^+ can be carried by I_{NaP} since it persists for longer time (Saint, 2008). It was previously reported that hypoxia increases I_{NaP} amplitude in neurons and cardiac cells (Hammarström and Gage 1998; Ju *et al*., 1996; Wang *et al.,* 2007). In contrast, hypoxia-induced small decrease of I_{NaT} was reported for neurons and myocytes (Hammarström and Gage 1998; Wang *et al.,* 2007). Importantly, increase in internal Na^+ concentration was reported as a result of hypoxia (Haigney *et al.,* 1994; Xiao and Allen, 1999). It was proposed that hypoxia could affect channel gating by formation or disruption of intermolecular disulfides

which causes conformational changes in VGSC protein (Hammarström and Gage 2002).

Therefore, in this chapter, we hypothesised that hypoxia would enhance MCBs of PCa cells by increasing the activity of VGSC, mainly through I_{NaP}.

3.1.1 Aims and scope of the present study

The main aim of this study was to investigate VGSC α- and β- subunit regulation by chronic hypoxia in strongly metastatic (Mat-LyLu) and weakly metastatic (AT2) rat prostate cancer cell lines. The specific aims were as follows:

1. To test if hypoxia was involved in regulation of VGSC α- and β- subunit mRNA and protein levels;
2. To test if hypoxia regulates metastatic cell behaviours (MCBs) - lateral motility, migration and invasion; and
3. To test if possible effects of hypoxia on MCBs could involve VGSC expression / activity.

3.2 Results

3.2.1 Some initial observations: Effects of chronic hypoxia on cell morphology

No change in the basic appearance or distribution of Mat-LyLu and AT2 cells in culture was observed under hypoxic (2 % O_2) condition over 24 h or 48 h (Figures 3.1A,C and 3.2A,C). Also, 24 h or 48 h treatment of Mat-LyLu and AT2 cells with 1 μM TTX under either normoxic or hypoxic conditions did not effect the cells' two-dimensional distribution (Figures 3.1B, D and 3.2B, D). On the other hand, the

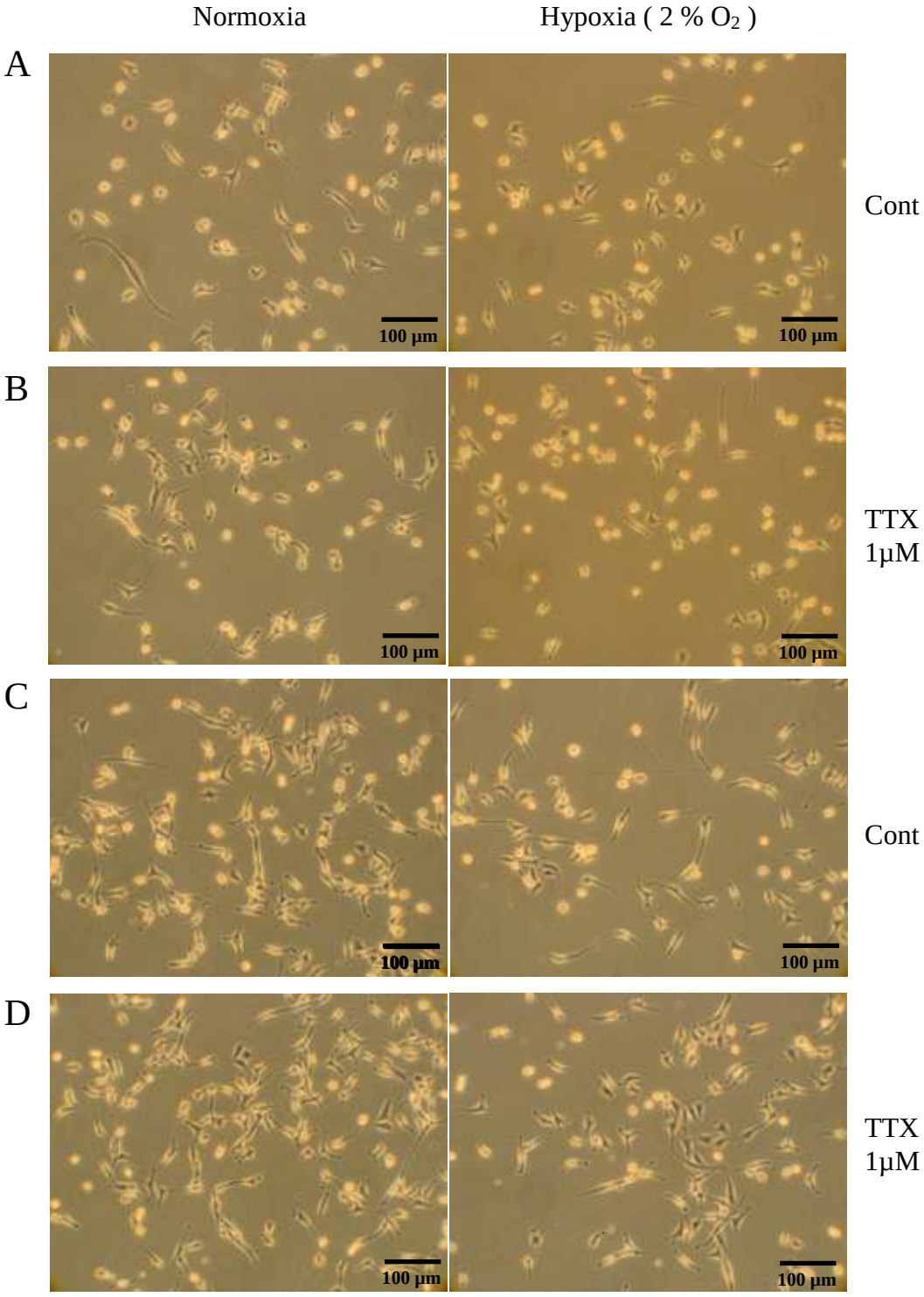


Figure 3.1 Phase-contrast light-photomicrography of Mat-LyLu cells.
Mat-LyLu cells were grown for 24 h (A & B) and 48 h (C & D) with (B & D) or without (A & C) 1µM TTX treatment in normoxia (left-hand pictures) or hypoxia (2 % O_2; right-hand pictures). Micrographs are typical of 3 experiments.

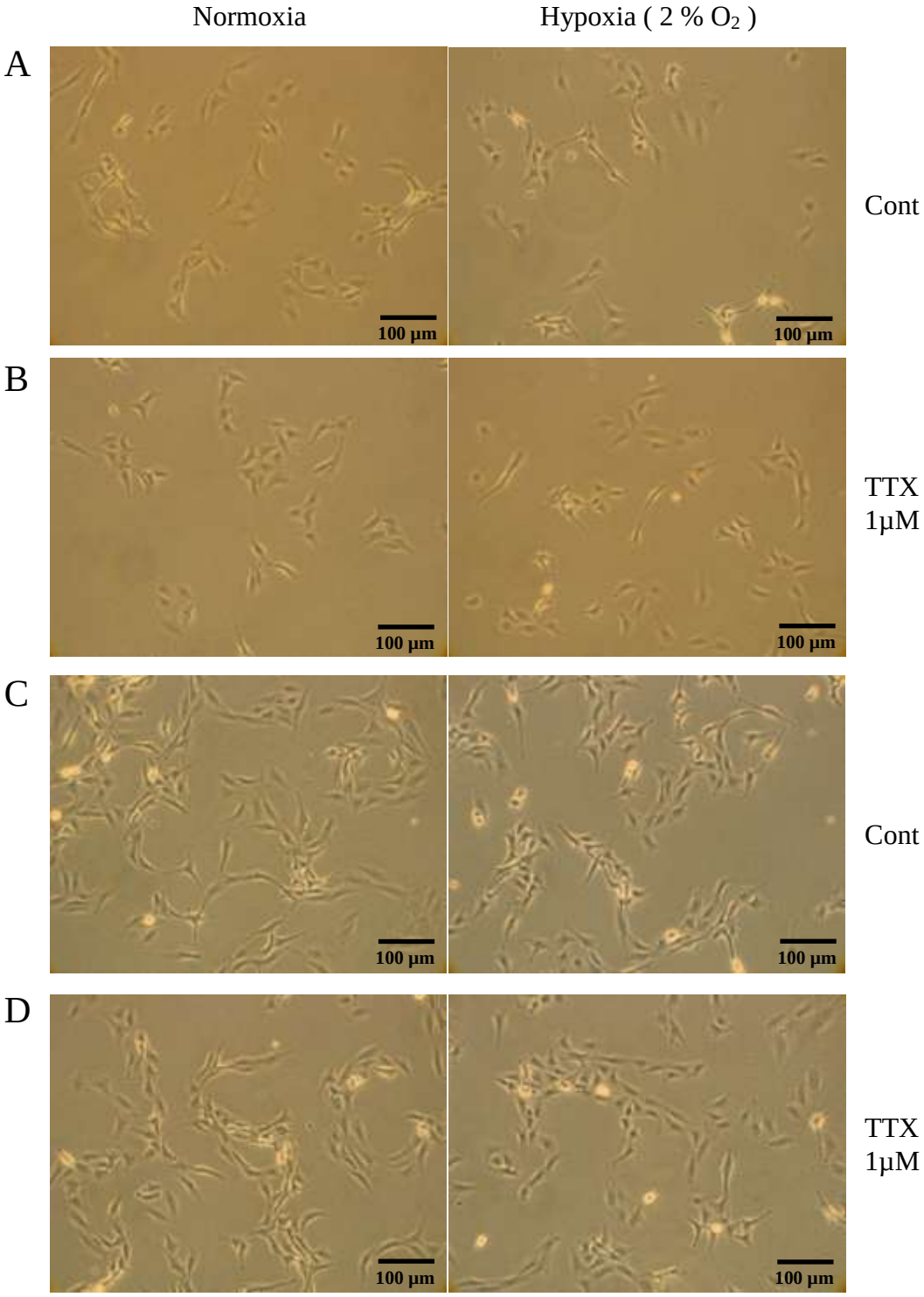


Figure 3.2 Phase-contrast light-photomicrography of AT2 cells.

AT2 cells were grown for 24 h (A & B) and 48 h (C & D) with (B & D) or without (A & C) 1µM TTX treatment in normoxia (left-hand pictures) or hypoxia (2 % $O_{2;}$ right-hand pictures). Micrographs are typical of 3 experiments.

number of Mat-LyLu cells in each field of view appeared less while no change was observed in AT2 cells when incubated under hypoxia for 48 h (Figures 3.1C, D and 3.2C, D).

Both Mat-LyLu and AT2 cells have extensive morphological heterogeneity. At the plating densities used, AT2 cells tended to form clusters, which dramatically reduced the number of single cells that could be used for morphological analysis (Figure 3.2). Therefore, morphological study of AT2 cells was not carried out. Morphological heterogeneity of Mat-LyLu cells were studied by subdividing cells into four groups: non-process bearing, monopolar, bipolar, multipolar, according to number of process possessed by the cells. Compared with normoxia, hypoxia did not change the percentage of non-process bearing cells (Figure 3.4A) both at 24 h (27.8 ± 7.3 % vs. 36.8 ± 6 %, respectively; $p > 0.05$; $n = 3$; Figures 3.3A and 3.4B; Table 3.1) and 48 h (18.0 ± 1.0 % vs. 11.4 ± 2.5 %, respectively; $p > 0.05$; $n = 3$; Figures 3.3C and 3.4C; Table 3.1). Treatment with 1 µM TTX for 24 h or 48 h also had no effect on percentage of non-process bearing cell in normoxia (26.2 ± 2.1 % vs. 6.4 ± 3.3 %, respectively; $p > 0.05$; $n = 3$; Figures 3.3 & 3.4B,C; Table 3.1) and hypoxia (30.5 ± 3.2 % vs. 16.8 ± 6.9 %, respectively; $p > 0.05$; $n = 3$; Figures 3.3 and 3.4B,C; Table 3.1). The percentage of monopolar cells (Figure 3.5A) also was not effected by 24 h incubation in normoxic condition with TTX (1 µM) and hypoxic conditions with or without 1µM TTX (29.8 ± 5.2 %, 26.6 ± 3.3 %, 26.2 ± 3.4 % and 25.3 ± 3.2 %, respectively; $p > 0.05$; $n = 3$; Figures 3.3A,B and 3.5B; Table 3.1). When the incubation period was increased to 48 h, 1 µM TTX or hypoxia again did not affect the proportion of monopolar cells ($p > 0.05$; $n = 3$; Figures 3.3C,D and 3.5C; Table 3.1). However, when hypoxia and TTX (1 µM) were co-applied for 24 h, monopolar cells decreased significantly from 17.8 ± 3.0 % to 9.8 ± 1.3 % ($p < 0.05$; $n = 3$;

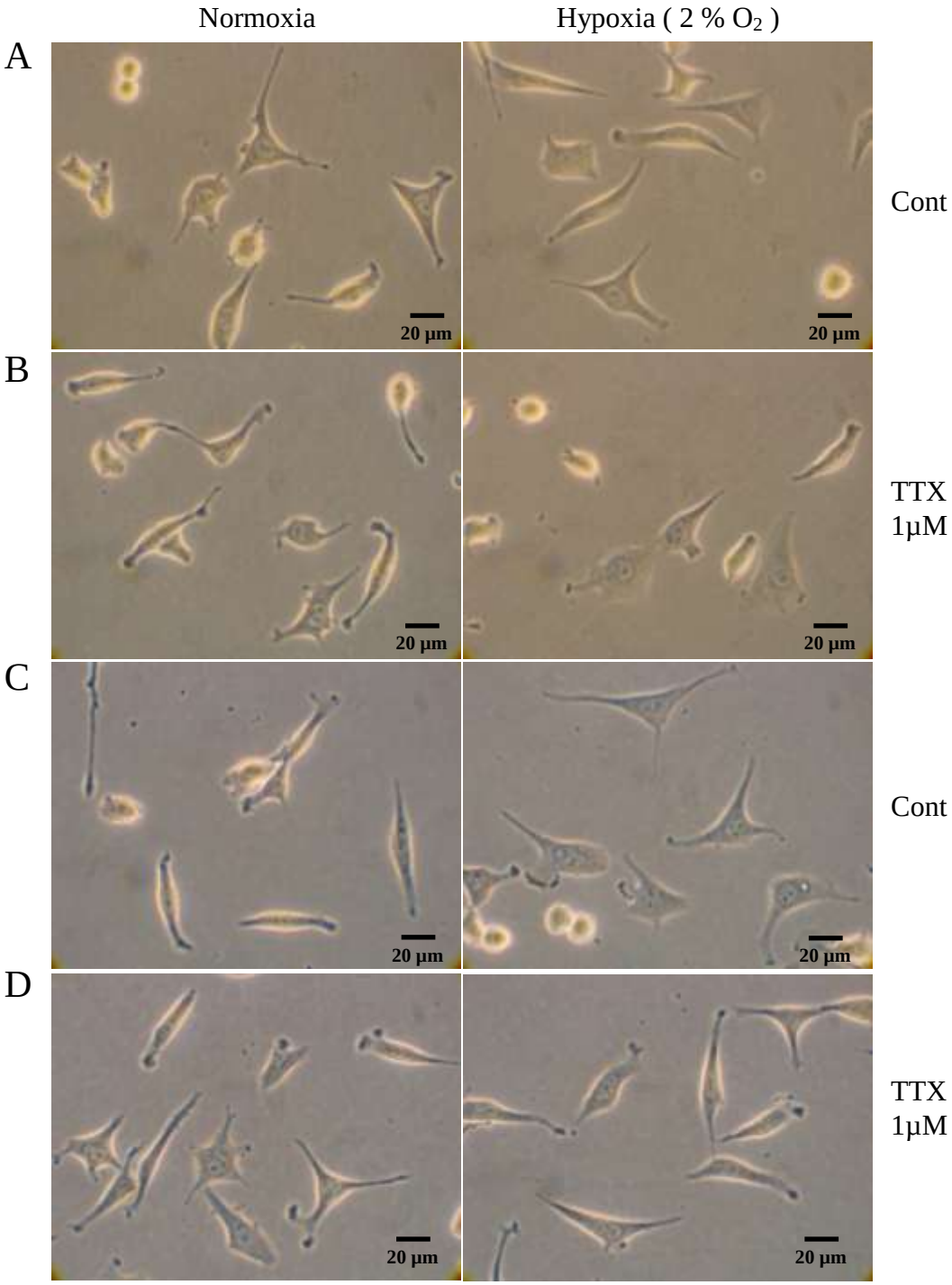
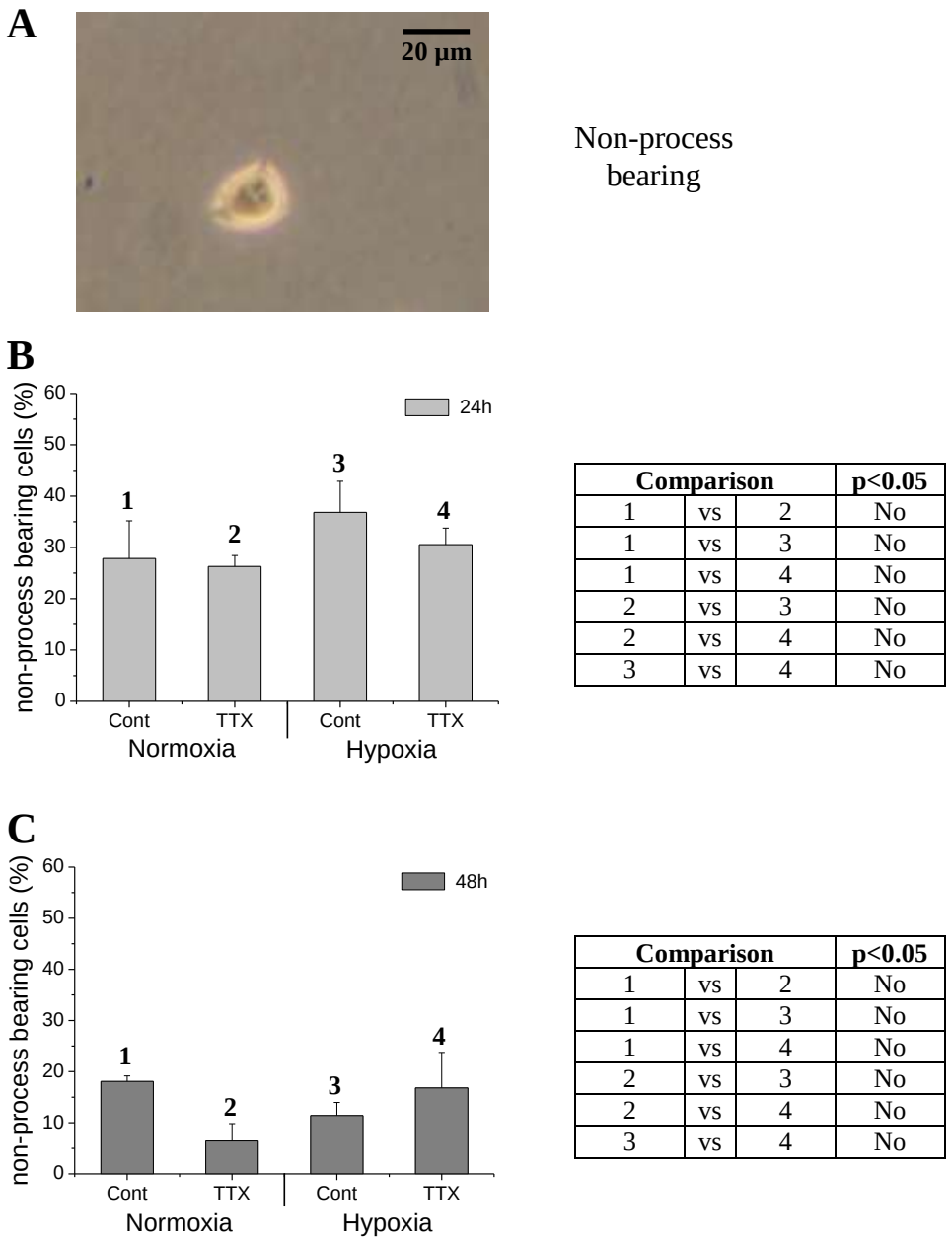


Figure 3.3 Phase-contrast light-photomicrography of Mat-LyLu cells in high magnification.

Mat-LyLu cells were grown for 24 h (A & B) and 48 h (C & D) with (B & D) or without (A & C) 1µM TTX treatment in normoxia (left-hand pictures) or hypoxia (2 % $O_{2;}$ right-hand pictures). Micrographs are typical of 3 experiments.

Table 3.1 Summary of effect of hypoxia on Mat-LyLu cell morphology and morphological heterogeneity. (↑) increase; (↓) decrease; (-) no change.

		Normoxia			Hypoxia			
		Control	TTX		Control		TTX	
Non-process bearing cells	**24h**	27.8±7.3 %	26.28±2.1 %	-	36.8±6.0 %	-	30.5±3.2 %	-
	48h	18.0±1.0 %	6.4±3.3 %	-	11.4±2.5 %	-	16.8±6.9 %	-
Monopolar cells	**24h**	29.8±5.2 %	26.6±3.3 %	-	26.2±3.4 %	-	25.3±3.27 %	-
	48h	17.7±3.0 %	20.5±2.7 %	-	19.6±1.6 %	-	9.8±1.3 %	↓
Bipolar cells	**24h**	37.6±5.7 %	39.0±3.3 %	-	30.6±5.6 %	-	39.5±6.0 %	-
	48h	49.1±7.2 %	56.4±3.0 %	-	47.1±4.2 %	-	45.6±3.1 %	-
Multipolar cells	**24h**	4.6±2.3 %	7.9±0.9 %	-	6.3±3.0 %	-	4.5±0.2 %	-
	48h	14.9±6.3 %	16.5±3.2 %	-	21.8±3.6 %	-	27.6±4.0 %	-
Cell body diameter	**24h**	15.0±0.2 µm	14.9±0.2 µm	-	16.3±0.2 µm	↑	15.8±0.3 µm	↑
	48h	14.4±0.2 µm	13.7±0.3 µm	-	15.7±0.3 µm	↑	15.6±0.3 µm	↑
Cell area	**24h**	4.8±0.1 x10^3 µm^2	4.8±0.1 x10^3 µm^2	-	5.2±0.2 x10^3 µm^2	-	5.3±0.2 x10^3 µm^2	-
	48h	5.4±0.1 x10^3 µm^2	6.2±0.2 x10^3 µm^2	↑	6.5±0.3 x10^3 µm^2	↑	6.6±0.2 x10^3 µm^2	↑
Process thickness	**24h**	5.5±0.2 µm	5.1±0.2 µm	-	5.2±0.2 µm	-	6.1±0.3 µm	-
	48h	5.6±0.3 µm	6.3±0.3 µm	-	5.6±0.3 µm	-	5.8±0.3 µm	-
Process length	**24h**	37.9±1.5 µm	38.8±1.4 µm	-	41.9±1.7 µm	-	38.3±1.3 µm	-
	48h	37.8±1.1 µm	39.5±1.2 µm	-	41.9±1.5 µm	-	42.7±1.3 µm	-

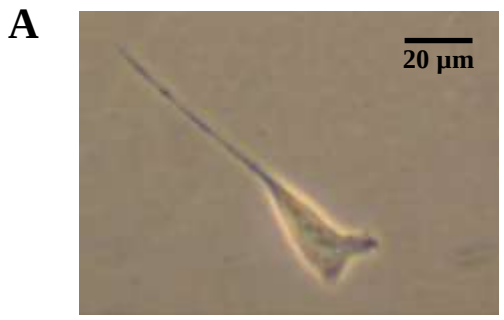


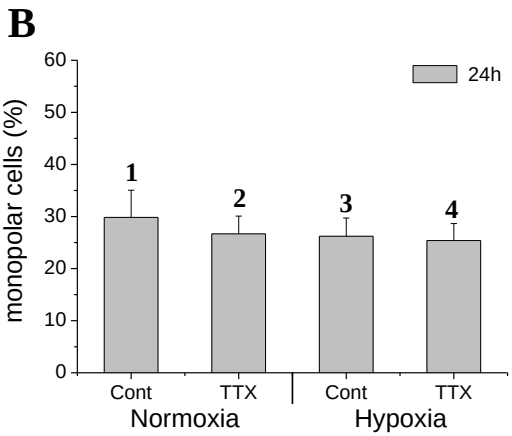
Comparison			p<0.05
1	vs	2	No
1	vs	3	No
1	vs	4	No
2	vs	3	No
2	vs	4	No
3	vs	4	No

Comparison			p<0.05
1	vs	2	No
1	vs	3	No
1	vs	4	No
2	vs	3	No
2	vs	4	No
3	vs	4	No

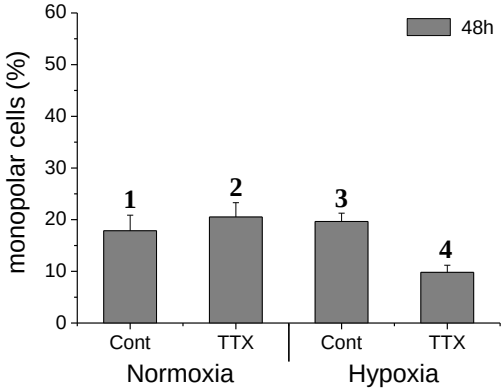
Figure 3.4 Studies effects of hypoxia on number of non-process bearing Mat-LyLu cells.

(A) Shows example phase-contrast light microscopy image of non-process bearing cells. Bar diagram show percentages of non-process bearing cells treated 24 h (B) or 48 h (C) ± TTX (1 µM) in normoxia or hypoxia (2 % O_2). Inset: table of multiple comparisons between treatments for statistical significance. Data are presented as means ± SEM and collected from ≥ 109 randomly selected individual cells (*n* = 3). Data were analysed by ANOVA followed by Newman-Keuls *post hoc* analysis.





Comparison			p<0.05
1	vs	2	No
1	vs	3	No
1	vs	4	No
2	vs	3	No
2	vs	4	No
3	vs	4	No

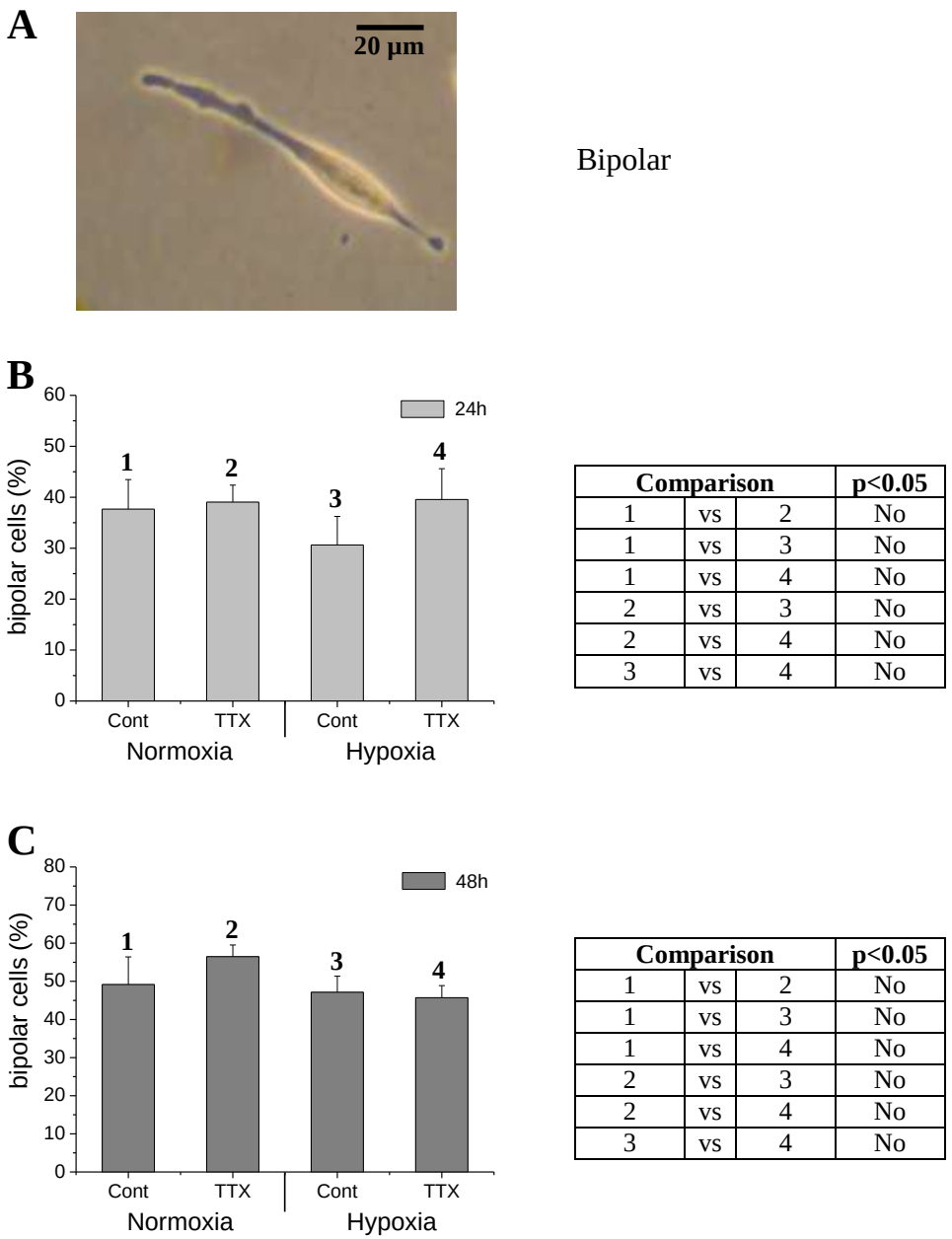


Comparison			p<0.05
1	vs	2	No
1	vs	3	No
1	vs	4	Yes
2	vs	3	No
2	vs	4	Yes
3	vs	4	Yes

Figure 3.5 Studies effects of hypoxia on number of monopolar Mat-LyLu cells. **(**A) Shows example phase-contrast light microscopy image of monopolar cells. Bar diagram show percentages of monopolar cells treated 24 h (B) or 48 h (C) ± TTX (1 µM) in normoxia or hypoxia (2 % O_2). Inset: table of multiple comparisons between treatments for statistical significance. Data are presented as means ± SEM and collected from ≥ 109 randomly selected individual cells (n = 3). Data were analysed by ANOVA followed by Newman-Keuls *post hoc* analysis.

Figures 3.3C,D and 3.5C; Table 3.1). The proportion of bipolar Mat-LyLu cells (Figure 3.6A) was not effected when incubated for 24 h or 48 h in normoxia with TTX (1 µM) or hypoxia with or without TTX (1 µM) ($p > 0.05$; $n = 3$; Figures 3.3 & 3.6B,C; Table 3.1). Under the same conditions, the percentage of multipolar cells (Figure 3.7A) remained unchanged ($n = 3$; Figures 3.3 and 3.7B,C; Table 3.1).

In addition to the analysis of the morphological diversity of MatLyLu cells, possible effects of the treatments on cell body diameter, cell-surface area, process length and process thickness were studied. When Mat-LyLu cells were treated for 24 h or 48 h with 1 µM TTX, there was no change in cell body diameter (Figure 3.8; Table 3.1). On the other hand, 24 h and 48 h incubation under hypoxic conditions increased Mat-LyLu cell body diameter from 15.0 ± 0.2 µm to 16.3 ± 0.2 µm and from 14.4 ± 0.2 µm to 15.7 ± 0.3 µm, respectively ($p < 0.05$; $n \geq 109$; Figure 3.8; Table3.1). Similarly, 24 h and 48 h incubation of MatLyLu cells in the presence of TTX (1 µM) under hypoxic conditions increased cell body diameter to 15.8 ± 0.3 µm and 15.6 ± 0.3 µm, respectively ($p < 0.05$; $n \geq 114$; Figure 3.8; Table 3.1). Mat-LyLu cell area (Figure 3.9A) did not change under both normoxic and hypoxic conditions with or without TTX (1 µM) over 24 h ($p > 0.05$; $n \geq 127$; Figure 3.9; Table 3.1). On the other hand, incubating Mat-LyLu cells under hypoxic conditions for 48 h increased their surface area from 5.4 ± 0.1 $x10^3$ μm^2 to 6.5 ± 0.3 $x10^3$ μm^2 ($p < 0.05$; $n \geq 109$; Figure 3.9; Table 3.1). In addition, 48 h treatment with TTX in normoxia and hypoxia increased cell-surface area to 6.2 ± 0.2 $x10^3$ and 6.6 ± 0.2 $x10^3$, respectively ($p < 0.05$; $n \geq 113$; Figure 3.9; Table 3.1). However, cell process thickness (Figure 3.10A) and process length (Figure 3.11A) were not affected by TTX (1µM) or hypoxia with or without TTX (1 µM) treatment ($p > 0.05$; $n \geq 84$; Figures 3.10 and 3.11; Table 3.1).



Comparison			p<0.05
1	vs	2	No
1	vs	3	No
1	vs	4	No
2	vs	3	No
2	vs	4	No
3	vs	4	No

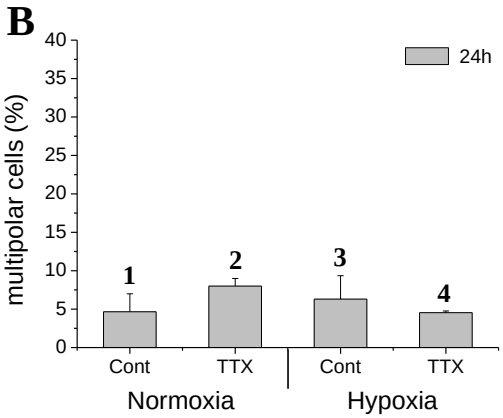
Comparison			p<0.05
1	vs	2	No
1	vs	3	No
1	vs	4	No
2	vs	3	No
2	vs	4	No
3	vs	4	No

Figure 3.6 Studies effects of hypoxia on number of bipolar Mat-LyLu cells.

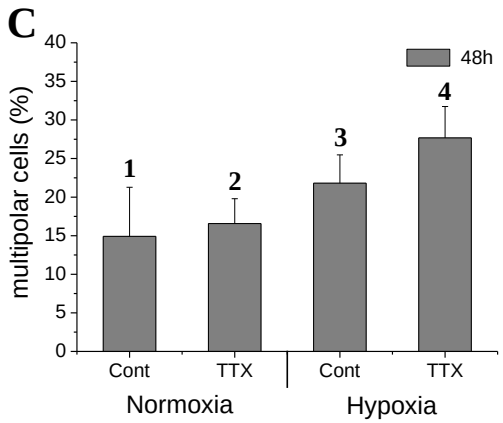
(A) Shows example phase-contrast light microscopy image of bipolar cells. Bar diagram show percentages of bipolar cells treated 24 h (B) or 48 h (C) ± TTX (1 µM) in normoxia or hypoxia (2 % O_2). Inset: table of multiple comparisons between treatments for statistical significance. Data are presented as means ± SEM and collected from ≥109 randomly selected individual cells (*n* = 3). Data were analysed by ANOVA followed by Newman-Keuls *post hoc* analysis.



Multipolar

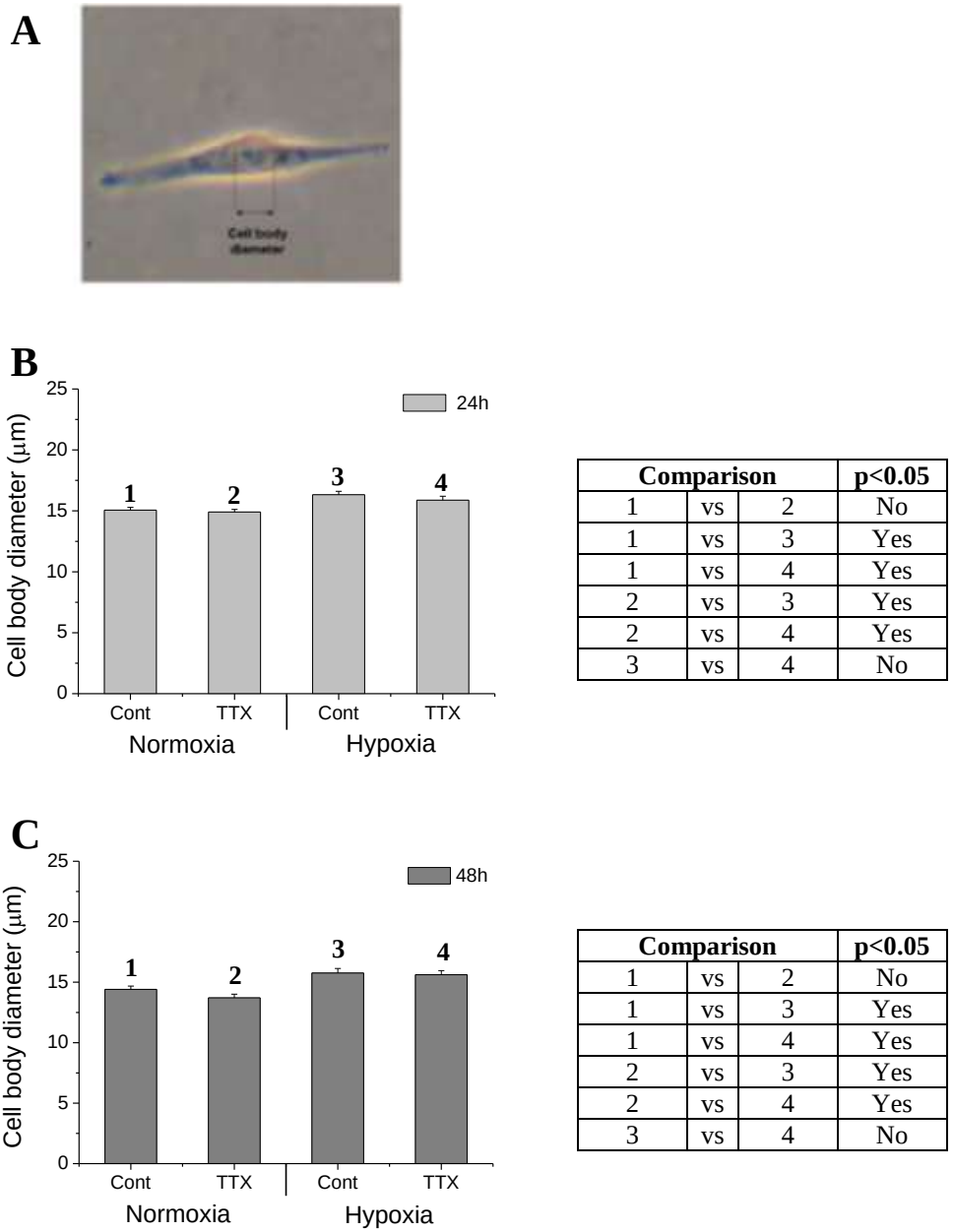


Comparison			p<0.05
1	vs	2	No
1	vs	3	No
1	vs	4	No
2	vs	3	No
2	vs	4	No
3	vs	4	No



Comparison			p<0.05
1	vs	2	No
1	vs	3	No
1	vs	4	No
2	vs	3	No
2	vs	4	No
3	vs	4	No

Figure 3.7 Studies effects of hypoxia on number of multipolar Mat-LyLu cells. **(**A) Shows example phase-contrast light microscopy image of multipolar cells. Bar diagram show percentages of multipolar cells treated 24 h (B) or 48 h (C) ± TTX (1 µM) in normoxia or hypoxia (2 % O_2). Inset: table of multiple comparisons between treatments for statistical significance. Data are presented as means ± SEM and collected from ≥109 randomly selected individual cells (*n* = 3). Data were analysed by ANOVA followed by Newman-Keuls *post hoc* analysis.



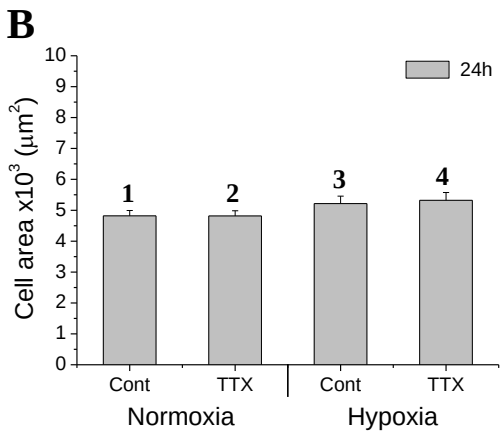
Comparison			p<0.05
1	vs	2	No
1	vs	3	Yes
1	vs	4	Yes
2	vs	3	Yes
2	vs	4	Yes
3	vs	4	No

Comparison			p<0.05
1	vs	2	No
1	vs	3	Yes
1	vs	4	Yes
2	vs	3	Yes
2	vs	4	Yes
3	vs	4	No

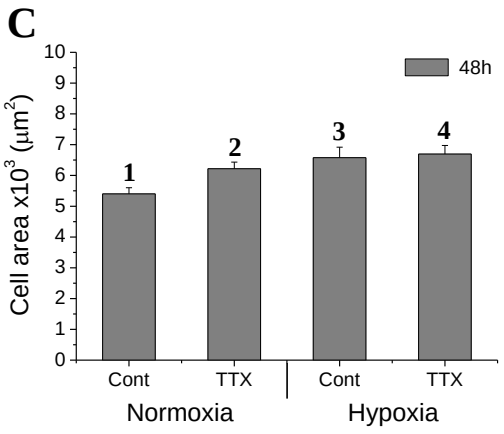
Figure 3.8 Bar diagram showing quantitative effect of hypoxia on cell body diameter.

(A)Image of a Mat-LyLu cells illustrating cell body diameter measurement. Histogram shows quantitative measurement of cell body diameter (µm) of Mat-LyLu cells which were treated 24h (B) or 48h (C) ± TTX (1 µM) in normoxia or hypoxia (2 % O_2). Inset: table of multiple comparisons between treatments for statistical significance. Data are presented as means ± SEM ($n \geq 109$). Data were analysed by ANOVA followed by Newman-Keuls *post hoc* analysis.



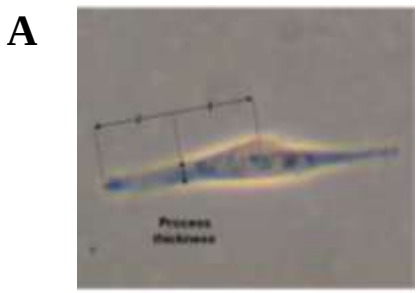


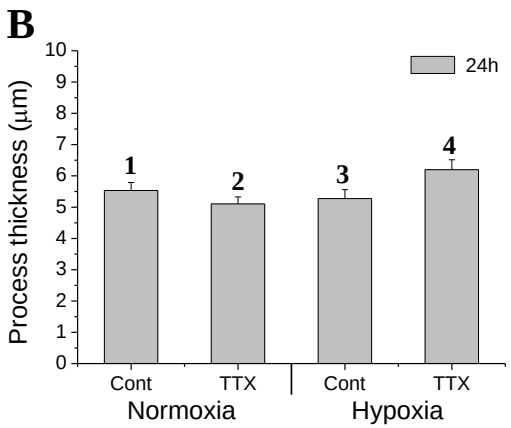
Comparison			p<0.05
1	vs	2	No
1	vs	3	No
1	vs	4	No
2	vs	3	No
2	vs	4	No
3	vs	4	No



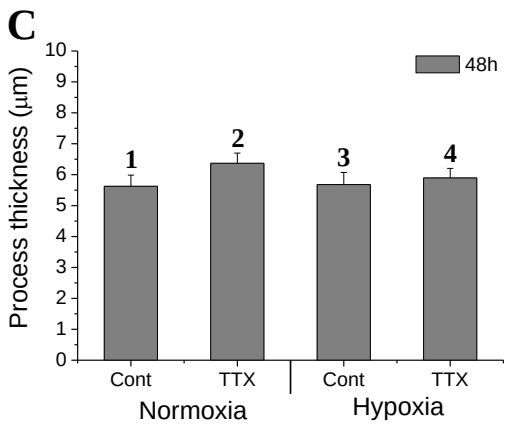
Comparison			p<0.05
1	vs	2	Yes
1	vs	3	Yes
1	vs	4	Yes
2	vs	3	No
2	vs	4	No
3	vs	4	No

Figure 3.9 Bar diagram showing quantitative effect of hypoxia on cell area.
(A)Image of a Mat-LyLu cells illustrating cell area measurement. Histogram shows quantitative measurement of cell area (µm^2) of Mat-LyLu cells which were treated 24h (B) or 48h (C) ± TTX (1 µM) in normoxia or hypoxia (2 % O_2). Inset: table of multiple comparisons between treatments for statistical significance. Data are presented as means ± SEM ($n \geq 109$). Data were analysed by ANOVA followed by Newman-Keuls *post hoc* analysis.





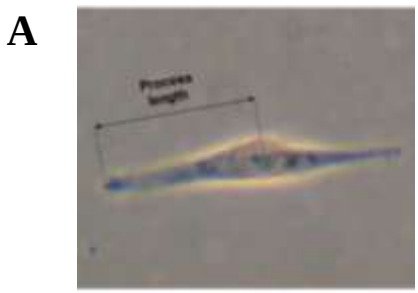
Comparison			p<0.05
1	vs	2	No
1	vs	3	No
1	vs	4	No
2	vs	3	No
2	vs	4	Yes
3	vs	4	No

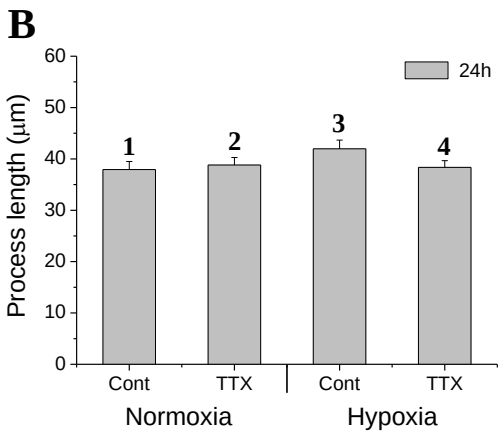


Comparison			p<0.05
1	vs	2	No
1	vs	3	No
1	vs	4	No
2	vs	3	No
2	vs	4	No
3	vs	4	No

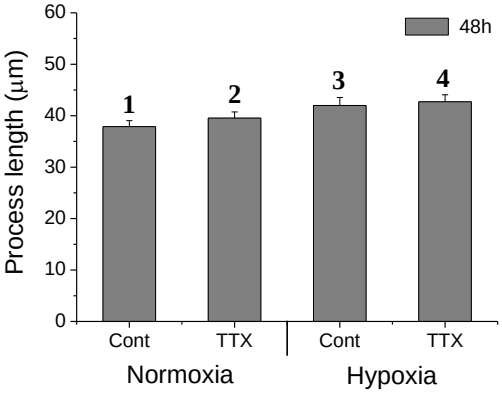
Figure 3.10 Histograms showing quantitative effect of hypoxia on process thickness.

(A)Image of a Mat-LyLu cells illustrating process thickness measurement. Bar diagram shows quantitative measurement of process thickness (µm) of Mat-LyLu cells which were treated 24h (B) or 48h (C) ± TTX (1 µM) in normoxia or hypoxia (2 % O_2). Inset: table of multiple comparisons between treatments for statistical significance. Data are presented as means ± SEM ($n \geq 84$). Data were analysed by ANOVA followed by Newman-Keuls *post hoc* analysis.





Comparison			p<0.05
1	vs	2	No
1	vs	3	No
1	vs	4	No
2	vs	3	No
2	vs	4	No
3	vs	4	No



Comparison			p<0.05
1	vs	2	No
1	vs	3	No
1	vs	4	No
2	vs	3	No
2	vs	4	No
3	vs	4	No

Figure 3.11 Histograms showing quantitative effect of hypoxia on process length.

(A)Image of a Mat-LyLu cells illustrating process length measurement. Bar diagram shows quantitative measurement of process length (µm) of Mat-LyLu cells which were treated 24h (B) or 48h (C) ± TTX (1 µM) in normoxia or hypoxia (2 % O_2). Inset: table of multiple comparisons between treatments for statistical significance. Data are presented as means ± SEM ($n \geq 84$). Data were analysed by ANOVA followed by Newman-Keuls *post hoc* analysis.

3.2.2 Effects of chronic hypoxia

3.2.2.1 Cell viability

Hypoxia was not toxic to Mat-LyLu and AT2 cells over 24 h and 48 h periods (Figure 3.12A&B). In addition, 24 and 48h treatment with TTX (1 μM) did not affect the viability of Mat-LyLu and AT2 cells under both normoxic and hypoxic conditions.

3.2.2.2 Cellular proliferation

Incubating Mat-LyLu cells for 24 h under hypoxic condition did not affect the cell number, compared with normoxia (Figure 3.13A). However, 48 and 72 h of hypoxia decreased number of Mat-LyLu cells significantly by 30 % and 59 %, respectively ($p < 0.05$ and $p < 0.001$, respectively; $n = 4$; Figure 3.13A). In contrast, hypoxia up to 72 h did not affect the number of AT2 cells ($p > 0.05$; $n = 3$; Figure 3.13B). Treating Mat-LyLu and AT2 cells with TTX (1 μM) up to 3 days did not affect cell numbers under both normoxic and hypoxic conditions ($p > 0.05$; $n \geq 3$; Figure 3.13C, D, E&F).

3.2.2.3 Nav1.7 mRNA expression

Expression of Nav1.7 and VGSCβ subunit mRNAs was studied using real-time PCR technique. Mat-LyLu and AT2 cells were incubated for 24 h under normoxic or hypoxic conditions. Agarose gel electrophoresis of Mat-LyLu cells confirmed specific single bands at the expected sizes for Nav1.7 and β-actin (414 nt and 362 nt respectively; Figure 3.14A). No Nav1.7 mRNA could be detected in AT2 cells, grown in normoxic or hypoxic conditions (Figure 3.14B). In both cells, no-template

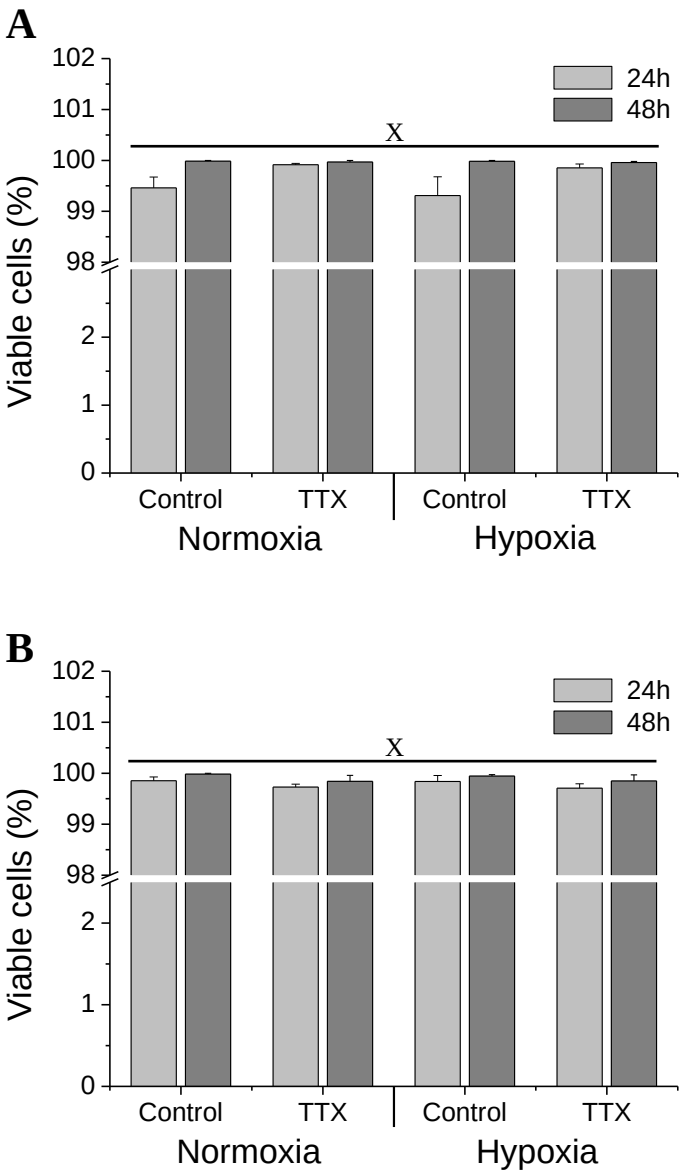


Figure 3.12 Bar diagram showing treatments had no toxic effect.

Possible toxic effects of 24h (light grey columns) or 48h (dark grey columns) treatment with or without TTX (1 µM) in normoxia or hypoxia (2 % O_2) was studied in Mat-LyLu (A) and AT2 (B) cells. Data are represented as means ± SEM (*n*=3). Data were analysed by ANOVA followed by Newman-Keuls *post hoc* analysis. (X) $p > 0.05$.

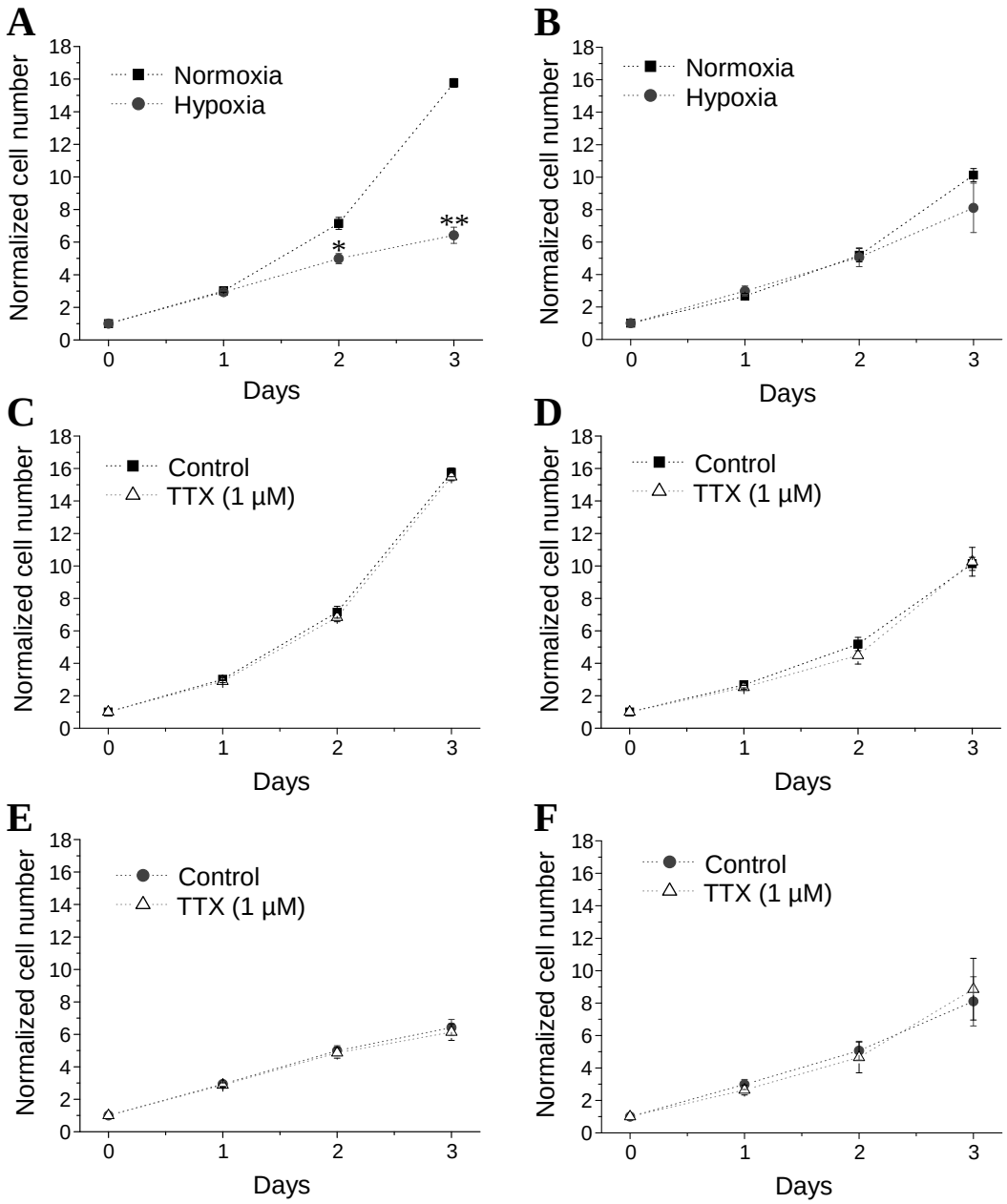


Figure 3.13 Time dependent effect of hypoxia (2 % O_2) on Mat-LyLu (A) and AT-2 (B) cell number.

TTX (1µM) do no effect cell number of Mat-LyLu (C & E) and AT-2 (D & F) in both normoxia (C & D) and hypoxia (E & F).Data are presented as means ± SEM ($n \geq 3$). Significance: (*) $p < 0.05$; (**) $p < 0.001$.

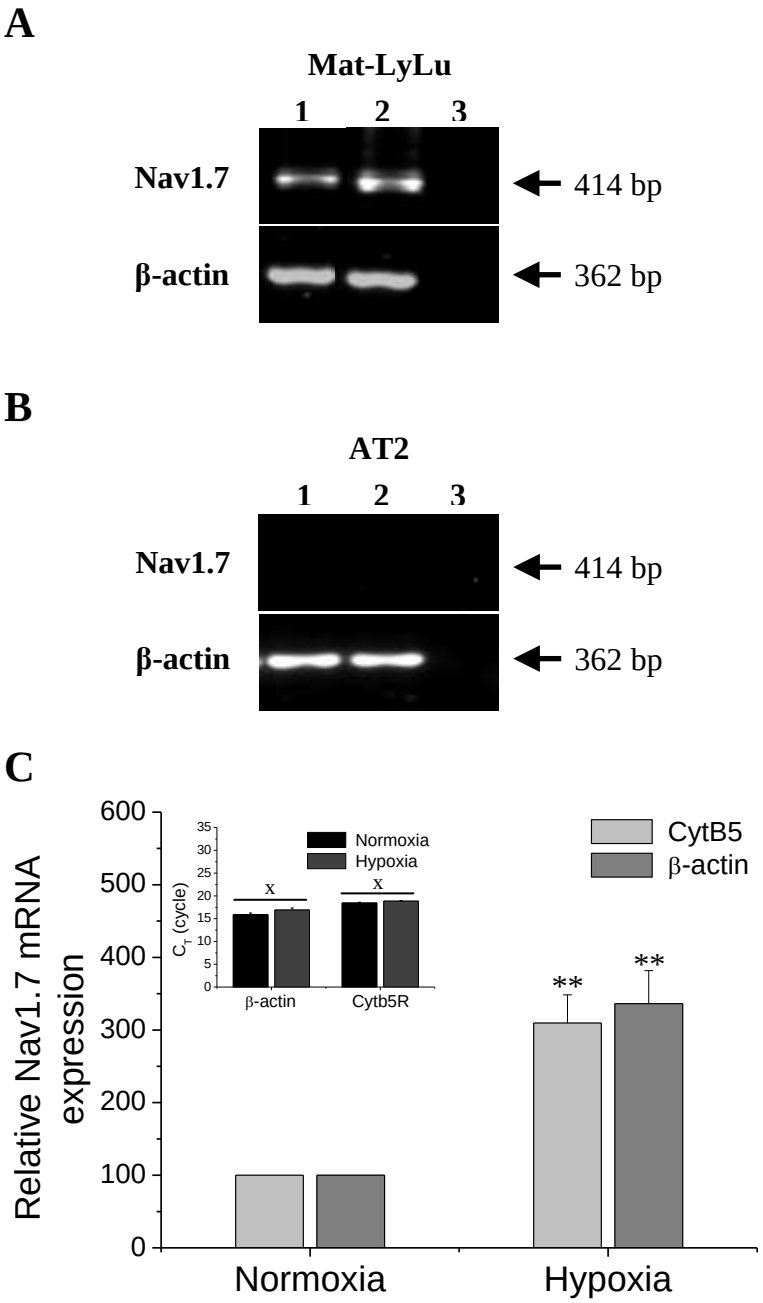


Figure 3.14 Effect of hypoxia (2 % O_2) on Mat-LyLu and AT-2 Nav1.7 mRNA expression.

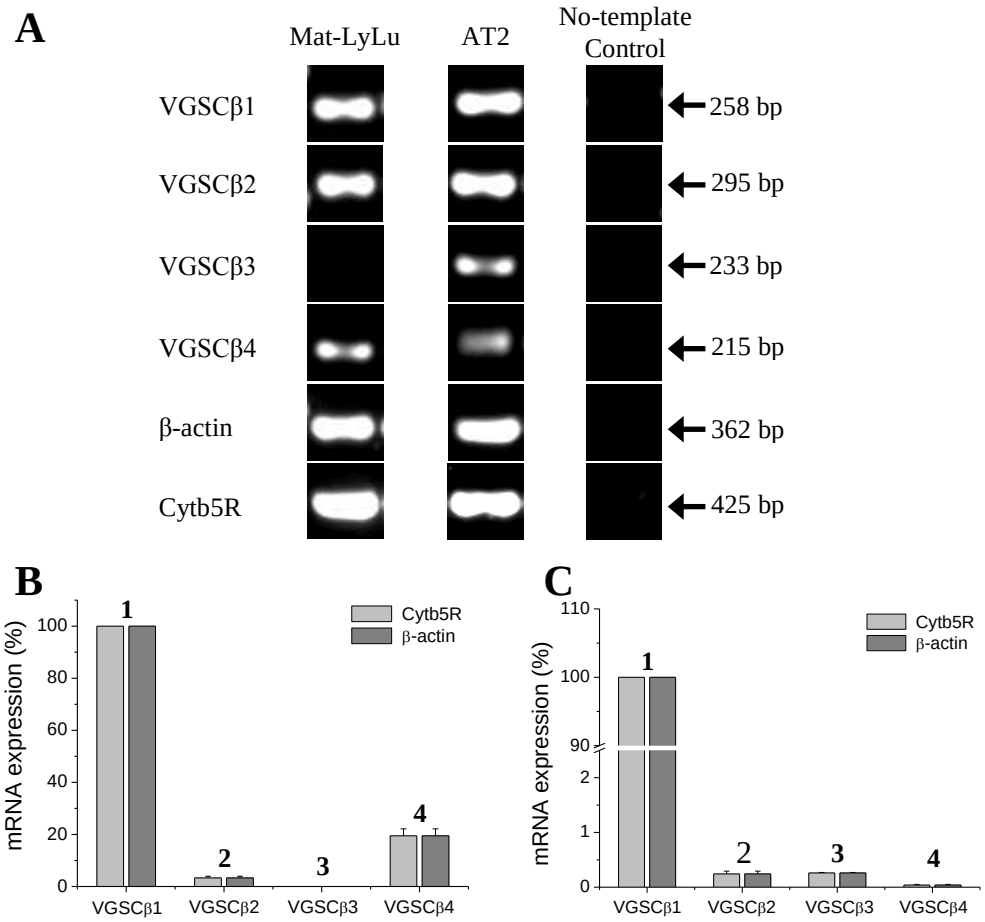
Agarose gel electrophoresis picture showing typical PCR product of Nav1.7 (414 bp) and normalising/control gene β-actin (362 bp) mRNA in Mat-LyLu (A) and AT2 (B) cells that was incubated under normoxic or hypoxic (2% O_2) conditions for 24 h. Lane (1) normoxia; (2) hypoxia; (3) no-template control. (C) Bar diagram showing result of real-time PCR experiment which effect of hypoxia on Nav1.7 mRNA expression was studied. The data were normalized to Cytb5R (light grey column) or β-actin (dark grey column) using the $2^{-\Delta\Delta C_T}$ method and described as relative to normoxic mRNA expression. Inset: bar diagram showing that both control/normalising genes C_T values was not affected by hypoxic treatment. Un-paired student t-test was used for statistic analysis. Data are presented as means ± SEM ($n \geq 3$). Significance: (**) $p < 0.001$; (X) $p > 0.05$.

controls did not give any signal (Figures 3.14 A&B). Hypoxia (24 h) significantly increased Nav1.7 mRNA expression by 309 ± 38.7 % (normalized to Cytb5R) / 336 ± 45.5 % (normalized to β-actin) ($p < 0.001$; $n = 12$; Figure 3.14C). Possible changes in the expression levels of the normalising/control genes, Cytb5R and β-actin (which should not be affect by treatments), were studied by plotting amplification threshold (C_T) values. Hypoxia did not have any significant effect on the Mat-LyLu normalising/control genes C_T values ($p > 0.05$; $n = 4$; Figure 3.14C inset).

3.2.2.4 VGSCβ subunit mRNA expression

3.2.2.4.1 Normoxia

Mat-LyLu and AT2 cells were incubated 24 h under normoxic conditions, and VGSCβ subunit mRNA expression was assessed by real-time PCR. Agarose gel electrophoresis of the PCR products of Mat-LyLu cells, grown in normoxic conditions, confirmed a specific single bands at the expected sizes for VGSCβ1, VGSCβ2, VGSCβ4, β-actin and Cytb5R (258 nt, 295 nt, 215 nt, 362 nt and 362 nt respectively; Figure 3.15A). However, no band was detected for VGSCβ3 (233 nt). On the other hand, a specific single band at the expected size for VGSCβ1, VGSCβ2, VGSCβ3, VGSCβ4, β-actin and Cytb5R (258 nt, 295 nt, 233 nt, 215 nt, 362 nt and 425 nt respectively) was detected for the PCR product of AT2 cells (Figure 3.15A). In both cells, no-template controls did not give any signal. VGSCβ1 was the predominant VGSCβ subunit that was expressed in both Mat-LyLu and AT2 cells. However, in Mat-LyLu cells, VGSCβ1 mRNA level was 30-fold and 5-fold higher than VGSCβ2 and VGSCβ4 mRNA levels, respectively; VGSCβ4 was ~6-fold



Comparison	p<0.05
1 vs 2	Yes
1 vs 3	Yes
1 vs 4	Yes
2 vs 3	Yes
2 vs 4	Yes
3 vs 4	Yes

Comparison	p<0.05
1 vs 2	Yes
1 vs 3	Yes
1 vs 4	Yes
2 vs 3	No
2 vs 4	Yes
3 vs 4	Yes

Figure 3.15 Basal mRNA expression profiles of VGSCβ subunits in Mat-LyLu and AT-2 cells.

(A)Agarose gel electrophoresis pictures showing typical PCR product of VGSCβ1 (258 bp), VGSCβ2 (295 bp), VGSCβ3 (233 bp), VGSCβ4 (215 bp) and normalising/control genes β-actin (362 bp) and Cytb5R (425 bp) mRNA in Mat-LyLu and AT2 cells that was incubated under normoxic conditions for 24 h. (B) Bar diagram showing result of real-time PCR experiment which basal mRNA expression of VGSCβ subunits were studied in Mat-LyLu cells. Inset: table of multiple comparisons between treatments for statistical significance. (C) Bar diagram showing result of real-time PCR experiment which basal mRNA expression of VGSCβ subunits were studied in AT2 cells. Inset: table of multiple comparisons between treatments for statistical significance. The data were normalized to Cytb5R (light grey column) or β-actin (dark grey column) using the $2^{-\Delta\Delta C_T}$ method and described as relative to VGSCβ1 mRNA expression. Data were analysed by ANOVA followed by Newman-Keuls *post hoc* analysis. Data are presented as means ± SEM ($n \geq 3$).

higher than VGSCβ2 ($p < 0.05$; $n = 6$; Figure 3.15B). Again, no VGSCβ3 expression was detected in Mat-LyLu cells (Figure 3.15B). In AT2 cells, the VGSCβ1 mRNA level was 411-fold, 384-fold and 2599-fold higher than the mRNA levels of VGSCβ2, VGSCβ3 and VGSCβ4, respectively ($p < 0.05$; $n = 3$; Figure 3.15C). VGSCβ2 and VGSCβ3 mRNA levels were same in AT2 cells while the VGSCβ4 mRNA level was significantly less (15-fold and 14-fold, respectively; $p < 0.05$; $n = 3$; Figure 3.15C).

AT2 cells had 9-fold higher VGSCβ1 mRNA than Mat-LyLu cells ($p < 0.05$; $n = 3$; Figure 3.16A&B). VGSCβ2 mRNA levels were not different in both cell lines ($p > 0.05$; $n = 3$; Figure 3.16A&C). VGSCβ3 was expressed in AT2 cells but not in Mat-LyLu cells ($p < 0.001$; $n = 3$; Figure 3.16A&D). Mat-LyLu cells had 39-fold higher VGSCβ4 mRNA than AT2 cells ($p < 0.05$; $n = 3$; Figure 3.16A&E). Essentially identical results were obtained when β-actin was used as the normalizing/control gene instead of Cytb5R (Figure 3.17).

3.2.2.4.2 Hypoxia

Agarose gel electrophoresis of the real-time PCR products from Mat-LyLu cells, grown in normoxic and hypoxic conditions, confirmed specific single bands at the expected size for VGSCβ1, VGSCβ2, VGSCβ4, β-actin and Cytb5R (258 nt, 295 nt, 215 nt, 362 nt and 425 nt, respectively; Figure 3.18A). However, no band was detected for VGSCβ3 (233 nt) in both conditions. No-template control experiment did not give any signal. When Mat-LyLu cells were incubated under hypoxic conditions, VGSCβ1 mRNA levels increased 1.9- and 2.1-fold when Cytb5R and β-actin were used as the control/normalising gene, respectively ($p < 0.05$; $n = 12$;

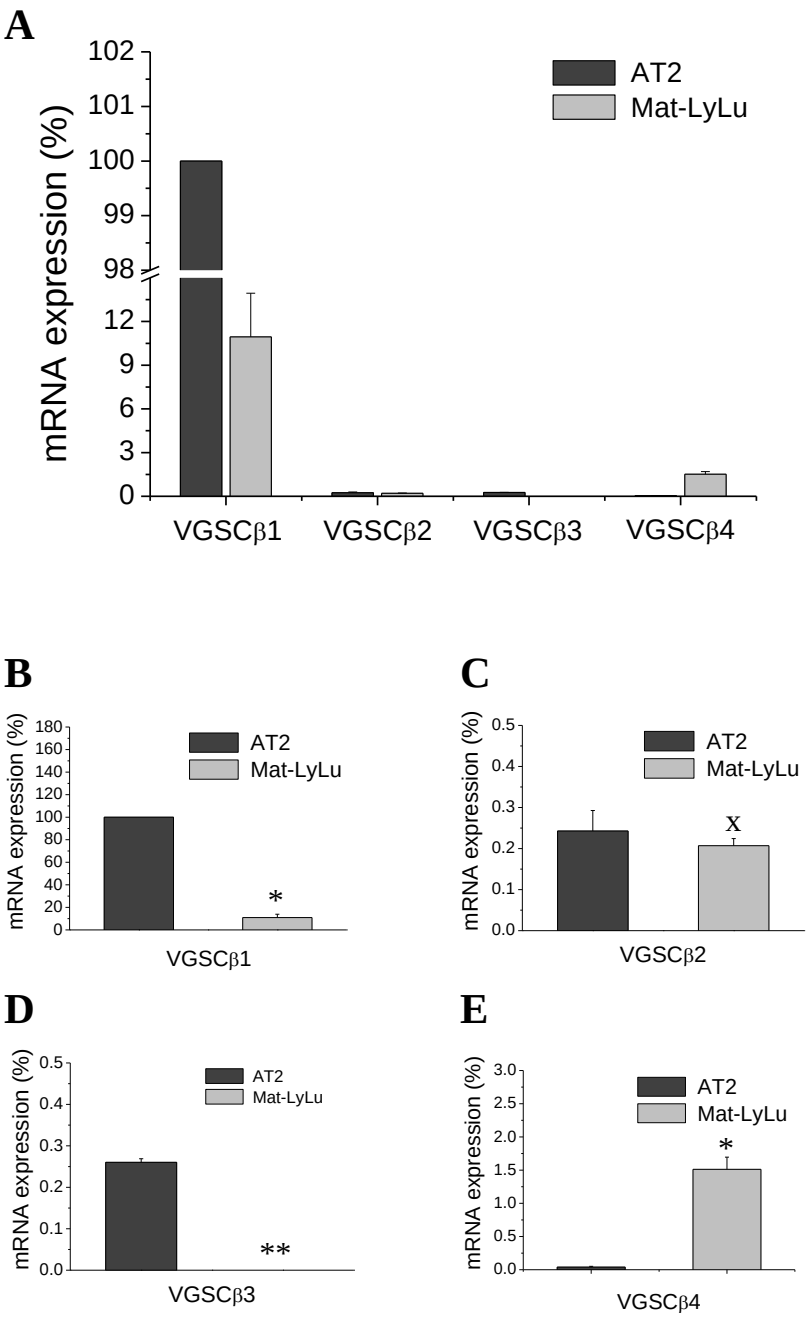


Figure 3.16 Comparison of VGSCβ subunits mRNA expression, using Cytb5R as normalising/control gene, between Mat-LyLu and AT-2 cells.

(A) Bar diagram showing result of real-time PCR experiment which basal mRNA expression of VGSCβ subunits in Mat-LyLu (light grey column) and AT2 (dark grey column) cells, incubated under control conditions for 24 h, were compared. Individual comparison of VGSCβ1 (B), VGSCβ2 (C), VGSCβ3 (D) and VGSCβ4 (E) mRNA between Mat-LyLu and AT2 cells. The data were normalized to Cytb5R using the $2^{-\Delta\Delta C_T}$ method and described as relative to VGSCβ1 mRNA expression of AT2 cells. Un-paired student t-test was used for statistic analysis. Data are presented as means ± SEM ($n \geq 3$). Significance: (*) $p < 0.05$; (**) $p < 0.001$; (X) $p > 0.05$.

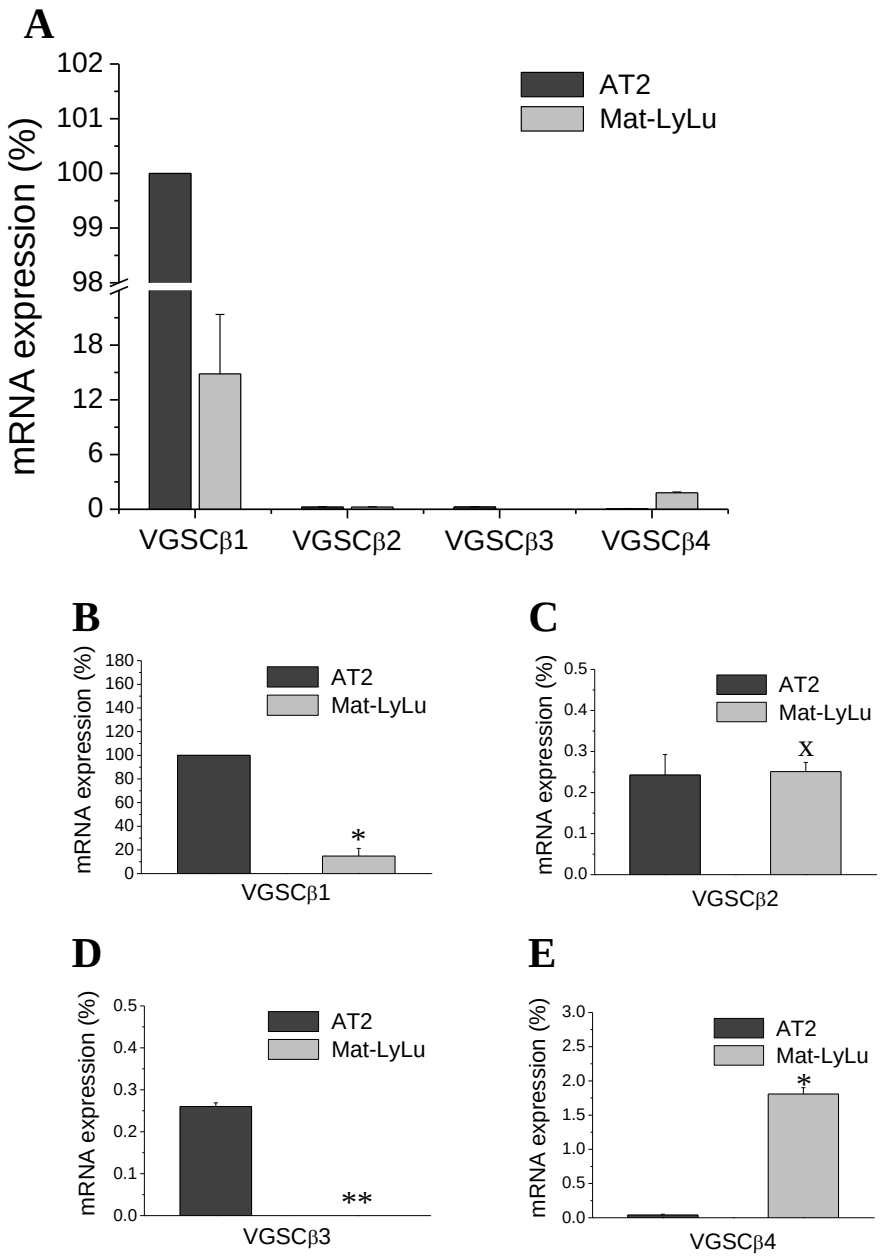


Figure 3.17 Comparison of VGSCβ subunits mRNA expression, using β-actin as normalising/control gene, between Mat-LyLu and AT-2 cells.
(A) Bar diagram showing result of real-time PCR experiment which basal mRNA expression of VGSCβ subunits in Mat-LyLu (light grey column) and AT2 (dark grey column) cells, incubated under control conditions for 24 h, were compared. Individual comparison of VGSCβ1 (B), VGSCβ2 (C), VGSCβ3 (D) and VGSCβ4 (E) mRNA between Mat-LyLu and AT2 cells. The data were normalized to β-actin using the $2^{-\Delta\Delta C_T}$ method and described as relative to VGSCβ1 mRNA expression of AT2 cells. Un-paired student t-test was used for statistic analysis. Data are presented as means ± SEM ($n \geq 3$). Significance: (*) $p < 0.05$; (**) $p < 0.001$; (X) $p > 0.05$.

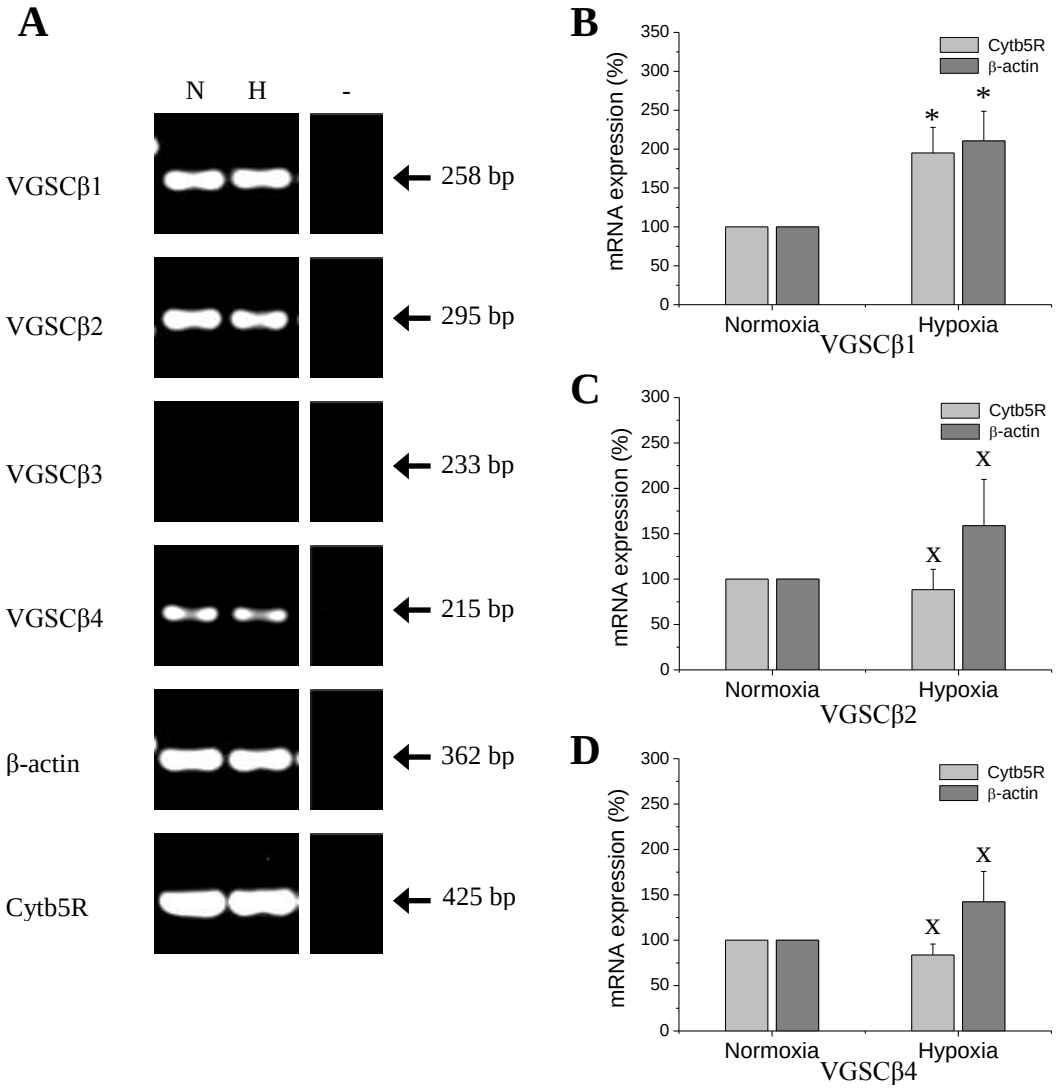


Figure 3.18 Effect of hypoxia (2 % O_2) on VGSCβ subunits mRNA expression in Mat-LyLu cells.

(A)Agarose gel electrophoresis pictures showing typical PCR product of VGSCβ1 (258 bp), VGSCβ2 (295 bp), VGSCβ3 (233 bp), VGSCβ4 (215 bp) and normalising/control genes β-actin (362 bp) and Cytb5R (425 bp) mRNA in Mat-LyLu cells that was incubated under normoxic or hypoxic conditions for 24 h. Lanes (N): normoxia; (H): hypoxia; -: no template control. Bar diagram showing result of real-time PCR experiment which effect of hypoxia on mRNA expression of VGSCβ1 (B), VGSCβ2 (C), VGSCβ3 (D), VGSCβ4 (E) subunits was studied in Mat-LyLu cells. The data were normalized to Cytb5R (light grey column) or β-actin (dark grey column) using the $2^{-\Delta\Delta C_T}$ method and described as relative to normoxic expression. Un-paired student t-test was used for statistic analysis. Data are presented as means ± SEM ($n \geq 3$). Significance: (**) $p < 0.05$; (X) $p > 0.05$.

Figure 3.18B). No change in VGSCβ2, VGSCβ3 and VGSCβ4 mRNA expression was detected following the hypoxic treatment ($p > 0.05$; $n = 6$; Figures 3.18A,C&D). Agarose gel electrophoresis of the real-time PCR products from AT2 cells, grown in normoxic and hypoxic conditions, confirmed specific single bands at the expected sizes for VGSCβ1, VGSCβ2, VGSCβ3, VGSCβ4, β-actin and Cytb5R (258 nt, 295 nt, 233 nt, 215 nt, 362 nt and 425 nt, respectively; Figure 3.19A). No-template control experiment did not give any signal. Hypoxia significantly increased VGSCβ1 mRNA levels by 199 ± 32 % (normalised to Cytb5R) / 311 ± 32 % (normalised to β-actin) ($p < 0.05$; $n = 3$; Figure 3.19B). VGSCβ2 mRNA levels increased by 123 ± 13 % (normalised to Cytb5R) / 195 ± 21 % (normalised to β-actin); the latter was statistically significant ($p < 0.05$; $n = 3$; Figure 3.19C). The VGSCβ3 mRNA level was unchanged by the hypoxic treatment ($p > 0.05$; $n = 3$; Figure 3.19D). In addition, VGSCβ4 mRNA levels increased significantly by ~4-fold (normalised to Cytb5R) / 6-fold (normalised to β-actin) ($p < 0.05$; $n = 3$; Figure 3.19E). Hypoxia did not have any effect on the C_T values of normalising/control genes, Cytb5R and β-actin, in Mat-LyLu cells ($p > 0.05$; $n = 3$; Figure 3.19F).

3.2.2.5 Expression of VGSCα protein

In preliminary Western blot experiments, expression of VGSC protein with a molecular weight of 220 kD was confirmed (Figure 3.20). However, the antibody proved difficult to handle in Western blots, so in the studies of hypoxia (2 % O_2) on subcellular distribution of VGSCα protein in Mat-LyLu cells quantitative data were obtained by immunocytochemistry and confocal image analyses, as follows (Figures 3.21-3.25).

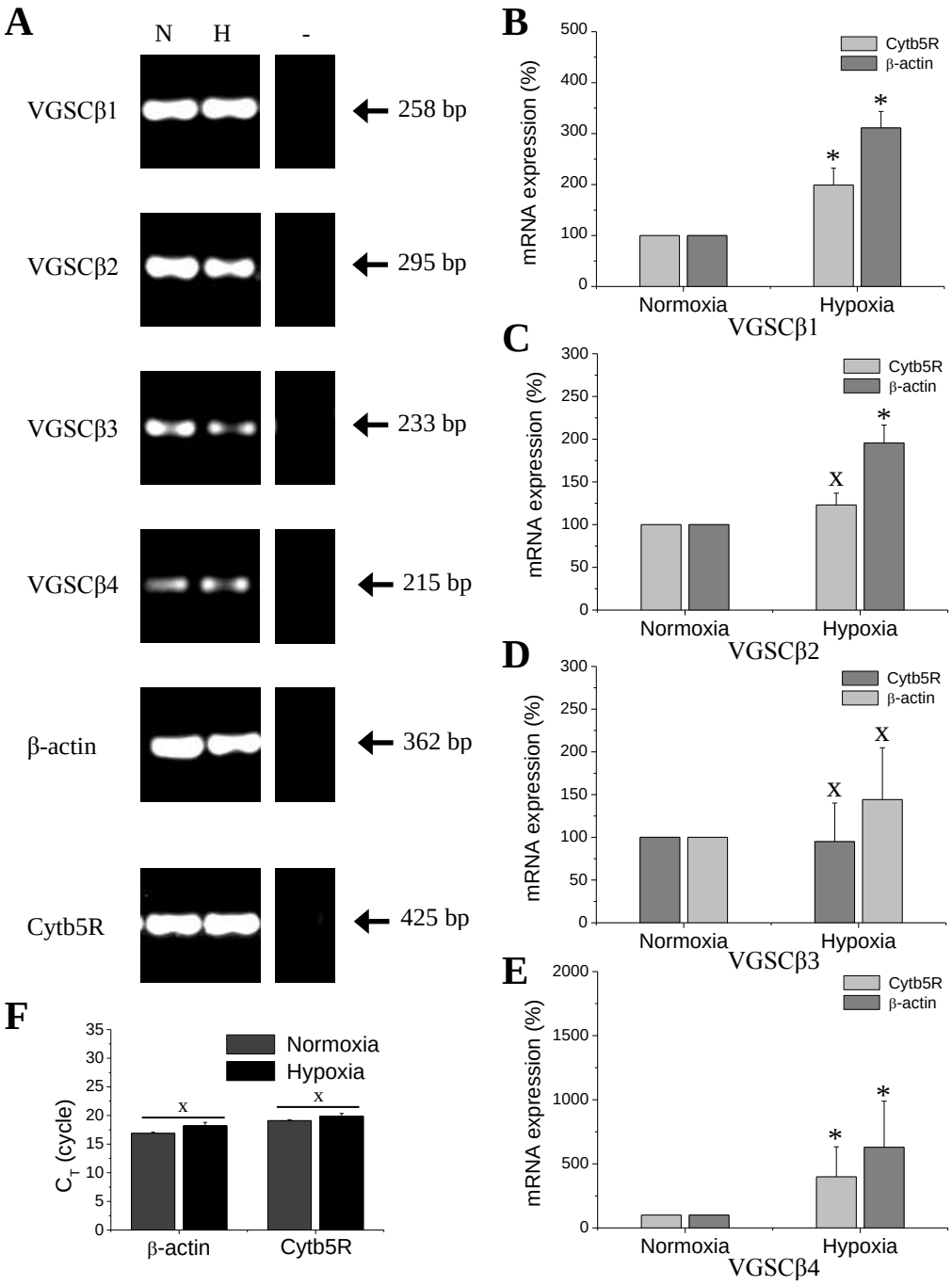


Figure 3.19 Effect of hypoxia (2 % O_2) on VGSCβ subunits mRNA expression in AT2 cells.

(A)Agarose gel electrophoresis pictures showing typical PCR product of VGSCβ1 (258 bp), VGSCβ2 (295 bp), VGSCβ3 (233 bp), VGSCβ4 (215 bp) and normalising/control genes β-actin (362 bp) and Cytb5R (425 bp) mRNA in AT2 cells that was incubated under normoxic or hypoxic conditions for 24 h. Lanes (N): normoxia; (H): hypoxia; -: no template control. Bar diagram showing result of real-time PCR experiment which effect of hypoxia on mRNA expression of VGSCβ1 (B), VGSCβ2 (C), VGSCβ3 (D), VGSCβ4 (E) subunits was studied in AT2. The data were normalized to Cytb5R (light grey column) or β-actin (dark grey column) using the $2^{-\Delta\Delta C_T}$ method and described as relative to normoxic expression. Man-Witney rank sum test was used for statistic analysis.(F) Histogram showing that both control/normalising genes C_T values was not affected by hypoxic treatment. Un-paired student t-test was used for statistic analysis. Data are presented as means ± SEM ($n \geq 3$). Significance: (*) $p < 0.05$; (X) $p > 0.05$.

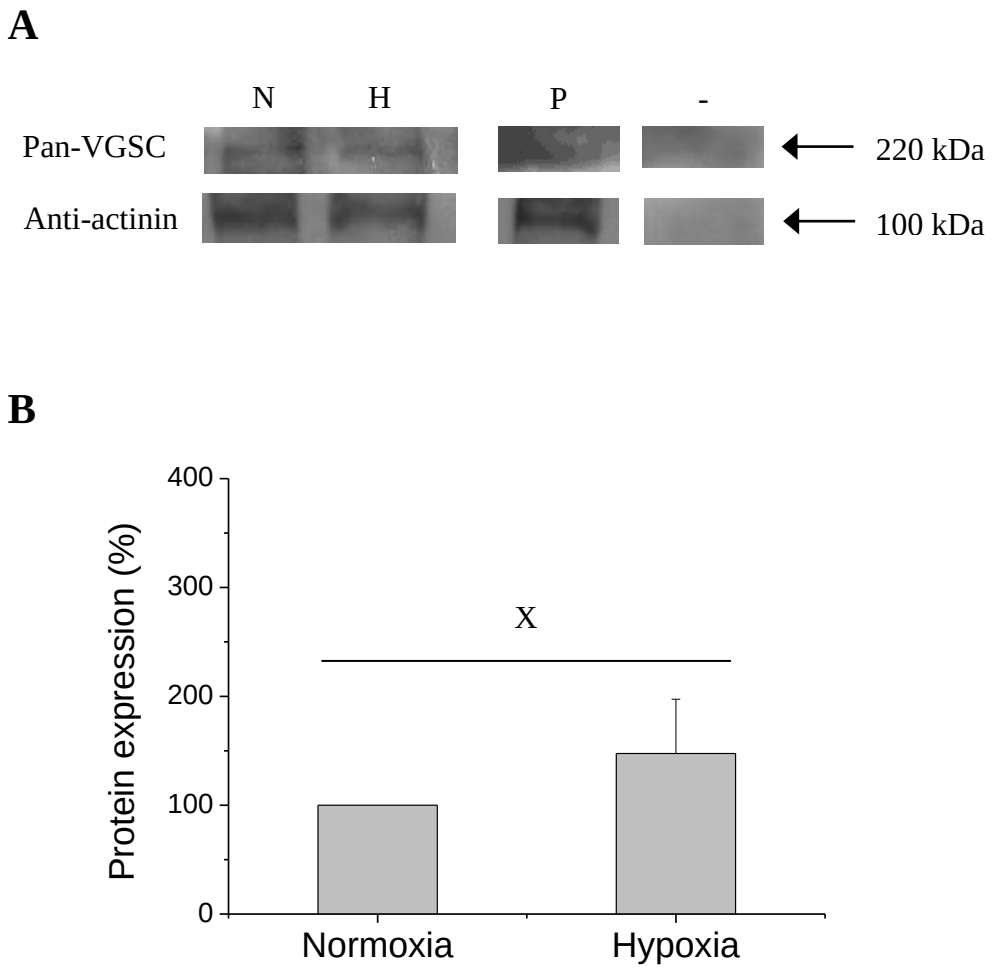


Figure 3.20 Effect of hypoxia (2 % O_2) on VGSCα protein expression in Mat-LyLu cells.
(A) Western blot of 50 µg of total protein per lane from Mat-LyLu cells. Lanes (N): normoxia; (H): hypoxia; (P): pre-absorbed with immunizing peptide; (-) no primary antibody. Bloats were immunostained with pan-VGSCα and anti-actinin antibodies. (B) Histogram showing relative VGSCα protein expression in normoxic and hypoxic conditions. The signal from pan-VGSC antibody was normalised to the respective anti-actinin signal. All data were represented as relative to normoxic VGSCα protein level. Un-paired student t-test was used for statistic analysis. Data are presented as means ± SEM (n = 4). Significance: (X) $p > 0.05$.

3.2.2.5.1 Control experiments

VGSCα protein expression was observed in intracellular and plasma membranes but not in nucleus of Mat-LyLu cells under control conditions (Figures 3.21A and 3.22). A number of control experiments were carried out for the immunocytochemical staining of Mat-LyLu cells with the pan-VGSC antibody (Figure 3.21B-D). No staining of Mat-LyLu cells was seen with the following treatments: i) a non-specific IgG used at the same concentration as the primary pan-VGSC antibody antibody (Figure 3.21B); ii) application of only the secondary antibody (Figure 3.21C); and iii) application of the pan-VGSC antibody pre-absorbed with the immunizing peptide, at x5 the antibody concentration (Figure 3.21D). These controls confirmed the specificity of the pan-VGSC antibody and the procedure used.

3.2.2.5.2 Plasma membrane VGSCα protein level

Quantification of VGSCα immunocytochemical staining in the cell periphery by "free form line profile" analysis of XYZ scans of Mat-LyLu cells revealed a decrease of plasma membrane VGSCα level, by ~15 %, from 208.7 ± 7.1 AU/µm to 176.7 ± 7.1 AU/µm by 24 h hypoxic (2 % O_2) treatment ($p < 0.05$; $n = 105$; Figure 3.23).

3.2.2.5.3 Intracellular VGSCα protein level

Quantification of VGSCα protein level by "area histogram" analysis of XYZ scans of Mat-LyLu cells revealed a decrease of internal VGSCα level by ~16 % from 22978 ± 587 AU to 19173 ± 389 AU by 24 h hypoxic (2 % O_2) treatment ($p < 0.001$; $n \geq 77$; Figure 3.24).

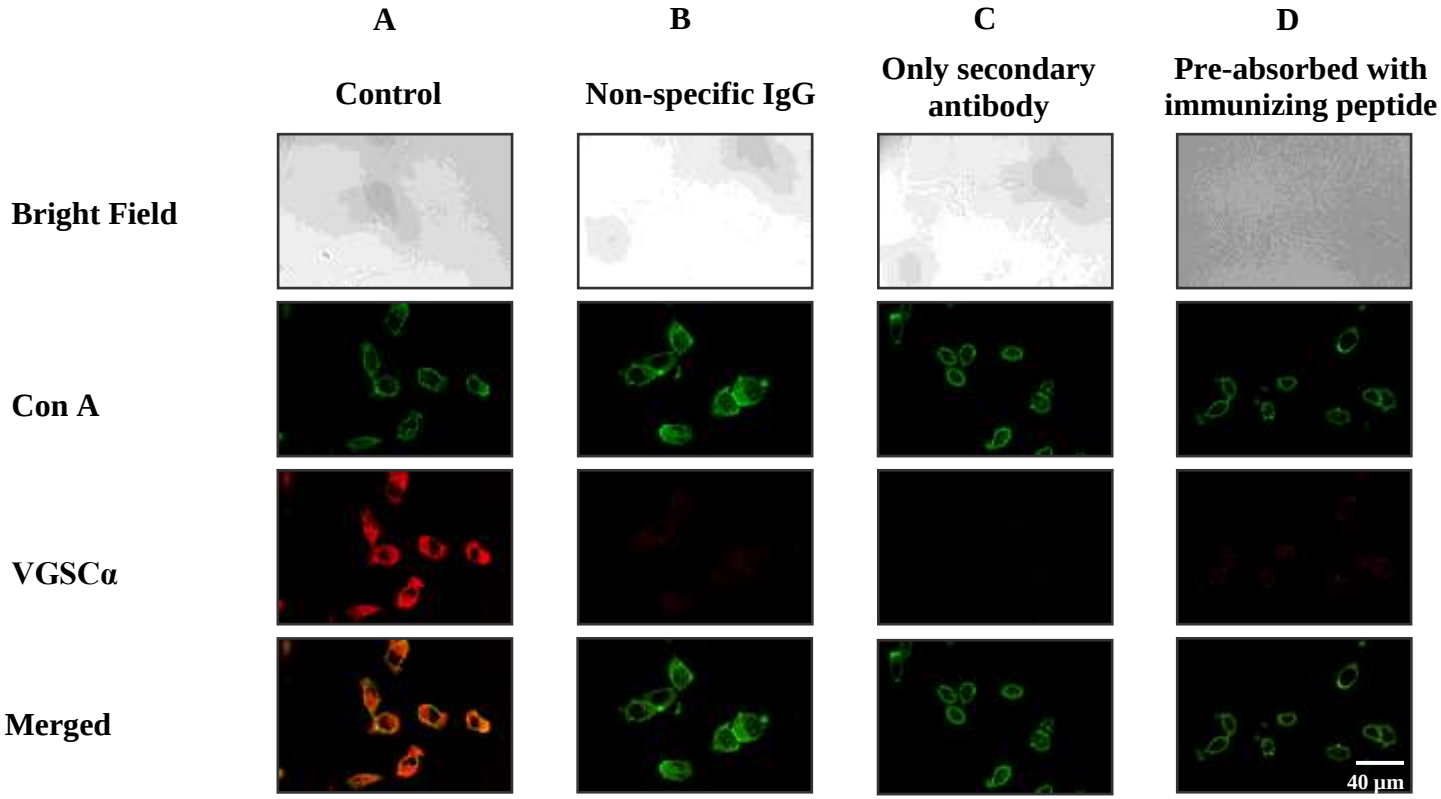


Figure 3.21 Controls for Immunocytochemistry with Mat-LyLu cells.
Typical confocal image of Mat-LyLu cells immunostained (A) pan-VGSC primary antibody, (B) instead of Pan-VGSC primary antibody equal amount of non-specific IgG, (C) instead of primary antibody equal amount of 5% BSA/PBS, (D) pan-VGSC antibody that was pre-absorbed with the immunizing peptide. Alexa-568 conjugated secondary antibody (red) was used in all samples. Slides were co-stained with FITCY conjugated Concanavalin A (Con A) plasma membrane marker (green). Scale bar (40 µm) applicable to all panels.

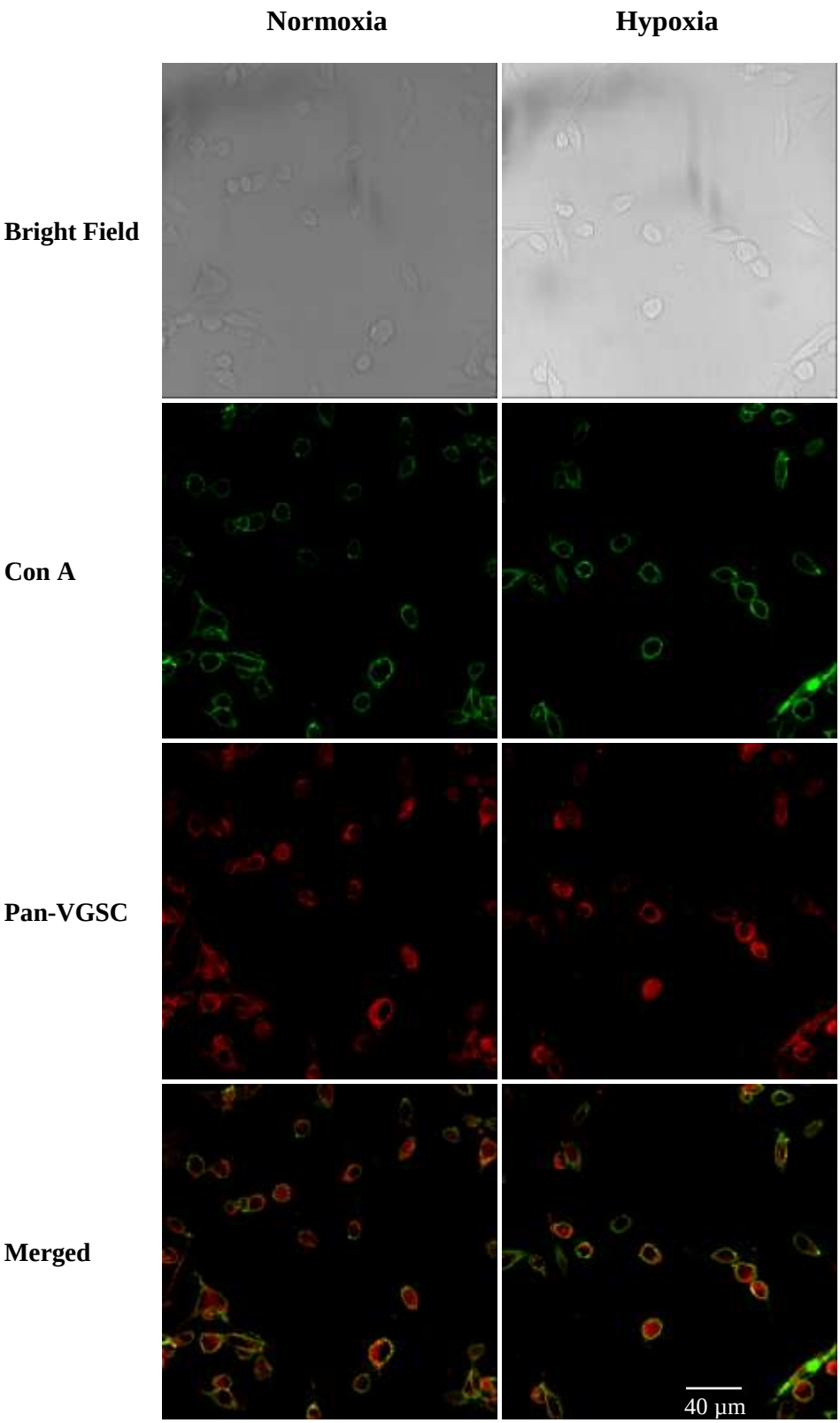


Figure 3.22 Confocal images from immunochemistry of Mat-LyLu cells incubated in normoxia and hypoxia (2 % O_2) with pan-VGSC antibody.
Typical XYZ confocal images of Mat-LyLu cells incubated 24 h under normoxic and hypoxic conditions. Signal from concanavalin A plasma membrane marker (green), pan-VGSC antibody (red) and overlay of both (merged image) are shown in addition to bright field image. Scale bar (40 µm) applicable to all panels.

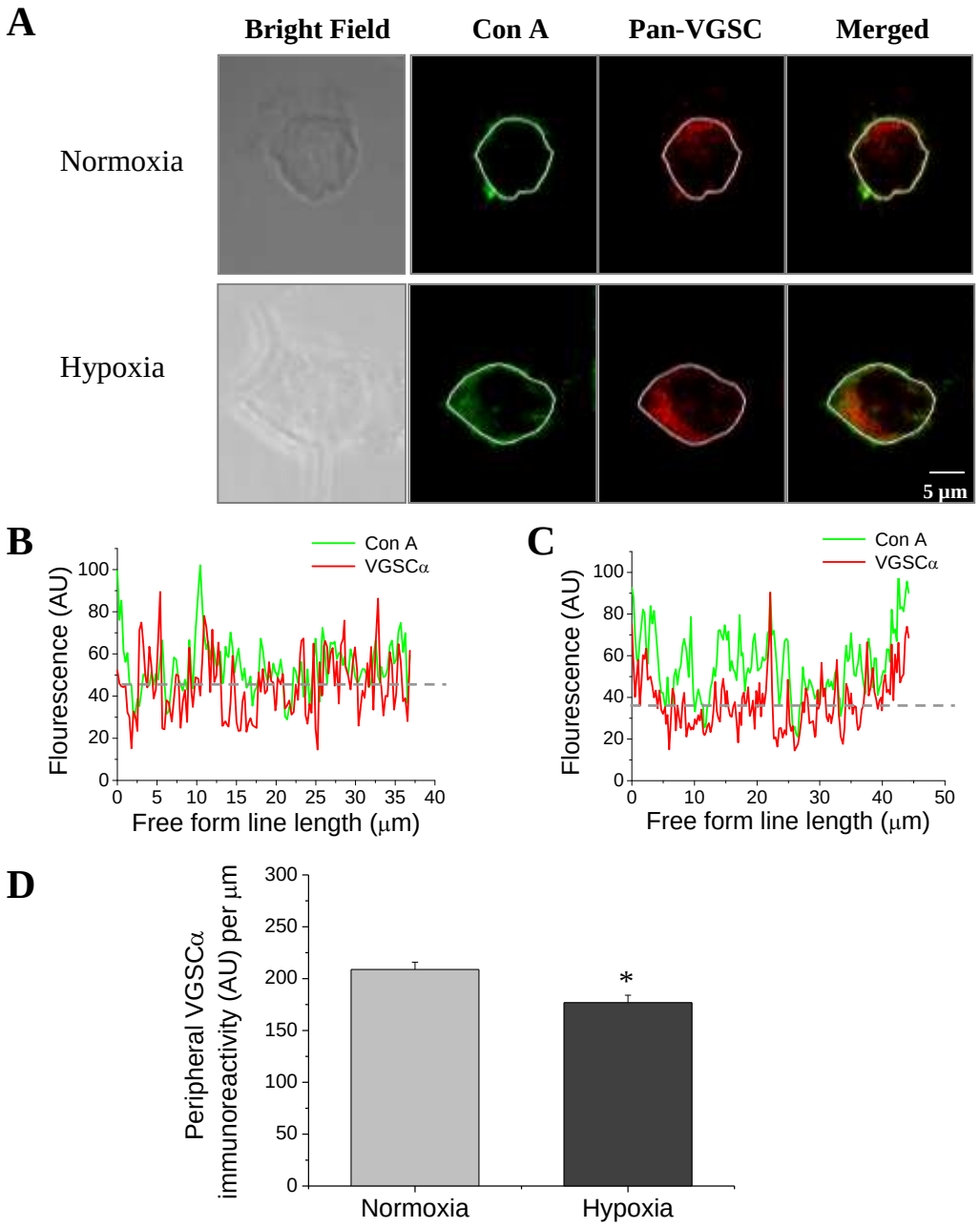


Figure 3.23 Effect of hypoxia (2 % O_2) on VGSCα protein levels in plasma membrane of Mat-LyLu cells.

(A) Typical XYZ confocal images of Mat-LyLu cells incubated 24 h under normoxic and hypoxic conditions. White lines indicate typical freeform line guided by Con A staining to measure cell surface protein level. Scale bar (5µm) applicable to all panels. (B) Representative trace showing signal intensity of Con A plasma membrane marker (green) and VGSCα (red) immunofluorescence along plasma membrane from typical cells incubated (24 h) in normoxic conditions (Figure 3.23A). (C) Representative trace showing signal intensity of Con A plasma membrane marker and VGSCα immunofluorescence along plasma membrane from typical cells incubated (24 h) in hypoxic conditions (Figure 3.23A). Dotted gray lines indicate mean pan-VGSC fluorescence. (D) Bar diagram showing level of VGSCα protein immunoreactivity along plasma membrane as a immunoreactivity (AU) per µm. Un-paired student t-test was used for statistic analysis. Data are presented as means ± SEM (n = 105). Significance: (*) $p < 0.05$.

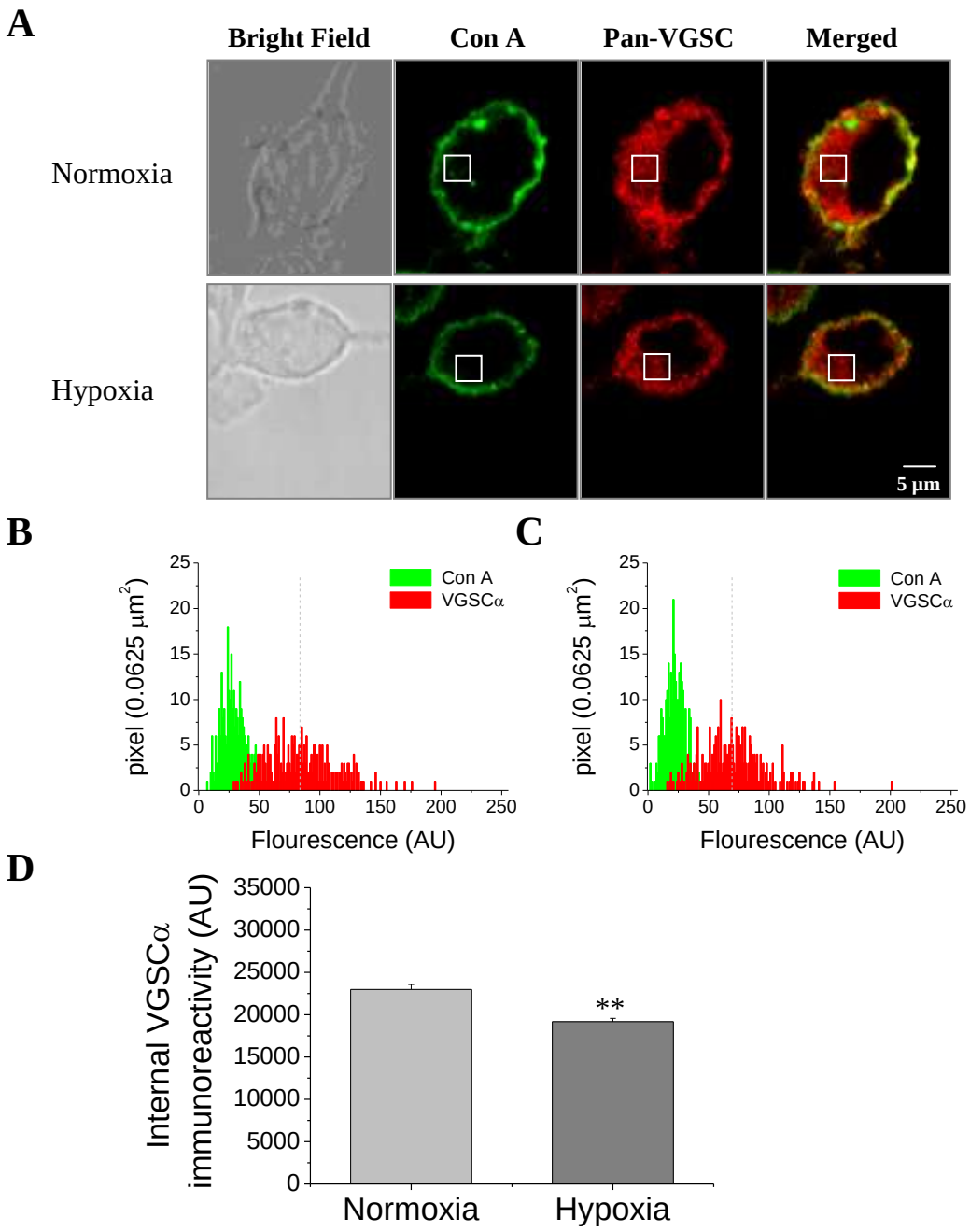


Figure 3.24 Effect of hypoxia (2 % O_2) on internal VGSCα protein levels of Mat-LyLu cells.

(A) Typical XYZ confocal images of Mat-LyLu cells incubated 24 h under normoxic and hypoxic conditions. White box indicates typical area covering 16 µm^2 square section of cytoplasm avoiding nucleus to measure internal protein level. Scale bar (5µm) applicable to all panels. (B) Representative histogram showing distribution of pixels (0.0625 µm^2) with signal intensity of Con A plasma membrane marker (green) and VGSCα (red) immunofluorescence in cytoplasm from typical cells incubated (24 h) in normoxic conditions (Figure 3.24A). (C) Representative histogram showing distribution of signal intensity of Con A plasma membrane marker (green) and VGSCα (red) immunofluorescence in cytoplasm from typicals cell incubated (24 h) in hypoxic conditions (Figure 3.24A). Dotted gray lines indicate mean pan-VGSC fluorescence. (D) Bar diagramt showing internal VGSCα protein immunoreactivity (AU). Un-paired student t-test was used for statistic analysis. Data are presented as means ± SEM ($n \geq 77$). Significance: (**) $p < 0.001$.

3.2.2.5.4 Subcellular distribution

The subcellular distribution of the VGSCα protein in Mat-LyLu cells was studied by "straight-line cross-sectional profile" analysis. This analysis revealed that the relative levels of plasma membrane and intracellular VGSCα protein were not affected by 24 h hypoxic (2 % O_2) treatment (10.5 ± 0.5 % and 11.2 ± 0.5 %, respectively; $p > 0.05$; $n = 61$; Figure 3.25). This result was consistent with the outcome of the "free form line profile" and "area histogram" analyses.

3.2.2.6 VGSCβ1 protein expression

Confocal immunocytochemistry with VGSCβ1 antibody was used to test possible effect of hypoxia (2 % O_2) on distribution of VGSCβ1 protein in Mat-LyLu cells (Figure 3.26-3.29). VGSCβ1 expression was observed in intracellular and plasma membrane but not in nucleus of Mat-LyLu cells under control conditions (Figure 3.26).

3.2.2.6.1 Plasma membrane VGSCβ1 protein level

Quantification of VGSCβ1 protein level by "free form line profile" analysis of XYZ scans of Mat-LyLu cells revealed no change in plasma membrane VGSCβ1 protein level after 24 h hypoxia (2 % O_2) treatment (245.8 ± 12.5 AU/µm and 245.5 ± 19.4 AU/µm, respectively; $p > 0.05$; $n = 86$; Figure 3.27).

3.2.2.6.2 Intracellular VGSCβ1 protein level

Quantification of VGSCβ1 protein level by "area histogram" analysis of XYZ scans of Mat-LyLu cells revealed no change of internal VGSCβ1 level by 24 h hypoxic (2

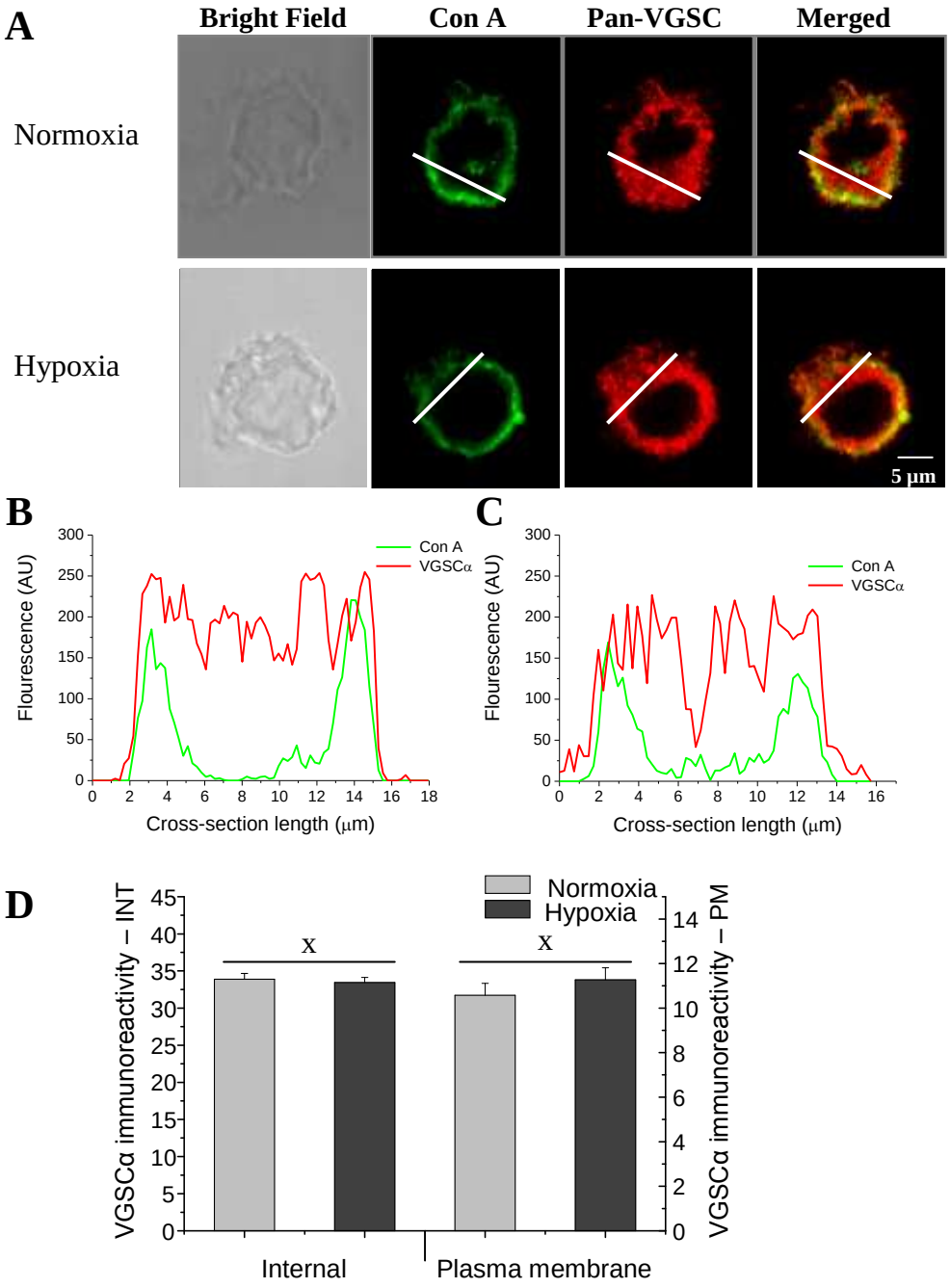


Figure 3.25 Effect of hypoxia (2 % O_2) on VGSCα protein distribution along typical cellular cross-section in Mat-LyLu cells.

(A) Typical XYZ confocal images of Mat-LyLu cells incubated 24 h under normoxic and hypoxic conditions. White line indicates typical cross-section. Scale bar (5µm) applicable to all panels. (B) Representative trace showing signal intensity of Con A plasma membrane marker (green) and VGSCα immunofluorescence (red) along cross-section from typical cells incubated (24 h) in normoxic conditions (Figure 3.22A). (C) Representative trace showing signal intensity of Con A plasma membrane marker and VGSCα immunofluorescence along cross-section from typical cells incubated (24 h) in hypoxic conditions (Figure 3.22A). (D) Bar diagram showing distribution of VGSCα protein immunoreactivity along subcellular cross-sections as a percentage of total (%). For plasma membrane (PM) immunoreactivity, 1.5 µm sections was measured inward from the edge of Con A staining. For internal (INT) immunoreactivity, middle 30 % of the cross-section was measured. Un-paired student t-test was used for statistic analysis. Data are presented as means ± SEM (n = 61). Significance: (X) $p > 0.05$.

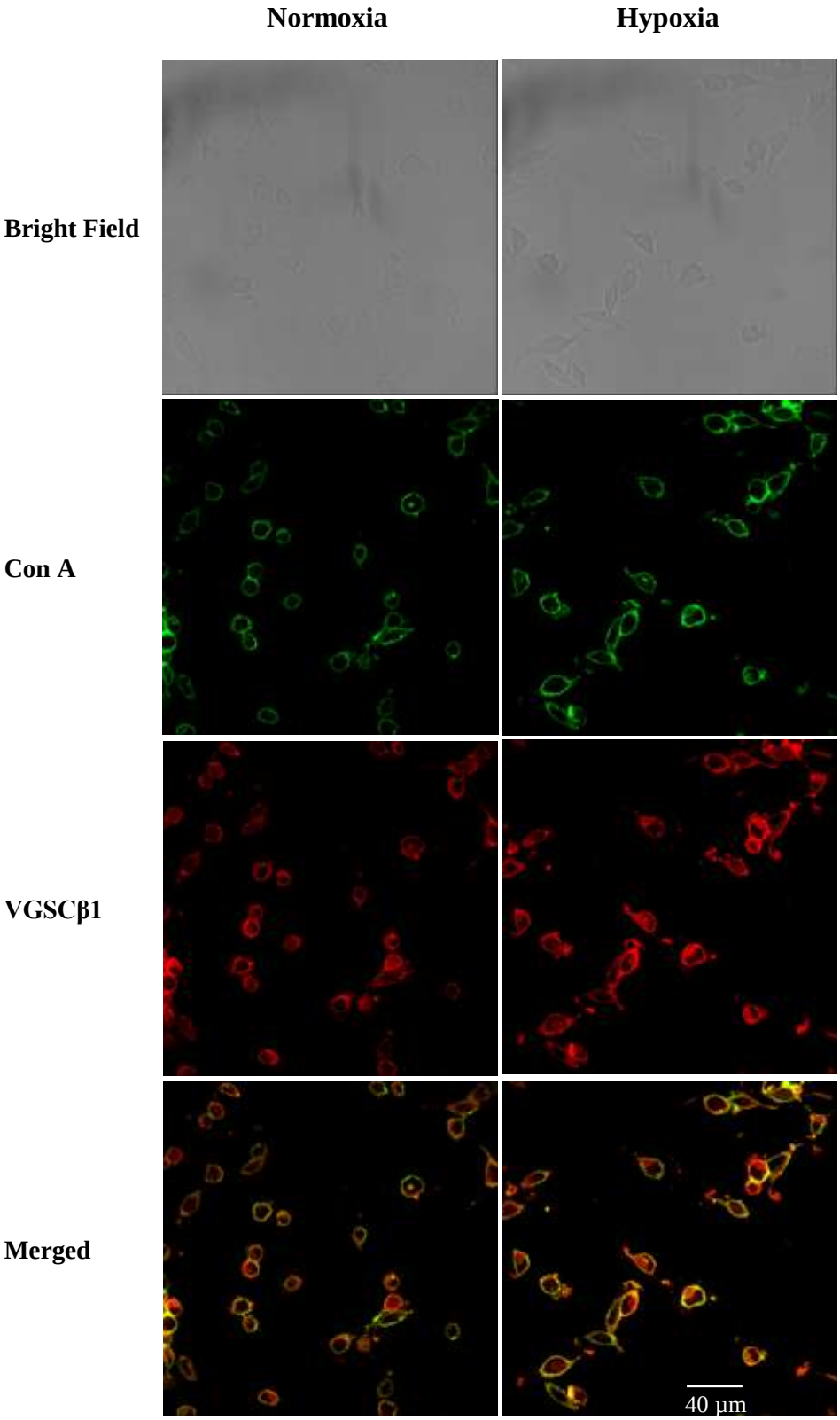


Figure 3.26 Confocal images from immunochemistry of Mat-LyLu cells incubated in normoxia and hypoxia (2 % O_2) with VGSCβ1 antibody.
Typical XYZ confocal images of Mat-LyLu cells incubated 24 h under normoxic and hypoxic conditions. Signal from concanavalin A plasma membrane marker (green), VGSCβ1 antibody (red) and overlay of both (merged image) are shown in addition to bright field image. Scale bar (40 µm) applicable to all panels.

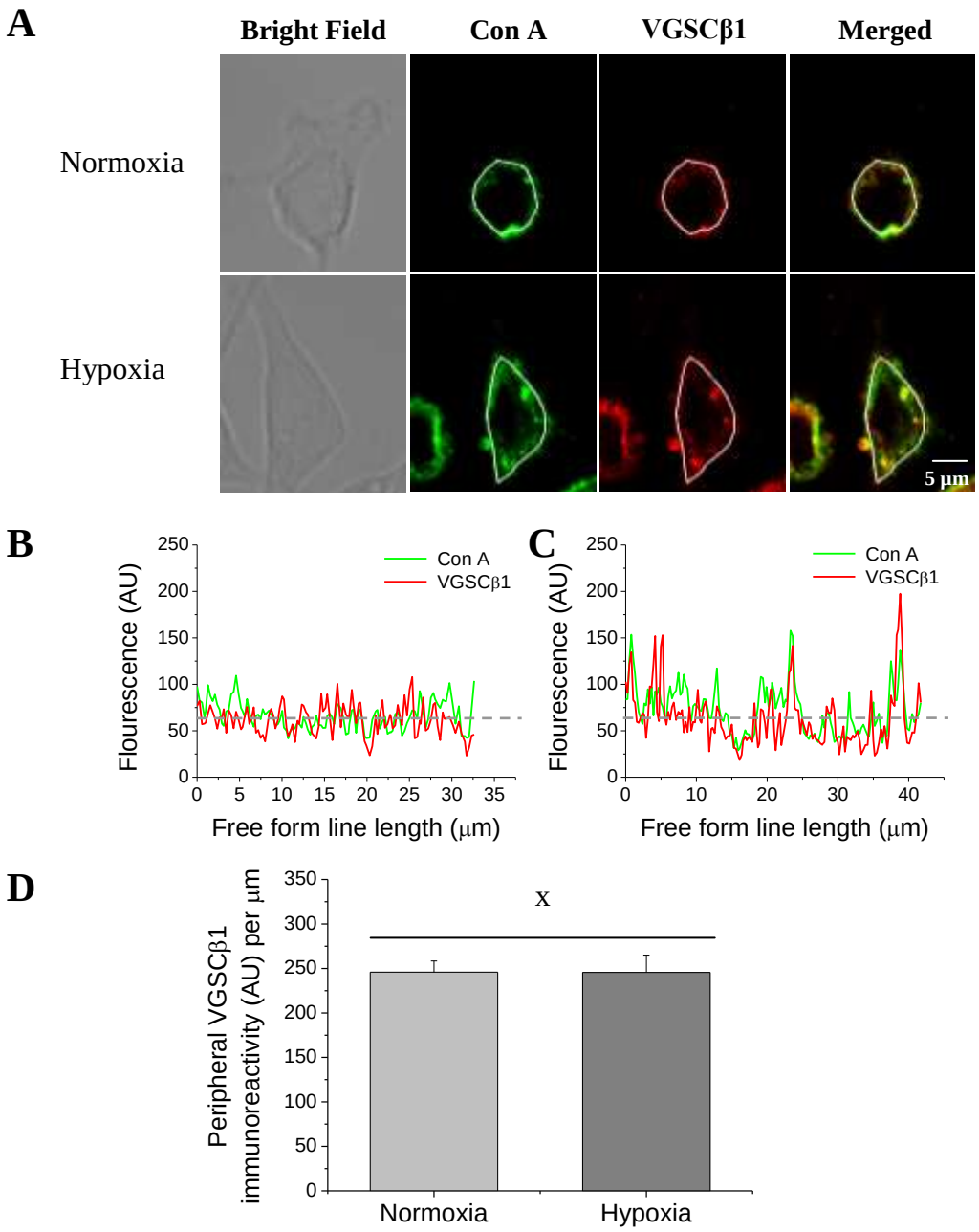


Figure 3.27 Effect of hypoxia (2 % O_2) on VGSCβ1 protein levels in plasma membrane of Mat-LyLu cells.

(A) Typical XYZ confocal images of Mat-LyLu cells incubated 24 h under normoxic and hypoxic conditions. White line indicates typical freeform line guided by Con A staining to measure cell surface protein level. Scale bar (5µm) applicable to all panels. (B) Representative trace showing signal intensity of Con A plasma membrane marker (green) and VGSCβ1 (red) immunofluorescence along plasma membrane from typical cells incubated (24 h) in normoxic conditions (Figure 3.27A). (C) Representative trace showing signal intensity of Con A plasma membrane marker and VGSCβ1 immunofluorescence along plasma membrane from typical cells incubated (24 h) in hypoxic conditions (Figure 3.27A). Dotted gray lines indicate mean VGSCβ1 fluorescence. (D) Bar diagram showing level of VGSCβ1 protein immunoreactivity along plasma membrane as a immunoreactivity (AU) per µm. Un-paired student t-test was used for statistic analysis. Data are presented as means ± SEM (n = 86). Significance: (x) $p > 0.05$.

% O_2) treatment (15562 ± 645 AU and 14197 ± 1203 AU, respectively; $p > 0.05$; n = 92; Figure 3.28).

3.2.2.6.3 Subcellular distribution

Quantification of VGSCβ1 protein distribution by 'straight line profile' analysis of XYZ scans of Mat-LyLu cells revealed that relative plasma membrane and intracellular VGSCβ1 distribution was not affected by 24 h hypoxic (2 % O_2) treatment (13.5 ± 0.5 % and 14.0 ± 0.7 % respectively; $p > 0.05$; n = 63; Figure 3.29). This result was consistent with the outcome of the "free form line profile" and "area histogram" analyses.

3.2.2.7 Studies on metastatic cell behaviours

3.2.2.7.1 Lateral motility

Effect of hypoxia on lateral motility of Mat-LyLu cells was studied using wound-heal assay. Chronic treatment (24 h) with hypoxia did not change Mat-LyLu motility index (MoI: 0.74 ± 0.11 and 0.75 ± 0.10, respectively; $p > 0.05$; n = 5; Figures 3.30A&B). In addition, 1 μM TTX treatment did not have effect on motility of Mat-LyLu cells under both normoxic and hypoxic conditions (MoI: 0.74 ± 0.11 and 0.68 ± 0.09, respectively; $p > 0.05$; n = 5; Figure 3.30A&B). In order to control for consistency of wound size, initial wound width were measured and plotted in Figure 3.30C. All wounds were 0.5 to 0.8 mm wide; there was no significant difference in the initial wound widths in all conditions tested (Figure 3.30C).

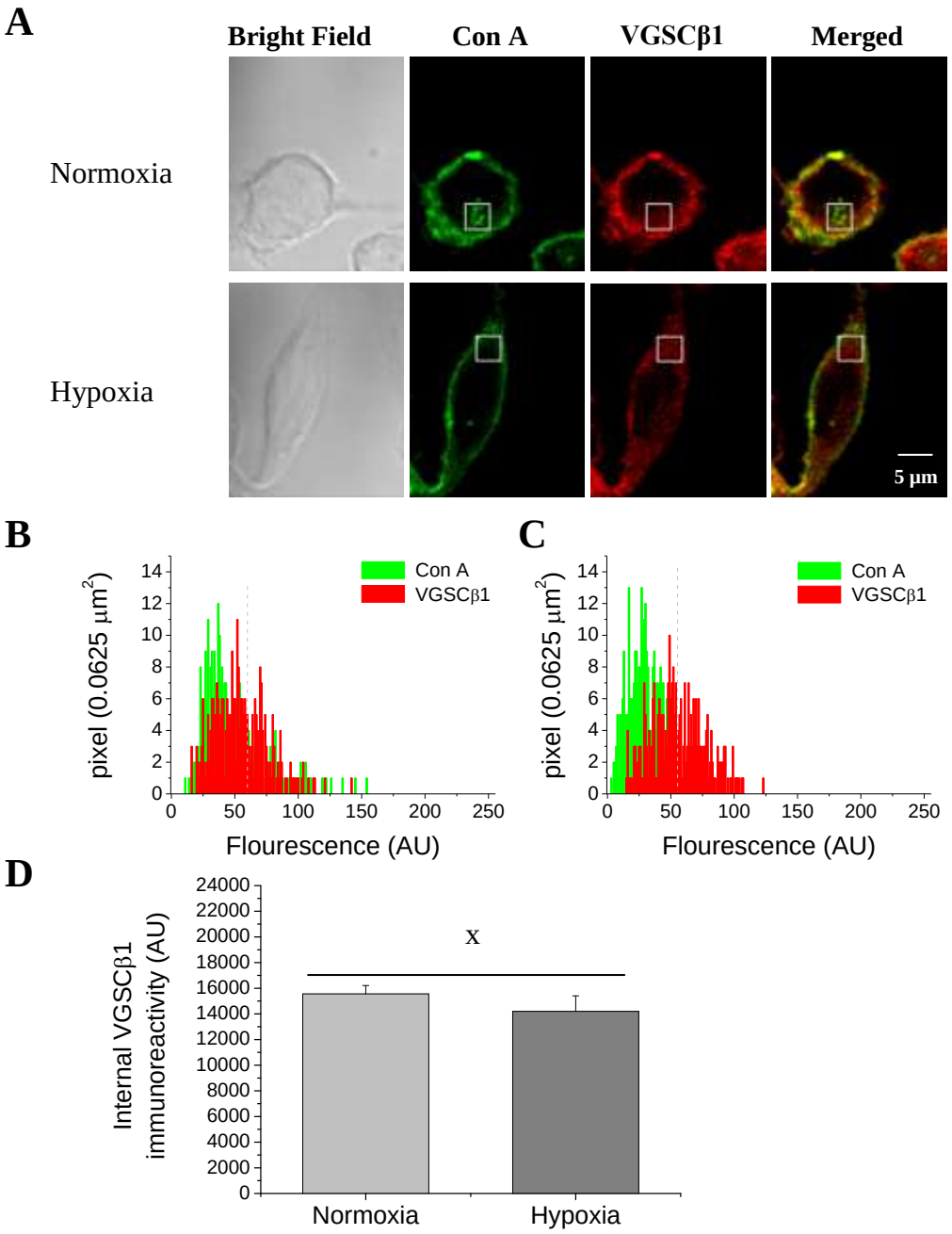


Figure 3.28 Effect of hypoxia (2 % O_2) on internal VGSCβ1 protein levels of Mat-LyLu cells.

(A) Typical XYZ confocal images of Mat-LyLu cells incubated 24 h under normoxic and hypoxic conditions. White box indicates typical area covering 16 µm^2 square section of cytoplasm avoiding nucleus to measure internal protein level. Scale bar (5µm) applicable to all panels. (B) Representative histogram showing distribution of pixels (0.0625 µm^2) with signal intensity of Con A plasma membrane marker (green) and VGSCβ1 (red) immunofluorescence in cytoplasm from typical cells incubated (24 h) in normoxic conditions (Figure 3.28A). (C) Representative histogram showing distribution of signal intensity of Con A plasma membrane marker (green) and VGSCβ1 (red) immunofluorescence in cytoplasm from typical cells incubated (24 h) in hypoxic conditions (Figure 3.28A). Dotted gray lines indicate mean pan-VGSC fluorescence. (D) Chart showing internal VGSCβ1 protein immunoreactivity (AU). Un-paired student t-test was used for statistic analysis. Data are presented as means ± SEM (*n* = 92). Significance: (x) p > 0.05.

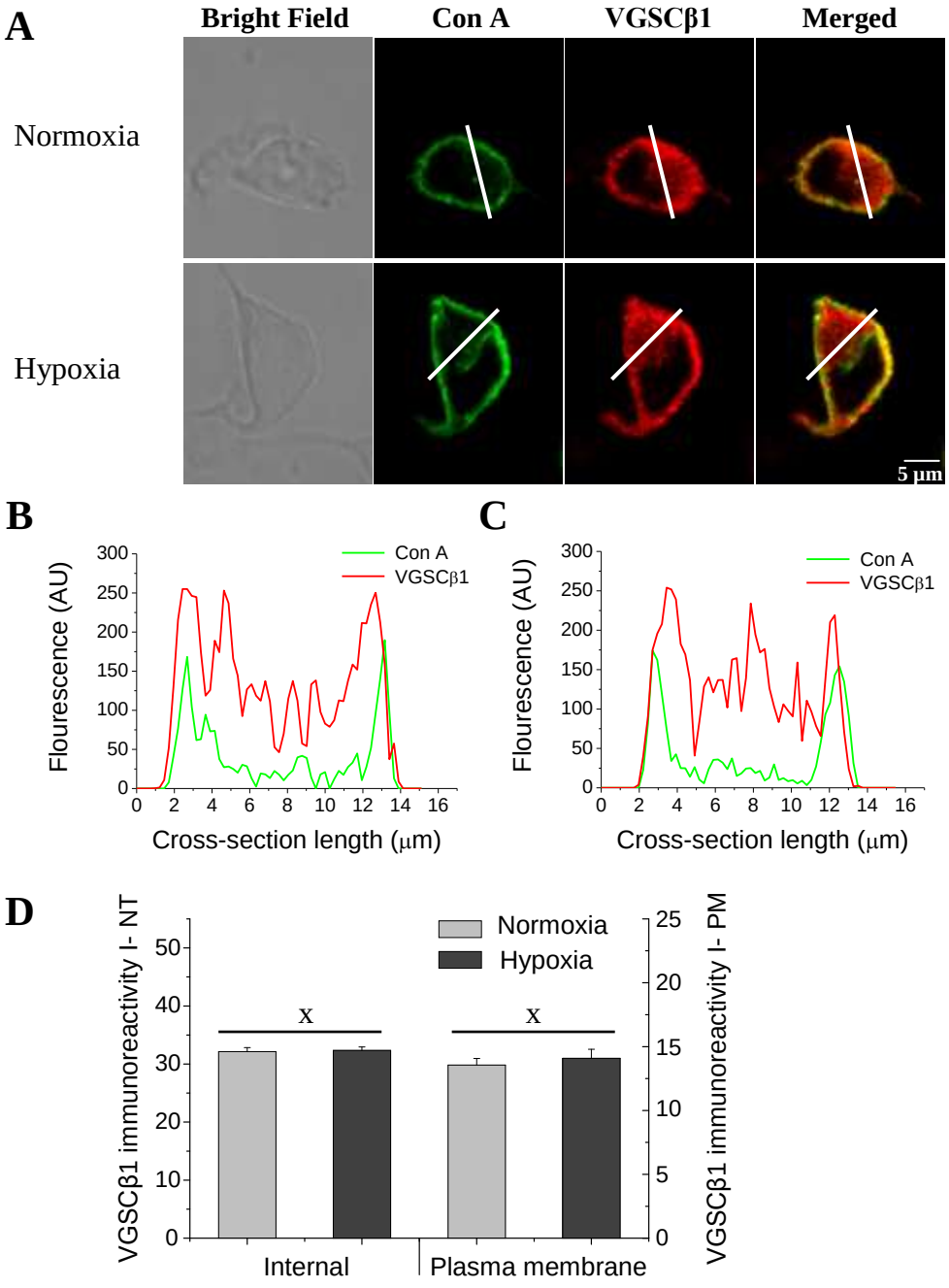


Figure 3.29 Effect of hypoxia (2 % O_2) on VGSCβ1 protein distribution along typical cellular cross-section in Mat-LyLu cells.
(A) Typical XYZ confocal images of Mat-LyLu cells incubated 24 h under normoxic and hypoxic conditions. White line indicates typical cross-section. Scale bar (5µm) applicable to all panels. (B) Representative trace showing signal intensity of Con A plasma membrane marker (green) and VGSCβ1 immunofluorescence (red) along cross-section from typical cells incubated (24 h) in normoxic conditions (Figure 3.26A). (C) Representative trace showing signal intensity of Con A plasma membrane marker and VGSCβ1 immunofluorescence along cross-section from typical cells incubated (24 h) in hypoxic conditions (Figure 3.26A). (D) Bar diagram showing distribution of VGSCβ1 protein immunoreactivity along subcellular cross-sections as a percentage of total (%). For plasma membrane (PM) immunoreactivity, 1.5 µm sections was measured inward from the edge of Con A staining. For internal (INT) immunoreactivity, middle 30 % of the cross-section was measured. Un-paired student t-test was used for statistic analysis. Data are presented as means ± SEM (n = 63). Significance: (X) $p > 0.05$.

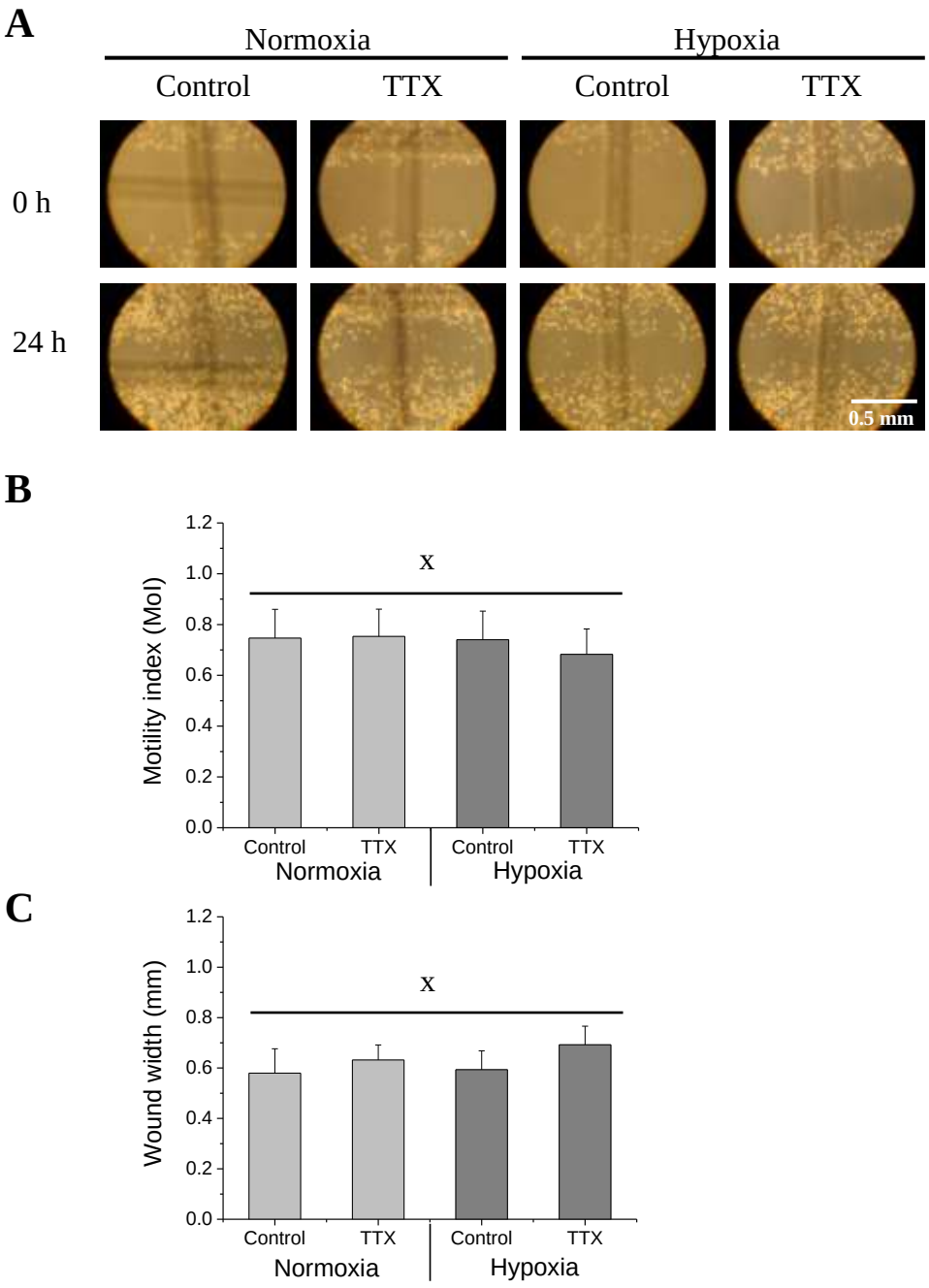


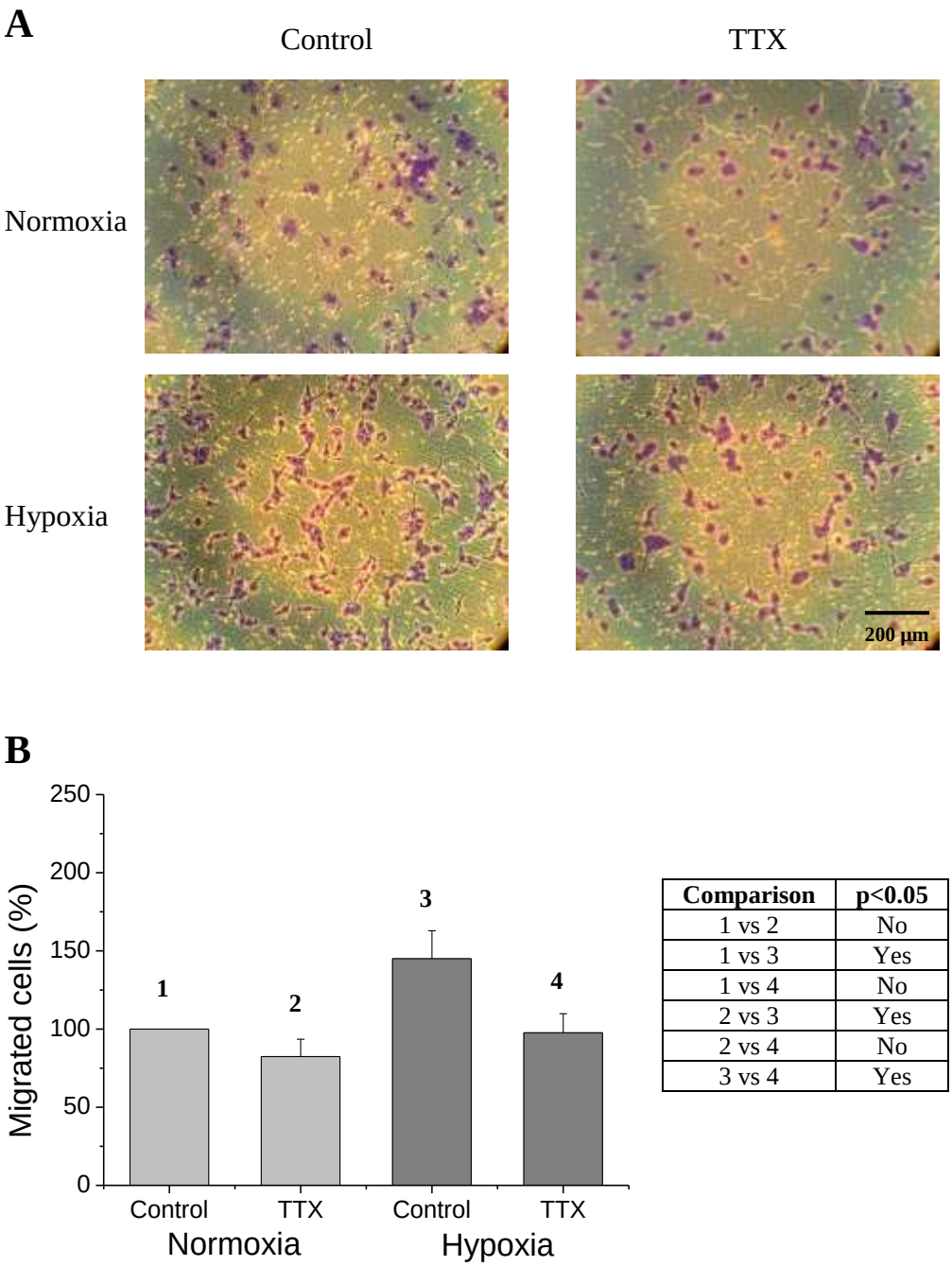
Figure 3.30 Effect of hypoxia (2 % O_2) on lateral motility of Mat-LyLu cells.
(A) Typical phase-contrast light-microscopy images obtained from wound-heal assay of Mat-LyLu cells incubated 24 h under normoxic and hypoxic conditions ± TTX (1 µM). Scale bar (0.5 mm) applicable to all panels. (B) Bar diagram showing motility index of Mat-LyLu cells, incubated in normoxia and hypoxia ± TTX (1 µM) for 24 h. (C) Bar diagram showing width of the wounds at 0 h of wound-heal assay. Data were analysed by analysis of variance followed by Newman-Keuls post hoc analysis. Data are presented as means ± SEM (n = 5). Significance: (x) $p > 0.05$.

3.2.2.7.2 Transwell migration

Transwell assays were used to study the effect of hypoxia on Mat-LyLu cell migration. Long-term treatment (24 h) with hypoxia significantly increased migration by 45 % ($p < 0.05$; $n = 9$; Figures 3.31). TTX (1 µM) treatment (24 h) did not change number of migrated Mat-LyLu cells under normoxic conditions ($p > 0.05$; $n = 9$; Figures 3.31). On the other hand, TTX (1 µM) treatment significantly decreased migrated cell number from 145 ± 17 % to 97 ± 12 % under hypoxic conditions ($p < 0.05$; $n = 9$; Figures 3.31). Interestingly, there was no difference between the migrated cell numbers for TTX treatment under hypoxic condition and the control condition in normoxia ($p > 0.05$; $n = 9$; Figures 3.31). Under hypoxic conditions TTX reduced migrated cell numbers to normoxic control levels ($p > 0.05$; $n = 9$; Figures 3.31).

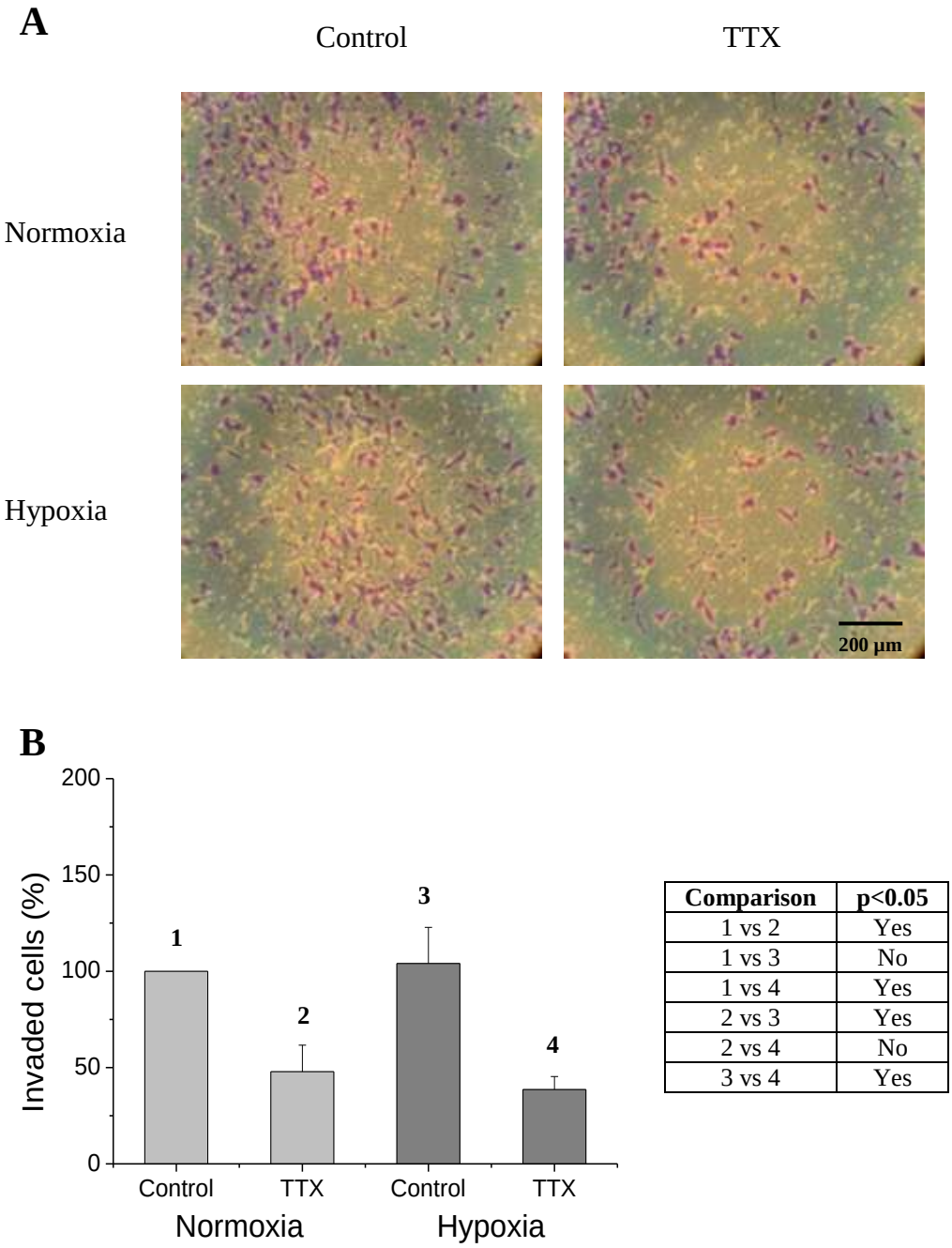
3.2.2.7.3 Matrigel™ invasion

Matrigel™ invasion assay was used to study effect of hypoxia on invasion of the Mat-LyLu cells. TTX (1 µM) significantly decreased invasion of Mat-LyLu cells under normoxic conditions to 47 ± 13 % of control ($p < 0.05$; $n \geq 4$; Figures 3.32). When Mat-LyLu cells were incubated under hypoxic conditions, the number of invaded cells was not changed (100 % and 104 ± 18 %, respectively; $p > 0.05$; $n = 8$; Figures 3.32). However, invasion of Mat-LyLu cells incubated under hypoxic conditions significantly decreased when treated with 1 µM TTX (104 ± 18 % and 38 ± 6 % respectively; $p > 0.05$; $n \geq 4$; Figures 3.32).



Comparison	p<0.05
1 vs 2	No
1 vs 3	Yes
1 vs 4	No
2 vs 3	Yes
2 vs 4	No
3 vs 4	Yes

Figure 3.31 Effect of hypoxia (2 % O_2) on migration of Mat-LyLu cells.
(A) Typical phase-contrast light-microscopy images of migrated cells obtained from transwell migration assay of Mat-LyLu cells incubated 24 h under normoxic and hypoxic conditions ± TTX (1 µM). Migrated cells were fixed and stained with crystal violet (purple). Scale bar (200 µm) applicable to all panels. (B) Histogram showing number of migrated Mat-LyLu cells, incubated in normoxia and hypoxia ± TTX (1 µM) for 24 h. Data were expressed as % relative to the control and presented as means ± SEM (*n* = 9). Data were analysed by ANOVA followed by Newman-Keuls *post hoc* analysis. Inset: table of multiple comparisons between treatments for statistical significance.



Comparison	p<0.05
1 vs 2	Yes
1 vs 3	No
1 vs 4	Yes
2 vs 3	Yes
2 vs 4	No
3 vs 4	Yes

Figure 3.32 Effect of hypoxia (2 % O_2) on invasion of Mat-LyLu cells.
(A) Typical phase-contrast light-microscopy images of invaded cells obtained from Matrigel™ invasion assays of Mat-LyLu cells incubated 24 h under normoxic and hypoxic conditions ± TTX (1 µM). Invaded cells were fixed and stained with crystal violet (purple). Scale bar (200 µm) applicable to all panels. (B) Bar diagram showing number of invaded Mat-LyLu cells, incubated in normoxia and hypoxia ± TTX (1 µM) for 24 h. Data were expressed as % relative to the control and presented as means ± SEM ($n \geq 4$). Data were analysed by ANOVA followed by Newman-Keuls *post hoc* analysis. Inset: table of multiple comparisons between treatments for statistical significance.

3.3 Discussion

The main findings of this study are as follows: (1) 24 h hypoxia or blocking VGSC activity with TTX (1 μM) did not affect the relative proportions of morphological subtypes (non-process bearing, monopolar, bipolar and multipolar) of Mat-LyLu cells. (2) Chronic hypoxia increased cell body diameter, whilst TTX had no effect. (3) Hypoxia decreased Mat-LyLu cell number when incubated for 48 - 72 h. (4) No effect of hypoxia was observed on proliferation of AT2 cells up to 72 h. (5) TTX had no effect on proliferation of both Mat-LyLu and AT2 cells. (6) Nav1.7 mRNA expression was increased after 24 h hypoxic treatment. (7) VGSCβ1 was the predominant subunit expressed in both AT2 and Mat-LyLu cells. (8) Hypoxia increased VGSCβ1 mRNA expression in both Mat-LyLu and AT2 cells. (9) Hypoxia decreased both internal and plasma membrane VGSCα protein level. (10) Hypoxia (24 h) had no effect on VGSCβ1 protein level. (11) Both hypoxia and TTX (1 μM) had no effect on lateral motility. (12) TTX (1 μM) had no effect on transverse migration under normoxic conditions. (13) Hypoxia increased Mat-LyLu cell transverse migration and TTX (1 μM) decreased it to normoxic levels. (14) Hypoxia had no effect on Mat-LyLu cell invasion but TTX (1 μM) decreased invasion under both normoxic and hypoxic conditions.

3.3.1 Effect of hypoxia on morphological development

Previously, it was reported that 72 h of hypoxia (3 % O_2) caused 'loosening' of cell contact and scattering from cell clusters of human hepatoblastoma, pancreatic cancer, colon cancer and breast cancer cells (Cannito *et al.,* 2008). However, no obvious such change in two dimensional distribution of Mat-LyLu and AT2 cells was

observed when treated with hypoxia (2 % O_2) for 24 h and 48 h. In addition, TTX had no effect on distribution of these cells both in hypoxia and normoxia.

Both Mat-LyLu and AT2 cells have extensive morphological heterogeneity. This heterogeneity was assessed by sub-dividing cells according their process number. No change in percentage of non-process bearing, monopolar, bipolar and multipolar cells was detected up to 48 h hypoxic treatment. In addition, blocking VGSC activity with TTX under hypoxic and normoxic conditions for 24 h had no effect on the morphological heterogeneity. However 48 hypoxia + TTX (1 µM) treatment significantly decreased percentage of monopolar cells. This was probably caused by the decrease in cell number with 48 h hypoxic treatment, which will be discussed in section 3.3.2.

It has been proposed that morphological change from epithelial to a spindle-shaped and fibroblast like morphology can be correlated with aggressiveness of cancer (Thiery, 2002). Furthermore, hypoxic transition to fibroblast like morphology was observed in various cancer cells such as human hepatoblastoma, pancreatic cancer, colon cancer and breast cancer cells (Cannito *et al.*, 2008; Lester *et al.*, 2007). A small, but significant increase in cell body diameter of Mat-LyLu cells treated with 24 h and 48 h hypoxia (2 % O_2) was detected. In addition, 48 h, but not 24 h, hypoxia increased Mat-LyLu cell size. Process length and process thickness were not affected by hypoxia (24 h and 48 h). Therefore, we can speculate that Mat-LyLu rat prostate cancer cell morphology did not change to fibroblast-like morphology with hypoxic treatment as was observed in other cancer cells. TTX (1 µM) had no effect on cell morphology in both hypoxic and normoxic conditions. The only exception was process thickness where 24 h hypoxia + TTX treatment increased process thickness slightly but significantly. On the other hand, a role for VGSC in

morphological development was established for Mat-LyLu cells by Fraser *et al.* (1999). It was shown that blocking VGSC with 6 µM TTX decreased cell process length and increased cell body diameter and process thickness (Fraser *et al.*, 1999). TTX (6 µM) used in Fraser *et al.* (1999) experiment was well above the necessary dose required to obtain complete blockage of Nav1.7. Therefore, we can speculate that morphologic effect seen by Fraser *et al.* (1999) can be caused by the high concentration of TTX used. In the same experiment, the cells were fixed by paraformaldehyde and stained by toluidine blue; on the other hand, in the current study morphological analyses were carried on images taken from live cells.

3.3.2 Effect of hypoxia on proliferation

Weakly metastatic rat prostate cancer AT2 cells were not affected by hypoxia up to 72 h. Incubation of Mat-LyLu cells in hypoxia for 24 h did not change the cell number. However, 48 h and 72 h hypoxia decreased Mat-LyLu cell number significantly compared to normoxia. Consistently, Alqawi *et al.* (2007) showed that only 5 % of Mat-LyLu cells survive after 3 weeks of hypoxia (1 % O_2). In addition, a decrease in human prostate cancer cell number after 72 h hypoxia (1 % O_2) was reported by Ackerstaff *et al.* (2007). Similarly, no change in tongue squamous carcinoma cell proliferation was observed at 24 h hypoxia but a decrease of proliferation was reported after 48 h and 72 h (Song *et al.*, 2009). On the other hand, no significant change in human hepatoblastoma, pancreatic cancer, colon cancer and breast cancer cell number was reported when treated with 72 h hypoxia (3 % O_2) (Cannito *et al.*, 2008). In the case of human prostate cancer, PC3 cells, Ackerstaff *et al.* (2007) proposed that hypoxia mediated down regulation of genes responsible for formation of the "pre-replicative complex".

We then investigated the possible involvement of VGSC activity in control of cell number. No change in AT2 and Mat-LyLu cell numbers was measured when VGSC was blocked by TTX (1 µM) under both hypoxic and normoxic conditions. Similarly, Fraser *et al.* (2000) documented that VGSC had no effect on the proliferation of either cell line. In other cancers also, VGSC activity was found not to affect cellular proliferation, e.g. breast cancer (Fraser *et al.,* 2005). Therefore, we can conclude that decrease in cell number by prolonged hypoxia was not controlled by VGSC activity.

Since hypoxia treatments longer than 24 h reduced cell number, subsequent experiments were restricted to 24h hypoxia, in order not to 'contaminate' any effect e.g. on cell motility. However, we should note that 24 h is still a nominal duration employed under 'model' experimental conditions. In reality, the clinical course of hypoxic (metastatic) tumours would run over months.

3.3.3 Regulation of VGSCα subunit expression by hypoxia

3.3.3.1 Nav1.7 mRNA expression

Nav1.7, the predominant VGSC functionally expressed in rat and human prostate cancer (Mat-LyLu and PC3) cells, was shown to enhance the cells' metastatic potential (Diss *et al.,* 2001; Grimes *et al.,* 1995; Nakajima *et al.,* 2009). The present study confirmed the previous work that strongly metastatic Mat-LyLu, but not the weakly metastatic AT2 cells, express Nav1.7 mRNA (Diss *et al.,* 2001). In Mat-LyLu cells, chronic hypoxia (24 h, 2 % O_2) significantly increased Nav1.7 mRNA levels. Consistently, prolong hypoxia induced increase in VGSCα mRNA level in developing rat cortex tissue (Zhang *et al.,* 2001). In addition, hypoxic regulation of

various ion channel mRNA expression was reported such as: voltage-gated potassium channel α-subunits (Kv1.1, Kv1.2, Kv1.5, Kv2.1, Kv4.3 and Kv9.3) and α_{1H} voltage-gated T type calcium channel (Platoshyn *et al.,* 2001; Conforti and Millhorn, 1997; Del Toro *et al.,* 2003). The mechanism of hypoxic upregulation of Nav1.7 mRNA expression is not known. However, there are several candidate pathways that can regulate gene expression by hypoxia, including: 3`-5` adenosine monophosphate (cAMP) / protein kinase A (PKA), Ca^{2+}-calmodulin, mitogen-activated protein kinase (MAPK) and hypoxia-inducible factors (HIF) pathway. There is evidence to suggest that the cAMP-PKA pathway could be involved in hypoxia mediated increase in Nav1.7 mRNA expression. Accordingly, hypoxia induced increase in PKA activity was reported in bone cells and endothelial cells (Zhang *et al.,* 2010). Offord and Catterall (1989) reported that 8-Br-cAMP, a membrane-permeant analogue of cAMP which activates PKA, increased the VGSC α-subunit mRNA expression in developing rat muscle cells. Conversely, treatment of Mat-LyLu cells with KT5720, a PKA inhibitor, for 48 h decreased Nav1.7 mRNA level (Brackenbury and Djamgoz, 2006). On the other hand, hypoxia induced HIF1α independent changes in genome-wide DNA methylation and histone acetylation, also known to regulate gene expression, was documented in human prostate cells (Watson *et al.,* 2009). Such genome-wide change in DNA methylation and histone acetylation may affect expression of a large number of genes, including those for ion channels.

3.3.3.2 VGSCα protein expression

Interestingly, increase in Nav1.7 mRNA expression by hypoxia was not reflected in VGSCα protein level. In fact, hypoxia decreased both internal and plasma membrane

VGSC α-subunit levels by ~ 15 %. There is evidence to suggest that mRNA regulation and protein levels can be controlled separately and independently (Orphanides and Reinberg, 2002). Discrepancy between VGSCα mRNA and protein expression in Mat-LyLu cells was also documented previously where TTX-induced decrease in Nav1.7 mRNA expression was not observed in total protein level (Brackenbury and Djamgoz, 2006). Similarly, difference in mRNA and protein expression was reported in a range of other pathophysiological conditions such as rheumatoid arthritis, psoriasis, B-chronic lymphoproliferative disorders (Sola *et al.,* 1999; Schedel *et al.,* 2004; Sano *et al.,* 2005 Gu *et al.,* 2006). It was speculated that this difference in mRNA and protein expression may be because of post-transcriptional disregulation or alterations in protein conformation (Sola *et al.,* 1999; Schedel *et al,* 2004).

Cellular mechanism underlying the decrease in VGSCα protein level is not known. This decrease in VGSCα protein level indicates change in protein turnover which can be because of decrease in protein synthesis and/or increase in protein degradation. Hypoxic reduction of VGSCα level is also reported in turtle brain (Pérez-Pinzón *et al.,* 1992). O'Reilly *et al.,* (1997) proposed that decreased VGSCα activity in hypoxic neuron cells is an adaptive mechanism to increase neuronal tolerance to hypoxia because it would reduce Na^+ influx and this would result in reduction in energy demand when energy supply is diminished during hypoxia.

3.3.3.3 Relative subcellular distribution of VGSC protein

In immunocytochemistry experiments, the relative percentages of intracellular and plasma membrane VGSCα protein levels did not change after 24 h of hypoxic treatment. This is consistent with the results obtained from the absolute

quantifications of intracellular and plasma membrane proteins, i.e. intracellular and plasma membrane VGSCα protein levels decreased similarly by ~ 15 %. These results suggest that the VGSCα protein cytoplasm-plasma membrane recycling, which has a turnover period of some 24 h, was not affected by hypoxia (2 % O_2).

3.3.4 VGSCβ subunit expression in Mat-LyLu and AT2 cells

All of the four known VGSC β-subunits mRNA expression was detected in the weakly metastatic rat prostate cancer cell line, AT2 where VGSCβ1 was the highest expressed subunit followed by VGSCβ3, VGSCβ2 and VGSCβ4. On the other hand, all but VGSCβ3 subunits mRNA expression was detected in strongly metastatic rat prostate cancer cell line, Mat-LyLu; VGSCβ1 was the highest expressed subunit followed by VGSCβ4 and VGSCβ2. High levels of VGSCβ1 mRNA expression in both AT2 and Mat-LyLu cell lines was consistent with previous finding on human prostate cancer cells, human breast cancer cells and human prostate tissue (Diss *et al.,* 2008; Chioni *et al.,* 2009; Candenas *et al.,* 2006). Similar to human prostate tissue, human prostate cancer cells and human breast cancer cells VGSCβ2 expression was low (Diss *et al.,* 2008; Chioni *et al.,* 2009; Candenas *et al.,* 2006). Interestingly, human breast cancer cells frequently express very low levels or no VGSCβ3 mRNA (Chioni *et al.,* 2009; Candenas *et al.,* 2006). VGSCβ4 mRNA expression in both AT2 and Mat-LyLu cell lines was consistent with previous finding on human prostate cancer cells, human breast cancer cells and human prostate tissue (Diss *et al.,* 2008; Chioni *et al.,* 2009; Candenas *et al.,* 2006).

AT2 cells expressed higher VGSCβ subunit mRNA than Mat-LyLu mainly due to higher VGSCβ1 expression. Similar result was documented in human breast cancer cells where weakly metastatic cells have higher VGSCβ expression (Chioni *et*

al., 2009). However, strongly metastatic human prostate cancer cells have higher VGSCβ expression than weakly metastatic cells (Diss *et al.,* 2008). On the other hand, no significance difference was observed between prostate cancer and non-cancerous human prostate tissues (Diss *et al.,* 2008). It is well documented that VGSCβ1 can interact with extracellular matrix proteins, cell adhesion molecules (CAM), cytoskeleton, and functions as CAMs (Isom and Catterall, 1996; Isom, 2002; Undrovinas *et al.,* 1995; Faissner 1997; Srinivasan *et al.,* 1998; Xiao *et al.,* 1999; Peles *et al.,* 1995; Malhotra *et al.,* 2000; Ratcliffe *et al.,* 2000; Isom, 2001; McEwen and Isom, 2004). Reduced adhesiveness in rat prostate cancer, in addition to human prostate and breast cancer cells was associated with higher metastatic potential, i.e. single-cell adhesion of weakly metastatic AT2 cells was lower than adhesion of strongly metastatic Mat-LyLu cells (Palmer *et al.,* 2008). Down regulation of VGSCβ1 with siRNA in weakly metastatic MCF-7 breast cancer cells decreased single-cell adhesion and increased Transwell migration (Chioni *et al.,* 2009). Over expression of VGSCβ1 in strongly metastatic MDA-MB-231 cells increased cell-cell adhesion and decreased lateral motility (Chioni *et al.,* 2009). Therefore, we can speculate, similar to human breast cells, that higher VGSCβ1 expression might be responsible for the higher adhesiveness of AT2 cells. On the other hand, it was shown that down regulation of VGSCβ1 cause increase in VGSCα mRNA expression (Chioni *et al.,* 2009). So, the lower VGSCβ1 expression in Mat-LyLu cells might take part in increased Nav1.7 mRNA expression. In fact, the cytoplasmic domain of VGSCβ1, when cleaved, can regulate gene expression (Brackenbury and Isom, 2008)

Low levels of VGSCβ2 expression were detected in both AT2 and Mat-LyLu cells. Expression of this subunit was not different between these strongly and weakly

metastatic cell lines. This result is consistent with previous finding on human prostate cell lines, where there was no difference in VGSCβ2 mRNA expression between strongly and weakly metastatic human prostate cancer cells, PNT2-C2, LnCaP, PC3 and PC3M (Diss *et al.,* 2008). Furthermore, a similar result was obtained in *in vivo* experiments on human tissues by Diss *et al.,* (2008). However, strongly metastatic MDA-MB-231 breast cancer cells have higher VGSCβ2 mRNA than weakly metastatic MCF-7 breast cancer cell line (Chioni *et al.,* 2009). VGSCβ2 was reported to regulate functional expression of VGSC α-subunit, channel gating, channel conductance and translocation of the channel (Isom *et al.,* 1995; Cruz *et al.,* 1999; Chen *et al.,* 2002; Pertin *et al.,* 2005). Therefore, VGSCβ2 expression in Mat-LyLu cells might be involved in regulation of VGSC expression / functioning.

VGSCβ3 mRNA expression was detected in AT2 cells but not in Mat-LyLu cells. A low level mRNA expression of this subunit was reported in human prostate cell lines, PNT2-C2, LnCaP, PC3 and PC-3M where no difference in expression between strongly and weakly metastatic cells was observed (Diss *et al.,* 2008). In the same study, no difference in VGSCβ3 mRNA expression was detected between prostate cancer and non-cancerous prostate tissue. However, Candenas *et al.,* (2006) did not find VGSCβ3 mRNA expression in human prostate tissue. In addition, similar to Mat-LyLu cells, no expression of VGSCβ3 was detected in human breast cancer cells. Interestingly, VGSCβ3 expression was correlated with p53 oncogene expression (Adachi *et al.,* 2004). VGSCβ3 gene contains two p53-response elements and was upregulated by overexpression of p53 (Adachi *et al.,* 2004). Thus, VGSCβ3 is a target gene for p53 and its minimised expression may give metastatic cancer cells an advantage against apoptosis, i.e. it is possible that diminishing VGSCβ3 expression may contribute to metastatic transformation.

A low level of VGSCβ4 mRNA expression was detected in both AT2 and Mat-LyLu cells, latter having higher expression. Studies on human prostate and breast cancer cell lines showed higher VGSCβ4 mRNA expression in weakly metastatic cell lines compared to strongly metastatic cell lines (Chioni *et al.,* 2009; Diss *et al.,* 2008). On the other hand, no difference in VGSCβ4 mRNA expression was detected between human prostate cancer and non-cancerous tissues (Diss *et al.,* 2008). VGSCβ4 was associated with changing activation voltage of Nav1.2 and Nav1.4 and was predicted to associate with extracellular matrix and CAMs (Yu *et al.,* 2003).

Further functiona studies are required to determine the possible pathophysiological role of VGSCβ expression in cancer and metastatic disease.

3.3.5 Regulation of VGSCβ expression by hypoxia

3.3.5.1 VGSCβ mRNA expression

Long-term hypoxia (24 h, 2 % O_2) increased VGSCβ1 mRNA expression of both weakly and strongly metastatic rat prostate cancer cell lines, AT2 and Mat-LyLu, respectively. The mechanism(s) underlying VGSCβ1 mRNA regulation in rat prostate cancer is not known. As discussed earlier, hypoxia may affect a number of signalling pathways in addition to genome-wide changes in methylation and acetilation (Seta *et al.,* 2002; Watson *et al.,* 2009). In addition, increase in VGSCβ1 mRNA expression in both strongly and weakly metastatic cell lines indicate that hypoxia influences similar mechanisms in these cell lines.

VGSCβ2 expression of Mat-LyLu cells was not affected by 24 h hypoxic treatment. On the other hand, VGSCβ2 mRNA level was elevated by 24 h hypoxic

treatment in AT2 cells. Hypoxia had no effect on VGSCβ3 mRNA expression of AT2 cells. No change in VGSCβ3 expression was observed in Mat-LyLu cells. VGSCβ4 subunit mRNA level of Mat-LyLu cells was not affected by chronic hypoxia. However, increase in VGSCβ4 was documented in AT2 cells in this study. It is evident from this result that VGSC β2, β3 and β4 subunit mRNA expressions were controlled differentially in weakly and strongly metastatic rat prostate cells and could result in different functional components, assuming that the mRNA changes were reflected at protein level.

3.3.5.2 VGSCβ1 protein expression

In this study, VGSCβ1 subunit protein expression was studied since this was found to be the predominant VGSCβ subunit expressed in rat prostate cancer, human prostate cancer and human breast cancer cell lines was VGSCβ1 (Chioni *et al.*, 2009; Diss *et al.*, 2008). Unfortunately, antibodies for VGSCβ2, VGSCβ3 and VGSCβ4 were not readily available. Interestingly, increase in VGSCβ1 mRNA expression by hypoxia was not reflected in VGSCβ1 protein level in Mat-LyLu cells. Hypoxia had no effect on both intracellular and plasma membrane levels of VGSCβ1 protein. As discussed previously, mRNA and protein levels can be controlled separately and independently (e.g. Orphanides and Reinberg, 2002).

3.3.5.3 Relative subcellular distribution of VGSCβ1 protein

The relative percentages of intracellular and plasma membrane VGSCβ1 protein levels did not change after 24 h hypoxic treatment. This is consistent with results obtained from ‘absolute’ quantification of intracellular and plasma membrane protein

levels, which also did not show any change. These results suggested that VGSCβ1 cytoplasm-plasma membrane protein cycling was not affected by hypoxia (2 % O_2).

3.3.6 Hypoxic regulation of metastatic activity of Mat-LyLu cells and possible involvement of VGSC activity

3.3.6.1 Lateral motility

It was reported that hypoxia (48 h) changed expression of various genes related to cellular motility in human prostate cancer PC3 cells (Ackerstaff *et al.,* 2007). In that study, upregulation of 8 genes and down regulation of 10 genes related to motility were detected. However, we found that lateral motility of Mat-LyLu cells was unchanged with 24 h hypoxia. In addition, no report on effect of hypoxia on lateral motility was found. Blocking VGSC for 24 h had no effect on lateral motility of Mat-LyLu cells in both hypoxic and normoxic conditions. On the other hand, previously, Fraser *et al.* (2003) suggested that functional VGSC expression enhances lateral motility. However, their results were based on assays lasting 48 h and no data was reported for 24 h TTX treatment. Taken together, these results would suggest that regulation of lateral motility by VGSC activity and the effect of hypoxia are time-dependent process.

3.3.6.2 Transverse migration

Increase in migration by hypoxia was reported previously for MDA-MB-231, MDA-MB-468, MCF7 and 4T1 breast cancer model cells (Cronin *et al.,* 2010, Lester *et al.,* 2007). In the present study, we also found that 24 h hypoxic treatment of Mat-LyLu

cells enhanced migration. This increase in migration was reduced to normoxic control levels when VGSC activity was blocked by TTX. However, blocking VGSC activity had no effect on migration in normoxic conditions. In contrast, Brackenbury and Djamgoz (2006) reported decrease of migration with TTX treatment in normoxic conditions. These contradicting results were probably caused by experimental conditions. Brackenbury and Djamgoz (2006) used 12 µm-pore Transwell filters in migration assay but 8 µm-pores Transwell filters were used in this study since former was no longer commercially available. It was also shown that serum factors may be required for VGSC dependent potentiation of migration where in presence of 0 % FBS TTX had no effect on Mat-LyLu cell migration (Brackenbury and Djamgoz 2007). Clearly, the increase in migration by hypoxia depended on VGSC activity. Accordingly, Onkal (2010) showed that hypoxia (2 % O_2, 24 h) significantly increased Na^+ peak current density in Mat-LyLu cells, so a follow-on increase in I_{NaT} may be expected (Appendix 1). In addition, it was previously reported that hypoxia increased I_{NaP} amplitude in neurons and cardiac cells (Hammarström and Gage 1998; Ju *et al.*, 1996). Although a small decrease in VGSC protein level was detected, hypoxic increase in I_{NaP} or I_{NAT} could be the reason for the VGSC-dependent increase in migration.

3.3.6.3 Matrigel™ invasion

Hypoxic treatment for 24 h did not have any affect on the invasion of Mat-LyLu cells. Consistently, Alqawi *et al.* (2007) reported that 5 h hypoxia (1 % O_2) did not effect invasion of Mat-LyLu cells. However in that study, increased invasion was reported for a hypoxia-resistant sub-clone of Mat-LyLu, surviving 8 weeks of hypoxia (1 % O_2). Watson *et al.* (2009) also reported increased invasiveness of a

hypoxia-resistant sub-clone of PwR-1E benign prostate epithelial cells maintained for 14 weeks in hypoxia. In contrast, Ackerstaff *et al.* (2007) reported decreased invasiveness of PC3 human prostate cancer cells after 72 h of hypoxia (1 % O_2). However, in the same study the cell number was found to decrease with hypoxia, which could explain the decrease in invasion capability. In addition to prostate cancer, many other studies on various type of cancer cell showed change in invasion by hypoxia. However, there is no general consensus on the direction of this effect. Increase of invasion with hypoxia was reported for MDA-MB-231, MDA-MB-468, MCF7 and 4T1 breast cancer cells, HCT116 and HT-29 human colon carcinoma, HepG2 human hepatoblastoma and PANC-1 pancreatic carcinoma cells (Cronin *et al.,* 2010; Lester *et al.,* 2007; Graham *et al.,* 1999, Krishnamachary *et al.,* 2003). On the other hand, no affect of hypoxia on invasion was reported for SiHa human cervical cancer, U2-OS human osteosarcoma cells, OW-1, SAU and SKA ovarian cancer cells (Pennacchietti *et al.,* 2003; Krtolica and Ludlow 1996). Decrease of invasion with hypoxic treatment was documented for choriocarcinoma cells (Sato *et al.,* 2002). Taking into account all these results, we can conclude that hypoxic regulation of invasion can change from one cancer type to another and may be time dependent.

Blocking VGSC with TTX decreased invasion of MatLyLu cells both in normoxic and hypoxic conditions. Similarly, role of VGSC on invasion of prostate cancer was extensively studied previously under normoxic conditions (Grimes *et al.,* 1995; Laniado *et al.,* 1997; Smith *et al.,* 1998; Bennett *et al.,* 2004; Nakajima *et al*.,2009). Bennett and colleagues (2004) proposed that functional expression of VGSC is “necessary and sufficient” for prostate cancer cell invasion. In the case of human strongly metastatic breast cancer cells, VGSC activity dependent increase in

invasiveness was proposed to be due to control of pH-dependent activation of cysteine cathepsins (Gillet *et al.,* 2009). Such an effect could explain why a role of VGSC activity in lateral motility and transverse migration was not always seen.

3.4 Concluding remarks

In the present study, we found differential regulation of mRNA and protein expression of VGSC α- and β1- subunit of Mat-LyLu cells when incubated in hypoxic conditions (24 h; 2 % O_2). Hypoxia increased both VGSC α- and β1- subunit mRNA expression but decreased or not effected the protein expression, respectively. No major effect of hypoxia on cell morphology was observed. In addition, hypoxia did not affect lateral motility and matrigel invasion of Mat-LyLu cells. On the other hand, VGSC activity-dependent enhancement of transverse migration was documented by chronic hypoxia (24 h; 2 % O_2). In overall conclusion, therefore, hypoxia mediated increase in transverse migration of Mat-LyLu cells was caused, at least in part, by increased VGSC activity which was probably regulated at a post-transcriptional level.

Chapter 4

EFFECTS OF PHARMACOLOGICAL BLOCKERS ON VOLTAGE-GATED Na^+ CHANNEL EXPRESSION AND METASTATIC CELL BEHAVIOURS OF DUNNING PROSTATE CANCER

4.1 Introduction

Functional expression of VGSCs has been associated with metastatic carcinomas as reviewed in Chapter 1 - General Introduction (also, Grimes *et al.,* 1995; Blandino *et al.,* 1995; Laniado *et al.,* 1997; Allen *et al.,* 1997; Grimes and Djamgoz, 1998; Abdul and Hoosein, 2002; Roger *et al.,* 2003; Fraser *et al.,* 2004; Ou *et al.,* 2005; Fraser *et al.,* 2005; Onganer and Djamgoz, 2005; Onganer *et al.,* 2005; Brackenbury and Djamgoz, 2006; Fulgenzi *et al.,* 2006; Roger *et al.,* 2007; Diaz *et al.,* 2007; Nakajima *et al.,* 2009; Gao *et al.,* 2009; Gao *et al.,* 2010; House *et al.,* 2010). It was reported that VGSC activity in rat strongly metastatic prostate cancer (PCa) Mat-LyLu cells can auto-regulate mRNA expression and protein trafficking via a positive feedback mechanism (Brackenbury and Djamgoz, 2006). In addition, VGSC activity was reported to contribute positively metastatic cell behaviours (MCBs), such as galvanotaxis, lateral motility, endocytotic membrane activity, transverse migration and invasion (Brackenbury and Djamgoz, 2006; Gillet *et al.,* 2009; Nakajima *et al.,* 2009; Fraser *et al.,* 2003; Mycielska *et al.,* 2003; Djamgoz *et al.,* 2001; Krasowska *et al.,* 2004; Grimes *et al.,* 1995; Laniado *et al.,* 1997; Smith *et al.,* 1998; Bennett *et al.,* 2004). Indeed, it was proposed that functional expression of VGSC is "necessary and sufficient" for cellular invasiveness in PCa (Bennett *et al.,* 2004). Finally, House *et al*. (2010) recently showed that functional VGSCs (Nav1.5) are a key regulator of invasiveness in colon cancer.

Because of their VGSC blocking activity, various pharmacological agents, including ranolazine, riluzole, procaine and lidocaine, have been used to treat a variety of pathological conditions, such as chronic angina, amyotropic lateral sclerosis, painful diabetic polyneuropathies, neuralgic pain and traumatic peripheral nerve injuries (Maier, 2009; Bensimon *et al.,* 1994; Lacomblez *et al.,* 2996). The

antianginal effect of ranolazine is thought to be through blockage of I_{NaP} (Antzelevitch *et al.,* 2004; Fredj *et al.,* 2006). Similarly, the neuroprotective property of riluzole was attributed to its ability to block I_{NaP} (Urbani and Belluzi, 2000; Zona *et al*., 1998). It was also proposed that I_{NaP} is more sensitive to VGSC blockers lidocaine and TTX than I_{NaT} in neurons (Hammarström and Gage, 1998). There is also some evidence that lidocaine and procaine may block embryonic VGSCs more than adult (Ribeiro and Costa, 2003). Ranolazine was proposed as a therapeutical agent in treatment of haematological malignancies and riluzole was suggested as a drug for advanced melanoma treatment (Samudio *et al.,* 2010; Le *et al.,* 2010). In addition, procaine was suggested as potential candidate for breast cancer therapy because of its reported anti-proliferative effects (Villar-Garea *et al.,* 2003). Procaine was also shown to enhance anti-tumoral activities of drugs used in cancer therapy (Chlebowski *et al.,* 1982; Esposito *et al.,* 1990; Viale *et al.,* 1998; Mizuno and Ishida, 1982). Furthermore, procaine and lidocaine were reported to radiosensitize hypoxic murine L5178Y cells (Yau and Kim, 1980). These findings would further suggest that clinical VGSC blockers could ultimately be useful as anti-cancer drugs.

Hypoxia occurs in many human solid cancers, including PCa, as tumours grow (Vaupel *et al.,* 2007; Harrison and Blackwell, 2004). Significant correlation with tissue hypoxia and clinical stage was reported in PCa (Movsas *et al.,* 2000). Development of hypoxia in growing tumours is crucial for inducing 'global' changes in gene expression, metabolic phenotype, ion haemostasis and, finally, angiogenesis (Higgins *et al.,* 2009; Ackerstaff *et al.,* 2007; Watson *et al.,* 2009, Haigney *et al.,* 1994; Xiao and Allen, 1999).

Interestingly, hypoxia can modulate VGSC activity by affecting channel gating by conformational changes caused by formation or disruption of

intermolecular disulfides (Hammarström and Gage, 2002). Accordingly, hypoxia induced increase in "persistent Na^+ current" (I_{NaP}) was reported in neurons and cardiac cells (Ju *et al*., 1996; Hammarström and Gage, 2002; Wang *et al.,* 2007). On the other hand, hypoxia reduced "transient Na^+ current" (I_{NaT}) in neurons and myocytes (Hammarström and Gage, 2002; Wang *et al.,* 2007). It was also reported that intracellular Na^+ concentration increased by hypoxia (Haigney *et al.,* 1994; Xiao and Allen, 1999).

In the light of these findings, it was hypothesised that targeting VGSC could be a novel and effective strategy to reduce metastatic potential of PCa. Therefore, in this chapter we proposed that pharmacological VGSC blockers, that are currently being used as 'safe' clinical drugs, could be used to decrease MCBs of PCa. In addition, tissue O_2 level could modify the effect of these drugs, since tissue O_2 level would affect VGSC activity.

4.1.1 Aims and scope of the present study

The main aim of this study was to evaluate possible effects of key pharmacological blockers on VGSCα expression and involvement in MCBs in the strongly metastatic rat PCa model, Mat-LyLu cells. The specific aims were as follows:

1. To test if ranolazine, riluzole (blockers of I_{NaP}) , procaine and lidocaine (general VGSC blockers) could regulate VGSCα mRNA and protein levels in normoxic and hypoxic conditions; and
2. To determine the possible effects of these pharmacological blockers on Matrigel™ invasion in normoxic and hypoxic conditions.

4.2 Results

Hypoxia treatments longer than 24 h reduced cell number, therefore all experiments were restricted to 24 h treatment, in order not to 'contaminate' any effect on Matrigel invasion. In addition, many previous experiments have been carried out using 24 h hypoxia (Ghafer *et al.,* 2003; Franovic *et al.,* 2007; Chen *et al.,* 2010; Dai *et al.,* 2011).

4.2.1 Effects of ranolazine

Ranolazine has been used extensively as an inhibitor of VGSC persistent currents, although it has a range of actions, depending on concentration (Chen *et al.,* 2009; Samudio *et al.,* 2010; Rajamani *et al.,* 2008; Antzelevitch *et al.,* 2004; Clarke *et al.,* 1996). In the present study, it was used in the concentration range 20 to 300 µM, since in this concentration range, ranolazine was shown to block I_{NaP} more effectively than I_{NaT} (Antzelevitch *et al.,* 2004).

4.2.1.1 Some initial observations: Cell morphology

No change in the basic appearance or distribution of Mat-LyLu cells in culture was observed when cultures were treated (24 h) with 20 µM and 50 µM ranolazine under both normoxic and hypoxic (2 % O_2) conditions (Figures 4.1A-C). On the other hand, after 300 µM ranolazine treatment, Mat-LyLu cells, maintained in either condition, appeared generally 'loose' and scattered (Figure 4.1D). Studying the cells under high magnification revealed that following 300 µM ranolazine treatment, cells lost their spindle-shaped / fibroblast-like morphology in both normoxic and hypoxic conditions (Figure 4.2D).

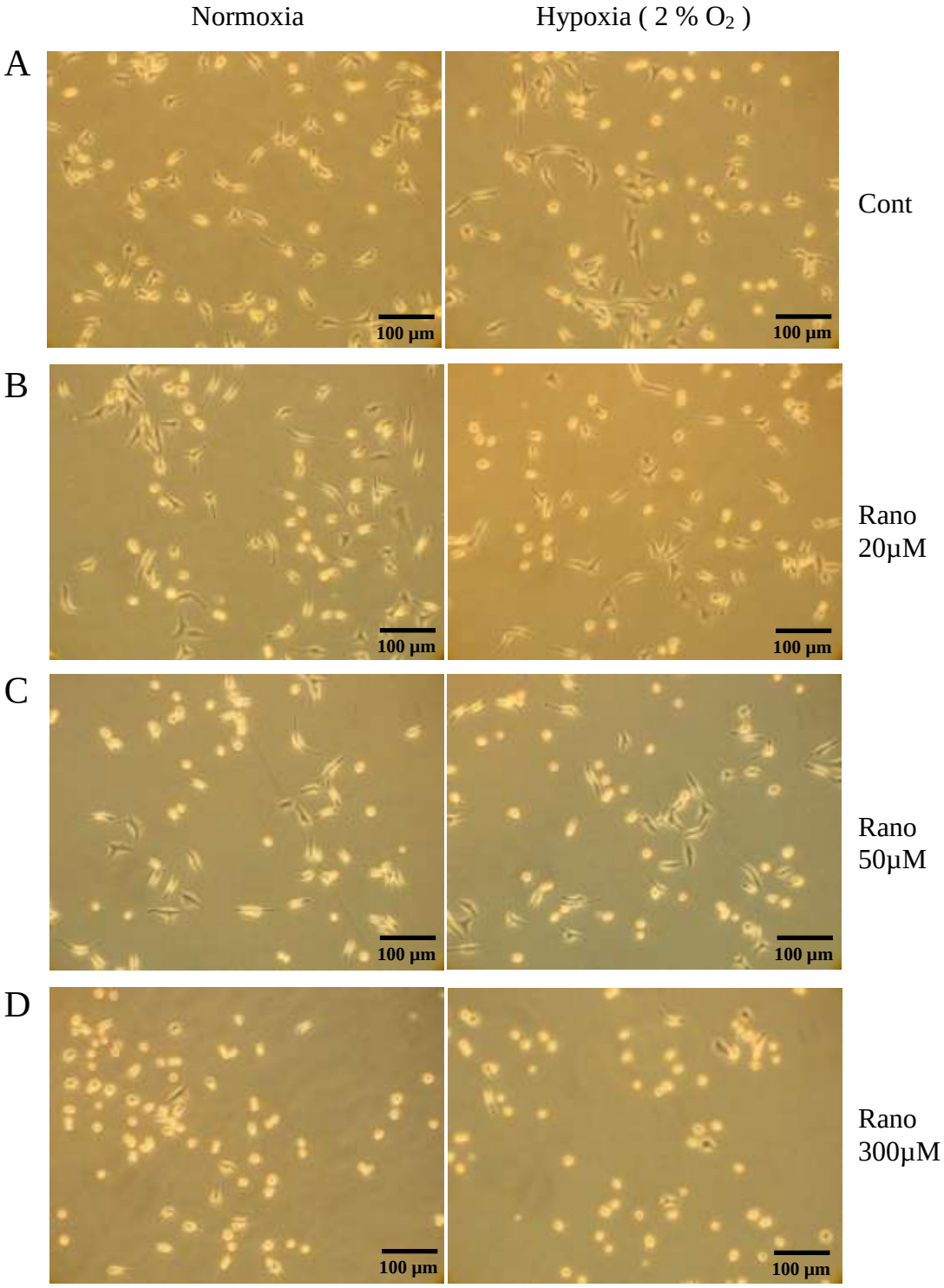


Figure 4.1 Phase-contrast light-photomicrography of Mat-LyLu cells treated with ranolazine.
Mat-LyLu cells were grown for 24 h under (A) control conditions, and in (B) 20µM ranolazine, (C) 50µM ranolazine, and (D) 300µM ranolazine treatment in normoxia (left hand pictures) and hypoxia (2 % O_2; right hand pictures). Micrographs are typical of 3 experiments.

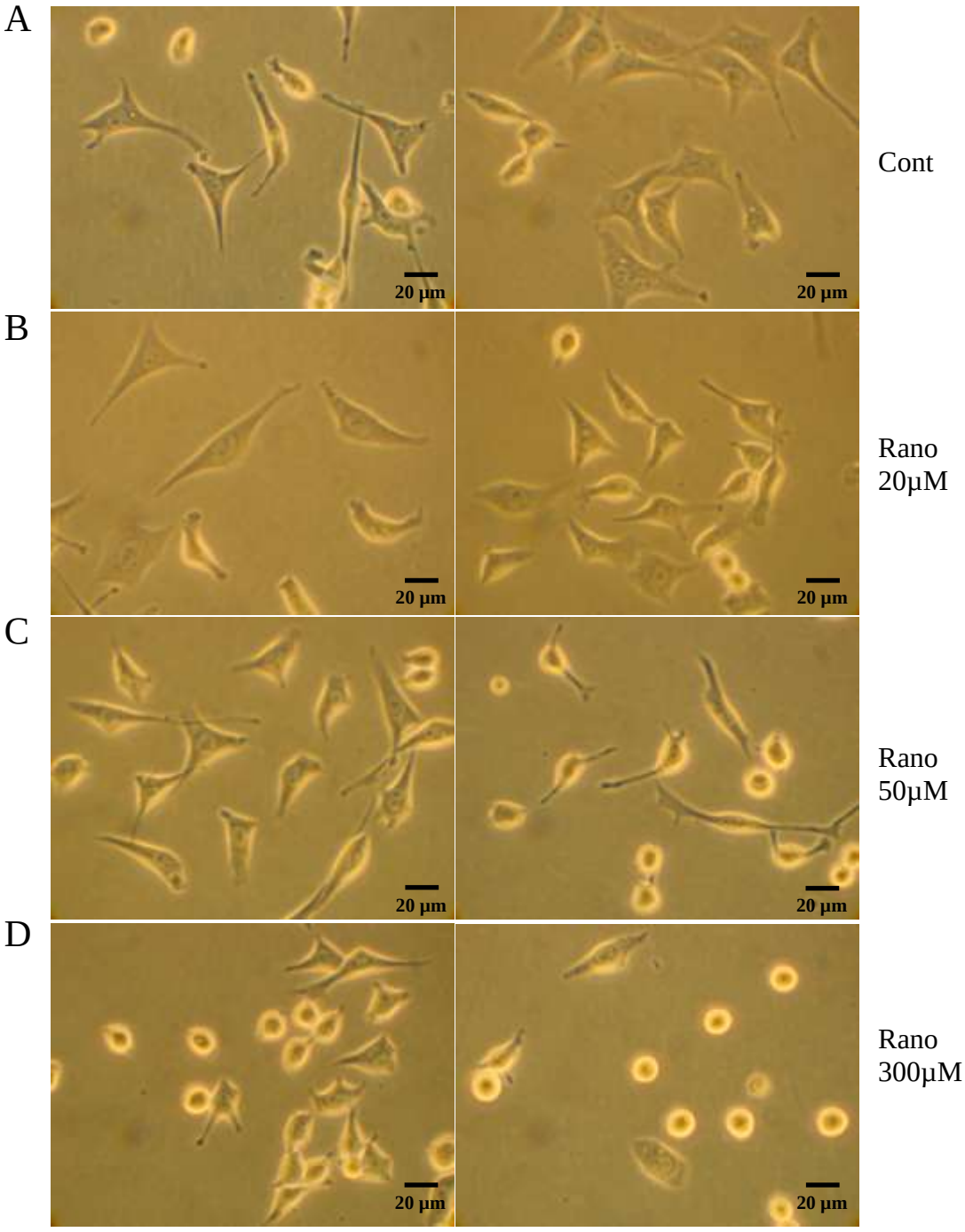


Figure 4.2 Phase-contrast light-photomicrography of Mat-LyLu cells, treated with ranolazine in high magnification.

Mat-LyLu cells were grown for 24 h under (A) control conditions, and in (B) 20µM ranolazine, (C) 50µM ranolazine, (D) 300µM ranolazine treatment in normoxia (left hand pictures) and hypoxia (2 % O_2; right hand pictures). Micrographs are typical of 3 experiments.

4.2.1.2 Cell viability

Treatment with concentrations of ranolazine up to 300 µM for 24 h had no effect on the viability of Mat-LyLu cells maintained in normoxic or hypoxic conditions (Figure 4.3).

4.2.1.3 Cellular proliferation

There was no change in Mat-LyLu cell number after treatment with ranolazine (20, 50 and 300 µM) over 24 h in normoxic conditions (Figure 4.4). Similarly, the cell number was not affected by 20 and 50 µM ranolazine treatment (24 h) in hypoxia (Figure 4.4). There was no effect when cell numbers were compared to the respective control. However, comparison of the cell number for 300 µM ranolazine in hypoxia with the normoxic control (~21 % O_2) suggested a statistically significant effect ($p < 0.05$; $n = 3$ each; Figure 4.4). Hypoxia by itself had no effect on cell number.

4.2.1.4 Nav1.7 mRNA expression

Expression of Nav1.7 mRNA was studied by real-time PCR. cDNAs were prepared from Mat-LyLu cells treated with 20 - 300 µM ranolazine for 24 h under normoxic or hypoxic conditions. Agarose gel electrophoresis confirmed specific single bands at the expected sizes for Nav1.7 and Cytb5R (414 nt and 425 nt, respectively; $n = 3$; Figure 4.5A). The "no-template control" did not give any signal ($n = 3$; Figure 4.5A). Significant decreases of Nav1.7 mRNA expression by 17 %, 20 % and 17 % were found to result from the treatment of the cells with 20, 50 and 300 µM ranolazine, respectively, under normoxic conditions ($p < 0.05$; $n = 3$ each; Figure 4.5B). Hypoxia (24 h) alone significantly increased Nav1.7 mRNA expression by 407 % ($p < 0.05$; $n = 3$; Figure 4.5B). Treatment of Mat-LyLu cells (24 h) with 20, 50 and 300

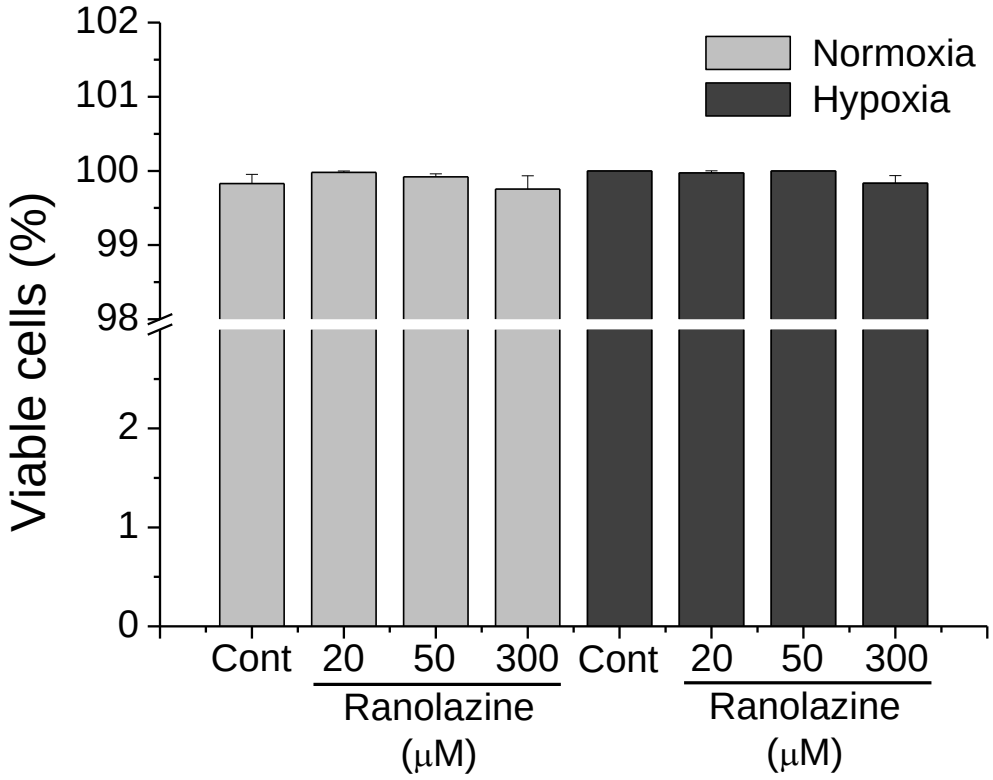
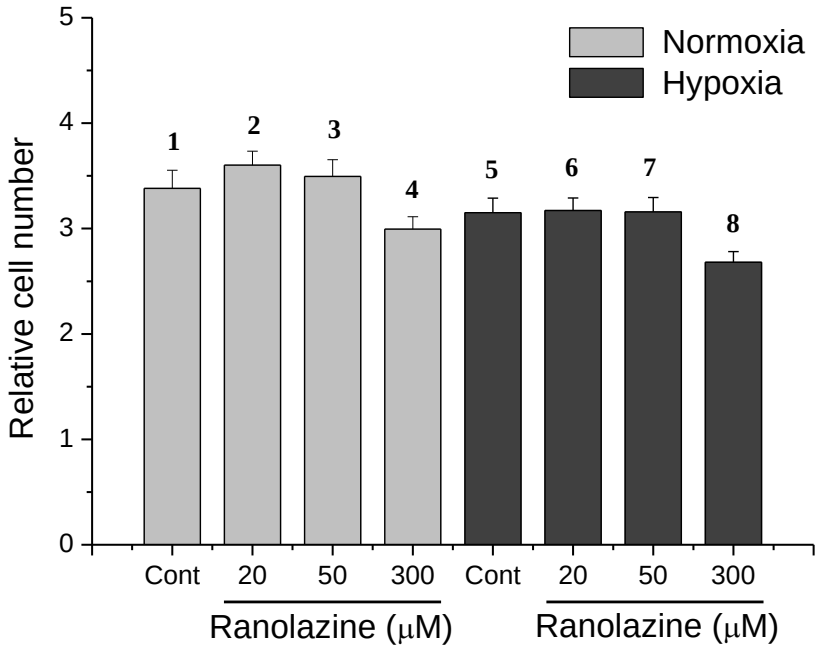


Figure 4.3 Bar diagram showing ranolazine treatments had no toxic effect.

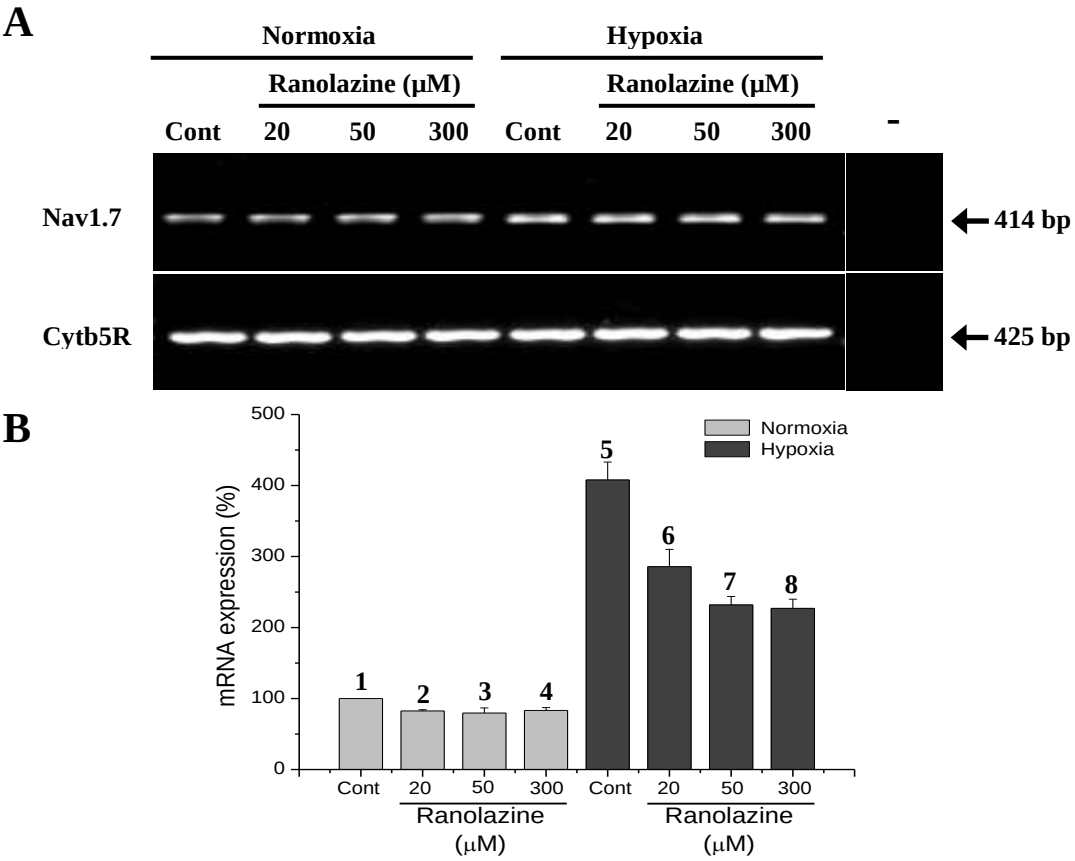
A possible effect of 20, 50 and 300 µM ranolazine on Mat-LyLu cell viability under normoxia (light grey columns) or hypoxia (2 % O_2; dark grey columns). Data are represented as means ± SEM (*n* = 3).



Comparison			p<0.05
1	vs	2	No
1	vs	3	No
1	vs	4	No
1	vs	5	No
1	vs	6	No
1	vs	7	No
1	vs	8	Yes
2	vs	3	No
2	vs	4	No
2	vs	5	No
2	vs	6	No
2	vs	7	No
2	vs	8	Yes
3	vs	4	No

Comparison			p<0.05
3	vs	5	No
3	vs	6	No
3	vs	7	No
3	vs	8	Yes
4	vs	5	No
4	vs	6	No
4	vs	7	No
4	vs	8	No
5	vs	6	No
5	vs	7	No
5	vs	8	No
6	vs	7	No
6	vs	8	No
7	vs	8	No

Figure 4.4 Dose dependent effect of ranolazine on Mat-LyLu cell number.
Bar diagram showing the effect of 20, 50 and 300 µM ranolazine on cell number of normoxic (light grey columns) or hypoxic (dark grey columns) Mat-LyLu cells. Data are presented as means ± SEM ($n \geq 3$). Data were analysed by ANOVA followed by Newman-Keuls *post hoc* analysis. Table of multiple comparisons between different treatments for statistical significance are shown underneath the bar diagram.



Comparison			p<0.05
1	vs	2	Yes
1	vs	3	Yes
1	vs	4	Yes
1	vs	5	Yes
1	vs	6	Yes
1	vs	7	Yes
1	vs	8	Yes
2	vs	3	No
2	vs	4	No
2	vs	5	Yes
2	vs	6	Yes
2	vs	7	Yes
2	vs	8	Yes
3	vs	4	No

Comparison			p<0.05
3	vs	5	Yes
3	vs	6	Yes
3	vs	7	Yes
3	vs	8	Yes
4	vs	5	Yes
4	vs	6	Yes
4	vs	7	Yes
4	vs	8	Yes
5	vs	6	No
5	vs	7	Yes
5	vs	8	Yes
6	vs	7	No
6	vs	8	No
7	vs	8	No

Figure 4.5 Effect of ranolazine on Mat-LyLu Nav1.7 mRNA expression.
(A) Typical PCR products of Nav1.7 (414 bp) and normalising/control gene Cytb5R (425 bp) mRNA in Mat-LyLu cells that was incubated with 20, 50 and 300 µM ranolazine under normoxic or hypoxic (2 % O_2) conditions for 24 h. (B) Bar diagram showing the result of real-time PCR experiment in which the effect of ranolazine on Nav1.7 mRNA expression was studied under normoxic (light grey column) or hypoxic (dark grey column) conditions. The data were normalized to Cytb5R using the $2^{-\Delta\Delta C_T}$ method and expressed relative to normoxic control Nav1.7 level. The table of multiple comparisons between different treatments for statistical significance are shown underneath the bar diagram. Kruskal-Wallis method was used for statistic analysis. Data are presented as means ± SEM (n = 3). (-): no template control

μM ranolazine reduced Nav1.7 mRNA expression levels significantly by 30 %, 43 % and 44 %, respectively, under hypoxic conditions ($p < 0.05$; $n = 3$; Figure 4.5B).

4.2.1.5 Subcellular VGSCα protein expression

4.2.1.5.1 Relative distribution

Confocal immunocytochemistry with a pan-VGSC antibody was used to test the possible effect of ranolazine (50 μM) on subcellular distribution of VGSCα protein in Mat-LyLu cells under normoxic or hypoxic (2 % O_2/ 24 h) conditions (Figure 4.6). VGSCα protein expression was detected in cytoplasm and plasma membrane but not in nucleus of Mat-LyLu cells (Figure 4.6). The subcellular distribution of the VGSCα protein was studied by 'straight line cross-sectional profile' analysis (Figure 4.7). In normoxia, relative to the total immunoreactivity (across the cell), plasma membrane VGSCα protein levels were 9.7 ± 0.4 % (control) and, 9.1 ± 0.3 % (ranolazine). In hypoxia, the corresponding values were 9.5 ± 0.5 % (hypoxia control) and 10.0 ± 0.5 % (ranolazine). Similar data were obtained for the internal VGSCα protein level: 35.2 ± 0.5 % (normoxia control), 35.6 ± 0.5 % (normoxia ranolazine), 35.6 ± 0.5 % (hypoxia control) and 34.7 ± 0.5 % (hypoxia ranolazine). There was no difference in the data for ranolazine *vs* corresponding control (for both: $p > 0.05$; $n \geq 63$; Figure 4.8A&B). It was concluded that ranolazine did not affect the relative subcellular distribution of VGSCα protein in normoxia or hypoxia.

4.2.1.5.2 Plasma membrane VGSCα protein level

Digital quantification of the peripheral VGSCα immunoreactivity (IR_{pm}) by 'free-form line profile' analysis of XYZ scans of Mat-LyLu cells treated (24 h) with

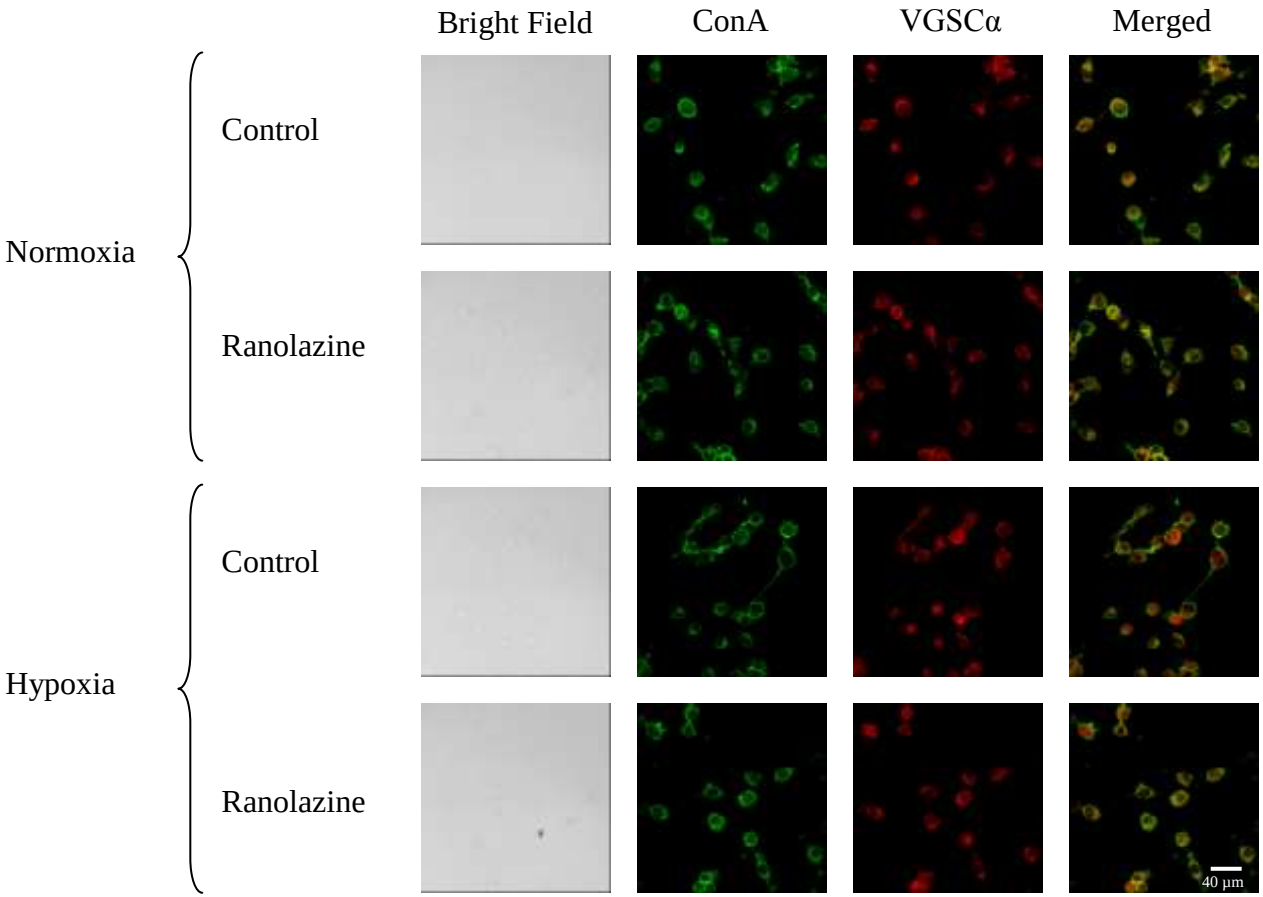


Figure 4.6 Confocal immunocytochemistry study of Mat-LyLu cells incubated with ranolazine.
Typical XYZ confocal images of Mat-LyLu cells incubated 24 h under normoxic and hypoxic (2 % O_2) conditions with or without ranolazine (50 µM). Signal from concanavalin A plasma membrane marker (green), pan-VGSC antibody (red) and overlay of both (merged image) are shown in addition to bright field image. Scale bar (40 µm) applicable to all panels.

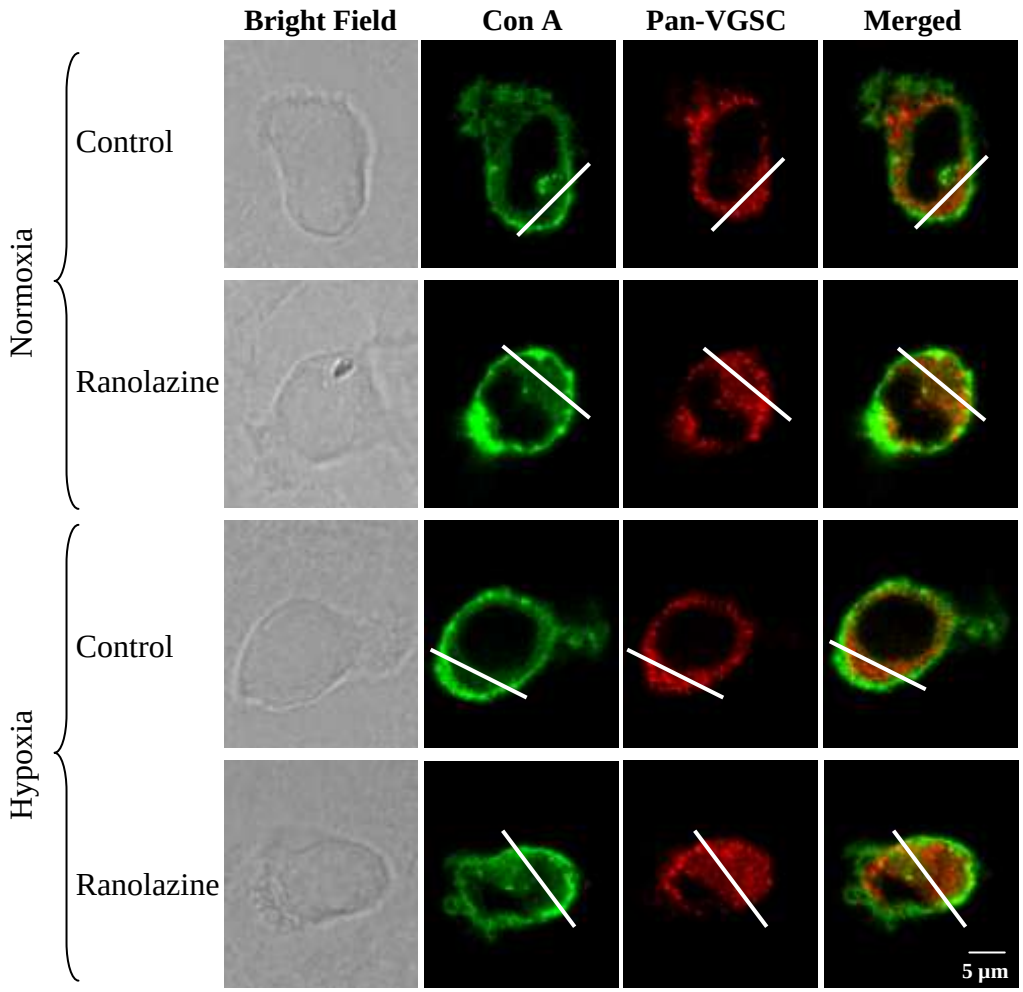


Figure 4.7 Typical image showing effect of ranolazine on VGSCα protein distribution along typical cellular cross-section in Mat-LyLu cells.
Representative XYZ confocal images of Mat-LyLu cells incubated 24 h under normoxic and hypoxic conditions with or without ranolazine (50 µM). White lines indicate typical cross-sections. Scale bar (5µm) applicable to all panels.

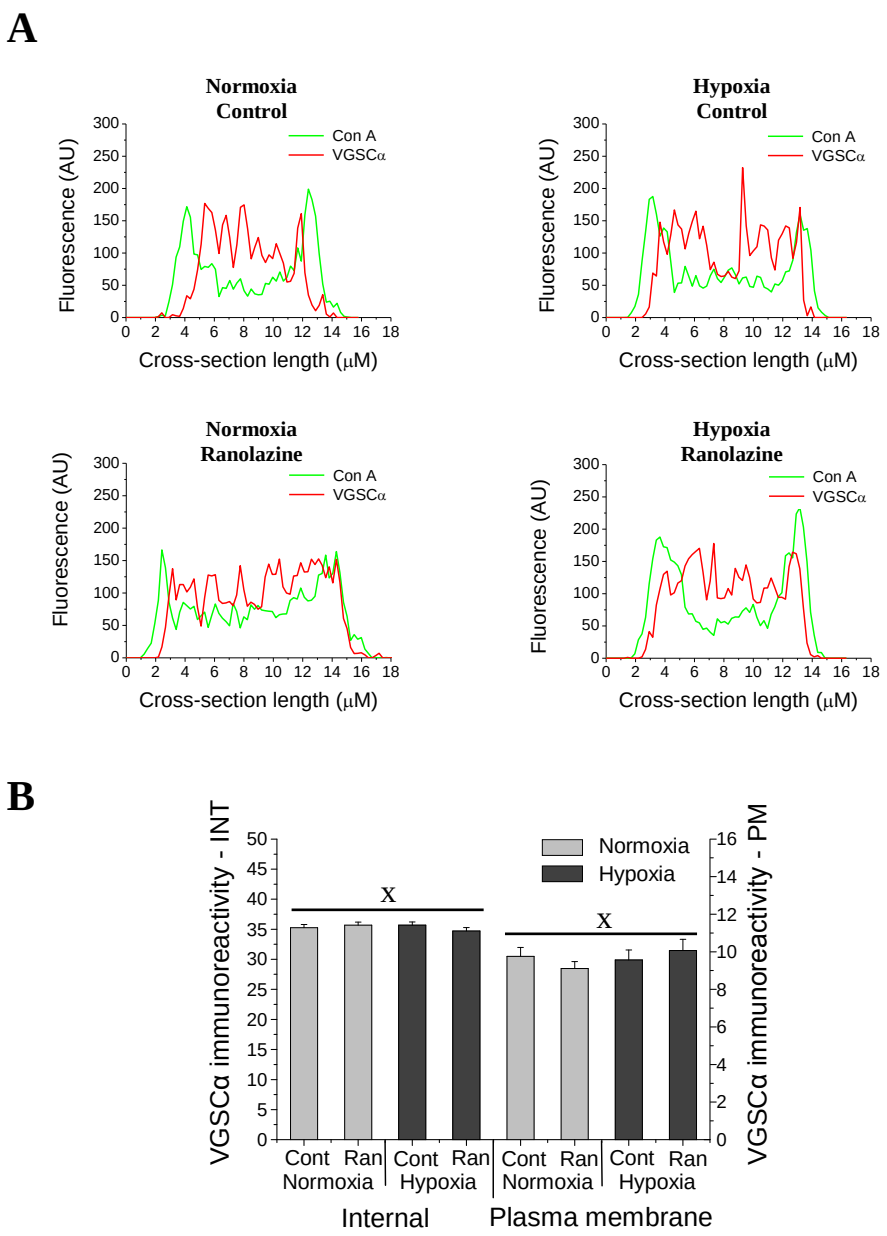


Figure 4.8 Effect of ranolazine on VGSCα protein distribution along typical cellular cross-section in Mat-LyLu cells.
(A) Representative traces showing signal intensity of Con A plasma membrane marker (green) and VGSCα immunofluorescence (red) along cross-section from typical cells (Figure 4.7) incubated (24 h) in normoxic or hypoxic conditions with or without ranolazine (50 µM). (B) Bar diagram showing distribution of VGSCα protein immunoreactivity along subcellular cross-sections as a percentage of total (%). For plasma membrane (PM) immunoreactivity, 1.5 µm sections was measured inward from the edge of Con A staining. For internal (INT) immunoreactivity, middle 30 % of the cross-section was measured. Data were analysed by ANOVA followed by Newman-Keuls post hoc analysis. Data are presented as means±SEM (*n* =63). Significance: (X) $p > 0.05$.

ranolazine (50 µM) revealed no change in plasma membrane VGSCα protein level under normoxic conditions (IR_{pm} = 155 ± 5 AU/µm and 144 ± 3 AU/µm, respectively; $p > 0.05$; $n \geq 63$; Figures 4.9 and 4.10A&B). Similarly, in Mat-LyLu cells treated with ranolazine and maintained in hypoxia, plasma membrane level of VGSCα protein did not change compared to hypoxia control (IR_{pm} = 121 ± 3 AU/µm and 131 ± 4 AU/µm, respectively; $p > 0.05$; $n \geq 63$; Figures 4.9 and 4.10A&B). On the other hand, hypoxia by itself caused a significant 22 % decrease in plasma membrane VGSCα protein level ($p < 0.05$; $n \geq 63$; Figures 4.9 and 4.10A&B) with no further effect of the ranolazine treatment.

4.2.1.5.3 Internal VGSCα protein level

Digital quantification of the 'internal' VGSCα immunoreactivity (IR_{int}) by the 'area histogram' analysis of XYZ scans of Mat-LyLu cells treated (24 h) with ranolazine (50 µM) under normoxic conditions revealed a significant (~ 9 %) decrease of internal VGSCα protein level, from 22978 ± 587 AU to 20934 ± 704 AU ($p < 0.05$; $n \geq 77$; Figures 4.11 and 4.12A&B). Hypoxia by itself caused a significant 16.5 % decrease in VGSCα immunoreactivity to 10173 ± 389 AU ($p < 0.05$; $n \geq 77$; Figures 4.11 and 4.12A&B). There was no further effect of the treatment with ranolazine under hypoxia (IR_{int} =18501 ± 682; $p < 0.05$; $n \geq 77$; Figures 4.11 and 4.12A&B).

4.2.1.6 Matrigel™ invasion

Matrigel™ invasion assays were used to assess the possible effect of ranolazine treatment on the invasiveness of Mat-LyLu cells maintained in normoxic and hypoxic conditions. Treatment with 20, 50 and 300 µM ranolazine significantly

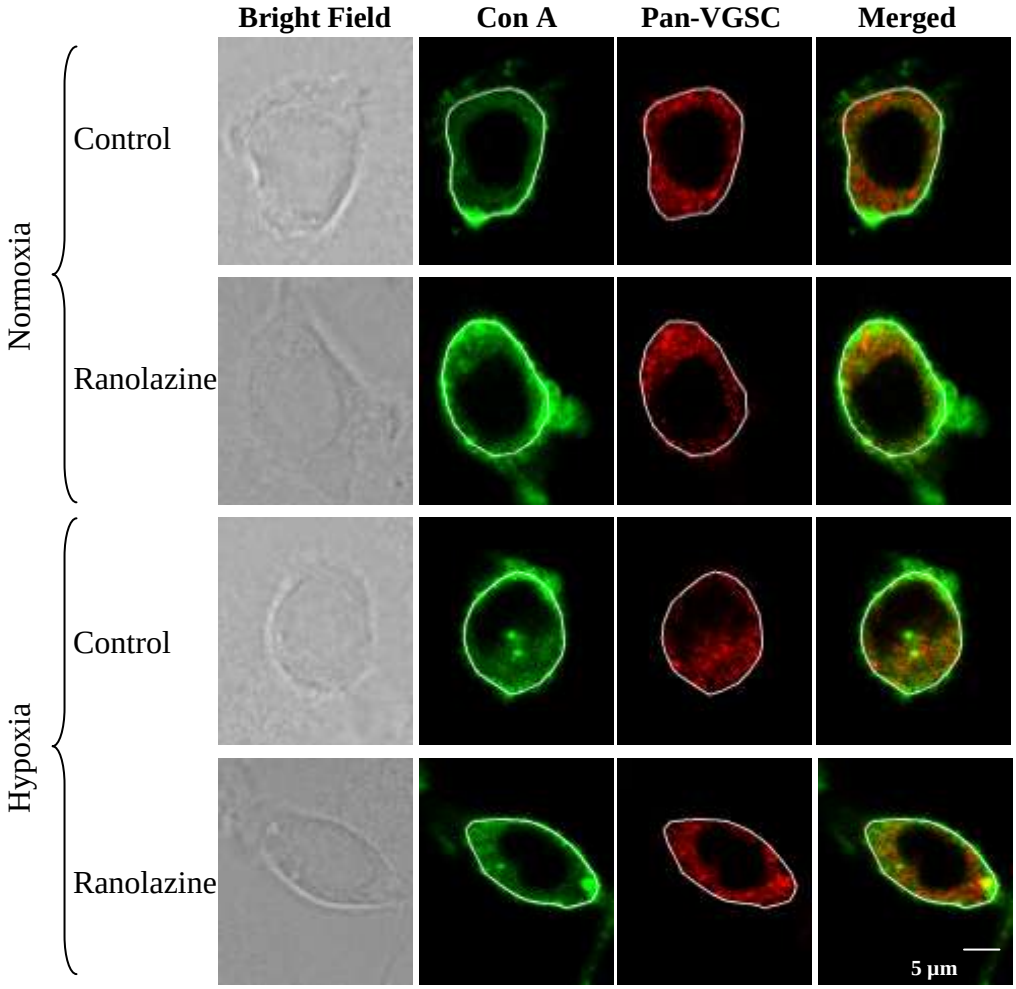
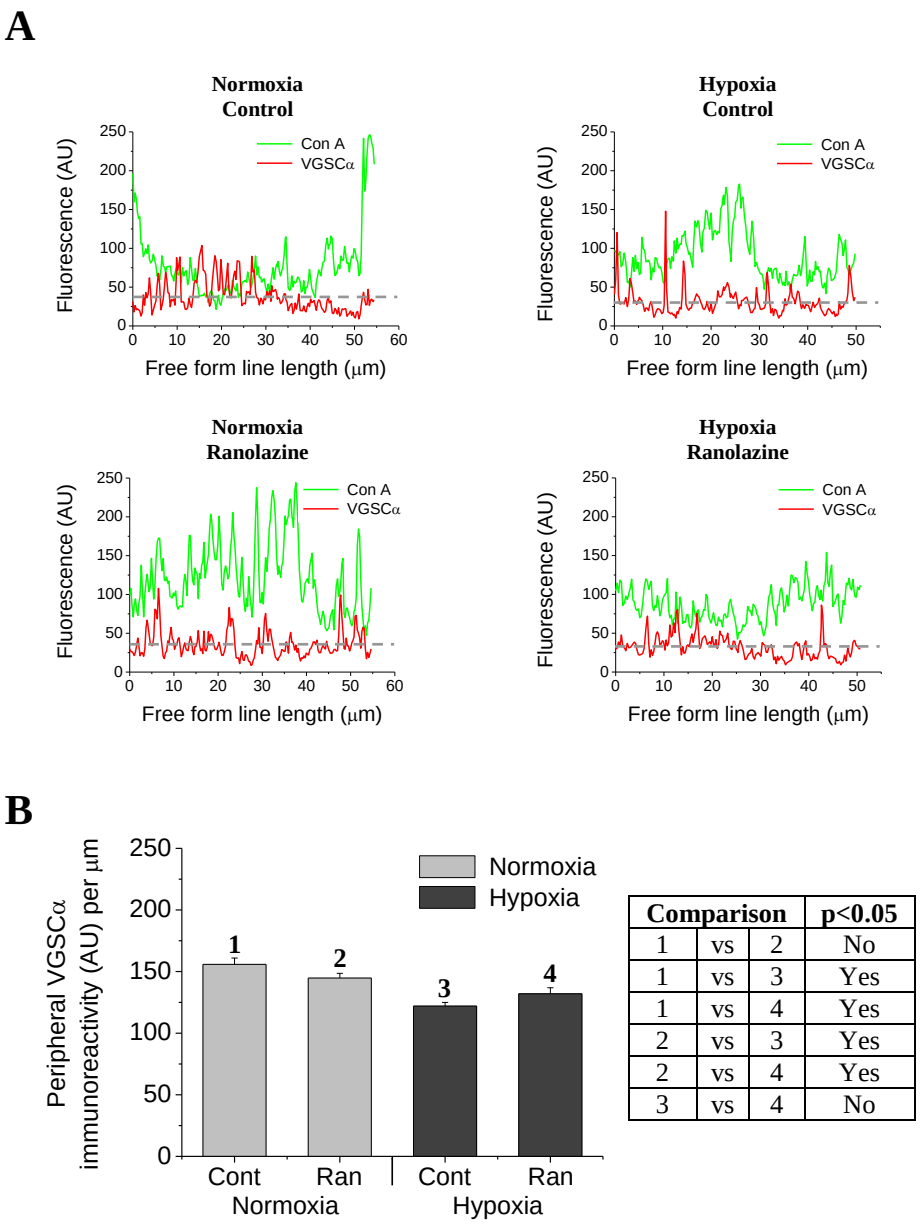


Figure 4.9 Typical image showing effect of ranolazine on VGSCα protein levels in plasma membrane of Mat-LyLu cells.
Representative XYZ confocal images of Mat-LyLu cells incubated 24 h under normoxic and hypoxic conditions with or without ranolazine (50 µM). White lines indicate typical freeform line guided by Con A staining to measure cell surface protein level. Scale bar (5µm) applicable to all panels.



Comparison			p<0.05
1	vs	2	No
1	vs	3	Yes
1	vs	4	Yes
2	vs	3	Yes
2	vs	4	Yes
3	vs	4	No

Figure 4.10 Effect of ranolazine on VGSCα protein levels in plasma membrane of Mat-LyLu cells.
(A) Representative trace showing signal intensity of Con A plasma membrane marker (green) and VGSCα (red) immunofluorescence along plasma membrane from a typical cells (Figure 4.9) incubated (24 h) in normoxic or hypoxic conditions with or without ranolazine (50 μM). Dotted gray lines indicate mean pan-VGSC fluorescence. (B) Bar diagram showing level of VGSCα protein immunoreactivity along plasma membrane as immunoreactivity (AU) per μm. Inset: table of multiple comparisons between treatments for statistical significance. Data were analysed by ANOVA followed by Newman-Keuls post hoc analysis. Data are presented as means ± SEM (n = 71).

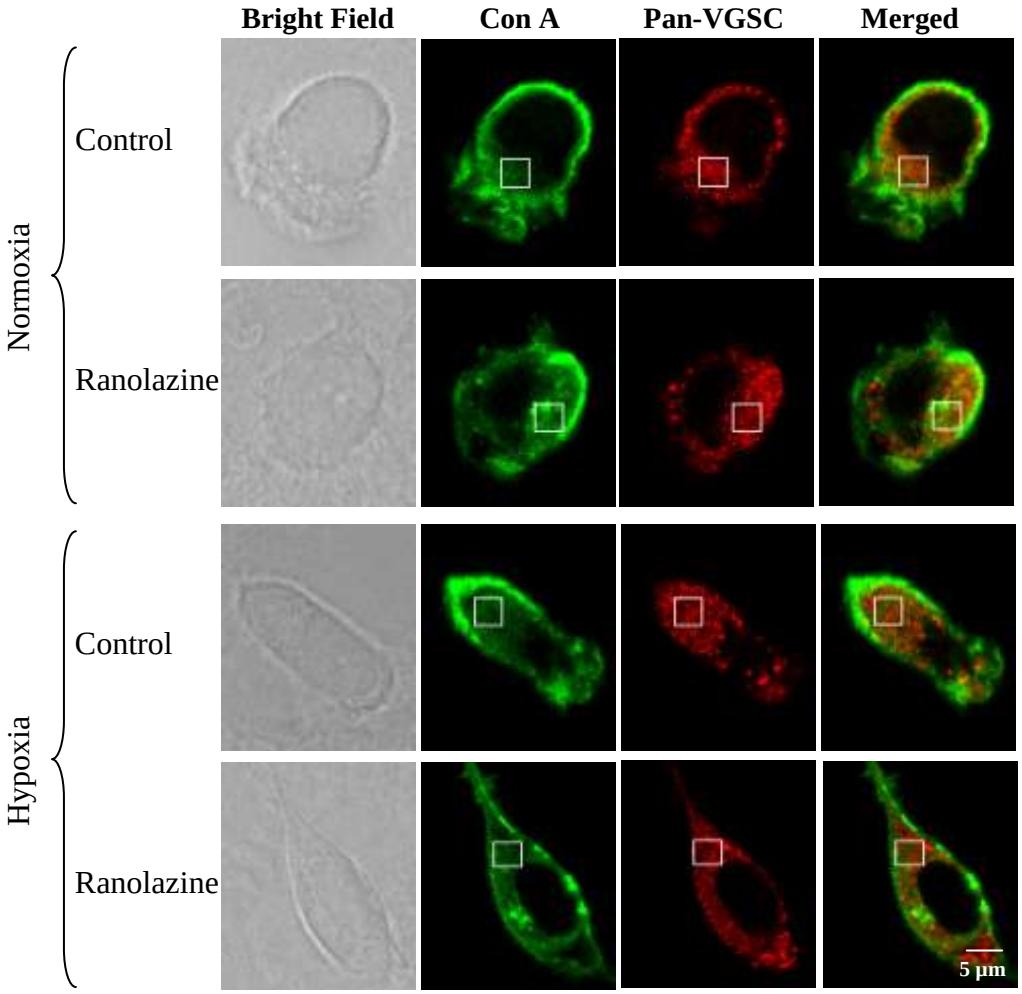
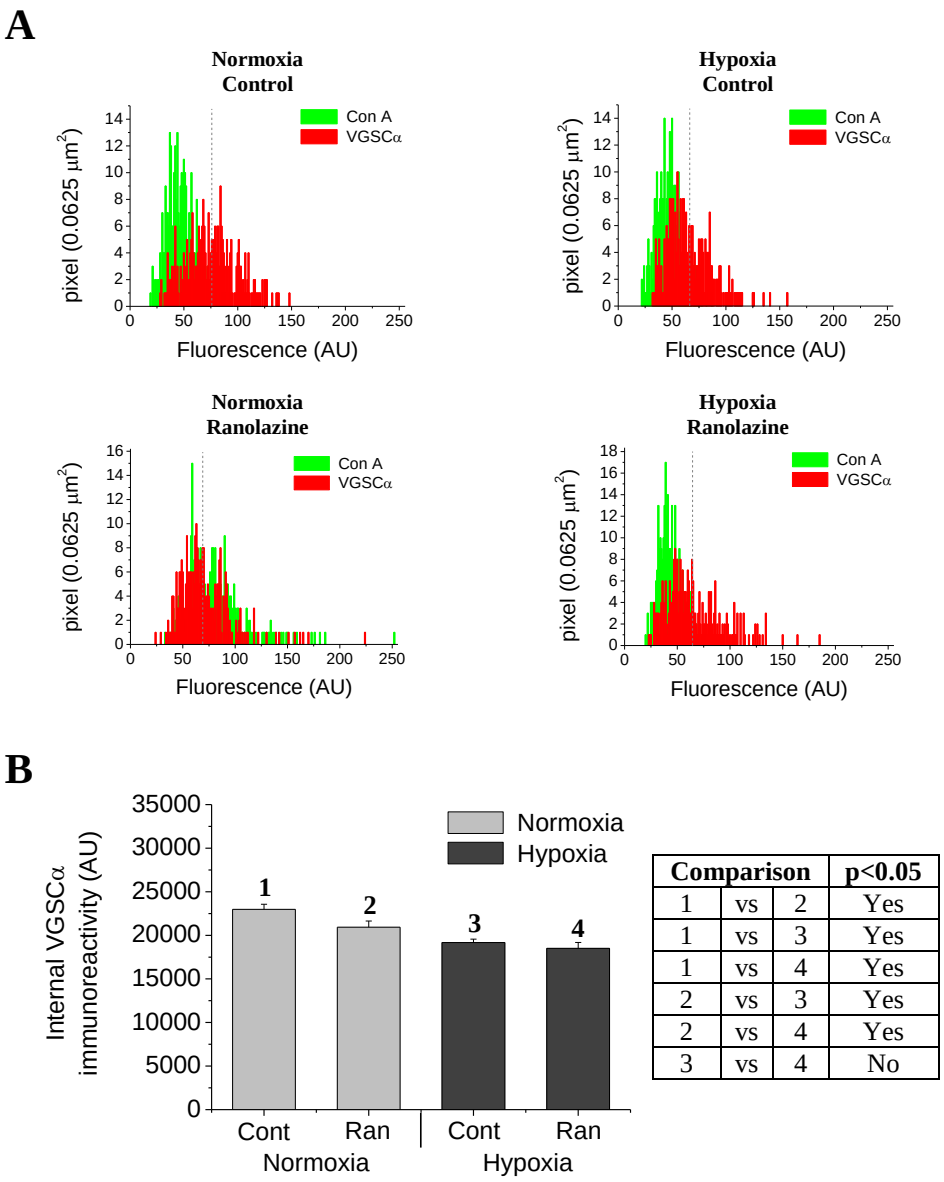


Figure 4.11 Typical image showing effect of ranolazine on internal VGSCα protein levels of Mat-LyLu cells.
Representative XYZ confocal images of Mat-LyLu cells incubated 24 h under normoxic and hypoxic conditions with or without ranolazine (50 µM). White box indicates typical area covering 16 μm^2 square section of cytoplasm avoiding nucleus to measure internal protein level. Scale bar (5µm) applicable to all panels.



Comparison			p<0.05
1	vs	2	Yes
1	vs	3	Yes
1	vs	4	Yes
2	vs	3	Yes
2	vs	4	Yes
3	vs	4	No

Figure 4.12 Effect of ranolazine on internal VGSCα protein levels of Mat-LyLu cells. (A) Representative histograms showing distribution of pixels (0.0625 µm^2) with signal intensity of Con A plasma membrane marker (green) and VGSCα (red) immunofluorescence in cytoplasm from typical cells (Figure 4.11) incubated (24 h) in normoxic or hypoxic conditions with or without ranolazine (50 µM). Dotted gray lines indicate mean pan-VGSC fluorescence. (B) Bar diagram showing internal VGSCα protein immunoreactivity (AU). Inset: table of multiple comparisons between treatments for statistical significance. Data were analysed by ANOVA followed by Newman-Keuls *post hoc* analysis. Data are presented as means ± SEM (n = 77).

decreased invaded cell number by 59 %, 55 %, 74 %, respectively ($p < 0.05$; $n \geq 4$ each; Figures 4.13 and 4.14) under normoxic conditions. Similarly, 24 h treatment of cells in hypoxic conditions with 20, 50 and 300 µM ranolazine significantly decreased invaded cell number by 63 %, 73 %, 87 %, respectively ($p < 0.05$; $n \geq 4$ each; Figures 4.13 and 4.14). Hypoxia alone had no effect on cellular invasion ($p > 0.05$; $n = 8$; Figures 4.13 and 4.14).

4.2.1.7 Summary of the effects of ranolazine

Hypoxia increased Nav1.7 mRNA expression whilst decreasing plasma membrane and intracellular VGSCα protein levels. The effects of ranolazine on Mat-LyLu cells were as follows: i) decreased Nav1.7 mRNA expression (both conditions); (ii) decreased intracellular VGSCα protein; and (iii) decreased invasion (both conditions). Some of these effects were concentration dependent. There was no effect on any of the other characteristics measured, including cell viability and number (proliferation) (Table 4.1).

4.2.2 Effects of riluzole

Riluzole has also been used as an inhibitor of VGSC persistent currents, although it too can have a range of actions, depending on concentration (Weiss *et al.*, 2010; Le *et al.*, 2010; Parihar *et al.*, 2003; Doble, 1996; Zona *et al.*, 1998; Frizzo *et al.*, 2004; Xu *et al.*, 2001). In the present study, riluzole (dissolved in DMSO) was used in the concentration range 1 to 100 µM. This concentration range was shown previously to block I_{NaP} more effectively than I_{NaT} (Weiss *et al.*, 2010; Urbani and Belluzi, 2000).

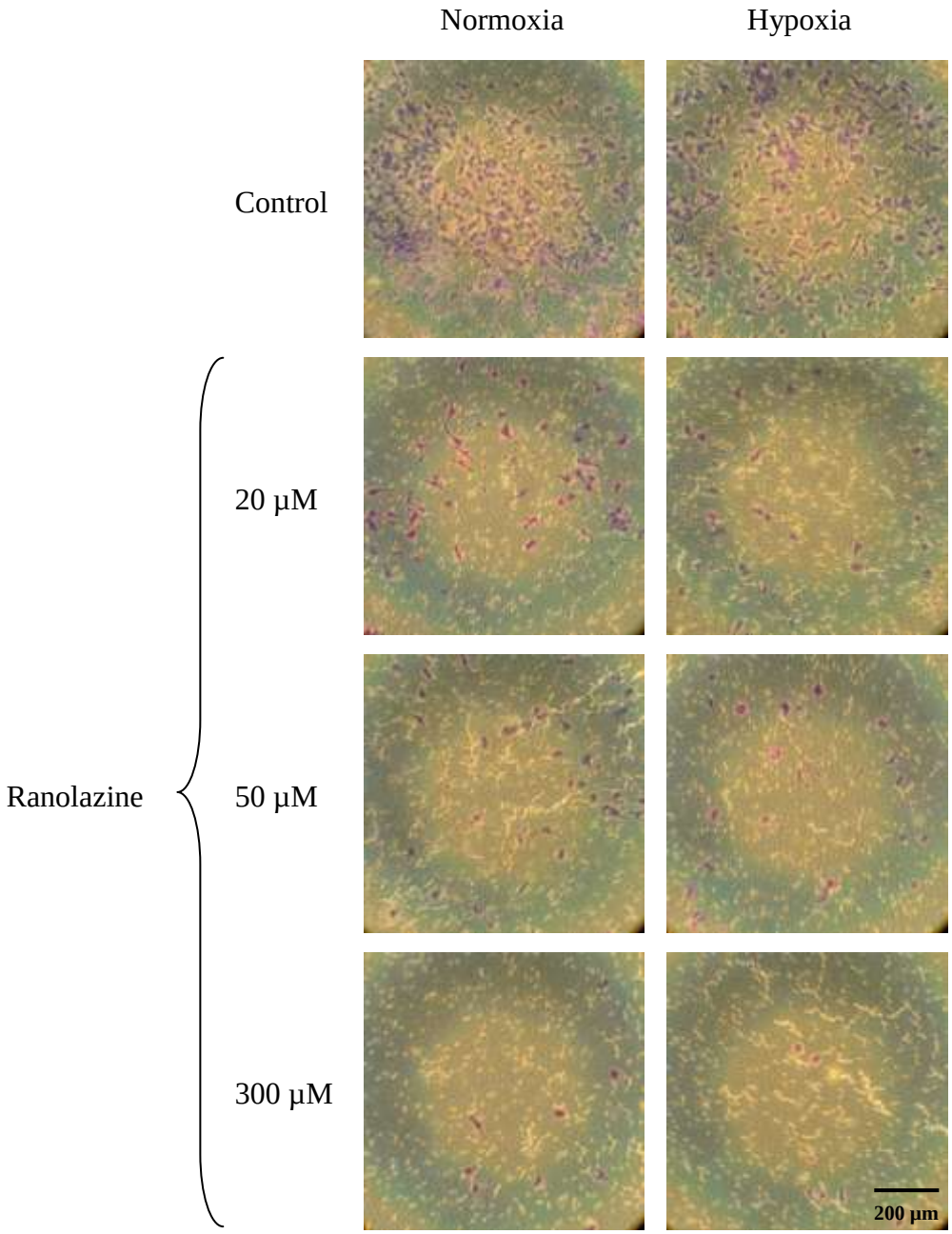
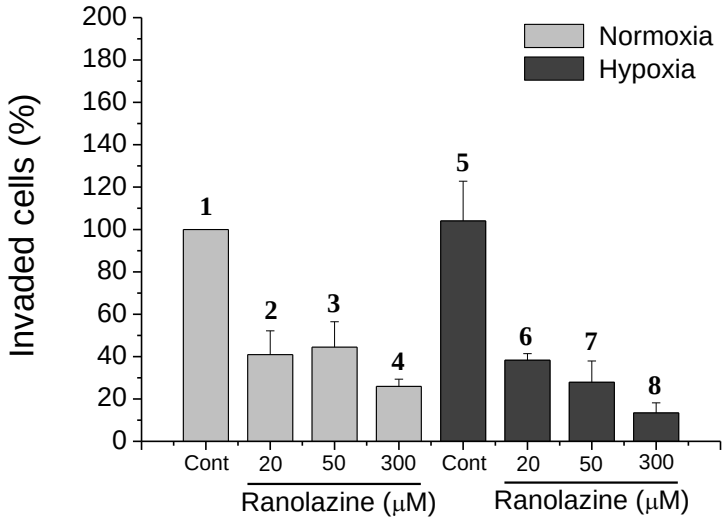


Figure 4.13 Typical images of invaded cells showing the effect of ranolazine on invasion of Mat-LyLu invesiveness.
Typical phase-contrast light-microscopy images of invaded cells obtained from Matrigel™ invasion assays of Mat-LyLu cells incubated 24 h under normoxic and hypoxic conditions with or without ranolazine (20, 50 and 300 µM). Invaded cells were fixed and stained with crystal violet (purple). Scale bar (200 µm) applicable to all panels.



Comparison			p<0.05
1	vs	2	Yes
1	vs	3	Yes
1	vs	4	Yes
1	vs	5	No
1	vs	6	Yes
1	vs	7	Yes
1	vs	8	Yes
2	vs	3	No
2	vs	4	No
2	vs	5	Yes
2	vs	6	No
2	vs	7	No
2	vs	8	Yes
3	vs	4	No

Comparison			p<0.05
3	vs	5	Yes
3	vs	6	No
3	vs	7	No
3	vs	8	Yes
4	vs	5	Yes
4	vs	6	No
4	vs	7	No
4	vs	8	No
5	vs	6	Yes
5	vs	7	Yes
5	vs	8	Yes
6	vs	7	No
6	vs	8	Yes
7	vs	8	No

Figure 4.14 Effect of ranolazine on invasion of Mat-LyLu cells.
Bar diagram showing number of invaded Mat-LyLu cells, incubated 24 h under normoxic and hypoxic conditions with or without ranolazine (20, 50 and 300 µM). Data were expressed relative to the control (%) and presented as means ± SEM ($n \geq 4$). Data were analysed by Kruskal-Wallis analysis of variance. Inset: table of multiple comparisons between treatments for statistical significance.

Table 4.1 Summary of results
(Nor) normoxia; (Hyp) hypoxia; (PM) plasma membrane; (/) concentration dependent; (+) increase; (-) decrease; (0) no change

STUDIES	HYPOXIA	RANOLAZINE		RILUZOLE		PROCAINE		LIDOCAINE	
		Nor	Hyp	Nor	Hyp	Nor	Hyp	Nor	Hyp
MORPHOLOGY	0	0 / +	0 / +	0	0	0	0 / +	0 / +	0 / +
VIABILITY	0	0	0	0	0	0	0	0	0
PROLIFERATION	0	0	0	0 / -	0 / -	0	0	0	0 / -
Nav1.7 mRNA	+	-	0 / -	0 / -	0 / -	0 / -	0	0 / -	0 / -
VGSCα PROTEIN									
(i) Subcellular	0	0	0	0	0	0	0	0	0
(ii) PM	-	0	0	0	+	-	0	-	0
(iii) Internal	-	-	0	-	-	-	0	-	-
INVASION	0	-	-	0	0	-	-	-	-

4.2.2.1 Some initial observations: Cell morphology

Treatment of Mat-LyLu cells in culture with 0.015 % DMSO, 10 µM and 30 µM riluzole for 24 h revealed no obvious change in the basic appearance or distribution of the cells under both normoxic and hypoxic (2 % O_2) conditions (Figures 4.15 A-D). A similar conclusion was reached after studying the cells under high magnification (Figures 4.16A-D).

4.2.2.2 Cell viability

Treatment with riluzole (up to 100 µM) or 0.05 % DMSO (corresponding concentration of solvent) for 24 h was not toxic to Mat-LyLu cells that were maintained in normoxic or hypoxic conditions (Figure 4.17).

4.2.2.3 Cellular proliferation

No significant change was recorded in Mat-LyLu cell number after treatments (24 h) with 0.015 % DMSO, 3 µM and 5 µM riluzole in normoxic and hypoxic conditions ($n \geq 3$ each; Figure 4.18). Also, DMSO by itself had no effect on cell number in either condition. However, some statistical variations were noted. For example, 10 µM and 30 µM riluzole treatments had no effect on cell number when compared to the respective DMSO control but cell numbers were significantly lower by 29 % and 48 %, respectively, when compared to the non-treated controls under normoxic conditions ($n \geq 3$ each; Figure 4.18). Under hypoxia, 10 µM riluzole treatment (24 h) decreased cell number by 26 % and 24 % when compared to non-treated and DMSO controls, respectively, the former change being significant ($p < 0.05$; $n \geq 3$ each; Figure 4.18). The highest concentration of riluzole tested (30 µM) significantly decreased cell number by 44 % and 41 % when compared to both non-treated and DMSO controls, respectively ($p < 0.05$; $n \geq 3$ each; Figure 4.18).

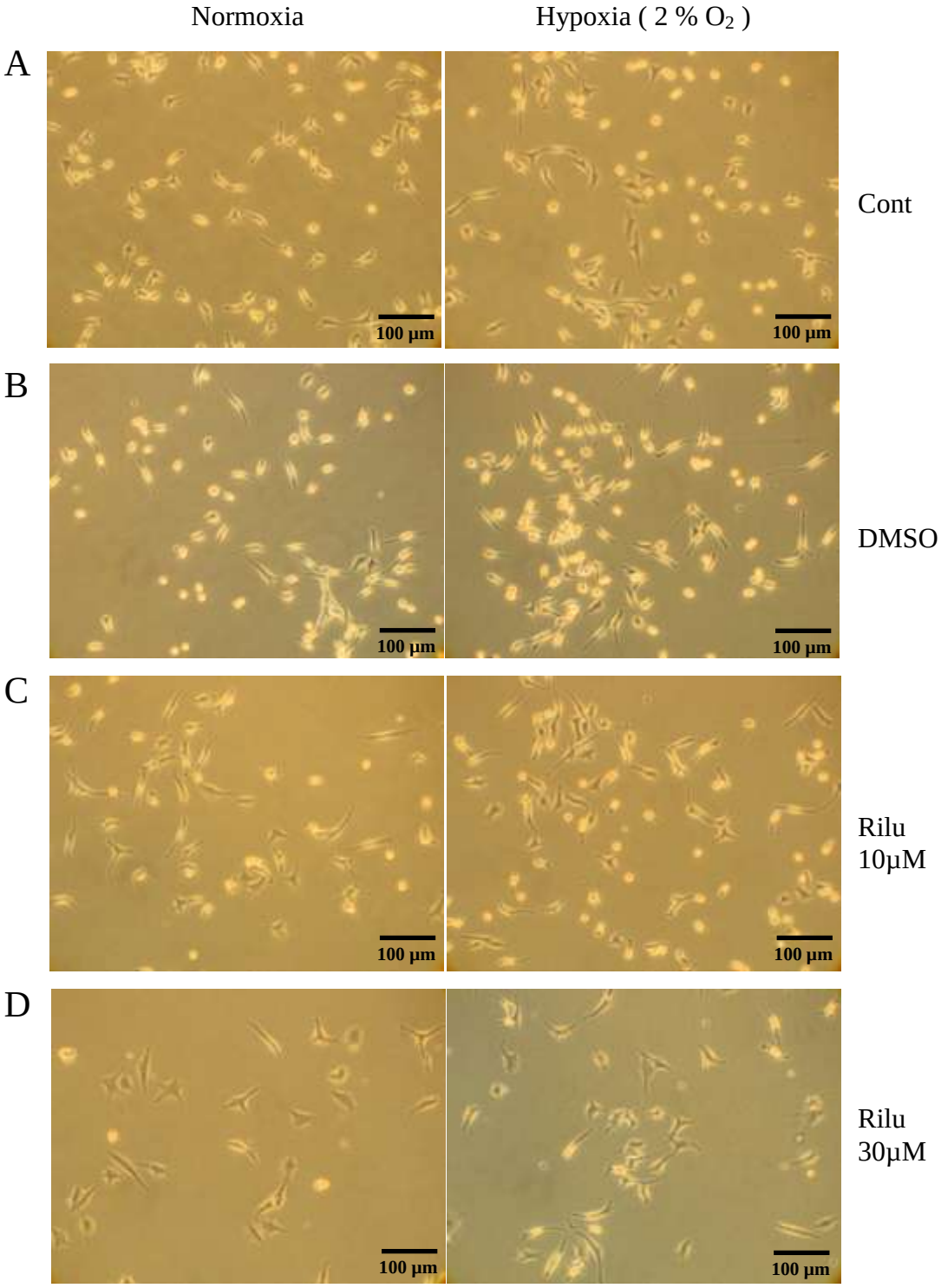


Figure 4.15 Phase-contrast light-photomicrography of Mat-LyLu cells, treated with riluzole.
Mat-LyLu cells were grown for 24 h under (A) control conditions, and in (B) 0.015 % DMSO, (C) 10 µM riluzole, and (D) 30 µM riluzole treatment in normoxia (left hand pictures) and hypoxia (2 % O_2; right hand pictures). Micrographs are typical of 3 experiments.

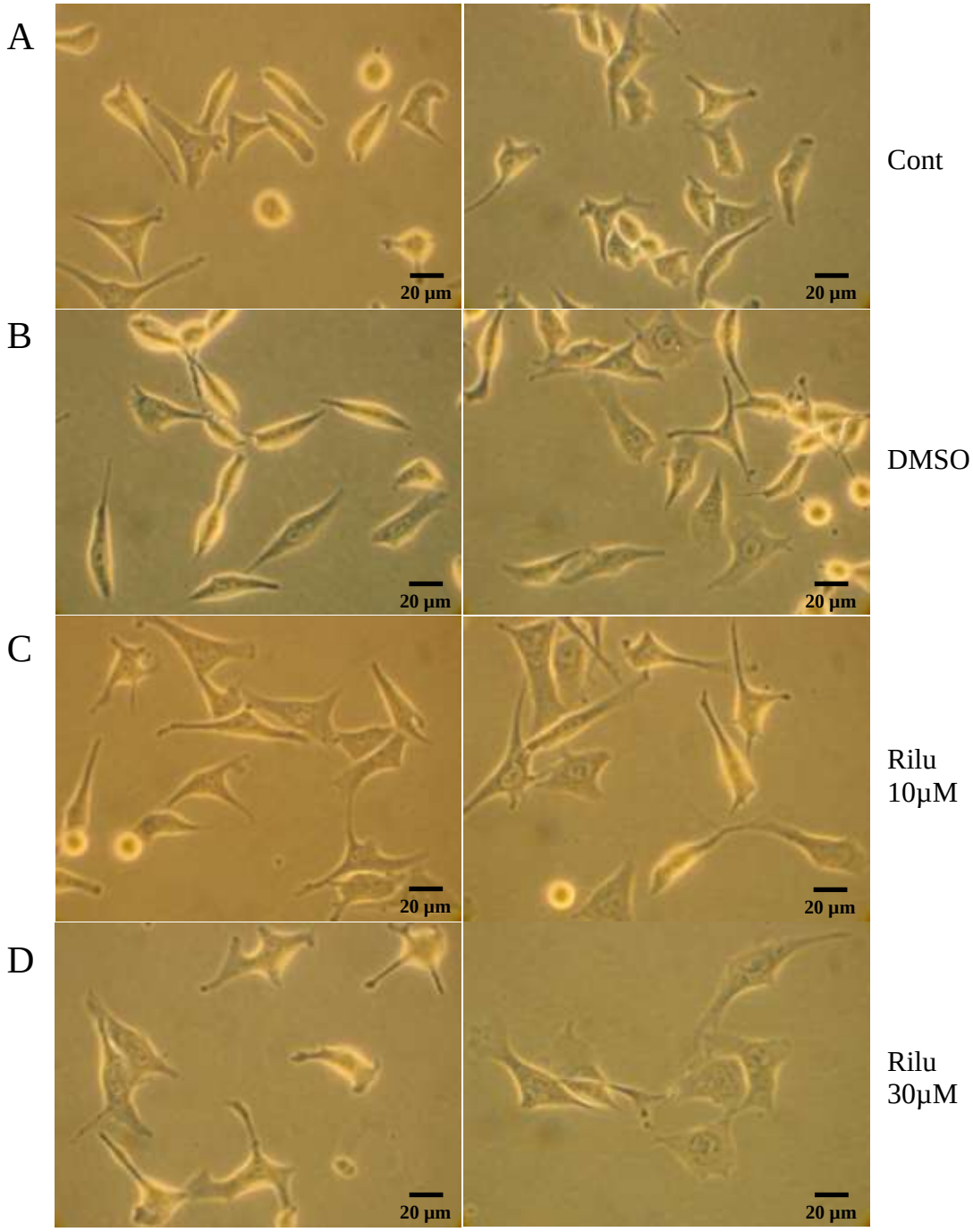


Figure 4.16 Phase-contrast light-photomicrography of Mat-LyLu cells, treated with riluzole, in high magnification.

Mat-LyLu cells were grown for 24 h under (A) control conditions, and in (B) 0.015 % DMSO, (C) 10 µM riluzole, and (D) 30 µM riluzole treatment in normoxia (left hand pictures) and hypoxia (2 % O_2; right hand pictures). Micrographs are typical of 3 experiments.

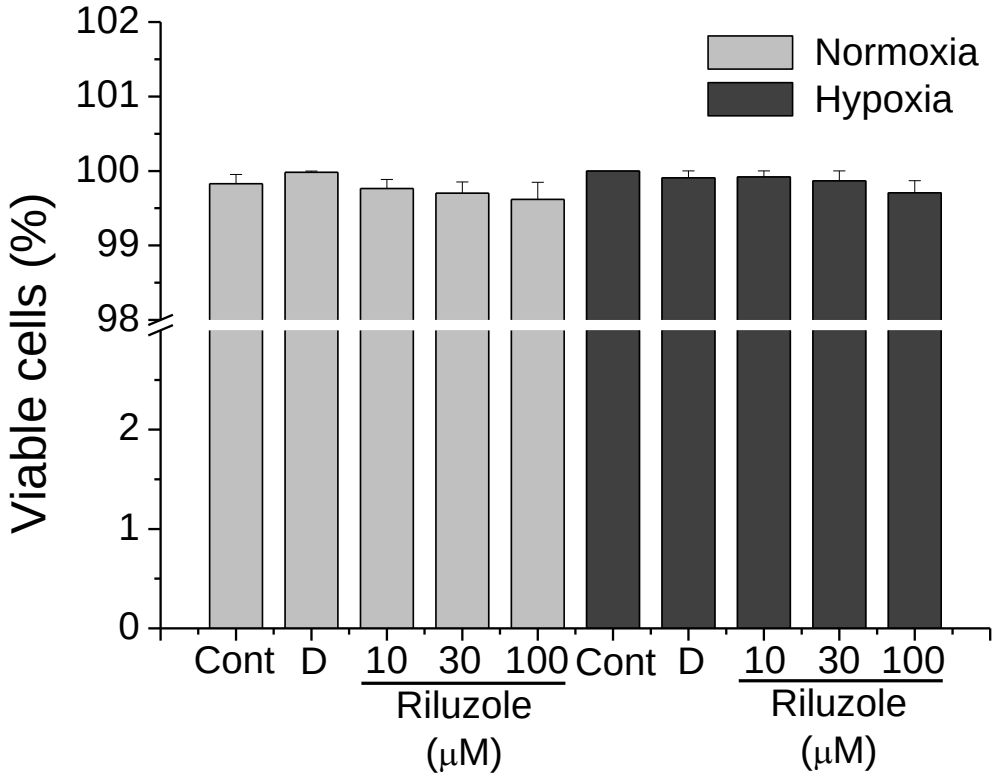
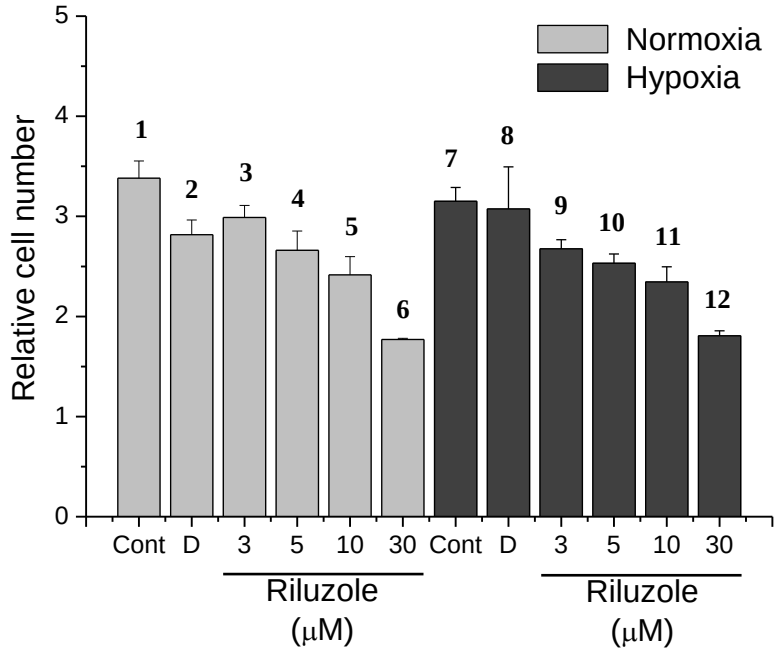


Figure 4.17 Bar diagram showing riluzole treatments had no toxic effect.

A possible effect of 0.05 % DMSO and 10, 30 and 100 µM ranolazine on Mat-LyLu cell viability under normoxia (light grey columns) or hypoxia (2 % O_2; dark grey columns). Data are represented as means ± SEM (n = 3).



Comparison			p<0.05
1	vs	2	No
1	vs	3	No
1	vs	4	No
1	vs	5	Yes
1	vs	6	Yes
1	vs	7	No
1	vs	8	No
1	vs	9	No
1	vs	10	No
1	vs	11	Yes
1	vs	12	Yes
2	vs	3	No
2	vs	4	No
2	vs	5	No
2	vs	6	No
2	vs	7	No
2	vs	8	No
2	vs	9	No
2	vs	10	No
2	vs	11	No
2	vs	12	No
3	vs	4	No

Comparison			p<0.05
3	vs	5	No
3	vs	6	Yes
3	vs	7	No
3	vs	8	No
3	vs	9	No
3	vs	10	No
3	vs	11	No
3	vs	12	Yes
4	vs	5	No
4	vs	6	No
4	vs	7	No
4	vs	8	No
4	vs	9	No
4	vs	10	No
4	vs	11	No
4	vs	12	No
5	vs	6	No
5	vs	7	No
5	vs	8	No
5	vs	9	No
5	vs	10	No
5	vs	11	No

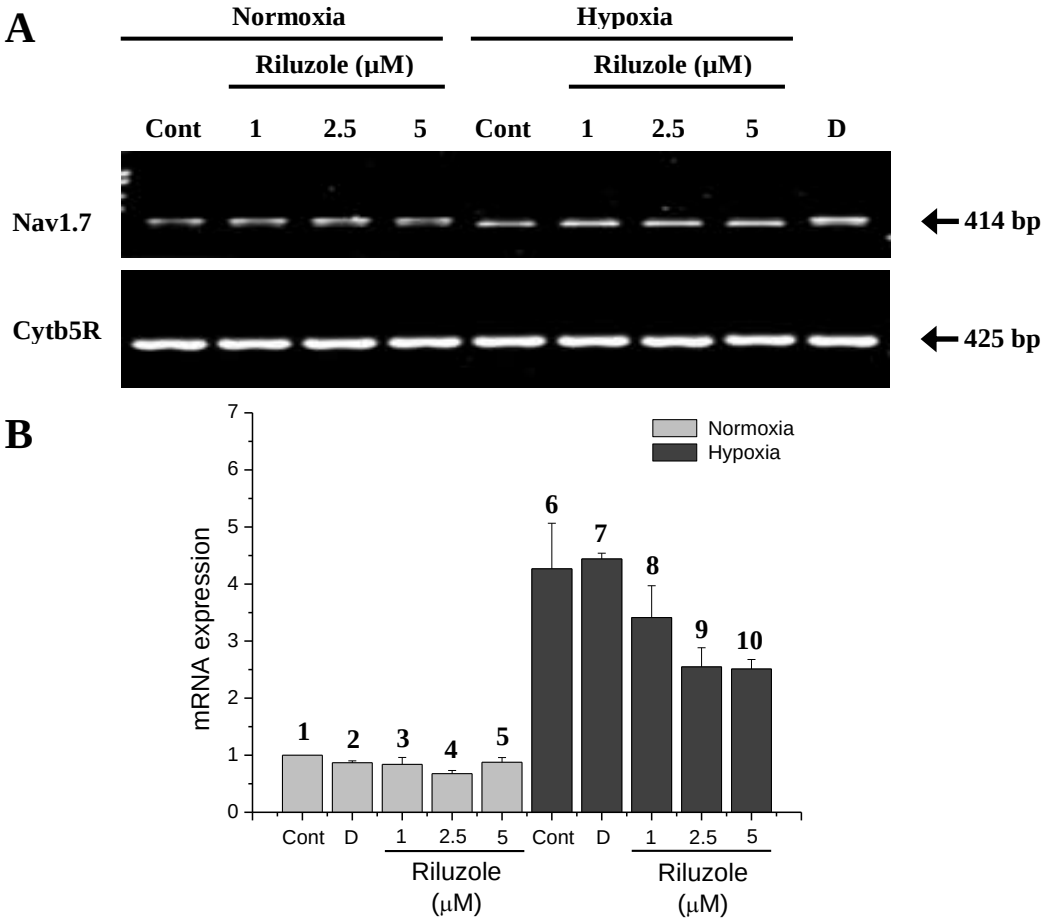
Comparison			p<0.05
5	vs	12	No
6	vs	7	Yes
6	vs	8	Yes
6	vs	9	No
6	vs	10	No
6	vs	11	No
6	vs	12	No
7	vs	8	No
7	vs	9	No
7	vs	10	No
7	vs	11	Yes
7	vs	12	Yes
8	vs	9	No
8	vs	10	No
8	vs	11	No
8	vs	12	Yes
9	vs	10	No
9	vs	11	No
9	vs	12	No
10	vs	11	No
10	vs	12	No
11	vs	12	No

Figure 4.18 Dose dependent effect of riluzole on Mat-LyLu cell number.
Bar diagram showing the effect of 3, 5, 10 and 30 µM riluzole on cell number of normoxic (light grey columns) or hypoxic (dark grey columns) Mat-LyLu cells. Data are presented as means ± SEM ($n \geq 3$). Data were analysed by ANOVA followed by Newman-Keuls *post hoc* analysis. Table of multiple comparisons between different treatments for statistical significance are shown underneath the bar diagram. (D) 0.015 % DMSO.

Because 24 h treatments with 10 µM riluzole consistently reduced cell number, subsequent experiments were restricted to 1 to 5 µM range, in order not to 'contaminate' any effect on Matrigel invasion.

4.2.2.4 Nav1.7 mRNA expression

Mat-LyLu cells were treated for 24 h with 1, 2.5 and 5 µM riluzole or 0.0025 % DMSO (highest concentration involved) under normoxic or hypoxic conditions and cDNAs were prepared for real-time PCRs. Agarose gel electrophoresis confirmed specific single bands at the expected sizes for Nav1.7 and Cytb5R (414 nt and 425 nt, respectively; $n = 3$ each; Figure 4.19A). The "no-template control" did not give any signal ($n = 3$; Figure 4.19A). No significant change in Nav1.7 mRNA expression was recorded when Mat-LyLu cells were treated (24 h) with 1 µM and 5 µM riluzole and 0.015 % DMSO ($p > 0.05$; $n = 3$ each; Figure 4.19B). On the other hand, 24 h treatment of Mat-LyLu cells, incubated with 2.5 µM riluzole under normoxic conditions, decreased Nav1.7 mRNA expression by 32 % and 22 % when compared to no treatment control (NTC) and DMSO controls, respectively, the former being statistically significant ($n = 3$ each; Figure 4.19B). Hypoxia itself readily increased Nav1.7 mRNA expression. Treatment with 1 µM riluzole for 24 h under hypoxic conditions had no significant effect on Nav1.7 mRNA level ($p > 0.05$; $n = 3$; Figure 4.19B). In contrast, under hypoxic conditions, 2.5 µM riluzole treatment (24 h) significantly decreased Nav1.7 mRNA level by 40 % and 43 % when compared to the NTC and DMSO controls, respectively ($p < 0.05$; $n = 3$ each; Figure 4.19B). Similarly, 5 µM riluzole treatment (24 h) in hypoxia significantly decreased Nav1.7 mRNA level by 41 % and 43 % when compared to the NTC and DMSO controls.



Comparison			p<0.05
1	vs	2	No
1	vs	3	No
1	vs	4	Yes
1	vs	5	No
1	vs	6	Yes
1	vs	7	Yes
1	vs	8	Yes
1	vs	9	Yes
1	vs	10	Yes
2	vs	3	No
2	vs	4	No
2	vs	5	No
2	vs	6	Yes
2	vs	7	Yes
2	vs	8	Yes

Comparison			p<0.05
2	vs	9	Yes
2	vs	10	Yes
3	vs	4	No
3	vs	5	No
3	vs	6	Yes
3	vs	7	Yes
3	vs	8	Yes
3	vs	9	Yes
3	vs	10	Yes
4	vs	5	No
4	vs	6	Yes
4	vs	7	Yes
4	vs	8	Yes
4	vs	9	Yes
4	vs	10	Yes

Comparison			p<0.05
5	vs	6	Yes
5	vs	7	Yes
5	vs	8	Yes
5	vs	9	Yes
5	vs	10	Yes
6	vs	7	No
6	vs	8	No
6	vs	9	Yes
6	vs	10	Yes
7	vs	8	No
7	vs	9	Yes
7	vs	10	Yes
8	vs	9	No
8	vs	10	No
9	vs	10	No

Figure 4.19 Effect of riluzole on Mat-LyLu Nav1.7 mRNA expression.
(A) Typical PCR products of Nav1.7 (414 bp) and normalising/control gene Cytb5R (425 bp) mRNA in Mat-LyLu cells that was incubated with 1, 2.5 and 5 µM riluzole under normoxic or hypoxic (2 % O_2) conditions for 24 h. (B) Bar diagram showing the result of real-time PCR experiment in which the effect of riluzole on Nav1.7 mRNA expression was studied under normoxic (light grey column) or hypoxic (dark grey column) conditions. The data were normalized to Cytb5R using the $2^{-\Delta\Delta C_T}$ method and expressed relative to normoxic control Nav1.7 level. The table of multiple comparisons between different treatments for statistical significance are shown underneath the bar diagram. Kruskal-Wallis method was used for statistic analysis. Data are presented as means ± SEM (n = 3). (D) 0.0025 % DMSO.

4.2.2.5 Subcellular VGSCα protein expression

4.2.2.5.1 Relative distribution

Confocal immunocytochemistry with the pan-VGSC antibody was used to test the possible effect of riluzole (2.5 µM) on subcellular distribution of VGSCα protein in Mat-LyLu cells under normoxic or hypoxic (2 % O_2) conditions (Figure 4.20). The relative subcellular distribution of the VGSCα protein was studied by 'straight line cross-sectional profile' analysis of Mat-LyLu cells (Figure 4.21). This analysis revealed that the relative level of plasma membrane and intracellular VGSCα protein was not affected by 24 h treatment with riluzole (2.5 µM) under both normoxic and hypoxic conditions ($p > 0.05$; $n \geq 63$; Figure 4.22). The relative plasma membrane VGSCα protein levels were as follows: 9.7 ± 0.4 % (normoxia control), 10.4 ± 0.4 % (normoxia + riluzole), 9.5 ± 0.5 % (hypoxia control), 10.6 ± 0.5 % (hypoxia + riluzole). Similarly, the relative intracellular VGSCα protein levels were as follows: 35.2 ± 0.5 % (normoxia control), 36.6 ± 0.4 % (normoxia + riluzole), 35.6 ± 0.5 % (hypoxic control) and 35.8 ± 0.5 % (hypoxia + riluzole). Thus, riluzole had no effect on relative levels of VGSCα protein in either cellular compartment.

4.2.2.5.2 Plasma membrane VGSCα protein level

Digital quantification of peripheral VGSCα immunoreactivity by 'free-form line profile' analysis of XYZ scans of Mat-LyLu cells, treated (24 h) with riluzole (2.5 µM), revealed no change in plasma membrane VGSCα level under normoxic conditions (IR_{pm} = 155 ± 5 AU/µm and 148 ± 3 AU/µm, respectively; $p > 0.05$; $n \geq 63$ each; Figures 4.23 and 4.24A&B). However, when Mat-LyLu cells were treated

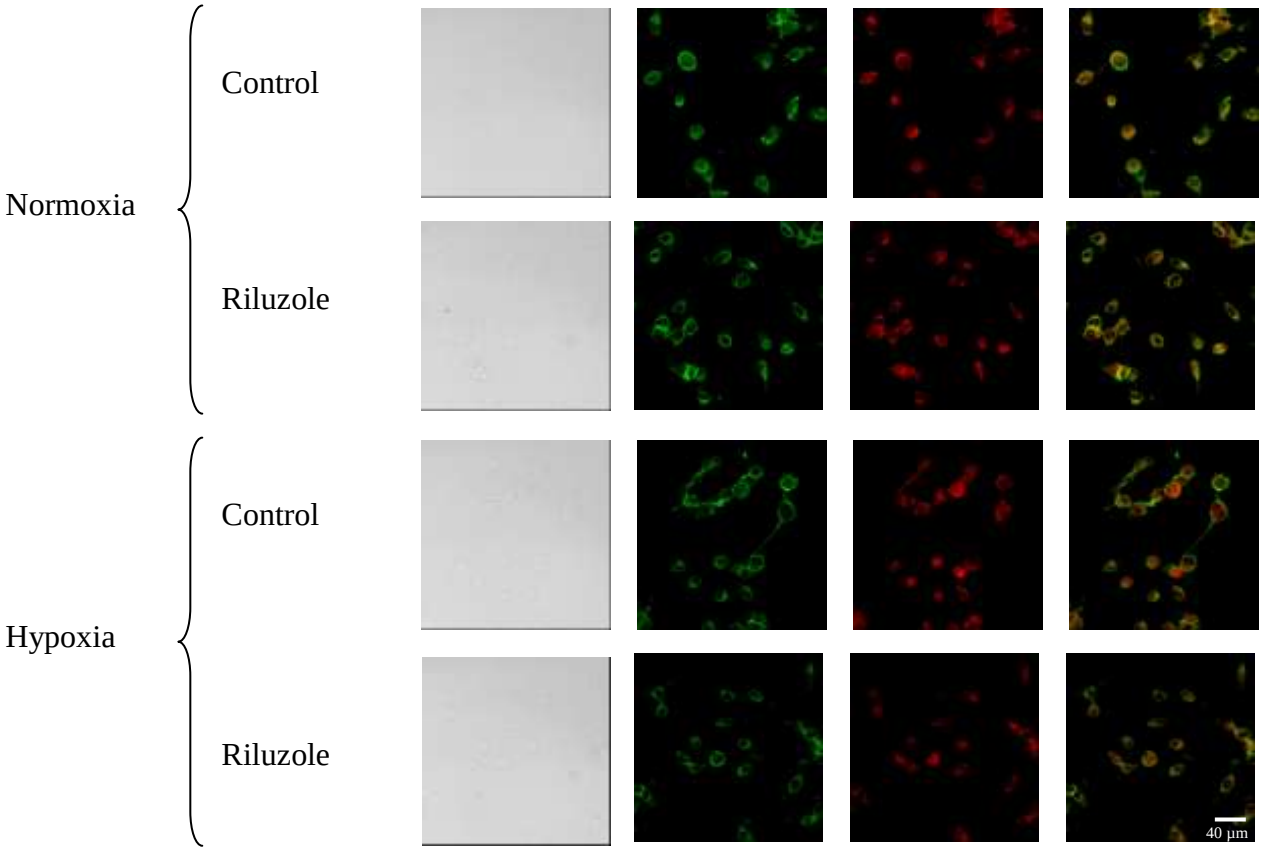


Figure 4.20 Confocal immunocytochemistry study of Mat-LyLu cells incubated with riluzole.
Typical XYZ confocal images of Mat-LyLu cells incubated 24 h under normoxic and hypoxic (2 % O_2) conditions with or without riluzole (2.5 µM). Signal from concanavalin A plasma membrane marker (green), pan-VGSC antibody (red) and overlay of both (merged image) are shown in addition to bright field image. Scale bar (40 µm) applicable to all panels.

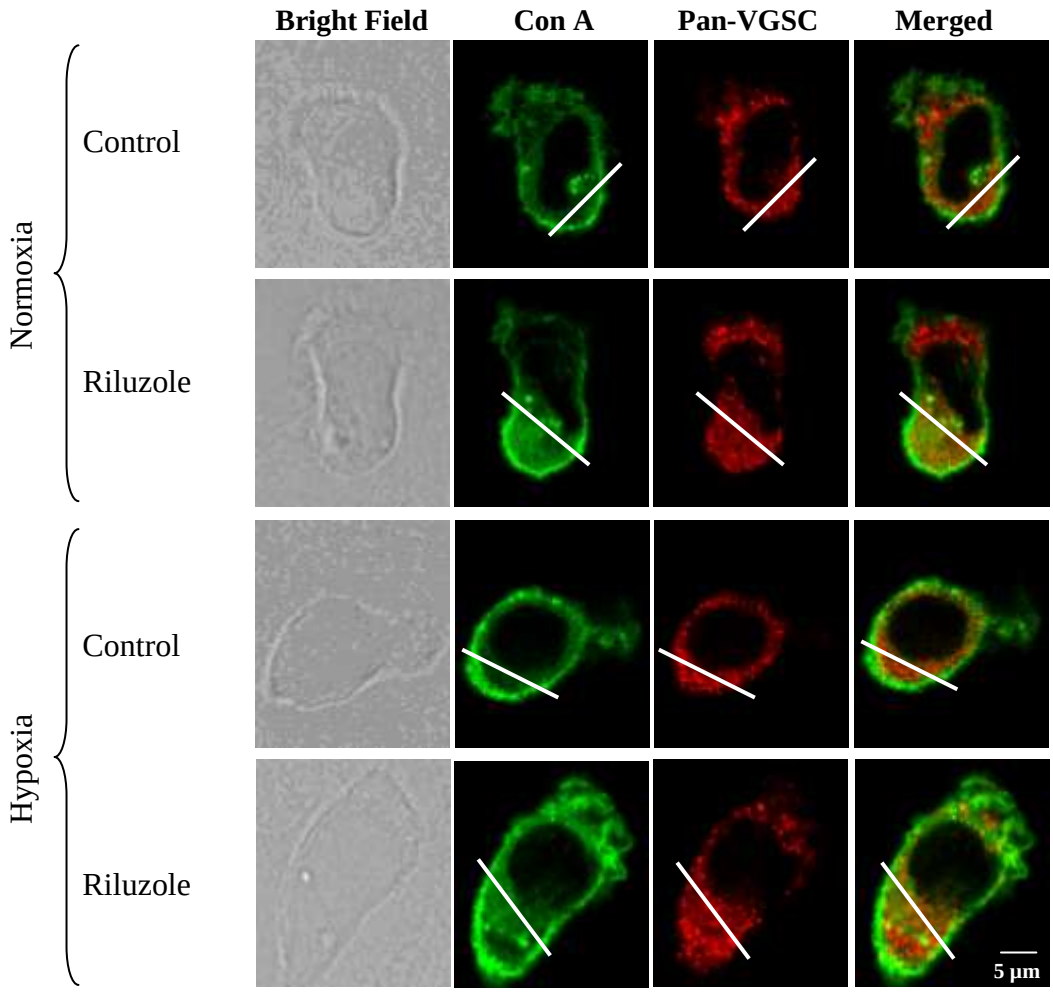


Figure 4.21 Typical image showing effect of riluzole on VGSCα protein distribution along typical cellular cross-section in Mat-LyLu cells.
Representative XYZ confocal images of Mat-LyLu cells incubated 24 h under normoxic and hypoxic conditions with or without riluzole (2.5 µM). White lines indicate typical cross-section. Scale bar (5µm) applicable to all panels.

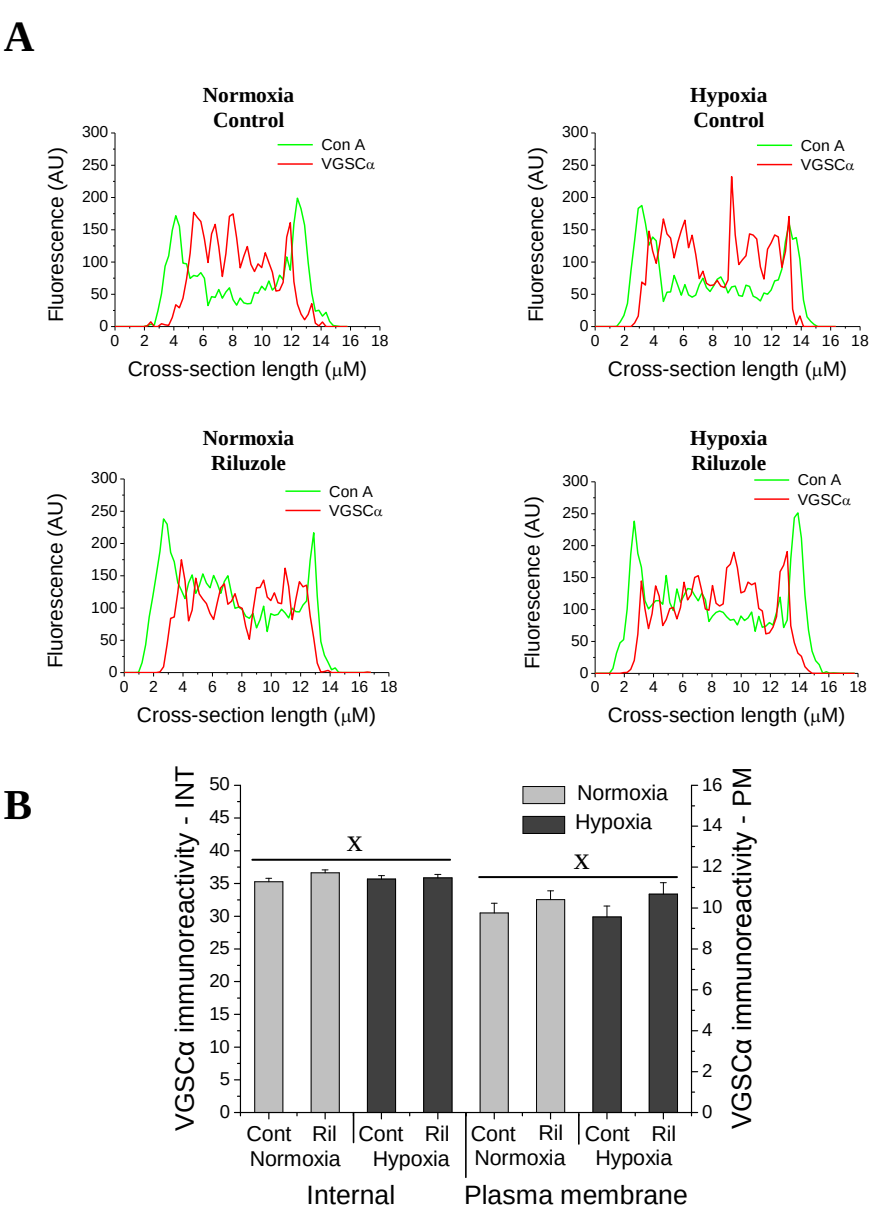


Figure 4.22 Effect of riluzole on VGSCα protein distribution along typical cellular cross-section in Mat-LyLu cells.
(A) Representative traces showing signal intensity of Con A plasma membrane marker (green) and VGSCα immunofluorescence (red) along cross-section from typical cells (Figure 4.21) incubated (24 h) in normoxic or hypoxic conditions with or without riluzole (2.5 μM). (B) Bar diagram showing distribution of VGSCα protein immunoreactivity along subcellular cross-sections as a percentage of total (%). For plasma membrane (PM) immunoreactivity, 1.5 μm sections was measured inward from the edge of Con A staining. For internal (INT) immunoreactivity, middle 30 % of the cross-section was measured. Data were analysed by ANOVA followed by Newman-Keuls *post hoc* analysis. Data are presented as means ± SEM (n = 63). Significance: (X) $p > 0.05$.

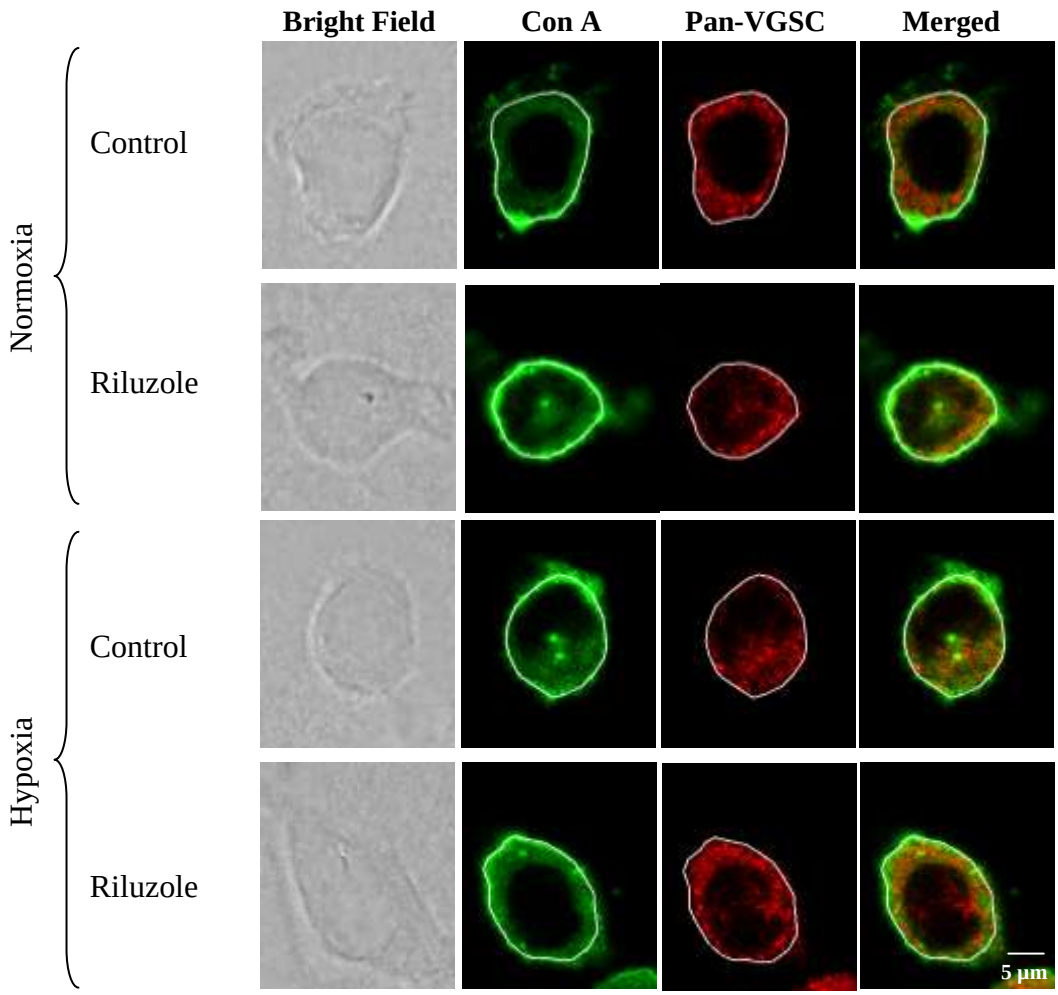
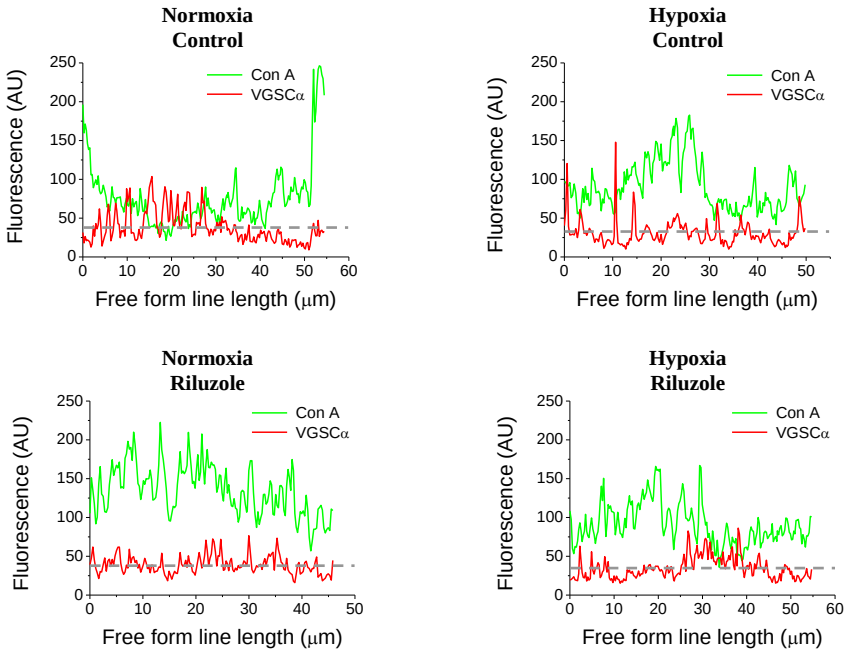
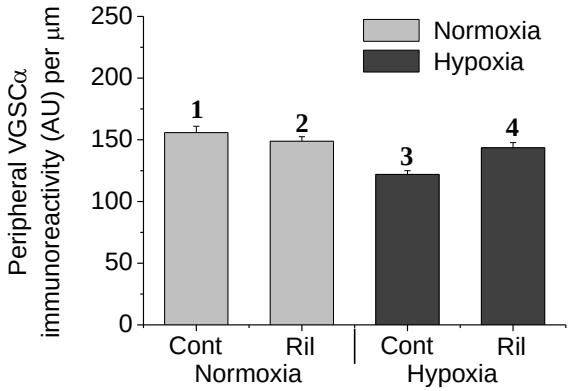


Figure 4.23 Typical image showing effect of riluzole on VGSCα protein levels in plasma membrane of Mat-LyLu cells.
Representative XYZ confocal images of Mat-LyLu cells incubated 24 h under normoxic and hypoxic conditions with or without riluzole (2.5 µM). White lines indicate typical freeform line guided by Con A staining to measure cell surface protein level. Scale bar (5µm) applicable to all panels.

A



B



Comparison			p<0.05
1	vs	2	No
1	vs	3	Yes
1	vs	4	No
2	vs	3	Yes
2	vs	4	No
3	vs	4	Yes

Figure 4.24 Effect of riluzole on VGSCα protein levels in plasma membrane of Mat-LyLu cells.
(A) Representative trace showing signal intensity of Con A plasma membrane marker (green) and VGSCα (red) immunofluorescence along plasma membrane from typical cells (Figure 4.23) incubated (24 h) in normoxic or hypoxic conditions with or without riluzole (2.5 μM). Dotted gray lines indicate mean pan-VGSC fluorescence. (B) Bar diagram showing level of VGSCα protein immunoreactivity along plasma membrane as an immunoreactivity (AU) per μm. Inset: table of multiple comparisons between treatments for statistical significance. Data were ANOVA of variance followed by Newman-Keuls *post hoc* analysis. Data are presented as means ± SEM (n = 74).

with riluzole (2.5 µM) under hypoxic conditions, plasma membrane level of VGSCα protein increased significantly: IR_{pm} = 121 ± 3 AU/µm (hypoxia control) *vs* 143 ± 4 AU/µm (hypoxia + riluzole) ($p < 0.05$; $n \geq 63$; Figures 4.23 and 4.24A&B). Hypoxia itself, again, reduced VGSCα protein level in plasma membrane: IR_{pm} = 121 ± 3 AU/µm (normoxia) *vs* 155 ± 5 AU/µm (hypoxia) ($p < 0.05$; $n \geq 63$ each; Figures 4.23 and 4.24A&B).

4.2.2.5.3 Internal VGSCα protein level

Quantification of 'internal' VGSCα immunoreactivity by 'area histogram' analysis of XYZ scans of Mat-LyLu cells revealed a significant decrease of internal VGSCα level (relative to normoxic control) by 9 %, 16 % and 17 % when incubated in (i) normoxic condition with riluzole (2.5 µM), (ii) hypoxic control condition and (iii) hypoxic condition with riluzole (2.5 µM), respectively ($p < 0.05$; $n \geq 77$ each; Figures 4.25 and 4.26A&B). On the other hand, internal VGSCα protein levels of cells maintained in hypoxia with or without riluzole (2.5 µM) for 24 h were not different ($p > 0.05$; $n \geq 77$ each; Figures 4.25 and 4.26A&B).

4.2.2.6 Matrigel™ invasion

Matrigel™ invasion assays were used to study the possible effects of riluzole treatment on invasiveness of Mat-LyLu cells maintained in normoxic and hypoxic conditions. Under normaxic conditions, 0.0025 % DMSO (control) and 1 µM and 2.5 µM riluzole treatments had no significant effect on invaded Mat-LyLu cell number ($p > 0.05$; $n \geq 4$ each; Figures 4.27 and 4.28). On the other hand, 5 µM riluzole treatment significantly reduced invaded cell number by 50 % when compared to the 'non-treated control' under normoxia ($p < 0.05$; $n \geq 4$; Figures 4.27

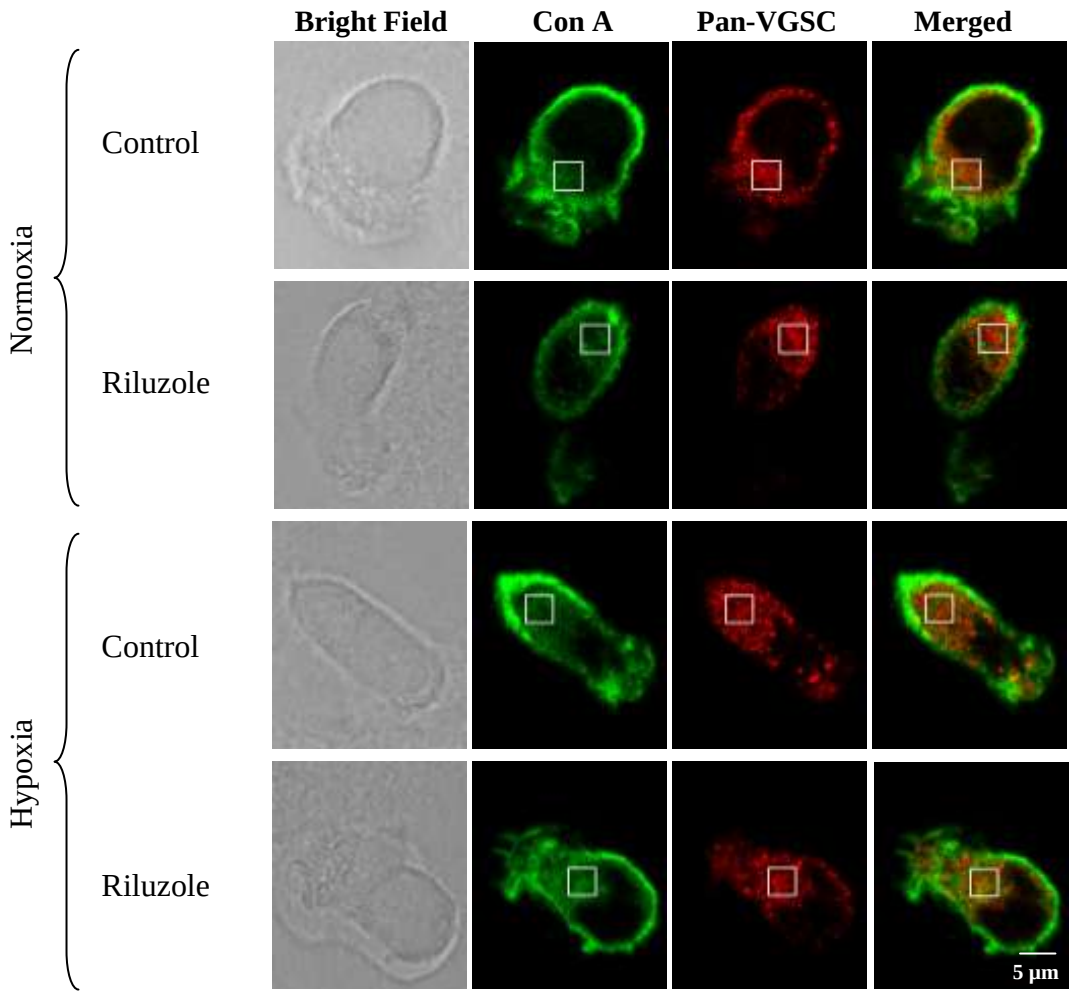
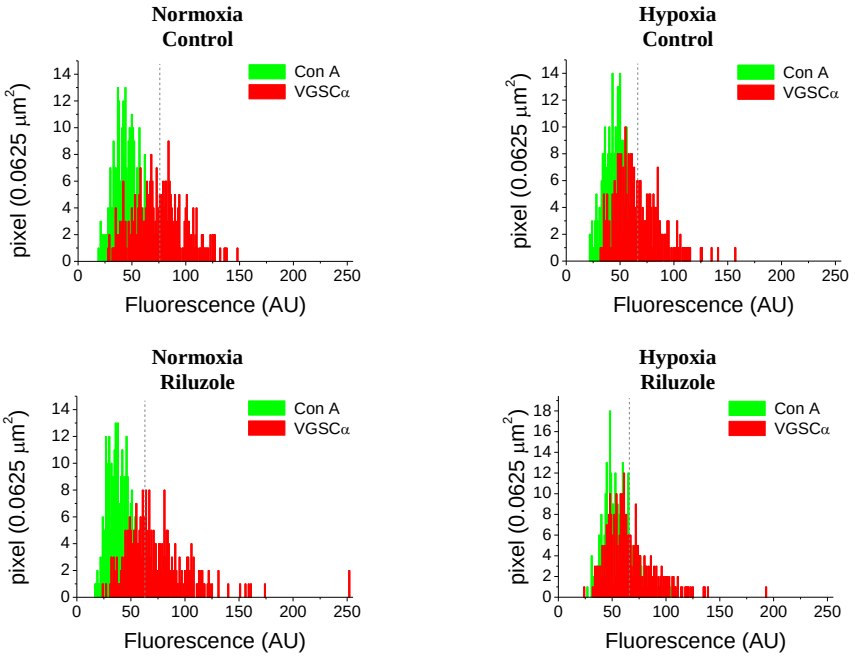
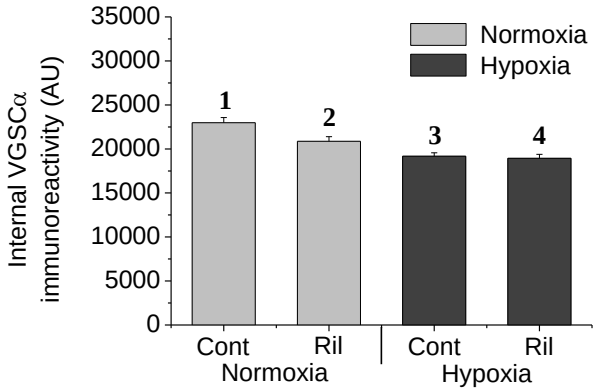


Figure 4.25 Typical image showing effect of riluzole on internal VGSCα protein levels of Mat-LyLu cells.
Representative XYZ confocal images of Mat-LyLu cells incubated 24 h under normoxic and hypoxic conditions with or without riluzole (2.5 µM). White box indicates typical area covering 16 μm^2 square section of cytoplasm avoiding nucleus to measure internal protein level. Scale bar (5µm) applicable to all panels.

A



B



Comparison			p<0.05
1	vs	2	Yes
1	vs	3	Yes
1	vs	4	Yes
2	vs	3	Yes
2	vs	4	Yes
3	vs	4	No

Figure 4.26 Effect of riluzole on internal VGSCα protein levels of Mat-LyLu cells.
(A) Representative histograms showing distribution of pixels (0.0625 µm^2) with signal intensity of Con A plasma membrane marker (green) and VGSCα (red) immunofluorescence in cytoplasm from typical cells (Figure 4.25) incubated (24 h) in normoxic or hypoxic conditions with or without riluzole (2.5 µM). Dotted gray lines indicate mean pan-VGSC fluorescence. (B) Bar diagram showing internal VGSCα protein immunoreactivity (AU). Inset: table of multiple comparisons between treatments for statistical significance. Data were analysed by ANOVA followed by Newman-Keuls *post hoc* analysis. Data are presented as means ± SEM (n = 77).

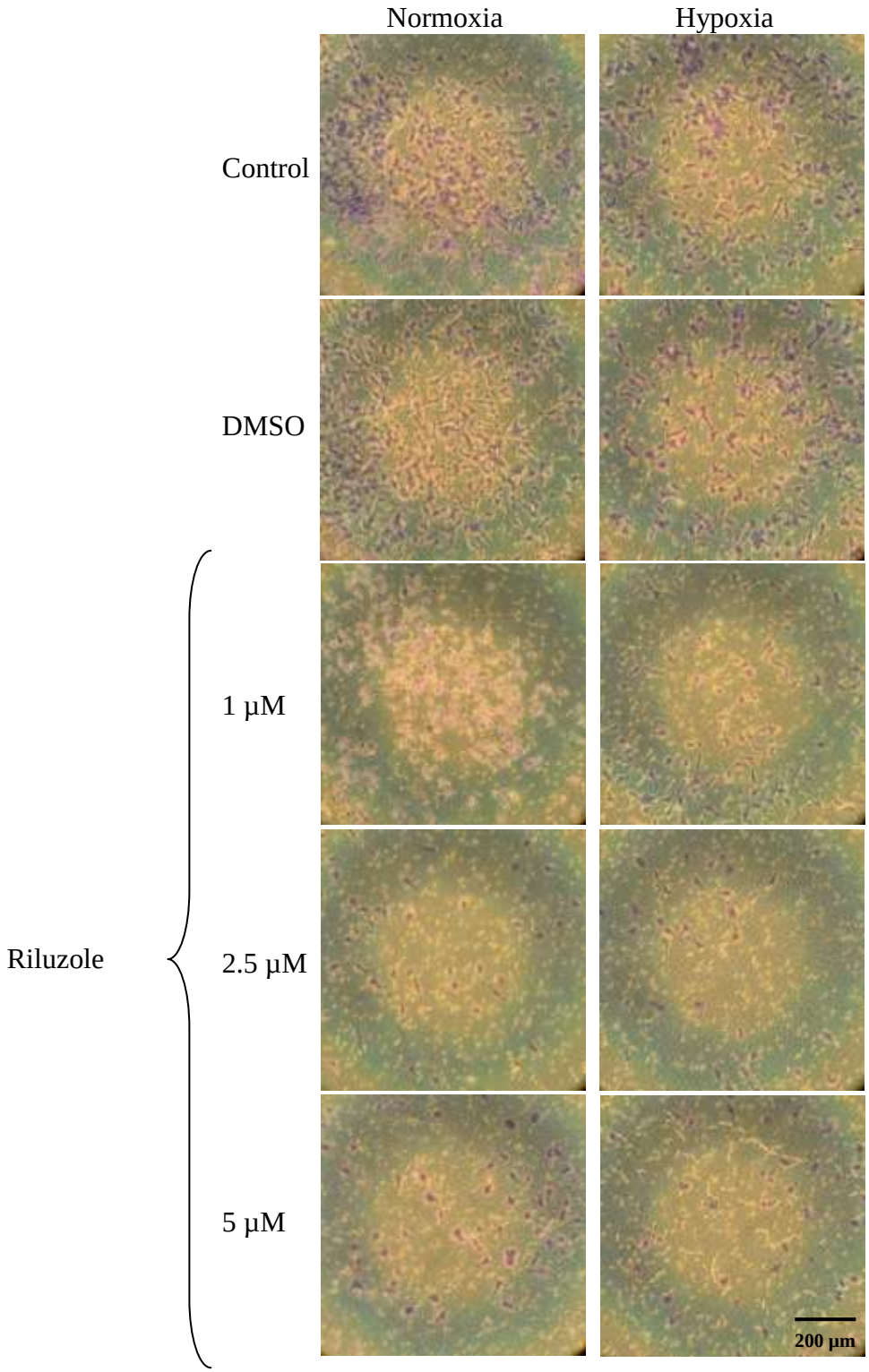
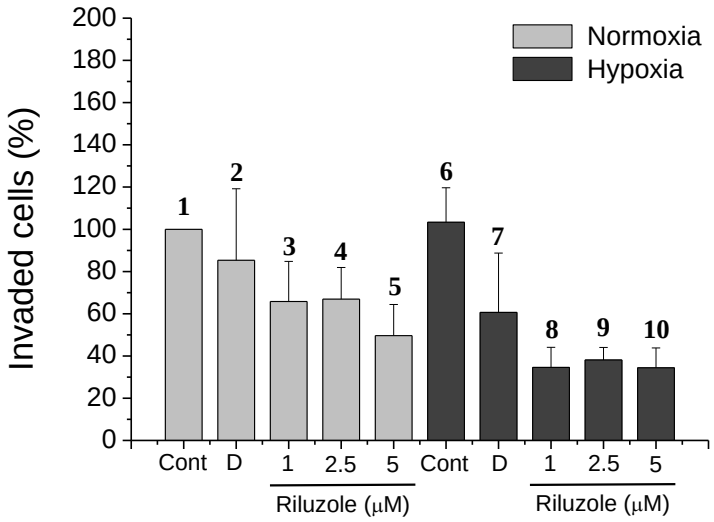


Figure 4.27 Typical images of invaded cells showing the effect of riluzole on invasion of Mat-LyLu invasiveness.
Typical phase-contrast light-microscopy images of invaded cells obtained from Matrigel™ invasion assays of Mat-LyLu cells incubated 24 h under normoxic and hypoxic conditions with or without riluzole (1, 2.5 and 5 µM). Invaded cells were fixed and stained with crystal violet (purple). Scale bar (200 µm) applicable to all panels. DMSO (0.0025 %).



Comparison			p<0.05
1	vs	2	No
1	vs	3	No
1	vs	4	No
1	vs	5	Yes
1	vs	6	No
1	vs	7	Yes
1	vs	8	Yes
1	vs	9	Yes
1	vs	10	Yes
2	vs	3	No
2	vs	4	No
2	vs	5	No
2	vs	6	No
2	vs	7	No
2	vs	8	Yes

Comparison			p<0.05
2	vs	9	Yes
2	vs	10	No
3	vs	4	No
3	vs	5	No
3	vs	6	No
3	vs	7	No
3	vs	8	No
3	vs	9	No
3	vs	10	No
4	vs	5	No
4	vs	6	No
4	vs	7	No
4	vs	8	No
4	vs	9	No
4	vs	10	No

Comparison			p<0.05
5	vs	6	Yes
5	vs	7	No
5	vs	8	No
5	vs	9	No
5	vs	10	No
6	vs	7	No
6	vs	8	Yes
6	vs	9	Yes
6	vs	10	Yes
7	vs	8	No
7	vs	9	No
7	vs	10	No
8	vs	9	No
8	vs	10	No
9	vs	10	No

Figure 4.28 Effect of riluzole on invasion of Mat-LyLu cells.
Histogram showing number of invaded Mat-LyLu cells, incubated 24 h under normoxic and hypoxic conditions with or without riluzole (1, 2.5 and 5 μM). Data were expressed relative to the control (%) and presented as means ± SEM ($n \geq 4$). Data were analysed by Kruskal-Wallis analysis of variance. The table of multiple comparisons between treatments for statistical significance shown underneath. D: DMSO (0.0025 %).

and 4.28). However, riluzole (1, 2.5 and 5 µM) had no significant effect on invasion when compared to DMSO controls under normoxic conditions ($p > 0.05$; $n \geq 4$; Figures 4.27 and 4.28). Treatment of Mat-LyLu cells for 24 h in hypoxic conditions with 1 , 2.5 and 5 µM riluzole significantly decreased invaded cell number by 66 %, 63 % and 66 %, respectively ($p < 0.05$; $n \geq 4$; Figures 4.27 and 4.28). Invaded cell number under hypoxia decreased by 41 % by 0.0025 % DMSO treatment; this change was not significant ($p > 0.05$; $n \geq 4$ each; Figures 4.27 and 4.28). Riluzole (1, 2.5 and 5 µM) had no significant effect on invasion when compared to the respective DMSO controls under hypoxic conditions ($p > 0.05$; $n \geq 4$ each; Figures 4.27 and 4.28). Again, hypoxia by itself had no effect on invasiveness.

4.2.2.7 Summary of effects of riluzole

Under normoxic conditions, riluzole had some inhibitory effect on cell proliferation and decreased intracellular VGSCα level and invasiveness. Hypoxia had no effect on invasion. DMSO introduced considerable variability in the invasion assays and under hypoxia, again, riluzole, had no effect on invasion (Table 4.1).

4.2.3 Effects of procaine

Procaine is a local anaesthetic that has been used as a non-selectively blocker of VGSCs. In the present study, it was used in the concentration range 1 to 1000 µM, since this concentration range was shown previously to block VGSC (Bräu *et al.*, 1998; Vlachová *et al.*, 1999).

4.2.3.1 Some initial observations: Cell morphology

No change in the basic appearance or distribution of Mat-LyLu cells in culture was observed when cultures were treated (24 h) with 100 µM and 500 µM procaine under

both normoxic and hypoxic (2 % O_2) conditions (Figures 4.29A-C). At the higher concentration of 1000 µM, also, procaine treatment in normoxia did not change the basic appearance or distribution of the cells. On the other hand, Mat-LyLu cells maintained in hypoxic conditions and treated similarly acquired generally to lose inter-cellular contacts and appear scattered (Figure 4.29D). Studying the effect of procaine treatment on Mat-LyLu cells under high magnification revealed that 1000 µM treatment caused loss of spindle-shaped fibroblast like morphology in hypoxic but not in normoxic conditions (Figure 4.30D). Thus, procaine treatment (24 h) of up to 500 µM had no obvious effect on cell morphology in normoxia or hypoxia (Figure 4.30A-C).

4.2.3.2 Cell viability

Procaine treatment (24 h) up to 1000 µM was not toxic to Mat-LyLu cells maintained in normoxic or hypoxic conditions (Figure 4.31).

4.2.3.3 Cellular proliferation

No significant change was recorded in Mat-LyLu cell number after 24 h procaine treatment (10, 100, 500, 700 and 1000 µM) in normoxic conditions ($p > 0.05$; $n \geq 3$ each; Figure 4.32). Hypoxia by itself had no effect, as before, and all concentrations of procaine used did not affect Mat-LyLu cell number (24 h) ($p > 0.05$; $n \geq 3$ each; Figure 4.32). However, when compared to the normoxic control, 700 and 1000 µM procaine in hypoxia appeared to reduce cell numbers by 32 % and 31 %, respectively ($p < 0.05$; $n \geq 3$ each; Figure 4.32).

Because 24 h treatments with 700 µM procaine under hypoxia reduced cell number, subsequent experiments were restricted to 1 to 500 µM range, in order not to 'contaminate' any effect on Matrigel invasion.

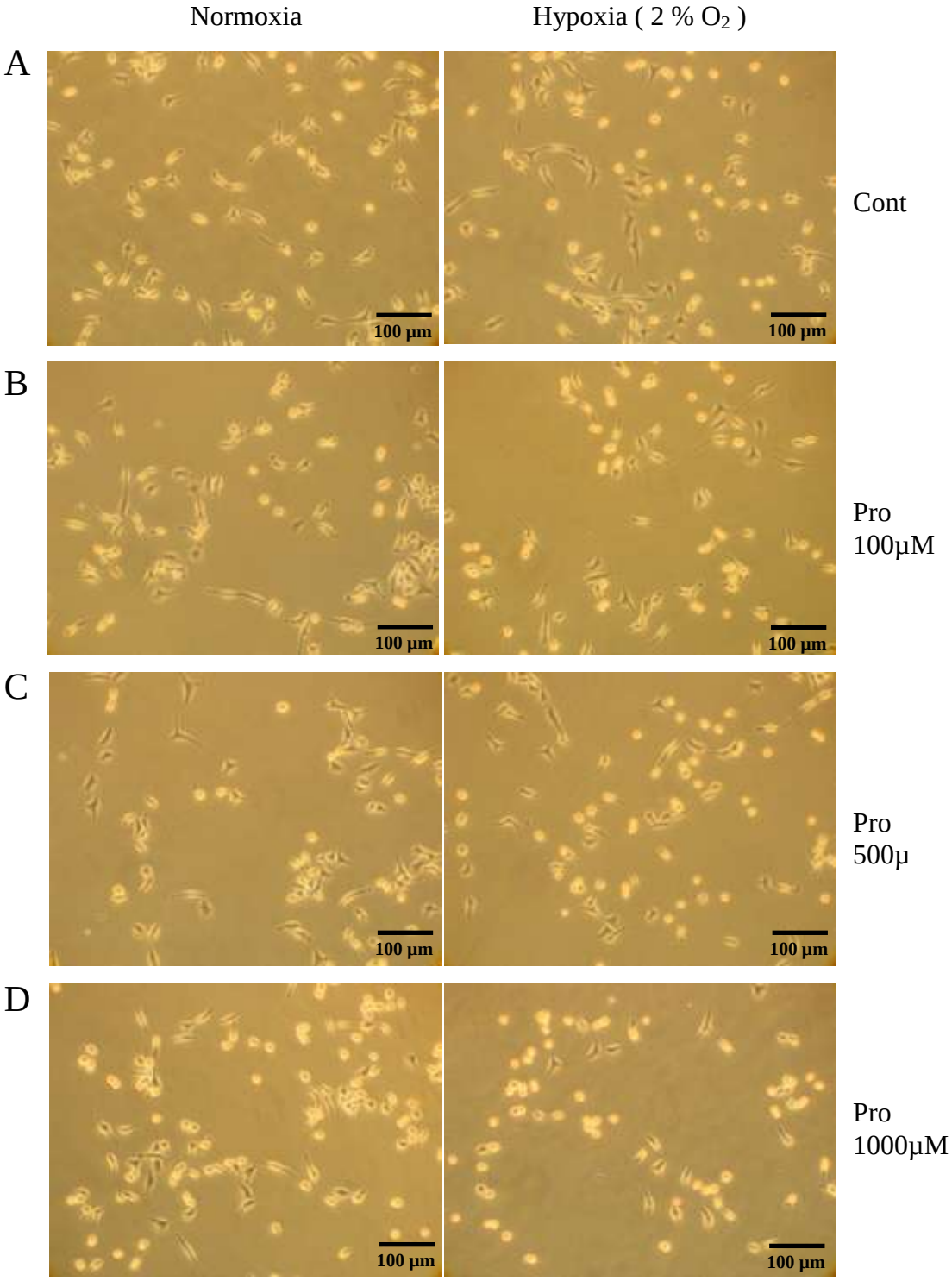


Figure 4.29 Phase-contrast light-photomicrography of Mat-LyLu cells, treated with procaine.

Mat-LyLu cells were grown for 24 h under (A) control conditions, and in (B) 100 µM procaine, (C) 500 µM procaine, (D) 1000 µM procaine treatment in normoxia (left hand pictures) and hypoxia (2 % O_2; right hand pictures). Micrographs are typical of 3 experiments.

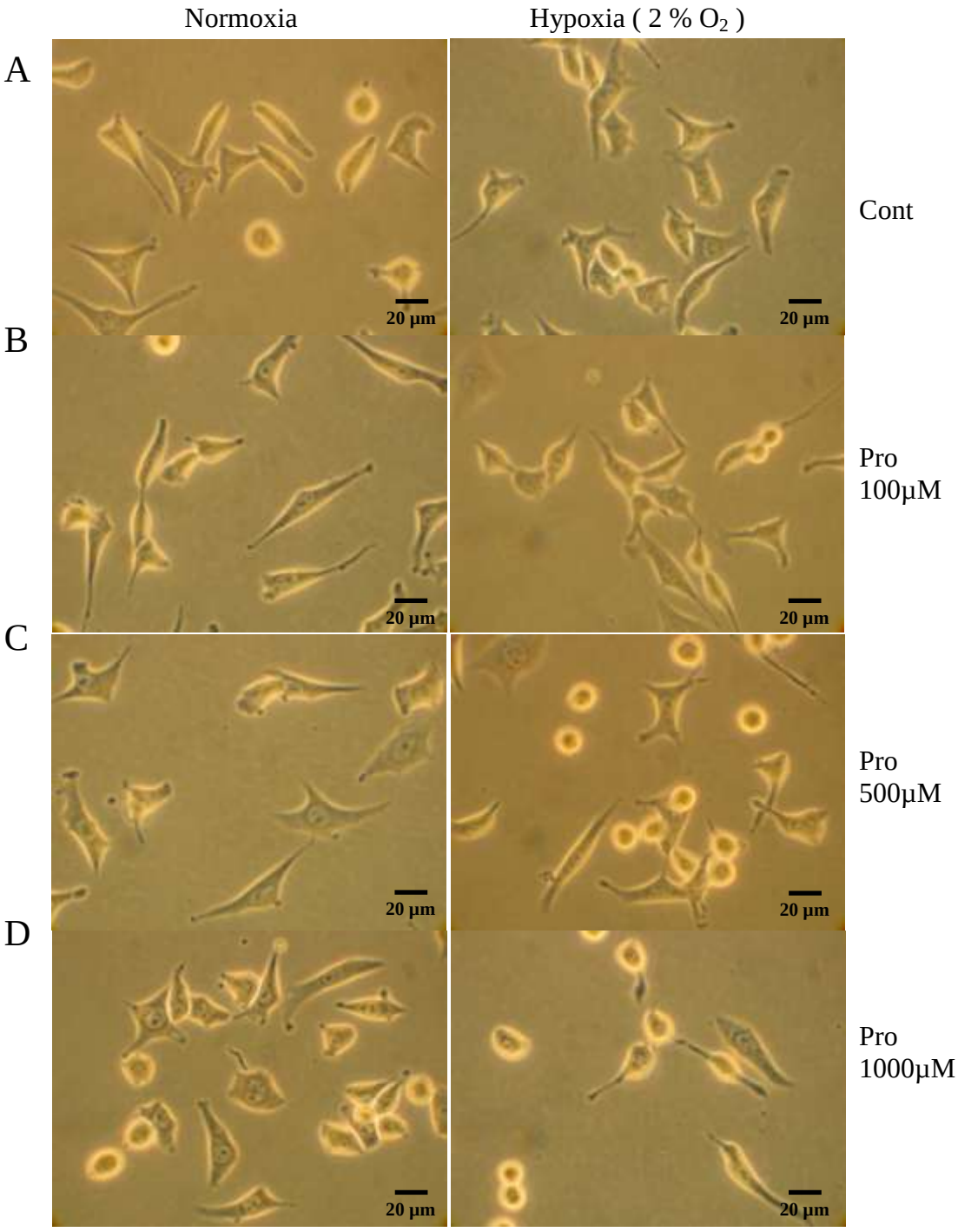


Figure 4.30 Phase-contrast light-photomicrography of Mat-LyLu cells, treated with procaine, in high magnification.

Mat-LyLu cells were grown for 24 h under (A) control conditions, and in (B) 100 µM procaine, (C) 500 µM procaine, (D) 1000 µM procaine treatment in normoxia (left hand pictures) and hypoxia (2 % O_2; right hand pictures). Micrographs are typical of 3 experiments.

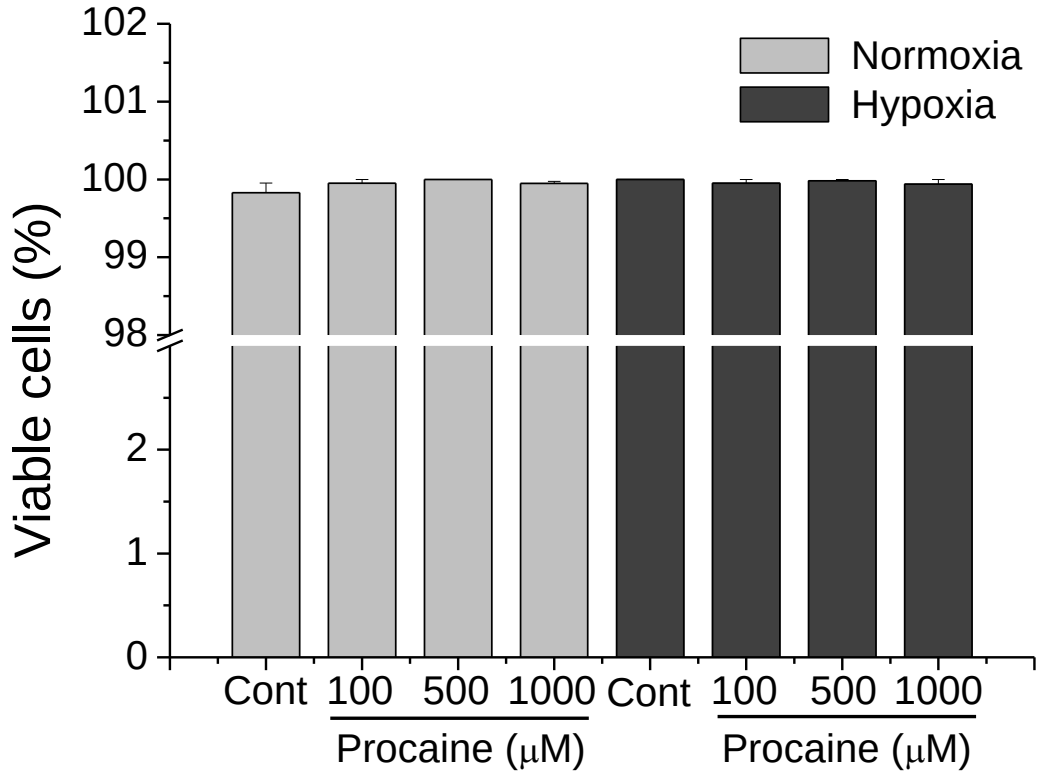
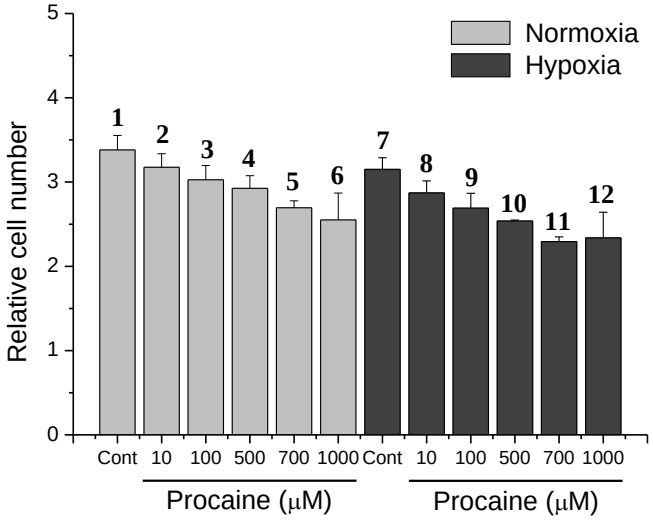


Figure 4.31 Bar diagram showing procaine treatments had no toxic effect.

A possible effect of 100, 500 and 1000 µM procaine on Mat-LyLu cell viability under normoxia (light grey columns) or hypoxia (2 % O_2; dark grey columns). Data are represented as means ± SEM (*n* = 3).



Comparison			p<0.05
1	vs	2	No
1	vs	3	No
1	vs	4	No
1	vs	5	No
1	vs	6	No
1	vs	7	No
1	vs	8	No
1	vs	9	No
1	vs	10	No
1	vs	11	Yes
1	vs	12	Yes
2	vs	3	No
2	vs	4	No
2	vs	5	No
2	vs	6	No
2	vs	7	No
2	vs	8	No
2	vs	9	No
2	vs	10	No
2	vs	11	No
2	vs	12	No
3	vs	4	No

Comparison			p<0.05
3	vs	5	No
3	vs	6	No
3	vs	7	No
3	vs	8	No
3	vs	9	No
3	vs	10	No
3	vs	11	No
3	vs	12	No
4	vs	5	No
4	vs	6	No
4	vs	7	No
4	vs	8	No
4	vs	9	No
4	vs	10	No
4	vs	11	No
4	vs	12	No
5	vs	6	No
5	vs	7	No
5	vs	8	No
5	vs	9	No
5	vs	10	No
5	vs	11	No

Comparison			p<0.05
5	vs	12	No
6	vs	7	No
6	vs	8	No
6	vs	9	No
6	vs	10	No
6	vs	11	No
6	vs	12	No
7	vs	8	No
7	vs	9	No
7	vs	10	No
7	vs	11	No
7	vs	12	No
8	vs	9	No
8	vs	10	No
8	vs	11	No
8	vs	12	No
9	vs	10	No
9	vs	11	No
9	vs	12	No
10	vs	11	No
10	vs	12	No
11	vs	12	No

Figure 4.32 Dose dependent effect of procaine on Mat-LyLu cell number.
Bar diagram showing the effect of 10, 100, 500 and 700 μM procaine on cell number of normoxic (light grey columns) or hypoxic (dark grey columns) Mat-LyLu cells. Data are presented as means ± SEM ($n \geq 3$). Data were analysed by ANOVA followed by Newman-Keuls *post hoc* analysis. Table of multiple comparisons between different treatments for statistical significance are shown underneath the bar diagram.

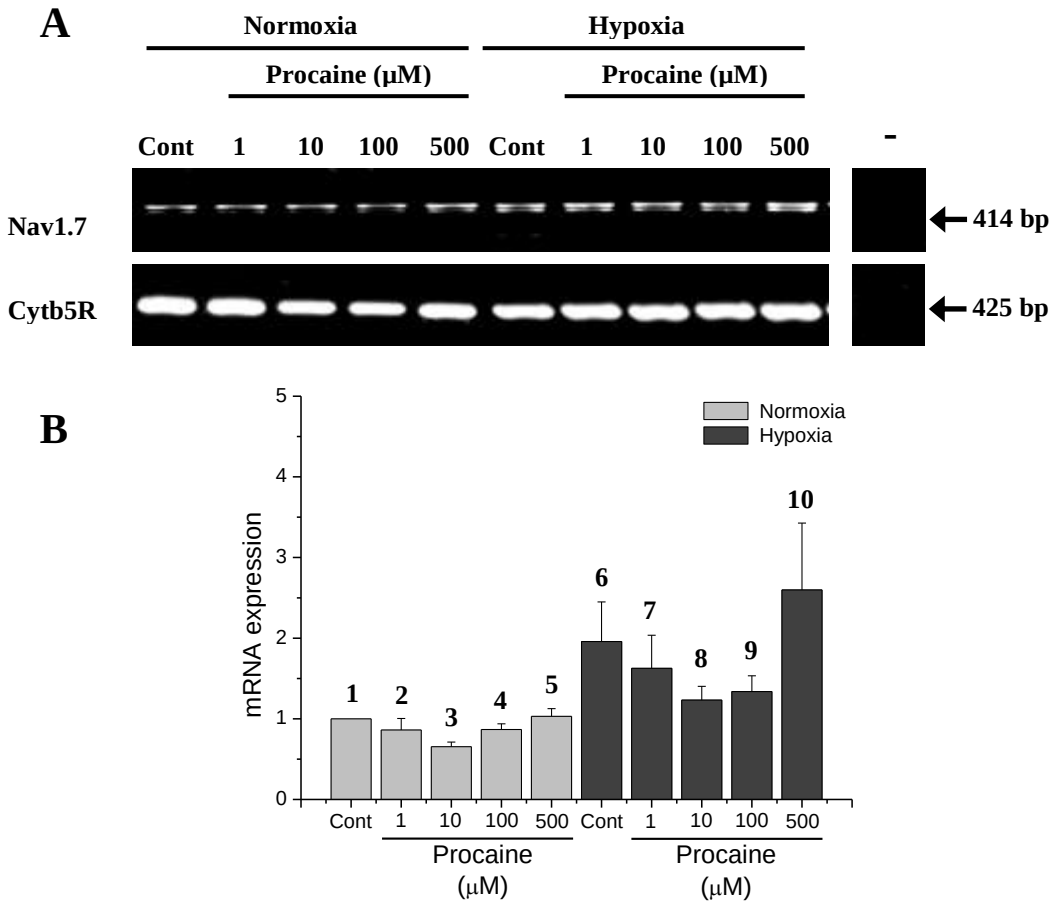
4.2.3.4 Nav1.7 mRNA expression

Mat-LyLu cells were treated for 24 h with 1, 10, 100 and 500 µM procaine under normoxic or hypoxic conditions, and cDNAs were prepared for real-time PCR analyses. Agarose gel electrophoresis confirmed specific single bands at the expected sizes for Nav1.7 and Cytb5R (414 nt and 425 nt, respectively; n = 3 each; Figure 4.33A). The "no-template control" did not give any signal (n = 3 each; Figure 4.33A). There was a dose dependent effect of procaine on Nav1.7 mRNA expression in normoxia. For 1, 100 or 500 µM procaine, there was no change in Nav1.7 mRNA expression in Mat-LyLu cells treated in normoxia for 24 h ($p > 0.05$; n = 3 each; Figure 4.33B). On the other hand, 10 µM procaine significantly decreased Nav1.7 mRNA by 35 % under normoxic conditions ($p < 0.05$; $n \geq 3$; Figure 4.33B). Hypoxia itself significantly increased Nav1.7 mRNA expression. On the other hand, in hypoxia, 24 h treatment with procaine (up to 500 µM) had no effect on the Nav1.7 mRNA level ($p > 0.05$; $n \geq 3$ each; Figure 4.33B).

4.2.3.5 Subcellular VGSCα protein expression

4.2.3.5.1 Relative distribution

Confocal immunocytochemistry and digital imaging of Mat-LyLu cells stained with the pan-VGSC antibody was used to test the possible effect of procaine (100 µM) on subcellular distribution of VGSCα protein under normoxic or hypoxic (2 % O_2) conditions (Figure 4.34). The subcellular distribution of the VGSCα protein was studied by 'straight line cross-sectional profile' analysis (Figure 4.35). The relative plasma membrane VGSCα protein levels were as follows: 9.7 ± 0.4 % (normoxia control), 10.6 ± 0.4 % (normoxia + procaine), 9.5 ± 0.5 % (hypoxia control), 9.0 ± 0.5 % (hypoxia + procaine). The corresponding internal VGSCα protein levels were



Comparison			p<0.05
1	vs	2	No
1	vs	3	Yes
1	vs	4	No
1	vs	5	No
1	vs	6	Yes
1	vs	7	Yes
1	vs	8	No
1	vs	9	No
1	vs	10	Yes
2	vs	3	No
2	vs	4	No
2	vs	5	No
2	vs	6	Yes
2	vs	7	Yes
2	vs	8	Yes

Comparison			p<0.05
2	vs	9	Yes
2	vs	10	Yes
3	vs	4	No
3	vs	5	Yes
3	vs	6	Yes
3	vs	7	Yes
3	vs	8	Yes
3	vs	9	Yes
3	vs	10	Yes
4	vs	5	No
4	vs	6	Yes
4	vs	7	Yes
4	vs	8	No
4	vs	9	Yes
4	vs	10	Yes

Comparison			p<0.05
5	vs	6	Yes
5	vs	7	Yes
5	vs	8	No
5	vs	9	No
5	vs	10	Yes
6	vs	7	No
6	vs	8	No
6	vs	9	No
6	vs	10	No
7	vs	8	No
7	vs	9	No
7	vs	10	No
8	vs	9	No
8	vs	10	Yes
9	vs	10	Yes

Figure 4.33 Effect of procaine on Mat-LyLu Nav1.7 mRNA expression.
(A) Typical PCR products of Nav1.7 (414 bp) and normalising/control gene Cytb5R (425 bp) mRNA in Mat-LyLu cells that was incubated with 1, 10, 100 and 500 μM procaine under normoxic or hypoxic (2 % O_2) conditions for 24 h. (B) Bar diagram showing the result of real-time PCR experiment in which the effect of procaine on Nav1.7 mRNA expression was studied under normoxic (light grey column) or hypoxic (dark grey column) conditions. The data were normalized to Cytb5R using the $2^{-\Delta\Delta C_T}$ method and expressed relative to normoxic control Nav1.7 level. The table of multiple comparisons between different treatments for statistical significance are shown underneath the bar diagram. Kruskal-Wallis method was used for statistic analysis. Data are presented as means ± SEM (n = 3). (-): no template control.

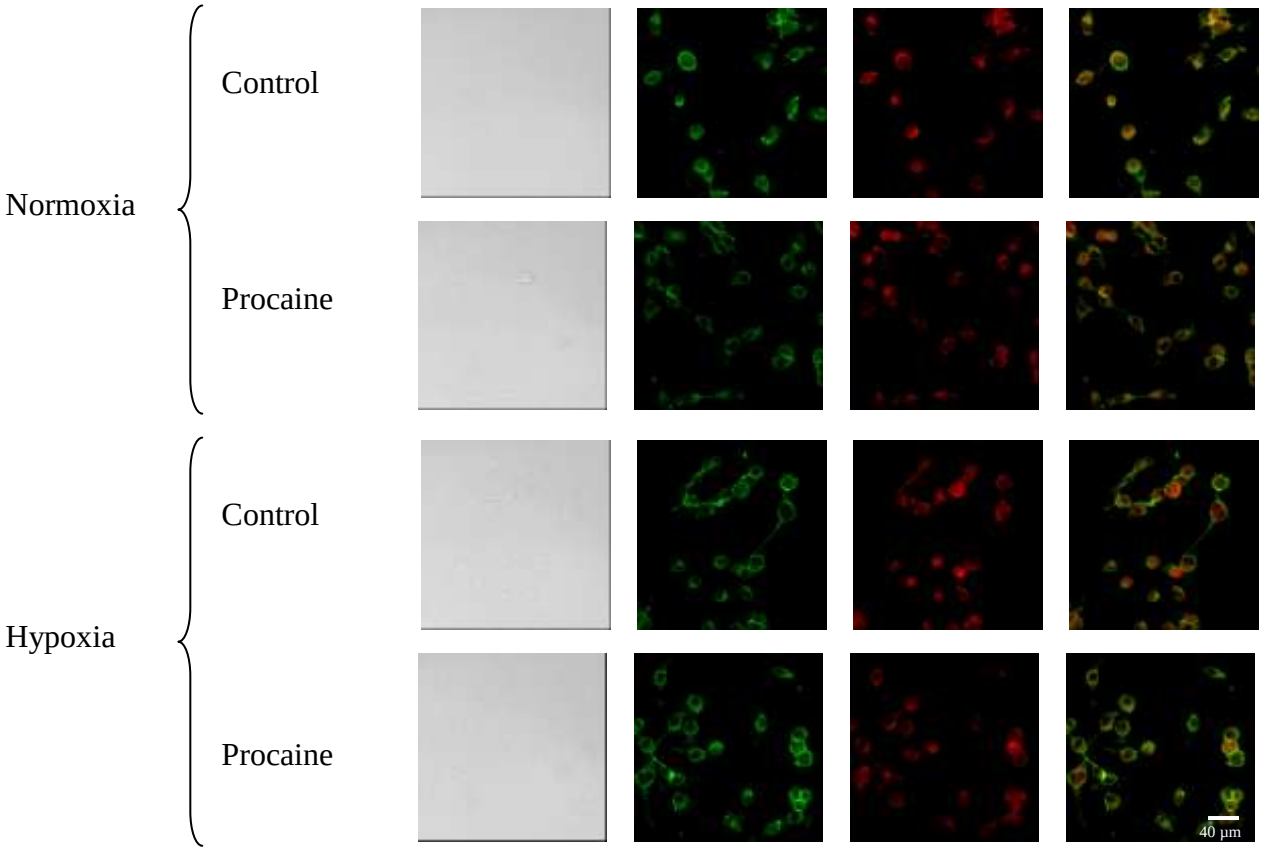


Figure 4.34 Confocal immunocytochemistry study of Mat-LyLu cells incubated with procaine.
Typical XYZ confocal images of Mat-LyLu cells incubated 24 h under normoxic and hypoxic (2 % O_2) conditions with or without procaine (100 µM). Signal from concanavalin A plasma membrane marker (green), pan-VGSC antibody (red) and overlay of both (merged image) are shown in addition to bright field image. Scale bar (40 µm) applicable to all panels.

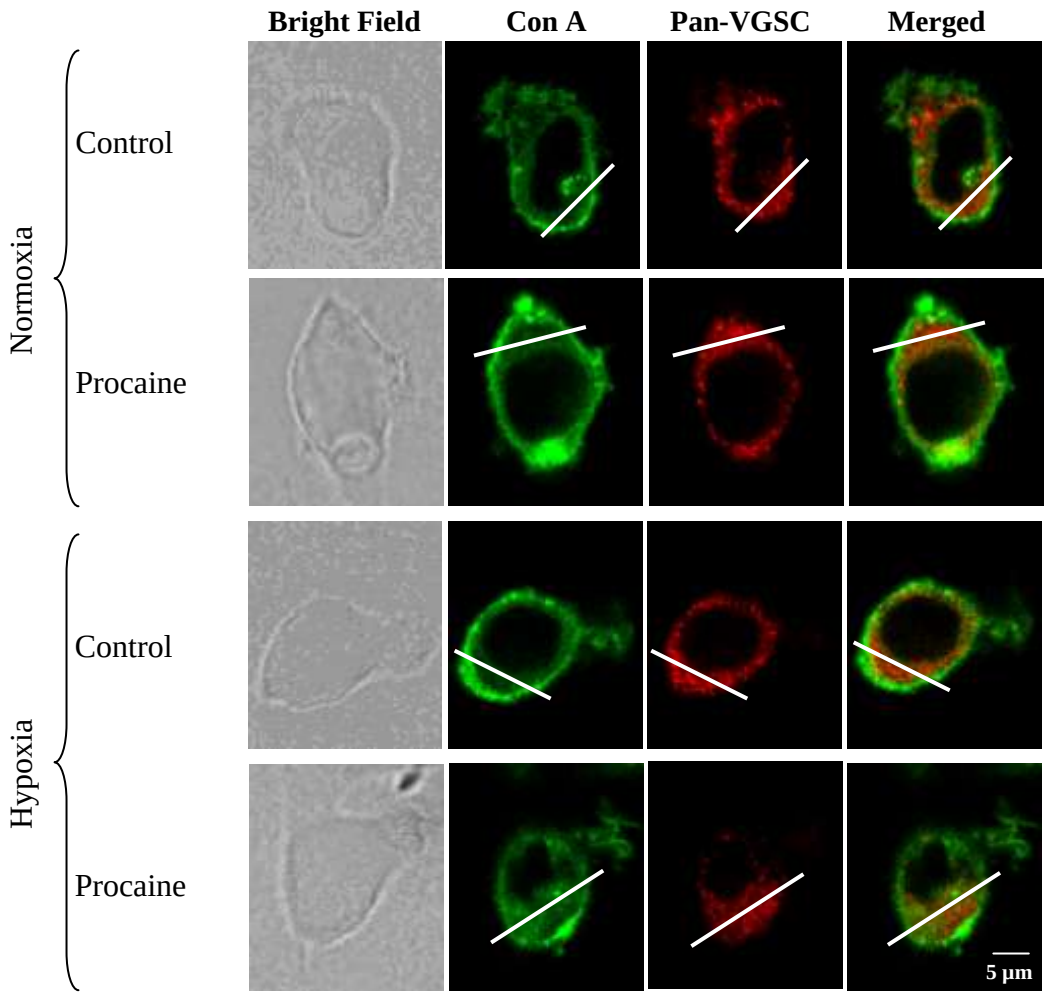


Figure 4.35 Typical image showing effect of procaine on VGSCα protein distribution along typical cellular cross-section in Mat-LyLu cells.
Representative XYZ confocal images of Mat-LyLu cells incubated 24 h under normoxic and hypoxic conditions with or without procaine (100 µM). White lines indicate typical cross-section. Scale bar (5µm) applicable to all panels.

as follows: 35.2 ± 0.5 % (normoxia control), 35.0 ± 0.4 % (normoxia + procaine), 35.6 ± 0.5 % (hypoxia) and 35.7 ± 0.5 % (hypoxia + procaine). This analysis revealed that the relative levels of plasma membrane and intracellular VGSCα protein were not affected by 24 h procaine (100 µM) treatment in both normoxic and hypoxic conditions (for both: $p > 0.05$; $n \geq 63$; Figure 4.36A&B).

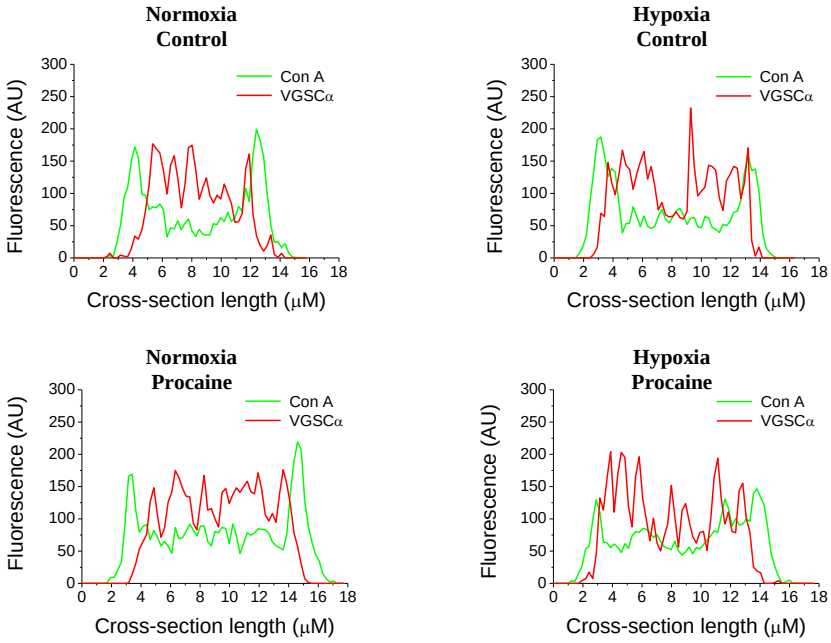
4.2.3.5.2 Plasma membrane VGSCα protein level

Digital quantification of VGSCα peripheral immunostaining by 'free-form line profile' analysis of XYZ scans of Mat-LyLu cells, treated (24 h) with procaine (100 µM), revealed a significantly lower level of plasma membrane VGSCα level under normoxic conditions: IR_{pm} = 155 ± 5 AU/µm vs 129 ± 4 AU/µm ($p < 0.05$; $n \geq 74$ each; Figures 4.37 and 4.38A&B). Hypoxia by itself significantly reduced the plasma membrane VGSCα level. On the other hand, 100 µM procaine treatment for 24 h in hypoxia had no effect ($p > 0.05$; $n \geq 74$ each; Figures 4.37 and 4.38A&B).

4.2.3.5.3 Internal VGSCα protein level

Digital quantification of intracellular VGSCα immunoreactivity by 'area histogram' analysis of XYZ scans of Mat-LyLu cells revealed a significant decreases in IR_{int} by 19 %, 16 % and 24 % when the cells were incubated in (i) normoxic condition with procaine (100 µM), (ii) hypoxic control condition and (iii) hypoxia with procaine (100 µM), respectively ($p < 0.05$; $n \geq 77$ each; Figures 4.39 and 4.40A&B). On the other hand, the internal VGSCα protein level of Mat-LyLu cells maintained in hypoxia with or without procaine (100 µM) treatment (24 h) remained unchanged ($p > 0.05$; $n \geq 77$ each; Figures 4.39 and 4.40A&B).

A



B

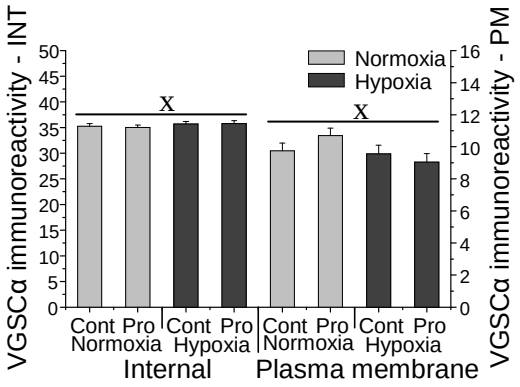


Figure 4.36 Effect of procaine on VGSCα protein distribution along typical cellular cross-section in Mat-LyLu cells.
(A) Representative traces showing signal intensity of Con A plasma membrane marker (green) and VGSCα immunofluorescence (red) along cross-section from typical cells (Figure 4.35) incubated (24 h) in normoxic or hypoxic conditions with or without procaine (100 μM). (B) Bar diagram showing distribution of VGSCα protein immunoreactivity along subcellular cross-sections as a percentage of total (%). For plasma membrane (PM) immunoreactivity, 1.5 μm sections was measured inward from the edge of Con A staining. For internal (INT) immunoreactivity, middle 30 % of the cross-section was measured. Data were analysed by ANOVA followed by Newman-Keuls *post hoc* analysis. Data are presented as means ± SEM (n = 63). Significance: (X) $p > 0.05$.

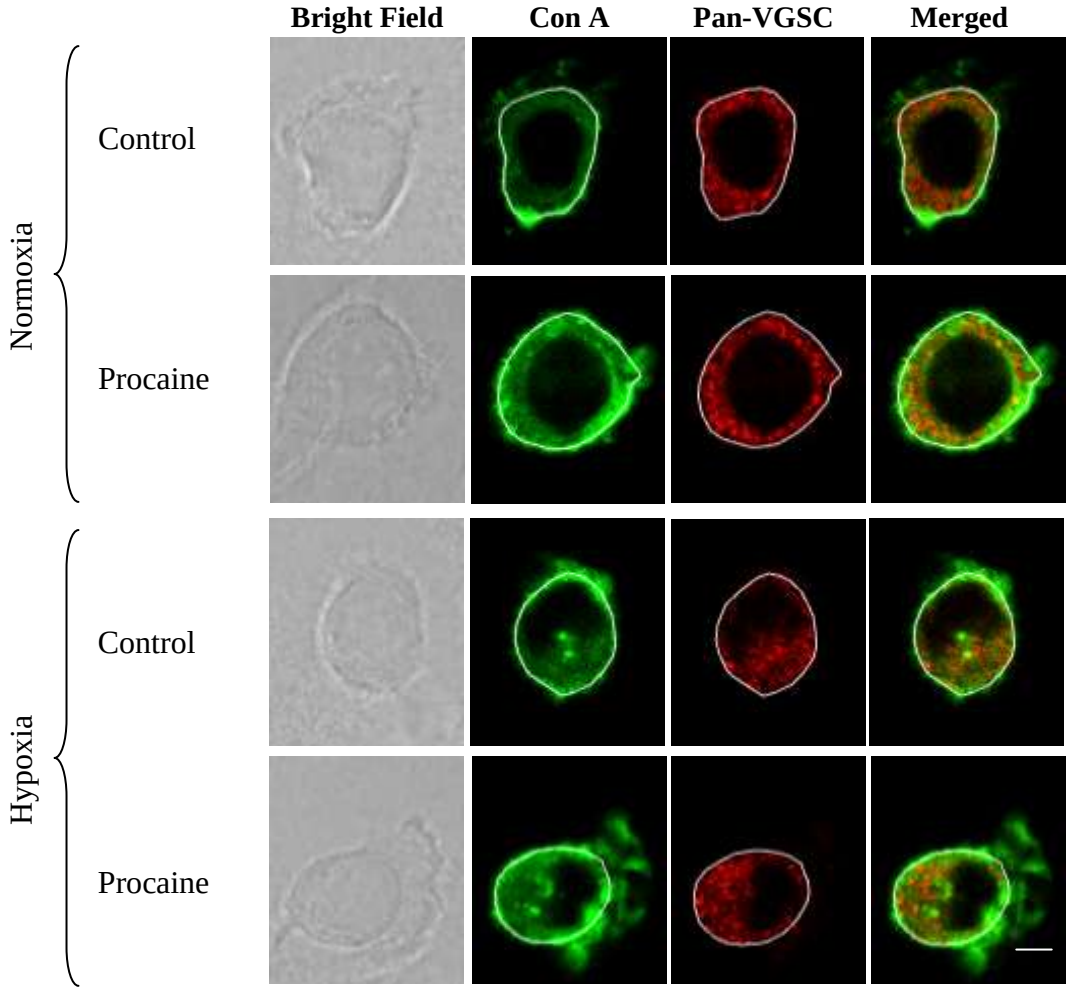
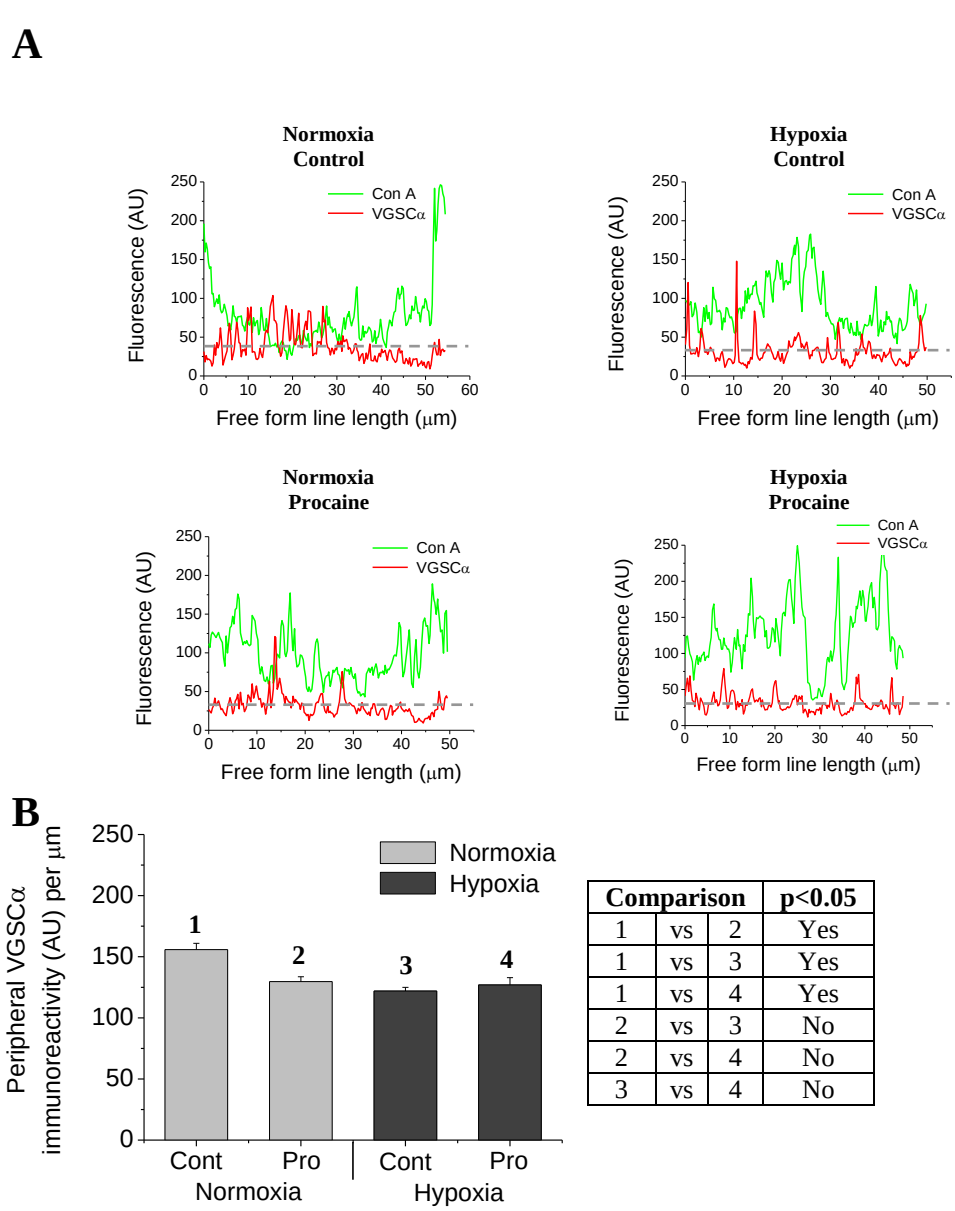


Figure 4.37 Typical image showing effect of procaine on VGSCα protein levels in plasma membrane of Mat-LyLu cells.
Representative XYZ confocal images of Mat-LyLu cells incubated 24 h under normoxic and hypoxic conditions with or without procaine (100 µM). White lines indicate typical freeform line guided by Con A staining to measure cell surface protein level. Scale bar (5µm) applicable to all panels.



Comparison			p<0.05
1	vs	2	Yes
1	vs	3	Yes
1	vs	4	Yes
2	vs	3	No
2	vs	4	No
3	vs	4	No

Figure 4.38 Effect of procaine on VGSCα protein levels in plasma membrane of Mat-LyLu cells.
(A) Representative trace showing signal intensity of Con A plasma membrane marker (green) and VGSCα (red) immunofluorescence along plasma membrane from typical cells (Figure 4.37) incubated (24 h) in normoxic or hypoxic conditions with or without procaine (100 μM). Dotted gray lines indicate mean pan-VGSC fluorescence. (B) Bar diagram showing level of VGSCα protein immunoreactivity along plasma membrane as immunoreactivity (AU) per μm. Inset: table of multiple comparisons between treatments for statistical significance. Data were analysed by ANOVA followed by Newman-Keuls *post hoc* analysis. Data are presented as means ± SEM (n = 74).

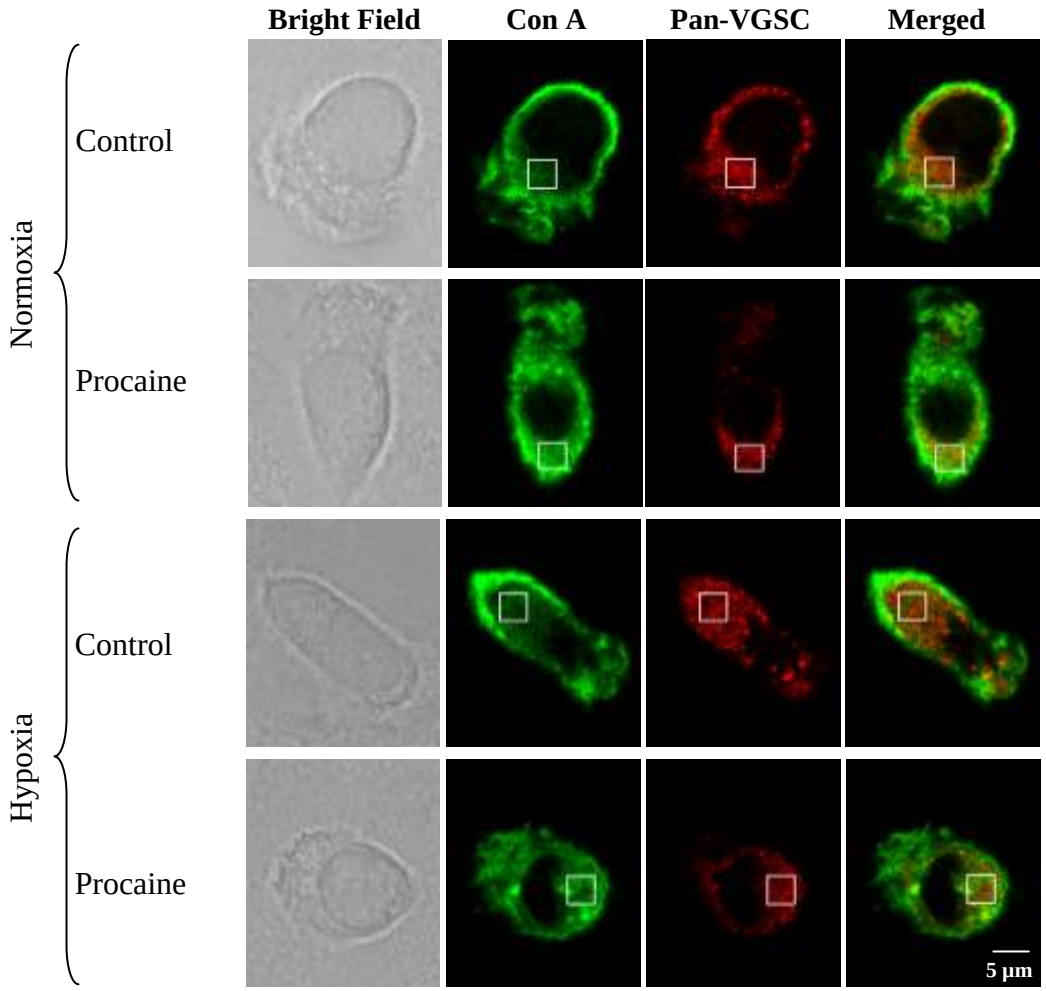
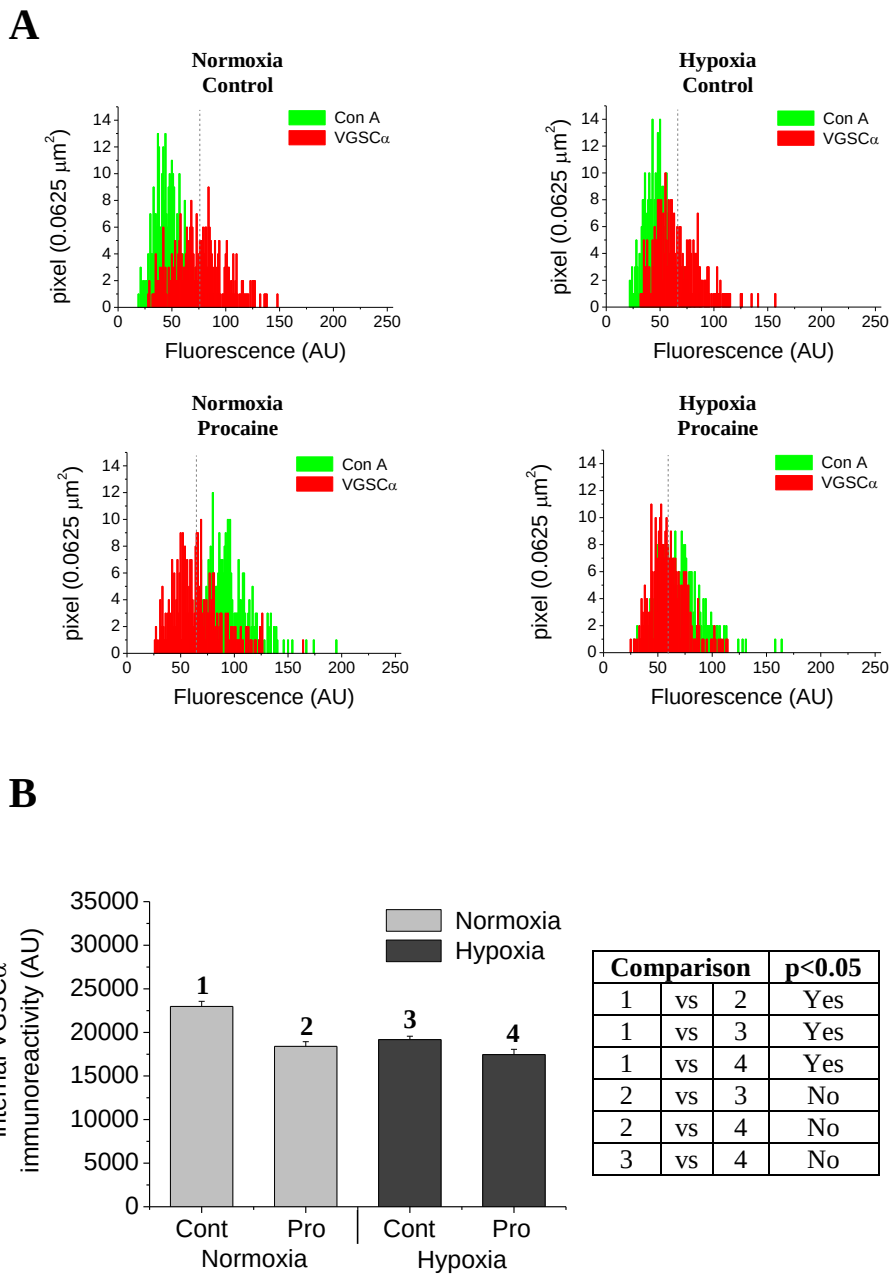


Figure 4.39 Typical image showing effect of procaine on internal VGSCα protein levels of Mat-LyLu cells.
Representative XYZ confocal images of Mat-LyLu cells incubated 24 h under normoxic and hypoxic conditions with or without procaine (100 µM). White box indicates typical area covering 16 μm^2 square section of cytoplasm avoiding nucleus to measure internal protein level. Scale bar (5µm) applicable to all panels.



Comparison			p<0.05
1	vs	2	Yes
1	vs	3	Yes
1	vs	4	Yes
2	vs	3	No
2	vs	4	No
3	vs	4	No

Figure 4.40 Effect of procaine on internal VGSC*α* protein levels of Mat-LyLu cells.
(A) Representative histograms showing distribution of pixels (0.0625 µm^2) with signal intensity of Con A plasma membrane marker (green) and VGSCα (red) immunofluorescence in cytoplasm from typical cells (Figure 4.39) incubated (24 h) in normoxic or hypoxic conditions with or without procaine (100 µM). Dotted gray lines indicate mean pan-VGSC fluorescence. (B) Bar diagram showing internal VGSCα protein immunoreactivity (AU). Inset: table of multiple comparisons between treatments for statistical significance. Data were analysed by ANOVA followed by Newman-Keuls *post hoc* analysis. Data are presented as means ± SEM (n = 77).

4.2.3.6 Matrigel™ invasion

Matrigel™ invasion assay was used to study effect of procaine treatment on the invasivenss of Mat-LyLu cells maintained in normoxic and hypoxic conditions. Treatment of 1, 10 and 100 µM procaine under normoxic conditions significantly decreased invaded cell number by 50 %, 57 %, 61 %, respectively ($p < 0.05$; $n \geq 4$ each; Figures 4.41 and 4.42). Hypoxia by itself had no effect. However, similar to normoxia, 24 h treatment of Mat-LyLu cells under hypoxia with 1, 10 and 100 µM procaine significantly decreased invaded cell number by 64 %, 69 %, 81 %, respectively ($p < 0.05$ each; $n \geq 4$; Figures 4.41 and 4.42). There was no difference in the effects of given concentrations of procaine in normoxia vs hypoxia (Figure 4.42 inset).

4.2.3.7 Summary of effects of procaine

Under normoxic (but not hypoxic) conditions, procaine inhibited Nav1.7 mRNA and protein expression in plasma membrane and cytoplasm. Invasion was inhibited by procaine under both normoxic and hypoxic conditions. Hypoxia itself had no effect on invasiveness (Table 4.1).

4.2.4 Effects of lidocaine

Lidocaine is another local anaesthetic that has been used extensively as a non-selectively blocker of VGSCs. In the present study, it was used in the concentration range 1 to 1000 µM, since this concentration range was shown to block I_{NaP} more effectively than I_{NaT} (Bräu *et al.,* 1998; Rajamani *et al.,* 2008; Fraser *et al.,* 2005; Hammarström and Gage, 1998).

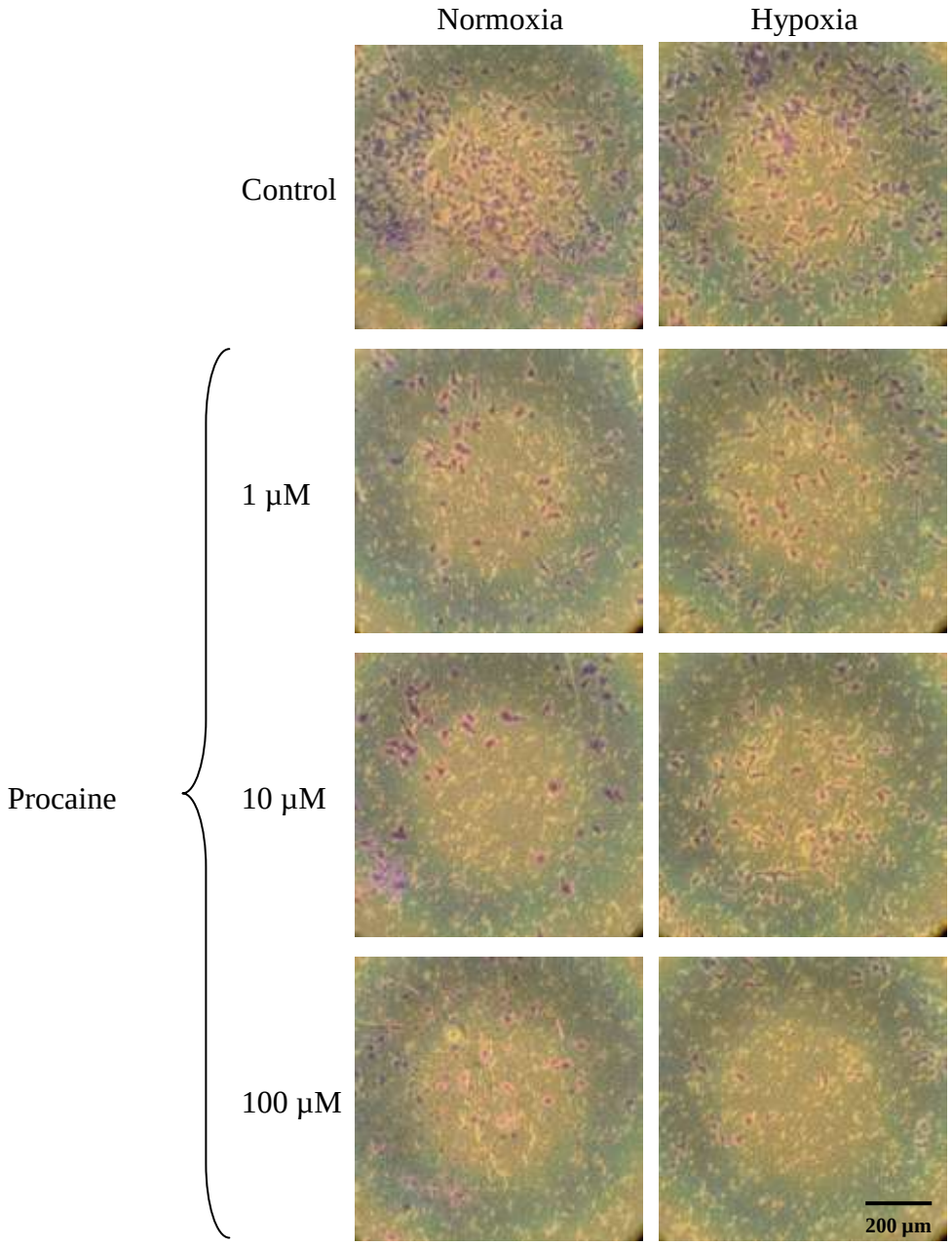
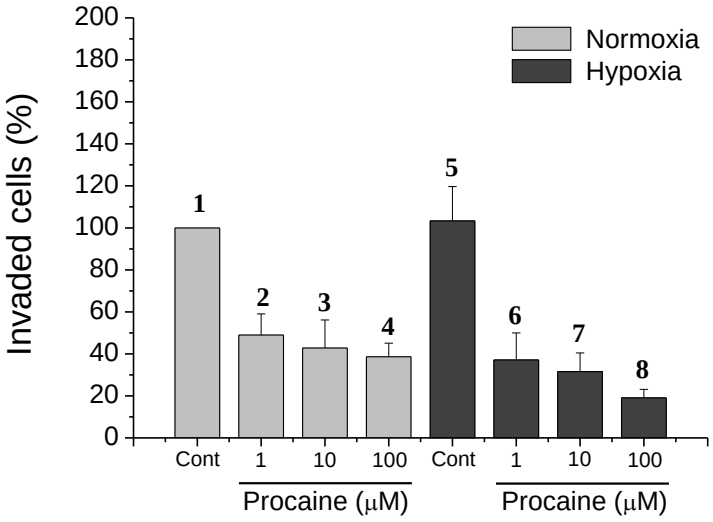


Figure 4.41 Typical images of invaded cells showing the effect of procaine on invasion of Mat-LyLu invasiveness.
Typical phase-contrast light-microscopy images of invaded cells obtained from Matrigel™ invasion assays of Mat-LyLu cells incubated 24 h under normoxic and hypoxic conditions with or without procaine (1, 10 and 100 µM). Invaded cells were fixed and stained with crystal violet (purple). Scale bar (200 µm) applicable to all panels.



Comparison			p<0.05
1	vs	2	Yes
1	vs	3	Yes
1	vs	4	Yes
1	vs	5	No
1	vs	6	Yes
1	vs	7	Yes
1	vs	8	Yes
2	vs	3	No
2	vs	4	No
2	vs	5	Yes
2	vs	6	No
2	vs	7	No
2	vs	8	Yes
3	vs	4	No

Comparison			p<0.05
3	vs	5	Yes
3	vs	6	No
3	vs	7	No
3	vs	8	No
4	vs	5	Yes
4	vs	6	No
4	vs	7	No
4	vs	8	No
5	vs	6	Yes
5	vs	7	Yes
5	vs	8	Yes
6	vs	7	No
6	vs	8	No
7	vs	8	No

Figure 4.42 Effect of procaine on invasion of Mat-LyLu cells.
Bar diagram showing number of invaded Mat-LyLu cells incubated 24 h under normoxic and hypoxic conditions with or without procaine (1, 10 and 100 µM). Data were expressed relative to the control (%) and presented as means ± SEM ($n \geq 4$). Data were analysed by Kruskal-Wallis analysis of variance. The table of multiple comparisons between treatments for statistical significance are shown underneath the bar diagram.

4.2.4.1 Some initial observations: Cell morphology

No change in the basic appearance or distribution of Mat-LyLu cells was observed when the cultures were treated (24 h) with up to 500 µM lidocaine under both normoxic and hypoxic (2 % O_2) conditions (Figures 4.43A-C). On the other hand, after 1000 µM lidocaine treatment, Mat-LyLu cells, maintained in normoxic or hypoxic conditions, appeared generally to 'lose' cell contacts and become scattered (Figure 4.43D). Studying effect of lidocaine treatment on Mat-LyLu cells in high magnification revealed that 1000 µM treatment caused loss of spindle-shaped fibroblast like morphology in both normoxic and hypoxic conditions (Figure 4.44D). Examination under higher magnification still revealed no obvious effect on cell morphology by the lower doses of lidocaine (100 and 500 µM) (Figures 4.44A-C).

4.2.4.2 Cell viability

Treatment (24 h) with lidocaine at concentrations up to 1000 µM was not toxic to Mat-LyLu cells maintained in normoxic or hypoxic conditions (Figure 4.45).

4.2.4.3 Cellular proliferation

No significant change was recorded in Mat-LyLu cell number after 24 h lidocaine treatment (10, 100, 500, 700 and 1000 µM) in normoxic conditions ($p > 0.05$; $n \geq 3$ each; Figure 4.46). Similarly, Mat-LyLu cell number was not affected by 10, 100 and 500 µM lidocaine treatment (24 h) in hypoxia ($p > 0.05$; $n \geq 3$ each; Figure 4.46). On the other hand, under hypoxia, 700 and 1000 µM lidocaine treatment (24 h) significantly decreased Mat-LyLu cell number by 37 and 35 %, respectively, when

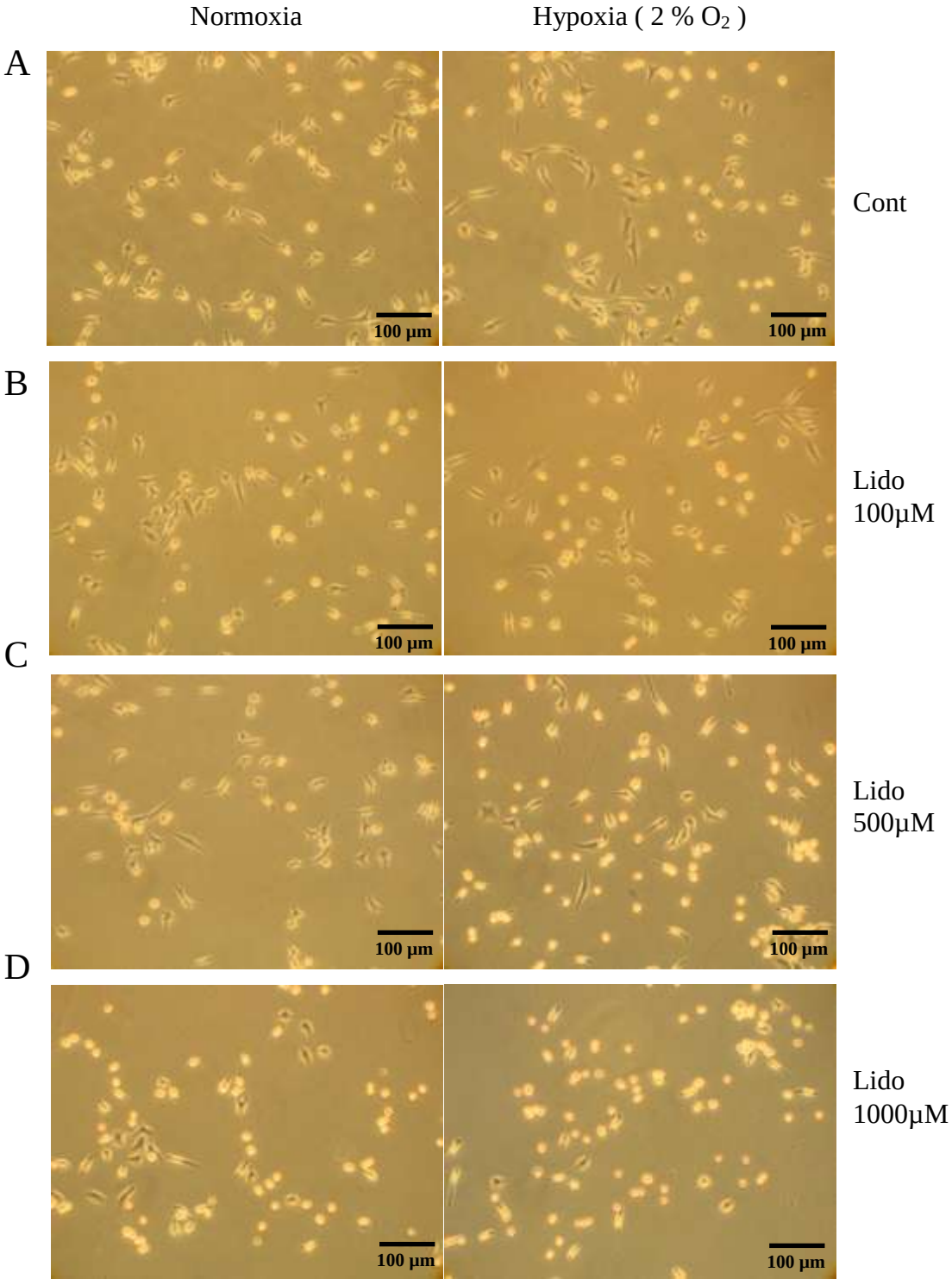


Figure 4.43 Phase-contrast light-photomicrography of Mat-LyLu cells treated with lidocaine.

Mat-LyLu cells were grown for 24 h under (A) control conditions, and in (B) 100 µM lidocaine, (C) 500 µM lidocaine, (D) 1000 µM lidocaine treatment in normoxia (left hand pictures) and hypoxia (2 % O_2; right hand pictures). Micrographs are typical of 3 experiments.

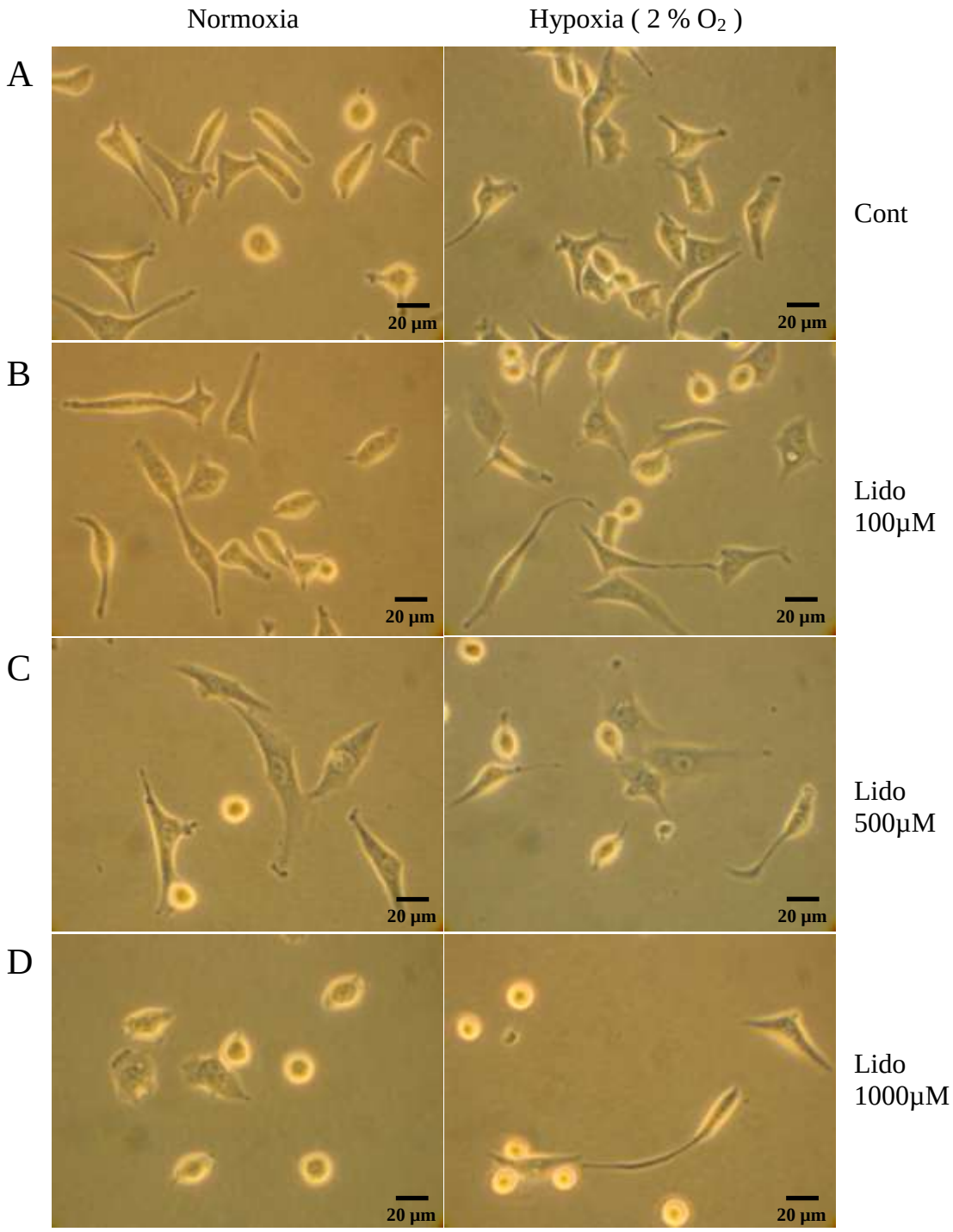


Figure 4.44 Phase-contrast light-photomicrography of Mat-LyLu cells, treated with lidocaine, in high magnification.

Mat-LyLu cells were grown for 24 h under (A) control conditions, and in (B) 100 µM lidocaine, (C) 500 µM lidocaine, (D) 1000 µM lidocaine treatment in normoxia (left hand pictures) and hypoxia (2 % O_2; right hand pictures). Micrographs are typical of 3 experiments.

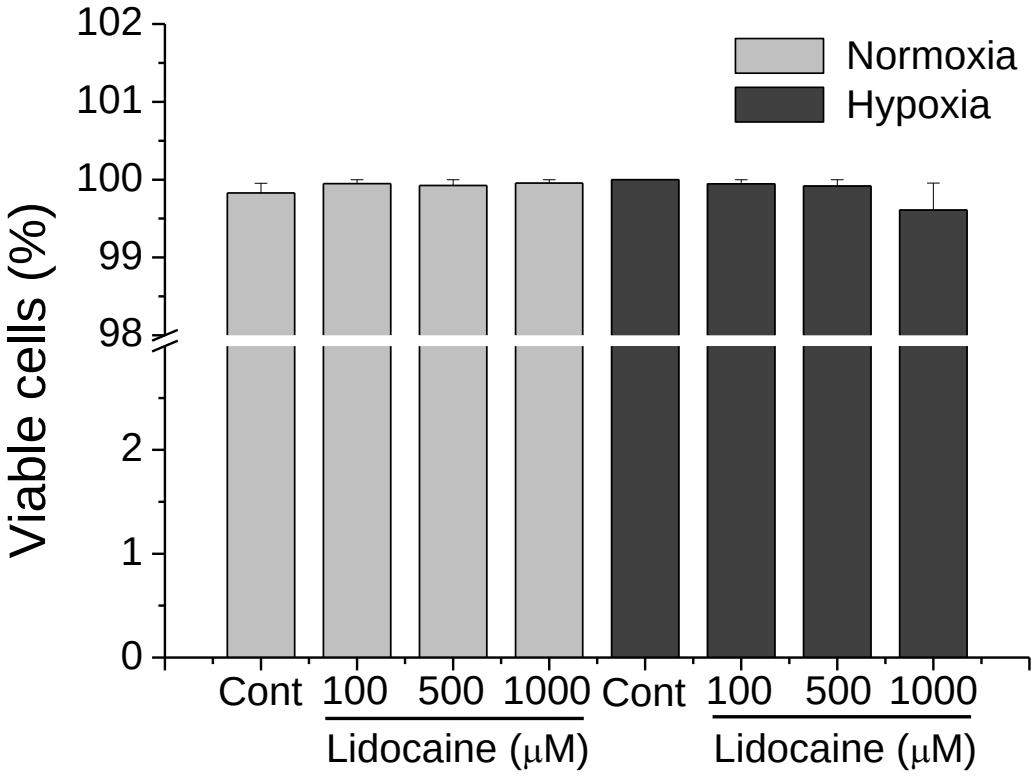
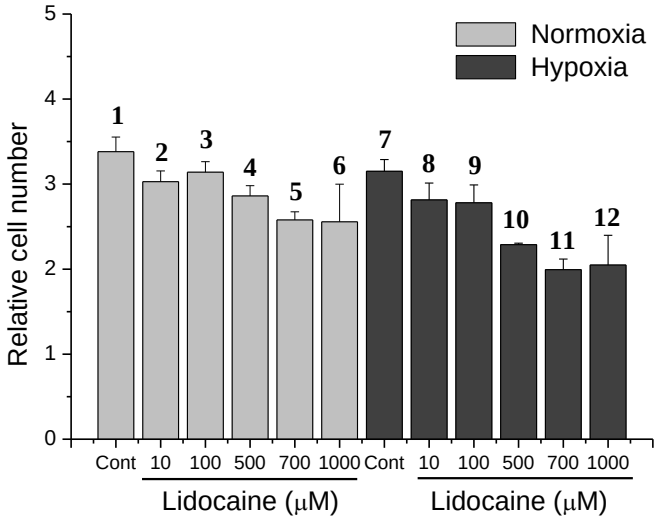


Figure 4.45 Bar diagram showing lidocaine treatments had no toxic effect.

A possible effect of 100, 500 and 1000 μM lidocaine on Mat-LyLu cell viability under normoxia (light grey columns) or hypoxia (2 % O_2; dark grey columns). Data are represented as means ± SEM (*n* = 3).



Comparison			p<0.05
1	vs	2	No
1	vs	3	No
1	vs	4	No
1	vs	5	No
1	vs	6	No
1	vs	7	No
1	vs	8	No
1	vs	9	No
1	vs	10	Yes
1	vs	11	Yes
1	vs	12	Yes
2	vs	3	No
2	vs	4	No
2	vs	5	No
2	vs	6	No
2	vs	7	No
2	vs	8	No
2	vs	9	No
2	vs	10	No
2	vs	11	No
2	vs	12	No
3	vs	4	No

Comparison			p<0.05
3	vs	5	No
3	vs	6	No
3	vs	7	No
3	vs	8	No
3	vs	9	No
3	vs	10	No
3	vs	11	Yes
3	vs	12	Yes
4	vs	5	No
4	vs	6	No
4	vs	7	No
4	vs	8	No
4	vs	9	No
4	vs	10	No
4	vs	11	No
4	vs	12	No
5	vs	6	No
5	vs	7	No
5	vs	8	No
5	vs	9	No
5	vs	10	No
5	vs	11	No

Comparison			p<0.05
5	vs	12	No
6	vs	7	No
6	vs	8	No
6	vs	9	No
6	vs	10	No
6	vs	11	No
6	vs	12	No
7	vs	8	No
7	vs	9	No
7	vs	10	No
7	vs	11	Yes
7	vs	12	Yes
8	vs	9	No
8	vs	10	No
8	vs	11	No
8	vs	12	No
9	vs	10	No
9	vs	11	No
9	vs	12	No
10	vs	11	No
10	vs	12	No
11	vs	12	No

Figure 4.46 Dose dependent effect of lidocaine on Mat-LyLu cell number.
Bar diagram showing the effect of 10, 100, 500 and 700 µM lidocaine on cell number of normoxic (light grey columns) or hypoxic (dark grey columns) Mat-LyLu cells. Data are presented as means ± SEM ($n \geq 3$). Data were analysed by ANOVA followed by Newman-Keuls *post hoc* analysis. Table of multiple comparisons between different treatments for statistical significance are shown underneath the bar diagram.

compared to the corresponding hypoxic control ($p < 0.05$; $n \geq 3$ each; Figure 4.46). Hypoxia by itself had no effect.

Because 24 h treatments with 700 µM lidocaine under hypoxia reduced cell number, subsequent experiments were restricted to 1 to 500 µM range, in order not to 'contaminate' any effect on Matrigel invasion.

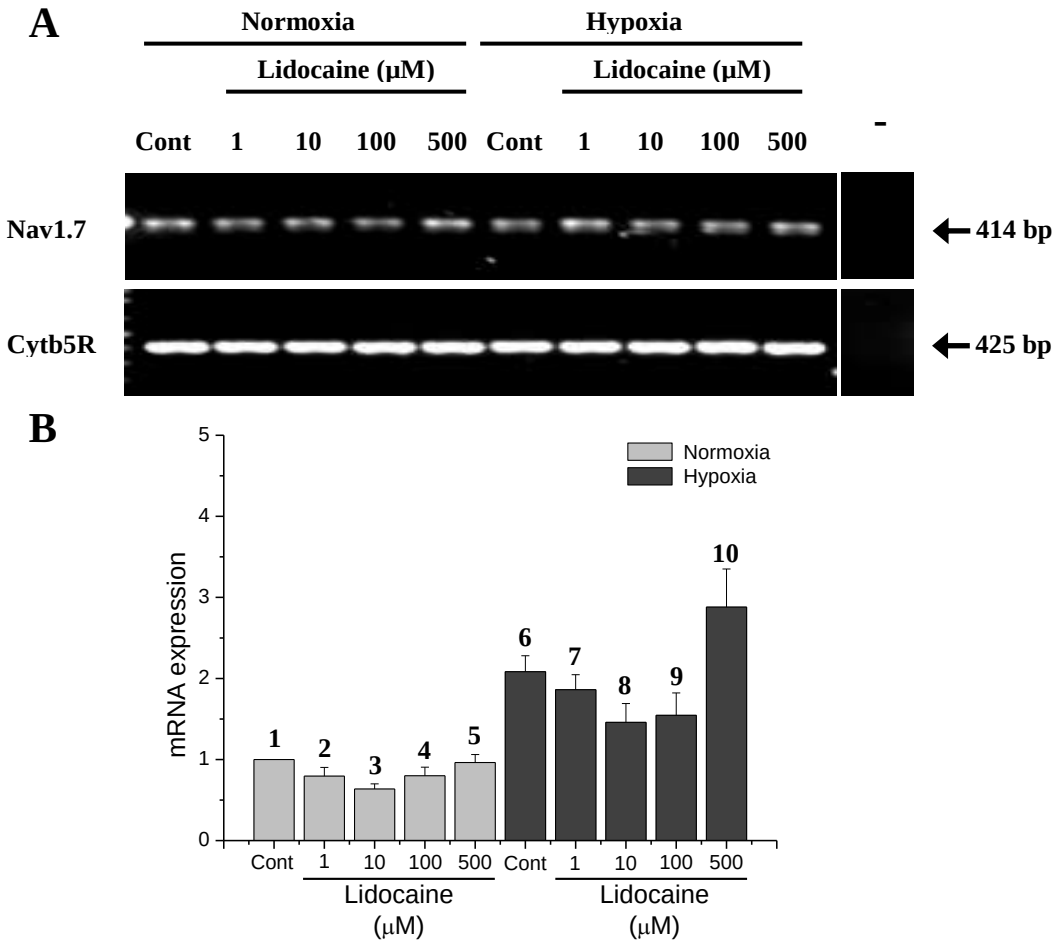
4.2.4.4 Nav1.7 mRNA expression

Mat-LyLu cells were treated for 24 h with 1, 10, 100 and 500 µM lidocaine under normoxic or hypoxic conditions and cDNAs were prepared for realtime PCR analyses. Agarose gel electrophoresis confirmed specific single bands at the expected sizes for Nav1.7 and Cytb5R (414 nt and 425 nt, respectively; $n = 3$ each; Figure 4.47A). The "no-template control" did not give any signal ($n = 3$ each; Figure 4.47A). Lidocaine treatment (24 h) had a dose-dependent, biphasic effect on Nav1.7 mRNA expression. No significant change was recorded for 1, 100 and 500 µM lidocaine under both normoxic and hypoxic conditions ($p > 0.05$; $n = 3$ each; Figure 4.47B). On the other hand, 10 µM lidocaine significantly decreased Nav1.7 mRNA under both conditions, by 36 % (compared to normoxic control) and 30 % (compared to hypoxic control) ($p < 0.05$; $n \geq 3$ each; Figure 4.47B). Hypoxia by itself increased Nav1.7 mRNA, as before.

4.2.4.5 Subcellular VGSCα protein expression

4.2.4.5.1 Relative distribution

Digital confocal analyses of the immunostaining obtained with the pan-VGSC antibody was used to test the possible effect of lidocaine (100 µM) on the subcellular



Comparison			p<0.05
1	vs	2	No
1	vs	3	Yes
1	vs	4	No
1	vs	5	No
1	vs	6	Yes
1	vs	7	Yes
1	vs	8	No
1	vs	9	No
1	vs	10	Yes
2	vs	3	No
2	vs	4	No
2	vs	5	No
2	vs	6	Yes
2	vs	7	Yes
2	vs	8	Yes

Comparison			p<0.05
2	vs	9	Yes
2	vs	10	Yes
3	vs	4	No
3	vs	5	Yes
3	vs	6	Yes
3	vs	7	Yes
3	vs	8	Yes
3	vs	9	Yes
3	vs	10	Yes
4	vs	5	No
4	vs	6	Yes
4	vs	7	Yes
4	vs	8	Yes
4	vs	9	Yes
4	vs	10	Yes

Comparison			p<0.05
5	vs	6	Yes
5	vs	7	Yes
5	vs	8	No
5	vs	9	Yes
5	vs	10	Yes
6	vs	7	No
6	vs	8	Yes
6	vs	9	No
6	vs	10	No
7	vs	8	No
7	vs	9	No
7	vs	10	No
8	vs	9	No
8	vs	10	Yes
9	vs	10	Yes

Figure 4.47 Effect of lidocaine on Mat-LyLu Nav1.7 mRNA expression.
(A) Typical PCR products of Nav1.7 (414 bp) and normalising/control gene Cytb5R (425 bp) mRNA in Mat-LyLu cells that was incubated with 1, 10, 100 and 500 µM lidocaine under normoxic or hypoxic (2 % O_2) conditions for 24 h. (B) Bar diagram showing the result of real-time PCR experiment in which the effect of lidocaine on Nav1.7 mRNA expression was studied under normoxic (light grey column) or hypoxic (dark grey column) conditions. The data were normalized to Cytb5R using the $2^{-\Delta\Delta C_T}$ method and expressed relative to normoxic control Nav1.7 level. The table of multiple comparisons between different treatments for statistical significance are shown underneath the bar diagram. Kruskal-Wallis method was used for statistic analysis. Data are presented as means ± SEM (n = 3). (-): no template control.

distribution of VGSCα protein in Mat-LyLu cells under normoxic or hypoxic (2 % O_2) conditions (Figure 4.48). The subcellular distribution of the VGSCα protein was studied by 'straight line cross-sectional profile' analysis (Figure 4.49). The relative plasma membrane VGSCα protein levels were as follows: 9.7 ± 0.4 % (normoxia control), 10.1 ± 0.5 % (normoxia + lidocaine), = 9.5 ± 0.5 % (hypoxic control) and 9.9 ± 0.4 % (hypoxia + lidocaine); the corresponding internal VGSCα protein levels were as follows: 35.2 ± 0.5 % (normoxia control), =34.0 ± 0.5 % (normoxia + lidocaine), 35.6 ± 0.5 % (hypoxic control) and 35.2 ± 0.5 % (hypoxia + lidocaine) (for all: $p > 0.05$; $n \geq 63$; Figure 4.50A&B). Thus, this method revealed that the relative level of plasma membrane and intracellular VGSCα protein was not affected by 24 h lidocaine (100 µM) treatment under both normoxic and hypoxic conditions.

4.2.4.5.2 Plasma membrane VGSCα protein level

Digital quantification of the VGSCα immunoreactivity protein level by 'free-form line profile' analysis of XYZ scans of Mat-LyLu cells, treated (24 h) with lidocaine (100 µM), revealed a significant decrease of plasma membrane VGSCα protein level: IR_{pm} = 155 ± 5 AU/µm (normoxic control) *vs* 129 ± 4 AU/µm (normoxic lidocaine) ($p < 0.05$; $n \geq 74$ each; Figures 4.51 and 4.52A&B). On the other hand, 100 µM lidocaine treatment for 24 h did not change plasma membrane VGSCα protein level when the Mat-LyLu cells were maintained in hypoxia ($p > 0.05$; $n \geq 74$; Figures 4.51 and 4.52A&B).

4.2.4.5.3 Internal VGSCα protein level

Digital quantification of the intracellular VGSCα immunoreactivity by 'area histogram' analysis of XYZ scans of Mat-LyLu cells revealed a significant decreases

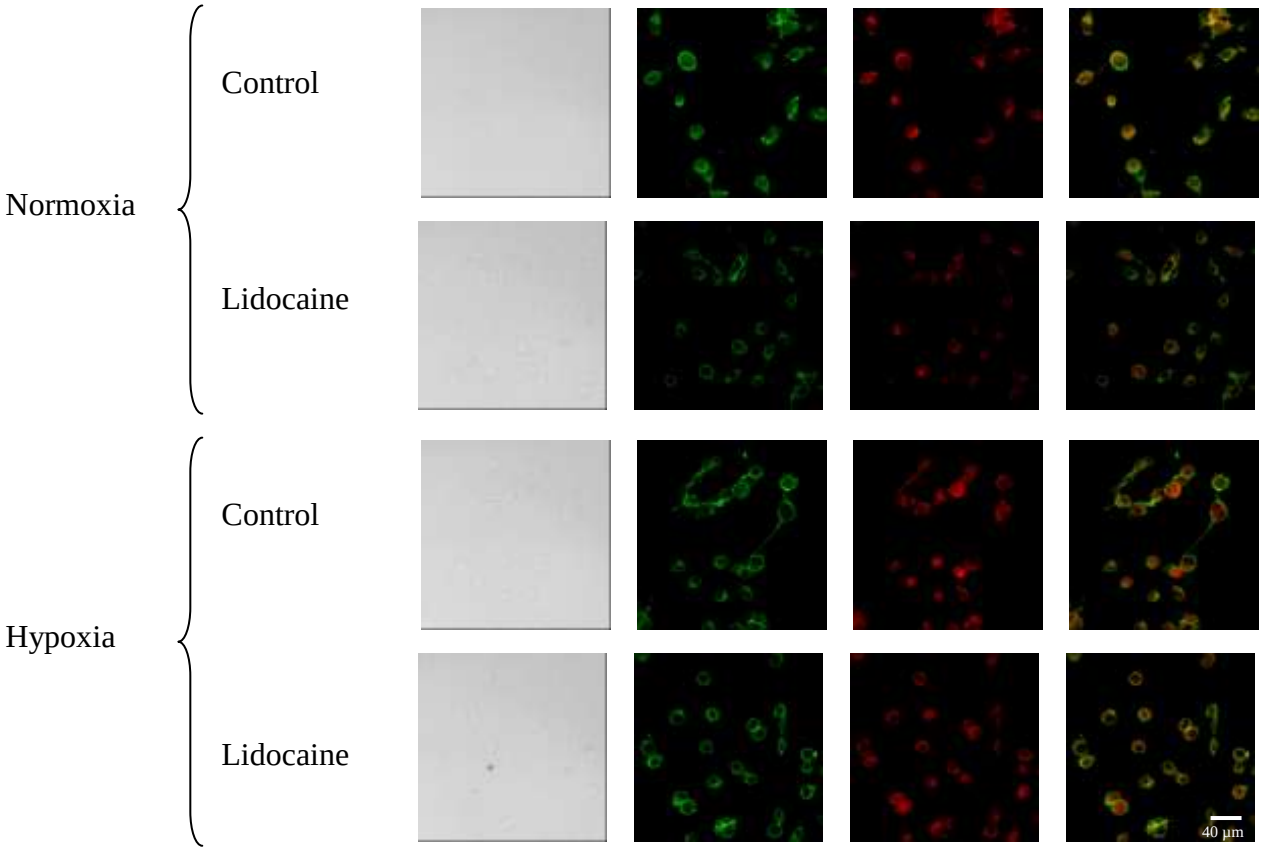


Figure 4.48 Confocal immunocytochemistry study of Mat-LyLu cells incubated with lidocaine.
Typical XYZ confocal images of Mat-LyLu cells incubated 24 h under normoxic and hypoxic (2 % O_2) conditions with or without lidocaine (100 µM). Signal from concanavalin A plasma membrane marker (green), pan-VGSC antibody (red) and overlay of both (merged image) are shown in addition to bright field image. Scale bar (40 µm) applicable to all panels.

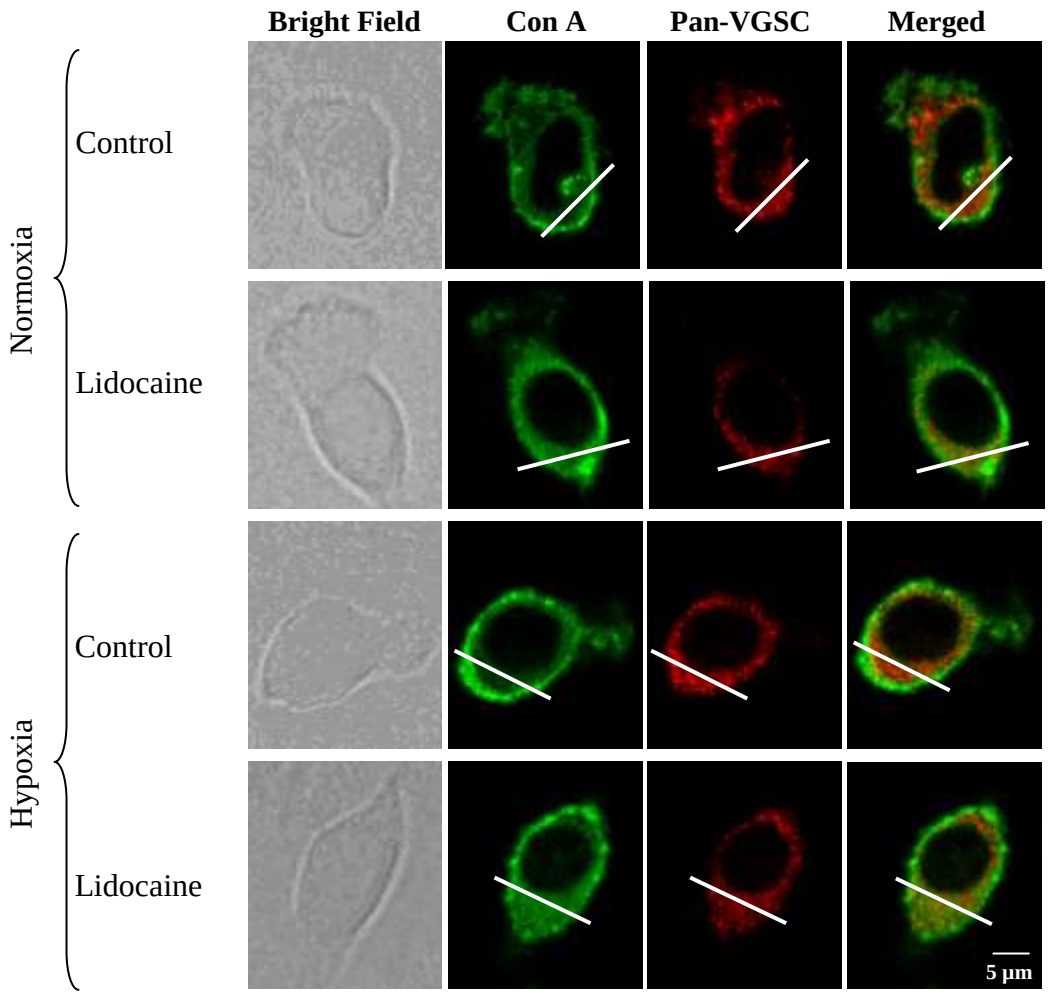
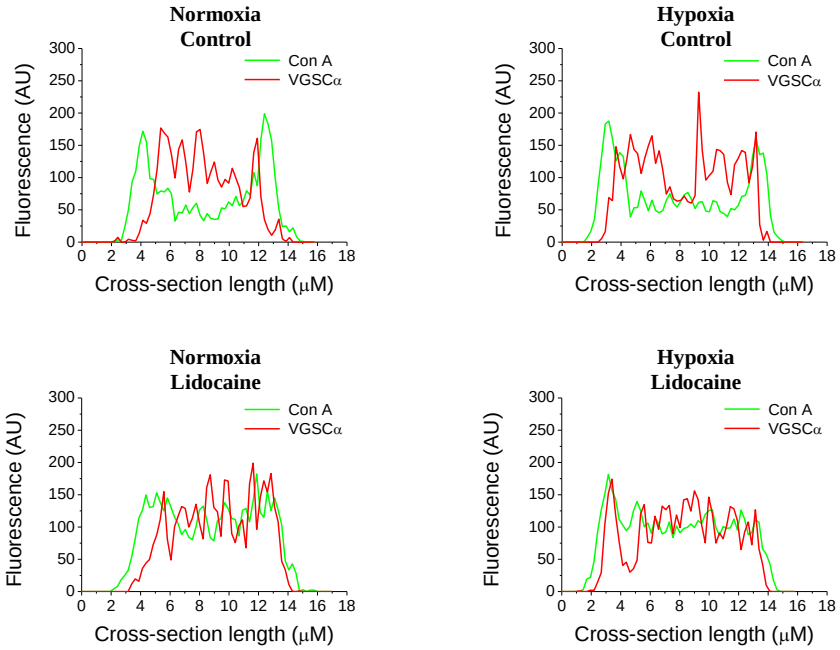


Figure 4.49 Typical image showing effect of lidocaine on VGSCα protein distribution along typical cellular cross-section in Mat-LyLu cells.
Representative XYZ confocal images of Mat-LyLu cells incubated 24 h under normoxic and hypoxic conditions with or without lidocaine (100 µM). White lines indicate typical cross-section. Scale bar (5µm) applicable to all panels.

A



B

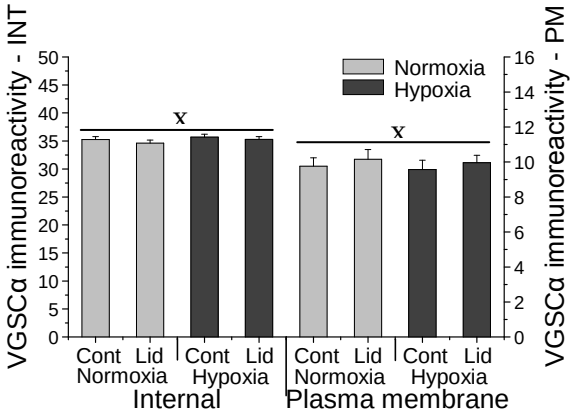


Figure 4.50 Effect of lidocaine on VGSCα protein distribution along typical cellular cross-section in Mat-LyLu cells.
(A) Representative traces showing signal intensity of Con A plasma membrane marker (green) and VGSCα immunofluorescence (red) along cross-section from typical cells (Figure 4.49) incubated (24 h) in normoxic or hypoxic conditions with or without lidocaine (100 µM). (B) Bar diagram showing distribution of VGSCα protein immunoreactivity along subcellular cross-sections as a percentage of total (%). For plasma membrane (PM) immunoreactivity, 1.5 µm sections was measured inward from the edge of Con A staining. For internal (INT) immunoreactivity, middle 30 % of the cross-section was measured. Data were analysed by ANOVA followed by Newman-Keuls *post hoc* analysis. Data are presented as means ± SEM (n = 63). Significance: (X) $p > 0.05$.

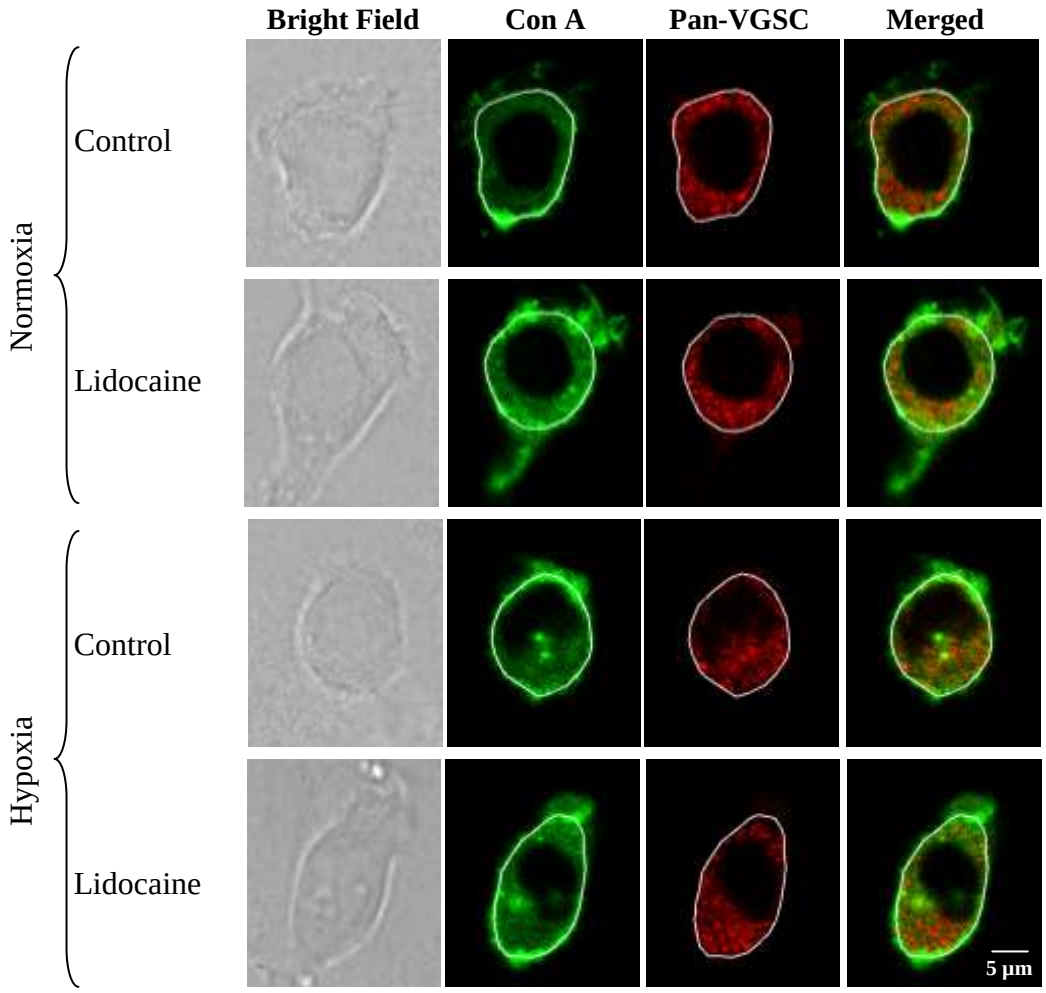
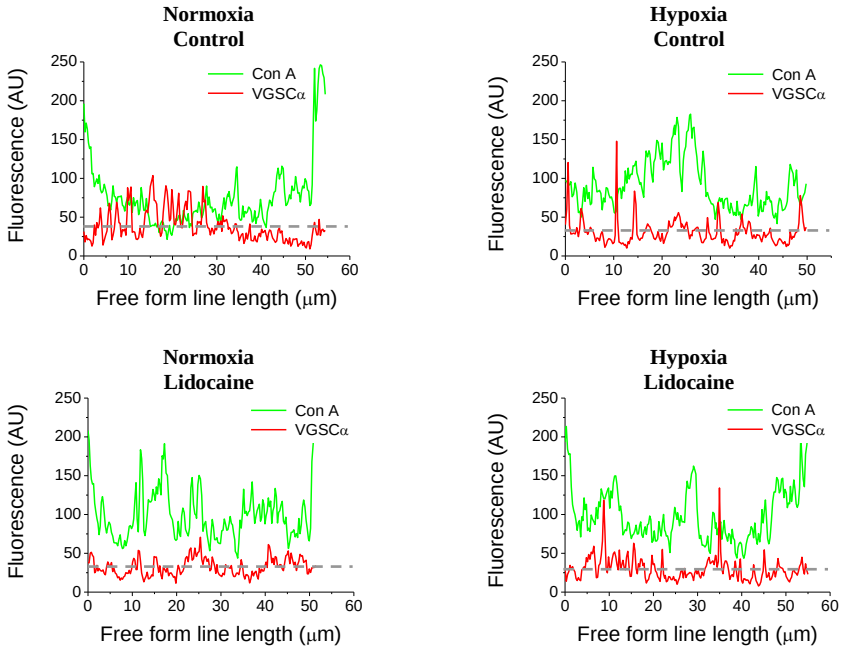
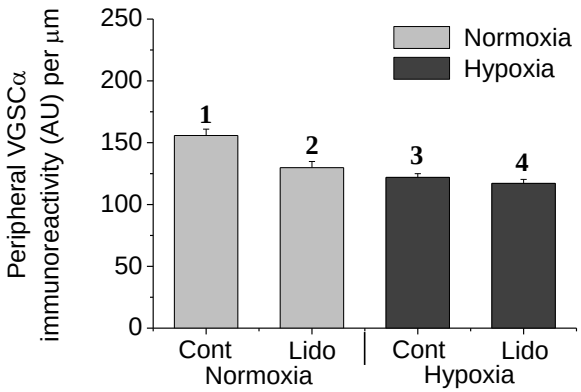


Figure 4.51 Typical image showing effect of lidocaine on VGSCα protein levels in plasma membrane of Mat-LyLu cells.
Representative XYZ confocal images of Mat-LyLu cells incubated 24 h under normoxic and hypoxic conditions with or without lidocaine (100 µM). White lines indicate typical freeform line guided by Con A staining to measure cell surface protein level. Scale bar (5µm) applicable to all panels.

A



B



Comparison			p<0.05
1	vs	2	Yes
1	vs	3	Yes
1	vs	4	Yes
2	vs	3	No
2	vs	4	No
3	vs	4	No

Figure 4.52 Effect of lidocaine on VGSCα protein levels in plasma membrane of Mat-LyLu cells.
(A) Representative trace showing signal intensity of Con A plasma membrane marker (green) and VGSCα (red) immunofluorescence along plasma membrane from typical cells (Figure 4.51) incubated (24 h) in normoxic or hypoxic conditions with or without lidocaine (100 μM). Dotted gray lines indicate mean pan-VGSC fluorescence. (B) Bar diagram showing level of VGSCα protein immunoreactivity along plasma membrane as immunoreactivity (AU) per μm. Inset: table of multiple comparisons between treatments for statistical significance. Data were analysed by ANOVA followed by Newman-Keuls *post hoc* analysis. Data are presented as means ± SEM (n = 74).

of internal VGSCα protein level by 17 %, 16 % and 27 % when the cells were incubated in (i) normoxic condition with lidocaine (100 µM), (ii) hypoxic control condition and (iii) hypoxic condition with lidocaine (100 µM), respectively (for all: $p < 0.05$; $n \geq 77$ each; Figures 4.53 and 4.54A&B)

4.2.4.6 Matrigel™ invasion

Matrigel™ invasion assays were used to study possible effects of lidocaine treatment on the invasiveness of Mat-LyLu cells maintained in normoxic or hypoxic conditions. There was some variability in the data obtained. Under normaxic conditions, although 1 µM lidocaine decreased the invaded cell number by 45 %, this change was not statistically significant ($p > 0.05$; $n \geq 4$ each; Figures 4.55 and 4.56). Treatment of 10 µM and 100 µM lidocaine significantly decreased invaded cell numbers by 46 % and 76 %, respectively, under normoxic conditions ($p < 0.05$; $n \geq 4$; Figures 4.55 and 4.56). Similarly, 24 h treatment of Mat-LyLu cells in hypoxic conditions with 1 , 10 and 100 µM procaine significantly decreased invaded cell number by 69 %, 74 % and 58 %, respectively ($p < 0.05$; $n \geq 4$ for all; Figures 4.55 and 4.56). Hypoxia by itself was not effective, as in all other assay sets.

4.3 Discussion

The main findings of this study on Mat-LyLu cells are as follows (Table 4.1):

1) Hypoxia, highly consistently, had no effect on cellular morphology, viability, proliferation or invasion. However, it increased Nav1.7 mRNA expression whilst decreasing VGSCα protein levels in plasma membrane and cytoplasm.

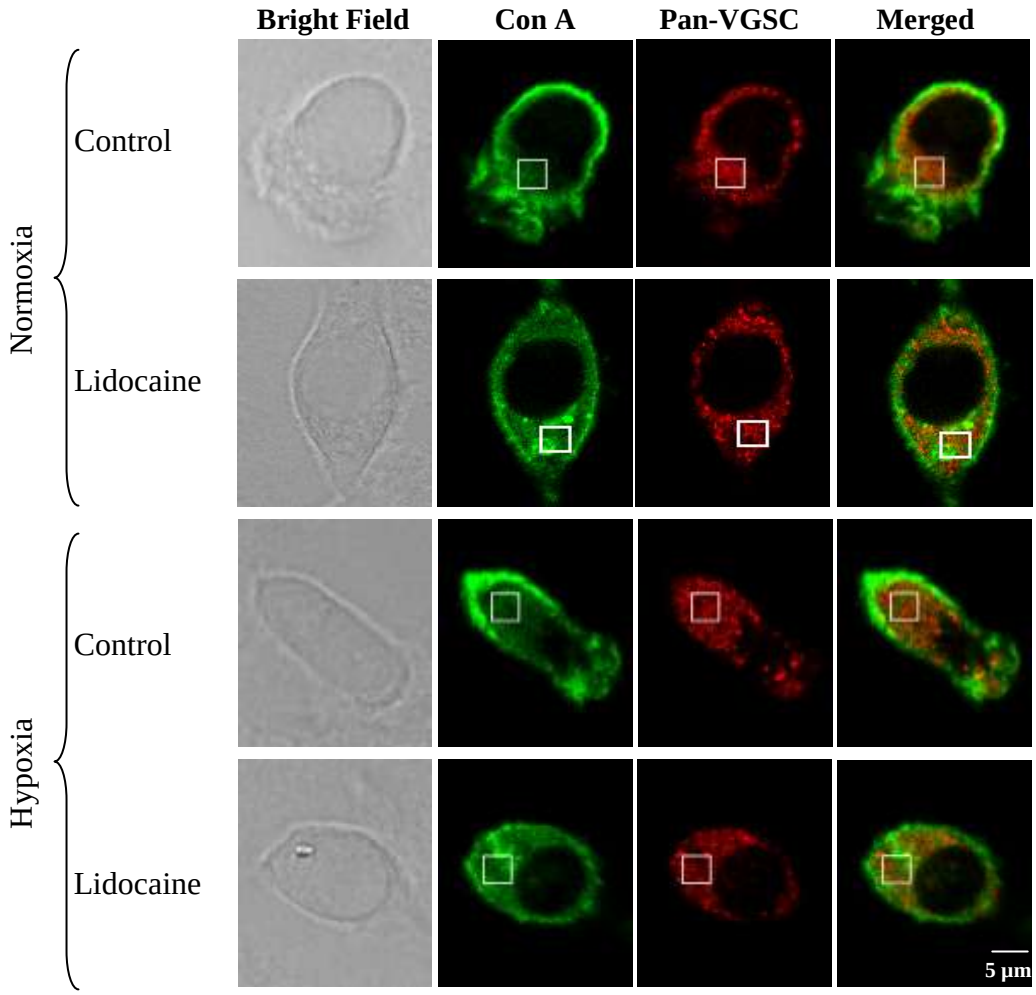
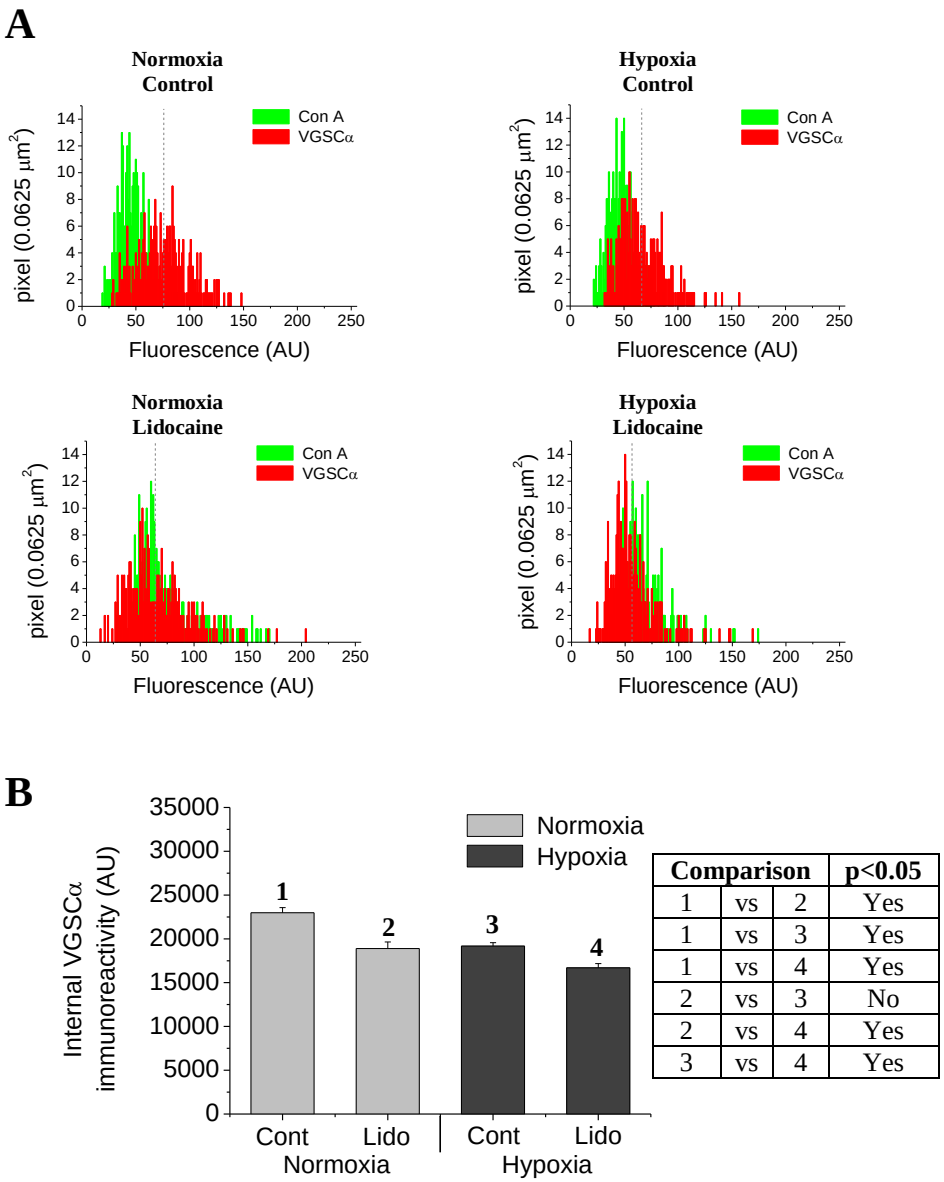


Figure 4.53 Typical image showing effect of lidocaine on internal VGSCα protein levels of Mat-LyLu cells.
Representative XYZ confocal images of Mat-LyLu cells incubated 24 h under normoxic and hypoxic conditions with or without lidocaine (100 µM). White box indicates typical area covering 16 μm^2 square section of cytoplasm avoiding nucleus to measure internal protein level. Scale bar (5µm) applicable to all panels.



Comparison			p<0.05
1	vs	2	Yes
1	vs	3	Yes
1	vs	4	Yes
2	vs	3	No
2	vs	4	Yes
3	vs	4	Yes

Figure 4.54 Effect of lidocaine on internal VGSCα protein levels of Mat-LyLu cells.
(A) Representative histograms showing distribution of pixels (0.0625 µm^2) with signal intensity of Con A plasma membrane marker (green) and VGSCα (red) immunofluorescence in cytoplasm from typical cells (Figure 4.53) incubated (24 h) in normoxic or hypoxic conditions with or without lidocaine (100 µM). Dotted gray lines indicate mean pan-VGSC fluorescence. (B) Bar diagram showing internal VGSCα protein immunoreactivity (AU). Inset: table of multiple comparisons between treatments for statistical significance. Data were analysed by ANOVA followed by Newman-Keuls *post hoc* analysis. Data are presented as means ± SEM (n = 77).

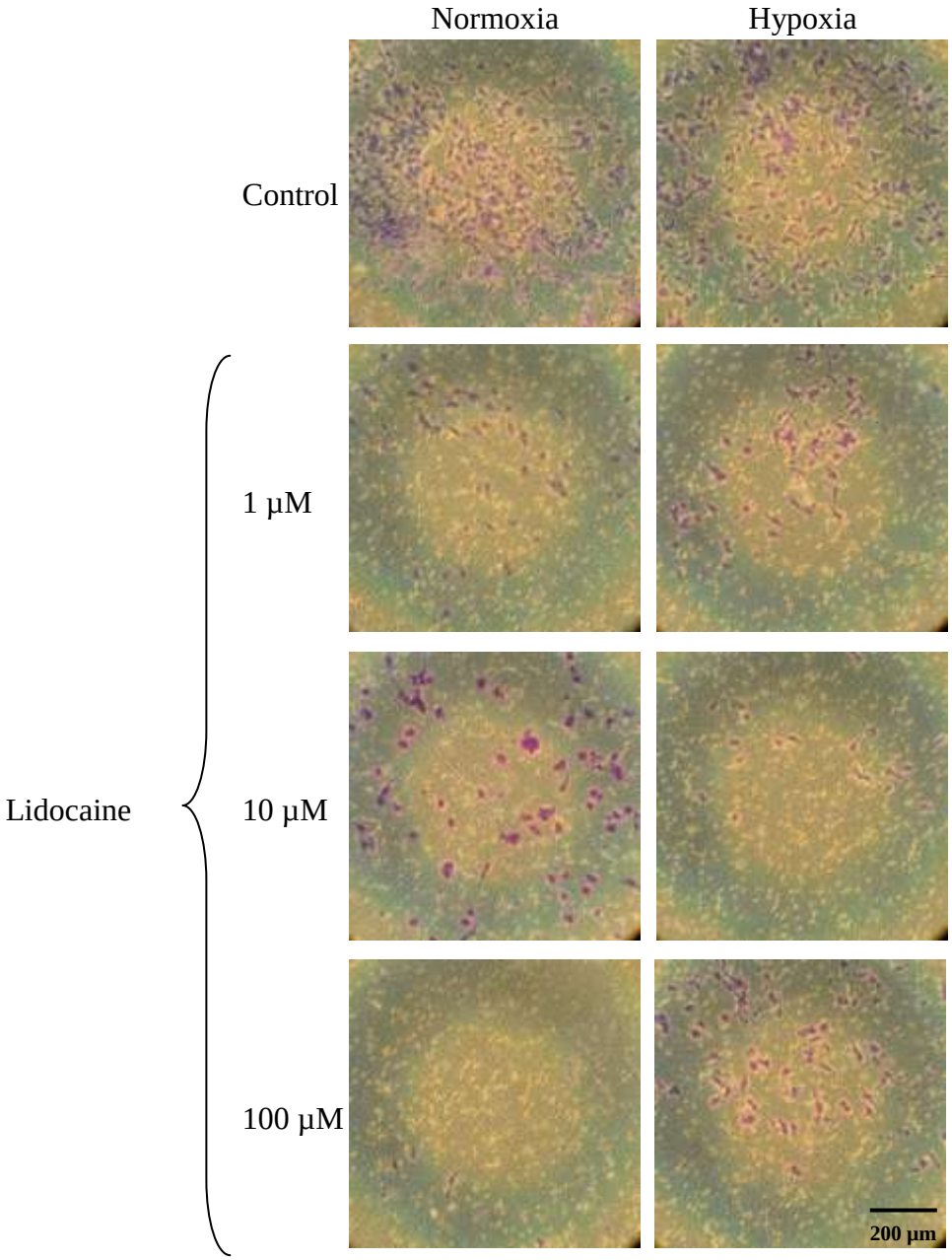
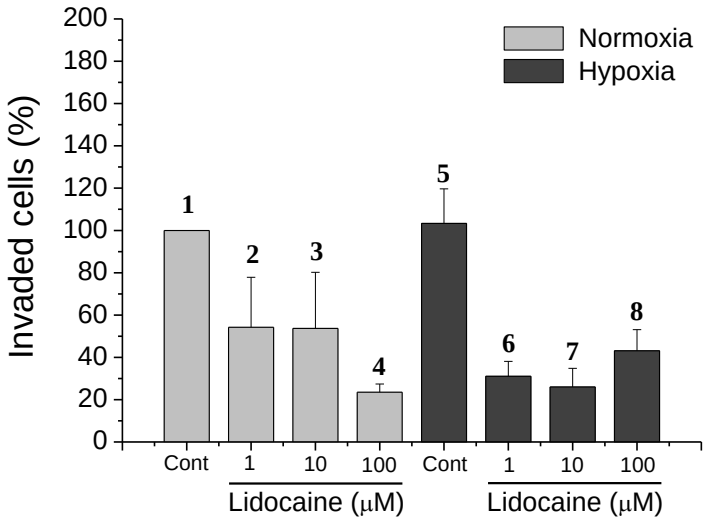


Figure 4.55 Typical images of invaded cells showing the effect of lidocaine on Mat-LyLu invasiveness.
Typical phase-contrast light-microscopy images of invaded cells obtained from Matrigel™ invasion assays of Mat-LyLu cells incubated 24 h under normoxic and hypoxic conditions with or without lidocaine (1, 10 and 100 µM). Invaded cells were fixed and stained with crystal violet (purple). Scale bar (200 µm) applicable to all panels.



Comparison			p<0.05
1	vs	2	No
1	vs	3	Yes
1	vs	4	Yes
1	vs	5	No
1	vs	6	Yes
1	vs	7	Yes
1	vs	8	Yes
2	vs	3	No
2	vs	4	No
2	vs	5	No
2	vs	6	No
2	vs	7	No
2	vs	8	No
3	vs	4	No

Comparison			p<0.05
3	vs	5	Yes
3	vs	6	No
3	vs	7	No
3	vs	8	No
4	vs	5	Yes
4	vs	6	No
4	vs	7	No
4	vs	8	No
5	vs	6	Yes
5	vs	7	Yes
5	vs	8	Yes
6	vs	7	No
6	vs	8	No
7	vs	8	No

Figure 4.56 Effect of lidocaine on invasion of Mat-LyLu cells.
Bar diagram showing number of invaded Mat-LyLu cells, incubated 24 h under normoxic and hypoxic conditions with or without lidocaine (1, 10 and 100 µM). Data were expressed relative to the control (%) and presented as means ± SEM ($n \geq 4$). Data were analysed by Kruskal-Wallis analysis of variance. The table of multiple comparisons between treatments for statistical significance are shown underneath the bar diagram.

2) Ranolazine treatment (20-300 μM; 24 h) had no effect on cellular viability or proliferation under both normoxic and hypoxic conditions. Nav1.7 mRNA expression was reduced in both conditions. There was no effect on plasma membrane VGSCα protein levels in both conditions, whilst internal VGSCα protein expression was reduced under normoxia. Importantly, ranolazine decreased invasiveness under both conditions with some dose dependency.
3) Riluzole treatment (1-5 μM; 24 h) had no effect on cellular morphology and viability; however, there was a tendency for reduction of cell number at high concentration (30 μM). Use of DMSO as a solvent introduced considerable variability in the data. There was some reduction of Nav1.7 mRNA and intracellular VGSC protein expression in normoxia. On the other hand, plasma membrane VGSCα protein level increased under hypoxia. Although there was a consistent trend in suppression of invasiveness by riluzole at concentrations that did not affect proliferation, the changes were not significant when compared to DMSO controls.
4) Procaine treatment (10-1000 μM; 24 h) slightly altered Mat-LyLu cell morphology under hypoxia; cell viability and numbers were not affected in both normoxia and hypoxia. Procaine decreased Nav1.7 mRNA expression and both internal and plasma membrane VGSCα protein levels were reduced by procaine under normoxic conditions; there was no effect on protein expression or distribution under hypoxia. Procaine decreased Mat-LyLu cell invasion both under normoxic and hypoxic conditions.
5) Lidocaine treatment (10 - 1000 μM; 24 h) had no effect on cell viability or cell numbers in normoxia; high doses had an inhibitory effect under

hypoxia. There was some reduction in Nav1.7 mRNA and VGSCα protein expression by lidocaine in both normoxic and hypoxic conditions, but, in hypoxia, only cytoplasmic protein level was reduced by lidocaine. Lidocaine (10 and 100 μM) decreased Mat-LyLu cell invasion under both normoxic and hypoxic conditions.

4.3.1 Effects of hypoxia alone

The effects of hypoxia alone were highly consistent: Thus, no effect was seen cellular morphology, viability or cell number. Interestingly, Nav1.7 mRNA expression was increased whilst both cytoplasmic and plasma membrane VGSCα protein levels were decreased. There was no effect on invasiveness.

4.3.2 Observations on cell morphology

None of the four pharmacological treatments had an obvious effect on the morphologies or distribution of Mat-LyLu cells. This was somewhat surprising since VGSC blockers have previously been shown to induce changes in morphologies of cells, including neurones (Wilkemeyer and Angelides, 1996; Sretavan *et al*., 1988) and Mat-LyLu cells (Fraser *et al*., 1999). These changes have generally been in the direction of making the cellular architecture appear less developed, e.g. retracted dendrites in the case of neurones (Friedman and Shatz, 1990). It is not clear why the observations of Fraser *et al*. (1999) could not be replicated here. Possible reasons for this include lack of fixing and staining of the cells, in the present study, which could have precluded some changes being clearly observed. However, some effects (loosening of cell contacts and lost of spindle-shaped / fibroblast-like morphology) were observed with the following treatments: i) 300 μM ranolazine (normoxia and

hypoxia). This could be due to inhibition of sodium - calcium exchanger activity (Antzelevitch *et al.,* 2004). (ii) 1000 µM procaine and lidocaine (normoxia and hypoxia). This could be due to changes in the physicochemical properties (e.g. membrane fluidity) of lipid membranes. Such effects of 7 mM procaine and 1000 µM lidocaine were demonstrated on 1,2-dipalmitoylphosphatidylcholine membrane by Tsuchiya *et al.* (2007).

4.3.3 Effects on cell number

Here, the term "cell number" rather than "proliferation" has been used since it was not possible to study systematically possible effects on apoptosis. Nevertheless, since the working concentrations of the agents used did not affect cell viability (as determined by trypan blue staining), it can be assumed that the measurements made represent mainly proliferative activity. At the lower end of the concentration ranges of all 4 pharmacological agents used, there was no effect on cell number. Assuming that these low concentrations would affect/block mainly VGSC activity, the results agree with the established notion that VGSCs are not involved in cellular proliferation of cancer cells (Nakajima *et al*., 2009; Fulgenzi *et al*., 2006; Fraser *et al*., 1999, 2000, 2005). On the other hand, it was previously reported that 250 and 500 µM ranolazine decreased leukemia cell proliferation via inhibition of fatty acid oxidation (Samudio *et al.,* 2010). Riluzole (3-10 µM) had no effect on proliferation of Mat-LyLu cells under both normoxic and hypoxic conditions. 30 µM riluzole decreased the Mat-LyLu cell number under both conditions. This decrease in Mat-LyLu cell number is not because of I_{NaP} block since riluzole concentration used was much higher than IC_{50} of I_{NaP} (IC_{50}=2 µM). It was also suggested that 25 µM riluzole treatment inhibits proliferation of melanoma cells via inhibition of glutamate release

(Le *et al.*, 2010). In addition, it was documented that riluzole (10-50 µM) decrease viable LNCaP and C4-2 prostate cancer cell number by inhibition of DNA synthesis and apoptotic cell death via ER stress (Akamatsu *et al.*, 2009). Therefore, following experiments were carried out at riluzole concentrations between 1 and 5 µM.

4.3.4 mRNA versus protein expression

It was clear from the results (and as summarised in Table 1) that the various treatments had differential effects on Nav1.7 and VGSCα protein expression in Mat-LyLu cells. In fact, it can be assumed that the VGSCα studied represented mainly Nav1.7 protein in these cells, since this is the main VGSC species expressed in rat (and human) PCa cells (Diss *et al.*, 2001,, 2005; Nakajima *et al*., 2009). It is now generally accepted that mRNA and protein expression can be regulated differentially and independently in cells, such that (i) mRNA can be produced and 'docked' without being translated and (ii) protein synthesis can occur from such stored mRNA without any transcription (Sola *et al*., 1999; Ropponen *et al*., 2001; Orphanides and Reinberg, 2002; Schedel *et al*., 2004; Gu *et al*., 2006; Martin and Zukin, 2006; Pfeiffer and Huber, 2006). Such differential regulation presumably is functionally expedient and depends on intracellular factors such as mRNA stability and protein lifetime (Brackenbury *et al*., 2007; Brackenbury and Djamgoz, 2006; Ben Fredj *et al*., 2004; St Johnston, 2005). This could be particulary important pathophysiologically in cancer cells exposed dynamically to a wide variety of micro-environmental conditions. Previously also, Brackenbury and Djamgoz (2006) showed in Mat-LyLu cells that nerve growth factor upregulated VGSC protein expression without any change in Nav1.7 mRNA expression.

In the following, we discuss further the effects of the pharmacological agent used, one by one, on VGSC expression and cellular invasiveness.

4.3.5 Effects of ranolazine

Ranolazine, (±)-4-[2-hydroxy-3-(o-methoxyphenoxy)propyl]-l-piperazineaceto-2',6'-xylidide, is a antianginal drug that does not affect heart rate or blood pressure (Maier, 2009). It is commercially available under the brand name of "Ranexa" and clinical usage was approved in the United States and European Union (Maier, 2009). Its main mode of action is thought to be blockage of persistent (late) Na^+ current (I_{NaP}) of VGSCs (Antzelevitch *et al.,* 2004; Fredj *et al.,* 2006). Therapeutic plasma concentrations during treatment of patients with ischemic heart disease have been estimated to be in the range 2-8 µM (Rajamani *et al.,* 2008). Depending on concentration, ranolazine can block both I_{NaP} and I_{NaT} but lower, clinical doses preferentially block I_{NaP} (Chen *et al.,* 2009; Wang *et al.,* 2008; Antzelevitch *et al.,* 2004; Fredj *et al.,* 2006). It was shown earlier that ranolazine thus blocks I_{NaP} of mouse myocytes and HEK-293 cells expressing long-QT syndrome 3 mutant VGSC with a half-maximum inhibitory concentration (IC_{50}) of ~15 µM (Fredj *et al.,* 2006). In the same study, the value of IC_{50} for block of I_{NaT} with ranolazine was 135 µM (Fredj *et al.,* 2006). In addition, Antzelevitch *et al*. (2004) found that ranolazine blocked I_{NaP} more effective than I_{NaT} of isolated canine ventricular myocytes (IC_{50}s = 5.9 and 296 µM, respectively). A similar effect of ranolazine was observed on human embryonic kidney 293T cells expressing inactivation-deficient rat Nav1.4, the values of IC_{50}s being 2.4 µM (I_{NaP}) and 225.4 µM (I_{NaT}) (Wang *et al.,* 2008). Block of Na^+ current by ranolazine was also documented for human Nav1.7 and rat Nav1.8 channels (Rajamani *et al.,* 2008; Wang *et al.,* 2008). Rajamani *et al.* (2008) also

documented that ranolazine blocked Na^+ current with IC_{50} value of 10.3 μM, when Nav1.7 was co-expressed with VGSCβ1 subunit in human embryonic kidney 293 cells. Various site-directed mutagenesis studies showed that ranolazine blocks VGSCs by binding to a conserved local anaesthetic site (D1/D3/D4:S6) on the inside of the membrane (Wang *et al.*, 2008; Fredj *et al.*, 2006). In addition to VGSC currents, however, ranolazine found to block the following ionic mechanisms: human Kv11.1 / human ether-a-go-go related gene, hERG (IC_{50}=11.5 μM), sodium-calcium exchanger (IC_{50}=91 μM), peak and late L-type voltage-gated Ca^+ channel (VGCC) currents (IC_{50} = 50 and 296 μM, respectively) in canine myocytes (Antzelevitch *et al.*, 2004). Kv11.1 was shown to be expressed in various cancer cell lines (Bianchi *et al.*, 1998; Wang *et al.*, 2002). However, there is no evidence of Kv11.1 expression in prostate cancer. Also, Ding *et al.* (2006) showed absence of VGCCs in Mat-LyLu cells. Initially, it was proposed that the antianginal effect of ranolazine occurred via inhibition of fatty acid oxidation (McCormack *et al*., 1996; Clarke *et al*., 1996). However, subsequently, it has been shown that ranolazine at therapeutical doses does not inhibit fatty acid oxidation (Hale *et al.*, 2008). Therefore, we can assume that the primary effect of ranolazine seen in this study is via blockage of VGSC.

As already noted, the predominant VGSC functionally expressed in rat and human prostate cancer cells, Nav1.7, was reported to increase the metastatic potential (Diss *et al.*, 2001; Grimes *et al.*, 1995; Nakajima *et al.*, 2009). Brackenbury and Djamgoz (2006) proposed that Nav1.7 mRNA is up-regulated at steady-state via positive feedback in Mat-LyLu cells. It was reported that blockage of VGSC activity with TTX reduced Nav1.7 mRNA expression in Mat-LyLu cells (Brackenbury and Djamgoz, 2006). Similarly, Mat-LyLu cell Nav1.7 mRNA expression decreased by 24 h ranolazine treatment (20-300 μM) under both hypoxic and normoxic conditions.

This indicates involvement of ranolazine on Nav1.7 mRNA regulation via inhibition of VGSC activity. Although ranolazine (50 μM) had no effect on plasma membrane VGSCα protein level, invasiveness was reduced significantly.

Previously, involvement of VGSC activity on invasive capacity of prostate cancer cells was studied extensively (Grimes *et al.*, 1995; Laniado *et al.*, 1997; Smith *et al.*, 1998; Bennett *et al.*, 2004; Nakajima *et al.*, 2009). It was also suggested that, functional expression of VGSC is "necessary and sufficient" for prostate cancer cell invasion (Bennett *et al.*, 2004). In addition, previously we showed that TTX decreased Mat-LyLu cell invasion under both normoxic and hypoxic conditions (Sections 3.2.2.7.3 and 3.3.6.3). Similarly, ranolazine (20-300 μM) decreased invasion of Mat-LyLu cells under both normoxic and hypoxic conditions probably via inhibition of VGSC / I_{NaP} activity.

These results raise the possibility that ranolazine may be useful as an anti-metastatic drug, especially as it is already in clinical use against angina (Maier, 2009). Interestingly, in the only *in vivo* study reported to date, ranolazine (30 mg/kg, twice daily), in fact, increased the number of tumours in $APC^{(Min/+)}$ mice and tumours become more invasive, thought to occur via inhibition of fatty acid oxidation (Suckow *et al.*, 2004). However, ranolazine used in that study was more than the maximum recommended dose for human: 500-1000 mg, twice daily (Chaitman, 2006).

4.3.6 Effects of riluzole

Riluzole (2-amino-6-trifluoromethoxy benzothiazole) is an anti-excitatory and neuroprotective agent. Its use, under the brand name "Rilutex", was approved for treatment of the fatal neurodegenerative disease Amyotrophic Lateral Sclerosis

(ALS) in USA and Europe (Bensimon *et al.,* 1994; Lacomblez *et al.,* 1996). Riluzole was shown to be not harmful in humans at concentrations up to 10 µM (Weiss *et al.,* 2010; Le Liboux *et al.,* 1999). It was proposed that the neuroprotective property of riluzole was via inhibition of I_{NaP} (Urbani and Belluzi, 2000; Zona *et al*., 1998). Indeed, riluzole was shown to protect against cardiac ischemia by inhibiting I_{NaP} (Weiss *et al.,* 2010). Riluzole would bind to VGSCα subunit (binding site is not known) and stabilize the channel in its inactivated formation (Doble, 1999; Hebert *et al.,* 1994).

Riluzole treatment had some inhibitory effect on Nav1.7 mRNA expression and intracellular VGSCα protein expression in both normoxia and hypoxia. Although riluzole caused some increase in VGSCα protein expression in plasma membrane under hypoxia, there was no effect on invasiveness. In fact, although there was a strong and consistent trend towards inhibition, riluzole had no effect on invasiveness at concentrations (1 – 5 µM) that did not affect cellular viability or proliferative activity. This is likely to be due the significant variability introduced by DMSO used as a solvent.

Riluzole had no effect on Nav1.7 mRNA expression in normoxia but decreased it significantly under hypoxia. It was previously reported that hypoxia would increase I_{NaP} amplitude and therefore increase internal Na^+ concentration in neurons and cardiac cells (Hammarström and Gage, 1998; Ju and Gage, 1996). As discussed earlier (Section 4.3.1.3), Nav1.7 mRNA was regulated by VGSC activity in Mat-LyLu cells (Brackenbury and Djamgoz, 2006). Therefore, we can speculate that the increase intracellular Na^+ and the subsequent increase in PKA activity could be the reasons of increase in Nav1.7 mRNA expression in Mat-LyLu cells.

The effect on VGSCα protein expression was studied with 2.5 μM riluzole which nevertheless increased plasma membrane expression. This was surprising considering the activity-dependent positive feedback hypothesis, involving intracellular trafficking, proposed by Brackenbury and Djamgoz (2006) according which a reduction would be expected. One possibility is that 2.5 μM riluzole was not sufficient to block I_{NaP} completely, since regulation may occur in all-or-none fashion (Brackenbury and Djamgoz, 2006).

Previously, effects of riluzole on human prostate cancer cells were investigated in 3 separate studies, as follows:

1. Abdul and Hoosein (2002) initially studied effects on four different cell lines, including the VGSC-expressing PC-3 cells and found that riluzole inhibited growth with an IC_{50} of 43-128 μM.

2. Parihar *et al*. (2003) found that riluzole (EC_{50} = 2 μM) evoked concentration-dependent increases in proliferation of PC-3 (and LNCaP) cells. However, this effect was proposed to be through intermediate-conductance Ca^{2+}-activated K^{+} channels.
3. Akamatsu *et al*. (2009) showed that riluzole (10-50 μM) induces inhibition of DNA synthesis and apoptotic cell death via endoplasmic reticulum stress in both LNCaP and C4-2 prostate cancer cell lines.

In conclusion, riluzole is likely to have anti-PCa effects via a number of ionic and cellular mechanisms. Further work is required to determine the role of I_{NaP} in the effects of riluzole. In particular, anti-invasive/metastatic effects would be worthwhile investigating further.

4.3.7 Effects of procaine

Procaine (4-aminobenzoic acid-2-diethylaminoethyl ester) is a clinically used local anaesthetic. It was documented that its main mode of action is via VGSC block by interacting with local anaesthetic binding site at D1/D3/D4:S6 of VGSCα subunit (Lilley and Robinson, 1998; Bräu *et al.,* 1998; Ragsdale *et al.,* 1994). However, procaine can also block voltage-dependent K^+ current in peripheral nerves with IC_{50} value of 6302 µM (Bräu *et al*., 1998).

Procaine (1 mM but not 0.5 mM) inhibited growth of breast cancer MCF-7 cells via DNA-demethylation (Villar-Garea *et al.,* 2003). In the present study, procaine (1 µM – 1 mM) had no effect on Mat-LyLu cell number under normoxia or hypoxia. This result is consistent with VGSC activity having no role in Mat-LyLu cell proliferation (Fraser *et al.,* 2000).

Procaine reduced Mat-LyLu cell invasion dose dependent manner under both normoxic and hypoxic conditions, consistent with involvement of VGSC activity. Overall, this agrees with previous work showing enhancement of prostate cancer cell invasiveness by functional VGSC expression (e.g. Grimes *et al.,* 1995; Laniado *et al.,* 1997; Smith *et al.,* 1998; Bennett *et al.,* 2004; Nakajima *et al.,* 2009). However, as well the presumed suppression of VGSC activity, procaine also had some inhibitory effects on Nav1.7 mRNA and VGSCα protein expression. Thus, procaine may have potential as an anti-metastatic drug. Interestingly, procaine was reported to enhance antitumoral activity of several drugs used in cancer therapy, such as cisplatin, mitomycine C, peplomycin and doxorubicin (Chlebowski *et al.,* 1982; Esposito *et al.,* 1990; Viale *et al.,* 1998; Mizuno and Ishida, 1982).

4.3.8 Effects of lidocaine

Lidocaine (2-diethylamino-N-(2,6-dimethylphenyl) acetamide), a structural analogue of ranolazine, is another clinically used local anaesthetic. It is reported to be useful in therapy of painful diabetic polyneuropathies, neuralgic pain and traumatic peripheral nerve injuries (Klinger *et al.*, 1997). Lidocaine achieves anaesthetic effect mainly by blocking VGSC activity by binding to local anaesthetic site located at D1/D3/D4:S6 region (Sheet *et al.*, 2007; Chevrier *et al.*, 2004; Lilley and Robinson, 1998; Bräu *et al.*, 1998; Ragsdale *et al.*, 1994). Lidocaine was also shown to block VGSC in MDA-MB-231 breast cancer cell line (Fraser *et al.*, 2005). It was also reported that lidocaine (200 µM) decrease endocytic membrane activity via VGSC channel blockage (Onganer and Djamgoz, 2005). In addition, similar to procaine, lidocaine can also block voltage-dependent K^+ currents in peripheral nerves with an IC_{50} of ~1118 µM (Bräu *et al.*, 1998). In the present study, lidocaine (10 and 100 µM) decreased invasion of Mat-LyLu cells under both normoxic and hypoxic conditions, thereby providing further evidence on involvement of VGSC in invasiveness of cancer cells. At these concentrations (in fact, up to 1 mM), lidocaine had no effect on Mat-LyLu cell number in normoxia. Only at high concentrations (700 and 1000 µM) was cell number reduced under hypoxic conditions.

At the concentrations used to suppress invasiveness, there was also a tendency to inhibit expression of Nav1.7 mRNA and VGSCα protein. These results agree generally with previous findings (i) that VGSC activity promotes cellular invasiveness without any involvement in proliferation and (ii) VGSC expression is under auto-controlling such that channel activity can have both transcriptional and post-translational effects (Brackenbury and Djamgoz, 2006).

Overall, the effects of lidocaine reported elucidated here would support the notion that lidocaine can also have anti-cancer/metastatic effects. It was shown earlier that that 3.5 mM lidocaine caused growth inhibition of SHG human melanoma cells (Chlebowski *et al.*, 1982). In another study, Mammoto *et al.* (2002) found that lidocaine inhibited the invasiveness of various human cancer cell lines but this was thought to be independent of any VGSC blockage.

4.4 Concluding remarks

In overall conclusion, 3 of the 4 VGSC blockers (ranolazine, procaine and lidocaine) employed in the present study produced inhibitory effects on metastatic cell behaviour (invasion) at concentrations that did not affect primary cell growth. These findings further support the following viewpoints. First, primary and secondary tumourigenesis are controlled differently, perhaps even independently (Hanahan and Weinberg, 2000; Welch *et al*., 2000; Welch, 2004; Welch, 2006). Second, VGSC blockers can be useful clinically as anti-metastatic drugs (Onkal and Djamgoz, 2009; Gillet *et al.*, 2009; Roger *et al.*, 2006; Prevarskaya *et al.*, 2007; Brackenbury and Djamgoz, 2006). The only apparent exception was riluzole which did not produce statistically significant effects in spite of the strong inhibitory trends. This was likely to be due to the obligatory use of DMSO as a solvent. Nevertheless, with further experimentation and optimization, it is possible that riluzole can also produce significant effects. We should emphasise, however, that blocking VGSC activity was accompanied by changes in Nav1.7 mRNA and protein expression, and these secondary effects will need to be taken into account when considering the full clinical potential of VGSC blockers as anti-metastatic agents.

Chapter 5

STUDY OF INTRACELLULAR Ca^{2+} OSCILLATIONS IN HUMAN METASTATIC PROSTATE CANCER PC-3M CELLS

5.1 Introduction

Ca^{2+} signalling is a key player in transmembrane activity and intracellular signal transmission. Ca^{2+} signalling regulates many cellular processes such as fertilization (Ozil and Swann, 1995), cell cycle (e.g. Ding *et al.*, 2010), apoptosis (Norberg *et al.*, 2008), mitochondrial redox state (Hajnóczky *et al.*, 1995), differential gene expression (Wang *et al.*, 2010; Liao *et al.*, 2006; Dolmetsch *et al.*, 1998; Li *et al.*, 1998; Haisenleder *et al.*, 2001; Buonanno and Fields, 1999; Olson and Williams, 2000), motility / invasion (Amuthan *et al.*, 2002; Wei *et al.*, 2009; Huang *et al.*, 2004; Komuro and Rakic, 1996), muscle contraction, pacemaker activity, growth-cone turning / migration (Gomez *et al.*, 1995; Gomez *et al.*, 2001), axonal growth (Tang *et al.*, 2003), development of neurotransmitter phenotype (Ciccolini *et al.*, 2003), formation of nodules in plant root hairs (Ehrhardt *et al.*, 1996), development of muscle (Ferrari *et al.*, 1998), release of cytokines (Uhlén *et al.*, 2000), exocytosis (Tse *et al.*, 1993), adhesion (Giannone *et al.*, 2002; Liao *et al.*, 2006), chemotaxis, and synaptic plasticity (Parkash and Asotra, 2010; Mycielska *et al.*, 2004 Berridge, 1998; Berridge, 2009). Ca^{2+} signalling has also been implicated in modulation of metastatic cell behaviours (MCBs) in various cancers, including prostate cancer (PCa), breast cancer, head and neck squamous cell carcinoma, pulmonary adenocarcinoma, rhabdomyoblasts, fibrosarcoma, and retinoblastoma (Wang *et al.*, 2010; Liao *et al.*, 2006; Huang *et al.*, 2004; Zhong *et al.*, 2010; Wu *et al.*, 1997; Amuthan *et al.*, 2002; Amuthan *et al.*, 2001; Cook and Lockyer, 2006; Wertz and Dixit, 2000; Lehen'kyi *et al.*, 2007). In addition, changes in expression profiles of Ca^{2+} channels and pumps in cancer cells were proposed to play important role in carcinogenesis (Parkash and Asotro 2010; Monteith *et al.*, 2007).

Since high levels of intracellular Ca^{2+} ($[Ca^{2+}]_i$) can be cytotoxic, cells spend considerable energy in order to maintain a basal $[Ca^{2+}]_i$ of $\leq$100 nM, while extracellular Ca^{2+} concentrations are at mM levels (Parkash and Asotro, 2010; Berridge *et al.*, 2003; Berridge *et al.*, 1998). This regulation of $[Ca^{2+}]_i$ is carried out by chelation / binding, compartmentalisation and extrusion of intracellular Ca^{2+} (Parkash and Asotro, 2010; Berridge *et al.*, 2003; Berridge *et al.*, 1998). On the whole, therefore, physiological changes in intracellular Ca^{2+} are brief (Parkash and Asotro 2010; Rey *et al.*, 2010; Clapham 2007; Berridge *et al.*, 1998).

Ca^{2+} signalling can be mediated by influx of Ca^{2+} through plasma membrane and/or release of Ca^{2+} from internal stores (Roderick and Cook, 2008; Clapham, 2007; Berridge *et al.*, 2003; Berridge *et al.*, 1998). In turn, Ca^{2+} influx can occur via many different membrane mechanisms including voltage-gated Ca^{2+} channels (VGCCs), receptor-operated and store-operated Ca^{2+} channels (Berridge *et al.*, 1998). However, a rise in $[Ca^{2+}]_i$ can also result from slowing or reversal of Na^+ - Ca^{2+} exchanger (NCX) activity (Poburko, *et al.*, 2007; Eder *et al.*, 2005; Rosker *et al.*, 2004; Arnon *et al.*, 2000). On the other hand, two main Ca^{2+}-release channels have been characterized in endoplasmic reticulum (ER): ryanodine receptor (RyR) and inositol-triphosphate receptor (IP_3R) (Campbell *et al.*, 1987; Streb *et al.*, 1983). In addition, several pumps have been implicated in Ca^{2+} signalling / $[Ca^{2+}]_i$ regulation, including sarcoplasmic-endoplasmic reticulum Ca^{2+}-ATPase (SERCA), plasma-membrane Ca^{2+}-ATPase (PMCA) and mitochondrial Ca^{2+} uniporter, as well as NCX (Berridge *et al.*, 2003; Berridge *et al.*, 1998).

Liao et al. (2006) proposed that extracellular Ca^{2+} is a mediator of PCa bone metastasis. In addition, PCa cell motility, including galvanotaxis, was suggested to be regulated by Ca^{2+} signalling (Wang *et al.*, 2010; Mycielska and Djamgoz, 2004).

In PCa, TRPC1, TRPC3, TRPC4, TRPV2, TRPV6, TRPM8 subtypes of transient receptor potential (TRP) cation (including Ca^{2+}) channel family were identified (Abeele *et al*., 2003a; Abeele *et al*., 2003b; Abeele *et al*., 2004; Fixemer *et al*., 2003; Schmidt *et al*., 2006). In addition, some involvement of TRPV2 and TRPM8 in MCBs in PCa was documented (Monet *et al*., 2010; Gkika *et al*., 2010). For example, silencing of TRPV2 by siRNA reduced growth and invasion of PC-3 cells (Monet *et al*., 2010). Furthermore, TRPM8 activation mediated reduction in PC-3 cell motility was recently documented (Gkika *et al*., 2010).

Functional expression of voltage-gated Na^+ channels (VGSCs) have been associated with initiation and progression of several metastatic carcinomas (Grimes *et al.,* 1995; Blandino *et al.,* 1995; Laniado *et al.,* 1997; Allen *et al.,* 1997; Grimes and Djamgoz, 1998; Abdul and Hoosein, 2002; Roger *et al.,* 2003; Fraser *et al.,* 2004; Ou *et al.,* 2005; Fraser *et al.,* 2005; Onganer and Djamgoz, 2005; Onganer *et al.,* 2005; Brackenbury and Djamgoz, 2006; Fulgenzi *et al.,* 2006; Roger *et al.,* 2007; Diaz *et al.,* 2007; Nakajima *et al.,* 2009; Gao *et al.,* 2009; Gao *et al.,* 2010; House *et al.,* 2010). VGSC activity was shown to potentiate galvanotaxis, lateral motility, endocytic membrane activity, transverse migration and invasion in cancer cells (Brackenbury and Djamgoz, 2006; Gillet *et al.,* 2009; Nakajima *et al.,* 2009; Fraser *et al.,* 2003; Mycielska *et al.,* 2003; Djamgoz *et al.,* 2001; Krasowska *et al.,* 2004; Grimes *et al.,* 1995; Laniado *et al.,* 1997; Smith *et al.,* 1998; Bennet *et al.,* 2004). Concurrently, it was shown that strongly metastatic hepatoma and mammary adenocarcinoma have higher internal Na^+ concentrations than corresponding nontumoural cells (Cameron *et al.,* 1980). Similarly, the Na^+ content is higher in advanced breast cancers than benign tumours (Ouwerkerk *et al.,* 2007).

Interestingly, influx of Na^+ through openings of VGSCs (Sagel *et al.*, 1991; Gosling *et al.*, 1998) as well as TRP channels (Poburka, *et al.*, 2007; Eder *et al.*, 2005; Rosker *et al.*, 2004; Arnon *et al.*, 2000) was proposed to mediate Ca^{2+} influx by slowing or reversing NCX activity.

Therefore, in this chapter we proposed the hypothesis that VGSC activity modulates the intracellular Ca^{2+} levels.

5.2 Aims and scope of the present study

The main aim was to elucidate some basic aspects of Ca^{2+} signalling in human metastatic PCa PC-3M cells. The specific aims were as follows:

3. To test whether spontaneous Ca^{2+} oscillations occurred;
4. To determine the possible role of VGSC activity in Ca^{2+} signalling; and
5. To gain an insight to the subcellular regulatory components involved in Ca^{2+} oscillations.

5.3 Results

Fluo-4, a Ca^{2+} indicator dye, and high-speed confocal digital imaging system were used to record changes in intracellular $[Ca^{2+}]$ levels in human metastatic PCa cell line PC3M, human weakly metastatic PCa cell line LNCaP and rat highly metastatic PCa cell line Mat-LyLu in a comparative approach. $[Ca^{2+}]_i$ was measured as "$\Delta F/F$" (as defined in the Materials and Methods" chapter) and plotted as a percentage of the value above the average baseline (treated as 0 %).

5.3.1 Spontaneous oscillations of intracellular Ca^{2+} in PCa cells: Basic characteristics and comparative aspects

Of PC-3M cells, 24 ± 6 % showed spontaneous Ca^{2+} oscillations (n = 6; Figure 5.1A; Supplementary Videos 1 and 2). A transient event was accepted as an "oscillation" if it (i) occurred a minimum of 3 times and (ii) reached a minimum amplitude of 50 %. The $[Ca^{2+}]_i$ oscillations did not appear to be localized to any particular part of the PC-3M cells. Both spontaneously oscillating and non-oscillating PC-3M cells responded to depolarization of membrane potential (induced by application of 100 mM KCl) with increase in $[Ca^{2+}]_i$ (Figure 5.1A&B). There was no noticeable change in oscillation frequency or amplitude over 30 min of recording (Figure 5.1A). The basic characteristics of the Ca^{2+} oscillations in PC-3M cells were as follows: amplitude = 172 ± 17 % and frequency = 0.5 ± 0.04 oscillation/min (n = 38). In some cases, cells discharged repetitively and cumulatively without returning to baseline. Such cells were excluded from the analyses.

In contrast to PC-3M, the weakly metastatic human PCa cell line LNCaP did not have any spontaneous Ca^{2+} activity (n = 3; Figure 5.2A; Supplementary Videos 3 and 4). Nevertheless, membrane potential depolarization (induced by 100 mM KCl) caused a rapid rise in $[Ca^{2+}]_i$ (n = 3; Figure 5.2A).

In strongly metastatic rat PCa Mat-LyLu cells, no spontaneous Ca^{2+} event was recorded (n = 3; Figure 5.2B; Supplementary Videos 5 and 6). In addition, membrane depolarization (induced by 100 µM KCl) had no effect on $[Ca^{2+}]_i$ (n = 3; Figure 5.2B). This result agreed generally with the data of Ding *et al*. (2006) showing lack of functional VGCC expression in Mat-LyLu cells.

In the remainder of the experiments, mainly the PC-3M cells were used.

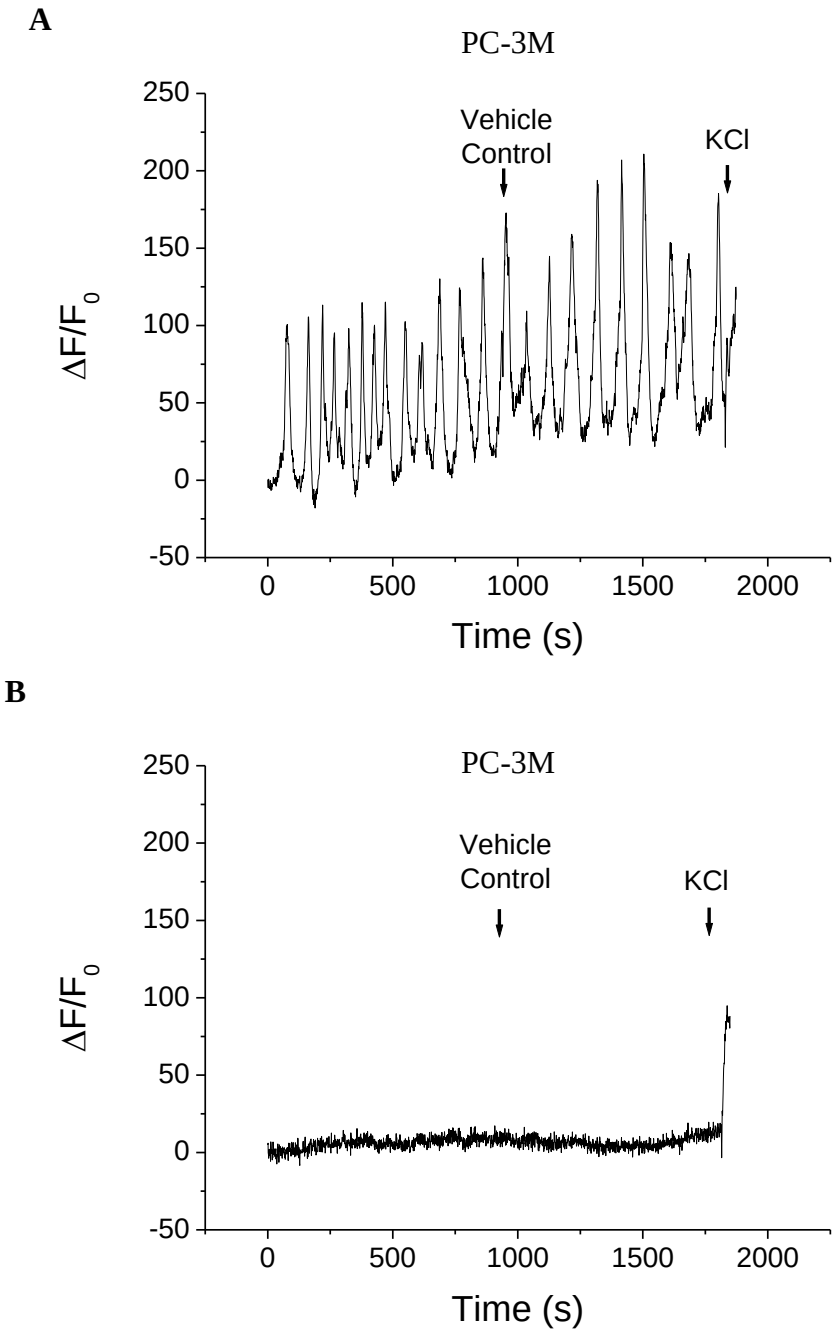


Figure 5.1 Spontaneous Ca^{2+} oscillations in PC3M cells.

Representative traces showing oscillatory changes in internal fluorescence intensity in PC-3M cells that were loaded with the Ca^{2+} indicator dye Fluo-4: (A) A typical oscillating cell; (B) A typical non oscillating cell. Changes in fluorescence intensity are expressed as $\Delta F/F_0$ (%). Applications of given treatments are indicated by arrows. Vehicle control, control buffer solution (MPS) without any treatment; KCl, potassium chloride (100 mM).

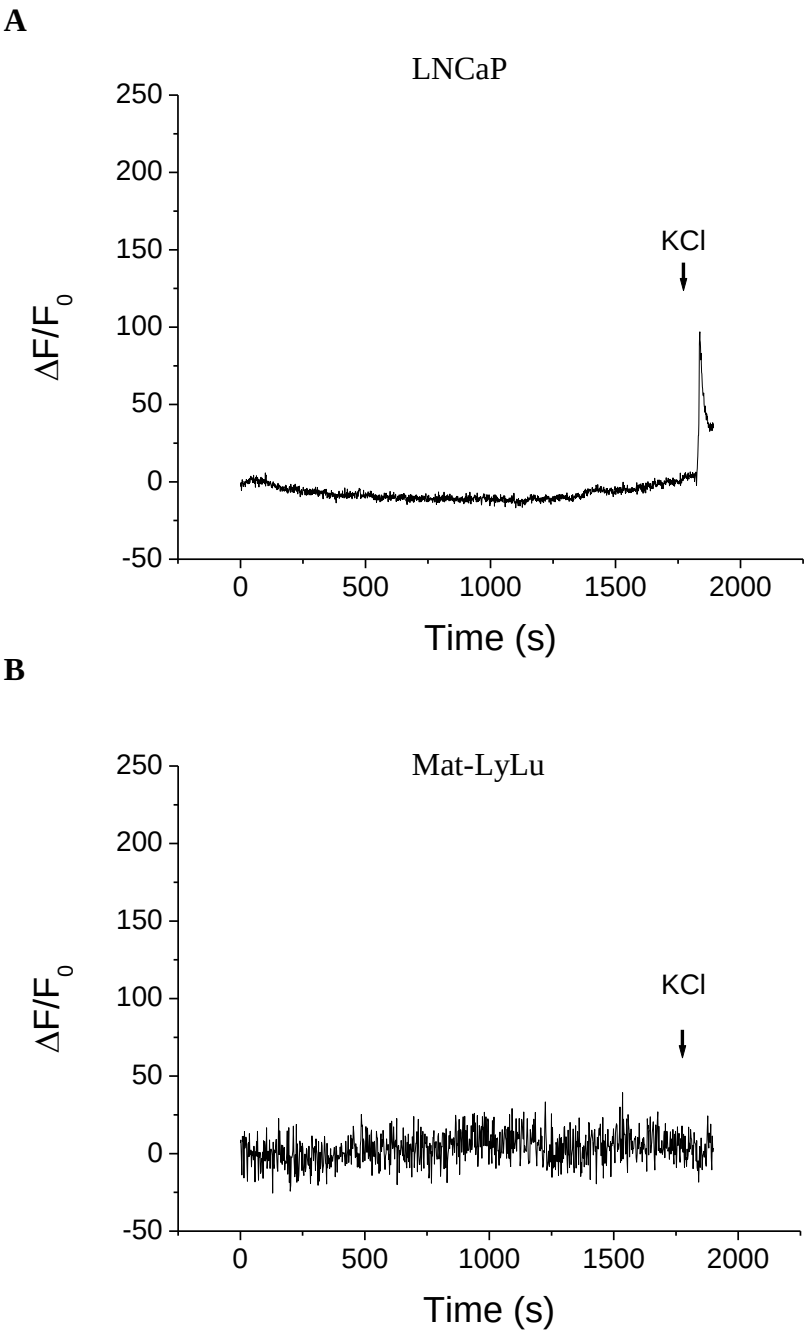


Figure 5.2 Spontaneous changes in $[Ca^{2+}]_i$ in LNCaP and Mat-LyLu cells

Typical recordings showing internal fluorescence intensity change over time in LNCaP (A) and Mat-LyLu (B) cells loaded with the Ca^{2+} indicator dye Fluo-4. Changes in fluorescence intensity are expressed as $\Delta F/F_0$ (%); black arrows indicate treatment application at shown time points. KCl was used at 100 mM.

5.3.2 Effects of VGSC blockers on Ca^{2+} oscillations in PC-3M cells

5.3.2.1 Effect of TTX

Blocking VGSC activity with 1 μM TTX significantly decreased amplitude of Ca^{2+} oscillations in PC-3M cells by some 47 %, from 137 ± 17 % to 73 ± 17 % ($p < 0.05$; $n = 23$; Figures 5.3A and 5.4A; Supplementary Videos 7 and 8). In addition, frequency of oscillations was significantly reduced by 59 %, from 0.39 ± 0.04 to 0.16 ± 0.03 oscillation/min ($p < 0.001$; $n = 23$; Figures 5.3A and 5.4B). There was no change in the number of oscillating PC-3M cells following the TTX treatment: 13 ± 6 % (control) and 13 ± 4 % (TTX-treated) ($p > 0.05$; $n = 3$; Figure 5.4C). TTX (1 μM) had no effect on the internal Ca^{2+} level in non-oscillating PC-3M cells ($n = 3$; Figure 5.3B). Depolarization of membrane potential (induced by 100 mM KCl) in the presence of TTX (1 μM) increased $[Ca^{2+}]_i$ in both oscillating and non-oscillating PC-3M cells ($n = 3$ each; Figure 5.3A&B).

5.3.2.2 Effect of ranolazine

Ranolazine was used as a selective blocker of the VGSC persistent current (I_{NaP}). Treatment with 20 μM ranolazine significantly reduced the Ca^{2+} oscillation amplitude by 43 %, from 149 ± 20 % to 85 ± 15 % ($p < 0.05$; $n = 17$; Figures 5.5A and 5.6A; Supplementary Videos 9 and 10). Oscillation frequency was also significantly decreased by 59 %, from 0.44 ± 0.04 to 0.18 ± 0.03 oscillation/min ($p < 0.001$; $n = 17$; Figures 5.5A and 5.6B). Also, similar to TTX, ranolazine (20 μM) had no significant effect on number of oscillating PC-3M cells: 25 ± 12 % (control) and 22 ± 13 % (ranolazine-treated) ($p > 0.05$; $n = 3$; Figure 5.6C). There was no

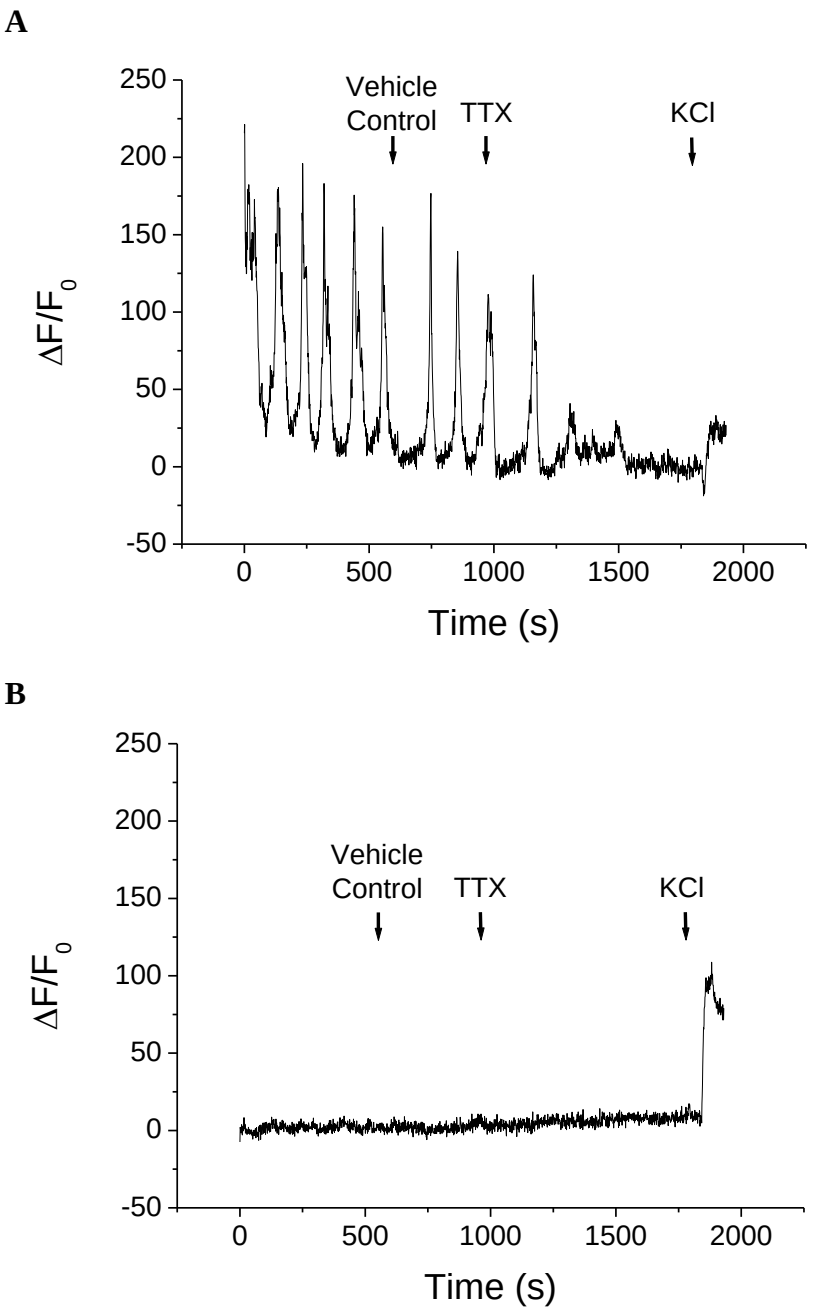


Figure 5.3 Effect of TTX on spontaneous Ca^{2+} oscillations in PC-3M cells

Representative traces showing the effect of TTX (1 µM) on spontaneous Ca^{2+} oscillations in a typical oscillating (A) and non-oscillating (B) PC-3M cell. Changes in fluorescence intensity are expressed as $\Delta F/F_0$ (%). Treatment application times are indicated by arrows. Vehicle control, buffer solution (MPS) without any treatment; KCl, potassium chloride (100 mM).

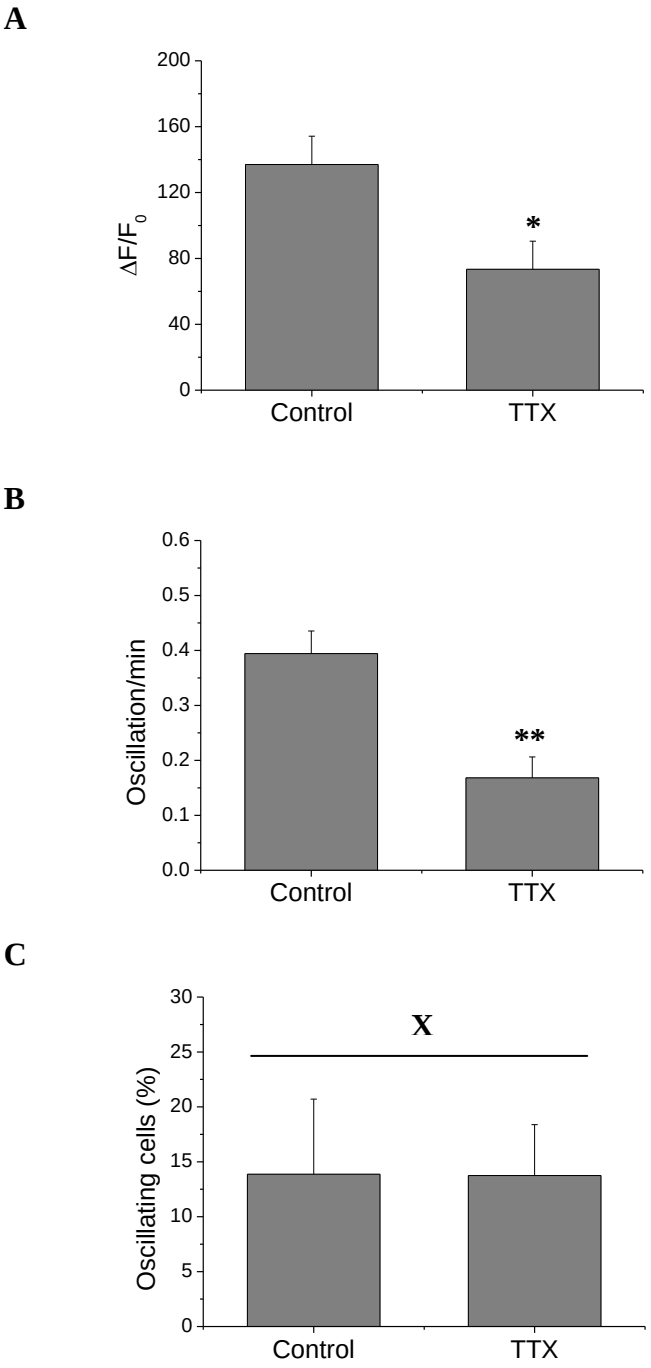


Figure 5.4 Summary of the effects of TTX on spontaneous Ca^{2+} oscillations in PC-3M cells.

Bar diagrams illustrates the effect of 1 µM TTX on the amplitude (A) and the frequency (B) of spontaneous Ca^{+2} oscillations recorded in PC-3M cells. Data were obtained in a 'matched' fashion (i.e. from the same cells) under control conditions and then in the presence of TTX (15 min each). Paired t-tests were used for statistical comparisons (n = 23). (C) Effect of TTX (1 µM) on the percentage of oscillating PC-3M cells. Paired t-test was used for statistical analysis (n = 3). Data are presented as mean ± SEM. Significance: (*) $p < 0.05$; (**) $p < 0.001$; (X) $p > 0.05$.

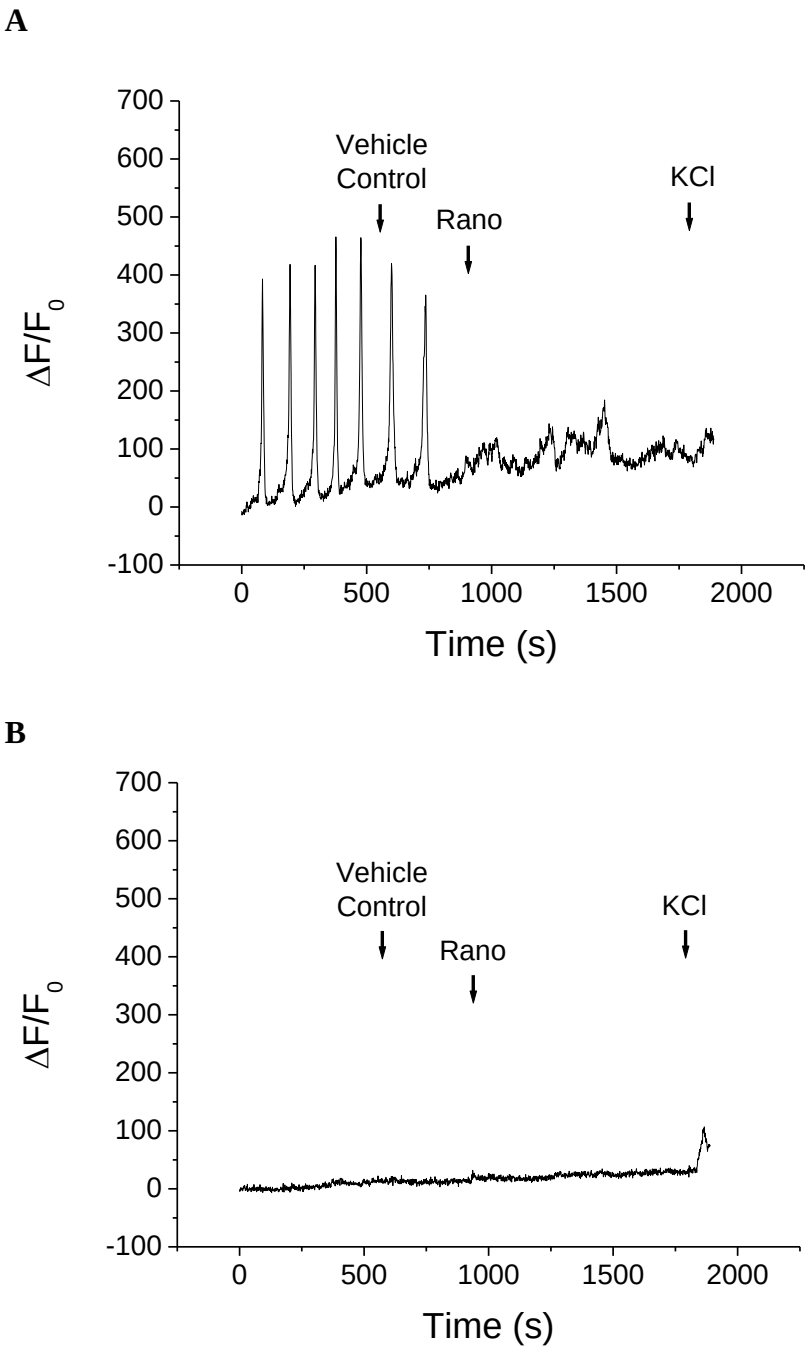


Figure 5.5 Effect of ranolazine on spontaneous Ca^{2+} oscillations in PC-3M cells. Representative traces showing the effect of 20 µM ranolazine on spontaneous Ca^{2+} oscillations in PC-3M cells: (A) an oscillating cell; (B) non-oscillating cell. Changes in fluorescence intensity are expressed as $\Delta F/F_0$ (%). Treatment application times are indicated with arrows. Vehicle control, buffer solution (MPS) without any treatment; KCl, potassium chloride (100mM); Rano, ranolazine (20 µM).

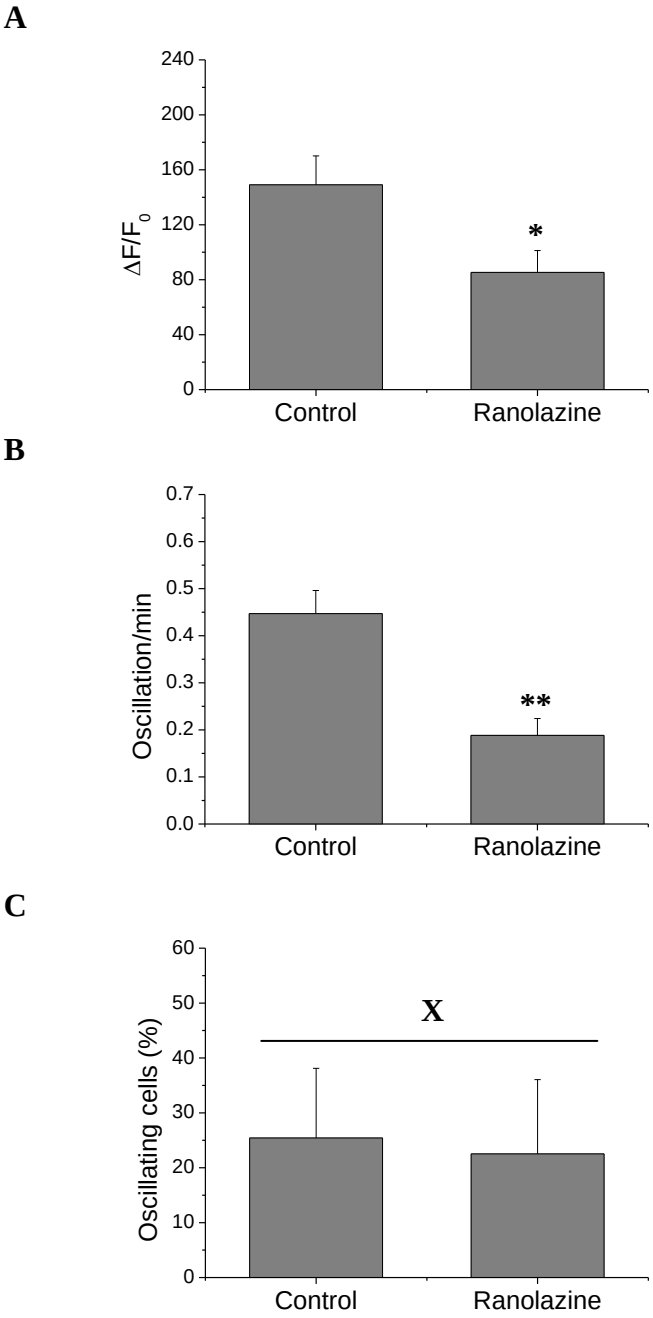


Figure 5.6 Summary of the effects of ranolazine on spontaneous Ca^{2+} oscillations in PC-3M cells.

Bar diagrams illustrating the effect of 20 µM ranolazine on the amplitude (A) and the frequency (B) of Ca^{2+} oscillations in PC-3M cells. Data were obtained in a 'matched' fashion (i.e. from the same cells) under control conditions and then in the presence of ranolazine (15 min each). Paired t-tests were used for statistical comparisons (n = 17). (C) Effect of ranolazine (20 µM) on the percentage of oscillating PC-3M cells. Paired t-test was used for statistical analysis (n = 3). Data are presented as mean ± SEM. Significance: (*) $p < 0.05$; (**) $p < 0.001$; (X) $p > 0.05$.

significant change of intracellular Ca^{2+} concentration in non-oscillating PC-3M cells after ranolazine treatment (n = 3; Figure 5.5B). Finally, increases in intracellular Ca^{2+} levels were recorded after depolarization of membrane potential with 100 µM KCl in the presence of ranolazine (20 µM) in both oscillating and non-oscillating PC-3M cells (n = 3; Figures 5.5A&B).

It was concluded that VGSC activity, in particular I_{NaP}, played a significant role in regulating the $[Ca^{2+}]_i$ oscillations in PC-3M cells.

5.3.3 Effects of Na^+-free conditions on Ca^{2+} oscillations

Role of extracellular Na^+ in Ca^{2+} oscillations were studied by substituting NaCl in the bathing solutions with equimolar LiCl or choline chloride.

5.3.3.1 Effect of Li^+-substituted Na^+-free solution

No change was recorded in the Ca^{2+} oscillation amplitude of PC-3M cells when maintained in control and Li^+-substituted Na^+-free conditions (165 ± 13 and 172 ± 17 %, respectively; $p > 0.05$; $n \geq 38$; Figures 5.7A and 5.8A; Supplementary Videos 11 and 12). In addition, there was no difference in frequency of Ca^{2+} oscillations: 0.52 ± 0.04 oscillation/min (control) and 0.52 ± 0.04 oscillation/min (Li^+-substituted) ($p > 0.05$; $n \geq 38$; Figures 5.7A and 5.8B). The number of oscillating cells also was not changed in the Li^+-substituted Na^+-free conditions: 24 ± 6 % (control) and 37 ± 4 % (Li^+-substituted) ($p > 0.05$; $n \geq 3$; Figure 5.8C). Depolarization of membrane potential (induced by 100 mM KCl) significantly increased intracellular Ca^{2+} levels in both oscillating and non-oscillating PC-3M cells under Li^+-substituted Na^+-free conditions (n = 3; Figure 5.7A&B).

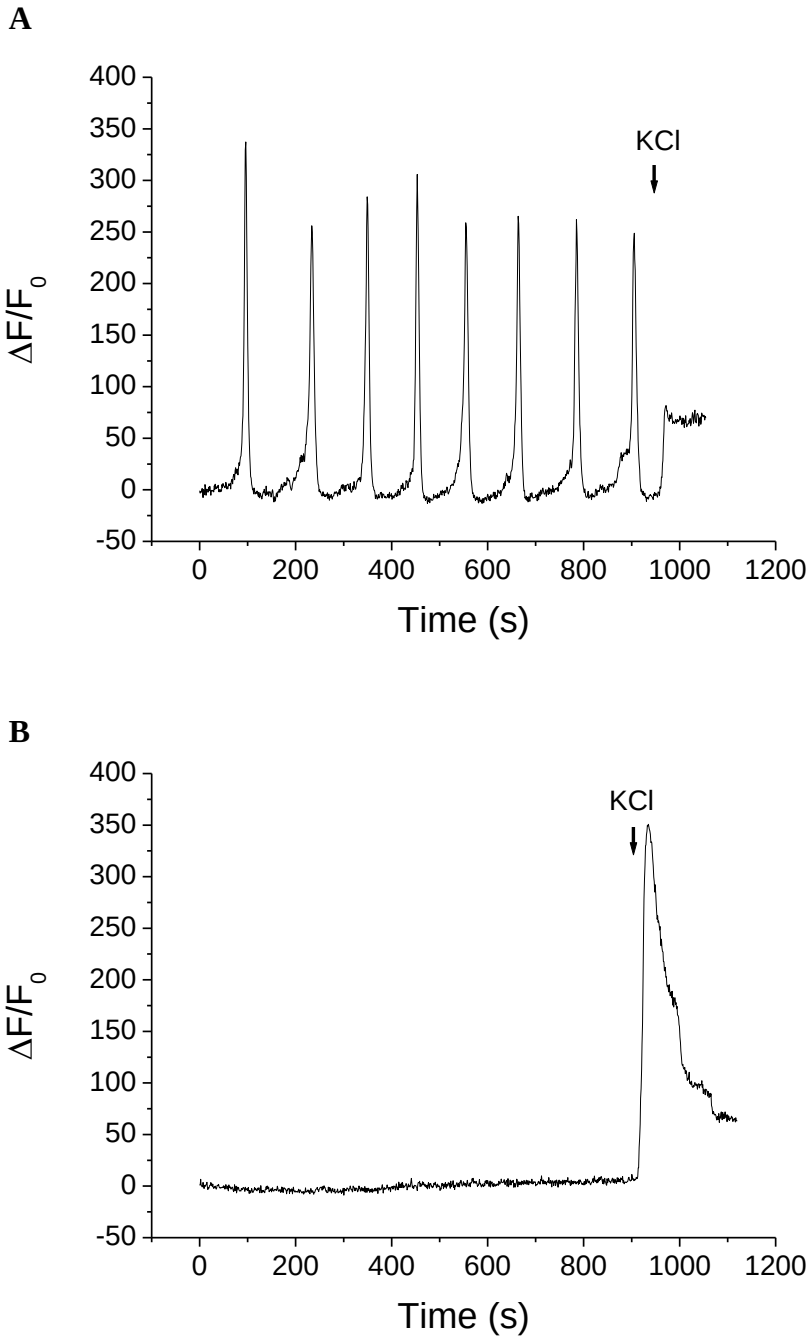
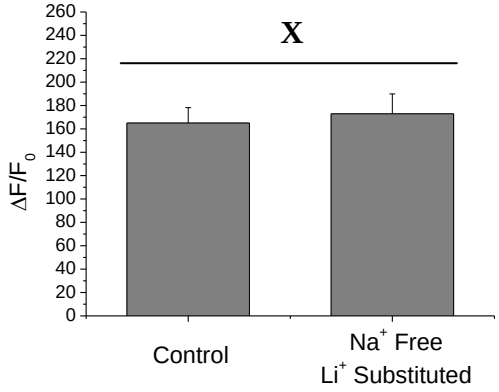


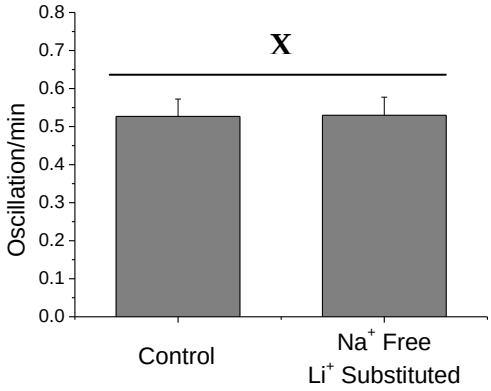
Figure 5.7 Effect of Na^+ free (Li^+ substituted) conditions on Ca^{2+} oscillations in PC-3M cells.

Exemplar recordings showing the effect of Li^+ substituted Na^+ free MPS on Ca^{2+} oscillations in oscillating (A) and non-oscillating (B) PC-3M cells. Changes in fluorescence intensity are expressed as $\Delta F/F_0$ (%). Treatment application times are indicated by arrows. KCl, potassium chloride (100 mM).

A



B



C

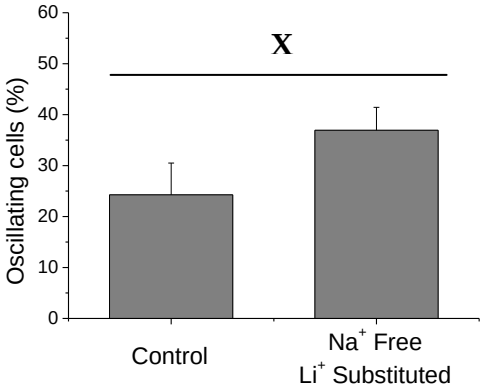


Figure 5.8 Summary of the effects of Na^+ free (Li^+- substituted) conditions on spontaneous Ca^{2+} oscillations in PC-3M cells.

Bar diagrams showing the effect of Na^+ free (Li^+-substituted) MPS on the amplitude (A) and the frequency (B) of Ca^{+2} oscillations in PC-3M cells. Data were obtained in a 'matched' fashion (i.e. from the same cells) under control conditions and then in the presence of Na^+-free MPS (15 min each). Paired t-tests were used for statistical comparisons ($n \geq 38$). (C) Effect of Li^+ substituted Na^+ free MPS on the percentage of oscillating PC-3M cells ($n = 3$). Paired t-test was used for statistical analysis. Data are presented as mean ± SEM. Significance: (X) $p > 0.05$.

5.3.3.2 Effect of choline-substituted Na^+-free solution

Choline-substituted Na^+-free conditions significantly decreased the amplitude of Ca^{2+} oscillations in PC-3M cells by 28 %, from 165 ± 13 to 119 ± 9 % ($p < 0.05$; $n \geq 34$; Figures 5.9A and 5.10A; Supplementary Videos 13 and 14). On the other hand, when the cells were exposed to the choline-substituted Na^+-free conditions, oscillation frequency was significantly elevated by 63 %, from 0.52 ± 0.04 oscillation/min (control) to 0.85 ± 0.09 oscillation/min (choline$^+$-substituted) ($p < 0.05$; $n \geq 34$; Figures 5.9A and 5.10B). However, there was no effect on the number of oscillating cells: 24 ± 6 % (control) and 47 ± 12 % (choline$^+$-substituted) ($p > 0.05$; $n \geq 3$; Figure 5.10C). Membrane depolarization (induced by 100 mM KCl) caused increases in the intracellular Ca^{2+} level in both oscillating and non-oscillating PC-3M cells under choline-substituted Na^+-free conditions, as in the control solution (n =3; Figures 5.9A&B).

It was concluded that extracellular Na^+ played a significant role in regulating the $[Ca^{2+}]_i$ oscillations in PC-3M cells.

5.3.4 Involvement of extracellular Ca^{2+} in spontaneous Ca^{2+} oscillations

In order to study the possible involvement of extracellular Ca^{2+} on the spontaneous Ca^{2+} oscillations, intracellular Ca^{2+} levels of PC-3M cells were recorded first under Ca^{2+}-free conditions in the presence of the Ca^{2+} chelating agent EGTA (5 μM). Then, 2.5 mM Ca^{2+} was re-admitted into the bath solution. In the absence of extracellular Ca^{2+}, there was no oscillation in PC-3M cells (n =3; Figures 5.11A&B; Supplementary Videos 15 and 16). After the application of Ca^{2+} (2.5 mM), however, the intracellular Ca^{2+} level showed a sharp rise and this was followed by a rapid fall

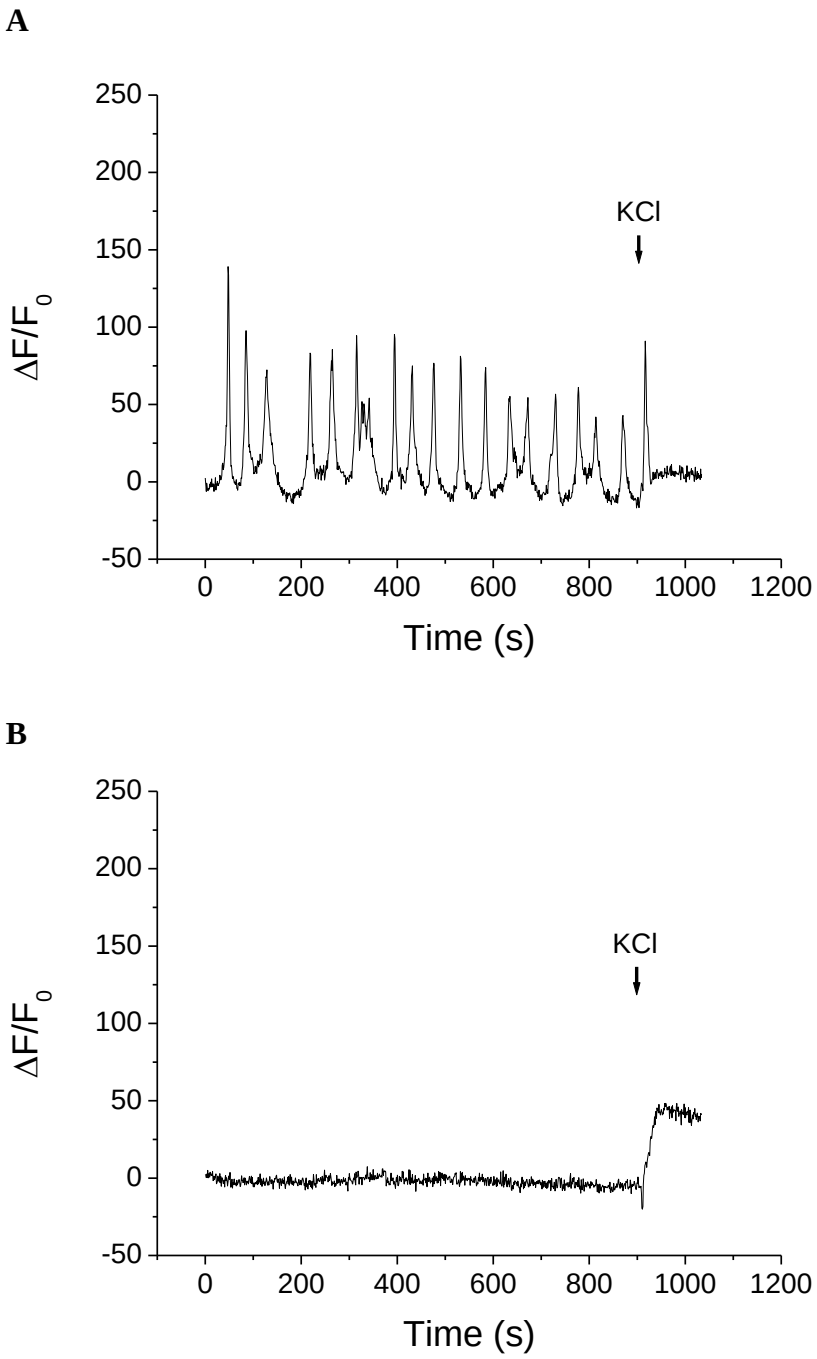


Figure 5.9 Effect of Na^+ free (choline-substituted) MPS on Ca^{2+} oscillations in PC-3M cells.

Typical recordings showing the effect choline-substituted Na^+ free MPS on Ca^{2+} oscillations in an oscillating (A) and non-oscillating (B) PC-3M cell. Changes in fluorescence intensity were expressed as $\Delta F/F_0$ (%). Treatment application times are indicated by arrows. KCl, potassium chloride (100 mM).

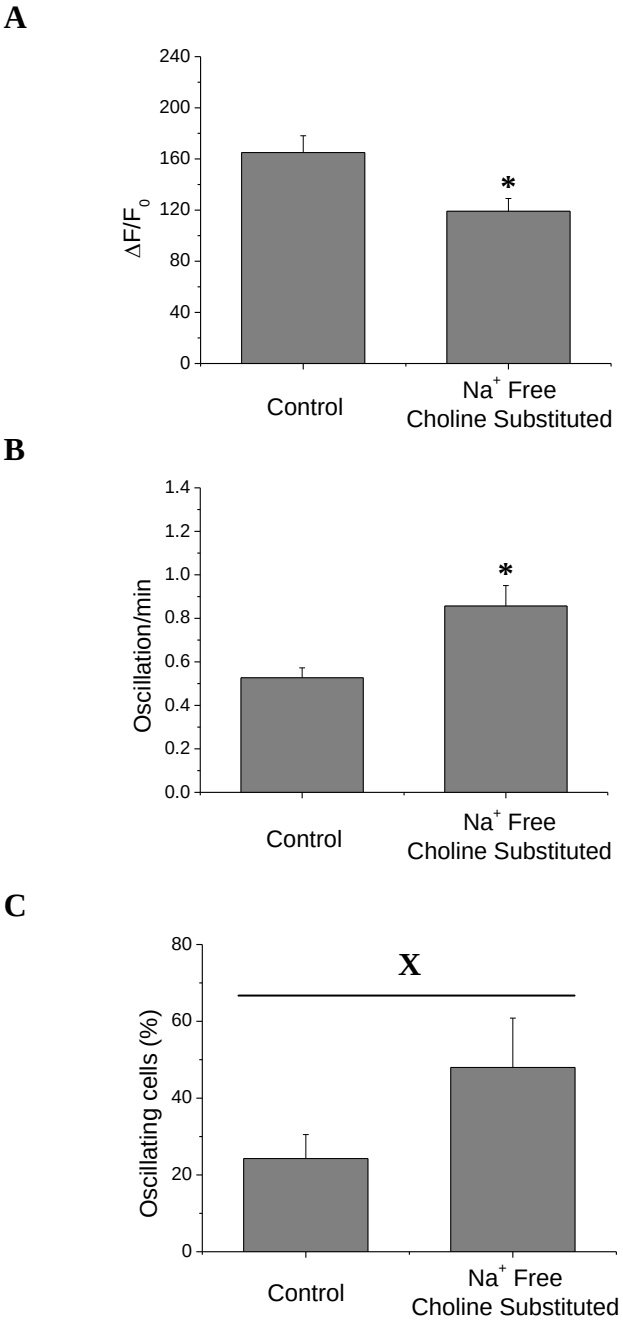


Figure 5.10 Summary of the effects of Na^+ free (choline-substituted) MPS on spontaneous Ca^{2+} oscillations in PC-3M cells.

Bar diagrams showing the effect of choline-substituted Na^+ free MPS on the amplitude (A) and the frequency (B) of Ca^{+2} oscillations in PC-3M cells. Data were obtained in a 'matched' fashion (i.e. from the same cells) under control conditions and then in the presence of Na^+-free MPS (15 min each). Paired t-tests were used for statistical comparisons ($n \geq 34$). (C) Effect of choline-substituted Na^+ free MPS on the percentage of oscillating PC-3M cells. Paired t-test was used for statistical analysis ($n = 3$). Data are presented as mean ± SEM. Significance: (*) $p < 0.05$; (X) $p > 0.05$.

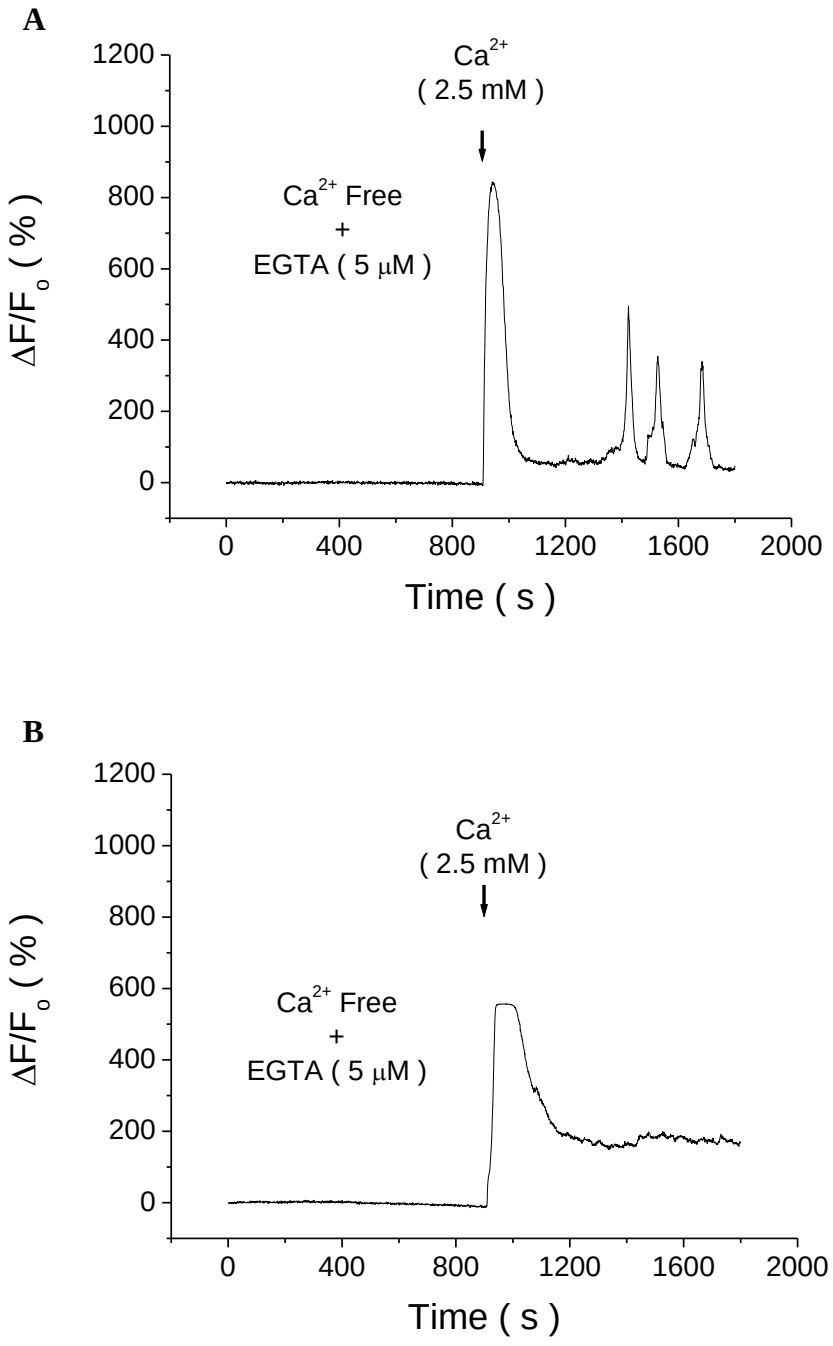


Figure 5.11 Effect of varying the extracellular [Ca^{2+}] on spontaneous Ca^{2+} oscillations in PC-3M cells.

Recordings showing that extracellular Ca^{2+} is necessary for spontaneous Ca^{2+} oscillations in PC-3M cells: (A) an oscillating cell. (B) a non-oscillating cell. Recordings were first taken in the presence of Ca^{2+}-free MPS supplied with 5 μM EGTA, and then in the presence of 2.5 mM Ca^{2+}. Changes in fluorescence intensity were expressed as $\Delta F/F_0$ (%). Treatment application times are indicated with arrows.

to a new level that was still above the original baseline (*n* =3; Figures 5.11). Subsequently, some PC-3M cells started to oscillate (*n* =3; Figures 5.11A).

It was concluded that extracellular Ca^{2+} played a significant role in generating the $[Ca^{2+}]_i$ oscillations in PC-3M cells.

5.3.5 Effects of thapsigargin and EGTA on spontaneous Ca^{2+} oscillations

Thapsigargin was used as an inhibitor of SERCA (Sagara and Inesi, 1999; Wei *et al*., 2009). First, the intracellular Ca^{2+} levels of PC-3M cells were recorded under control conditions for 10 min. Then, thapsigargin (5 μM) was added to the bathing solution and $[Ca^{2+}]_i$ was recorded for a further 40 min. Finally, effect of membrane depolarization was monitored by applying 100 mM KCl. Immediately after thapsigargin application, intracellular Ca^{2+} level elevated sharply and this was followed by a small drop and then a second elevation of intracellular Ca^{2+} level; this sequence of events was seen in both oscillating and non-oscillating PC-3M cells (*n* = 3; Figure 5.12; Supplementary Videos 17 and 18). Following the second rise, $[Ca^{2+}]_i$ steadily fell to a new level that was higher than the original baseline (*n* = 3; Figure 5.12). Interestingly, depolarization of membrane potential in the presence of thapsigargin caused decreases in intracellular Ca^{2+} level in both oscillating and non-oscillating PC-3M cells (*n* = 3 each; Figure 5.12).

Next, intracellular Ca^{2+} levels were recorded under Ca^{2+}-free conditions with EGTA (5 μM) added for 10 min followed by application of (i) thapsigargin (5 μM) and/or (ii) after 40 min, membrane depolarization using 100 mM KCl. Under the initial Ca^{2+}-free conditions, there was no $[Ca^{2+}]_i$ oscillations (*n* = 3; Figure 5.13A). After thapsigargin application, the internal Ca^{2+} level increased sharply followed by a fast decline to baseline that was maintained for at least 40 min of recording (*n* = 3;

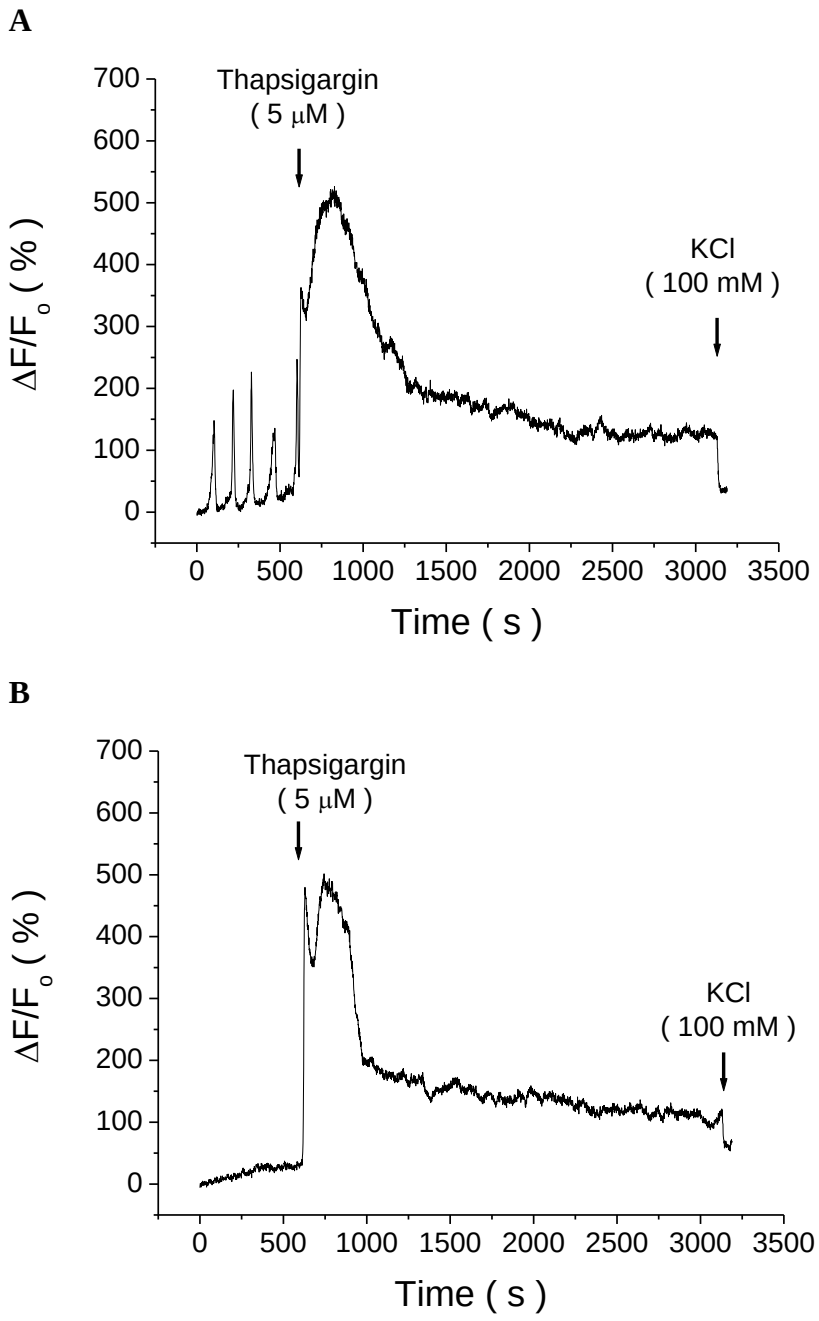


Figure 5.12 Effect of thapsigargin on Ca^{2+} oscillations in PC-3M cells.

Example recordings showing the effect of thapsigargin (depletes the Ca^{2+} store in ER) on Ca^{2+} signalling in oscillating (A) and non-oscillating (B) PC-3M cells. Changes in fluorescence intensity were expressed as $\Delta F/F_0$ (%). Treatment application times are indicated by arrows. KCl, potassium chloride (100 mM).

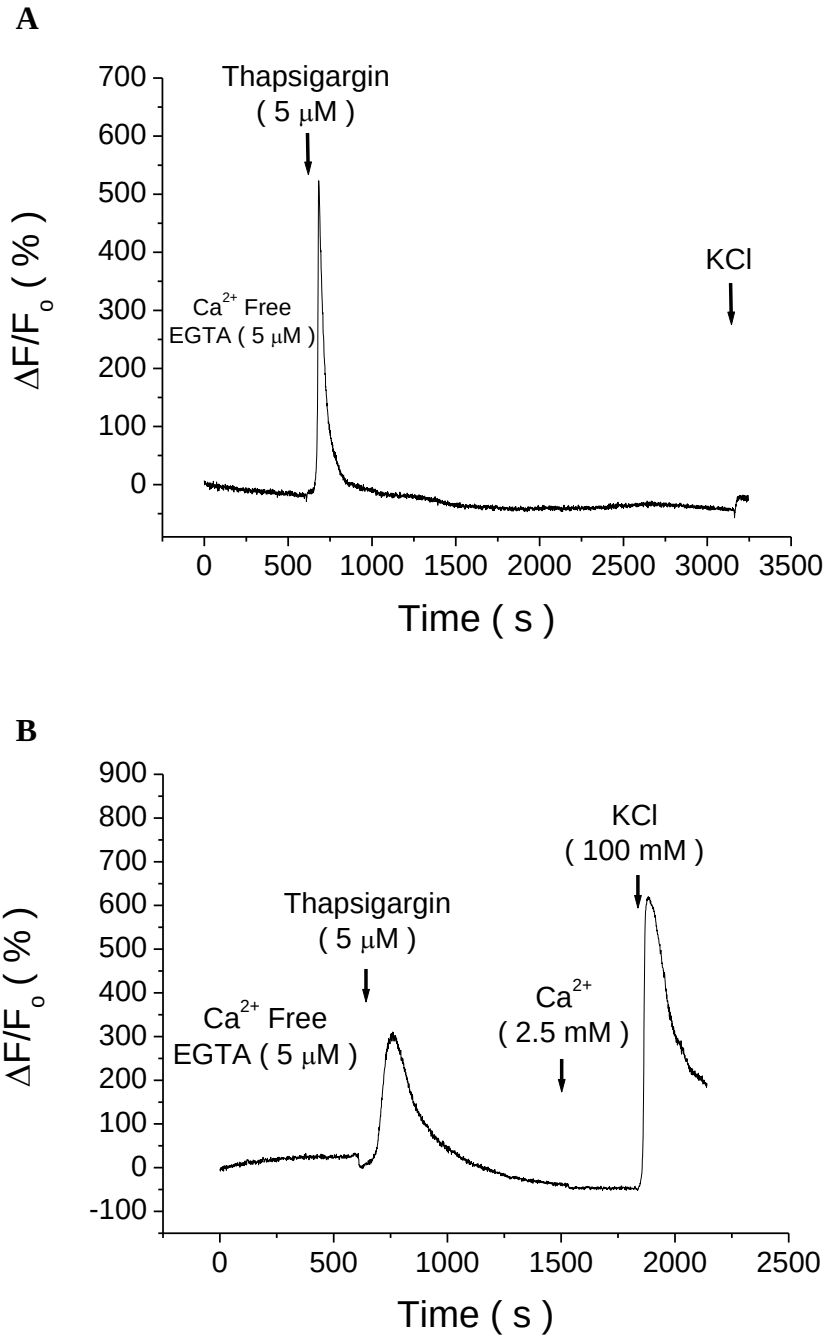


Figure 5.13 Effect of extracellular and intracellular [Ca^{2+}] on Ca^{2+} oscillations in PC-3M cells.

(A) Traces showing the effect of thapsigargin on spontaneous Ca^{2+} oscillations in PC-3M cells in the presence of Ca^{2+}-free MPS (supplied with 5μM EGTA). (B) Same as part A but 2.5 mM Ca^{2+} was added following thapsigargin application. Changes in fluorescence intensity were expressed as $\Delta F/F_0$ (%). Treatment application times are indicated with arrows. KCl, potassium chloride (100 mM).

Figure 5.13A; Supplementary Videos 19 and 20). Membrane depolarization with 100 mM KCl caused a small increase in $[Ca^{2+}]_i$ (n = 3; Figure 5.13A).

Next, Ca^{2+} oscillations were recorded under Ca^{2+}-free conditions in the presence of EGTA (5 µM) applied for 10 min followed by treatment with thapsigargin (5 µM) to deplete ER Ca^{2+} stores. Finally, 15 mins after thapsigargin application, 2.5 mM Ca^{2+} was reintroduced into the external bath and recordings were continued for a further 5 min. Finally, the membrane was depolarized with 100 mM KCl application. Again, under the initial Ca^{2+}-free conditions, there was no Ca^{2+} oscillations in PC-3M cells (n = 3; Figure 5.13B). After addition of thapsigargin, a sharp $[Ca^{2+}]_i$ transient was generated which then returned back to baseline and no further change was recorded (n = 3; Figure 5.13B). After the re-addition of Ca^{2+} into the external bath solution, there was no change in $[Ca^{2+}]_i$ (n = 3; Figure 5.13B). Finally, depolarizing the membrane potential caused an increase in internal Ca^{2+} concentration (n = 3; Figure 5.13B).

It was concluded (i) that release from internal stores contributed to the $[Ca^{2+}]_i$ oscillations in PC-3M cells and (ii) that SERCA had a significant role in this process.

5.3.6 Effects of caffeine and ryanodine on spontaneous Ca^{2+} oscillations

The possible involvement of RyR-induced release of Ca^{2+} from internal stores in the $[Ca^{2+}]_i$ oscillations was studied using caffeine and micromolar ryanodine as an activator and inhibitor of RyR, respectively (Williams and Sims, 2007; Mariot *et al*., 2000).

Intracellular Ca^{2+} levels of PC-3M cells were recorded under control conditions for 10 min. Then, 10 mM caffeine was added to the external bath solution. Finally, the membrane potential was depolarized by 100 mM KCl. In oscillating PC-

3M cells, caffeine (10 mM) suppressed Ca^{2+} oscillations without significantly changing the steady-state baseline level (*n* = 3; Figures 5.14A; Supplementary Videos 21 and 22). In non-oscillating cells, application of caffeine significantly elevated the $[Ca^{2+}]_i$ level without inducing oscillations (*n* = 3; Figure 5.14B). Depolarization caused increases in $[Ca^{2+}]_i$ in both oscillating and non-oscillating PC-3M cells (*n* = 3; Figures 5.14A&B).

Inhibition of RyR with 50 μM ryanodine significantly decreased the amplitude of the Ca^{2+} oscillations in PC-3M cells by 59 %, from 204 ± 23 % to 84 ± 17 % ($p < 0.001$; *n* = 26; Figures 5.15A and 5.16A; Supplementary Videos 23 and 24). In addition, oscillation frequency was significantly reduced by 72 %, from 0.71 ± 0.08 to 0.20 ± 0.05 oscillation/min ($p < 0.001$; *n* = 26; Figures 5.15A and 5.16B). There was no significant change in number of oscillating PC-3M cells by 50 μM ryanodine treatment ($p > 0.05$; *n* = 3; Figure 5.16C). Ryanodine (50 μM) had no effect on $[Ca^{2+}]_i$ in non-oscillating PC-3M cells (*n* = 3; Figure 5.15B). Depolarization of membrane potential (with 100 mM KCl) in the presence of ryanodine (50 μM) increased internal Ca^{2+} levels in both oscillating and non-oscillating cells (*n* = 3; Figure 5.15A&B).

It was concluded that RyR had a significant role in regulating the $[Ca^{2+}]_i$ oscillations in PC-3M cells.

5.4 Discussion

The main findings of this study are as follows: (1) A subpopulation (~25 %) of human strongly metastatic PC-3M cells generated spontaneous, 'global' Ca^{2+} oscillations; (2) no such activity was found in human weakly metastatic LNCaP cells

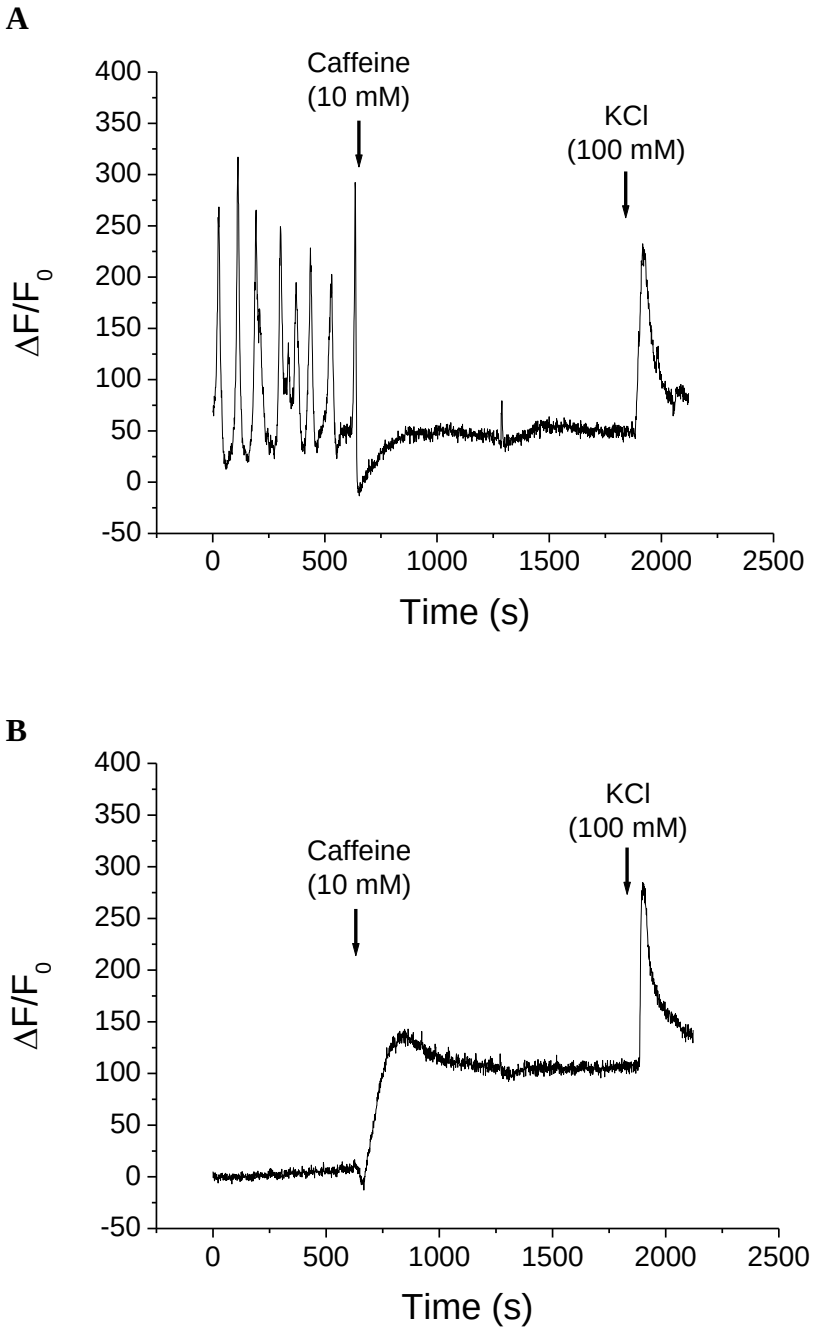


Figure 5.14 Effect of caffeine on Ca^{2+} oscillations in PC-3M cells.

Representative traces showing the effect of 10 mM caffeine on Ca^{2+} oscillations in PC-3M cells: (A) an oscillating cell; (B) a non oscillating cell. Changes in fluorescence intensity were expressed as $\Delta F/F_0$ (%). Treatment application times are indicated with arrow. KCl, potassium chloride (100 mM).

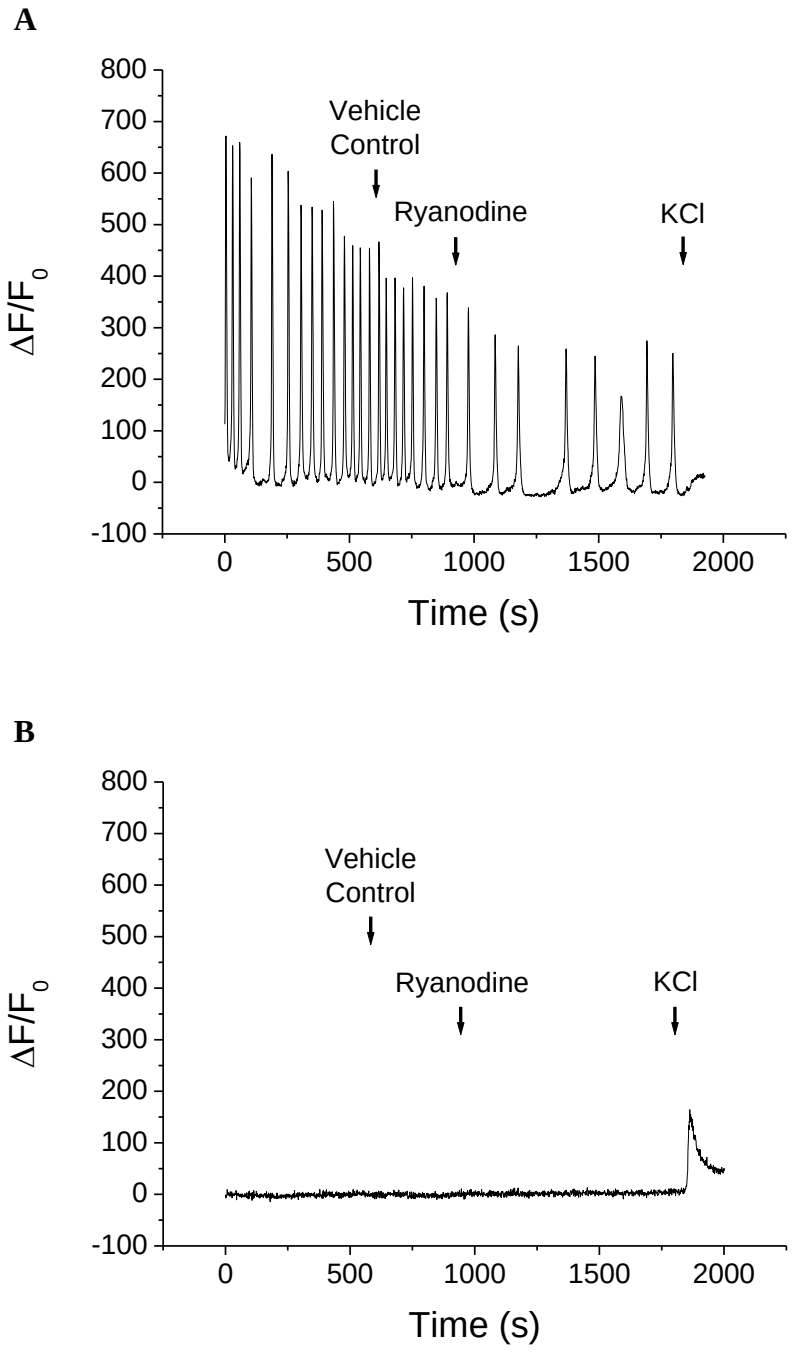
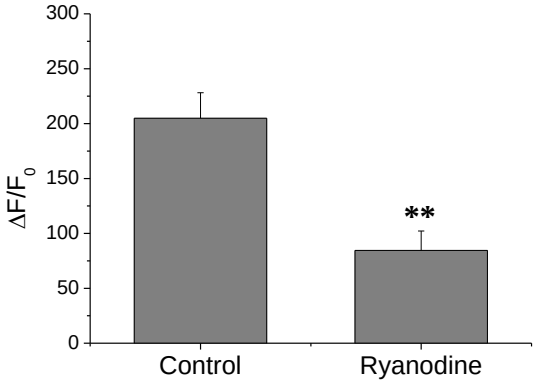
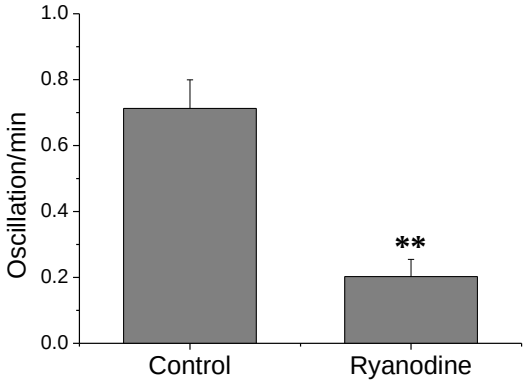


Figure 5.15 Effect of ryanodine on Ca^{2+} oscillations in PC-3M cells.
Typical recordings showing the effect of ryanodine (50 µM) on Ca^{2+} oscillations in PC-3M cells: (A) an oscillating cell; (B) a non-oscillating cell. Changes in fluorescence intensity were expressed as $\Delta F/F_0$ (%). Treatment application times are indicated by arrows. Vehicle control, buffer solution (MPS) without any treatment; KCl, potassium chloride (100 mM).

A



B



C

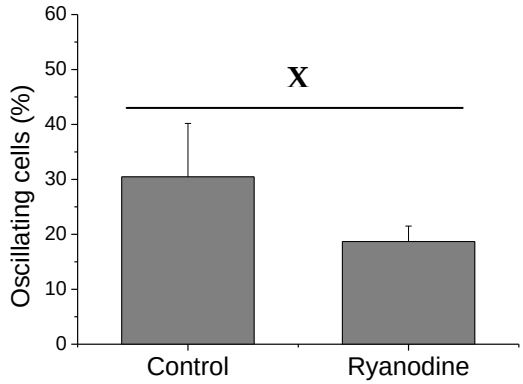


Figure 5.16 Summary of the effects of ryanodine on spontaneous Ca^{2+} oscillations in PC-3M cells.

Bar diagrams showing the effects of 50 µM ryanodine on the amplitude (A) and the frequency (B) of Ca^{2+} oscillations in PC-3M cells. Data were obtained in a 'matched' fashion (i.e. from the same cells) under control conditions and then in the presence of ryanodine (15 min each). Paired t-tests were used for statistical analysis (n = 26). (C) Effect of ryanodine (50 µM) on the percentage of oscillating PC-3M cells. Paired t-test was used for statistical analysis (n = 3). Data are presented as mean ± SEM. Significance: (**) $p < 0.001$; (X) $p > 0.05$.

or the strongly metastatic rat PCa cell line, Mat-LyLu. (3) The averages of the basic characteristics of the $[Ca^{2+}]_i$ oscillations in PC-3M cells were as follows: 172 % (amplitude) and 0.5 oscillation/min (frequency). (4) TTX and ranolazine reduced both frequency and amplitude of Ca^{2+} oscillations but did not affect the percentage of oscillating cells. (5) Substituting extracellular Na^+ with equimolar Li^+ had no effect on frequency and amplitude of Ca^{2+} oscillations or the number of oscillating cells. (6) Substituting extracellular Na^+ with equimolar $choline^+$ reduced the amplitude but increased the frequency of Ca^{2+} oscillations (7) Under Ca^{2+} free conditions, no oscillations were detected in PC-3M cells but after addition of Ca^{2+} some cells started to oscillate (but not after also thapsigargin pre-treatment). (8) Efflux of Ca^{2+} from internal stores by thapsigargin treatment induced influx of external Ca^{2+}. (9) Stimulating RyR caused an increase in intracellular Ca^{2+}, whilst inhibiting RyR decreased both amplitude and frequency of Ca^{2+} oscillations. These results are summarised qualitatively in Table 5.1.

5.4.1 Calcium signalling in PCa cells

Intracellular Ca^{2+} signalling regulates many cellular processes, particularly, motility, invasion, transcription, cell cycle/proliferation and apoptosis, which are also relate directly to the metastatic potential of cancer cells, as in PCa, breast cancer; head and neck squamous cell carcinoma, pulmonary adenocarcinoma, rhabdomyoblasts, fibrosarcoma and retinoblastoma (Wang *et al.,* 2010; Liao *et al.*, 2006; Huang *et al.,* 2004; Zhong *et al.,* 2010; Wu *et al.,* 1997; Amuthan *et al.,* 2002; Amuthan *et al.,* 2001; Cook and Lockyer, 2006; Wertz and Dixit, 2000; Lehen'kyi *et al.,* 2007). Here, we studied Ca^{2+} signalling in several PCa cell lines, PC-3M, LNCaP (both human) and Mat-LyLu (rat), in a comparative approach.

Table 5.1 Synopsis of results

TREATMENT	AMPLITUDE	FREQUENCY	RESPONSE TO KCl
TTX	-	-	0
Ranolazine	-	-	0
Na^+-free: Li^+	0	0	0
Na^+-free: choline$^+$	-	+	0
Ca^{2+}-free	-	ND	ND
Thapsigargin	(locked)	-	(baseline reduction)
Caffeine	-	-	0
Ryanodine	-	-	0

- : DECREASE
+ : INCREASE
0 : NO CHANGE
ND: NOT DETERMINED

The results depended on the cells' metastatic potential as well as species of origin. Thus, only human strongly metastatic PC-3M cells generated spontaneous Ca^{2+} oscillations. It is not clear why the analogous rat PCa cell line did not show Ca^{2+} oscillations, although Mat-LyLu cells share many of the ionic characteristics of PC-3 cells, including the subtypes of VGSC (Nav1.7) and voltage-gated K^+ channel (Kv1.3) expression (Diss *et al*., 2001; Fraser *et al*., 2003). Nevertheless, the present results on Mat-LyLu cells complement the previous findings of Ding *et al.* (2006) who also could not reveal any spontaneous activity of $[Ca^{2+}]_i$ and showed additionally (i) that Mat-LyLu cell membranes were insensitive to changes in extracellular Ca^{2+} levels and (ii) that membrane depolarization had no effect on $[Ca^{2+}]_i$. Taken together, these results would imply that the Dunning cells may not be a valid model of human PCa, at least as far as intracellular Ca^{2+} signalling and regulation are concerned.

Interestingly, only ~25 % of PC-3M cells showed spontaneous $[Ca^{2+}]_i$ oscillations. This is in line with the well known heterogeneity of cancer cell lines. In the case of functional VGSC expression also, only subpopulations of prostate cancer cells were positive, 10 % and 50 % of human and rat strongly metastatic cells, respectively (Laniado *et al.,* 1997; Grimes *et al.,* 1995). It could be suggested that 25 % expression of VGSC cannot make significant changes in MCBs. However, it is well established that blocking VGSC activity does cause significant suppression of MCBs of these cells. For instance, Laniado *et al.* (1997) showed that 10 % of the 'parent' strongly metastatic human prostate cancer PC-3 cells expressed functional VGSCs. On the other hand, blocking VGSC in these cells using nanomolar concentration of the specific VGSC blocker, TTX, caused 31 % reduction in invasiveness. Although, our data and current literature taken together would suggest

that Ca^{2+} oscillations could be important in modulating VGSC-dependent MCBs (e.g. directional motility and invasion), further experiments are required to establish the precise role of Ca^{2+} oscillations in MCBs.

The present study is the first characterization of $[Ca^{2+}]_i$ oscillations in human PCa cells. As discussed earlier, Ca^{2+} signalling is important generally for functioning of cells. On the other hand, prolonged increase in $[Ca^{2+}]_i$ can cause cell death (Roderick and Cook, 2008; Wertz and Dixit, 2000). Accordingly, Berridge *et al.* (1998) proposed that cells avoids cell death by delivering Ca^{2+} signals that has to be relayed over long time periods as repetitive brief 'transients', i.e. as "Ca^{2+} oscillations". It was suggested that cellular information can be encoded in the frequency and/or amplitude of the Ca^{2+} oscillations (Berridge *et al.*, 2003; Berridge *et al.*, 1998).

No change in intracellular Ca^{2+} levels under control condition was recorded in weakly metastatic human PCa cell line, LNCaP. Previously, a store-operated Ca^{2+} entry mechanism was described in LNCaP cells (Lallet-Daher *et al.*, 2009; Lehen'kyi *et al.*, 2007; Gackière *et al.*, 2006; Abeele *et al.*, 2004; Abeele *et al.*, 2003a; Abeele *et al.*, 2003b; Gutierrez *et al.*, 1999). However, similar to our results, no spontaneous oscillation was reported in LNCaP cells. On the other hand, here, we demonstrated that membrane depolarization can regulate the intracellular Ca^{2+} level in LNCaP cells. In contrast, Lallet-Daher *et al.* (2009) reported that hyperpolarisation via activation of Ca^{2+}-activated K^+ channels, would cause influx of Ca^{2+} in PCa cell lines. In addition, Gutierrez *et al.* (1999) showed that fluctuations in membrane potential between -80 and +80 mV did not affect the Ca^{2+} permeability of LNCaP cells. Further work is necessary to decipher these apparent inconsistencies.

5.4.2 A model of intracellular Ca^{2+} oscillations in PC-3M cells

From the present findings, taken together with published data, a working model of spontaneous Ca^{2+} oscillations in PC-3M cells can be proposed, as illustrated in Figure 5.17. In this model, the oscillations in $[Ca^{2+}]_i$ are generated and modulated, and these occur in compartmentalised fashion (i.e. in a cellular micro-environment), as follows:

1. PC-3M cell membranes are tonically depolarized at rest and, consequently, VGSCs spend a significant time in open state. This is consistent with the highly reproducible effects of TTX (an open-channel blocker) on strongly metastatic, including PC-3/M cells, reported over many years (Grimes *et al*., 1995; Nakajima *et al*., 2009; Onganer *et al*., 2007; Mycielska *et al*., 2005; Scorey *et al*., 2006; Laniado *et al*., 1997).

2. The VGSC activity leads to Na^+ influx, possibly mainly via I_{NaP} and further depolarize the membrane potential (V_m). Indeed, Cameron *et al*. (1980) have shown that strongly metastatic cells have higher levels of Na^+, and malignant *versus* benign tumours are also higher in their Na^+ content (Ouwerkerk *et al*., 2007).

3. The influx of Na^+ (and the depolarization of V_m) can raise $[Ca^{2+}]_i$ by slowing or reversing NCX activity (Poburko, *et al.,* 2007; Eder *et al.,* 2005; Rosker *et al.,* 2004; Arnon *et al.,* 2000; Blaustein and Lederer, 1999; Matsuoka and Hilgemann, 1992; Miura and Kimura, 1989). The latter is electrogenic with a stoichiometry of $3Na^+$: 1 Ca^{2+} (Blaustein and Lederer 1999).

4. The increase in $[Ca^{2+}]_i$ can activate RyR receptors and result in further rise in $[Ca^{2+}]_i$ (Berridge *et al.,* 2003).

Steps 1 – 4 can explain the rising phase of given Ca^{2+} 'spike'. In order to return $[Ca^{2+}]_i$ back to baseline and repeat the cycle, a Ca^{2+}-sensitive negative

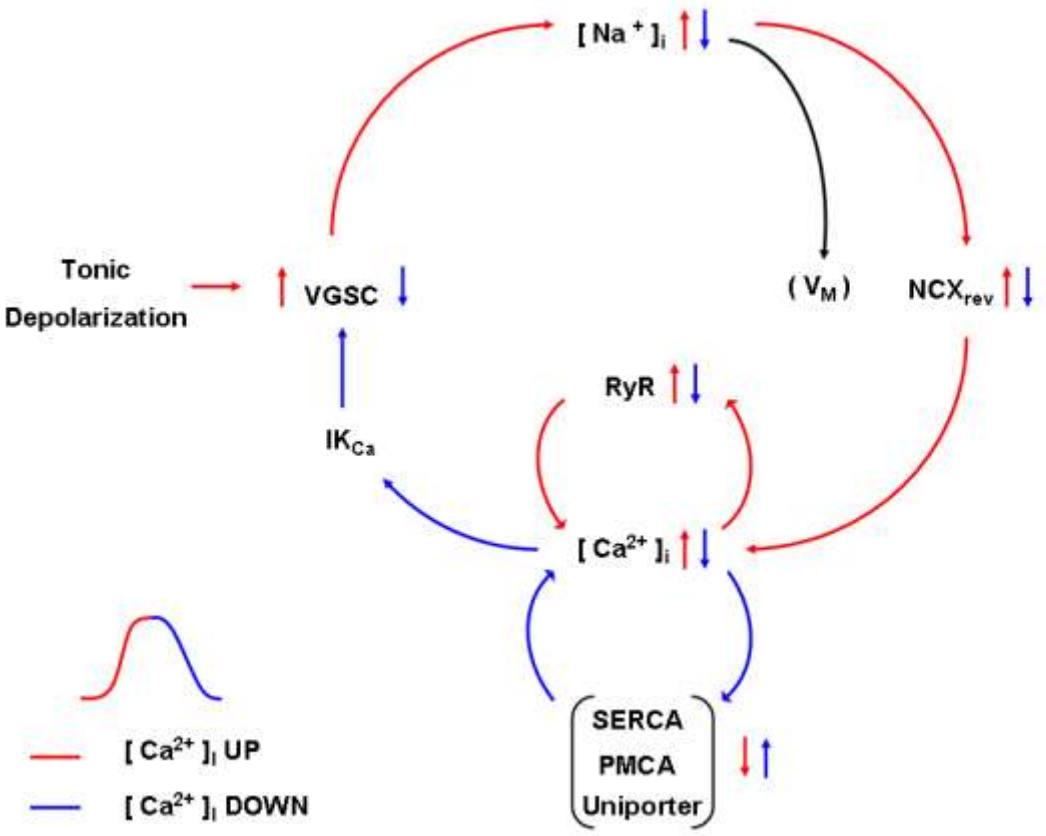


Figure 5.17 A basic model explaining possible mechanisms underlying spontaneous Ca^{2+} oscillations in PC3M cells.
Influx of Na^+ through VGSC activates NCX_{rev}. Extracellular Ca^{2+} is exchanged with intracellular Na^+ by NCX_{rev} therefore $[Ca^{2+}]_i$ increases. Increased $[Ca^{2+}]_i$ activates RyR and more Ca^{2+} is released in to the cell and produces growth phase of Ca^{2+} transient. Plasma-membrane is hyperpolarized by IK_{Ca} channel which is activated by increased $[Ca^{2+}]_i$. Membrane hyperpolarization inactivates VGSC. At the same time, cytoplasmic Ca^{2+} was removed by PMCA, SERCA and Uniporter to extracellular solution, into ER and into mitochondria, respectively, until $[Ca^{2+}]_i$ reaches equilibrium. $[Na^+]_i$, intracellular Na^+ concentration; $[Ca^{2+}]_i$ intracellular Ca^{2+} concentration, VGSC, voltage-gated Na^+ channel; NCX_{rev}, Na^+-Ca^{2+} exchanger working in reverse mode; RyR, ryanodine receptor; SERCA, sarcoplasmic-endoplasmic reticulum Ca^{2+} ATPase; PMCA, plasma-membrane Ca^{2+} ATPase; Uniporter, mitochondrial uniporter; IK_{Ca}, Ca^{2+} activated potassium channels; ↑ increase activity; ↓ decrease activity; V_M, membrane potential . Red line shows actions in activation/growth phase of a Ca^{2+} transient (inset) and blue line shows actions in decay phase of a Ca^{2+} transient.

'feedback' mechanism is required. In oscillating networks, such feedback is frequently provided by Ca^{2+}-activated K^+ (g_{KCa}) channels (Fridlyand *et al*., 2009). $K_{Ca}3.1$ and $K_{Ca}1.1$ subtypes of g_{KCa} (I_{KCa}) channels are also expressed in PC-3/M cells (Yan and Aldrich, 2010; Bloch *et al* 2007; Lallet-Daher *et al*., 2009; Parihar *et al*., 2003; Laniado *et al*., 2001).

5. Increased intracellular Ca^{2+} up to a level would activate g_{KCa} channels which would then hyperpolarize the plasma membrane V_m and thus reduce VGSC activity (Lallet-Daher *et al*., 2009; Félétou, 2009).

6. The increased $[Ca^{2+}]_i$ (locally up to mM level) would result in inhibition of RyR (Berridge *et al*., 2003). At the same time, further decrease of $[Ca^{2+}]_i$ would result from (i) extrusion of Ca^{2+} from the cell by PMCA, and (ii) uptake into ER and mitochondria by SERCA and uniporter, respectively.

7. As $[Ca^{2+}]_i$ recovers back towards baseline, g_{KCa} channels are inactivated, V_m starts to depolarize and the condition in (1) is re-established, leading to repeat of the cycle and resulting in the $[Ca^{2+}]_i$ oscillations.

In this model, amplitude would be increased by activities of VGSC and RyR, and decreased by all Ca^{2+} sequestration mechanisms (PMCA, SERCA etc.). On the other hand, frequency would be controlled in a complex manner by all mechanisms. In addition, we cannot rule out the possibility that other Ca^{2+} entry and / or efflux mechanisms are involved in the model of Figure 5.17. Such additional mechanisms could include TRPC1, TRPC3, TRPC4, TRPV2, TRPV6, and TRPM8.

5.4.3 Role of the various subcellular mechanisms in Ca^{2+} signalling / oscillations

In the following, with reference to Table 5.1, we discuss / re-evaluate the role played by the various subcellular mechanisms investigated in the Ca^{2+} oscillations in PC-3M cells.

5.4.3.1 VGSC and cation (Na^+) influx

Blocking VGSC activity with TTX or ranolazine produced similar effects, indicating that it was I_{NaP} that was mainly responsible for the involvement of VGSC activity in the Ca^{2+} oscillations. Thus, both frequency and amplitude of Ca^{2+} oscillations were reduced. On the other hand, when extracellular Na^+ was substituted with equimolar Li^+, there was no change in the amplitude or frequency of the oscillations but rise and decay time constants were reduced. These effects can be due to multiple reasons. First, it is well known VGSCs are permeable to Li^+ (Blaustein and Santiago, 1977; Hille, 1972). Therefore, we can assume that Li^+ influx occurred and V_m depolarized as normal. Second, in the absence of extracellular Na^+, NCX will initially work in reverse (driven by the Ca^{2+} and Na^+ gradient) and this mode will be facilitated by the V_m depolarization. Subsequently, however, intracellular Li^+ would not be able substitute for Na^+ in NCX which will be inhibited (Blaustein and Lederer, 1999). Nevertheless, the initial rise in $[Ca^{2+}]_i$ with RyR can enable $[Ca^{2+}]_i$ to reach normal amplitude and oscillations may continue with regular frequency.

Interestingly, when extracellular Na^+ was replaced by the large organic $choline^+$, there was a decrease in amplitude but an increase in frequency of oscillations. These effects can be explained by the facts (i) that NCX again would tend to work in reverse (Palty *et al.*, 2004; Blaustein and Lederer, 1999) but (ii) that

since there will have been no V_m depolarization (due to the VGSC impermeability of choline$^+$), and hence any rise in $[Ca^{2+}]_i$ would be limited. As regards the frequency, return of $[Ca^{2+}]_i$ back to baseline might be quicker without the V_m depolarization, so the cycle would be repeated more frequently.

5.4.3.2 Extracellular Ca^{2+}

In the absence of extracellular Ca^{2+}, PC-3M cells had no spontaneous Ca^{2+} oscillations. After re-administering Ca^{2+} into the external bath solution, however, an increase in internal Ca^{2+} was observed which, after some delay, returned to a new baseline (higher than the original). Following the return to new baseline Ca^{2+} levels, some cells did start to oscillate. These results are consistent with the proposed role of NCX. Previously, Lehen'kyi *et al.* (2007) demonstrated in LNCaP cells that increased extracellular Ca^{2+} would induce an increase in intracellular Ca^{2+}. However, when the cationic channel TRPV6 was knocked down by siRNA, extracellular Ca^{2+} did not affect the intracellular Ca^{2+} levels (Lehen'kyi *et al.*, 2007). Therefore it was proposed that TRPV6 was 'constitutively open' and mediated tonic Ca^{2+} influx into LNCaP cells (Lehen'kyi *et al.*, 2007). A similar mechanism could also be involved in the role of extracellular Ca^{2+} in PC-3M cell $[Ca^{2+}]_i$ oscillations.

5.4.3.3 Thapsigargin

Possible role of sarcoplasmic-endoplasmic reticulum Ca^{2+} pump (SERCA) on the spontaneous Ca^{2+} oscillations was investigated using thapsigargin as a specific inhibitor (Sagara and Inesi, 1991). Thapsigargin caused a significant rise in basal intracellular Ca^{2+} level in PC-3M cells indicating that SERCA was active tonically in PC-3M cells. This initial increase was immediately followed by a second Ca^{2+} peak

and then $[Ca^{2+}]_i$ decreased and levelled off higher than the initial resting condition. On the other hand, when PC-3M cells were maintained in Ca^{2+}-free conditions, which would result in the emptying of Ca^{2+} from ER stores, thapsigargin did not produce the second peak and $[Ca^{2+}]_i$ returned to baseline. This suggested strongly that the secondary peak and elevation of $[Ca^{2+}]_i$ were mediated by influx of extracellular Ca^{2+}. Previously, a store-operated Ca^{2+} entry mechanism was described in LNCaP, DU145 and PC-3 PCa cells where ER depletion indeed caused influx of Ca^{2+} from extracellular solution (Lallet-Daher *et al.,* 2009; Lehen'kyi *et al.,* 2007; Gackière *et al.,* 2006; Abeele *et al.,* 2004; Abeele *et al.,* 2003a; Abeele *et al.,* 2003b; Gutierrez *et al.,* 1999). Furthermore, Lallet-Daher *et al.* (2009) proposed that activation of an intermediate-conductance Ca^{2+}- -activated K^+ channel ($IK_{Ca,}$ KCa3.1) would hyperpolarize plasma membrane and this change in V_m mediated store-operated Ca^{2+} entry via TRPV6 cation channels in PCa cells. Similarly, depolarizing plasma membrane of PC-3M cells after efflux of Ca^{2+} from ER caused decrease in internal Ca^{2+} level. Therefore, similar to LNCaP, DU145 and PC-3 cells, PC-3M cells are also likely to possess a store-operated Ca^{2+} entry mechanism.

Following inhibition of SERCA, no spontaneous Ca^{2+} oscillations were observed in PC-3M cells. This was probably due to 'swamping' of the Ca^{2+} homeostasis resulting from Ca^{2+} release and influx. Consistent with this, the secondary elevated of $[Ca^{2+}]_i$ was close to the peak reached by the oscillations.

5.4.3.4 Ryanodine receptor

Ca^{2+} signalling works mostly by producing brief changes in intracellular Ca^{2+} levels. These changes in intracellular Ca^{2+} can be mediated by influx of Ca^{2+} through plasma membrane and/or release of Ca^{2+} from internal stores (Roderick and Cook,

2008; Clapham, 2007; Berridge *et al.,* 2003; Berridge *et al.,* 1998). Two families of Ca^{2+} release channels were identified in the primary Ca^{2+} storing organelle, ER: RyR and IP_3R. Rayanodine receptor is generally found in excitable cells (Chen *et al*., 2009). However, expression of RyR was shown in breast and prostate cancer cells (Abdul *et al.,* 2008; Mariot *et al.,* 2000). This agrees with the notion that metastatic cells possess some of the characteristics typical of excitable cells such as neurones (e.g. Onganer *et al*., 2005). Furthermore, strong correlation between RyR expression and breast cancer grade was reported (Abdul *et al.,* 2008). It was shown that LNCaP cells express functional RyR and the caffeine can mediate Ca^{2+} efflux from intracellular Ca^{2+} stores via RyR (Mariot *et al.,* 2000). Accordingly, in the present study, caffeine was used to confirm the presence of functional RyRs in PC-3M cells. Indeed, caffeine (at 10 mM concentrations that would stimulate RyRs) increased $[Ca^{2+}]_i$ and suppressed Ca^{2+} oscillations. Conversely, inhibiting RyR with a high concentration of ryanodine reduced both amplitude and frequency of the spontaneous Ca^{2+} oscillations, without affecting the baseline level. These results suggested (i) that functional RyRs were present in PC-3M cells and (ii) that RyR activity plays a significant role in generation of the spontaneous Ca^{2+} oscillations.

5.4.4 Possible pathophysiolgical consequence of Ca^{2+} oscillations in PCa (PC-3M) cells and future perspectives

As already noted in this chapter, Ca^{2+} signalling is important for both the physiology and pathophysiology of cells. In particular, since prolonged increases in $[Ca^{2+}]_i$ would be cytotoxic, Berridge *et al.* (1998) suggested that intracellular Ca^{2+} signalling would be more expedient as repetitive brief 'transients' (i.e. as "Ca^{2+} oscillations") that can be allowed to occur over long time periods. Importantly, Berridge *et al.*

(1998, 2003) also suggested that cellular information can be encoded in the frequency and/or amplitude of Ca^{2+} oscillations. Such oscillations can subserve a wide range of cellular functions from fundamental gene expression to proliferation and motility/migration (e.g. Dolmetsch *et al*., 1998; Ding *et al*., 2010; Komura and Rakic, 1996). Most such processes are common also to cancer cells and most probably relate to the metastasis. Accordingly, $[Ca^{2+}]_i$ oscillated in the strongly metastatic PC-3M but not the weakly/non-metastatic LNCaP cells (Figures 5.1A *vs* 5.2A). It was proposed that information of Ca^{2+} signal can be encoded in the frequency and/or amplitude of oscillations (Berridge *et al.*, 2003; Berridge *et al.*, 1998). For example, De Koninck and Schulman (1998), showed that amplitude and frequency of $[Ca^{2+}]_i$ spikes can modulate CaM kinase II activity. Further work is required to relate the amplitude / frequency characteristics of the $[Ca^{2+}]_i$ oscillations to the different components of the metastatic cascade.

Here, we presented a simple cycling model of $[Ca^{2+}]_i$ oscillations in PC-3M cells. Whilst the model is well supported by the pharmacological evidence presented, it should be tested further and possibly expanded at least along the lines of the following:

1. At present, the $[Ca^{2+}]_i$ signal is treated as 'global'. Higher temporal and spatial resolution would be useful (i) to determine if the proposed spatial compartmentalization of the signalling components indeed exists and (ii) to reveal if $[Ca^{2+}]_i$ travels intracellular as 'waves' (Subramanian *et al*., 2001; Wei *et al*., 2009).
2. The possible role of the membrane potential (V_m) should be elucidated experimentally using voltage-sensitive dyes, such Di-8-ANEPPS (Valverde et al., 2010). Similarly, whether the proposed influx of Na^+

indeed occurs can be tested using Na^+-sensitive dyes, CoroNa Green or SBFI (Meier et al., 2006).

3. The proposed role of NCX (in forward and reverse modes) can be tested using mode-selective pharmacological blockers (Hobai and O'Rourke, 2004; Laskowski and Medler, 2009).
4. The possible role of other cation channels, such as TRPV6 (Fixemer *et al*., 2003), should also be investigated. However, exposing the cells to 100 mM KCl consistently elevated the $[Ca^{2+}]_i$ level. This is not consistent with the role of such a passive mechanism. In turn, this raises the possibility of V_m having effects upon other electrogenic mechanisms. These would be additional to NCX since the KCl treatment was still potently effective under Na^+-free conditions when NCX activity would be expected to be impaired.
5. Finally, it is possible that the proposed Na^+ influx and/or the Ca^{2+} itself can activate kinases and these may modulate the $[Ca^{2+}]_i$ oscillations by phosphorylating the regulatory components. In particular, Na^+ can stimulate PKA (Brackenbury and Djamgoz, 2006) and Ca^{2+} is a substrate for CaM kinase (Colomer and Means, 2007).

Chapter 6

GENERAL DISCUSSION

According to Office for National Statistics (2010), 1 in 4 deaths in the UK were caused by cancer in 2008 and prostate cancer (PCa) is second commonest cause of cancer death in man. Ionic mechanisms, such as voltage-gated sodium channel (VGSC) activity and Ca^{2+} signalling, were shown to play important role in metastatic behaviour of PCa, as reviewed by Onkal and Djamgoz (2009) and Prevarskaya *et al.* (2010). Therefore, it was proposed that targeting these mechanisms could be a novel and effective strategy to tackle cancer, including PCa (Onkal and Djamgoz, 2009; Prevarskaya *et al.,* 2010). On the other hand, microenvironmental effects such as O_2 and Ca^{2+} levels could modulate metastatic cell behaviours (MCBs) in PCa (Alqawi *et al.,* 2007; Watson *et al.,* 2008; Ackerstaff *et al.,* 2007; Liao *et al.,* 2006). Importantly, hypoxia has been detected in cancerous tissue of prostate (Movsas *et al.,* 2000). Therefore, the main aims of this thesis were (i) to study effect of 'long-term' (24 h or longer) hypoxia (2 % O_2) on VGSC expression and possible consequent effect on MCBs in a comparative approach to strongly and weakly metastatic PCa cell lines, Mat-LyLu and AT-2, respectively; (ii) to investigate effects of clinically approved pharmacological VGSC blockers on VGSC expression and Matrigel invasion in Mat-LyLu cells to evaluate their anti-cancer potential; and (iii) to characterise transient changes in intracellular Ca^{2+} level ("Ca^{2+} oscillations") and possible involvement of VGSC in this signalling in strongly metastatic human and rat PCa cells (PC-3M and Mat-LyLu, respectively) and weakly metastatic human PCa LNCaP cells.

6.1 Summary of key findings

The main findings of the studies described in this Thesis are as follows:

1. Hypoxia (2 % O_2) longer than 24 h significantly decreased the number of Mat-LyLu cells while not effecting AT-2 cell number. On the other hand, Nav1.7 and VGSCβ1 subunits (predominant VGSC α- and β- subunits expressed in PCa) mRNA levels increased significantly by long-term hypoxia (2 % O_2, 24 h). However, a small but significant decrease in VGSC α-subunit level was detected in the hypoxic Mat-LyLu cells; VGSCβ1 protein level was not affected. Similar hypoxia had no effect on lateral motility and Matrigel invasion of Mat-LyLu cells but transverse migration was increased by in a VGSC dependent manner.
2. At micromolar concentration, clinically used pharmacological VGSC blockers (ranolazine, riluzole, procaine and lidocaine) (i) reduced Nav1.7 mRNA expression, (ii) decreased VGSCα protein level and (iii) decreased Matrigel invasion of Mat-LyLu cells under both normoxia (21 % O_2, 24 h) and hypoxia (2 % O_2, 24 h).
3. Spontaneous transient changes in intracellular calcium activity ($[Ca^{2+}]_i$), - "Ca^{2+} oscillations" - occurred in ~25 % of PC-3M cells; no such activity was detectable in LNCaP and Mat-LyLu cells. Ranolazine and TTX modulated both oscillation frequency and amplitude in PC-3M cells. Both extracellular and endoplasmic reticulum (ER) Ca^{2+} played a significant role in the oscillation process. Ryanodine receptor (RyR) was also involved in the Ca^{2+} oscillations.

6.2 Hypoxic regulation of VGSC expression and MCB in PCa

Tumour microenvironment plays important role in MCB of PCa cells and it was proposed that cancerous cells would not be able to acquire metastatic phenotype by only genetic alteration without the impact of microenvironmental factors (e.g. Chung *et al.,* 2005). One of the distinct characteristic of the microenvironment in PCa is decreased tissue O_2 level, ~1.5 % vs. ~4 %, in cancerous and normal tissue, respectively (Movsas *et al.,* 2000). In addition, androgen-deprivation therapy was proposed to cause tissue hypoxia (Rudolfsson and Bergh, 2009). Accordingly, changes in MCB were detected in hypoxic PCa (Alqawi *et al.,* 2007; Watson *et al.,* 2008; Ackerstaff *et al.,* 2007). VGSC expression and function were correlated earlier with metastatic potential of PCa (e.g. Grimes *et al.,* 1995; Laniado *et al.,* 1997; Diss *et al.,* 2005). In a different area of research, it was shown that hypoxia in neurons and cardiac cells increased the persistent sodium current of VGSC, and, therefore, could increase intracellular Na^+ concentration and thus lead to intracellular Ca^{2+} overload (Hammarström and Gage, 1998; Ju *et al.,* 1996; Wang *et al.,* 2007). Increased intracellular Na^+ was also shown to increase Nav1.7 mRNA and plasma membrane (PM) trafficking of VGSC α-subunit while having no effect on total protein level in Mat-LyLu cells; these effects were largely mediated by the adenylate cyclise (AC) / protein kinase A (PKA) pathway (Brackenbury and Djamgoz, 2006). The increased Nav1.7 mRNA expression in Mat-LyLu cells under hypoxic conditions shown in the present study is consistent with the earlier work (Brackenbury and Djamgoz, 2006). However, decreased VGSCα protein level in PM was detected in hypoxic Mat-LyLu cells. Similarly, Préze-Pinzón *et al.* (1992) showed that reduced O_2 level decreased VGSC α-subunit protein expression in turtle brain and O'Reilly *et al.* (1997) proposed that reduced O_2 level could cause a decrease in VGSC expression in

neurones, as a part of a process to conserve energy during metabolic stress. Consequently, the metabolic phenotypes of PCa cells were shown to be effected by hypoxic stress (Higgins *et al.,* 2009). In addition, mRNA and protein could be differentially regulated (e.g. Orphanides and Reinberg, 2002). On the other hand, Onkal (2010) showed that peak current density of VGSC in Mat-LyLu cells increased significantly in hypoxic (2 % O_2, 24 h). This would imply that VGSC could be regulated post-translationally, independently of protein expression. Thus, it would be appear that VGSC expression in Mat-LyLu cells can be regulated independently, at least partially, at a hierarchy of levels (from transcription to post-translation).

Increased VGSC activity was shown to enhance lateral motility, transverse migration and Matrigel invasion of Mat-LyLu cells (Fraser *et al.,* 2003; Brackenbury and Djamgoz, 2006; Grimes *et al.,* 1995). Accordingly, in the present study, transverse migration of Mat-LyLu cells increased with hypoxia (2 % O_2, 24 h) and this effect was VGSC dependent. However, the hypoxia-mediated increased VGSC activity did not cause any effect on lateral motility and Matrigel invasion. These observations suggest that, under the hypoxic conditions induced, the effect on MCBs was specific to transverse migration, paralleling intra/extravasation, which has been suggested to be one of the critical components of the metastatic cascade (Wyckoff *et al.,* 2000). Importantly, TTX decreased both normoxic and hypoxic Mat-LyLu cell invasiveness equally, supporting the proposed role of VGSC in invasion (Grimes *et al.,* 1995; Laniado *et al.,* 1997; Smith *et al.,* 1998; Bennett *et al.,* 2004; Nakajima *et al.,* 2009). On the other hand, the hypoxia-mediated increase in VGSC activity did not further increase the invasiveness of Mat-LyLu cells probably because VGSC was already working maximally under normoxic condition, as suggested earlier

(Brackenbury and Djamgoz, 2006). In addition, Gillet *et al.* (2009) showed that VGSC activity leads to intracellular alkalization and perimembrane acidification. In same study, they showed that VGSC activity dependent increase in invasiveness of strongly metastatic human breast cancer (BCa) MDA-MB-231 cells was caused by pH-dependent activation of cysteine cathepsins, which play crucial role in BCa cell invasion (Gillet *et al.,* 2009). Since, hypoxia was shown to be involved in changes in lactic acid production (Higgins *et al.,* 2009), the resulting acidification of intracellular pH could be one reason for not detecting VGSC activity dependent increase in invasion of hypoxic Mat-LyLu cells.

Similar to the results presented here, Alqawi *et al.* (2007) reported that 5 h hypoxia (1 % O_2) had no affect on Mat-LyLu cells invasion. On the other hand, they showed that after 3 weeks of hypoxia (1 % O_2) only 5 % of Mat-LyLu cells survived and after 8 weeks (1 % O_2), the surviving cells were found to be significantly more invasive than normoxic cells. Therefore, it was proposed that hypoxia acts as a selective pressure on cancerous cells and selects for highly invasive and apoptosis-resistant phenotype (Alqawi *et al.,* 2007). In addition, these results, taken together, clearly show that different periods of hypoxia can have different affects on PCa cells.

6.3 Ca^{2+} signalling downstream to VGSC activity possibly leading to MCB regulation

Like hypoxia, other microenvironmental factors can also play important role in cancer development and progression. In particular, the high Ca^{2+} concentration in bone environment was proposed to facilitate metastasis of PCa to bone (Liado *et al.,* 2006). Interestingly, Mat-LyLu cells, which spread to lymph node and lung but not to bone, was shown to be not responsive to extracellular Ca^{2+} (Ding *et al.,* 2008).

Accordingly, no $[Ca^{2+}]_i$ oscillations were detected in the present study. This result alone may indicate that Mat-LyLu cells are only a limited model of metastatic PCa. Also, LnCaP cells, which are weakly (and non-skeletal) metastatic, did not show any spontaneous $[Ca^{2+}]_i$ activity. On the other hand, 25 % of PC-3M cells, which are skeletal metastatic, had spontaneous Ca^{2+} oscillations. These Ca^{2+} oscillations were dependent on extracellular Ca^{2+}. Accordingly, the parental cell line of PC-3M, PC3, which is also skeletal metastatic, was shown to be more adhesive when extracellular Ca^{2+} concentration was elevated (Liado *et al.,* 2006). In addition, increase in extracellular Ca^{2+} level was reported to induce increase in proliferation of PC3 and C4-2B (a metastatic variant of LnCaP) cells but not the parent LNCaP cell line (Liado *et al.,* 2006). These results would indicate that Ca^{2+} signalling / oscillations could be important for metastasis of human PCa cells to bone.

It was proposed earlier that Ca^{2+} signalling could be downstream to VGSC activity leading to MCB, including galvanotaxis (Mycielska and Djamgoz 2004; Mycielska and Djamgoz 2003; Onkal and Djamgoz, 2009). Therefore, having studied this hypothesis, we found that VGSC activity was indeed involved in modulation of Ca^{2+} oscillations. Accordingly, Na^+ entry via VGSC was proposed to mediate increase in $[Ca^{2+}]_i$ by slowing or reversing Na^+/Ca^{2+} exchanger (NCX) (Poburko *et al.,* 2007; Eder *et al.,* 2005; Rosker *et al.,* 2004; Arnon *et al.,* 2000; Blaustein and Lederer, 1999; Matsuka and Hilgemann; Miura and Kimura, 1989). In addition, this local increase in $[Ca^{2+}]_i$ could be amplified by activation of ER Ca^{2+} release channels including ryanodine receptor (Berridge *et al.,* 2003). In the present study, we showed that disruption of ryanodine receptor or depletion of ER Ca^{2+} stores had negative effect on Ca^{2+} signalling. Therefore, our results taken together with the current

literature further support the notion that Ca^{2+} signalling is downstream to VGSC activity and has important consequences for metastasis.

6.4 Pharmacological VGSC inhibition and clinical implications.

As described above, tumour microenvironment, in addition to genetic modifications, can play a key role in the acquisition of metastatic phenotype (Chung *et al.*, 2005). Indeed, reduced O_2 level is one of the characteristics of cancerous tissue (Vaupel *et al.*, 2007; Harrison and Blackwell). In addition, Movsas *et al.* (2000) reported a positive correlation between hypoxia and clinical stage of cancer and patient age in PCa patients. Therefore, non invasive imaging of tissue O_2 levels was proposed as a promising tool for cancer diagnosis. Long-term hypoxia, could lead to cell death in Mat-LyLu cells, as shown by Alqawi *et al.* (2007). Accordingly, androgen deprivation therapy was shown to cause prostate tissue hypoxia leading to cell death due to changes in O_2 supply and demand (Rudolfsson and Bergh, 2009). However, this hypoxic microenvironment would select for apoptosis-resistant cells and increased metastatic ability which could be a cause of the relapse and re-emergence of metastasis in PCa undergoing prolonged androgen downregulation (Rudolfsson and Bergh, 2009; Koochekpour, 2010). Since the aim of research is to understand and establish novel therapeutically strategies for cancer and metastatic disease, *in vitro* studies should be carried out under microenvironmental conditions similar to those found *in vivo*.

Because VGSC activity was shown to increase MCBs, it was proposed as a novel and promising target for cancer therapy (Onkal and Djamgoz, 2009). However, when pharmacological VGSC blocker used at a concentration necessary for complete block of both transient and persistent currents of VGSC (I_{NaP} and I_{NaT}), they would

be lethal, e.g. by stopping heartbeat. However, at lower concentrations, these pharmacological blockers were shown to preferentially block I_{NaP} (Chen *et al.,* 2009; Samudio *et al.,* 2010; Rajamani *et al.,* 2008; Antzelevitch *et al.,* 2004; Weiss *et al.,* 2010; Le *et al.,* 2010; Parihar *et al.,* 2003; Doble, 1996; Zona *et al.,* 1998; Hammarström and Gage, 1998). Specifically, ranolazine and riluzole were proposed to mediate anti-anginal and neuroprotective effects by blocking I_{NaP} (Antzelevitch *et al.,* 2004; Fredj *et al.,* 2006; Urbani and Belluzi, 2000; Zona *et al.,* 1998). In addition, low doses of lidocaine were shown to preferentially block I_{NaP} (Hammarström and Gage, 1998). Therefore, here, we used clinically approved pharmacological VGSC blockers - ranolazine, riluzole, procaine and lidocaine - at clinically safe micromolar doses, to study their possible effects on VGSC expression and Matigel invasion of Mat-LyLu cells. We concluded that these agents reduced invasiveness of PCa cells and thus could be used as anti-cancer drug.

6.5 Future perspective.

There are still many aspects of PCa that need to be elucidated, as follows:

I. We showed here that hypoxia increased mRNA levels of VGSC and transverse migration (by VGSC-dependent mechanism). Brackenbury and Djamgoz (2006), proposed that VGSC activity increased VGSC mRNA expression and migration via the AC/PKA. Therefore, involvement of this pathway in hypoxia induced increase in migration could be studied.

II. Previously, the hypoxia-induced increase in VGSC peak current density was reported in Mat-LyLu cells (Onkal, 2010). In addition, enhancement I_{NaP} was reported in hypoxic cardiac and neuronal cells (Hammarström and Gage, 1998; Ju and Gage, 1996). However, there is no electrophysiological

evidence on hypoxic effect on I_{NaP} in our model cells. Therefore, I_{NaP} activity can be further examined in both normoxia and hypoxia using electrophysiological techniques.

III. I_{NaP} and I_{NaT} components of VGSCs in various cell types were shown to have different sensitivity to ranolazine, riluzole, procaine and lidocaine, depending on concentration (Chen *et al.,* 2009; Samudio *et al.,* 2010; Rajamani *et al.,* 2008; Antzelevitch *et al.,* 2004; Weiss *et al.,* 2010; Le *et al.,* 2010; Parihar *et al.,* 2003; Doble, 1996; Zona *et al.,* 1998; Hammarström and Gage, 1998). However, differential effect of these drugs on I_{NaP} and I_{NaT} was not studied in Mat-LyLu cells. Therefore, dose-dependent effects of these drugs on I_{NaP} and I_{NaT} in Mat-LyLu cells could be examined by electrophysiology.

IV. *In vivo* effects of these pharmacological VGSC blockers on PCa metastasis can be studied using appropriate animal models. Such models could be the Copenhagen rat (Lamb and Zhang, 2005; Blouin *et al.,* 2005) or the TRAMP transgenic mouse model (Gingrich *et al.,* 1996; Kaplan-Lefko *et al.,* 2003). Such studies could further validate the anti-cancer potential of these drugs and asses their safety.

V. In the present study, we showed that 25 % of PCa (PC-3M) cells showed spontaneous Ca^{2+} oscillations. Such Ca^{2+} signalling was shown to play important role in many cellular processes including invasion, migration, motility, adhesion, galvanotaxis, and secretion (Amuthan *et al.,* 2002; Wei *et al.,* 2009; Huang *et al.,* 2004; Komuro and Rakic, 1996; Giannone *et al.,* 2002; Liao *et al.,* 2006; Tse *et al.,* 1993; Giannone *et al.,* 2002; Liao *et al.,* 2006; Mycielska and Djamgoz 2003; Mycielska and Djamgoz 2004).

Therefore, the role of the oscillations in PCa can be determined by investigating differences in MCBs of oscillating vs. non-oscillating cells.

VI. of VGSC activity in Ca^{2+} signalling could be further examined by (i) measurement of changes in intracellular Na^{+} concentrations, (ii) examining changes in membrane potentials and (iii) observing changes in $[Ca^{2+}]_i$ following increase in intracellular Na^{+}.

VII. Other proposed component of this Ca^{2+} oscillation signalling including NCX and Ca^{2+}-activated K^{+} channels could be further studied by (i) using selective mode dependent pharmacological inhibitors and (ii) colocalization of VGSC and NCX (e.g. in caveolae).

References

Aalami OO, Fang TD, Song HM, Nacamuli RP. (2003). Physiological features of aging persons. *Arch Surg.* **138**(10):1068-76.

Abdul M, Hoosein N. (2001) Inhibition by anticonvulsants of prostate-specific antigen and interleukin-6 secretion by human prostate cancer cells. *Anticancer Res* **21**(3B):2045-8.

Abdul M & Hoosein N. (2002). Voltage-gated sodium ion channels in prostate cancer: expression and activity. *Anticancer Res* **22**, 1727-1730.

Abdul M, Ramlal S, Hoosein N. (2008). Ryanodine receptor expression correlates with tumor grade in breast cancer. *Pathol Oncol Res.***14**(2):157-60.

Abeele F V, Shuba Y, Roudbaraki M, Lemonnier L, Vanoverberghe K, Mariot P, Skryma R, Prevarskaya N. (2003a) Store-operated Ca2+ channels in prostate cancer epithelial cells: function, regulation, and role in carcinogenesis. *Cell Calcium* **33**(5-6):357-73.

Abeele F V, Roudbaraki M, Shuba Y, Skryma R, Prevarskaya N. (2003b) Store-operated Ca2+ current in prostate cancer epithelial cells. Role of endogenous Ca2+ transporter type 1. *J Biol Chem* **278**(17):15381-9.

Abeele F V, Lemonnier L, Thébault S, Lepage G, Parys JB, Shuba Y, Skryma R, Prevarskaya N. (2004) Two types of store-operated Ca2+ channels with

different activation modes and molecular origin in LNCaP human prostate cancer epithelial cells. *J Biol Chem* **279**(29):30326-37.

Abriel H, Kamynina E, Horisberger JD & Staub O. (2000). Regulation of the cardiac voltagegated Na+ channel (H1) by the ubiquitin-protein ligase Nedd4. *FEBS Lett* **466**, 377-380.

Ackerstaff E, Artemov D, Gillies RJ, Bhujwalla ZM. (2007). Hypoxia and the presence of human vascular endothelial cells affect prostate cancer cell invasion and metabolism. *Neoplasia* **9**(12):1138-51.

Adachi K, Toyota M, Sasaki Y, Yamashita T, Ishida S, Ohe-Toyota M, Maruyama R, Hinoda Y, Saito T, Imai K, Kudo R & Tokino T. (2004). Identification of SCN3B as a novel p53-inducible proapoptotic gene. *Oncogene* **23**, 7791-7798.

Akamatsu K, Shibata MA, Ito Y, Sohma Y, Azuma H, Otsuki Y. (2009). Riluzole induces apoptotic cell death in human prostate cancer cells via endoplasmic reticulum stress. *Anticancer Res* **29**(6):2195-204.

Akopian AN, Okuse K, Souslova V, England S, Ogata N & Wood JN. (1999). Trans-splicing of a voltage-gated sodium channel is regulated by nerve growth factor. *FEBS Lett* **445**, 177- 182.

Alqawi O, Wang HP, Espiritu M, Singh G. (2007). Chronic hypoxia promotes an aggressive phenotype in rat prostate cancer cells. *Free Radic Res.* **41**(7):788-97.

Allen DH, Lepple-Wienhues A & Cahalan MD. (1997). Ion channel phenotype of melanoma cell lines. *J Membr Biol* **155**, 27-34.

Aman TK, Grieco-Calub TM, Chen C, Rusconi R, Slat EA, Isom LL & Raman IM. (2009). Regulation of persistent Na current by interactions between beta subunits of voltage-gated Na channels. *J Neurosci* **29**, 2027-2042.

Arnon A, Hamlyn JM, Blaustein MP. (200). Na(+) entry via store-operated channels modulates Ca(2+) signaling in arterial myocytes. *Am J Physiol Cell Physiol.* **278**(1):C163-73.

Amuthan G, Biswas G, Zhang SY, Klein-Szanto A, Vijayasarathy C, Avadhani NG. (2001). Mitochondria-to-nucleus stress signaling induces phenotypic changes, tumor progression and cell invasion. *EMBO J.* **20**(8):1910-20.

Amuthan G, Biswas G, Ananadatheerthavarada HK, Vijayasarathy C, Shephard HM, Avadhani NG. (2002). Mitochondrial stress-induced calcium signaling, phenotypic changes and invasive behavior in human lung carcinoma A549 cells. *Oncogene.* **21**(51):7839-49.

Anderson JD, Hansen TP, Lenkowski PW, Walls AM, Choudhury IM, Schenck HA, Friehling M, Höll GM, Patel MK, Sikes RA, Brown ML. (2003). Voltage-gated sodium channel blockers as cytostatic inhibitors of the androgen-independent prostate cancer cell line PC-3. *Mol Cancer Ther*. **2**(11):1149-54.

Andrés ME, Burger C, Peral-Rubio MJ, Battaglioli E, Anderson ME, Grimes J, Dallman J, Ballas N & Mandel G. (1999). CoREST: a functional corepressor required for regulation of neural-specific gene expression. *Proc Natl Acad Sci USA* **96**, 9873-9878.

Antzelevitch C, Belardinelli L, Wu L, Fraser H, Zygmunt AC, Burashnikov A, Di Diego JM, Fish JM, Cordeiro JM, Goodrow RJ Jr, Scornik F & Perez G. (2004). Electrophysiologic properties and antiarrhythmic actions of a novel antianginal agent. *J Cardiovasc Pharmacol Ther* **9**, S65-83.

Bacac M & Stamenkovic I. (2008). Metastatic cancer cell. *Annu Rev Pathol* **3**, 221-247.

Baylor SM, Hollingworth S. (2010). Calcium indicators and calcium signalling in skeletal muscle fibres during excitation-contraction coupling. *Prog Biophys Mol Biol.* **105**(3):162-79.

Belcher SM, Zerillo CA, Levenson R, Ritchie JM & Howe JR. (1995). Cloning of a sodium channel alpha subunit from rabbit Schwann cells. *Proc Natl Acad Sci USA* **92**, 11034-11038.

Bendahhou S, Cummins TR, Potts JF, Tong J & Agnew WS. (1995). Serine-1321-independent regulation of the mu 1 adult skeletal muscle Na+ channel by protein kinase C. *Proc Natl Acad Sci USA* **92**, 12003-12007.

Ben Fredj N., Grange J., Sadoul R., Richard S., Goldberg Y. and Boyer V. (2004). Depolarization-induced translocation of the RNA-binding protein Sam68 to the dendrites of hippocampal neurons. *J Cell Sci* **117**: 1079-90.

Bennett PB, Yazawa K, Makita N & George AL Jr. (1995). Molecular mechanism for an inherited cardiac arrhythmia. *Nature* **376**, 683-685.

Bennett E, Urcan MS, Tinkle SS, Koszowski AG & Levinson SR. (1997). Contribution of sialic acid to the voltage dependence of sodium channel gating. A possible electrostatic mechanism. *J Gen Physiol* **109**, 327-343.

Bennett ES. (2002). Isoform-specific effects of sialic acid on voltage-dependent Na+ channel gating: functional sialic acids are localized to the S5-S6 loop of domain I. *J Physiol* **538**, 675-690.

Bennett ES, Smith BA & Harper JM. (2004). Voltage-gated Na^+ channels confer invasive properties on human prostate cancer cells. *Pflugers Arch* **447**, 908-914.

Bensimon G, Lacomblez L, Meininger V. (1994). A controlled trial of riluzole in amyotrophic lateral sclerosis. ALS/Riluzole Study Group. *N Engl J Med* **330**(9):585-91.

Berger JC, Vander-Griend D, Stadler WM & Rinker-Schaeffer C. (2004). Metastasis suppressor genes: signal transduction, cross-talk and the potential for modulating the behavior of metastatic cells. *Anticancer Drugs* **15**, 559-568.

Bernards R & Weinberg RA. (2002). A progression puzzle. *Nature* **418**, 823.

Berridge MJ. (1998). Neuronal calcium signaling. *Neuron.* **21**(1):13-26.

Berridge MJ, Bootman MD, Lipp P. (1998). Calcium--a life and death signal. *Nature.* **395**(6703):645-8.

Berridge MJ, Bootman MD, Roderick HL. (2003). Calcium signalling: dynamics, homeostasis and remodelling. *Nat Rev Mol Cell Biol.* **4**(7):517-29.

Berridge MJ. (2009). Calcium hypothesis of Alzheimer's disease. *Pflugers Arch.* **459**(3):441-9.

Bertout JA, Patel SA & Simon MC. (2008). The impact of O2 availability on human cancer. *Nat Rev Cancer* **8**, 967-975.

Bianchi L, Wible B, Arcangeli A, Taglialatela M, Morra F, Castaldo P, Crociani O, Rosati B, Faravelli L, Olivotto M, Wanke E. (1998). herg encodes a K+ current highly conserved in tumors of different histogenesis: a selective advantage for cancer cells? *Cancer Res* **58**(4):815-22.

Black JA, Langworthy K, Hinson AW, Dib-Hajj SD & Waxman SG. (1997). NGF has opposing effects on Na+ channel III and SNS gene expression in spinal sensory neurons. *Neuroreport* **8**, 2331-2335.

Black JA, Cummins TR, Plumpton C, Chen YH, Hormuzdiar W, Clare JJ & Waxman SG. (1999). Upregulation of a silent sodium channel after peripheral, but not central, nerve injury in DRG neurons. *J Neurophysiol* **82**, 2776-2785.

Blouin S, Baslé MF, Chappard D. (2005). Rat models of bone metastases. *Clin Exp Metastasis.* **22**(8):605-14

Blaustein MP, Santiago EM. (1977). Effects of internal and external cations and of ATP on sodium-calcium and calcium-calcium exchange in squid axons. *Biophys J.* **20**(1):79-111.

Blaustein MP, Lederer WJ. (1999). Sodium/calcium exchange: its physiological implications. *Physiol Rev.* **79**(3):763-854.

Blandino JK, Viglione MP, Bradley WA, Oie HK & Kim YI. (1995). Voltage-dependent sodium channels in human small-cell lung cancer cells: role in

action potentials and inhibition by Lambert-Eaton syndrome IgG. *J Membr Biol* **143**, 153-163.

Blencowe BJ. (2006). Alternative splicing: new insights from global analyses. *Cell* **126**, 37-47.

Bloch M, Ousingsawat J, Simon R, Schraml P, Gasser TC, Mihatsch MJ, Kunzelmann K, Bubendorf L. KCNMA1 gene amplification promotes tumor cell proliferation in human prostate cancer. *Oncogene.* **26**(17):2525-34.

Bostwick DG, Qian J. (2004). High-grade prostatic intraepithelial neoplasia. *Mod Pathol.* **17**(3):360-79.

Brackenbury WJ & Djamgoz MB. (2006). Activity-dependent regulation of voltage-gated Na^+ channel expression in Mat-LyLu rat prostate cancer cell line. *J Physiol* **573**, 343-356.

Brackenbury WJ, Chioni AM, Diss JKJ, Djamgoz MB. (2007). The neonatal splice variant of Nav1.5 potentiates in vitro invasive behaviour of MDA-MB-231 human breast cancer cells. *Breast Cancer Res Treat* **101**, 149-160.

Brackenbury WJ & Djamgoz MB. (2007). Nerve growth factor enhances voltage-gated Na^+ channel activity and Transwell migration in Mat-LyLu rat prostate cancer cell line. *J Cell Physiol* **210**, 602-608.

Brackenbury WJ & Isom LL. (2008). Voltage-gated Na+ channels: potential for beta subunits as therapeutic targets. *Expert Opin Ther Targets* **12**, 1191-1203.

Brackenbury WJ, Djamgoz MB & Isom LL. (2008). An emerging role for voltage-gated Na+ channels in cellular migration: regulation of central nervous system development and potentiation of invasive cancers. *Neuroscientist* **14**, 571-583.

Brat DJ, Castellano-Sanchez AA, Hunter SB, Pecot M, Cohen C, Hammond EH, Devi SN, Kaur B & Van Meir EG. (2004). Pseudopalisades in glioblastoma are hypoxic, express extracellular matrix proteases, and are formed by an actively migrating cell population. *Cancer Res* **64**, 920-927.

Bräu ME, Vogel W, Hempelmann G. (1998). Fundamental properties of local anesthetics: half-maximal blocking concentrations for tonic block of Na+ and K+ channels in peripheral nerve. *Anesth Analg* **87**(4):885-9.

Brawer MK. (2010). New treatments for castration-resistant prostate cancer: highlights from the 44th annual meeting of the american society of clinical oncology, may 30-june 3, 2008, chicago, IL. *Rev Urol.* **10**(4):294-6.

Brouland JP, Gélébart P, Kovàcs T, Enouf J, Grossmann J, Papp B. (2005). The loss of sarco/endoplasmic reticulum calcium transport ATPase 3 expression is an early event during the multistep process of colon carcinogenesis. *Am J Pathol.* **167**(1):233-42.

Buonanno A, Fields RD. (1999). Gene regulation by patterned electrical activity during neural and skeletal muscle development. *Curr Opin Neurobiol*. **9**(1):110-20.

Burke B, Giannoudis A, Corke KP, Gill D, Wells M, Ziegler-Heitbrock L & Lewis CE. (2003). Hypoxia-induced gene expression in human macrophages: implications for ischemic tissues and hypoxia-regulated gene therapy. *Am J Pathol* **163**, 1233-1243.

Butterworth KT, McCarthy HO, Devlin A, Ming L, Robson T, McKeown SR, Worthington J. (2008). Hypoxia selects for androgen independent LNCaP cells with a more malignant geno- and phenotype. *Int J Cancer*. **123**(4):760-8.

Cairns RA, Kalliomaki T, Hill RP. (2001). Acute (cyclic) hypoxia enhances spontaneous metastasis of KHT murine tumors. *Cancer Res.* **61**(24):8903-8.

Camacho JA, Hensellek S, Rougier JS, Blechschmidt S, Abriel H, Benndorf K & Zimmer T. (2006). Modulation of Nav1.5 channel function by an alternatively spliced sequence in the DII/DIII linker region. *J Biol Chem* **281**, 9498-9506.

Cameron IL, Smith NK, Pool TB, Sparks RL. (1980). Intracellular concentration of sodium and other elements as related to mitogenesis and oncogenesis in vivo. *Cancer Res.* **40**(5):1493-500.

Campbell KP, Knudson CM, Imagawa T, Leung AT, Sutko JL, Kahl SD, Raab CR, Madson L. (1987). Identification and characterization of the high affinity [3H]ryanodine receptor of the junctional sarcoplasmic reticulum Ca2+ release channel. *J Biol Chem.* **262**(14):6460-3.

Candenas L, Seda M, Noheda P, Buschmann H, Cintado CG, Martin JD, Pinto FM. (2006). Molecular diversity of voltage-gated sodium channel alpha and beta subunit mRNAs in human tissues. *Eur J Pharmacol.* **541**(1-2):9-16.

Cannito S, Novo E, Compagnone A, Valfrè di Bonzo L, Busletta C, Zamara E, Paternostro C, Povero D, Bandino A, Bozzo F, Cravanzola C, Bravoco V, Colombatto S, Parola M. (2008). Redox mechanisms switch on hypoxia-dependent epithelial-mesenchymal transition in cancer cells. *Carcinogenesis.* **29**(12):2267-78.

Canning MT, Postovit LM, Clarke SH & Graham CH. (2001). Oxygen-mediated regulation of gelatinase and tissue inhibitor of metalloproteinases-1 expression by invasive cells. *Exp Cell Res* **267**, 88-94.

Cantrell AR, Ma JY, Scheuer T & Catterall WA. (1996). Muscarinic modulation of sodium current by activation of protein kinase C in rat hippocampal neurons. *Neuron* **16**, 1019- 1026.

Cantrell AR & Catterall WA. (2001). Neuromodulation of Na+ channels: an unexpected form of cellular plasticity. *Nat Rev Neurosci* **2**, 397-407.

Cantrell AR, Tibbs VC, Yu FH, Murphy BJ, Sharp EM, Qu Y, Catterall WA & Scheuer T. (2002). Molecular mechanism of convergent regulation of brain Na(+) channels by protein kinase C and protein kinase A anchored to AKAP-15. *Mol Cell Neurosci* **21**, 63- 80.

Carr DB, Day M, Cantrell AR, Held J, Scheuer T, Catterall WA & Surmeier DJ. (2003). Transmitter modulation of slow, activity-dependent alterations in sodium channel availability endows neurons with a novel form of cellular plasticity. *Neuron* **39**, 793-806.

Catterall WA. (2000). From ionic currents to molecular mechanisms: the structure and function of voltage-gated sodium channels. *Neuron* **26**, 13-25.

Catterall WA. (2001). A 3D view of sodium channels. *Nature* **409**, 988-991.

Catterall WA, Goldin AL & Waxman SG. (2005). International Union of Pharmacology. XLVII. Nomenclature and structure-function relationships of voltage-gated sodium channels. *Pharmacol Rev* **57**, 397-409.

Catterall WA, Cestèle S, Yarov-Yarovoy V, Yu FH, Konoki K & Scheuer T. (2007). Voltage-gated ion channels and gating modifier toxins. *Toxicon* **49**, 124-141.

Catterall WA. (2010). Ion Channel Voltage Sensors: Structure, Function, and Pathophysiology. *Neuron* **67**, 915-928.

Cestèle S & Catterall WA. (2000). Molecular mechanisms of neurotoxin action on voltage-gated sodium channels. *Biochimie* **82**, 883-892.

Chahine M, Plante E & Kallen RG. (1996). Sea anemone toxin (ATX II) modulation of heart and skeletal muscle sodium channel alpha-subunits expressed in tsA201 cells. *J Membr Biol* **152**, 39-48.

Chahine M, Ziane R, Vijayaragavan K & Okamura Y. (2005). Regulation of Nav channels in sensory neurons. *Trends Pharmacol Sci* **26**, 496-502.

Chaitman BR. (2006). Ranolazine for the treatment of chronic angina and potential use in other cardiovascular conditions. *Circulation* **113**(20):2462-72.

Chen C, Bharucha V, Chen Y, Westenbroek RE, Brown A, Malhotra JD, Jones D, Avery C, Gillespie PJ 3rd, Kazen-Gillespie KA, Kazarinova-Noyes K, Shrager P, Saunders TL, Macdonald RL, Ransom BR, Scheuer T, Catterall WA & Isom LL. (2002). Reduced sodium channel density, altered voltage dependence of inactivation, and increased susceptibility to seizures in mice lacking sodium channel beta 2-subunits. *Proc Natl Acad Sci USA* **99**, 17072-17077.

Chen Y, Yu FH, Surmeier DJ, Scheuer T & Catterall WA. (2006). Neuromodulation of Na+ channel slow inactivation via cAMP-dependent protein kinase and protein kinase C. *Neuron* **49**, 409-420.

Chen BS, Lo YC, Peng H, Hsu TI, Wu SN. (2009). Effects of ranolazine, a novel anti-anginal drug, on ion currents and membrane potential in pituitary tumor GH(3) cells and NG108-15 neuronal cells. *J Pharmacol Sci* **110**(3):295-305.

Chen M & Manley JL. (2009). Mechanisms of alternative splicing regulation: insights from molecular and genomics approaches. *Nat Rev Mol Cell Biol* **10**, 741-754.

Chen J, Imanaka N, Chen J, Griffin JD. (2010). Hypoxia potentiates Notch signaling in breast cancer leading to decreased E-cadherin expression and increased cell migration and invasion. *Br J Cancer*. **102**(2):351-60.

Chevrier P, Vijayaragavan K & Chahine M. (2004). Differential modulation of Nav1.7 and Nav1.8 peripheral nerve sodium channels by the local anesthetic lidocaine. *Br J Pharmacol* **142**, 576-584.

Chioni AM, Fraser SP, Pani F, Foran P, Wilkin GP, Diss JKJ & Djamgoz MB. (2005). A novel polyclonal antibody specific for the Nav1.5 voltage-gated Na^+ channel 'neonatal' isoform. *J Neurosci Methods* **147**, 88-98.

Chioni AM, Brackenbury WJ, Calhoun JD, Isom LL & Djamgoz MB. (2009). A novel adhesion molecule in human breast cancer cells: voltage-gated Na+ channel beta1 subunit. *Int J Biochem* **41**, 1216-1227.

Chioni AM, Shao D, Grose R & Djamgoz MB. (2010). Protein kinase A and regulation of neonatal Nav1.5 expression in human breast cancer cells: activity-dependent positive feedback and cellular migration. *Int J Biochem Cell Biol* **42,** 346-358.

Chlebowski RT, Block JB, Cundiff D, Dietrich MF. (1982). Doxorubicin cytotoxicity enhanced by local anesthetics in a human melanoma cell line. *Cancer Treat Rep*. **66**(1):121-5.

Choi DY, Toledo-Aral JJ, Segal R, Halegoua S. (2001). Sustained signaling by phospholipase C-gamma mediates nerve growth factor-triggered gene expression. *Mol Cell Biol.* **21**(8):2695-705.

Chong JA, Tapia-Ramírez J, Kim S, Toledo-Aral JJ, Zheng Y, Boutros MC, Altshuller YM, Frohman MA, Kraner SD & Mandel G. (1995). REST: a mammalian silencer protein that restricts sodium channel gene expression to neurons. *Cell* **80,** 949-957.

Chu LW, Pettaway CA & Liang JC. (2001). Genetic abnormalities specifically associated with varying metastatic potential of prostate cancer cell lines as detected by comparative genomic hybridization. *Cancer Genet Cytogenet* **127**, 161-167.

Chung LW, Baseman A, Assikis V, Zhau HE. (2005). Molecular insights into prostate cancer progression: the missing link of tumor microenvironment. *J Urol.* **173**(1):10-20.

Chung FY, Lin SR, Lu CY, Yeh CS, Chen FM, Hsieh JS, Huang TJ, Wang JY. (2006). Sarco/endoplasmic reticulum calcium-ATPase 2 expression as a tumor marker in colorectal cancer. *Am J Surg Pathol* **30**(8):969-74

Ciccolini F, Collins TJ, Sudhoelter J, Lipp P, Berridge MJ, Bootman MD. (2003). Local and global spontaneous calcium events regulate neurite outgrowth and onset of GABAergic phenotype during neural precursor differentiation. *J Neurosci.* **23**(1):103-11.

Clapham DE. (2007). Calcium signaling. *Cell.* **131**(6):1047-58.

Clare JJ. (2010) Targeting voltage-gated sodium channels for pain therapy. *Expert Opin Investig Drugs* **19**, 45-62.

Clarke B, Wyatt KM, McCormack JG. (1996). Ranolazine increases active pyruvate dehydrogenase in perfused normoxic rat hearts: evidence for an indirect mechanism. *J Mol Cell Cardiol* **28**(2):341-50.

Schulman CC, Irani J, Morote J, Schalken JA, Montorsi F, Chlosta PL, Heidenreich A. (2010) Androgen-deprivation therapy in prostate cancer: a European expert panel review. *Eur Urol* **9**:675-91.

Colomer J, Means AR. (2007). Physiological roles of the Ca2+/CaM-dependent protein kinase cascade in health and disease. *Subcell Biochem.* **45**:169-214.

Conforti L, Millhorn DE. (1997). Selective inhibition of a slow-inactivating voltage-dependent K+ channel in rat PC12 cells by hypoxia. *J Physiol.* **502** (Pt 2):293-305.

Contassot E, Wilmotte R, Tenan M, Belkouch MC, Schnüriger V, de Tribolet N, Burkhardt K, Dietrich PY. (2004). Arachidonylethanolamide induces apoptosis of human glioma cells through vanilloid receptor-1. *J Neuropathol Exp Neurol* **63**(11):1114.

Cook SJ, Lockyer PJ. (2006). Recent advances in Ca(2+)-dependent Ras regulation and cell proliferation. *Cell Calcium.* **39**(2):101-12.

Copley RR. (2004). Evolutionary convergence of alternative splicing in ion channels. *Trends Genet* **20**, 171-176.

Crill WE. (1996). Persistent sodium current in mammalian central neurons. *Annu Rev Physiol* **58**, 349-362.

Cronin PA, Wang JH, Redmond HP. (2010). Hypoxia increases the metastatic ability of breast cancer cells via upregulation of CXCR4. *BMC Cancer.* **10**:225.

Cronin NB, O'Reilly A, Duclohier H & Wallace BA. (2005). Effects of deglycosylation of sodium channels on their structure and function. *Biochemistry* **44,** 441-449.

Cruz J., Santana L., Frederick C., Isom L., Malhotra J., Mattei L., Kass R., Xia J., An R.-H. and Lederer W. (1999). Whether "slip-mode conductance" occurs. *Science* **284**: 711a.

Dai Y, Bae K, Siemann DW. (2011). Impact of Hypoxia on the Metastatic Potential of Human Prostate Cancer Cells. Int J Radiat Oncol Biol Phys. Epub ahead of print.

Dargent B & Couraud F. (1990). Down-regulation of voltage-dependent sodium channels initiated by sodium influx in developing neurons. *Proc Natl Acad Sci USA* **87**, 5907- 5911.

Dargent B, Paillart C, Carlier E, Alcaraz G, Martin-Eauclaire MF & Couraud F. (1994). Sodium channel internalization in developing neurons. *Neuron* **13**, 683-690.

De Koninck P, Schulman H. (1998). Sensitivity of CaM kinase II to the frequency of Ca2+ oscillations. *Science.* **279**(5348):227-30.

Deeds J, Cronin F, Duncan LM. (2000). Patterns of melastatin mRNA expression in melanocytic tumors. *Hum Pathol* **31**(11):1346-56.

Del Toro R, Levitsky KL, López-Barneo J, Chiara MD. (2003). Induction of T-type calcium channel gene expression by chronic hypoxia. *J Biol Chem.* **278**(25):22316-24.

Diaz D, Delgadillo DM, Hernández-Gallegos E, Ramírez-Domínguez ME, Hinojosa LM, Ortiz CS, Berumen J, Camacho J & Gomora JC. (2007). Functional expression of voltage-gated sodium channels in primary cultures of human cervical cancer. *J Cell Physiol* **210**, 469-478.

Dib-Hajj SD, Tyrrell L, Black JA & Waxman SG. (1998). NaN, a novel voltage-gated Na channel, is expressed preferentially in peripheral sensory neurons and down-regulated after axotomy. *Proc Natl Acad Sci USA* **95**, 8963-8968.

Dietrich PS, McGivern JG, Delgado SG, Koch BD, Eglen RM, Hunter JC & Sangameswaran L. (1998). Functional analysis of a voltage-gated sodium channel and its splice variant from rat dorsal root ganglia. *J Neurochem* **70**, 2262–2272.

Ding Y & Djamgoz MB. (2004). Serum concentration modifies amplitude and kinetics of voltage-gated Na^+ current in the Mat-LyLu cell line of rat prostate cancer. *Int J Biochem Cell Biol* **36**, 1249-1260.

Ding Y, Robbins J, Fraser SP, Grimes JA, Djamgoz MB. (2006). Comparative studies of intracellular Ca2+ in strongly and weakly metastatic rat prostate cancer cell lines. *Int J Biochem Cell Biol.* **38**(3):366-75.

Ding Y, Brackenbury WJ, Onganer PU, Montano X, Porter LM, Bates LF & Djamgoz MB. (2008). Epidermal growth factor upregulates motility of Mat-LyLu rat prostate cancer cells partially via voltage-gated Na+ channel activity. *J Cell Physiol* **215**, 77-81.

Ding X, He Z, Zhou K, Cheng J, Yao H, Lu D, Cai R, Jin Y, Dong B, Xu Y, Wang Y. (2010). Essential role of TRPC6 channels in G2/M phase transition and development of human glioma. *J Natl Cancer Inst.* **102**(14):1052-68.

Diss JK, Archer SN, Hirano J, Fraser SP & Djamgoz MB. (2001). Expression profiles of voltage-gated Na(+) channel alpha-subunit genes in rat and human prostate cancer cell lines. *Prostate* **48**, 165-178.

Diss JK, Fraser SP & Djamgoz MB. (2004). Voltage-gated Na+ channels: multiplicity of expression, plasticity, functional implications and pathophysiological aspects. *Eur Biophys J* **33**, 180-193.

Diss JK, Stewart D, Pani F, Foster CS, Walker MM, Patel A & Djamgoz MB. (2005). A potential novel marker for human prostate cancer: voltage-gated sodium channel expression in vivo. *Prostate Cancer Prostatic Dis* **8**, 266-273.

Diss JK, Faulkes DJ, Walker MM, Patel A, Foster CS, Budhram-Mahadeo V, Djamgoz MB, Latchman DS. (2006). Brn-3a neuronal transcription factor

functional expression in human prostate cancer. *Prostate Cancer Prostatic Dis.* **9**(1):83-91.

Diss JKJ, Fraser SP, Walker MM, Patel A, Latchman DS & Djamgoz MB. (2008). Beta-subunits of voltage-gated sodium channels in human prostate cancer: quantitative in vitro and in vivo analyses of mRNA expression. *Prostate Cancer Prostatic Dis* **11**, 325-333.

Djamgoz MBA, Mycielska M, Madeja Z, Fraser SP & Korohoda W. (2001). Directional movement of rat prostate cancer cells in direct-current electric field: involvement of voltage gated Na^+ channel activity. *J Cell Sci* **114**, 2697-2705.

Djamgoz MBA & Isbilen B. (2006). Dietary compounds as anti-cancer agents: A preliminary evaluation of ion channels and membrane excitability as possible target mechanisms. *Turk. J Biochem* **31**, 57-68.

Doble A. (1996). The pharmacology and mechanism of action of riluzole. *Neurology* **47**(6 Suppl 4):S233-41.

Dolmetsch RE, Xu K, Lewis RS. (1998). Calcium oscillations increase the efficiency and specificity of gene expression. *Nature.* **392**(6679):933-6.

Dunning WF. (1963) Prostate cancer in the rat. *Natl Cancer Inst Monogr* **12**:351-69.

Duprat F, Lesage F, Patel AJ, Fink M, Romey G, Lazdunski M. (2000). The neuroprotective agent riluzole activates the two P domain K(+) channels TREK-1 and TRAAK. *Mol Pharmacol.* **57**(5):906-12.

Eder P, Poteser M, Romanin C, Groschner K. (2005). Na(+) entry and modulation of Na(+)/Ca(2+) exchange as a key mechanism of TRPC signaling. *Pflugers Arch.* **451**(1):99-104.

Edwards BK, Brown ML, Wingo PA, Howe HL, Ward E, Ries LA, Schrag D, Jamison PM, Jemal A, Wu XC, Friedman C, Harlan L, Warren J, Anderson RN & Pickle LW. (2005). Annual report to the nation on the status of cancer, 1975-2002, featuring population-based trends in cancer treatment. *J Natl Cancer Inst* **97**, 1407-1427.

Egeblad M, Werb Z. (2002). New functions for the matrix metalloproteinases in cancer progression. *Nat Rev Cancer* **2**(3):161-74.

Ehrhardt DW, Wais R, Long SR. (1996). Calcium spiking in plant root hairs responding to Rhizobium nodulation signals. *Cell.* **85**(5):673-81.

Endo Y, Uzawa K, Mochida Y, Shiiba M, Bukawa H, Yokoe H, Tanzawa. (2004). Sarcoendoplasmic reticulum Ca(2+) ATPase type 2 downregulated in human oral squamous cell carcinoma. *Int J Cancer.* **110**(2):225-31.

England S, Bevan S & Docherty RJ. (1996). PGE2 modulates the tetrodotoxin-resistant sodium current in neonatal rat dorsal root ganglion neurones via the cyclic AMP-protein kinase A cascade. *J Physiol* **495**, 429-440.

England S. (2008). Voltage-gated sodium channels: the search for subtype-selective analgesics. *Expert Opin Investig Drugs* **17**, 1849-1864.

Esposito M, Fulco RA, Collecchi P, Zicca A, Cadoni A, Merlo F, Rosso R, Sobrero A. (1990). Improved therapeutic index of cisplatin by procaine hydrochloride. *J Natl Cancer Inst* **82**(8):677-84.

Faissner A. (1997). The tenascin gene family in axon growth and guidance. *Cell Tissue Res.* **290**(2):331-41.

Fanger GR, Vaillancourt RR, Heasley LE, Montmayeur JP, Johnson GL, Maue RA. (1997). Analysis of mutant platelet-derived growth factor receptors expressed in PC12 cells identifies signals governing sodium channel induction during neuronal differentiation. *Mol Cell Biol.* **17**(1):89-99.

Félétou M. (2009). Calcium-activated potassium channels and endothelial dysfunction: therapeutic options? *Br J Pharmacol.***156**(4):545-62.

Ferrari MB, Ribbeck K, Hagler DJ, Spitzer NC. (1998). A calcium signaling cascade essential for myosin thick filament assembly in Xenopus myocytes. *J Cell Biol.* **141**(6):1349-56.

Fidler IJ & Kripke ML. (1977). Metastasis results from preexisting variant cells within a malignant tumor. *Science* **197**, 893-895.

Fidler IJ. (2002). Critical determinants of metastasis. *Semin Cancer Biol* **12**, 89-96.

Fidler IJ. (2003). The pathogenesis of cancer metastasis: the 'seed and soil' hypothesis revisited. *Nat Rev Cancer* **3**, 453-458.

Fixemer T, Wissenbach U, Flockerzi V, Bonkhoff H. (2003). Expression of the Ca2+-selective cation channel TRPV6 in human prostate cancer: a novel prognostic marker for tumor progression. *Oncogene* **22**(49):7858-61.

Fotia AB, Ekberg J, Adams DJ, Cook DI, Poronnik P & Kumar S. (2004). Regulation of neuronal voltage-gated sodium channels by the ubiquitin-protein ligases Nedd4 and Nedd4-2. *J Biol Chem* **279**, 28930-28935.

Fozzard HA & Lipkind GM. (2010). The tetrodotoxin binding site is within the outer vestibule of the sodium channel. *Mar Drugs* **8**, 219-234.

Frankel S, Smith GD, Donovan J, Neal D. (2003). Screening for prostate cancer. *Lancet* **361**(9363):1122-8.

Franovic A, Gunaratnam L, Smith K, Robert I, Patten D, Lee S. (2007). Translational up-regulation of the EGFR by tumor hypoxia provides a nonmutational

explanation for its overexpression in human cancer. *Proc Natl Acad Sci U S A*. **104**(32):13092-7.

Fraser SP, Ding Y, Liu A, Foster CS & Djamgoz MB. (1999). Tetrodotoxin suppresses morphological enhancement of the metastatic Mat-LyLu rat prostate cancer cell line. *Cell Tissue Res* **295**, 505-512.

Fraser SP, Grimes JA, Djamgoz MB. (2000). Effects of voltage-gated ion channel modulators on rat prostatic cancer cell proliferation: comparison of strongly and weakly metastatic cell lines. *Prostate* **44**(1):61-76.

Fraser SP, Salvador V, Manning EA, Mizal J, Altun S, Raza M, Berridge RJ & Djamgoz MB. (2003). Contribution of functional voltage-gated Na+ channel expression to cell behaviors involved in the metastatic cascade in rat prostate cancer: I. lateral motility. *J Cell Physiol* **195**, 479-487.

Fraser SP, Diss JK, Lloyd LJ, Pani F, Chioni AM, George AJ & Djamgoz MB. (2004). T-lymphocyte invasiveness: control by voltage-gated Na^+ channel activity. *FEBS Lett* **569**, 191-194.

Fraser SP, Diss JKJ, Chioni AM, Mycielska ME, Pan H, Yamaci RF, Pani F, Siwy Z, Krakowska M, Grzywna Z, Brackenbury WJ, Theodorou D, Koyutűrk M, Kaya H, Battaloğlu E, Tamburo De Bella M, Slade MJ, Tolhurst R, Palmieri C, Jiang J, Latchman DS, Coombes RC & Djamgoz MB. (2005). Voltage-gated

sodium channel expression and potentiation of human breast cancer metastasis. *Clin Cancer Res* **11**, 5381-5389.

Fredj S, Sampson KJ, Liu H & Kass RS. (2006). Molecular basis of ranolazine block of LQT-3 mutant sodium channels: evidence for site of action. *Br J Pharmacol* **148**, 16-24.

Fridlyand LE, Jacobson DA, Kuznetsov A, Philipson LH. (2009). A model of action potentials and fast Ca2+ dynamics in pancreatic beta-cells. *Biophys J* **96**(8):3126-39

Friedman S, Shatz CJ. (1990). The Effects of Prenatal Intracranial Infusion of Tetrodotoxin on Naturally Occurring Retinal Ganglion Cell Death and Optic Nerve Ultrastructure. *Eur J Neurosci* **2**(3):243-253.

Frizzo ME, Dall'Onder LP, Dalcin KB, Souza DO. (2004). Riluzole enhances glutamate uptake in rat astrocyte cultures. *Cell Mol Neurobiol* **24**(1):123-8.

Frohnwieser B, Chen LQ, Schreibmayer W & Kallen RG. (1997). Modulation of the human cardiac sodium channel alpha-subunit by cAMP-dependent protein kinase and the responsible sequence domain. *J Physiol* **498**, 309-318.

Fuessel S, Sickert D, Meye A, Klenk U, Schmidt U, Schmitz M, Rost AK, Weigle B, Kiessling A, Wirth MP. (2003). Multiple tumor marker analyses (PSA, hK2,

PSCA, trp-p8) in primary prostate cancers using quantitative RT-PCR. *Int J Oncol* **23**(1):221-8.

Fulgenzi G, Graciotti L, Faronato M, Soldovieri MV, Miceli F, Amoroso S, Annunziato L, Procopio A & Taglialatela M. (2006). Human neoplastic mesothelial cells express voltage-gated sodium channels involved in cell motility. *Int J Biochem Cell Biol* **38**, 1146-1159.

Gackière F, Bidaux G, Lory P, Prevarskaya N, Mariot P. (2006). A role for voltage gated T-type calcium channels in mediating "capacitative" calcium entry? *Cell Calcium.* **39**(4):357-66.

Ghafar MA, Anastasiadis AG, Chen MW, Burchardt M, Olsson LE, Xie H, Benson MC, Buttyan R. (2003). Acute hypoxia increases the aggressive characteristics and survival properties of prostate cancer cells. *Prostate.* **54**(1):58-67.

Gao R, Wang J, Shen Y, Lei M, Wang Z. (2009). Functional expression of voltage-gated sodium channels Nav1.5 in human breast cancer cell line MDA-MB-231. *J Huazhong Univ Sci Technolog Med Sci*. **29**(1):64-7.

Gao R, Shen Y, Cai J, Lei M & Wang Z. (2010). Expression of voltage-gated sodium channel alpha subunit in human ovarian cancer. *Oncol Rep*. **23**, 1293-1299.

Gastaldi M, Bartolomei F, Massacrier A, Planells R, Robaglia-Schlupp A, Cau P. (1997). Increase in mRNAs encoding neonatal II and III sodium channel alpha-

isoforms during kainate-induced seizures in adult rat hippocampus. *Brain Res Mol Brain Res* **44**(2):179-90.

Gauthier ML, Torretto C, Ly J, Francescutti V, O'Day DH. (2003). Protein kinase Calpha negatively regulates cell spreading and motility in MDA-MB-231 human breast cancer cells downstream of epidermal growth factor receptor. *Biochem Biophys Res Commun* **307**(4):839-46.

Gellens ME, George AL Jr, Chen LQ, Chahine M, Horn R, Barchi RL & Kallen RG. (1992). Primary structure and functional expression of the human cardiac tetrodotoxin-insensitive voltage-dependent sodium channel. *Proc Natl Acad Sci USA* **89**, 554-558.

Gersdorff Korsgaard MP, Christophersen P, Ahring PK & Olesen SP. (2001). Identification of a novel voltage-gated Na+ channel rNa(v)1.5a in the rat hippocampal progenitor stem cell line HiB5. *Pflugers Arch* **443**, 18-30.

Ghafar MA, Anastasiadis AG, Chen MW, Burchardt M, Olsson LE, Xie H, Benson MC, Buttyan R. (2003). Acute hypoxia increases the aggressive characteristics and survival properties of prostate cancer cells. *Prostate.* **54**(1):58-67.

Giannone G, Rondé P, Gaire M, Haiech J, Takeda K. (2002). Calcium oscillations trigger focal adhesion disassembly in human U87 astrocytoma cells. *J Biol Chem.* **277**(29):26364-71.

Gillet L, Roger S, Besson P, Lecaille F, Gore J, Bougnoux P, Lalmanach G & Le Guennec JY. (2009). Voltage-gated sodium channel activity promotes cysteine cathepsin-dependent invasiveness and colony growth of human cancer cells. *J Biol Chem* **284**, 8680-8691.

Gillet L, Roger S, Bougnoux P, Le Guennec JY, Besson P. (2011). Beneficial effects of omega-3 long-chain fatty acids in breast cancer and cardiovascular diseases: voltage-gated sodium channels as a common feature? *Biochimie.* **93**(1):4-6.

Gingrich JR, Barrios RJ, Morton RA, Boyce BF, Demayo FJ, Finegold MJ, Angelopoulou R, Rosen JM, Greenberg NM. (1996). Metastatic prostate cancer in a transgenic mouse. *Cancer Res.* **56**(18):4096-4102.

Gkika D, Flourakis M, Lemonnier L, Prevarskaya N. (2010). PSA reduces prostate cancer cell motility by stimulating TRPM8 activity and plasma membrane expression. *Oncogene* **29**(32):4611-6.

Gold MS, Levine JD & Correa AM. (1998). Modulation of TTX-R INa by PKC and PKA and their role in PGE2-induced sensitization of rat sensory neurons in vitro. *J Neurosci* **18**, 10345-10355.

Goldin AL, Barchi RL, Caldwell JH, Hofmann F, Howe JR, Hunter JC, Kallen RG, Mandel G, Meisler MH, Netter YB, Noda M, Tamkun MM, Waxman SG, Wood JN & Catterall WA. (2000). Nomenclature of voltage-gated sodium channels. *Neuron* **28**, 365-368.

Goldin AL. (2001). Resurgence of sodium channel research. *Annu Rev Physiol* **63**, 871-894.

Goldin AL. (2003). Mechanisms of sodium channel inactivation. *Curr Opin Neurobiol* **13**, 284-290.

Gomez TM, Snow DM, Letourneau PC. (1995). Characterization of spontaneous calcium transients in nerve growth cones and their effect on growth cone migration. *Neuron.* **14**(6):1233-46.

Gomez TM, Robles E, Poo M, Spitzer NC. (2001). Filopodial calcium transients promote substrate-dependent growth cone turning. *Science.* **291**(5510):1983-7.

Goodison S, Viars C, Urquidi V. (2005). Molecular cytogenetic analysis of a human breast metastasis model: identification of phenotype-specific chromosomal rearrangements. *Cancer Genet Cytogenet* **156**: 37-48.

Gosling M, Harley SL, Turner RJ, Carey N & Powell JT. (1998). Human saphenous vein endothelial cells express a tetrodotoxin-resistant, voltage-gated sodium current. *J Biol Chem* **273**, 21084-21090.

Graeber TG, Osmanian C, Jacks T, Housman DE, Koch CJ, Lowe SW, Giaccia AJ. (1996). Hypoxia-mediated selection of cells with diminished apoptotic potential in solid tumours. *Nature.* **379**(6560):88-91.

Gregory CW, Fei X, Ponguta LA, He B, Bill HM, French FS, Wilson EM. (2004). Epidermal growth factor increases coactivation of the androgen receptor in recurrent prostate cancer. *J Biol Chem* **279**(8):7119-30.

Graham CH, Forsdike J, Fitzgerald CJ, Macdonald-Goodfellow S. (1999). Hypoxia-mediated stimulation of carcinoma cell invasiveness via upregulation of urokinase receptor expression. *Int J Cancer.* **80**(4):617-23.

Grimes JA, Fraser SP, Stephens GJ, Downing JEG, Laniado ME, Foster CS, Abel PD & Djamgoz MB. (1995). Differential expression of voltage-activated Na^+ currents in two prostatic tumour cell lines: contribution to invasiveness in vitro. *FEBS Letts* **369**, 290-294.

Grimes JA & Djamgoz MB. (1998). Electrophysiological characterization of voltage-gated Na^+ current expressed in the highly metastatic Mat-LyLu cell line of rat prostate cancer. *J Cell Physiol* **175**, 50-58.

Grimes JA, Nielsen SJ, Battaglioli E, Miska EA, Speh JC, Berry DL, Atouf F, Holdener BC, Mandel G & Kouzarides T. (2000). The co-repressor mSin3A is a functional component of the REST-CoREST repressor complex. *J Biol Chem* **275**, 9461-9467.

Gu X., Lundqvist E. N., Coates P. J., Thurfjell N., Wettersand E. and Nylander K. (2006). Dysregulation of TAp63 mRNA and protein levels in psoriasis. *J Invest Dermatol* **126**: 137-41.

Gupta GP, Perk J, Acharyya S, de Candia P, Mittal V, Todorova-Manova K, Gerald WL, Brogi E, Benezra R & Massagué J. (2007). ID genes mediate tumor reinitiation during breast cancer lung metastasis. *Proc Natl Acad Sci USA* **104,** 19506-19511.

Gustafson TA, Clevinger EC, Oneill TJ, Yarowsky PJ & Krueger BK. (1993). Mutually exclusive exon splicing of type-III brain sodium channel-alpha subunit RNA generates developmentally-regulated isoforms in rat-brain. *J Biol Chem* **268,** 18648-18653.

Gutierrez AA, Arias JM, García L, Mas-Oliva J, Guerrero-Hernández A. (1999). Activation of a Ca2+-permeable cation channel by two different inducers of apoptosis in a human prostatic cancer cell line. *J Physiol.* **517** (Pt 1):95-107.

Hagel C & Stavrou D. (2007). Neuronal markers in non-neuronal tissues. *Prog Exp Tumor Res* **39**, 64-77.

Haigney MC, Lakatta EG, Stern MD & Silverman HS. (1994). Sodium channel blockade reduces hypoxic sodium loading and sodium-dependent calcium loading. *Circulation* **90**, 391-399.

Haisenleder DJ, Workman LJ, Burger LL, Aylor KW, Dalkin AC, Marshall JC. (2001). Gonadotropin subunit transcriptional responses to calcium signals in the rat: evidence for regulation by pulse frequency. *Biol Reprod.* **65**(6):1789-93.

Hajnóczky G, Robb-Gaspers LD, Seitz MB, Thomas AP. (1995). Decoding of cytosolic calcium oscillations in the mitochondria. *Cell.* **82**(3):415-24.

Hale SL, Shryock JC, Belardinelli L, Sweeney M, Kloner RA. (2008). Late sodium current inhibition as a new cardioprotective approach. *J Mol Cell Cardiol.* **44**(6):954-67.

Hammarström AK & Gage PW. (1998). Inhibition of oxidative metabolism increases persistent sodium current in rat CA1 hippocampal neurons. *J Physiol.* **510** (Pt 3):735-41.

Hammarström AK & Gage PW. (2000). Oxygen-sensing persistent sodium channels in rat hippocampus. *J Physiol* **529**, 107-118.

Hammarström AK & Gage PW. (2002). Hypoxia and persistent sodium current. *Eur Biophys J* **31**, 323-330.

Hanahan D & Weinberg RA. (2000). The hallmarks of cancer. *Cell* **100**, 57-70.

Harris AL. (2002). Hypoxia--a key regulatory factor in tumour growth. *Nat Rev Cancer*. **2**(1):38-47.

Harrison L, Blackwell K. (2004). Hypoxia and anemia: factors in decreased sensitivity to radiation therapy and chemotherapy? *Oncologist* **9** Suppl 5:31-40.

Hebert T, Drapeau P, Pradier L, Dunn RJ. (1994). Block of the rat brain IIA sodium channel alpha subunit by the neuroprotective drug riluzole. *Mol Pharmacol.* **45**(5):1055-60.

Heighway J, Betticher DC, Hoban PR, Altermatt HJ, Cowen R. (1996). Coamplification in tumors of KRAS2, type 2 inositol 1,4,5 triphosphate receptor gene, and a novel human gene, KRAG. *Genomics* **35**(1):207-14.

Heinemann SH, Terlau H, Stuhmer W, Imoto K & Numa S. (1992). Calcium channel characteristics conferred on the sodium channel by single mutations. *Nature* **356,** 441-443.

Heinlein CA, Chang C. (2004) Androgen receptor in prostate cancer. *Endocr Rev* **25**(2):276-308.

Herfst LJ, Rook MB & Jongsma HJ. (2004). Trafficking and functional expression of cardiac Na+ channels. *J Mol Cell Cardiol* **36**, 185-193.

Higgins LH, Withers HG, Garbens A, Love HD, Magnoni L, Hayward SW, Moyes CD. (2009). Hypoxia and the metabolic phenotype of prostate cancer cells. *Biochim Biophys Acta* **1787**(12):1433-43.

Hille B. (1971). The permeability of the sodium channel to organic cations in myelinated nerve. *J Gen Physiol* **58**, 599-619.

Hille B. (1972). The permeability of the sodium channel to metal cations in myelinated nerve. *J Gen Physiol* **59**, 637-658.

Hille B. (2001). Ionic channels of excitable membranes (third edition). Sinauer Associates Inc., Sunderland (Massachusetts), USA.

Hobai IA, O'Rourke B. (2004). The potential of Na+/Ca2+ exchange blockers in the treatment of cardiac disease. *Expert Opin Investig Drugs.* **13**(6):653-64.

Horoszewicz JS, Leong SS, Chu TM, Wajsman ZL, Friedman M, Papsidero L, Kim U, Chai LS, Kakati S, Arya SK, Sandberg AA. (1980). The LNCaP cell line--a new model for studies on human prostatic carcinoma. *Prog Clin Biol Res* **37**:115-32.

House CD, Vaske CJ, Schwartz AM, Obias V, Frank B, Luu T, Sarvazyan N, Irby R, Strausberg RL, Hales TG, Stuart JM & Lee NH. (2010). Voltage-gated Na+ channel SCN5A is a key regulator of a gene transcriptional network that controls colon cancer invasion. *Cancer Res* **70**, 6957-6967.

Huang JB, Kindzelskii AL, Clark AJ, Petty HR. (2004). Identification of channels promoting calcium spikes and waves in HT1080 tumor cells: their apparent roles in cell motility and invasion. *Cancer Res.* **64**(7):2482-9.

Huggins C & Hodges CV *(*1941) Studies on prostatic cancer: I. The effect of castration, of estrogen and of androgen injection on serum phosphatases in metastatic carcinoma of the prostate. *Cancer Research **1** 293*–297.

Hunter KW. (2004). Host genetics and tumour metastasis. *Br J Cancer* **90**, 752-755.

Hynes RO. (2003). Metastatic potential: generic predisposition of the primary tumor or rare, metastatic variants-or both? *Cell* **113**, 821-823.

Ingham RJ, Gish G & Pawson T. (2004). The Nedd4 family of E3 ubiquitin ligases: functional diversity within a common modular architecture. *Oncogene* **23**, 1972-1984.

Isaacs JT, Yu GW, Coffey DS. (1981). The characterization of a newly identified, highly metastatic variety of Dunning R 3327 rat prostatic adenocarcinoma system: the MAT LyLu tumor. *Invest Urol* **19**(1):20-3.

Isom LL, De Jongh KS, Patton DE, Reber BF, Offord J, Charbonneau H, Walsh K, Goldin AL & Catterall WA. (1992). Primary structure and functional

expression of the beta 1 subunit of the rat brain sodium channel. *Science*. **256**, 839-842.

Isom LL, De Jongh KS & Catterall WA. (1994). Auxiliary subunits of voltage-gated ion channels. *Neuron* **12**, 1183-1194.

Isom LL, Ragsdale DS, De Jongh KS, Westenbroek RE, Reber BF, Scheuer T & Catterall WA. (1995). Structure and function of the beta 2 subunit of brain sodium channels, a transmembrane glycoprotein with a CAM motif. *Cell* **83**, 433-442.

Isom LL & Catterall WA. (1996). Na+ channel subunits and Ig domains. *Nature* **383**, 307-308.

Isom LL. (2001). Sodium channel beta subunits: anything but auxiliary. *Neuroscientist* **7**, 42-54.

Isom LL. (2002). The role of sodium channels in cell adhesion. *Front Biosci* **7**, 12-23.

Ito M, Xu H, Guffanti AA, Wei Y, Zvi L, Clapham DE, Krulwich TA. (2004). The voltage-gated Na+ channel NaVBP has a role in motility, chemotaxis, and pH homeostasis of an alkaliphilic Bacillus. *Proc Natl Acad Sci U S A.* **101**(29):10566-71.

Iwahashi Y, Furuyama T, Inagaki S, Morita Y & Takagi H. (1994). Distinct regulation of sodium channel types I, II and III following nerve transection. *Brain Res Mol Brain Res.* **22**, 341-345.

Jemal A, Siegel R, Xu J & Ward E. (2010). Cancer statistics, 2010. *CA Cancer J Clin* **60**, 277-300.

Jeong SY, Goto J, Hashida H, Suzuki T, Ogata K, Masuda N, Hirai M, Isahara K, Uchiyama Y & Kanazawa I. (2000). Identification of a novel human voltage-gated sodium channel alpha subunit gene, SCN12A. *Biochem Biophys Res Commun* **267**, 262-270.

Johnson D, Montpetit ML, Stocker PJ & Bennett ES. (2004). The sialic acid component of the beta1 subunit modulates voltage-gated sodium channel function. *J Biol Chem* **279**, 44303-44310.

Ju YK, Saint DA & Gage PW. (1996). Hypoxia increases persistent sodium current in rat ventricular myocytes. *J Physiol* **497**, 337-347.

Kaplan RN, Riba RD, Zacharoulis S, Bramley AH, Vincent L, Costa C, MacDonald DD, Jin DK, Shido K, Kerns SA, Zhu Z, Hicklin D, Wu Y, Port JL, Altorki N, Port ER, Ruggero D, Shmelkov SV, Jensen KK, Rafii S, Lyden D. (2005). VEGFR1-positive haematopoietic bone marrow progenitors initiate the pre-metastatic niche. *Nature* **438**: 820-7.

Kaplan-Lefko PJ, Chen TM, Ittmann MM, Barrios RJ, Ayala GE, Huss WJ, Maddison LA, Foster BA, Greenberg NM. (2003). Pathobiology of autochthonous prostate cancer in a pre-clinical transgenic mouse model. *Prostate.* **55**(3):219-237.

Kaighn ME, Narayan KS, Ohnuki Y, Lechner JF & Jones LW. (1979). Establishment and characterization of a human prostatic carcinoma cell line (PC-3). *Invest Urol* **17**, 16-23.

Kazarinova-Noyes K, Malhotra JD, McEwen DP, Mattei LN, Berglund EO, Ranscht B, Levinson SR, Schachner M, Shrager P, Isom LL & Xiao ZC. (2001). Contactin associates with Na+ channels and increases their functional expression. *J Neurosci* **21**, 7517-7525.

Kazen-Gillespie KA, Ragsdale DS, D'Andrea MR, Mattei LN, Rogers KE & Isom LL. (2000). Cloning, localization, and functional expression of sodium channel beta1A subunits. *J Biol Chem* **275**, 1079-1088.

Keller ET, Zhang J, Cooper CR, Smith PC, McCauley LK, Pienta KJ, Taichman RS. (2001). Prostate carcinoma skeletal metastases: cross-talk between tumor and bone. *Cancer Metastasis Rev* **20**(3-4):333-49.

Kerr NC, Holmes FE & Wynick D. (2004). Novel isoforms of the sodium channels Nav1.8 and Nav1.5 are produced by a conserved mechanism in mouse and rat. *J Biol Chem* **279**, 24826-24833.

Kim J, Adam RM, Freeman MR. (2002). Activation of the Erk mitogen-activated protein kinase pathway stimulates neuroendocrine differentiation in LNCaP cells independently of cell cycle withdrawal and STAT3 phosphorylation. *Cancer Res* **62**(5):1549-54.

Klinger R, Denecke H, Glier B, Kröner-Herwig B, Nilges P, Redegeld M, Weiss L. (1997). Quality control in the therapy of chronic pain. Results obtained by a task force of the German Section of the International Association for the Study of Pain on psychological assessment of chronic pain. XI. Assessment and multiaxial classification of pain. *Schmerz* **11**(6):378-85.

Klugbauer N, Lacinova L, Flockerzi V & Hofmann F. (1995). Structure and functional expression of a new member of the tetrodotoxin-sensitive voltage-activated sodiumchannel family from human neuroendocrine cells. *EMBO J* **14**, 1084–1090.

Kobayashi H, Shiraishi S, Yanagita T, Yokoo H, Yamamoto R, Minami S, Saitoh T & Wada A. (2002). Regulation of voltage-dependent sodium channel expression in adrenal chromaffin cells: involvement of multiple calcium signaling pathways. *Ann NY Acad Sci* **971**,127-134.

Komuro H, Rakic P. (1996). Intracellular Ca2+ fluctuations modulate the rate of neuronal migration. *Neuron.* **17**(2):275-85.

Kontis KJ & Goldin AL. (1997). Sodium channel inactivation is altered by substitution of voltage sensor positive charges. *J Gen Physiol* **110**, 403-413.

Koochekpour S. (2010). Androgen receptor signaling and mutations in prostate cancer. *Asian J Androl.* **12**(5):639-57.

Korosec B, Glavac D, Rott T, Ravnik-Glavac M. (2006). Alterations in the ATP2A2 gene in correlation with colon and lung cancer. *Cancer Genet Cytogenet* **171**(2):105-11.

Kozlowski JM, Fidler IJ, Campbell D, Xu ZL, Kaighn ME, Hart IR. (1984). Metastatic behavior of human tumor cell lines grown in the nude mouse. *Cancer Res* **44**(8):3522-9.

Kraner S, Yang J & Barchi R. (1989). Structural inferences for the native skeletal muscle sodium channel as derived from patterns of endogenous proteolysis. *J Biol Chem* **264**, 13273-13280.

Krasowska M, Grzywna ZJ, Mycielska ME & Djamgoz MB. (2004). Patterning of endocytic vesicles and its control by voltage-gated Na^+ channel activity in rat prostate cancer cells: fractal analyses. *Eur Biophys J* **33**, 535-542.

Krawetz S (2009) Bioinformatics for systems biology. New York, USA Humane Press

Krishnamachary B, Berg-Dixon S, Kelly B, Agani F, Feldser D, Ferreira G, Iyer N, LaRusch J, Pak B, Taghavi P, Semenza GL. (2003). Regulation of colon carcinoma cell invasion by hypoxia-inducible factor 1. *Cancer Res.* **63**(5):1138-43.

Kuo CC, Bean BP. (1994). Na^+ channels must deactivate to recover from inactivation. *Neuron* **12**: 819-29.

Krtolica A, Ludlow JW. (1996). Hypoxia arrests ovarian carcinoma cell cycle progression, but invasion is unaffected. *Cancer Res.* **56**(5):1168-73.

Kusner LL, Mygland A, Kaminski HJ. (1998). Ryanodine receptor gene expression thymomas. *Muscle Nerve* **21**(10):1299-303.

Lacomblez L, Bensimon G, Leigh PN, Guillet P, Meininger V. (1996). Dose-ranging study of riluzole in amyotrophic lateral sclerosis. Amyotrophic Lateral Sclerosis/Riluzole Study Group II. *Lancet* **347**(9013):1425-31.

Lallet-Daher H, Roudbaraki M, Bavencoffe A, Mariot P, Gackière F, Bidaux G, Urbain R, Gosset P, Delcourt P, Fleurisse L, Slomianny C, Dewailly E, Mauroy B, Bonnal JL, Skryma R, Prevarskaya N. (2009). Intermediate-conductance Ca2+-activated K+ channels (IKCa1) regulate human prostate cancer cell proliferation through a close control of calcium entry. *Oncogene.* **28**(15):1792-806.

Lamb DJ, Zhang L. (2005). Challenges in prostate cancer research: animal models for nutritional studies of chemoprevention and disease progression. *J Nutr.* **135**(12 Suppl):3009S-3015S.

Langley R, Price P, Pollock P, Abel PD. (2010) Osteoporosis in patients with prostate cancer on long-term androgen deprivation therapy: an increasing but under-recognised problem. *BJU Int.* **106**(5):726-7

Laniado ME, Lalani EN, Fraser SP, Grimes JA, Bhangal G, Djamgoz MB & Abel PD. (1997). Expression and functional analysis of voltage-activated Na^+ channels in human prostate cancer cell lines and their contribution to invasion in vitro. *Am J Pathol* **150**, 1213-1221.

Laniado ME, Fraser SP & Djamgoz MB. (2001). Voltage-gated K(+) channel activity in human prostate cancer cell lines of markedly different metastatic potential: distinguishing characteristics of PC-3 and LNCaP cells. *Prostate* **46**, 262-274.

Laskowski AI, Medler KF. (2009). Sodium-calcium exchangers contribute to the regulation of cytosolic calcium levels in mouse taste cells. *J Physiol.* **587**(Pt 16):4077-89.

Latour I, Louw DF, Beedle AM, Hamid J, Sutherland GR, Zamponi GW. (2004). Expression of T-type calcium channel splice variants in human glioma. *Glia* **48**(2):112-9.

Lazzeri M, Vannucchi MG, Spinelli M, Bizzoco E, Beneforti P, Turini D, Faussone-Pellegrini MS. (2005). Transient receptor potential vanilloid type 1 (TRPV1) expression changes from normal urothelium to transitional cell carcinoma of human bladder. *Eur Urol* **48**(4):691-8.

Le MN, Chan JL, Rosenberg SA, Nabatian AS, Merrigan KT, Cohen-Solal KA, Goydos JS. (2010). The glutamate release inhibitor Riluzole decreases migration, invasion, and proliferation of melanoma cells. *J Invest Dermatol* **130**(9):2240-9.

Lee WJ, Roberts-Thomson SJ, Holman NA, May FJ, Lehrbach GM, Monteith GR. (2002). Expression of plasma membrane calcium pump isoform mRNAs in breast cancer cell lines. *Cell Signal* **14**(12):1015-22.

Lee WJ, Roberts-Thomson SJ, Monteith GR. (2005). Plasma membrane calcium-ATPase 2 and 4 in human breast cancer cell lines. *Biochem Biophys Res Commun* **337**(3):779-83.

Le Liboux A, Cachia JP, Kirkesseli S, Gautier JY, Guimart C, Montay G, Peeters PA, Groen E, Jonkman JH, Wemer J. (1999). A comparison of the pharmacokinetics and tolerability of riluzole after repeat dose administration in healthy elderly and young volunteers. *J Clin Pharmacol* **39**(5):480-6.

Lehen'kyi V, Flourakis M, Skryma R, Prevarskaya N. (2007). TRPV6 channel controls prostate cancer cell proliferation via Ca(2+)/NFAT-dependent pathways. *Oncogene.* **26**(52):7380-5.

Lester RD, Jo M, Montel V, Takimoto S, Gonias SL. (2007). uPAR induces epithelial-mesenchymal transition in hypoxic breast cancer cells. *J Cell Biol.* **178**(3):425-36.

Li M, West JW, Lai Y, Scheuer T & Catterall WA. (1992). Functional modulation of brain sodium channels by cAMP-dependent phosphorylation. *Neuron* **8**, 1151-1159.

Li M, West JW, Numann R, Murphy BJ, Scheuer T & Catterall WA. (1993). Convergent regulation of sodium channels by protein kinase C and cAMP-dependent protein kinase. *Science* **261**, 1439-1442.

Li W, Llopis J, Whitney M, Zlokarnik G, Tsien RY. (1998). Cell-permeant caged InsP3 ester shows that Ca2+ spike frequency can optimize gene expression. *Nature.* **392**(6679):936-41.

Li Y, Tu C, Wang H, Silverman DN, Frost SC. (2011). Catalysis and pH control by membrane-associated carbonic anhydrase IX in MDA-MB-231 breast cancer cells. *J Biol Chem*. **6**;286(18):15789-96.

Liao J, Schneider A, Datta NS, McCauley LK. (2006). Extracellular calcium as a candidate mediator of prostate cancer skeletal metastasis. *Cancer Res* **66**(18):9065-73.

Lilley SJ, Robbins J. (1998).The action of local anaesthetics on the compound action potential is altered by the nature of the permeant ion in frog nerve. *Neurosci Lett* **252**(1):41-4.

Liotta LA & Clair T. (2000). Cancer. Checkpoint for invasion. *Nature* **405**, 287-288.

Lioudyno MI, Kozak JA, Penna A, Safrina O, Zhang SL, Sen D, Roos J, Stauderman KA, Cahalan MD. (2008). Orai1 and STIM1 move to the immunological synapse and are up-regulated during T cell activation. *Proc Natl Acad Sci U S A.***105**(6):2011-6.

Livak KJ & Schmittgen TD. (2001). Analysis of relative gene expression data using real-time quantitative PCR and the 2^{-ddCt} method. *Methods* **25**, 402-408.

Magistretti J, Ragsdale DS & Alonso A. (1999). Direct demonstration of persistent Na+ channel activity in dendritic processes of mammalian cortical neurones. *J Physiol* **521**, 629-636.

Meier SD, Kovalchuk Y, Rose CR. (2006). Properties of the new fluorescent Na+ indicator CoroNa Green: comparison with SBFI and confocal Na+ imaging. *J Neurosci Methods.* **155**(2):251-9.

Maier LS. (2009). A novel mechanism for the treatment of angina, arrhythmias, and diastolic dysfunction: inhibition of late I(Na) using ranolazine. *J Cardiovasc Pharmacol* **54**(4):279-86.

Maitland NJ, Collins A. (2005). A tumour stem cell hypothesis for the origins of prostate cancer. *BJU Int* **96**(9):1219-23.

Makielski JC, Ye B, Valdivia CR, Pagel MD, Pu J, Tester DJ & Ackerman MJ. (2003). A ubiquitous splice variant and a common polymorphism affect heterologous expression of recombinant human SCN5A heart sodium channels. *Circ Res* **93**, 821-828.

Malhotra JD, Kazen-Gillespie K, Hortsch M & Isom LL. (2000). Sodium channel beta subunits mediate homophilic cell adhesion and recruit ankyrin to points of cell-cell contact. *J Biol Chem* **275**, 11383-11388.

Malhotra JD, Koopmann MC, Kazen-Gillespie KA, Fettman N, Hortsch M & Isom L. (2002). Structural requirements for interaction of sodium channel beta 1 subunits with ankyrin. *J Biol Chem* **277**, 26681-26688.

Maltsev VA, Sabbah HN, Higgins RS, Silverman N, Lesch M & Undrovinas AI. (1998). Novel, ultraslow inactivating sodium current in human ventricular cardiomyocytes. *Circulation* **98**, 2545-2552.

Maltsev VA & Undrovinas AI. (2006). A multi-modal composition of the late Na+ current in human ventricular cardiomyocytes. *Cardiovasc Res* **69**, 116-127.

Mammoto T, Mukai M, Mammoto A, Yamanaka Y, Hayashi Y, Mashimo T, Kishi Y, Nakamura H. (2002). Intravenous anesthetic, propofol inhibits invasion of cancer cells. *Cancer Lett* **184**(2):165-70.

Mantegazza M, Curia G, Biagini G, Ragsdale DS & Avoli M. (2010). Voltage-gated sodium channels as therapeutic targets in epilepsy and other neurological disorders. *Lancet Neurol* **9**, 413-424.

Marban E, Yamagishi T & Tomaselli GF. (1998). Structure and function of voltage-gated sodium channels. *J Physiol* **508**, 647-657.

Mariot P, Prevarskaya N, Roudbaraki MM, Le Bourhis X, Van Coppenolle F, Vanoverberghe K, Skryma R. (2000). Evidence of functional ryanodine receptor involved in apoptosis of prostate cancer (LNCaP) cells. *Prostate*. **43**(3):205-14.

Mariot P, Vanoverberghe K, Lalevee N, Rossier MF, Prevarskaya N. (2002). Overexpression of an alpha 1H (Cav3.2) T-type calcium channel during neuroendocrine differentiation of human prostate cancer cells. *J Biol Chem* **277**(13):10824-33.

Martin KC, Zukin RS. (2006). RNA trafficking and local protein synthesis in dendrites: an overview. *J Neurosci* **26**(27):7131-4.

Matsuoka S, Hilgemann DW. (1992). Steady-state and dynamic properties of cardiac sodium-calcium exchange. Ion and voltage dependencies of the transport cycle. *J Gen Physiol.* **100**(6):963-1001.

McCormack JG, Baracos VE, Barr R, Lopaschuk GD. (1996). Effects of ranolazine on oxidative substrate preference in epitrochlearis muscle. *J Appl Physiol* **81**(2):905-10.

McEwen DP & Isom LL. (2004). Heterophilic interactions of sodium channel beta1 subunits with axonal and glial cell adhesion molecules. *J Biol Chem* **279**, 52744-52752.

McEwen DP, Meadows LS, Chen C, Thyagarajan V & Isom LL. (2004). Sodium channel beta1 subunit-mediated modulation of Nav1.2 currents and cell surface density is dependent on interactions with contactin and ankyrin. *J Biol Chem* **279**, 16044-16049.

McKeown M. (1992). Alternative mRNA splicing. *Annu Rev Cell Biol.* **8**:133-55.

Meadows LS & Isom LL. (2005). Sodium channels as macromolecular complexes: implications for inherited arrhythmia syndromes. *Cardiovasc Res* **67**, 448-458.

Meisler MH, Kearney JA, Sprunger LK, MacDonald BT, Buchner DA, Escayg A. (2002). Mutations of voltage-gated sodium channels in movement disorders and epilepsy. *Novart Fdn Symp* **241**: 72–86.

Méry A, Aimond F, Ménard C, Mikoshiba K, Michalak M, Pucéat M. (2005). Initiation of embryonic cardiac pacemaker activity by inositol 1,4,5-trisphosphate-dependent calcium signaling. *Mol Biol Cell.* **16**(5):2414-23.

Miura Y, Kimura J. (1989). Sodium-calcium exchange current. Dependence on internal Ca and Na and competitive binding of external Na and Ca. *J Gen Physiol.* **93**(6):1129-45.

Mizuno S, Ishida A. (1982). Selective enhancement of the cytotoxicity of the bleomycin derivative, peplomycin, by local anesthetics alone and combined with hyperthermia. *Cancer Res* **42**(11):4726-9.

Mohler PJ, Rivolta I, Napolitano C, LeMaillet G, Lambert S, Priori SG & Bennett V. (2004). Nav1.5 E1053K mutation causing Brugada syndrome blocks binding to ankyrin-G and expression of Nav1.5 on the surface of cardiomyocytes. *Proc Natl Acad Sci USA* **101**, 17533-17538.

Monet M, Lehen'kyi V, Gackiere F, Firlej V, Vandenberghe M, Roudbaraki M, Gkika D, Pourtier A, Bidaux G, Slomianny C, Delcourt P, Rassendren F, Bergerat JP, Ceraline J, Cabon F, Humez S, Prevarskaya N. (2010). Role of

cationic channel TRPV2 in promoting prostate cancer migration and progression to androgen resistance. *Cancer Res* **70**(3):1225-35.

Monteith GR, McAndrew D, Faddy HM, Roberts-Thomson SJ. (2007). Calcium and cancer: targeting Ca2+ transport. *Nat Rev Cancer* **7**(7):519-30.

Mollenhauer HH, Morré DJ & Rowe LD. (1990). Alteration of intracellular traffic by monensin; mechanism, specificity and relationship to toxicity. *Biochim Biophys Acta* **1031**, 225-246.

Morgan K, Stevens EB, Shah B, Cox PJ, Dixon AK, Lee K, Pinnock RD, Hughes J, Richardson PJ, Mizuguchi K & Jackson AP. (2000). beta 3: an additional auxiliary subunit of the voltage-sensitive sodium channel that modulates channel gating with distinct kinetics. *Proc Natl Acad Sci USA* **97**, 2308-2313.

Movsas B, Chapman JD, Greenberg RE, Hanlon AL, Horwitz EM, Pinover WH, Stobbe C, Hanks GE. (2000). Increasing levels of hypoxia in prostate carcinoma correlate significantly with increasing clinical stage and patient age: an Eppendorf pO(2) study. *Cancer* **89**(9):2018-24.

Muniz M, Alonso M, Hidalgo J & Velasco A. (1996). A regulatory role for cAMP-dependent protein kinase in protein traffic along the exocytic route. *J Biol Chem* **271**, 30935- 30941.

Muniz M, Martin ME, Hidalgo J & Velasco A. (1997). Protein kinase A activity is required for the budding of constitutive transport vesicles from the trans-Golgi network. *Proc Natl Acad Sci USA* **94**, 14461-14466.

Murphy BJ, Rossie S, De Jongh KS & Catterall WA. (1993). Identification of the sites of selective phosphorylation and dephosphorylation of the rat brain Na+ channel alpha subunit by cAMP-dependent protein kinase and phosphoprotein phosphatases. *J Biol Chem* **268**, 27355-27362.

Murray KT, Hu NN, Daw JR, Shin HG, Watson MT, Mashburn AB & George AL Jr. (1997). Functional effects of protein kinase C activation on the human cardiac Na+ channel. *Circ Res* **80**, 370-376.

Mycielska ME, Fraser SP, Szatkowski M & Djamgoz MB. (2003). Contribution of functional voltage-gated Na^+ channel expression to cell behaviors involved in the metastatic cascade in rat prostate cancer: II. Secretory membrane activity. *J Cell Physiol* **195**, 461-469.

Mycielska ME, Djamgoz MB. (2004). Cellular mechanisms of direct-current electric field effects: galvanotaxis and metastatic disease. *J Cell Sci* **117**: 1631-9.

Mycielska ME, Palmer CP, Brackenbury WJ & Djamgoz MB. (2005). Expression of Na+-dependent citrate transport in a strongly metastatic human prostate cancer PC-3M cell line: regulation by voltage-gated Na+ channel activity. *J Physiol* **563**, 393-408.

Nakajima T, Kubota N, Tsutsumi T, Oguri A, Imuta H, Jo T, Oonuma H, Soma M, Meguro K, Takano H, Nagase T & Nagata T, (2009). Eicosapentaenoic acid inhibits voltage-gated sodium channels and invasiveness in prostate cancer cells. *Br J Pharmacol* **56**, 420-431.

Nguyen DX & Massagué J. (2007). Genetic determinants of cancer metastasis. *Nat Rev Genet* **8**, 341-352.

Norberg E, Gogvadze V, Ott M, Horn M, Uhlén P, Orrenius S, Zhivotovsky B. (2008). An increase in intracellular Ca2+ is required for the activation of mitochondrial calpain to release AIF during cell death. *Cell Death Differ*. **15**(12):1857-64.

Offord J & Catterall WA. (1989). Electrical activity, cAMP, and cytosolic calcium regulate mRNA encoding sodium channel alpha subunits in rat muscle cells. *Neuron* **2,** 1447-1452.

Ogata N & Ohishi Y. (2002). Molecular diversity of structure and function of the voltage-gated Na+ channels. *Jpn J Pharmacol* **88**, 365-377.

Oh Y & Waxman SG. (1998). Novel splice variants of the voltage-sensitive sodium channel alpha subunit. *Neuroreport* **9**, 1267-1272.

Okuse K, Malik-Hall M, Baker MD, Poon WY, Kong H, Chao MV & Wood JN. (2002). Annexin II light chain regulates sensory neuron-specific sodium channel expression. *Nature* **417**, 653-656.

Olson EN, Williams RS. (2000). Calcineurin signaling and muscle remodeling. *Cell.* **101**(7):689-92.

Onganer PU & Djamgoz MB. (2005). Small-cell lung cancer (human): potentiation of endocytic membrane activity by voltage-gated Na^+ channel expression in vitro. *J Membr Biol* **204**, 67-75.

Onganer PU, Seckl MJ & Djamgoz MB. (2005). Neuronal characteristics of small-cell lung cancer. *Br J Cancer* **93**, 1197-1201.

Onganer PU, Djamgoz MB. (2007). Epidermal growth factor potentiates in vitro metastatic behaviour of human prostate cancer PC-3M cells: involvement of voltage-gated sodium channel. *Mol Cancer.* **6**:76.

Onkal R, Mattis JH, Fraser SP, Diss JK, Shao D, Okuse K & Djamgoz MB. (2008). Alternative splicing of Nav1.5: an electrophysiological comparison of 'neonatal' and 'adult' isoforms and critical involvement of a lysine residue. *J Cell Physiol* **216**, 716-726.

Onkal R & Djamgoz MB. (2009). Molecular pharmacology of voltage-gated sodium channel expression in metastatic disease: clinical potential of neonatal Nav1.5 in breast cancer. *Eur J Pharmacol* **625**, 206-219.

Onkal R. (2010). Neonatal Nav1.5 voltage-gated Na+ channel: regulation, electrophysiology and pharmacology. .*PhD. Thesis* **Imperial College London.**

Orphanides G. and Reinberg D. (2002). A unified theory of gene expression. *Cell* **108**: 439-51.

O'Reilly JP, Cummins TR & Haddad GG. (1997). Oxygen deprivation inhibits Na+ current in rat hippocampal neurones via protein kinase. *C J Physiol* **503**, 479-488.

Ou Y, Strege P, Miller SM, Makielski J, Ackerman M, Gibbons SJ, Farrugia G. (2003). Syntrophin gamma 2 regulates SCN5A gating by a PDZ domain-mediated interaction. *J Biol Chem.* **278**(3):1915-23.

Ou SW, Kameyama A, Hao LY, Horiuchi M, Minobe E, Wang WY, Makita N & Kameyama M. (2005). Tetrodotoxin-resistant Na^+ channels in human neuroblastoma cells are encoded by new variants of Nav1.5/SCN5A. *Eur J Neurosci* **22**, 793-801.

Ouadid-Ahidouch H, Chaussade F, Roudbaraki M, Slomianny C, Dewailly E, Delcourt P, Prevarskaya N. (2000). KV1.1 K(+) channels identification in

human breast carcinoma cells: involvement in cell proliferation. *Biochem Biophys Res Commun.* **278**(2):272-7.

Ouwerkerk R, Jacobs MA, Macura KJ, Wolff AC, Stearns V, Mezban SD, Khouri NF, Bluemke DA, Bottomley PA. (2007). Elevated tissue sodium concentration in malignant breast lesions detected with non-invasive 23Na MRI. *Breast Cancer Res Treat.* **106**(2):151-60.

Ozil JP, Swann K. (1995). Stimulation of repetitive calcium transients in mouse eggs. *J Physiol.* **483** (Pt 2):331-46.

Pacifico F, Ulianich L, De Micheli S, Treglia S, Leonardi A, Vito P, Formisano S, Consiglio E, Di Jeso B. (2003). The expression of the sarco/endoplasmic reticulum Ca2+-ATPases in thyroid and its down-regulation following neoplastic transformation. *J Mol Endocrinol* **30**(3):399-409.

Paget S. (1889). The distribution of secondary growths in cancer of the breast - 1889. *Cancer Metastasis Rev* **8**: 98-101.

Paillart C, Boudier JL, Boudier JA, Rochat H, Couraud F & Dargent B. (1996). Activityinduced internalization and rapid degradation of sodium channels in cultured fetal neurons. *J Cell Biol* **134**, 499-509.

Palmer CP, Mycielska ME, Burcu H, Osman K, Collins T, Beckerman R, Perrett R, Johnson H, Aydar E & Djamgoz MB. (2008). Single cell adhesion measuring

apparatus (SCAMA): application to cancer cell lines of different metastatic potential and voltage-gated Na+ channel expression. *Eur Biophys J* **37**, 359-368.

Palty R, Ohana E, Hershfinkel M, Volokita M, Elgazar V, Beharier O, Silverman WF, Argaman M, Sekler I. (2004). Lithium-calcium exchange is mediated by a distinct potassium-independent sodium-calcium exchanger. *J Biol Chem.* **279**(24):25234-40.

Pantel K, Brakenhoff RH. (2004). Dissecting the metastatic cascade. *Nat Rev Cancer* **4**: 448-56.

Pardo LA, Contreras-Jurado C, Zientkowska M, Alves F, Stühmer W. (2005). Role of voltage-gated potassium channels in cancer. *J Membr Biol.* **205**(3):115-24.

Parihar AS, Coghlan MJ, Gopalakrishnan M, Shieh CC. (2003). Effects of intermediate-conductance Ca2+-activated K+ channel modulators on human prostate cancer cell proliferation. *Eur J Pharmacol* **471**(3):157-64.

Parkash J, Asotra K. (2010) Calcium wave signaling in cancer cells. *Life Sci*. in print.

Paz MF, Wei S, Cigudosa JC, Rodriguez-Perales S, Peinado MA, Huang TH, Esteller M. (2003). Genetic unmasking of epigenetically silenced tumor suppressor genes in colon cancer cells deficient in DNA methyltransferases. *Hum Mol Genet* **12**(17):2209-19.

Peles E, Nativ M, Campbell PL, Sakurai T, Martinez R, Lev S, Clary DO, Schilling J, Barnea G, Plowman GD, Grumet M, Schlessinger J. (1995). The carbonic anhydrase domain of receptor tyrosine phosphatase beta is a functional ligand for the axonal cell recognition molecule contactin. *Cell.* **82**(2):251-60.

Peng JB, Zhuang L, Berger UV, Adam RM, Williams BJ, Brown EM, Hediger MA, Freeman MR. (2001). CaT1 expression correlates with tumor grade in prostate cancer. *Biochem Biophys Res Commun* **282**(3):729-34.

Pennacchietti S, Michieli P, Galluzzo M, Mazzone M, Giordano S, Comoglio PM. (2003). Hypoxia promotes invasive growth by transcriptional activation of the met protooncogene. *Cancer Cell.* **3**(4):347-61.

Pérez-Pinzón MA, Rosenthal M, Sick TJ, Lutz PL, Pablo J, Mash D. Downregulation of sodium channels during anoxia: a putative survival strategy of turtle brain. *Am J Physiol.* **262**(4 Pt 2):R712-5.

Pertin M, Ji RR, Berta T, Powell AJ, Karchewski L, Tate SN, Isom LL, Woolf CJ, Gilliard N, Spahn DR, Decosterd I. (2005). Upregulation of the voltage-gated sodium channel beta2 subunit in neuropathic pain models: characterization of expression in injured and non-injured primary sensory neurons. *J Neurosci.* **25**(47):10970-80.

Pfeiffer BE, Huber KM. (2006). Current advances in local protein synthesis and synaptic plasticity. *J Neurosci* **26**(27):7147-50.

Platoshyn O, Yu Y, Golovina VA, McDaniel SS, Krick S, Li L, Wang JY, Rubin LJ, Yuan JX. (2001). Chronic hypoxia decreases K(V) channel expression and function in pulmonary artery myocytes. *Am J Physiol Lung Cell Mol Physiol*. **280**(4):L801-12.

Plummer NW, McBurney MW & Meisler MH. (1997). Alternative splicing of the sodium channel SCN8A predicts a truncated two-domain protein in fetal brain and non-neuronal cells. *J Biol Chem* **272**, 24008-24015.

Plummer NW, Galt J, Jones JM, Burgess DL, Sprunger LK, Kohrman DC & Meisler MH. (1998). Exon organization, coding sequence, physical mapping, and polymorphic intragenic markers for the human neuronal sodium channel gene SCN8A. *Genomics* **54**, 287–296.

Plummer NW & Meisler MH. (1999). Evolution and diversity of mammalian sodium channel genes. *Genomics* **57**, 323-331.

Poburko D, Liao CH, Lemos VS, Lin E, Maruyama Y, Cole WC, van Breemen C. (2007). Transient receptor potential channel 6-mediated, localized cytosolic [Na+] transients drive Na+/Ca2+ exchanger-mediated Ca2+ entry in purinergically stimulated aorta smooth muscle cells. *Circ Res.* **101**(10):1030-8.

Poste G & Fidler IJ. (1980). The pathogenesis of cancer metastasis. *Nature* **283**, 139-146.

Pouysségur J, Dayan F & Mazure NM. (2006). Hypoxia signalling in cancer and approaches to enforce tumour regression. *Nature* **441,** 437-443.

Prevarskaya N, Skryma R, Bidaux G, Flourakis M & Shuba Y. (2007). Ion channels in death and differentiation of prostate cancer cells. *Cell Death Differ* **14**, 1295-1304.

Prevarskaya N, Skryma R, Shuba Y. (2010). Ion channels and the hallmarks of cancer. *Trends Mol Med.* **16**(3):107-21.

Pruthi S, Brandt KR, Degnim AC, Goetz MP, Perez EA, Reynolds CA, Schomberg PJ, Dy GK, Ingle JN. (2007). A multidisciplinary approach to the management of breast cancer, part 1: prevention and diagnosis. *Mayo Clin Proc* **82**: 999-1012.

Qu Y, Curtis R, Lawson D, Gilbride K, Ge P, DiStefano PS, Silos-Santiago I, Catterall WA & Scheuer T. (2001). Differential modulation of sodium channel gating and persistent sodium currents by the beta1, beta2, and beta3 subunits. *Mol Cell Neurosci* **18**, 570-580.

Ragsdale DS, McPhee JC, Scheuer T, Catterall WA. (1994). Molecular determinants of state-dependent block of Na+ channels by local anesthetics. *Science.* **265**(5179):1724-8.

Rajamani S, Shryock JC & Belardinelli L. (2008). Block of tetrodotoxin-sensitive, Na(V)1.7 and tetrodotoxin-resistant, Na(V)1.8, Na+ channels by ranolazine. *Channels (Austin)* **2**, 449-460.

Ramaswamy S, Ross KN, Lander ES & Golub TR. (2003). A molecular signature of metastasis in primary solid tumors. *Nat Genet* **33**, 49-54.

Ratcliffe CF, Qu Y, McCormick KA, Tibbs VC, Dixon JE, Scheuer T & Catterall WA. (2000). A sodium channel signaling complex: modulation by associated receptor protein tyrosine phosphatase beta. *Nat Neurosci* **3**, 437-444.

Raymond CK, Castle J, Garrett-Engele P, Armour CD, Kan Z, Tsinoremas N & Johnson JM. (2004). Expression of alternatively spliced sodium channel alpha-subunit genes: Unique splicing patterns are observed in dorsal root ganglia. *J Biol Chem* **279**, 46234–46241.

Reisner PD, Brandt PC, Vanaman TC. (1997). Analysis of plasma membrane Ca(2+)-ATPase expression in control and SV40-transformed human fibroblasts. *Cell Calcium* **21**(1):53-62.

Rey O, Young SH, Jacamo R, Moyer MP, Rozengurt E. (2010). Extracellular calcium sensing receptor stimulation in human colonic epithelial cells induces intracellular calcium oscillations and proliferation inhibition. *J Cell Physiol.* **225**(1):73-83.

Ribeiro MA, Costa PF. (2003). The sensitivity of sodium channels in immature and mature rat CA1 neurones to the local anaesthetics procaine and lidocaine. *Brain Res Dev Brain Res.* ***146***(1-2):59-70.

Ridgway PF, Ziprin P, Alkhamesi N, Paraskeva PA, Peck DH & Darzi AW. (2005). Hypoxia augments gelatinase activity in a variety of adenocarcinomas in vitro. *J Surg Res* **124**, 180-186.

Roderick HL, Cook SJ. (2008). Ca2+ signalling checkpoints in cancer: remodelling Ca2+ for cancer cell proliferation and survival. *Nat Rev Cancer.* **8**(5):361-75.

Roger S, Besson P & Le Guennec JY. (2003). Involvement of a novel fast inward sodium current in the invasion capacity of a breast cancer cell line. *Biochim Biophys Acta* **1616**, 107-11.

Roger S, Potier M, Vandier C, Besson P & Le Guennec JY. (2006). Voltage-gated sodium channels: new targets in cancer therapy? *Curr Pharm Des* **12**, 3681-3695.

Roger S, Rollin J, Barascu A, Besson P, Raynal PI, Iochmann S, Lei M, Bougnoux P, Gruel Y & Le Guennec JY. (2007). Voltage-gated sodium channels potentiate

the invasive capacities of human non-small-cell lung cancer cell lines. *Int J Biochem Cell Biol* **39,** 774-786.

Rogers M, Tang L, Madge DJ, Stevens EB. (2006). The role of sodium channels in neuropathic pain. *Semin Cell Dev Biol.* **17**(5):571-81.

Ropponen KM, Kellokoski JK, Pirinen RT, Moisio KI, Eskelinen MJ, Alhava EM, Kosma VM. (2001). Expression of transcription factor AP-2 in colorectal adenomas and adenocarcinomas; comparison of immunohistochemistry and in situ hybridisation. *J Clin Pathol* **54**(7):533-8.

Rosenthal SA, Sandler HM. (2010). Treatment strategies for high-risk locally advanced prostate cancer. *Nat Rev Urol.* **7**(1):31-8.

Rosker C, Graziani A, Lukas M, Eder P, Zhu MX, Romanin C, Groschner K. (2004). Ca(2+) signaling by TRPC3 involves Na(+) entry and local coupling to the Na(+)/Ca(2+) exchanger. *J Biol Chem.* **279**(14):13696-704.

Rougier JS, van Bemmelen MX, Bruce MC, Jespersen T, Gavillet B, Apothéloz F, Cordonier S, Staub O, Rotin D & Abriel H. (2005). Molecular determinants of voltage-gated sodium channel regulation by the Nedd4/Nedd4-like proteins. *Am J Physiol Cell Physiol* **288**, 692-701.

Rudolfsson SH, Bergh A. (2009). Hypoxia drives prostate tumour progression and impairs the effectiveness of therapy, but can also promote cell death and serve as a therapeutic target. *Expert Opin Ther Targets.* **13**(2):219-25.

Rudy B. (1978). Slow inactivation of the sodium conductance in squid giant axons. Pronase resistance. *J Physiol* **283**,1-21.

Sagara Y, Inesi G. (1991). Inhibition of the sarcoplasmic reticulum Ca2+ transport ATPase by thapsigargin at subnanomolar concentrations. *J Biol Chem.* **266**(21):13503-6.

Sage SO, van Breemen C & Cannell MB. (1991). Sodium-calcium exchange in cultured bovine pulmonary artery endothelial cells. *J Physiol* **440**, 569-580.

Saint DA, Ju YK & Gage PW. (1992). A persistent sodium current in rat ventricular myocytes. *J Physiol* **453**, 219-231.

Saint DA. (2006). The role of the persistent Na(+) current during cardiac ischemia and hypoxia. *J Cardiovasc Electrophysiol* **1**, 96-103.

Saint DA. (2008). The cardiac persistent sodium current: an appealing therapeutic target? *Br J Pharmacol* **153**, 1133-1142.

Saito K, Uzawa K, Endo Y, Kato Y, Nakashima D, Ogawara K, Shiba M, Bukawa H, Yokoe H, Tanzawa H. (2006). Plasma membrane Ca2+ ATPase isoform 1 down-regulated in human oral cancer. *Oncol Rep.* **15**(1):49-55.

Sakakura C, Hagiwara A, Fukuda K, Shimomura K, Takagi T, Kin S, Nakase Y, Fujiyama J, Mikoshiba K, Okazaki Y, Yamagishi H. (2003). Possible involvement of inositol 1,4,5-trisphosphate receptor type 3 (IP3R3) in the peritoneal dissemination of gastric cancers. *Anticancer Res* **23**(5A):3691-7.

Salnikow K, Costa M, Figg WD, Blagosklonny MV. (2000). Hyperinducibility of hypoxia-responsive genes without p53/p21-dependent checkpoint in aggressive prostate cancer. *Cancer Res.* **60**(20):5630-4.

Sambrook J, Fritsch EF & Maniatis T. (1989). Molecular cloning: a laboratory manual, Cold Spring Harbor Laboratory Press.

Samudio I, Harmancey R, Fiegl M, Kantarjian H, Konopleva M, Korchin B, Kaluarachchi K, Bornmann W, Duvvuri S, Taegtmeyer H, Andreeff M. (2010). Pharmacologic inhibition of fatty acid oxidation sensitizes human leukemia cells to apoptosis induction. *J Clin Invest* **120**(1):142-56.

Sano S, Chan KS, Carbajal S, Clifford J, Peavey M, Kiguchi K, Itami S, Nickoloff BJ, DiGiovanni J. (2005). Stat3 links activated keratinocytes and immunocytes required for development of psoriasis in a novel transgenic mouse model. *Nat Med.* **11**(1):43-9.

Sarao R, Gupta SK, Auld VJ & Dunn RJ. (1991). Developmentally regulated alternative RNA splicing of rat-brain sodium-channel messenger-RNAs. *Nucleic Acids Res* **19**, 5673-5679.

Sashihara S, Yanagihara N, Izumi F, Murai Y & Mita T. (1994). Differential up-regulation of voltage-dependent Na+ channels induced by phenytoin in brains of genetically seizuresusceptible (E1) and control (ddY) mice. *Neuroscience* **62**, 803-811.

Satin J, Kyle JW, Chen M, Bell P, Cribbs LL, Fozzard HA & Rogart RB. (1992). A mutant of TTX-resistant cardiac sodium channels with TTX-sensitive properties. *Science* **256**, 1202-1205.

Sato C, Ueno Y, Asai K, Takahashi K, Sato M, Engel A & Fujiyoshi Y. (2001). The voltage-sensitive sodium channel is a bell-shaped molecule with several cavities. *Nature* **409**, 1047-1051.

Sato Y, Fujiwara H, Higuchi T, Yoshioka S, Tatsumi K, Maeda M, Fujii S. (2002). Involvement of dipeptidyl peptidase IV in extravillous trophoblast invasion and differentiation. *J Clin Endocrinol Metab.* **87**(9):4287-96.

Schaller KL, Krzemien DM, McKenna NM & Caldwell JH. (1992). Alternatively spliced sodium channel transcripts in brain and muscle. *J Neurosci* **12**, 1370-1381.

Schaller KL, Krzemien DM, Yarowsky PJ, Krueger BK & Caldwell JH. (1995). A novel, abundant sodium channel expressed in neurons and glia. *J Neurosci* **15**, 3231-3242.

Schedel J., Distler O., Woenckhaus M., Gay R. E., Simmen B., Michel B. A., Muller-Ladner U. and Gay S. (2004). Discrepancy between mRNA and protein expression of tumour suppressor maspin in synovial tissue may contribute to synovial hyperplasia in rheumatoid arthritis. *Ann Rheum Dis* **63**: 1205-11.

Schmidt U, Fuessel S, Koch R, Baretton GB, Lohse A, Tomasetti S, Unversucht S, Froehner M, Wirth MP, Meye A. (2006). Quantitative multi-gene expression profiling of primary prostate cancer. *Prostate* **66**(14):1521-34.

Schreibmayer W, Dascal N, Lotan I, Wallner M & Weigl L. (1991). Molecular mechanism of protein kinase C modulation of sodium channel alpha-subunits expressed in Xenopus oocytes. *FEBS Lett* **291**, 341-344.

Schroeter A, Walzik S, Blechschmidt S, Haufe V, Benndorf K & Zimmer T. (2010). Structure and function of splice variants of the cardiac voltage-gated sodium channel Na(v)1.5. *J Mol Cell Cardiol* **49**, 16-24.

Schwirzke M, Schiemann S, Gnirke AU & Weidle UH. (1999). New genes potentially involved in breast cancer metastasis. *Anticancer Res* **19**, 1801-1814.

Scorey N, Fraser SP, Patel P, Pridgeon C, Dallman MJ, Djamgoz MB. (2006). Notch signalling and voltage-gated Na+ channel activity in human prostate cancer cells: independent modulation of in vitro motility. *Prostate Cancer Prostatic Dis.* **9**(4):399-406.

Seda M, Pinto FM, Wray S, Cintado CG, Noheda P, Buschmann H, Candenas L. (2007). Functional and molecular characterization of voltage-gated sodium channels in uteri from nonpregnant rats. *Biol Reprod* **77**(5):855-63.

Seta K, Kim HW, Ferguson T, Kim R, Pathrose P, Yuan Y, Lu G, Spicer Z, Millhorn DE. (2002). Genomic and physiological analysis of oxygen sensitivity and hypoxia tolerance in PC12 cells. *Ann N Y Acad Sci.* **971**:379-88.

Shah BS, Rush AM, Liu S, Tyrrell L, Black JA, Dib-Hajj SD & Waxman SG. (2004). Contactin associates with sodium channel Nav1.3 in native tissues and increases channel density at the cell surface. *J Neurosci* **24**, 7387-7399.

Shao D, Okuse K & Djamgoz MB. (2009). Protein-protein interactions involving voltage-gated sodium channels: Post-translational regulation, intracellular trafficking and functional expression. *Int J Biochem Cell Biol* **41**, 1471-1481.

Sheets MF & Hanck DA. (2007). Outward stabilization of the S4 segments in domains III and IV enhances lidocaine block of sodium channels. *J Physiol* **582**, 317-334.

Shipston MJ. (2001). Alternative splicing of potassium channels: a dynamic switch of cellular excitability. *Trends Cell Biol*. **11**(9):353-8.

Shiraishi S, Shibuya I, Uezono Y, Yokoo H, Toyohira Y, Yamamoto R, Yanagita T, Kobayashi H & Wada A. (2001a). Heterogeneous increases of cytoplasmic calcium: distinct effects on down-regulation of cell surface sodium channels and sodium channel subunit mRNA levels. *Br J Pharmacol* **132**, 1455-1466.

Shiraishi S, Yanagita T, Kobayashi H, Uezono Y, Yokoo H, Minami SI, Takasaki M & Wada A. (2001b). Up-regulation of cell surface sodium channels by cyclosporin A, FK506, and rapamycin in adrenal chromaffin cells. *J Pharmacol Exp Ther* **297**, 657-665.

Sikes RA, Walls AM, Brennen WN, Anderson JD, Choudhury-Mukherjee I, Schenck HA & Brown ML. (2003). Therapeutic approaches targeting prostate cancer progression using novel voltage-gated ion channel blockers. *Clin Prostate Cancer* **2**, 181-187.

Simone G, Mangia A, Petroni S, Trotti I, Paradiso A, Marzullo F, De Lena M & Leone A. (1998). nm23 expression in human breast cancer: correlation with cell proliferation (S-phase) as observed with a double-labeling immunocytochemical-autoradiographic technique. *Int J Oncol* **12**, 1055-1059.

Skryma RN, Prevarskaya NB, Dufy-Barbe L, Odessa MF, Audin J, Dufy B. (1997). Potassium conductance in the androgen-sensitive prostate cancer cell line, LNCaP: involvement in cell proliferation. *Prostate* **33**(2):112-22.

Smith RD & Goldin AL. (1997). Phosphorylation at a single site in the rat brain sodium channel is necessary and sufficient for current reduction by protein kinase A. *J Neurosci* **17**, 6086-6093.

Smith RD & Goldin AL. (1998). Functional analysis of the rat I sodium channel in xenopus oocytes. *J Neurosci* **18**, 811-820.

Smith P, Rhodes NP, Shortland AP, Fraser SP, Djamgoz MB, Ke Y & Foster CS. (1998). Sodium channel protein expression enhances the invasiveness of rat and human prostate cancer cells. *FEBS Lett* **423**, 19-24.

Sola B., Salaun V., Ballet J. J. and Troussard X. (1999). Transcriptional and post-transcriptional mechanisms induce cyclin-D1 over-expression in B-chronic lymphoproliferative disorders. *Int J Cancer* **83**: 230-4.

Song Y, Wang W, Qu X, Sun S. (2009). Effects of hypoxia inducible factor-1alpha (HIF-1alpha) on the growth & adhesion in tongue squamous cell carcinoma cells. *Indian J Med Res.***129**(2):154-63.

Sporn MB. (1996). The war on cancer. *Lancet* **347**: 1377-81.

Sretavan DW, Shatz CJ, Stryker MP. (1988). Modification of retinal ganglion cell axon morphology by prenatal infusion of tetrodotoxin. *Nature* **336**(6198):468-71.

Srinivasan J, Schachner M & Catterall WA. (1998). Interaction of voltage-gated sodium channels with the extracellular matrix molecules tenascin-C and tenascin-R. *Proc Natl Acad Sci USA* **95**, 15753-15757.

Stamey TA, Johnstone IM, McNeal JE, Lu AY, Yemoto CM. (2002). Preoperative serum prostate specific antigen levels between 2 and 22 ng./ml. correlate poorly with post-radical prostatectomy cancer morphology: prostate specific antigen cure rates appear constant between 2 and 9 ng./ml. *J Urol* **167**(1):103-11.

Steeg PS, Ouatas T, Halverson D, Palmieri D & Salerno M. (2003). Metastasis suppressor genes: basic biology and potential clinical use. *Clin Breast Cancer* **4**, 51-62.

Steinsapir J, Socci R, Reinach P. (1991). Effects of androgen on intracellular calcium of LNCaP cells. *Biochem Biophys Res Commun* **179**(1):90-6.

Stetler-Stevenson WG, Aznavoorian S, Liotta LA. (1993). Tumor cell interactions with the extracellular matrix during invasion and metastasis. *Annu Rev Cell Biol* **9**: 541-73.

St Johnston D. (2005). Moving messages: the intracellular localization of mRNAs. *Nat Rev Mol Cell Biol* **6**: 363-75.

Streb H, Irvine RF, Berridge MJ, Schulz I. (1983). Release of Ca2+ from a nonmitochondrial intracellular store in pancreatic acinar cells by inositol-1,4,5-trisphosphate. *Nature*. **306**(5938):67-9.

Subarsky P & Hill RP. (2003). The hypoxic tumour microenvironment and metastatic progression. *Clin Exp Metastasis.* **20**(3):237-50.

Subarsky P & Hill RP. (2008). Graded hypoxia modulates the invasive potential of HT1080 fibrosarcoma and MDA MB231 carcinoma cells. *Clin Exp Metastasis* **25**, 253-264.

Subramanian S, Viatchenko-Karpinski S, Lukyanenko V, Györke S, Wiesner TF. (2001). Underlying mechanisms of symmetric calcium wave propagation in rat ventricular myocytes. *Biophys J.* **80**(1):1-11.

Suckow MA, Gutierrez LS, Risatti CA, Wolter WR, Taylor RE, Pollard M, Navari RM, Castellino FJ, Paoni NF. (2004). The anti-ischemia agent ranolazine promotes the development of intestinal tumors in APC(Min/+) mice. *Cancer Lett* **209**(2):165-9.

Sun YM, Favre I, Schild L & Moczydlowski E. (1997). On the structural basis for size-selective permeation of organic cations through the voltage-gated sodium

channel. Effect of alanine mutations at the DEKA locus on selectivity, inhibition by Ca2+ and H+, and molecular sieving. *J Gen Physiol* **110**, 693-715.

Swartz KJ. (2008). Sensing voltage across lipid membranes. *Nature* **456**, 891-897.

Tabb JS, Fanger GR, Wilson EM, Maue RA & Henderson LP. (1994). Suppression of sodium channel function in differentiating C2 muscle cells stably overexpressing rat androgen receptors. *J Neurosci* **14**, 763-773.

Taddese A & Bean BP. (2002). Subthreshold sodium current from rapidly inactivating sodium channels drives spontaneous firing of tuberomammillary neurons. *Neuron* **33**, 587-600.

Tanaka T, Kato H, Kojima I, Ohse T, Son D, Tawakami T, Yatagawa T, Inagi R, Fujita T, Nangaku M. (2006). Hypoxia and expression of hypoxia-inducible factor in the aging kidney. *J Gerontol A Biol Sci Med Sci.* **61**(8):795-805.

Tang F, Dent EW, Kalil K. (2003). Spontaneous calcium transients in developing cortical neurons regulate axon outgrowth. *J Neurosci.* **23**(3):927-36.

Tateyama M, Rivolta I, Clancy CE & Kass RS. (2003). Modulation of cardiac sodium channel gating by protein kinase A can be altered by disease-linked mutation. *J Biol Chem* **278**, 46718-46726.

Tennant TR, Kim H, Sokoloff M, Rinker-Schaeffer CW. (2000). The Dunning model. *Prostate* **43**(4):295-302.

Thebault S, Lemonnier L, Bidaux G, Flourakis M, Bavencoffe A, Gordienko D, Roudbaraki M, Delcourt P, Panchin Y, Shuba Y, Skryma R, Prevarskaya N. (2005). Novel role of cold/menthol-sensitive transient receptor potential melastatine family member 8 (TRPM8) in the activation of store-operated channels in LNCaP human prostate cancer epithelial cells. *J Biol Chem* **280**(47):39423-35.

Thiery JP. (2002). Epithelial-mesenchymal transitions in tumour progression. *Nat Rev Cancer.* **2**(6):442-54.

Thimmapaya R, Neelands T, Niforatos W, Davis-Taber RA, Choi W, Putman CB, Kroeger PE, Packer J, Gopalakrishnan M, Faltynek CR, Surowy CS & Scott VE. (2005). Distribution and functional characterization of human Nav1.3 splice variants. *Eur J Neurosci* **22**, 1-9.

Tietze C, Schlesinger P & Stahl P. (1980). Chloroquine and ammonium ion inhibit receptormediated endocytosis of mannose-glycoconjugates by macrophages: apparent inhibition of receptor recycling. *Biochem Biophys Res Commun* **93**, 1-8.

Tikhonov DB & Zhorov BS. (2007). Sodium channels: ionic model of slow inactivation and state-dependent drug binding. *Biophys J* **93**, 1557-1570.

Toledo-Aral JJ, Brehm P, Halegoua S & Mandel GA. (1995). Single pulse of nerve growth factor triggers long-term neuronal excitability through sodium channel gene induction. *Neuron* **14**, 607-11.

Toledo-Aral JJ, Moss BL, He ZJ, Koszowski AG, Whisenand T, Levinson SR, Wolf JJ, Silos-Santiago I, Halegoua S & Mandel G. (1997). Identification of PN1, a predominant voltage-dependent sodium channel expressed principally in peripheral neurons. *Proc Natl Acad Sci USA* **94**, 1527-1532.

Tombola F, Pathak MM & Isacoff EY. (2006). How does voltage open an ion channel? *Annu Rev Cell Dev Biol* **22**, 23-52.

Toyota M, Ho C, Ohe-Toyota M, Baylin SB, Issa JP. (1999). Inactivation of CACNA1G, a T-type calcium channel gene, by aberrant methylation of its 5' CpG island in human tumors. *Cancer Res* **59**(18):4535-41.

Trimmer JS & Rhodes KJ. (2004). Localization of voltage-gated ion channels in mammalian brain. *Annu Rev Physiol* **66**, 477-519.

Tsavaler L, Shapero MH, Morkowski S, Laus R. (2001). Trp-p8, a novel prostate-specific gene, is up-regulated in prostate cancer and other malignancies and shares high homology with transient receptor potential calcium channel proteins. *Cancer Res* **61**(9):3760-9.

Tse A, Tse FW, Almers W, Hille B. (1993). Rhythmic exocytosis stimulated by GnRH-induced calcium oscillations in rat gonadotropes. *Science.* **260**(5104):82-4.

Tsuchiya H, Mizogami M, Ueno T, Takakura K. (2007). Interaction of local anaesthetics with lipid membranes under inflammatory acidic conditions. *Inflammopharmacology* **15**(4):164-70.

Tyrrell L, Renganathan M, Dib-Hajj SD & Waxman SG. (2001). Glycosylation alters steadystate inactivation of sodium channel Nav1.9/NaN in dorsal root ganglion neurons and is developmentally regulated. *J Neurosci* **21**, 9629-9637.

Uhlén P, Laestadius A, Jahnukainen T, Söderblom T, Bäckhed F, Celsi G, Brismar H, Normark S, Aperia A, Richter-Dahlfors A. (2000). Alpha-haemolysin of uropathogenic E. coli induces Ca2+ oscillations in renal epithelial cells. *Nature.* **405**(6787):694-7.

Undrovinas AI, Shander GS, Makielski JC. (1995). Cytoskeleton modulates gating of voltage-dependent sodium channel in heart. *Am J Physiol.* **269**(1 Pt 2):H203-14.

Urbani A, Belluzzi O. (2000). Riluzole inhibits the persistent sodium current in mammalian CNS neurons. *Eur J Neurosci* **12**(10):3567-74.

Vaidya KS & Welch DR. (2007). Metastasis suppressors and their roles in breast carcinoma. *J Mammary Gland Biol Neoplasia* **12**, 175-190.

Valverde CA, Kornyeyev D, Ferreiro M, Petrosky AD, Mattiazzi A, Escobar AL. (2010). Transient Ca2+ depletion of the sarcoplasmic reticulum at the onset of reperfusion. *Cardiovasc Res.* **85**(4):671-80.

van Bemmelen MX, Rougier JS, Gavillet B, Apothéloz F, Daidié D, Tateyama M, Rivolta I, Thomas MA, Kass RS, Staub O & Abriel H. (2004). Cardiac voltage-gated sodium channel Nav1.5 is regulated by Nedd4-2 mediated ubiquitination. *Circ Res* **95**, 284-291.

Vaupel P, Höckel M, Mayer A. (2007). Detection and characterization of tumor hypoxia using pO2 histography. *Antioxid Redox Signal* **9**(8):1221-35.

Vecchi M, Confalonieri S, Nuciforo P, Viganò MA, Capra M, Bianchi M, Nicosia D, Bianchi F, Galimberti V, Viale G, Palermo G, Riccardi A, Campanini R, Daidone MG, Pierotti MA, Pece S & Di Fiore PP. (2008). Breast cancer metastases are molecularly distinct from their primary tumors. *Oncogene* **27**, 2148-2158.

Viale M, Pastrone I, Pellecchia C, Vannozzi MO, Cafaggi S, Esposito M. (1998). Combination of cisplatin-procaine complex DPR with anticancer drugs increases cytotoxicity against ovarian cancer cell lines. *Anticancer Drugs* **9**(5):457-63.

Vijayaragavan K, Boutjdir M & Chahine M. (2004). Modulation of Nav1.7 and Nav1.8 peripheral nerve sodium channels by protein kinase A and protein kinase C. *J Neurophysiol* **91**, 1556-1569.

Vilin YY & Ruben PC. (2001). Slow inactivation in voltage-gated sodium channels: molecular substrates and contributions to channelopathies. *Cell Biochem Biophys* **35**, 171-190.

Villar-Garea A, Fraga MF, Espada J, Esteller M.(2003). Procaine is a DNA-demethylating agent with growth-inhibitory effects in human cancer cells. *Cancer Res* **63**(16):4984-9.

Vlachová V, Vitásková Z, Vyklický L, Orkand RK. (1999). Procaine excites nociceptors in cultures from dorsal root ganglion of the rat. *Neurosci Lett.* **263**(1):49-52.

Wang XT, Nagaba Y, Cross HS, Wrba F, Zhang L, Guggino SE. (2000) The mRNA of L-type calcium channel elevated in colon cancer: protein distribution in normal and cancerous colon. *Am J Pathol* **157**(5):1549-62.

Wang H, Zhang Y, Cao L, Han H, Wang J, Yang B, Nattel S, Wang Z. (2002). HERG K+ channel, a regulator of tumor cell apoptosis and proliferation. *Cancer Res* **62**(17):4843-8.

Wang W, Ma J, Zhang P & Luo A. (2007). Redox reaction modulates transient and persistent sodium current during hypoxia in guinea pig ventricular myocytes. *Pflugers Arch* **454**, 461-475.

Wang GK, Calderon J & Wang SY. (2008). State- and use-dependent block of muscle Nav1.4 and neuronal Nav1.7 voltage-gated Na+ channel isoforms by ranolazine. *Mol Pharmacol* **73**, 940-948.

Wang Q, Symes AJ, Kane CA, Freeman A, Nariculam J, Munson P, Thrasivoulou C, Masters JR, Ahmed A. (2010). A novel role for Wnt/Ca2+ signaling in actin cytoskeleton remodeling and cell motility in prostate cancer. *PLoS One* **5**(5):e10456.

Watson JA, Watson CJ, McCrohan AM, Woodfine K, Tosetto M, McDaid J, Gallagher E, Betts D, Baugh J, O'Sullivan J, Murrell A, Watson RW, McCann A. (2009). Generation of an epigenetic signature by chronic hypoxia in prostate cells. *Hum Mol Genet* **18**(19):3594-604.

Waxman SG, Kocsis JD & Black JA. (1994). Type III sodium channel mRNA is expressed in embryonic but not adult spinal sensory neurons, and is reexpressed following axotomy. *J Neurophysiol* **72**, 466-470.

Waxman SG. (2007). Channel, neuronal and clinical function in sodium channelopathies: from genotype to phenotype. *Nat Neurosci* **10**, 405-409.

Wei C, Wang X, Chen M, Ouyang K, Song LS, Cheng H. (2009). Calcium flickers steer cell migration. *Nature.* **457**(7231):901-5. Epub 2008 Dec 31.

Weigelt B, Hu Z, He X, Livasy C, Carey LA, Ewend MG, Glas AM, Perou CM & Van't Veer LJ. (2005). Molecular portraits and 70-gene prognosis signature are preserved throughout the metastatic process of breast cancer. *Cancer Res* **65**, 9155-9158.

Weiss S, Benoist D, White E, Teng W & Saint DA. (2010). Riluzole protects against cardiac ischaemia and reperfusion damage via block of the persistent sodium current. *Br J Pharmacol* **160**, 1072-1082.

Welch DR, Steeg PS & Rinker-Schaeffer CW. (2000). Molecular biology of breast cancer metastasis. Genetic regulation of human breast carcinoma metastasis. *Breast Cancer Res* **2**, 408-416.

Welch DR. (2004). Microarrays bring new insights into understanding of breast cancer metastasis to bone. *Breast Cancer Res* **6**, 61-64.

Welch DR. (2006). Do we need to redefine a cancer metastasis and staging definitions? *Breast Dis* **26**, 3-12.

Wertz IE, Dixit VM. (2000). Characterization of calcium release-activated apoptosis of LNCaP prostate cancer cells. *J Biol Chem.* **275**(15):11470-7.

West JW, Numann R, Murphy BJ, Scheuer T & Catterall WA. (1991). A phosphorylation site in the Na+ channel required for modulation by protein kinase C. *Science* **254**, 866-868.

West JW, Patton DE, Scheuer T, Wang Y, Goldin AL & Catterall WA. (1992). A cluster of hydrophobic amino acid residues required for fast Na(+)-channel inactivation. *Proc Natl Acad Sci USA* **89**, 10910-10914.

Whitaker WR, Faull RL, Waldvogel HJ, Plumpton CJ, Emson PC & Clare JJ. (2001). Comparative distribution of voltage-gated sodium channel proteins in human brain. *Brain Res Mol Brain Res* **88**, 37-53.

Wilkemeyer MF, Angelides KJ. (1996). Addition of tetrodotoxin alters the morphology of thalamocortical axons in organotypic cocultures. *J Neurosci Res* **43**(6):707-18.

Williams BA, Sims SM. (2007). Calcium sparks activate calcium-dependent Cl- current in rat corpus cavernosum smooth muscle cells. *Am J Physiol Cell Physiol.* **293**(4):C1239-51.

Wissenbach U, Niemeyer BA, Fixemer T, Schneidewind A, Trost C, Cavalie A, Reus K, Meese E, Bonkhoff H, Flockerzi V. (2001). Expression of CaT-like, a novel calcium-selective channel, correlates with the malignancy of prostate cancer. *J Biol Chem* **276**(22):19461-8.

Wonderlin WF, Strobl JS. (1996). Potassium channels, proliferation and G1 progression. *Membr Biol.* **154**(2):91-107.

Wu Y, Palad AJ, Wasilenko WJ, Blackmore PF, Pincus WA, Schechter GL, Spoonster JR, Kohn EC, Somers KD. (1997). Inhibition of head and neck squamous cell carcinoma growth and invasion by the calcium influx inhibitor carboxyamido-triazole. *Clin Cancer Res.* **3**(11):1915-21.

Wychoff JB, Jones JG, Condeelis JS, Segall JE. (2000). A critical step in metastasis: in vivo analysis of intravasation at the primary tunor. Cancer Res. 60(9):2504-11.

Xiao XH & Allen DG. (1999). Role of Na(+)/H(+) exchanger during ischemia and preconditioning in the isolated rat heart. *Circ Res* **85**, 723-730.

Xiao ZC, Ragsdale DS, Malhotra JD, Mattei LN, Braun PE, Schachner M & Isom LL. (1999). Tenascin-R is a functional modulator of sodium channel beta subunits. *J Biol Chem* **274**, 26511-26517.

Xie J & Black DL. (2001). A CaMK IV responsive RNA element mediates depolarizationinduced alternative splicing of ion channels. *Nature* **410**, 936-939.

Xu L, Enyeart JA, Enyeart JJ. (2001). Neuroprotective agent riluzole dramatically slows inactivation of Kv1.4 potassium channels by a voltage-dependent oxidative mechanism. *J Pharmacol Exp Ther* **299**(1):227-37.

Yan J, Aldrich RW. (2010). LRRC26 auxiliary protein allows BK channel activation at resting voltage without calcium. *Nature.* **466**(7305):513-6.

Yanagita T, Kobayashi H, Yamamoto R, Kataoka H, Yokoo H, Shiraishi S, Minami S, Koono M & Wada A. (2000). Protein kinase C-alpha and -epsilon down-regulate cell surface sodium channels via differential mechanisms in adrenal chromaffin cells. *J Neurochem* **74**, 1674-1684.

Yau TM, Kim SC. (1980). Local anaesthetics as hypoxic radiosensitizers, oxic radioprotectors and potentiators of hyperthermic killing in mammalian cells. *Br J Radiol* **53**(631):687-92.

Yu JL, Rak JW, Coomber BL, Hicklin DJ, Kerbel RS. (2002). Effect of p53 status on tumor response to antiangiogenic therapy. *Science.* **295**(5559):1526-8.

Yu FH, Westenbroek RE, Silos-Santiago I, McCormick KA, Lawson D, Ge P, Ferriera H, Lilly J, DiStefano PS, Catterall WA, Scheuer T & Curtis R. (2003). Sodium channel beta4, a new disulfide-linked auxiliary subunit with similarity to beta2. *J Neurosci* **23**, 7577-7585.

Yu FH & Catterall WA. (2003). Overview of the voltage-gated sodium channel family. *Genome Biol* **4**, 207.

Yuhi T, Wada A, Kobayashi H, Yamamoto R, Yanagita T & Niina H. (1996). Up-regulation of functional voltage-dependent sodium channels by cyclic AMP-dependent protein kinase in adrenal medulla. *Brain Res* **709**, 37-43.

Zhang L, Zhou W, Velculescu VE, Kern SE, Hruban RH, Hamilton SR, Vogelstein B, Kinzler KW. (1997) Gene expression profiles in normal and cancer cells. *Science* **276**(5316):1268-72.

Zhang JH, Gibney GT, Xia Y. (2001). Effect of prolonged hypoxia on Na+ channel mRNA subtypes in the developing rat cortex. *Brain Res Mol Brain Res.* **91**(1-2):154-8.

Zhang ZN, Li Q, Liu C, Wang HB, Wang Q & Bao L. (2008). The voltage-gated Na+ channel Nav1.8 contains an ER-retention/retrieval signal antagonized by the beta3 subunit. *J Cell Sci* **121**, 3243-3452.

Zhang YL, Tavakoli H, Chachisvilis M. (2010). Apparent PKA activity responds to intermittent hypoxia in bone cells: a redox pathway? *Am J Physiol Heart Circ Physiol.* **299**(1):H225-35.

Zhu W, Ou Y, Li Y, Xiao R, Shu M, Zhou Y, Xie J, He S, Qiu P, Yan G. (2009). A small-molecule triptolide suppresses angiogenesis and invasion of human

anaplastic thyroid carcinoma cells via down-regulation of the nuclear factor-kappa B pathway. *Mol Pharmacol.* **75**(4):812-9.

Zhuang L, Peng JB, Tou L, Takanaga H, Adam RM, Hediger MA, Freeman MR. (2002). Calcium-selective ion channel, CaT1, is apically localized in gastrointestinal tract epithelia and is aberrantly expressed in human malignancies. *Lab Invest* **82**(12):1755-64.

Zimmer T, Biskup C, Bollensdorff C & Benndorf K. (2002a) The beta1 subunit but not the beta2 subunit colocalizes with the human heart Na+ channel (hH1) already within the endoplasmic reticulum. *J Membr Biol* **186**, 13-21.

Zimmer T, Bollensdorff C, Haufe V, Birch-Hirschfeld E & Benndorf K. (2002b) Mouse heart Na+ channels: primary structure and function of two isoforms and alternatively spliced variants. *Am J Physiol Heart Circ Physiol* **282**, 1007-1017.

Zona C, Siniscalchi A, Mercuri NB, Bernardi G. (1998). Riluzole interacts with voltage-activated sodium and potassium currents in cultured rat cortical neurons. *Neuroscience* **85**(3):931-8.

Zhong Z, Yeow WS, Zou C, Wassell R, Wang C, Pestell RG, Quong JN, Quong AA. (2010). Cyclin D1/cyclin-dependent kinase 4 interacts with filamin A and affects the migration and invasion potential of breast cancer cells. *Cancer Res.***70**(5):2105-14.

Zhou D, Lambert S, Malen PL, Carpenter S, Boland LM & Bennett V. (1998). AnkyrinG is required for clustering of voltage-gated Na channels at axon initial segments and for normal action potential firing. *J Cell Biol* **143**, 1295-1304.

Zhou J, Yi J, Hu N, George AL Jr & Murray KT. (2000). Activation of protein kinase A modulates trafficking of the human cardiac sodium channel in Xenopus oocytes. *Circ Res* **87**, 33-38.

Zhou J, Shin HG, Yi J, Shen W, Williams CP & Murray KT. (2002). Phosphorylation and putative ER retention signals are required for protein kinase A-mediated potentiation of cardiac sodium current. *Circ Res* **91**, 540-546.

Zygmunt AC, Eddlestone GT, Thomas GP, Nesterenko VV & Antzelevitch C. (2001). Larger late sodium conductance in M cells contributes to electrical heterogeneity in canine ventricle. *Am J Physiol Heart Circ Physiol* **281**, 689-697.

Publications

Refereed/full/archival papers

Mazurek MP, Prasad PD, Gopal E, Fraser SP, Bolt L, Rizaner N, Palmer CP, Foster CS, Palmieri F, Ganapathy V, Stühmer W, Djamgoz MB, Mycielska ME.

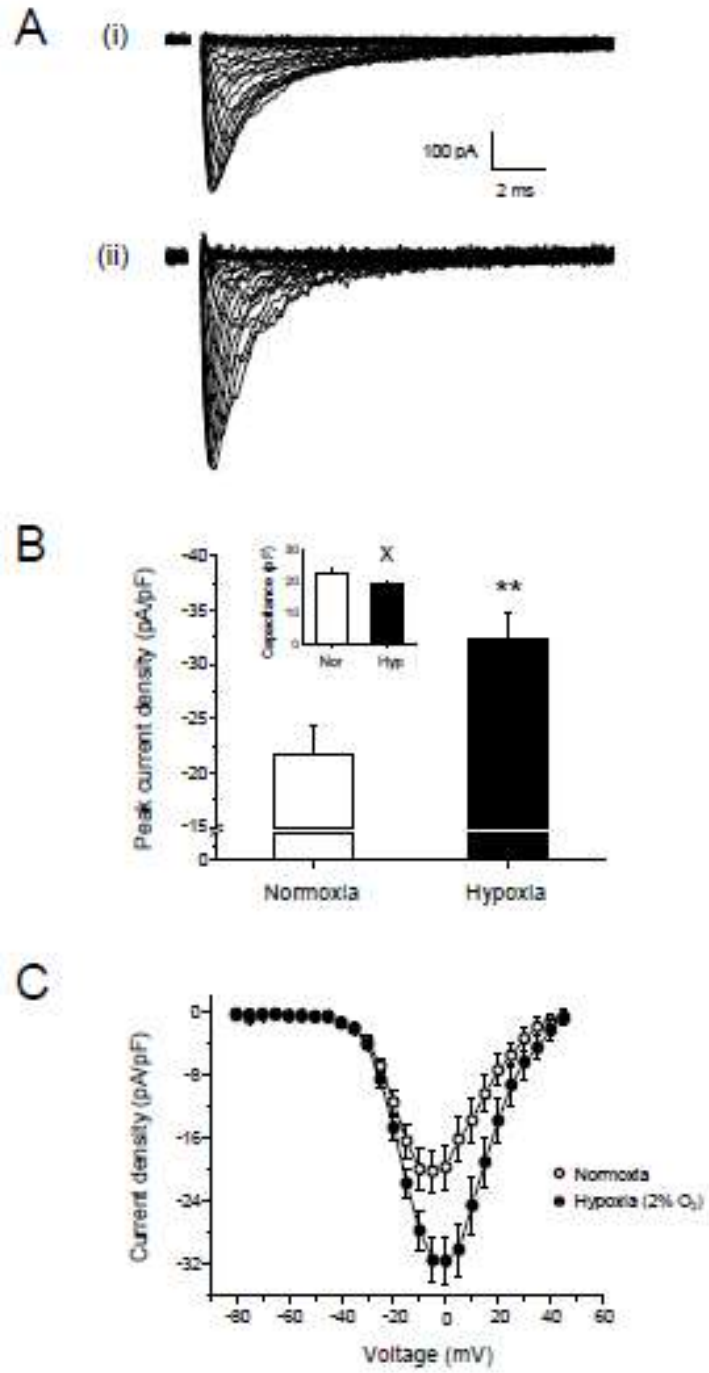
(2010). Molecular origin of plasma membrane citrate transporter in human prostate epithelial cells. *EMBO Rep* **11**(6):431-7.

Mycielska ME, Patel A, Rizaner N, Mazurek MP, Keun H, Patel A, Ganapathy V, Djamgoz MB. (2009). Citrate transport and metabolism in mammalian cells: prostate epithelial cells and prostate cancer. *Bioessays* **31**(1):10-20.

Manuscripts in preparation

Onkal R, Fraser SP, Diss JKJ, Rizaner N, Shao D and Djamgoz MBA. Hypoxic modulation of voltage-gated sodium channel expression and activity in strongly metastatic MDA-MB-231 human breast cancer cells: Enhancement of invasiveness *in vitro*.

Appendices



Appendix 1 Hypoxia (2 % O_2, 24 h) increased peak Na^+ current density in Mat-LyLu cells.

(A) Typical whole-cell VGSC current in (i) normoxic (~21 % O_2, 24h) and (ii) hypoxic (2 % O_2, 24h) Mat-LyLu cells, elicited by 60 ms pulses to between -80 mV and +45 mV from a holding potential of -100 mV; interpulse duration was 2 s. (B) Bar diagram showing average peak current density in normoxic and hypoxic Mat-LyLu cells. Inset: bar deagram showing whole-cell capacitance in normoxic and hypoxic Mat-LyLu cells. (C) Mean *I-V* relationship for normoxic and hypoxic Mat-LyLu cells. Current density was larger in hypoxic Mat-LyLu cells in the voltage range -15 to +15 mV. Un-paired student t-test was used for statistic analysis. Data are presented as means ± SEM (n = 21 - 25). Significance: (**) $p < 0.01$; (X) $p > 0.05$. (Modified from Onkal, 2010)